Caractérisation des propriétés d'emploi des aciers thixoforgés : vers la maîtrise du processus de fabrication

Guochao Gu

2013-ENAM-0002

École doctorale n° 432 : Sciences des Métiers de l'Ingénieur

Doctorat ParisTech
T H È S E

pour obtenir le grade de docteur délivré par

l'École Nationale Supérieure d'Arts et Métiers

Spécialité " Génie mécanique – procédés de fabrication (AM) "

présentée et soutenue publiquement par

Guochao GU

le 18 janvier 2013

Metallurgical characterization of thixoforged steel parts for a better controlled manufacturing process

~ ~ ~

Caractérisation des propriétés d'emploi des aciers thixoforgés : vers la maîtrise du processus de fabrication

Directeur de thèse : **Régis BIGOT**
Co-encadrement de la thèse : **Raphaël PESCI et Laurent LANGLOIS**

Jury

M. Hervé COMBEAU, Professeur des Universités, Ecole des Mines de Nancy	Président
Mme. Helen Valerie ATKINSON, Professeur, University of Leicester	Rapporteur
M. Kaikun WANG, Professeur, University of Science & Technology Beijing	Rapporteur
M. Eric MAIRE, Directeur de recherche CNRS, INSA de Lyon	Examinateur
Mme. Véronique FAVIER, Professeur des Universités, Arts et Métiers ParisTech – Centre de Paris	Invité
M. Régis BIGOT, Professeur, Arts et Métiers ParisTech – Centre de Metz	Examinateur
M. Laurent LANGLOIS, Maître de conférences, Arts et Métiers ParisTech – Centre de Metz	Examinateur
M. Raphaël PESCI, Maître de conférences, Arts et Métiers ParisTech – Centre de Metz	Examinateur

T H È S E

Arts et Métiers ParisTech - Centre de Metz
LCFC EA CNRS 4495 et LEM3 UMR CNRS 7239

Remerciements / Acknowledgements

I would like to thank everybody who has helped me getting to this day in any kind of way.

First of all, I am extremely grateful to my supervisor, Régis BIGOT for giving me the opportunity to achieve this work. I also appreciated his continual support and immense help throughout the past three years. Régis's wisdom, enthusiasm inspired me to undertake further studies in metal forming. I hope that someday I could be as energetic, enthusiastic and lively as Régis.

I also want to thank the members of my PhD committee, Helen Valerie Atkinson, Kaikun Wang, Hervé Combeau, Eric Maire and Véronique Favier for their helpful suggestions in general. I thank the jury for participating in this Ph.D. defense as well. Special thanks to professors Atkinson and Wang for taking time to read carefully my manuscript and giving back their constructive advice.

I am extremely grateful to my co-supervisors, Raphaël Pesci and Laurent Langlois. Raphaël has been supportive and has given me the freedom to pursue various experiments without objection. He has accompanied me on numerous observing sessions and has been an excellent teacher of many aspects of microstructure observations. He has also provided insightful discussions about the research. I have also appreciated the immense help that Rahaël has given me not only in research activities but also in daily life. I am also eternally grateful to Laurent for his scientific advice and knowledge and many insightful discussions and suggestions. Laurent is a good teacher that encouraged and expected me to think more independently about our experiments and results. He was and remains my role model for a scientist, and teacher.

It is a pleasure for me to thank Eric Becker, whose encouragement and crazy humour lifted my spirits above the technical skills. I still remember the wonderful gala during the conference ICTP 2 years ago where he managed to teach me to speak German and encouraged me to speak with German girls. In addition, he helped me enormously on thixoforging tests and macrostructure characterization.

For surviving and staying sane in a PhD program, it is important to have a good support team. I was lucky to be a part of it – Régis group in LCFC, who nourished my work. I couldn't have survived the thixoforging experiment without Olivier Gyss, Alexandre Fendler and Emerik Henrion. I also thank people who were not part of the Régis group but helped me out, including Marc Wary and Denis Bouscaud, who helped me enormously on microstructure characterization. I know that I could always ask them for advice and opinions on lab related issues. I would also like to thank Luc Morhain, who is now working in another lab. He answered my numerous questions on induction heating process and helped me with the DSC experiments.

I would like to extend my appreciation to all of the staff at ENSAM Metz for giving me friendship and encouragement throughout the course of this work. Special mention to administrative crew: Stéphanie Schiappa and Véronique Ernest for their great help and good mood.

I shall not forget my friends who have contributed to nice times in Metz. Special mention is made here to the Chinese team at ENSAM, with whom I had the pleasure to work and share some outdoor activities. Many thanks to my friends who supported me from a distance.

Last but not least, I would like to take this opportunity to thank the dearest people in the world to me, my parents. They have always believed in me and supported me. They have sacrificed their lives for my brother, sister and my self and provided unconditional love and care. Without their support and encouragement during my study in France, I wouldn't have get to this day. These past several years have not been an easy ride, both academically and personally. I truly thank my parents, especially my dad for encouraging me when I was irritable and depressed. I feel that I learned a lot about the life and love.

Table of contents

I Résumé en français……..……1

Chapitre 1 : Bibliographie sur les procédés de fabrication des métaux à l'état semi-solide……...……3

1. Introduction…….……..……4
2. Procédé à l'état semi-solide……..…….……5

2.1 Principe des procédés de mise en forme à l'état semi-solide……6

2.2 Préparation des alliages……..……7

2.3 Les avantages des procédés de mise en forme à l'état semi-solide……8

3. Comportement des matériaux semi-solides…...……...9

3.1 Comportement des alliages avec une faible fraction de solide……9

3.2 Comportement des alliages avec de fortes fractions de solide……14

4. Evolution de la microstructure au cours de la préparation du ……18

4.1 Caractérisation de la microstructure……18

4.2 Influence du mode de préparation de l'alliage semi-solide sur la morphologie de la structure liquide solide……24

5. Développement des alliages pour les procédés de mise en forme à l'état semi-solide……....33

5.1 Différentes technologies……..……33

5.2 Influence du processus de fabrication……34

6. Application industriel de la mise en forme à l'état semi-solide...……....35
7. Conclusions……...39

Références……..……....40

Chapitre 2 : Méthodologie de caractérisation de la microstructure des semi-solides et thixoforgeage des aciers ……..……45

1. Introduction…….……46
2. Matériaux étudiés……47

2.1 Choix des matériaux……47

2.2 Compositions chimiques……48

2.3 Evaluation de la fraction liquide à l'état semi-solide……48

2.4 Propriétés physiques……49

3. Thixoforgeage des aciers ……50
3.1 Dispositif de chauffage ……51
3.2 La presse……58
3.3 Système d'acquisition……60
4. Evaluation de la fraction liquide et caractérisation de la microstructure……61
4.1 Détermination directe de la fraction liquide par l'utilisation de données thermodynamiques ……61
4.2 Détermination de la fraction liquide par analyse thermique……62
4.3 Evaluation de la fraction liquide par métallographie quantitative (2D et 3D)……65
4.4 Observation in situ par CLSM……75
5. Conclusions……79

Références……80

Chapitre 3: Analyse des résultats expérimentaux concernant la caractérisation de l'évolution de la fraction liquide et de la microstructure……83

1. Introduction……84
2. Evaluation de la fraction liquide par Thermo-Calc et DSC……84
3. Analyse de la fraction volumique de liquide par DSC……87
4. Analyse métallographique 2D d'un lopin trempé depuis l'état semi-solide……89
4.1 Analyse de la microstructure……91
4.2 Caractérisation de la microstructure par analyse d'image……94
5. Evaluation de la fraction liquide par microtomographie aux rayons X……97
5.1 Etat de livraison ……97
5.2Microstructure du matériau trempé depuis l'état semi-solide……98
6. Observations in situ des aciers M2, 100Cr6 et C38LTT……103
7. Conclusions……109

Chapitre 4: Etude des résultats de thixoforgeage ……111

1. Thixoforgeage de l'acier M2……112
1.1 Influence des paramètres de thixoforgeage ……116
1.2 Influence des paramètres du procédé sur l'effort de mise en forme……117
1.3 Observations macro et microscopiques……120

2. Thixoforgeage des autres nuances d'acier (100Cr6 et C38LTT)……127

Conclusion Générale ……129

II English version……..……133

General introduction……...……..135

Chapter 1
Bibliography of semi-solid Processing……..……...……..……139

1. Introduction…….……..……..141

2. Semi-solid processing…….……..…..……..……...142

2.1 Semi-solid processing routes …….……144

2.2 Different slurry or billet preparation routes……..……145

2.3 Advantages of semi-solid processing……149

3. Rheology of semi-solid materials……..……150

3.1 Behavior of alloys at low solid fractions……151

3.2 Behavior of alloys at high solid fractions……..……157

4. Microstructure evolution during material preparation and forming process……161

4.1 Microstructure characterization……161

4.2 Influence of slurry preparation conditions on morphology……169

5. Alloy development for SSM processing …….……178

5.1 Different technologies for SSM……178

5.2 Influence of manufacturing process on materials……..……180

6. Industrial applications of SSM……181

7. Conclusions……185

References……186

Chapter 2
Methodology of microstructure characterization and steel thixoforging……195

1. Introduction…….……..……197

2. Materials……198

2.1 Material selection……199

2.2 Chemical compositions……199

2.3 Evaluation of liquid fraction in the semi-solid state……199

2.4 Physical properties……200

3. Steel thixoforging……202

3.1 Heating system……202

3.2 The press……210

3.3 Acquisition systems……212

4. Evaluation of liquid fraction and microstructure characterization……213

4.1 Direct evaluation of the liquid fraction using thermodynamic data……214

4.2 Determination of volume fraction of liquid by thermal analysis……215

4.3 Evaluation of liquid fraction by quantitative metallography in 2D and 3D……217

4.4 In situ observations with CSLM……229

5. Conclusions……233

References ……235

Chapter 3
Liquid fraction evaluation and microstructure characterization……237

1. Introduction……239

2. Liquid fraction evaluation by Thermo-Calc……240

3. DSC analysis of liquid volume fraction……243

3.1 DSC curves……243

3.2 Liquid fraction obtained by partial area integration……244

3.3 Comparison between the DSC and equilibrium results……247

4. 2-Dimentional image analysis on the billet quenched from the semi-solid state……247

4.1 Heating cycle……248

4.2 Microstructure analysis……250

4.3 Microstructure characterization by image analysis……255

4.4 Microstructure characterization on C38LTT and 100Cr6……..*261*

4.5 Summary……..*261*

5. Evaluation of liquid fraction by X-ray microtomography…….....261

5.1 As-received state……..*261*

5.2 Microstructure of M2 quenched from the semi-solid state……..*263*

5.3 X-ray tomography on other steel grades……..*270*

5.4 Summary……..*270*

6. In situ observation on M2, 100Cr6 and C38LTT……270

6.1 Heating cycles for the grades……..*270*

6.2 Microstructure evolution of M2……..*271*

6.3 Microstructure evolution of 100Cr6……..*273*

6.4 Microstructure evolution of C38LTT……..*275*

6.5 Summary……..*276*

7. Conclusions…….277

References…….279

Chapter 4
Thixoforging - experimental results……..……..……281

1. Thixoforging of M2…….283

1.1 Introduction of the thixoforging process……..*283*

1.2 Final geometry of the thixoforged parts……..*283*

1.3 Influence of process parameters on final part shape……..*293*

1.4 Influence of the process parameters on the forming load……..*295*

1.5. Macroscopic & microscopic observations……..*301*

1.6 Conclusions……..*311*

2. Thixoforming of other steel grades……..312

2.1 Thixoforged parts of 100Cr6 steel grade……..*313*

2.2 Thixoforged parts of C38LTT steel grade……..*317*

2.3 Conclusions……..……..324

Conclusions……326

References……..…328

General conclusion……..329

Part I
Résumé Étendu en Français

Chapitre 1. Bibliographie sur les procédés de fabrication des métaux à l'état semi-solide

1. Introduction

De façon générale, la capacité à mettre en forme des pièces à l'état semi-solide dépend notamment de la maîtrise du comportement rhéologique et de l'écoulement du matériau lors de la mise en forme. Ces conditions ne dépendent pas seulement des paramètres de mise en forme mais également de la microstructure du matériau à l'état semi-solide. Nombre de paramètres comme la vitesse de mise en forme, les températures initiales de l'outil et du lopin ont une grande influence sur le procédé de thixoforgeage. Ils peuvent principalement modifier les échanges thermiques entre la pièce mise en forme et l'outil, ce qui en retour affecte la structure du lopin (notamment la fraction de liquide, la distribution des zones liquides et par conséquence la viscosité et la consistance du matériau) et influence les propriétés finales de la pièce [1, 2].

Il a été établi que le comportement rhéologique d'un matériau à l'état semi-solide dépend de la fraction volumique de liquide, de la taille, de la forme et de la distribution des particules solides. De plus, la microstructure à l'état semi-solide dépend de la nature du matériau, de son mode d'élaboration, de son histoire thermique (thermomécanique) ainsi que de son mode de chauffage au travers de paramètres comme la vitesse de chauffage, le temps de maintien…

La Fig. 1.1 illustre le synoptique typique de la gamme de thixoforgeage. Dans un premier temps, le lopin est découpé dans une barre qui est fabriquée à partir de différents procédés. Après chauffage à la température désirée, le lopin est transféré sous la presse de mise en forme pour être thixoforgé sous différentes conditions.

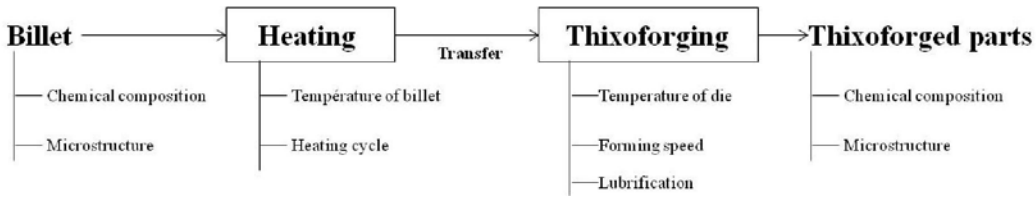

Fig. 1.1. Synoptique de la gamme de thixoforgeage.

Cependant, l'influence des conditions de mise en forme sur la microstructure et les propriétés mécaniques des pièces thixoforgées n'a toujours pas été clairement explicitée et caractérisée du fait de la complexité de la microstructure et de la rhéologie d'une telle structure. Les objectifs de cette étude sont de comprendre l'évolution de la microstructure au cours du processus complet de thixoforgeage :

- l'évolution de la microstructure au cours du chauffage depuis l'état initial jusqu'à l'état semi-solide.
- l'évolution de la microstructure au cours du thixoforgeage et l'influence des paramètres de mise en forme sur la microstructure.
- la structure finale de la pièce après refroidissement et les propriétés mécaniques associées.

La structure semi-solide de l'alliage apparaît comme un paramètre clef du thixoforgeage. Il est donc nécessaire de caractériser cette microstructure aux différents stades du processus de thixoforgeage.

Les avancées technologiques internationales dans le domaine de la mise en forme semi-solide sont discutées dans ce chapitre constitué de quatre parties axées respectivement sur la rhéologie, le développement technologique, les aspects matériaux et les applications industrielles.

2. Procédé à l'état semi-solide

La mise en forme à l'état semi-solide est un procédé dit "near net-shape" au cours duquel le matériau et partiellement à l'état liquide. Ce procédé permet l'obtention de pièces de forme complexe avec de bonnes propriétés mécaniques en une seule opération. La Fig. 1.2 illustre les domaines de températures typiques des procédés de fonderie, de mise en forme semi-solide et de forgeage. La microstructure pour le procédé semi-solide est également présentée dans la Fig. 1.2 : elle est constituée (dans le cas étudié) de particules solides entourées par la phase liquide.

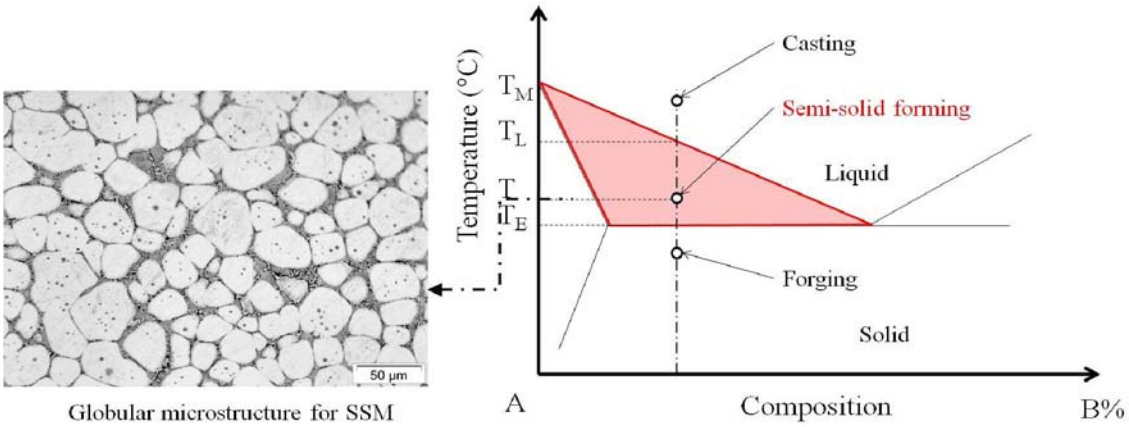

Fig. 1.2. Domaine de température typique pour les différents procédés.

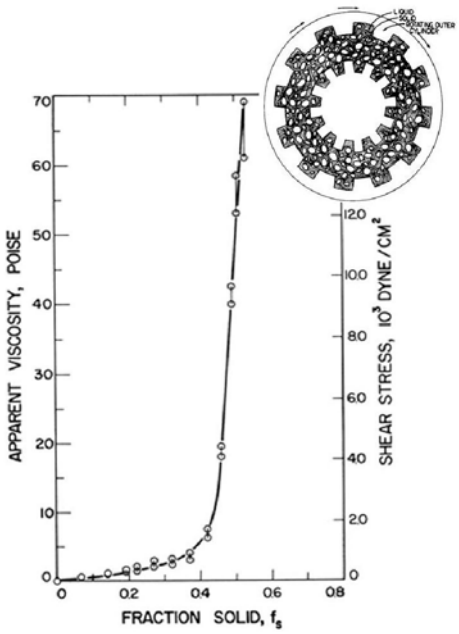

Fig. 1.3. Viscosité apparente en fonction de la fraction solide d'alliage Sn-15Pb cisaillé en continu et refroidi à -20°C/heure. Vitesse de rotation 500rpm [4].

Il y a quarante ans, en étudiant le comportement de l'alliage Sn-Pb partiellement solidifié, David Spencer [3] a découvert que les alliages à l'état semi-solide avaient un comportement thixotrope (Fig. 1.3). La viscosité augmente lentement avec l'accroissement de la fraction de solide pour des fractions de solide faibles (de 0 à 0,5) et fortement pour des fractions de solide supérieures. L'alliage partiellement solidifié peut donc être coulé pour les faibles taux de solide ou forgé pour les fort taux de solide [4]. L'aspect thixotrope de la mise en forme provient de l'évolution de la structure semi-solide de l'alliage depuis une structure dendritique vers une structure globulaire (ou non dendritique) par rupture des dendrites.

2.1. Principe des procédés de mise en forme à l'état semi-solide

Jusqu'à aujourd'hui, un grand nombre de procédés de mise en forme à l'état semi-solide ont été développés. La plupart d'entre eux peuvent être classés en deux catégories : le « rhéoformage » et le « thixoformage ». Dans le cas du « thixoformage », le matériau est chauffé jusqu'à l'état semi-solide puis mis en forme. En « rhéoformage », une structure semi-solide globulaire est obtenue par refroidissement depuis l'état liquide puis injectée dans un moule. La Fig. 1.4. illustre différents procédés de mise en forme à l'état semi-solide.

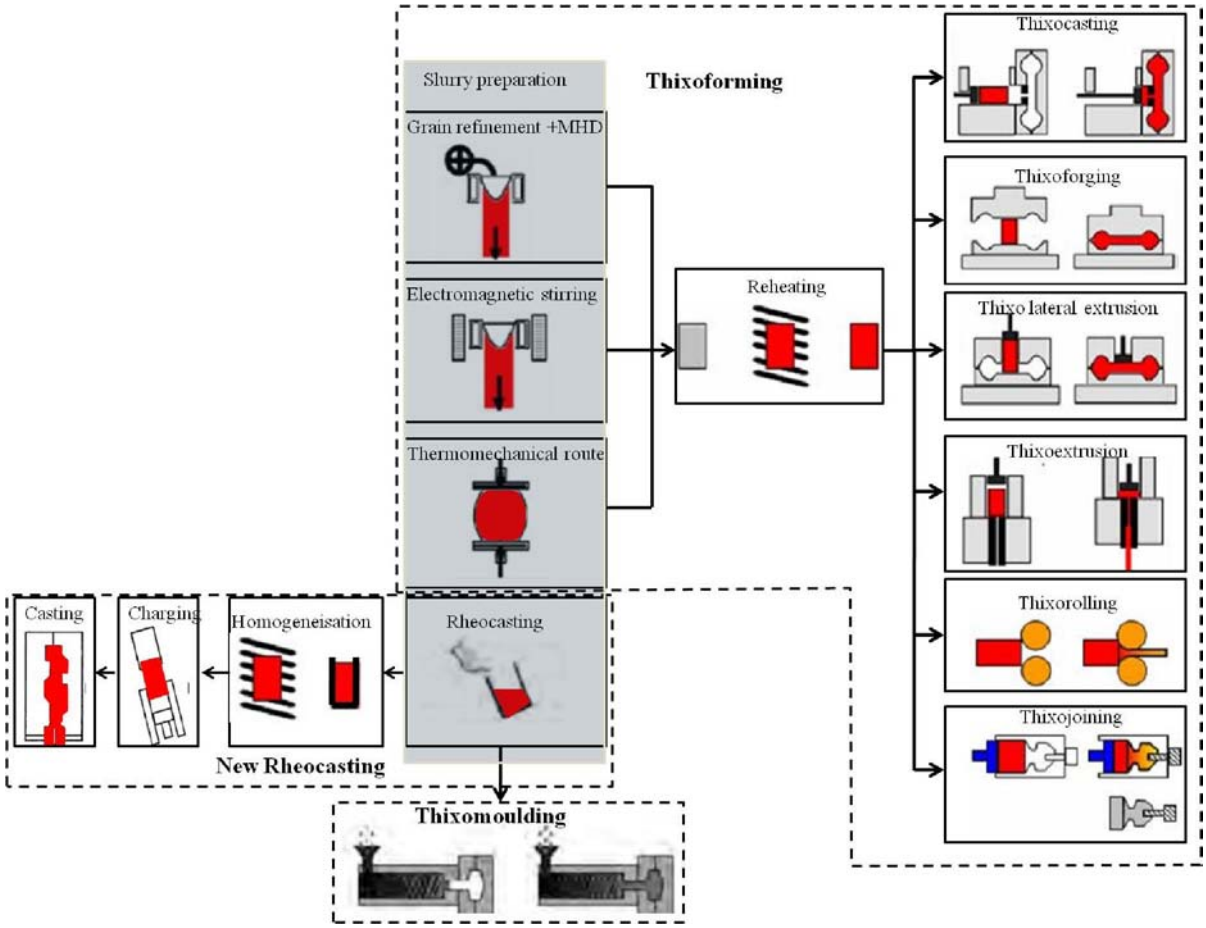

Fig. 1.4. Illustration de différents procédés de mise en forme à l'état semi-solide [1, 3].

2.2. Préparation des alliages

Le comportement rhéologique de l'alliage dépend très fortement de la structure semi-solide (dendritique ou globulaire,…). Cette dernière est obtenue par l'étape de préparation du lopin qui s'avère donc essentielle dans le processus de thixo- ou rhéoformage.

Afin de produire la microstructure semi-solide désirée, plusieurs modes de préparation ont été développés. On peut citer notamment le malaxage mécanique, l'agitation électromagnétique, le grossissement isotherme à partir d'une structure semi-solide dendritique, la fusion de poudre, la décharge électrique au travers de la structure semi-solide dendritique… Deux principes généraux sont à la base de ces procédés : casser la structure dendritique ou empêcher la formation de dendrite.

2.3. Les avantages des procédés de mise en forme à l'état semi-solide

Les travaux de recherche ainsi que les applications industrielles ont montré les avantages suivants :

Par rapport au procédé de fonderie conventionnel. Le caractère laminaire de l'écoulement au cours de la mise en forme dû à la plus grande viscosité du matériau permet de réduire considérablement les défauts dans les pièces. Les propriétés mécaniques des pièces obtenues sont par conséquent meilleures. De plus, les porosités et le retrait sont fortement réduits. La réduction du volume de porosités permet d'améliorer la soudabilité [40] et la résistance à la corrosion [4] des pièces produites. La plus faible température de mise en forme permet d'espérer une plus grande durée de vie des outillages. Une économie d'énergie peut également être attendue du fait du moindre chauffage de l'alliage.

Par rapport au procédé conventionnel de forgeage. Le thixoforgeage est un procédé de mise en forme « near net shape » avec lequel il est possible de produire des pièces de forme complexe. Les efforts de mise en forme sont fortement réduits ou pour un même effort de mise en forme, les taux de déformation accessibles sont plus importants. De plus, des pièces plus fines peuvent être obtenues avec de bonnes propriétés mécaniques permettant ainsi de se substituer au procédé de fonderie.

Avantage des procédés de mise en forme à l'état semi-solide pour différents matériaux. La mise en forme à l'état semi-solide peut s'appliquer à tous les métaux. Toutefois, les bénéfices attendus diffèrent d'un alliage à l'autre. Pour les alliages d'aluminium, le bénéfice attendu concerne les propriétés mécaniques des pièces par rapport à la fonderie. La faible température de fusion des alliages d'aluminium fait que le gain en durée de vie des outils est faible. Cependant, pour les alliages à haut point de fusion comme les aciers, le gain en durée de vie d'outillage peut devenir significatif. En ce qui concerne la compétition entre le thixoforgeage et le forgeage, la réduction du nombre de frappes pour l'obtention de forme complexe représente un gain important.

La mise en forme à l'état semi-solide des alliages légers est déjà mise en oeuvre industriellement. Le thixoforgeage des aciers et son industrialisation en est par contre encore au stade de la recherche.

3. Comportement des matériaux semi-solides

De façon générale, le comportement des matériaux semi-solides à structure globulaire présente deux propriétés rhéologiques: thixotropie et pseudoplasticté [5]. La thixotropie se définit comme la dépendance de la viscosité vi-à-vis du temps pour une même vitesse de déformation. La pseudoplasticité décrit la dépendance de la viscosité vis-à-vis de la vitesse de déformation. Selon les articles [6-8], il existe deux types de comportement semi-solide en fonction de la fraction de solide : comportement « liquide » pour les faibles taux de solide et le comportement « solide » pour les forts taux de solides dû à l'interconnexion entre les particules solides. Les mécanismes de déformation de ces deux types de structures sont fondamentalement différents. Le comportement des matériaux semi-solides à faible fraction de solide est décrit en terme de viscosité apparente. Cette dernière correspond à la viscosité d'un fluide homogène équivalent. Pour les forts taux de solide, le comportement doit tenir compte des deux phases et de leur interaction (agglomération et désagglomération).

Les techniques et les moyens expérimentaux de caractérisation à l'état semi-solide sont présentés dans les deux parties qui suivent en fonction de la fraction de solide.

3.1. Comportement des alliages avec une faible fraction de solide

3.1.1. Techniques expérimentales

Dans cette partie, on ne considère que les matériaux semi-solides avec structure globulaire. Dans ce cas, la viscosité est le paramètre déterminant du comportement du matériau [9].

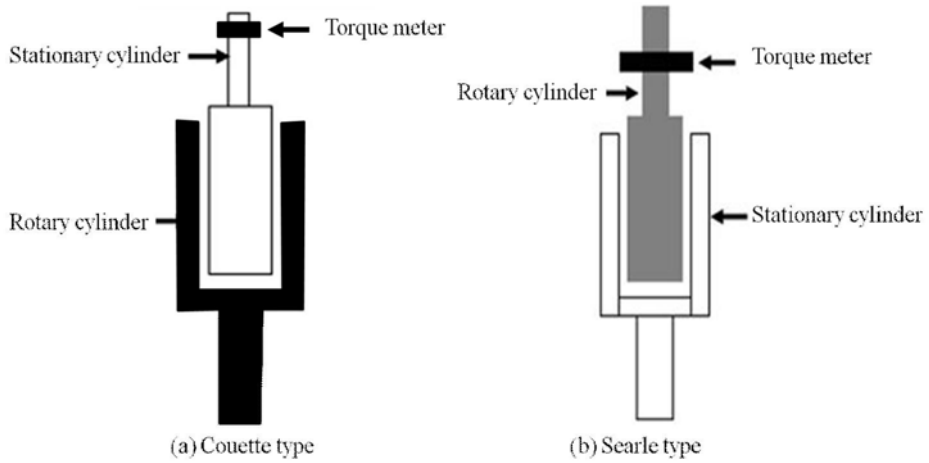

Fig. 1.5. Schéma de principe de deux types de viscomètre. (a) Couette et (b) Searle.

Il existe plusieurs méthodes pour caractériser le comportement de tels semi-solides. La plus simple consiste à utiliser un viscosimètre à cylindres concentriques et à mesurer le couple nécessaire pour assurer une vitesse de rotation relative entre les deux cylindres. Le schéma de deux types de viscosimètre (« Couette » et « Searle ») est présenté à la Fig. 1.5 [5, 10]. La contrainte de cisaillement et la vitesse de cisaillement peuvent être déduites de la mesure du couple et de la vitesse angulaire du cylindre mobile.

Grâce aux équations (1, 2 ,3), la viscosité apparente peut être estimée [10].

$$\tau = \frac{T}{2\pi r^2 L} \qquad \text{(Eq. 1.1)}$$

$$\dot{\gamma} = \frac{2\omega}{r^2}\left(\frac{r_i^2 r_0^2}{r_0^2 - r_i^2}\right) \qquad \text{(Eq. 1.2)}$$

$$\eta = \frac{T}{4\pi L\omega}\left(\frac{1}{r_i^2} - \frac{1}{r_0^2}\right) \qquad \text{(Eq. 1.3)}$$

où **T** est le couple mesuré, **L** est la hauteur de liquide entre les cylindres, $\dot{\gamma}$ est la vitesse de cisaillement apparente, **ω** est la vitesse angulaire du cylindre mobile, **η** est la viscosité apparente, $\mathbf{r_i}$ est le rayon du cylindre intérieur, $\mathbf{r_0}$ est le rayon du cylindre extérieur et **r** est le rayon considéré.

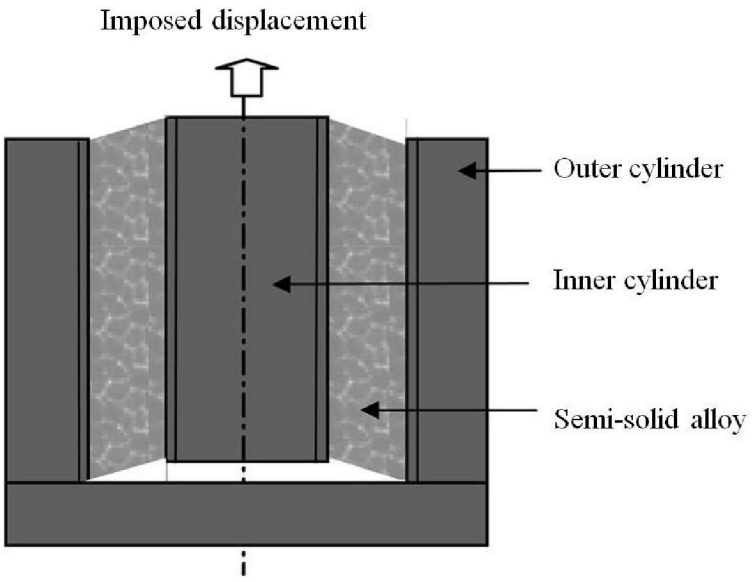

Fig. 1.6. Schéma du montage expérimental de cisaillement en translation.

Les avantages de cette technique résident dans la possibilité de générer directement l'état semi-solide dans le viscosimètre ainsi que dans la possibilité de changer les conditions de l'essai. Cependant, cette technique possède des limites en terme de contrôle de l'essai (température…), de vitesse de cisaillement [11]…

D'autres essais peuvent être conduits comme l'essai de cisaillement en translation dont un schéma est présenté sur la Fig. 1.6 [12].

3.1.2. Phénoménologie

Les premières investigations expérimentales sur les semi-solides ont été conduites sur l'alliage étain-plomb par Spencer [3]. Les résultats montrent que le semi-solide cisaillé avec une fraction solide supérieure à 0.2 se comporte comme un fluide non newtonien avec une viscosité bien plus faible que celle du semi-solide à structure dendritique.

Les courbes caractéristiques donnant la viscosité apparente du semi-solide en fonction de la fraction de solide sont présentées sur la figure 1.7 [5]. A une vitesse de cisaillement et une vitesse de refroidissement données, la viscosité augmente avec la fraction de solide. La viscosité augmente faiblement aux faibles fractions de solide et augmente plus fortement aux fortes fractions de solide. De plus, la viscosité diminue avec l'augmentation de la vitesse de cisaillement. Des résultats similaires ont été obtenus par d'autres auteurs [13-16].

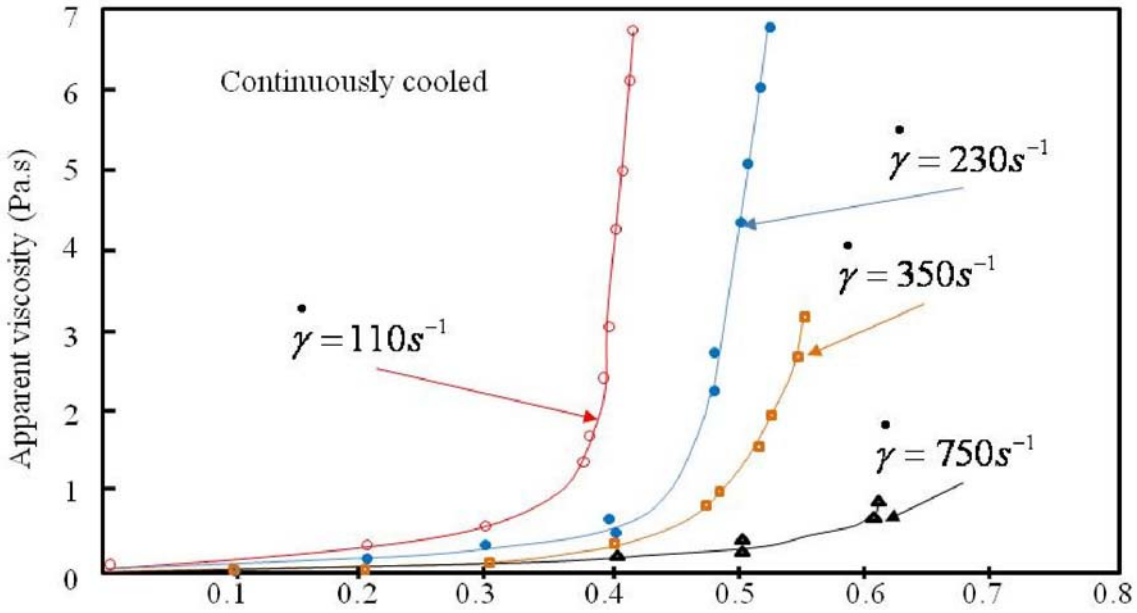

Fig. 1.7. Viscosité en fonction de la fraction solide pour un alliage Sn -15Pb cisaillé en continu et refroidi à 0.33K/min à différentes vitesses de cisaillement.

Les essais de cisaillement durant un maintien isotherme permettent d'obtenir des résultats plus précis. Comme illustré sur la Fig. 1.8, la viscosité décroît avec l'augmentation de la vitesse de cisaillement. De plus, en fonction de la fraction solide, la viscosité atteint une valeur relativement constante après un certain temps de cisaillement. Ce comportement est connu sous le nom de pseudoplasticité. Un tel comportement a également été constaté pour différents alliages [13, 15, 17]. La pseudoplasticité peut s'expliquer par la désagglomération des particules solides au cours du cisaillement. Ces explications ont été confirmées par des observations expérimentales sur des alliages Al-Si cisaillés à différente vitesse de déformation.

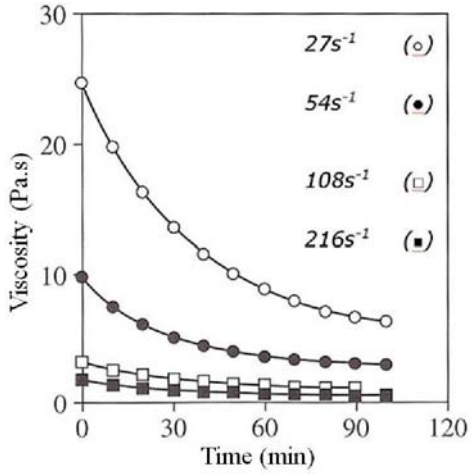

Fig. 1.8. Viscosité de l'alliage AlSi7Lg0.3 partiellement solidifié (fs = 0.35) en fonction du temps à 590°C [16] et pour différentes vitesses de cisaillement.

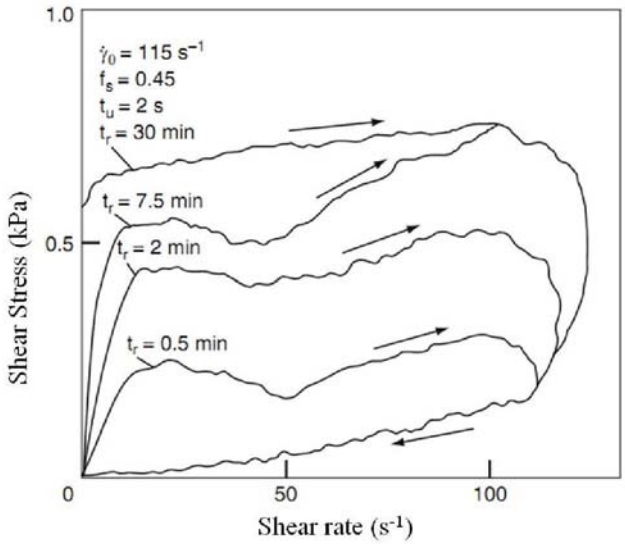

Fig. 1.9. Effet du temps de maintien (tr) sur la boucle d'hystérésis de l'alliage Sn-15Pb[5] ; tu est le temps nécessaire pour atteindre la vitesse de cisaillement de 115 s^{-1}.

Le comportement thixotrope est un autre phénomène rhéologique essentiel. Il a été mis en évidence la première fois par Joly et Mehrabian [42]. La Fig. 1.9 montre l'effet du temps d'attente sur la boucle d'hystérésis de l'alliage Sn-15Pb obtenu par Joly et Mehrabian. Toutes les courbes reviennent au point initial, ce qui indique pour cet alliage le caractère réversible de l'évolution de la microstructure. De plus, puisque la durée de l'essai est relativement courte, la croissance significative de particules solides ne s'est pas produite. Il a été remarqué que le processus d'agglomération influence la vitesse de cisaillement plus que la solidification des particules.

La Fig. 1.10 [18] montre l'influence du temps d'attente sur la contrainte d'écoulement du matériau. Cette dernière augmente avec le temps d'attente. Ce phénomène peut s'expliquer par l'accroissement de l'agglomération des particules solides et l'augmentation de leur taille. Toutefois, l'augmentation de la contrainte d'écoulement avec le temps de maintien n'est pas toujours vraie. Par exemple, pour les expériences conduites sur l'alliage AZ91D, la tendance da la variation de la contrainte de cisaillement avec le temps d'attente change en fonction de la valeur de la fraction solide. Ceci est illustré sur Fig. 1.11 [19]. Les auteurs expliquent cette différence de comportement comme la différence entre le mécanisme de grossissement des particules et le comportement du liquide piégé. Pour les fortes fractions de solide, il est plus « facile » pour la structure solide de piéger le liquide.

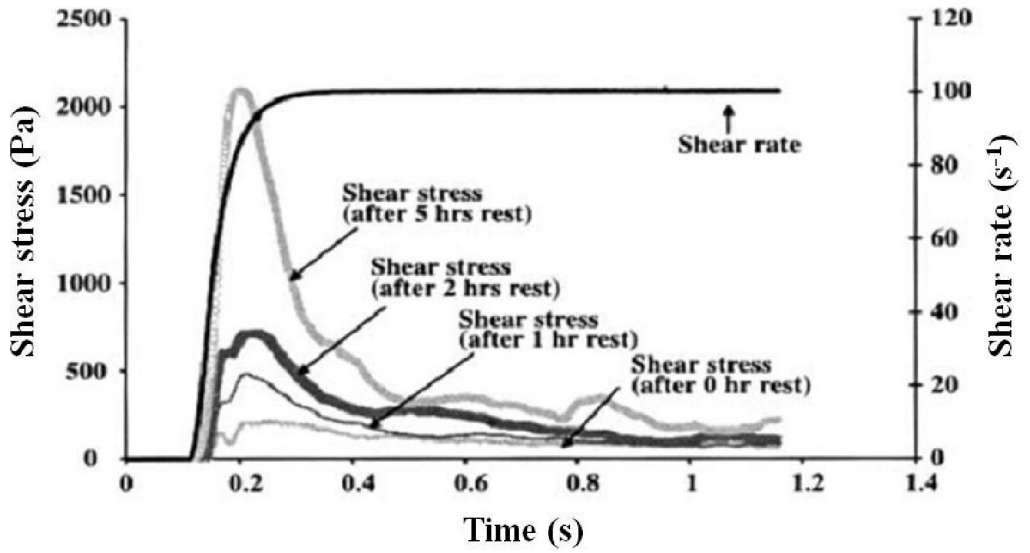

Fig. 1.10. Saut en vitesse de cisaillement de 0 à 100 s^{-1} après différents temps d'attente sur un alliage Sn-15Pb avec une fraction solide de 0.36 [18].

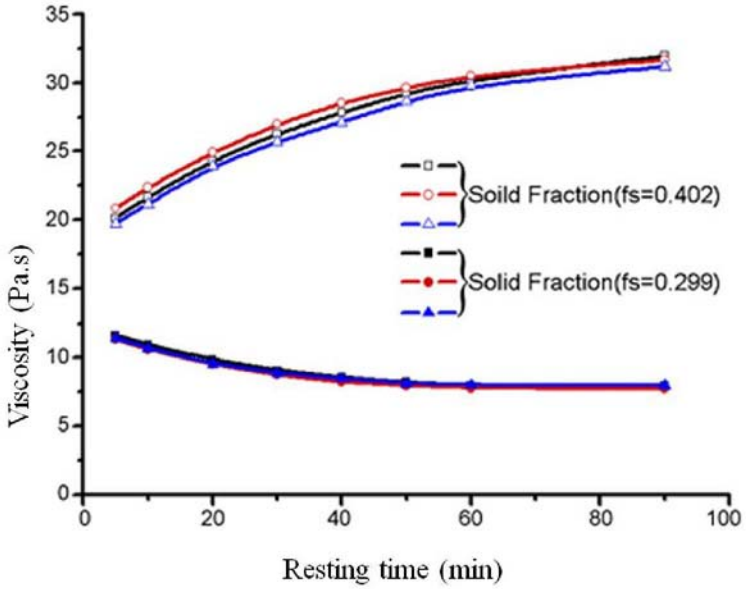

Fig. 1.11. Influence de la fraction solide et du temps d'attente sur la viscosité apparente [19].

Les résultats présentés dans cette partie concernent essentiellement les semi-solides avec une faible fraction de solide.

3.2. Comportement des alliages avec de fortes fractions de solide

Pour les alliages métalliques semi-solides avec une forte fraction de solide, le comportement est proche de celui des solides, avec une contrainte d'écoulement clairement définie due à l'existence d'un squelette solide.

3.2.1. Techniques expérimentales

Plusieurs méthodes expérimentales ont été employées pour caractériser le comportement des semi-solides à haute fraction de solide. La plus simple correspond à la compression entre plaques parallèles. Ce test correspondant à une opération de forgeage en matrices ouvertes : il donne des informations intéressantes sur le comportement de l'alliage au cours de ce type d'opération de mise en forme. Des expériences ont été menées sur diverses nuances d'alliages [20-23]. Les résultats obtenus peuvent être exploités pour caractériser le comportement rhéologique du matériau sur la base d'une hypothèse de fluide Newtonien ou non-Newtonien. Pour un fluide newtonien, l'équation de Stefan est appliquée au viscosimètre à plateaux parallèles :

$$F = -\frac{3\mu V^2}{2\pi h^5}\left(\frac{dh}{dt}\right) \qquad \text{(Eq. 1.4)}$$

où **μ** est la viscosité, **V** est le volume de matière, **h** est la hauteur instantanée de l'échantillon et **t** le temps.

La relation entre la viscosité et le temps peut s'écrire de la façon suivante :

$$\frac{1}{h^4} - \frac{1}{h_0^4} = \frac{8\pi F t}{3\eta V^2} \qquad \text{(Eq. 1.5)}$$

$$\frac{3Vh_0}{8\pi P_0}\left(\frac{1}{h^4} - \frac{1}{h_0^4}\right) = \frac{t}{\eta} \qquad \text{(Eq. 1.6)}$$

La vitesse de cisaillement moyenne d'un fluide Newtonien $\dot{\gamma}_{av}$ à chaque instant de l'essai de compression est donnée par la relation (Eq. 1.7) :

$$\dot{\gamma}_{av} = -\sqrt{\frac{V}{\pi}}\left(\frac{dh/dt}{2h^{2.5}}\right) \qquad \text{(Eq. 1.7)}$$

Si l'alliage semi-solide est supposé non-newtonien, les résultats sont interprétés en termes de loi puissance, liant la contrainte de cisaillement (τ) à la vitesse de cisaillement moyenne ($\dot{\gamma}_{av}$) avec $\tau = m\left(\dot{\lambda}\right)^n$, où **m** et **n** sont deux paramètres de la loi [22]. En fonction de la relation entre la viscosité, la contrainte de cisaillement et la vitesse de cisaillement, l'expression de la viscosité peut être obtenue sous la forme de Eq. 1.8. Le résultat final peut être donné par l'équation (Eq. 1.9) :

$$\eta = m\left(\dot{\lambda}\right)^{n-1} \qquad \text{(Eq. 1.8)}$$

$$\frac{h_0}{h} = \left\{1 + \left(\frac{3n+5}{2n}\right)h_0^{(n+1)/n}kt\right\}^{2n/(3n+5)} \qquad \text{(Eq. 1.9)}$$

où

$$k = \left\{\left(\frac{2n}{2n+1}\right)^n \frac{4F}{\pi d_0^{n+3} m}(n+3)\right\}^{1/n}$$

Pour étudier le comportement rhéologique des semi-solides sous des vitesses de déformation de l'ordre de celles rencontrées en thixoforgeage, un viscosimètre de compression a été développé par Yuko [24]. Son dispositif permet des vitesses de cisaillement jusqu'à 10^3 s^{-1}.

Des tests d'extrusion peuvent également être mis en œuvre pour étudier la viscosité des semi-solides. Par rapport au viscosimètre décrit ci-dessus, des vitesses de déformation supérieures à > $10s^{-1}$ peuvent être obtenues. De plus, ce test peut permettre d'observer les phénomènes de ségrégation de liquide où les écoulements de matière, ce test reproduisant des conditions de mise en forme similaires à celles rencontrées en thixoformage [25]. La Fig 1.12 présente le schéma d'un dispositif d'extrusion. Dans le cas d'une extrusion avant, le semi-solide est amené à s'écouler dans la filière (voir Fig. 1.12 (a)). La viscosité et la vitesse d'écoulement sont fonction de la vitesse et de la force de mise en forme. Cet essai permet d'étudier l'éjection de liquide et les phénomènes de ségrégation [26]. Le principal inconvénient provient du frottement entre le piston et la paroi du cylindre qui ne permet pas une mesure précise de l'effort de mise en forme et donc de la contrainte d'écoulement. Dans le cas de l'extrusion inverse (voir Fig. 1.12 (b)), l'effet des frottements est évité. Au cours de la mise en forme, le piston pénètre dans la matière et la matière s'écoule entre le piston et la paroi du cylindre extérieur.

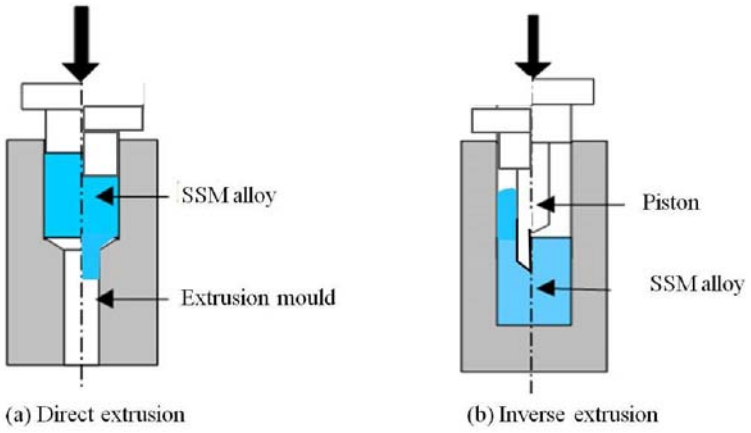

Fig. 1.12. Schéma des dispositifs d'extrusion. (a) extrusion avant et (b) extrusion inverse.

Le test d'indentation est également une méthode simple permettant la caractérisation des semi-solides. Il consiste à faire pénétrer dans la matière une aiguille avec une géométrie donnée. Cette méthode a été utilisée dans un premier temps pour évaluer la dureté de l'alliage avant injection. La rhéologie de l'alliage n'est pas facile à obtenir du fait de la complexité de l'état de contrainte sous et autour de l'aiguille ; la forme de l'indenteur a en outre une influence importante sur les résultats [27]. Du fait de la faible tenue des alliages à l'état semi-solide, l'essai de traction n'est pas utilisé pour étudier la rhéologie. Cette méthode ne convient pas pour les fractions solide inférieures à 0.85 [28].

3.2.2. Phénoménologie

A partir des résultats expérimentaux (Fig. 1.13), du fait de l'existence du « squelette » solide, le comportement du matériau peut être caractérisé comme suit :

- une grande limite d'écoulement existe au cours de la mise en forme3
- rupture du squelette solide et séparation des phases.

A partir de la mesure de l'effort de mise en forme et du déplacement, on constate un premier pic d'effort correspondant à la rupture du squelette solide. Ce pic est suivi d'une chute de l'effort du fait de la faible limite d'écoulement du matériau. A la fin de l'écrasement, l'effort de mise en forme augmente rapidement.

Lorsque la fraction de solide est élevée au cours de la mise en forme, la phase solide est soumise à une pression hydrostatique du fait du réarrangement des particules solides ou par leur faible déformation [66]. De plus, le gradient de pression hydrostatique dans la phase liquide causé par la réduction des volumes interstitiels entre les particules solides peut produire une séparation des phases [29]. De façon générale, la ségrégation du liquide peut être limitée par de fortes vitesses de déformation, des gradients de pression faibles, une faible fraction de solide et des particules solides sphériques et fines [8].

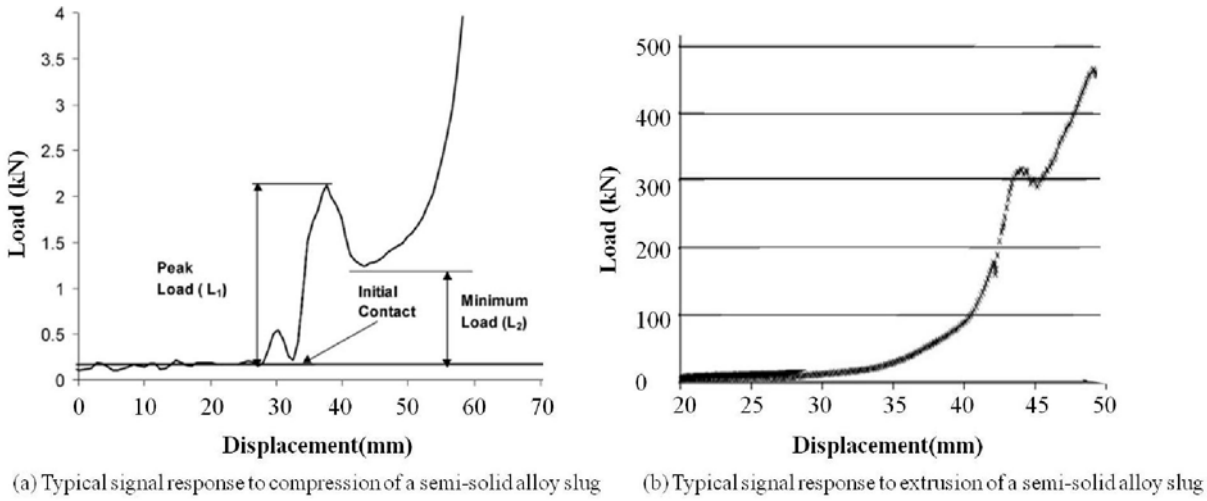

Fig. 1.13. Courbe effort déplacement typique d'un essai de compression. (a) [30] et extrusion (b) [25] d'un alliage semi-solide avec un fort taux de solide.

Suery et Fleming [23] ont procédé à des essais de compression sur des échantillons en Sn-15Pb avec une structure non-dendritique et dendritique fine. Les résultats obtenus à des vitesses de déformation identiques sont très différents, mettant en évidence l'influence de la

structure liquide-solide sur le comportement de l'alliage. Il est donc important d'étudier la microstructure du matériau aux différents stades du procédé.

4. Evolution de la microstructure au cours de la préparation du matériau et du procédé de mise en forme

Spencer et Fleming [31] stipulent que le matériau idéal pour la mise en forme à l'état semi-solide doit être mise en œuvre avec une fraction de solide précise constituée de particules solides sphériques uniformément réparties dans le matériau.

4.1. Caractérisation de la microstructure

Il a été montré que le comportement des alliages à l'état semi-solide dépend de la fraction volumique, la taille, la forme et la distribution des particules solides.

Fraction volumique de solide (F_S)

Il est très important de connaître la fraction liquide ou solide à l'état semi solide dans la mesure où elle représente un paramètre fondamental déterminant le comportement du matériau. La fraction solide est fonction de la température. Pour un alliage donné, elle ne peut être déterminée uniquement à une température donnée dans les conditions d'équilibre thermodynamique. Dans les autres cas, elle dépend de l'histoire thermique subie par le matériau. Tzimas et Zavaliangos ont listé différentes méthodes pour l'évaluation de la fraction solide [32]. Brièvement, les méthodes suivantes peuvent être utilisées pour la détermination de la fraction solide, soit directement soit par son effet sur des propriétés physiques de l'alliage :

- évaluation par des données thermodynamiques comme le diagramme d'équilibre.
- techniques d'analyse thermique comme la DTA ou la DSC.
- techniques de métallographie quantitative sur des microstructures trempées depuis l'état semi-solide.
- microtomographie aux rayons X in situ ou sur des microstructures trempées.
- contrôle par ultrasons par mesure de la vitesse de propagation des ondes.
- mesure de la résistivité électrique ou de la perméabilité magnétique.
- mesure des propriétés mécaniques par indentation ou extrusion.

Les trois dernières méthodes ne sont pas communément utilisées car il n'y a pas de correspondance unique entre la caractéristique mesurée et la fraction solide. Les trois premières sont les plus utilisées dans la pratique même si chacune d'elle possède ses limites :

- chaque méthode est approximative.
- l'utilisation de données thermodynamiques nécessite des informations supplémentaires concernant l'histoire thermique de l'alliage.
- les vitesses de chauffe accessibles par DSC sont bien inférieures à celles obtenues en mise en forme en conditions industrielles.

La microtomographie aux rayons X permet de dépasser les limitations des autres techniques ci-dessus car la mesure en 3D est appliquée directement sur le semi-solide obtenu avec de fortes vitesses de chauffe (Fig 1.14). Toutefois, il est difficile d'accéder à cette technique.

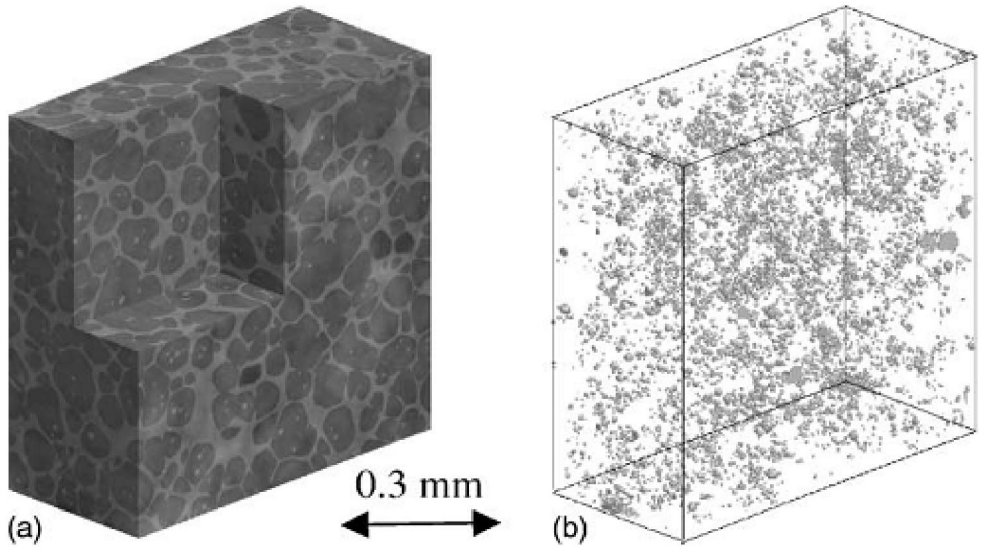

Fig. 1.14. (a) 3D visualisation d'un alliage Al-Si. (b) Liquide piégé extrait du volume présenté en (a) [33].

Par fraction liquide, on considère le liquide intergranulaire entourant les particules solides et pouvant contribuer au glissement des particules solides et le liquide intragranulaire piégé dans les particules solides et qui ne contribue pas à la déformation. Pour la mesure de fraction de liquide piégé, les mesures en 2D sur des sections réalisées aléatoirement peuvent être source d'erreur. Une mesure plus précise peut être effectuée en 3D par microtomographie aux rayons X sur des échantillons trempés ou in situ sur des échantillons à l'état semi-solide (directement à haute température).

Sensibilité à la température S* Techniquement, tous les alliages ne pas propres à être mis en forme à l'état semi-solide. L'aptitude à la mise en forme pour un alliage donné peut être caractérisée par la sensibilité de la fraction solide à la variation de la température. Celle-ci peut être exprimée par la dérivée de la fraction solide par rapport à la température, ceci à l'équilibre (Eq. 1. 10) [34] :

$$S^* = -\frac{df_s^*}{dT} \qquad \text{(Eq. 1.10)}$$

où f_s^* est la fraction solide, ***T*** est la température.

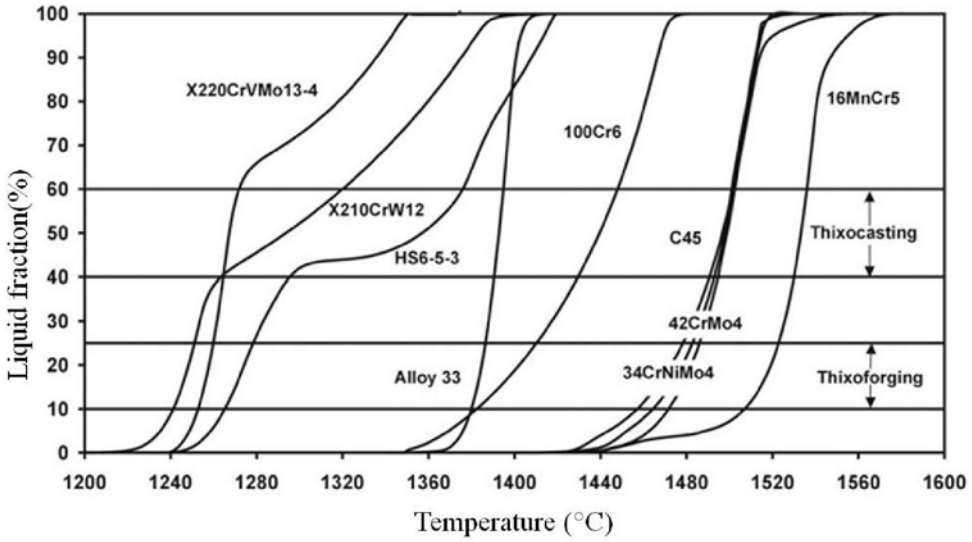

Fig. 1.15. Courbes de fraction liquide en fonction de la température déterminée par DTA à une vitesse de chauffage de 10K/min pour différents aciers [35].

Lors d'une opération réelle de thixoforgeage, la température n'est pas uniforme dans le lopin initial et au cours de sa déformation. Elle n'est pas constante dans le temps, évoluant au cours de l'opération et d'une opération à l'autre du fait de la dispersion liée au moyen de chauffage. De ce fait, une faible sensibilité à la température de la fraction solide voulue va dans le sens de la stabilité du procédé. Un intervalle liquide-solide important à une température faible est préférable. Au regard de l'étendue du domaine liquide-solide et de la sensibilité de la fraction solide, l'aptitude à la mise en forme des alliages d'aluminium et de magnésium a été confirmée. L'aptitude des aciers est plus difficile à établir. Le fer pur ou les aciers proches de l'eutectique ont une température de fusion spécifique sans intervalle liquide-solide [36]. Comme illustré sur la figure Fig. 1.15 (évolution de la fraction solide à l'état semi-solide évaluée par DTA ou DSC), les aciers fortement alliés avec une fusion complexe

montrent un large intervalle semi-solide à une température relativement faible et présente donc la meilleure aptitude à la mise en forme à l'état semi-solide.

L'intervalle semi-solide et la sensibilité à la température peuvent également être sensible à la variation de composition chimique. La Fig. 1.16 montre l'évolution de la fraction liquide en fonction de la température pour les aciers 100Cr6 et 100Cr6 LTT (Low Temperature for Thixoforming) obtenue par DSC [2]. Dans ce cas, la différence est due à une différence de stabilité des carbures due à la variation de teneur en élément d'alliage. La composition chimique des deux alliages est donnée dans le tableau 1.1.

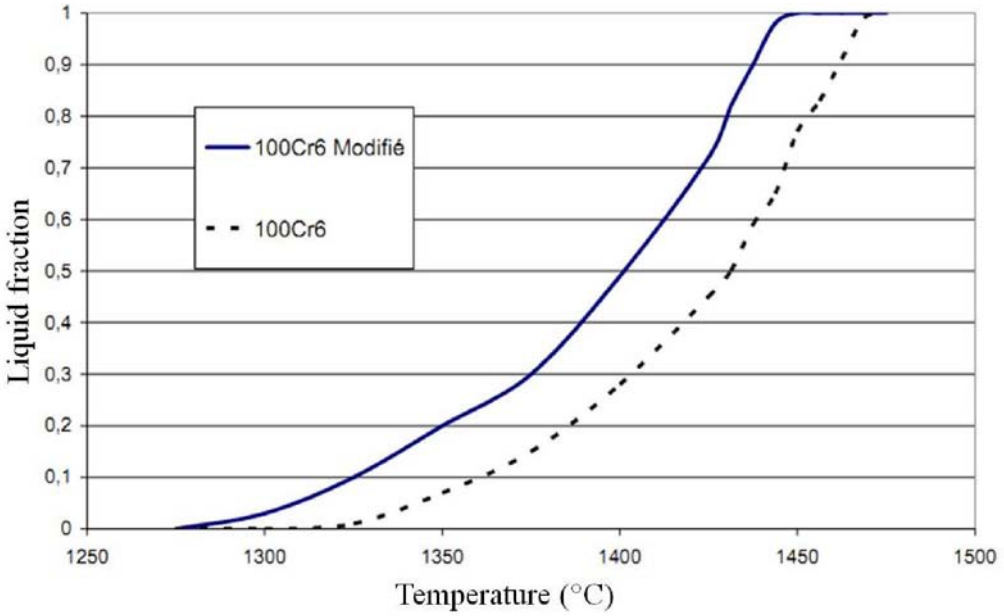

Fig. 1.16. Courbes de fraction de liquide en fonction de la température déterminée par DSC [2].

Tableau 1.1. Composition chimique des aciers étudiés dans la figure Fig. 1.16.

Mass 10^{-3}%	C	Si	Mn	S	P	Ni	Cr	Mo	Cu	Al	Sn	As	B*	V	Ti	Nb	Ca*	N*
100C6LTT	1055	1215	910	11	13	176	1306	43	177	29	12	20	3	6	3	3	8	66
100C6	988	230	326	6	7	210	1428	82	194	31	13	10	2	4	3	1	2	109

La morphologie de la microstructure liquide-solide revêt une importance majeure. La morphologie de la microstructure peut être caractérisée par plusieurs paramètres comme la taille, la forme et la distribution des particules solides.

Facteur de forme (F) Il est important de décrire de façon quantitative les particules solides. Généralement, les structures 3D sont caractérisées sur la base de mesures sur des sections 2D. Le facteur de forme (F) est défini par l'équation (Eq. 1.11) :

$$F = \frac{4\pi A}{P^2} \qquad \text{(Eq. 1.11)}$$

où A est l'aire de la section de la particule et P son périmètre.

F varie entre 0 pour des particules avec une section infiniment allongée et 1 pour les particules avec une section circulaire. Toutefois, une section 2D d'une particule peut conduire à plusieurs formes apparentes. Comme illustré dans la figure Fig. 1.17, une structure dendritique complexe conduit en fonction de l'orientation des sections considérées à une forte anisotropie et/ou variation du facteur de forme [11].

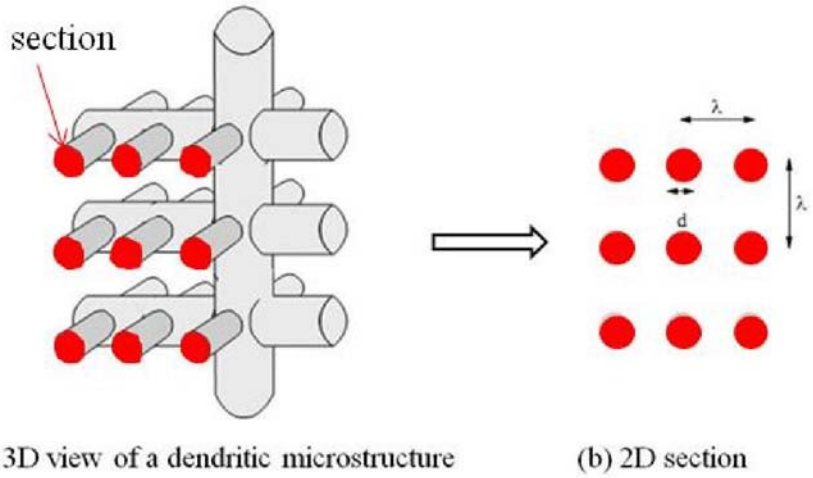

Fig. 1.17. Représentation d'une structure dendritique complexe. (a) vue 3D et (b) section 2D [11].

Loue et Suery ont introduit un facteur de forme spécifique sans dimension, $\mathbf{F_g}$, défini par l'équation Eq. 1.12 [37] :

$$F_g = \frac{1}{6\pi f_s}\frac{S_V^2}{N_A} \qquad \text{(Eq. 1.12)}$$

où $\mathbf{S_v}$ représente la surface d'interface solide-liquide par unité de volume, $\mathbf{N_A}$ est le nombre de grains par unité de surface et $\mathbf{F_s}$ est la fraction solide.

Comme démontré par les auteurs, F_g caractérise de façon plus précise la morphologie des particules que le facteur de forme usuel F. Toutefois, le paramètre $\mathbf{N_A}$ mesuré par analyse d'images peut ne pas représenter la vraie densité de particules du fait de la mesure 2D.

Taille de grain et distribution de la taille de grain

La taille de particules a un effet sur le comportement rhéologique du semi-solide et sur les propriétés mécaniques obtenues après mise en forme comme montré sur la figure Fig. 1.18.

La dimension fractale D est propose par Qin et Fan [38] pour décrire la morphologie de dendrites équiaxes.

Liu [18] met en évidence le fait qu'une augmentation de la taille des particules et du degré d'agglomération au cours de la mise en forme freinerait le mouvement relative des particules et conduirait donc à une augmentation de la contrainte d'écoulement et de la viscosité. L'augmentation de la contrainte d'écoulement peut être provoquée uniquement par l'augmentation du degré d'agglomération. Ceci peut s'expliquer de la façon suivante : pour une même masse de particules avec un même degré d'agglomération, en diminuant la taille des particules on augmente leur nombre. Ceci conduit à une augmentation du nombre d'interactions et, par la même, à une augmentation de la résistance à l'écoulement. Si la déformation croît, les interactions disparaissent provocant une chute de la viscosité.

Pour les procédés de mise en forme à l'état semi-solide, Uggowitzer et al. [39] suggèrent une taille de grain moyenne inférieure à 100 micromètres et un facteur de forme calculé par Eq. 1.1 [3] supérieur à 0.5 [11].

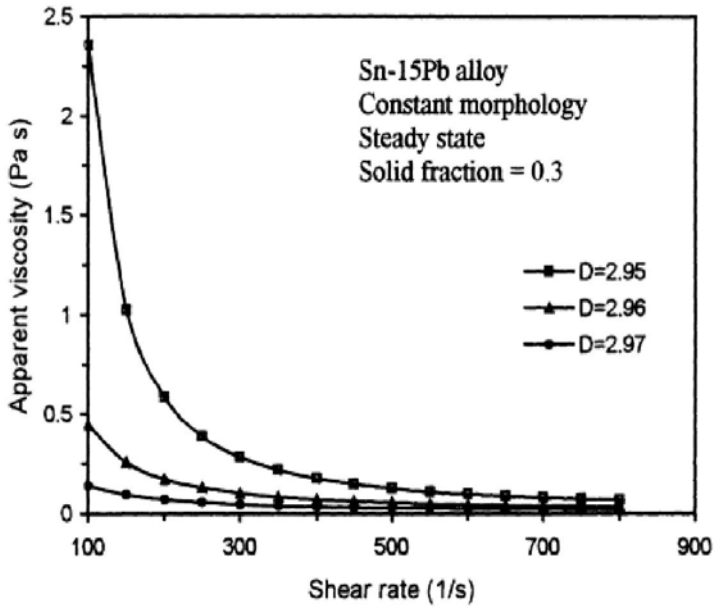

Fig. 1.18. Viscosité en fonction de la vitesse de cisaillement d'un alliage Sn-15Pb avec différentes dimensions fractales.

Contiguïté et volume contigüe Pour une structure liquide-solide avec une fraction solide fixée, l'arrangement des particules solides représente un facteur important pour le procédé de mise en forme. La contiguïté et la continuité peuvent être utilisées pour la caractérisation de la distribution des particules solides ou leur arrangement. La contiguïté Cf_s caractérise

l'arrangement ou plutôt la cohésion des particules solides et peut être définie comme la proportion moyenne de surface des particules solides correspondant à une interaction solide-solide. La contiguïté est donnée par l'équation suivante (Eq. 1.13) :

$$Cf_s = \frac{2S_V^{ss}}{2S_V^{ss} + S_V^{sl}} \quad \text{(Eq. 1.13)}$$

où Cf_s est la valeur de la contiguïté de la phase solide, S_V^{ss} est la valeur de la surface des particules solides, S_V^{sl} est la valeur de la surface des particules solides en contact avec le liquide.

La contiguïté peut être calculée à partir de la mesure des interfaces solide-solide et solide-liquide d'une métallographie. La résistance du squelette liquide dépend non seulement de la contiguïté mais également de la fraction solide. Pour cela, on peut utiliser le volume contigu C_sF_s tel que défini par l'équation (Eq. 1.14) [40] :

$$C_s f_s = V_s Cf_s, \quad \text{(Eq. 1.14)}$$

où $C_s f_s$ est le volume contigu, V_s est la fraction volumique de la phase solide et Cf_s est la valeur de la contiguïté de la phase solide.

Le nombre de particules par agglomérat est utilisé par Chen et Fan [41] pour décrire l'agglomération des particules dans un alliage à l'état semi-solide. En réalité, la contiguïté est en paramètre 3D qui ne peut être déterminé qu'en 3D. Grâce à la microtomographie aux rayons X, les connections et la distribution des particules peut être observées directement [33, 42-44].

4.2. Influence du mode de préparation de l'alliage semi-solide sur la morphologie de la structure liquide solide

Comme mentionné plus avant, un alliage peut être amené à un état semi-solide par solidification partielle ou par fusion partielle. Chaque cas est traité séparément dans ce qui suit.

4.2.1. Structure solide liquide obtenue par solidification partielle

Il a été établi que la formation d'une structure dendritique peut être évitée par agitation du matériau. A partir des études de différents auteurs sur plusieurs alliages (principalement

alliages de Sn-Pb, aluminium et magnésium), l'influence du mode d'obtention du semi-solide peut être résumé comme suit [5, 19, 45-48] :

- avec un temps d'agitation prolongé, une morphologie sphérique peut être obtenue par la rupture des dendrites suivie d'une sphéroïdisation des particules obtenues.
- l'augmentation de la vitesse de déformation accélère la transition des dendrites vers une structure avec des particules sphériques. Elle réduit également la quantité de liquide piégé dans les particules solides.
- un écoulement turbulent a un effet plus prononcé sur la structure qu'un écoulement laminaire.

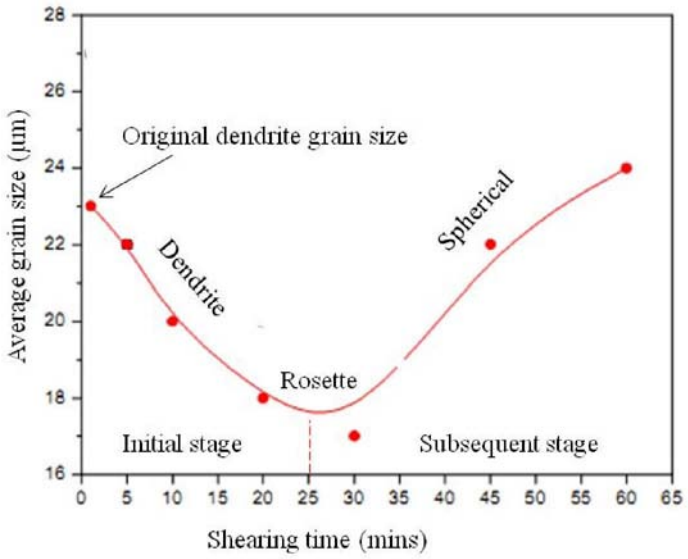

Fig. 1.19. Taille de grain en fonction du temps d'un alliage Al-5.2Si à une vitesse de déformation de 210 s^{-1} à 615°C [48].

Au cours de leurs investigations sur des alliages Al-Si, Yang et Tsao ont défini une durée critique d'agitation pour lequel la taille des particules solides connaît un minimum [46]. Un comportement similaire a été obtenu pour d'autres alliages par d'autres auteurs (voir Fig. 1.19). Ce phénomène peut être expliqué de la façon suivante : pour les alliages partiellement solidifiés avec une structure dendritique, au premier stade de l'agitation, les dendrites sont fragmentées par la déformation conduisant à une diminution de la dimension des particules et à une forte densité de particules. Si l'agitation est maintenue, la taille des particules sphériques augmente par "Osweld ripening" et on observe une coalescence des particules.

Pour une vitesse d'agitation donnée, la durée du traitement n'affecte pas seulement la taille des particules mais aussi leur facteur de forme, la fraction solide et la densité de particules.

Aucune évolution significative de la fraction solide ou du facteur de forme ne peut être mis en évidence au cours d'une agitation isotherme alors que la taille des particules évolue : la densité de particules décroît au cours du temps. Des résultats similaires sont décrits pour d'autres alliages [47].

La vitesse de déformation est un autre paramètre affectant la morphologie de la structure semi-solide. Avec une vitesse de déformation plus grande, on obtient des particules plus petites : la densité de particules augmente en conséquence [49]. Ji et Fan[50] ont également trouvé que des particules sphériques peuvent être obtenues rapidement sous des conditions d'écoulement fortement turbulent. De plus, Ji et Fan, Ryoo et Kim [51] ont aussi découvert que la taille de particules diminue rapidement avec l'augmentation de la vitesse de cisaillement sous la zone basse de vitesse de cisaillement, alors que la taille de particules se stabilise lorsque ces dernières sont soumises à des vitesses de cisaillement élevées, comme illustré Fig. 1.20.

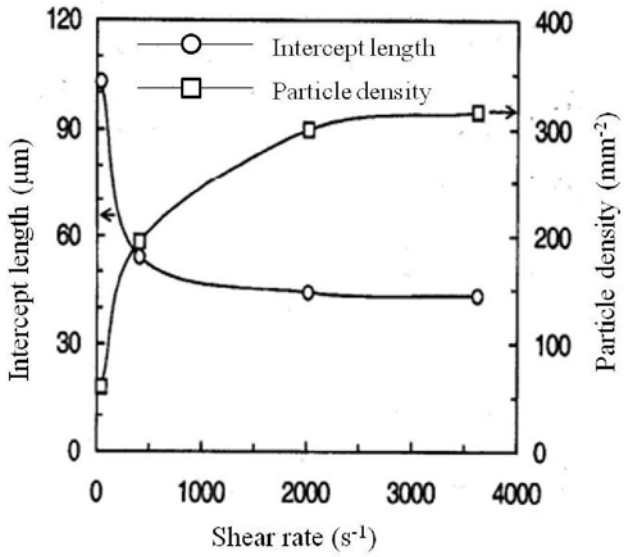

Fig. 1.20. Effet de la vitesse de déformation sur la taille des particules et leur densité pour un alliage Sn-15Pb refroidi de 215°C à 205°C avec une vitesse de refroidissement de 0.5°C/min [50].

Un autre résultat intéressant concerne l'influence de la vitesse de déformation sur la vitesse de grossissement des particules. Le grossissement des particules est proportionnel à la vitesse de déformation [52, 53]. Ceci peut s'expliquer en considérant les mécanismes d'"Ostwald ripening" et de coalescence des particules, tous deux gouvernés par la diffusion. La diffusivité est plus élevée pour les forts taux de cisaillement, donc, à l'accroissement de la vitesse de déformation est associé l'augmentation de vitesse de grossissement des particules.

La figure Fig. 1.21 illustre de façon schématique la transition morphologique que subit l'alliage depuis une structure dendritique jusqu'à une structure globulaire. Pour un alliage donné avec une structure liquide-solide dendritique, les dendrites sont dans un premier temps brisées par la déformation, les fragments évoluant ensuite vers une forme sphérique. Quand l'alliage semi-solide est agité de façon continue, les plus petites particules sphériques sont séparées par déformation et collision. Le grossissement des particules peut être expliqué par deux mécanismes : "Ostwald ripening" et la coalescence de particules. Par diffusion, les petites particules sont dissoutes au profit des grosses. Les particules agglomérées vont coalescer de manière à réduire leur énergie de surface. Quand les mécanismes d'agglomération et de séparation s'équilibrent, "Ostwald ripening" pourrait devenir le mécanisme prédominant.

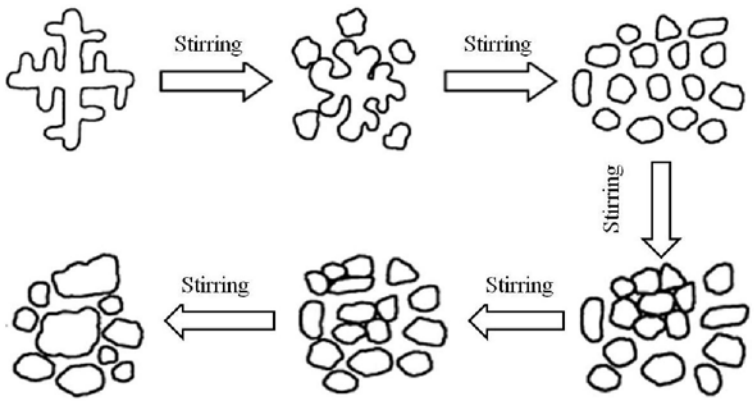

Fig. 1.21. Transition de morphologie durant le malaxage.

4.2.2. Structure obtenue par fusion partielle

De façon générale, l'évolution de la microstructure au cours de la chauffe est gouvernée par les processus de diffusion. La force motrice de la transformation de la phase solide en particules sphériques est la réduction de l'énergie d'interface entre les phases solide et liquide. Dans un processus de mise en forme, d'un côté, il est nécessaire d'allonger le temps de chauffage pour obtenir une structure globulaire, et d'un autre côté, le temps de chauffe et de maintien doit être faible pour des raison de coût et pour éviter un grossissement des grains qui aurait un effet négatif sur les propriétés de la pièce thixoforgée.

L'évolution de la microstructure au cours d'une fusion partielle dépend de la structure initiale de l'alliage. Wang et al. [54] ont étudié l'évolution de la microstructure de différents alliages d'aluminium durant leur fusion partielle. Ils ont observé que la structure obtenue

dépendait fortement de la structure initiale et de la durée de maintien. Fig. 1.22 illustre les différents comportements lors de la fusion partielle de divers alliages.

Un autre phénomène observé au cours de la chauffe est la formation du liquide piégé. Pour un matériau avec une structure dendritique, du liquide va être piégé dans le solide par une rapide coalescence des dendrites et des particules solides. Pour les matériaux ayant une structure équiaxe obtenue par extrusion ou laminage, du fait de phénomènes autobloquants [55], du liquide demeure piégé dans la phase solide durant le chauffage et le maintien. Au cours du chauffage et du maintien, il semble que le "Oswald ripening" et la coalescence des particules affectent le processus de formation du liquide piégé mais avec des effets opposés. La coalescence des particules provoque le piégeage du liquide alors que le "Ostwald ripening" conduit à une libération de liquide piégé [56-58].

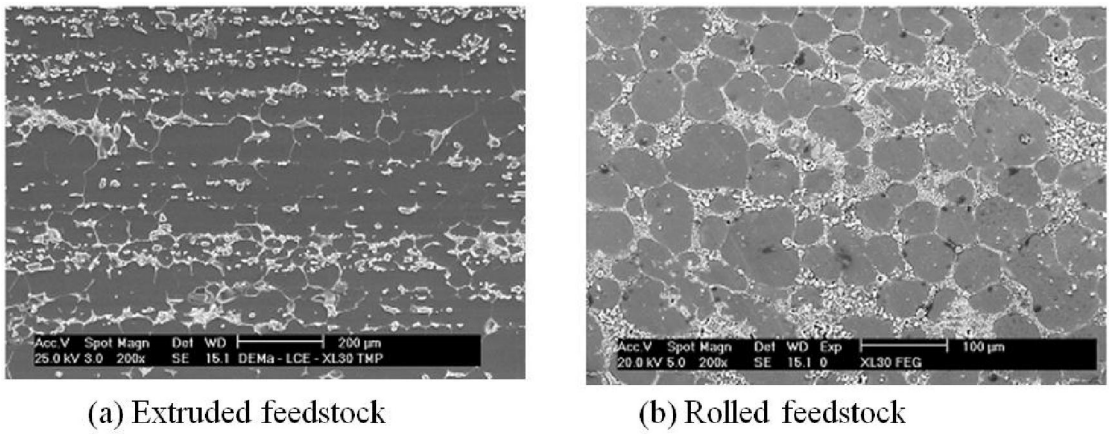

Fig. 1.22. Microstructure de l'A356 à 575°C après maintien isotherme pendant 2 min. (a) Matériau extrudé et (b) matériau traité thermiquement [59].

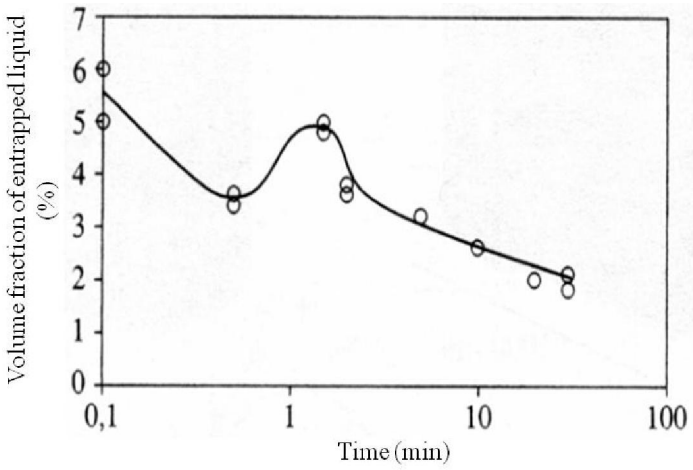

Fig. 1.23. Evolution de la fraction de liquide piégé en fonction du temps dans un alliage AS7U3 maintenu de façon isotherme à 573°C [62].

Au cours du maintien isotherme à l'état semi-solide, indépendamment de la morphologie initiale des particules, la phase solide évolue toujours vers une structure globulaire [54, 60, 61]. La taille de grain augmente avec le temps de maintien, ceci sans évolution notable de fraction de solide. Bien que la fraction de solide totale évolue légèrement, la fraction de liquide piégé décroît avec le temps de maintien du fait de l'"Ostwald ripening", comme illustré sur la Fig. 1.23 [62].

Plus le facteur de forme initial (Eq.12) est grand, plus la cinétique de globulisation est rapide et plus le temps nécessaire pour obtenir une structure globulaire est long (Fig. 1.24). Deux processus de grossissement sont actifs durant le maintien : la globulisation et le "Ostwald ripening". De façon générale, la globulisation commence plus tôt que le ripening.

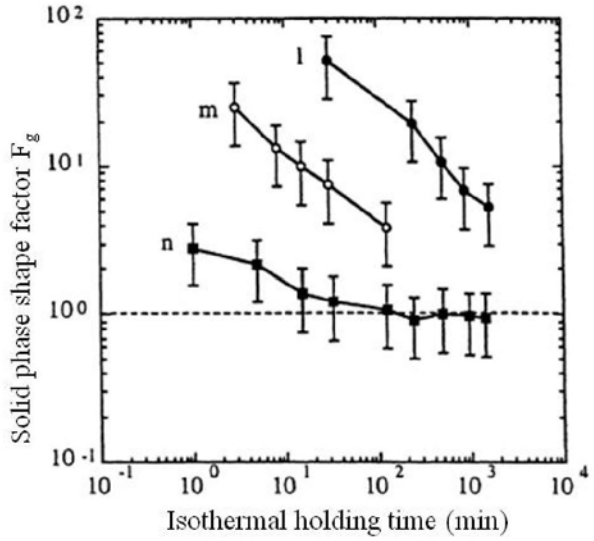

Fig. 1.24. Facteur de forme des particules 1/Fg en fonction du temps de maintien à 580°C (fs=0·5) pour un alliage Al-7Si-0·6Mg moulé, sans (l) et avec (m) affinement des grains, et par MHD agitation (n) [63].

La fraction solide qui dépend de la température influence la cinétique d'évolution de la microstructure. La vitesse de grossissement diminue lorsque diminue la fraction de solide. Basés sur des résultats expérimentaux, Sannes et al. [64] supposent que le grossissement des particules par coalescence est le mécanisme principal aux fortes fractions de solide alors qu'à faibles fractions de solide, l'évolution de structure serait principalement due à l'"Ostwald ripening".

De façon générale, la cinétique de grossissement pour des fractions de solide faibles, pour lesquelles les particules solides sont nettement séparées, suit un loi de Lifshitz-Slyozov-Wagner (LSW) [65] de la forme de l'équation (Eq. 1.15) :

$$d^3 - d_0^3 = Kt \qquad \text{(Eq. 1.15)}$$

où **d** est le diamètre moyen des particules à l'instant **t**, $\mathbf{d_0}$ est le diamètre moyen des particules à l'instant **t**=0 et **K** est la constante de vitesse de grossissement.

Pour des fractions solides plus élevées, pour lesquelles les champs de diffusion des particules sont en interaction, un modèle de migration du film liquide est a été proposé par Annavarapu et Dooherty [57]. Ce modèle indique que la vitesse de grossissement devrait croître avec la fraction solide. Cependant, les résultats expérimentaux montrent que pour les fortes fractions de solide ($\boldsymbol{F_s}$ > 0.7), la vitesse de grossissement décroît lorsque croît la fraction solide. Cependant, un modèle modifié de migration de film liquide a été proposé par Manson-Whitton [66].

4.2.3. Influence de la morphologie de la structure liquide solide sur le comportement rhéologique

Les effets de la morphologie de la phase solide sur le comportement rhéologique peuvent être déterminés par différents tests mécaniques appliqués sur le semi-solide. Les effets de la morphologie sont toujours liés à l'influence des conditions d'essai sur les contraintes ou la viscosité.

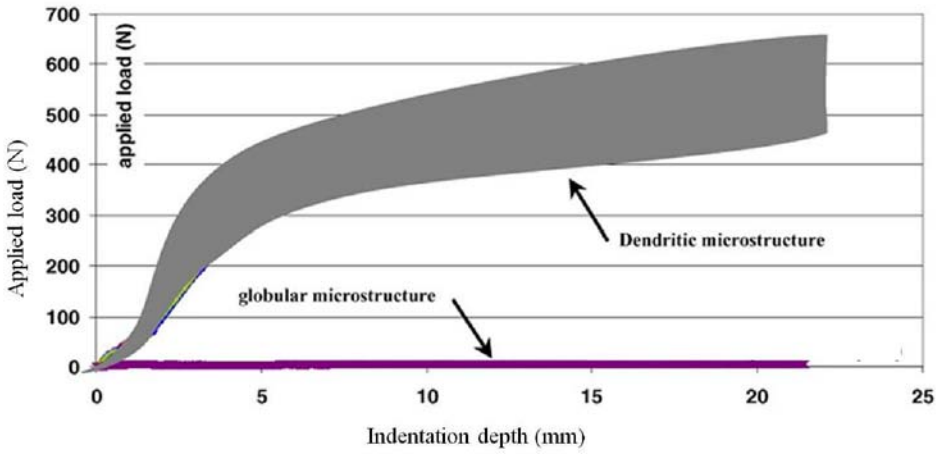

Fig. 1.25. Evolution de l'effort en fonction de la profondeur pour un essai de pénétration à une vitesse de 1mm/s, sur un alliage Sn-Pb15% avec deux microstructures [27].

L'étude de l'influence de la morphologie du semi-solide sur son comportement rhéologique se fait au travers d'essais de compression, d'extrusion ou d'indentation. Bigot et al. [27] ont comparé l'effort nécessaire à la pénétration dans le matériau avec différentes morphologie de semi-solide. Comme illustré par les résultats de la figure (Fig. 1.25), l'effort

de pénétration dans la structure dendritique est beaucoup plus élevé que celui nécessaire pour une structure globulisée.

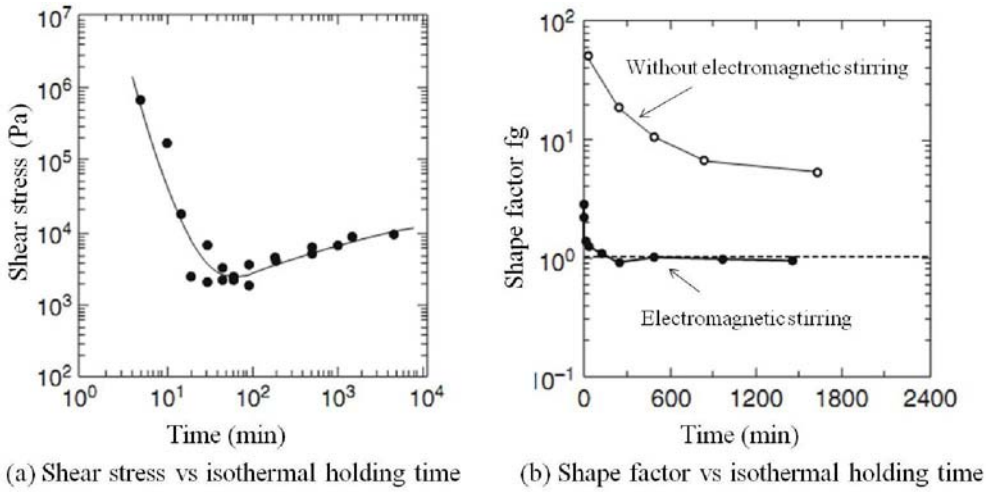

(a) Shear stress vs isothermal holding time (b) Shape factor vs isothermal holding time

Fig. 1.26. Influence du temps de maintien isotherme sur (a) la contrainte de cisaillement, (b) le facteur de forme [11, 37].

L'influence du facteur de forme des particules solides sur la viscosité peut être étudiée par différents tests mécaniques. Comme mentionné ci-dessus, pour les procédés de fusion partielle, le facteur de forme diminue avec l'augmentation du temps de maintien. Fig. 1.26 (a) présente la variation de contrainte de cisaillement déduite d'un essai de compression réalisé sur un alliage A357 obtenu par solidification avec agitation électromagnétique. L'influence du temps de maintien sur le facteur de forme est donnée sur la figure Fig. 1.26 (b). La contrainte de cisaillement décroît rapidement pour des temps de maintien court et augmente faiblement pour des temps longs. La chute de la contrainte d'écoulement résulte de la globulisation (voir Fig. 1.26 (b)). L'accroissement de la viscosité peut s'expliquer par l'effet d'agglomération.

L'influence de la morphologie de la phase solide peut également être obtenue en utilisant un viscosimètre. L'évolution de la viscosité en fonction du temps de malaxage est illustrée sur la figure Fig. 1.27 : l'essai a été réalisé sur un alliage AZ91D partiellement solidifié. La chute brutale de la contrainte de cisaillement en début d'essai correspond à la rupture des dendrites. Des temps de déformation isothermes longs provoquent l'agglomération des particules et à leur grossissement à l'origine d'une augmentation de la viscosité. Dans le même temps, Loué et al. décrivent l'influence du facteur de forme sur la viscosité, cette dernière étant une fonction décroissante du facteur de forme (Fig. 1.28).

La viscosité diminue lorsque la fraction de liquide augmente. Ceci est vrai si on considère la fraction de liquide effective ne tenant pas compte de la fraction de liquide piégé. Le liquide piégé ne participe pas au réarrangement des particules au cours de la déformation. A une température donnée, un accroissement de la fraction de liquide piégé revient à diminuer la fraction de liquide effective et donc à un accroissement de la viscosité.

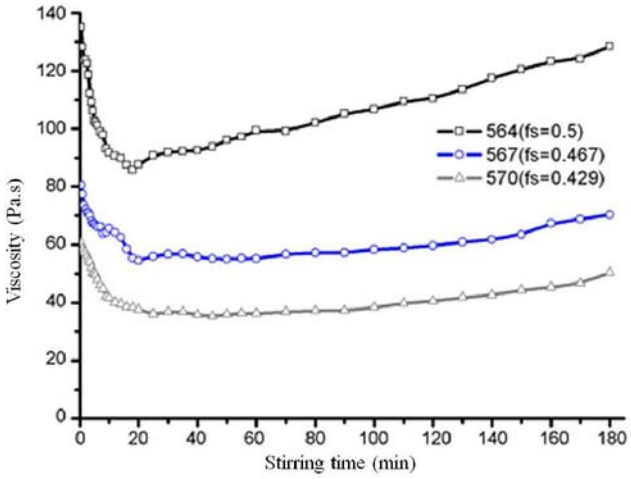

Fig. 1.27. Influence du temps de malaxage sur la viscosité apparente, essai réalisé sur un alliage AZ91D [19].

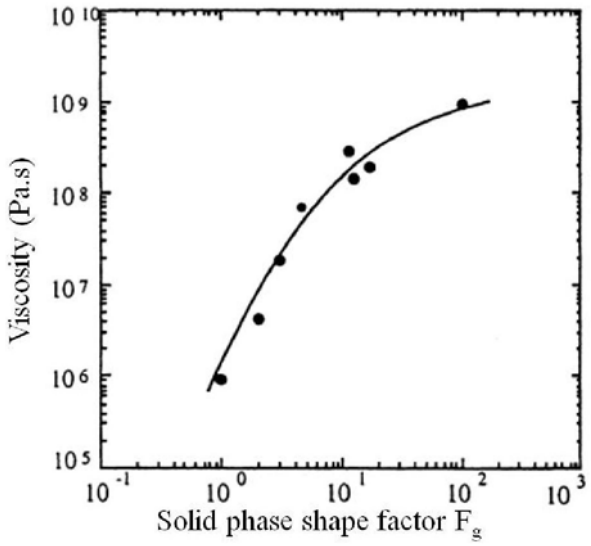

Fig. 1.28. Viscosité d'un alliage Al-7Si-0.6Mg avec une fraction solide de 0.5 en fonction du facteur de forme des particules (1/Fg, voir Eq. 1.12) [67].

Un autre facteur influent est la connectivité des particules solides [68]. L'auteur met en évidence qu'une déformation homogène est obtenue pour un volume contigu plus petit que 0.3.

5. Développement des alliages pour les procédés de mise en forme à l'état semi-solide

5.1. Différentes technologies

Depuis 40 ans, les procédés de mise en forme à l'état semi-solide ont été l'objet de recherches et de développements importants. Ces procédés se sont imposés comme des technologies sures pour produire des pièces complexes avec des propriétés mécaniques améliorées et un fort taux d'intégrité. Les alliages utilisés pour la mise en forme à l'état semi-solide sont optimisés pour les procédés conventionnels de forge ou fonderie. Or, les procédés de mise en forme à l'état semi-solide nécessitent une structure non dendritique. Ceci en fait un procédé unique nécessitant le développement d'alliages spécifiques. Ces alliages ont une aptitude à la mise en forme à l'état semi-solide accrue tout en assurant de bonnes propriétés mécaniques des pièces fabriquées. Ils ont, entre autres, une faible sensibilité de leur fraction solide à la température, un large intervalle liquide-solide avec une relative faible température de solidus, une certaine aptitude au vieillissement, des propriétés rhéologiques favorables, une sensibilité faible des propriétés aux variations de composition chimique. Parmi ces propriétés, la morphologie de la phase solide, le comportement rhéologique et l'aptitude à la mise en forme dépendent également des conditions de mise en œuvre. La sensibilité à la température, l'intervalle liquide solide et la température de solidus sont essentiellement fonction de la composition de l'alliage.

De façon générale, les outils thermodynamiques sont toujours appliqués à l'étude de l'influence des variations de composition sur la sensibilité à la température, l'intervalle de solidification et le potentiel de vieillissement de l'alliage. Liu et al. ont utilisé l'approche par l'outil thermodynamique CALPHAD pour évaluer la faisabilité d'une fabrication commerciale d'alliages d'aluminium [109, 110] et d'alliages de magnésium [69]. Lors d'une étude sur l'effet de la composition chimique sur les propriétés thermophysiques des aciers en utilisant le logiciel IDS (Fig. 1.29), Puttgen et al. soulignent le fait que les températures de solidus et liquidus dépendent du taux de carbone et de la dissolution des différents carbures. Fig. 1.30 rassemble les courbes donnant la fraction liquide en fonction de la température de plusieurs aciers obtenues par DTA.

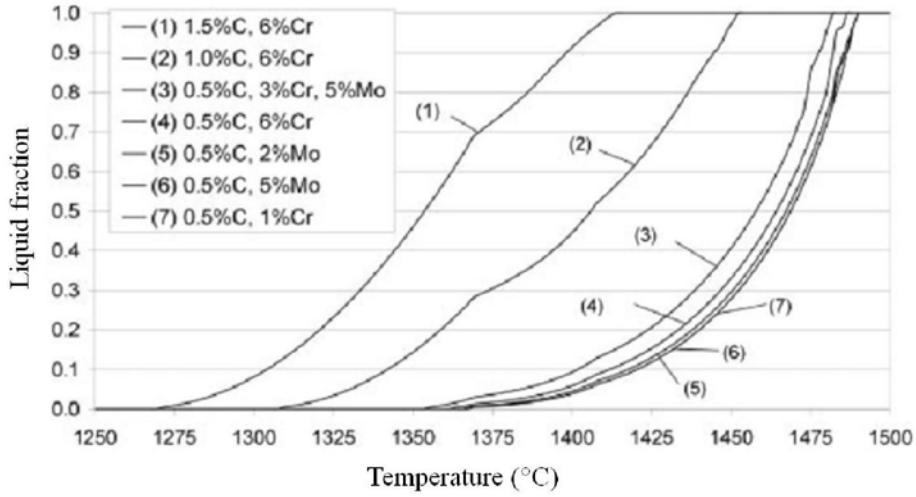

Fig. 1.29. Fraction liquide en fonction de la température pour différentes compositions chimique d'acier: calcul par IDS [70].

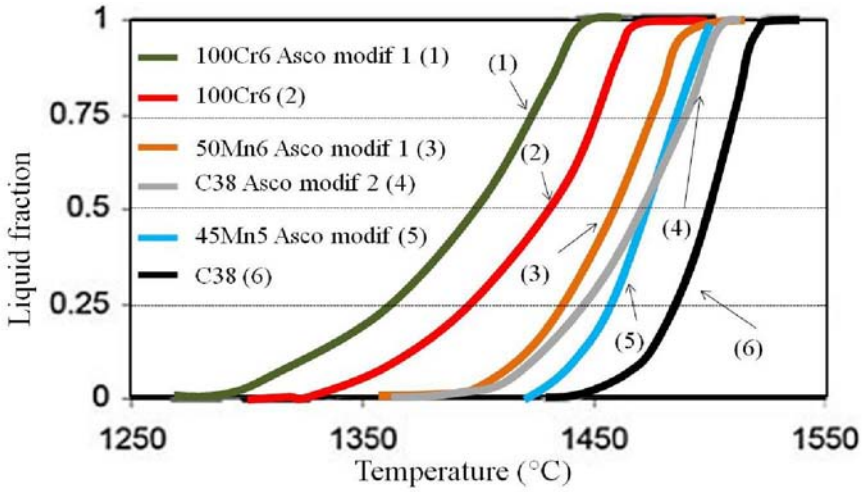

Fig. 1.30. Fraction liquide en fonction de la température de différents aciers obtenue par DSC[71, 72].

Les deux nuances d'acier fortement allié, X210CrW12 et HS 6-5-3, ont un large intervalle liquide-solide de même que l'acier à roulement 100Cr6. De plus, ASCOMETAL a développé plusieurs aciers avec une température de solidus faible et un large intervalle de fusion spécifiquement pour la mise en forme à l'état semi-solide. Li et al. [73] explique que la globularisation se produira toujours dans les alliages pour lesquels il existe une transformation péritectique à l'état solide.

5.2. Influence du processus de fabrication

La structure initiale de l'alliage peut être de morphologie multiple en fonction de son mode d'élaboration (fonderie, laminage, extrusion, etc.). Du fait de l'effet de multiples facteurs

intervenant au cours de l'obtention du lopin (thermique, chimique…), la structure initiale avant mise en forme n'est pratiquement jamais uniforme. La figure Fig. 1.31 illustre les trois zones de la structure obtenue dans un lopin issu de fonderie.

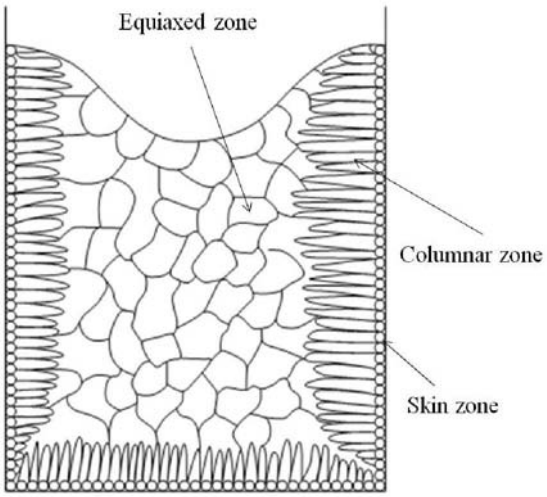

Fig. 1.31. Microstructure classique d'un lingot issu de fonderie [74].

6. Application industriel de la mise en forme à l'état semi-solide

La mise en forme à l'état semi-solide des alliages d'aluminium est déjà industrialisée alors que celle des aciers est encore en développement. Plusieurs aspects doivent être bien contrôlés pour le développement industriel du thixoforgeage des aciers :

- matériau : l'identification des aciers ayant la meilleure aptitude à la mise en forme semi-solide, l'évolution de la microstructure au cours chauffage et de la mise en forme.
- procédé : les conditions de mise en forme (vitesse de mise en forme, température du lopin et des outils, temps de maintien), mode de chauffage du lopin, transfert.

Le chauffage du lopin est toujours réalisé par induction du fait des grandes vitesses de chauffe accessibles et de sa répétabilité. Cependant, du fait de l'effet de peau, il est nécessaire de procéder à un cycle de chauffage comportant plusieurs paliers de puissance pour obtenir un champ de température dans le lopin le plus uniforme possible. Dans un contexte industriel, il n'est pas possible de contrôler la température par thermocouples. Pour cette raison, Becker et al. [26] suggèrent de chauffer les lopins sans mesure de température à partir d'un cycle de chauffage établi statistiquement sur un nombre important de tests préalables. Cette méthode n'est toutefois pas robuste face aux éventuels changements de conditions de production.

D'autres approches de contrôle de température sans thermocouple ont été proposées [75] utilisant par exemple des pyromètres sans contact.

Pour atteindre des objectifs de productivité et de reproductibilité, des robots industriels sont nécessaires pour le transfert et de maniement des lopins. Après son transfert et sa mise en position, le lopin doit pouvoir être déformé par le procédé de thixoforgeage piloté en position ou en effort. Il est conseillé de mettre en forme le métal à l'état semi-solide à grande vitesse, notamment pour limiter les échanges thermiques avec les outillages.

Différents composants en acier thixoforgé sont présentés dans le tableau table 1.2.

Tableau 1.2. Différentes pièces produites par mise en forme à l'état semi-solide.

Procédé	Photos	Nuance	Réf.
Thixoforgeage	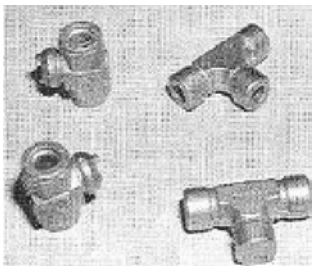	X105CrMo17, X5CrNi18-10	[76]
		M2, CoCr28MoNi	[77]
		FC-10/20/30, FCD-45	[78]
		C38, C70, C80	[79]
		C38, C60, C80, HS6-5-3	[80]
	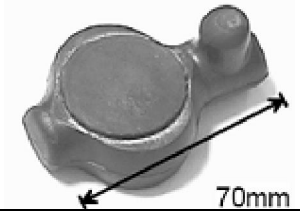	C38, C50, 100Cr6	[81]

		X210CrW12 100Cr6	[36]
Rhéoformage	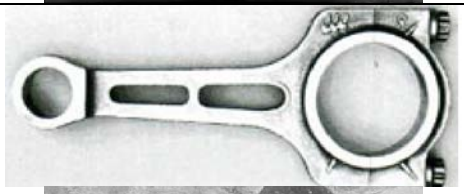 	C70, 100Cr6, HS6-5-2	[82]
		FCD450-10 Co-base alloy	[83]
	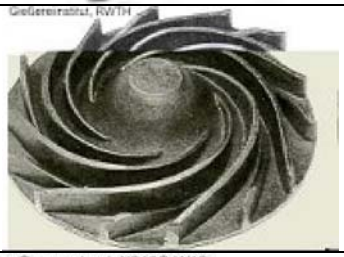	X210CrW12 X38CrMoV5-1 Laser sintered direct steel powder	[84, 85]
	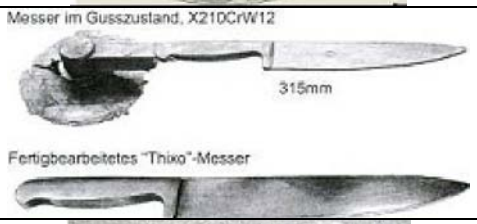	X210CrW12 X38CrMoV5-1 Laser sintered direct steel powder	[85]
Thixoextrusion		100Cr6, HS6-5-2	[70]
		HS6-5-3, X210CrW12, 100Cr6, C60	[86]

	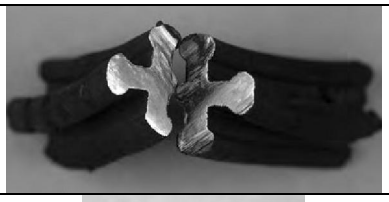	X210CrW12	[3]
	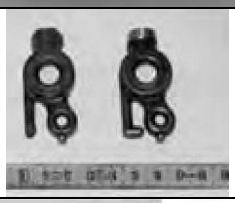	HS6-5-3 100Cr6,	[36]
Thixoassemblage	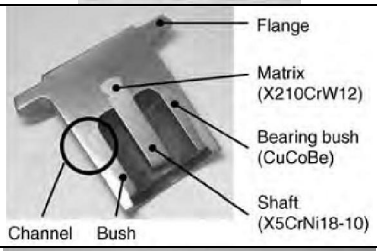	X210CrW12	
		HS6-5-3 100Cr6,	[86]
Rhéoforgeage		X210CrW12 100Cr6	

7. Conclusions

Un état de l'art sur les procédés de mise en forme à l'état semi-solide a été présenté dans ce chapitre.

Dans un premier temps, le comportement thixotrope des alliages semi-solides à microstructure globulaire et dendritique a été décrit. Le caractère thixotrope du comportement est dû aux cinétiques d'agrégation et de rupture des particules solides. L'importance de la structure liquide-solide au travers de la fraction solide, de la taille des particules et de leur facteur de forme est mise en évidence. Une structure globulaire est celle qui sera visée pour les procédés de mise en forme à l'état semi-solide. Les différents processus de préparation du semi-solide sont présentés.

Dans un deuxième temps, le comportement rhéologique du semi-solide à structure globulaire est étudié. Le comportement rhéologique résulte de la fraction liquide, de la taille et de la contiguïté des particules solides en relation avec la vitesse de déformation. L'influence du procédé sur la morphologie de la structure liquide-solide et le comportement rhéologique associé ont été présentés. Différents mécanismes d'évolution de la microstructure à l'état semi-solide ont été décrits. Le temps de chauffage, la fraction liquide obtenue et la microstructure initiale ont une influence importante sur la morphologie de la microstructure semi-solide et sur le comportement rhéologique du matériau.

L'état de l'art a mis en exergue l'importance de la structure liquide solide sur le comportement rhéologique des semi-solides et donc leur comportement en mise en forme. Il est donc nécessaire de développer et/ou de mettre en place des méthodologies de caractérisation de cette microstructure aux différentes étapes du processus complet de thixoforgeage. Le chapitre qui suit est consacré aux outils de caractérisation des semi-solides. Ce chapitre doit permettre de faire un premier choix des techniques qui vont constituer la méthodologie globale de caractérisation.

Références

1. Becker E: **Investigations experimentales et numeriques pour l'identification des parametres clefs du procede de thixoforgeage de l'acier sur le produit mis en forme.** Thesis. L'Ecole Nationale Supériure d'Arts et Métiers, Docteur de L'Ecole National Supérieure d'Arts et Métiers; 2008.
2. Cézard P: **Impact des effets thermiques sur le comportement du matériau lors de la mise en forme des aciers à l'état semi-solide : Analyses expérimentale et numérique.** Thesis. L'Ecole Nationale Supériure d'Arts et Métiers, Docteur de l'Ecole National Supérieure d'Arts et Métiers; 2006.
3. Hirt G, Kopp R (Eds.): **Thixoforming - semi-solid metal processing**. Aachen: Wiley-VCH Verlag GmbH & Co. KGaA; 2009.
4. Lebeau S, Decker R: **Microstructural design of thixomolded magnesium alloys.** In *5th International Conference on Semi-Solid Processing of Alloys and Composites; Colorado, USA*. Edited by Bhasin AK, Moore JJ, Young KP, Midson S. Colorado School of Mines; 1998: 217-224.
5. Joly PA, Mehrabian R: **The rheology of a partially solid alloy.** *Journal of Materials Science* 1976, **11:**1393-1418.
6. Flemings M: **Behavior of metal alloys in the semisolid state.** *Metallurgical and Materials Transactions A* 1991, **22:**957-981.
7. Kirkwood DH: **Semisolid metal processing.** *International Materials Reviews* 1994, **39:**173-189.
8. Fan Z: **Semisolid metal processing.** *International Materials Reviews* 2002, **47:**49-85.
9. Lashkari O, Ghomashchi R: **The implication of rheology in semi-solid metal processes: An overview.** *Journal of Materials Processing Technology* 2007, **182:**229-240.
10. Brabazon D, Browne DJ, Carr AJ: **Experimental investigation of the transient and steady state rheological behaviour of Al–Si alloys in the mushy state.** *Materials Science and Engineering: A* 2003, **356:**69-80.
11. Kirkwood DH, Suéry M, Kapranos P, Atkinson HV, Young KP: *Semi-solid Processing of Alloys*. Springer; 2010.
12. Ludwig O, Drezet JM, Martin C, Suéry M: **Rheological behavior of Al-Cu alloys during solidification constitutive modeling, experimental identification, and numerical study.** *Metallurgical and Materials Transactions A* 2005, **36:**1525-1535.
13. Lehuy H, Masounave J, Blain J: **Rheological behaviour and microstructure of stir-casting zinc-aluminium alloys.** *Journal of Materials Science* 1985, **20:**105-113.
14. Nan WS, Guangji S, Hanguo Y: **Rheological study of partially solidified Tin-Lead and Aluminium-Zinc alloys for stir-casting.** *Materials Transactions* 1990, **31:**715-722.
15. Kattamis TZ, Piccone TJ: **Rheology of semisolid Al-4.5%Cu-1.5%Mg alloy.** *Materials Science and Engineering: A* 1991, **131:**265-272.
16. Loue WR, Landkroon S, Kool WH: **Rheology of partially solidified AlSi7Mg0.3 and the influence of SiC additions.** *Materials Science & Engineering A, Structural materials : properties, microstructure and processing* 1992, **151:**255-262.
17. Turng LS, Wang KK: **Rheological behaviour and modelling of semi-solid Sn-15% Pb alloy.** *Journal of Materials Science* 1991, **26:**2173-2183.

18. Liu T, Ward P, Atkinson H, Kirkwood D: **Response of semi-solid Sn-15 pct Pb to rapid shear-rate changes.** *Metallurgical and Materials Transactions A* 2003, **34:**409-417.

19. Chen H-I, Chen J-C, Liao J-J: **The influence of shearing conditions on the rheology of semi-solid magnesium alloy.** *Materials Science and Engineering: A* 2008, **487:**114-119.

20. Azzi L, Ajersch F: **Development of alumnium base alloys for forming in semi solid state.** In *TransAL Conference; Lyon, France*. 2002: 23-33.

21. Lashkari O, Ghomashchi R: **The implication of rheological principles for characterization of semi-solid Al–Si cast billets.** *Journal of Materials Science* 2006, **41:**5958-5965.

22. Laxmanan V, Flemings M: **Deformation of semi-solid Sn-15 Pct Pb alloy.** *Metallurgical and Materials Transactions A* 1980, **11:**1927-1937.

23. Suery M, Flemings M: **Effect of Strain Rate on Deformation Behavior of Semi-Solid Dendritic Alloys.** *Metallurgical and Materials Transactions A* 1982, **13:**1809-1819.

24. Yurko J, Flemings M: **Rheology and microstructure of semi-solid aluminum alloys compressed in the drop-forge viscometer.** *Metallurgical and Materials Transactions A* 2002, **33:**2737-2746.

25. Becker E, Favier V, Bigot R, Cezard P, Langlois L: **Impact of experimental conditions on material response during forming of steel in semi-solid state.** *Journal of Materials Processing Technology* 2010, **210:**1482-1492.

26. Becker E, Bigot R, Langlois L: **Thermal exchange effects on steel thixoforming processes.** *The International Journal of Advanced Manufacturing Technology* 2009, **48:**913-924.

27. Bigot R, Favier V, Rouff C: **Characterisation of semi-solid material mechanical behaviour by indentation test.** *Journal of Materials Processing Technology* 2005, **160:**43-53.

28. Ferrante M, deFreitas E, Monilha M, Sinka V: **Rheological properties and microstructural evolution of semi-solid aluminum alloys inoculated with mischmetal and with titanium.** In *5th International Conference Semisolid Processing of Alloys and Composites; Colorado, USA*. Edited by Bhasin AK, Moore JJ, Young KP, Midson S. Colorado School of Mines; 1998: 35-42.

29. Suery M, Zavaliangos A: **Key problems in rheology of semi-solid alloys.** In *Proceedings of the 6th International Conference on Semi-solid Processing of Alloys and Composites; Turin*. Edited by Chiarmetta GL, Rosso M. Edimet Spa; 2000: 129-135.

30. Kapranos P, Liu TY, Atkinson HV, Kirkwood DH: **Investigation into the rapid compression of semi-solid alloy slugs.** *Journal of Materials Processing Technology* 2001, **111:**31-36.

31. Spencer D, Mehrabian R, Flemings MC: **Rheological behavior of Sn-15 pct Pb in the crystallization range.** *Metallurgical and Materials Transactions B* 1972, **3:**1925-1932.

32. Tzimas E, Zavaliangos A: **Evaluation of volume fraction of solid in alloys formed by semisolid processing.** *Journal of Materials Science* 2000, **35:**5319-5329.

33. Salvo L, Cloetens P, Maire E, Zabler S, Blandin JJ, Buffière JY, Ludwig W, Boller E, Bellet D, Josserond C: **X-ray micro-tomography an attractive characterisation technique in materials science.** *Nuclear Instruments and Methods in Physics Research Section B: Beam Interactions with Materials and Atoms* 2003, **200:**273-286.

34. Liu D, Atkinson HV, Jones H: **Thermodynamic prediction of thixoformability in alloys based on the Al–Si–Cu and Al–Si–Cu–Mg systems.** *Acta Materialia* 2005, **53:**3807-3819.

35. Püttgen W, Bleck W: **Thixoforming/semi-solid forming : DTA-measurements to determine the thixoformability of steels.** *Steel Research International* 2004, **75:**531-536.

36. Püttgen W, Bleck W, Hirt G, Shimahara H: **Thixoforming of steels – A status report.** *Advanced Engineering Materials* 2007, **9:**231-245.

37. Loue WR, Suery M: **Microstructural evolution during partial remelting of Al-Si7Mg alloys.** *Materials Science and Engineering: A* 1995, **203:**1-13.

38. Qin RS, Fan Z: **Fractal theory study on morphological dependence of viscosity of semisolid slurries.** *Materials Science and Technology* 2001, **17:**1149-1152.

39. **Metallkundliche Aspekte bei der semi-solid Formgebung von Leichtmetallen**

40. Gurland J: **A structural approach to the yield strength of two-phase alloys with coarse microstructures.** *Materials Science and Engineering* 1979, **40:**59-71.

41. Chen JY, Fan Z: **Modelling of rheological behaviour of semisolid metal slurries Part 1- Theory.** *Materials Science and Technology* 2002, **18:**237-242.

42. Zabler S, Rueda A, Rack A, Riesemeier H, Zaslansky P, Manke I, Garciamoreno F, Banhart J: **Coarsening of grain-refined semi-solid Al–Ge32 alloy: X-ray microtomography and in situ radiography.** *Acta Materialia* 2007, **55:**5045-5055.

43. Limodin N, Salvo L, Suéry M, DiMichiel M: **In situ investigation by X-ray tomography of the overall and local microstructural changes occurring during partial remelting of an Al–15.8wt.% Cu alloy.** *Acta Materialia* 2007, **55:**3177-3191.

44. Terzi S, Salvo L, Suery M, Dahle AK, Boller E: **Coarsening mechanisms in a dendritic Al–10% Cu alloy.** *Acta Materialia* 2010, **58:**20-30.

45. Kumar P, Martin C, Brown S: **Shear rate thickening flow behavior of semisolid slurries.** *Metallurgical and Materials Transactions A* 1993, **24:**1107-1116.

46. Yang Y, Tsao CY: **Viscosity and structure variations of Al–Si alloy in the semi-solid state.** *Journal of Materials Science* 1997, **32:**2087-2092.

47. Fan Z, Liu G, Hitchcock M: **Solidification behaviour under intensive forced convection.** *Materials Science and Engineering: A* 2005, **413-414:**229-235.

48. Sukumaran K, Pai BC, Chakraborty M: **The effect of isothermal mechanical stirring on an Al–Si alloy in the semisolid condition.** *Materials Science and Engineering: A* 2004, **369:**275-283.

49. Smith D, Eady J, Hogan L, Irwin D: **Crystallization of a faceted primary phase in a stirred slurry.** *Metallurgical and Materials Transactions A* 1991, **22:**575-584.

50. Ji S, Fan Z: **Solidification behaviour of Sn-15Pb alloy under high shear rate and high intensity of turbulence.** *Met Mater Trans* 2002, **33A:**3511-3520.

51. Ryoo YH, Kim DH: **Evolution of microstructure during semi-solid state processing of Mg-Al-Zn-X alloys.** In *3rd Int Conf on semisolid processing of alloys and composites; University of Tokyo, Japan*. Edited by Kiuchi M. Tokyo Institute of Industrial Science; 1994: 95-104.

52. Wan G, Sahm PR: **Particle growth by coalescence and Ostwald ripening in rheocasting of PbSn.** *Acta Metallurgica et Materialia* 1990, **38:**2367-2372.

53. Ji S, Roberts K, Fan Z: **Isothermal coarsening of fine and spherical particles in semisolid slurry of Mg– 9Al–1Zn alloy under low shear.** *Scripta Materialia* 2006, **55:**971-974.

54. Wang HY, Davidson CJ, Stjohn DH: **Semisolid microstructural evolution of AlSi7Mg during partial remelting.** *Materials Science and Engineering A* 2004, **368:**159-167.

55. Kleiner S, Beffort O, Uggowitzer PJ: **Microstructure evolution during reheating of an extruded Mg–Al–Zn alloy into the semisolid state.** *Scripta Materialia* 2004, **51:**405-410.

56. Secondé JF, Suéry M: **Effect of solidification conditions on deformation behaviour of semi-solid Sn-Pb alloys.** *Journal of Materials Science* 1984, **19:**3995-4006.

57. Annavarapu S, Doherty RD: **Inhibited coarsening of solid-liquid microstructures in spray casting at high volume fractions of solid.** *Acta Metallurgica et Materialia* 1995, **43:**3207-3230.

58. Chen TJ, Hao Y, Sun J, Li YD: **Phenomenological observations on thixoformability of a zinc alloy ZA27 and the resulting microstructures.** *Materials Science and Engineering: A* 2005, **396:**213-222.

59. Kliauga AM, Ferrante M: **The influence of deformation mode on the semi-solid state microstructure of an A356 aluminium alloy.** *Jornadas SAM-Conamet* 2001**:**91-98.

60. Chen TJ, Hao Y, Sun J, Li YD: **Effects of Mg and RE additions on the semi-solid microstructure of a zinc alloy ZA27.** *Science and Technology of Advanced Materials* 2003, **4:**495-502.

61. Amin-Ahmadi B, Aashuri H: **Globular Structure of M2 High Speed Steel by Thermomechanical Treatment in the Semisolid State.** *Steel Research International* 2010, **81:**381-386.

62. Suery M: *Mise en forme des alliages métalliques à l'état semi-solide.* Paris: Hemès Science Publications; 2002.

63. Blais S, Loue WR, Pluchon C: **Structure control by electromagnetic stirring and reheating at semi-solid state.** In *Proceedings of 4th International Conference on Semi-solid Processing of Alloys and Components; Sheffield, UK*. Edited by Kirkwood DH, Kapranos P. University of Sheffield; 1996: 187-192.

64. Laukli H, Lohne O, Sannes S, Gjestland H, Arnberg L: **Grain size distribution in a complex AM60 magesium alloy die casting.** *Int J Cast Metals Research* 2003, **6:**515-521.

65. Lifshitz IM, Slyozov VV: **The kinetics of precipitation from supersaturated solid solutions.** *J Chem Phys Solids* 1961, **19:**35-50.

66. Manson-Whitton ED, Stone IC, Jones JR, Grant PS, Cantor B: **Isothermal grain coarsening of spray formed alloys in the semi-solid state.** *Acta Materialia* 2002, **50:**2517-2535.

67. Loue WR, Suery M, Querbes JL: **Microstructure and rheology of partially remelted AlSi-alloys.** In *Proc 2nd Int Conf on the Processing of Semi-Solid Alloys and Composites; Cambridge, USA*. Edited by Brown SB, Flemings MC. TMS, Warrendale; 1992: 266.

68. Gullo GC, Steinhoff K, Uggowitzer PJ: **Microstructural changes during reheating of semi-solid alloy AA 6082.** In *6th International Conference Semi-Solid Processing of Alloys and Composites; Turin*. Edited by Chiarmetta GL, Rosso M. Edimet Spa; 2000: 367-372.

69. Liu YQ, Fan Z: **Magnesium alloy selections for semisolid metal processing.** In *7th S2P International Conference on Semi-solid Processing of Alloys and Composites; Tokyo, Japan*. Edited by Tsutsui Y, Kiuchi M, Ichikawa K. National Institute of Advanced Industrial Science and Technology and the Japan Society for Technology of Plasticity; 2002: 587-592.

70. Püttgen W, Bleck W, Seidl I, Kopp R, Bertrand C: **Thixoforged damper brackets made of the steel grades HS6-5-3 and 100Cr6.** *Advanced Engineering Materials* 2005, **7:**726-735.

71. Robelet M, Rassili A, Fischer D: **Steel grades adapted to the thixoforging process: metallurgical structures and mechanical properties.** *Solid State Phenomena* 2006, **Semi-Solid Processing of Alloys and Composites,116-117:**712-716.

72. Lecomte-Beckers J, Rassili A, Carton M, Robelet M, Koeune R: **Study of the liquid fraction and thermophysical properties of semi-solid steels and application to the simulation of inductive heating for thixoforming.** In *Advanced Methods in Material Forming*: Springer Berlin Heidelberg; 2005.

73. Li J, Sugiyama S, Yanagimoto J, Chen Y, Fan G: **Effect of inverse peritectic reaction on microstructural spheroidization in semi-solid state.** *Journal of Materials Processing Technology* 2008, **208:**165-170.

74. Smallman RE, Ngan AHW: *Physical Metallurgy and Advanced Materials.* Elsevier; 2007.

75. Gasper R, Schönbohm A, Enning M, Abel D: **Flatness Based Control of Inductive Heating of X210CrW12 into the Semi Solid State.** *Semi-Solid Processing of Alloys and Composites X* 2008, **141-143:**127-132.

76. Midson SP, Nicholas NH, Nichting RA, Young KP: **Semi-solid forming high temperature alloys. .** In *the 2nd International Conference on the Processing of Semi-Solid Alloys and Composites; Cambridge, MA, USA*. Edited by Brown SB, Flemings MC. TMS, Warrendale; 1992: 140-148.

77. Kapranos P, Kirkwood DH, Sellars CM: **Semi-solid processing of tool steel.** *Le Journal de Physique IV* 1993, **3:**835-840.

78. Kiuchi M, Sugiyama S, Arai M: **Experimental study on mushy metal forming.** *Journal of the Japan Society for Technology of Plasticity* 1996, **37:**1219-1224.

79. Rassili A, Fischer D, Robelet M, Dermurger J, Cucatto A, Klemn H, Walkin B, Kalsson M, Flüß A: **Improvement of materials and tools for thixoforming of steels.** In *8th International Conference on Semi-Solid Processing of Alloys and Composites* (Alexandrou GG, Jorstad J, Makhlouf M eds.). pp. 533-543. Limassol, Cyprus: NADCA (North American Die Casting Association); 2004:533-543.

80. Behrens B, Haller B, Fischer D: **Thixoforming/semi-solid forming : Thixoforging of steel using ceramic tool materials.** *Steel Research International* 2004, **75:**561-568.

81. Behrens B, Fischer D, Haller B, Rassili A, Jean-Christophe P, klemm H, Studinski A, Walkin B, Kalsson M, Robelet M, et al: **Series Production of Thixoformed Steel Parts.** *Solid State Phenomena* 2006, **Semi-Solid Processing of Alloys and Composites:**686-689.

82. Nohm B, Morjan U, Hartmann D: **Thixoforming of steel.** In *6th Inter Conf on Semi-solid Processing of Alloys and Composites; Turin, Italy*. Edited by Chiarmetta GL, Rosso M. Edimet Spa; 2000

83. Tsuchiya M, Ueno H, Takagi I: **Research of semi solid casting of iron.** *JSAE Review* 2003, **24:**205-214.

84. Bramann H, Fehlbier M, Sahm P, Buhrig-polaczek A: **Casting of a cold work steel alloy in semi-solid state.** *Journal of Materials Processing Technology* 2004**:**1357-1364.

85. Hirt G, Bleck W, Buhrig-Polaczek A, Shimahara H, Puttgen W, Afrath C: **Semi solid casting and forging of steel.** *Solid State Phenomena* 2006, **116-117:**34-43.

86. Kopp R, Kallweit J, Möller T, Seidl I: **Forming and joining of commercial steel grades in the semi-solid state.** *Journal of Materials Processing Technology* 2002, **130–131:**562-568.

Chapitre 2. Méthodologie de caractérisation de la microstructure des semi-solides et thixoforgeage des aciers

1. Introduction

Le chapitre précédent a mis en exergue la nécessité de caractériser la microstructure formée par les phases liquide et solide. Celle-ci est en effet déterminante pour le comportement de matériau au cours de la mise en forme et les propriétés mécaniques des pièces produites. La caractérisation du semi-solide concerne la fraction liquide ainsi que la taille et la forme des particules solides.

Dans ce chapitre sont présentées les techniques de caractérisation des structures semi-solides dans les aciers. Celles-ci sont soit conventionnelles, soit nouvelles. Il s'agit de décrire le principe de chaque technique pour en définir ensuite les potentiels et les limites. Ceci doit permettre de construire une méthodologie de caractérisation des semi-solides.

Les techniques étudiées sont la Calorimétrie Différentielle à Balayage (DSC), la microscopie optique, la microscopie électronique à balayage avec spectrométrie à dispersion d'énergie (MEB-EDS), la tomographie aux rayons X à haute énergie et la microscopie confocale laser à balayage (CLSM). La première technique est globale : elle permet la mesure de la fraction de liquide, mais ne donne aucun élément sur la morphologie de la structure liquide-solide. Les autres techniques permettent d'observer la microstructure. Les deux dernières technologies permettent des observations in situ alors que les technique de microscopie optique ou par MEB ne permettent que des observations post-mortem après refroidissement.

Le choix des techniques de caractérisation va fortement dépendre du matériau considéré. Dans notre cas, le travail se restreint aux aciers, dont trois nuances en particulier : l'acier fortement allié M2, l'acier non allié C38LTT et l'acier faiblement allié 100Cr6. Le premier alliage ne présente pas de grand intérêt industriel en termes d'application. Par contre, sa teneur en éléments lourds comme le tungstène ou le molybdène ainsi que son fort taux de carbures le rendent sensible à certaines techniques. Les deux autres alliages présentent quant à eux un intérêt industriel.

L'ensemble des techniques de caractérisation étudiées pour chaque matériau est donné dans le tableau 2.1.

Tableau 2.1. Différentes techniques appliquées à l'étude du procédé de thixoforgeage.

	M2	100Cr6	C38LTT	C38
Etat initial	MO, MEB-EDS, Microtomographie aux rayons X	MO, MEB-EDS, Microtomographie aux rayons X	MO, MEB-EDS	MO, MEB-EDS, Microtomographie aux rayons X
Etat semi-solide	DSC, MO, MEB-EDS, Microtomographie aux rayons X, CLSM	MO, MEB-EDS, Microtomographie aux rayons X, CLSM	MO, MEB-EDS, Microtomographie aux rayons X, CLSM	MO, MEB-EDS, Microtomographie aux rayons X, CLSM
Thixoforgeage	Essais de thixoforgeage MO, MEB-EDS	No	Essais de thixoforgeage, MO, MEB-EDS	No

Le comportement du matériau au cours d'une opération de thixoforgeage dépend de sa structure liquide solide, celle-ci étant fortement dépendant de la structure initiale et les conditions opératoires. Il existe un couplage fort entre le comportement du matériau et son mode de sollicitation thermomécanique au cours de la mise en forme. Pour étudier ces couplages et éprouver les techniques de caractérisations décrites ci-dessus des essais de thixoforgeage en conditions industrielles ou semi-industrielles ont été conduits. Ils concernent les trois aciers étudiés.

2. Matériaux étudiés

Les travaux de thèse se concentrent sur le thixoforgeage des aciers. La difficulté principale de l'étude et de la mise en œuvre du thixoforgeage des aciers provient du haut niveau de température. La conception des outillages et le comportement de l'acier à l'état semi-solide sont des points freinant le développement industriel du thixoforgeage des aciers.

L'analyse à température ambiante de la microstructure à l'état semi-solide est rendue difficile du fait de la diffusion des éléments d'alliage et de la transformation allotropique des aciers (structure CFC vers structure CC).

2.1. Choix des matériaux

Trois alliages ont été choisis : l'acier non allié C38LTT, l'acier faiblement allié 100Cr6 et l'acier fortement allié M2. Les deux premiers aciers ont un intérêt industriel. Leur aptitude à la mise en forme par thixoforgeage a été démontrée [1, 2]. Ces aciers présentent toutefois l'inconvénient de faibles teneurs en éléments d'alliage et des vitesses de diffusion des éléments rendant difficile la fixation de la répartition des éléments par un traitement thermique de trempe.

L'acier rapide M2 a été choisi non pas pour son intérêt industriel, mais pour l'avantage qu'il présente de permettre la caractérisation des structures liquide-solide à chaud par l'observation de la microstructure de l'alliage après trempe. En effet, les principaux éléments d'alliage comme le tungstène et le molybdène sont des éléments lourds dont la diffusion est lente. La structure initiale de l'alliage comporte des carbures dont la température de fusion est différente de celle de l'acier et qui vont conférer au matériau le comportement d'un matériau à deux phases solides distinctes.

2.2. Compositions chimiques

Tableau. 2.2. Composition chimique des aciers étudiés.

	Composition chimique (wt 10^{-3}%)																		
	C	**Si**	**Mn**	**S**	**P**	**Ni**	**Cr**	**Mo**	**Cu**	**Al**	**Sn**	**As**	**B***	**V**	**Ti**	**Nb**	**Ca***	**N***	**W**
C38	372	209	757	27	15	144	205	47	212	21	17	13	2	2	1	2	6	67	0
C38LTT	399	596	1424	83	77	91	130	29	114	3	9	9	4	89	15	0	10		0
100C6	988	230	326	6	7	210	1428	82	194	31	13	10	2	4	3	1	2	109	0
M2	850	35	250	≤40	≤40	200	4100	5000	100					1900					6400

La composition chimique des alliages peut varier pour une même nuance. Or, les variations de composition peuvent induire des différences notables dans le comportement à l'état semi-solide. La composition chimique de chaque nuance est donnée dans le tableau 2.2.

2.3. Evaluation de la fraction liquide à l'état semi-solide

La Fig. 2.1 présente l'évolution de la fraction volumique de liquide en fonction de la température obtenue par DSC/DTA. On peut remarquer que cette technique permet d'estimer la température de solidus et de liquidus de chaque acier. En comparant les courbes, on peut noter que l'acier M2 a le plus grand intervalle liquide-solide. Ceci provient de la fusion d'une teneur importante de carbures lors du chauffage. L'intervalle liquide-solide de l'acier 100Cr6 est relativement grand, ce qui va dans le sens d'une meilleure aptitude à la mise en forme à l'état semi-solide. En modifiant légèrement la composition de l'acier, on peut obtenir une température de solidus plus faible pour un plus large intervalle de fusion comme dans le cas des aciers C38LTT et C38. La pente des courbes à 10% et à 30% est relativement faible, traduisant une sensibilité de la fraction liquide aux variations de température modérée. Ceci va également dans le sens d'une bonne aptitude à la mise en forme à l'état semi-solide par thixoforgeage.

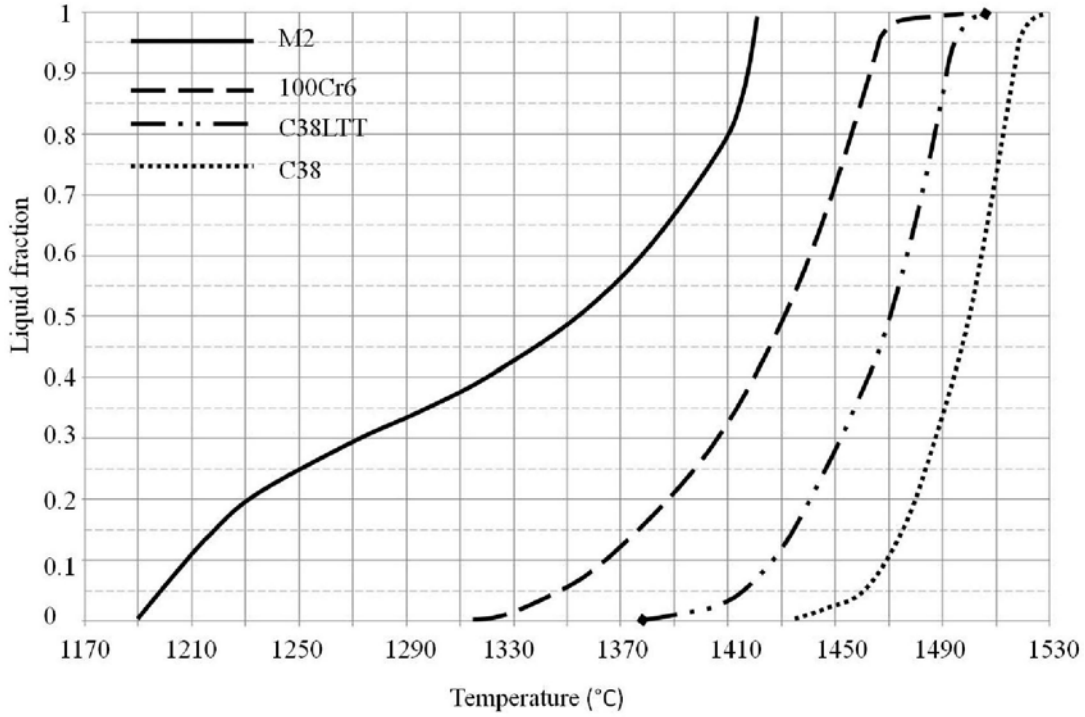

Fig. 2.1. Courbes de fraction liquide pour différentes nuances d'aciers en fonction de la température au moyen de mesures DSC/DTA obtenues par différents chercheurs [2-5].

2.4. Propriétés physiques

Dans un contexte industriel, les lopins sont chauffés jusqu'à l'état semi-solide par chauffage par induction. Du fait de la concentration de la génération de chaleur en surface de pièce, il est nécessaire de procéder à des cycles de chauffage en plusieurs étapes. Deux périodes de chauffe sont séparées par un temps d'attente permettant à la chaleur de diffuser vers le centre du lopin par conduction. De ce fait, il apparaît que l'évaluation des propriétés thermiques du matériau est essentielle. Les propriétés physiques des aciers étudiés à température ambiante sont données dans le tableau 2.3.

Table 2.3. Propriétés physiques à température ambiante des aciers étudiés.

Nuance	**Module d'élasticité**	**Densité**	**Limite élastique**	**Contrainte à rupture**	**Allongement**	**Conductivité thermique**	**Capacité tehrique spécifique**
	E (GPa)	ρ (g/cm^3)	σ_s (MPa)	σ_b (MPa)	A (%)	λ (W/m.°K)	Cp (J/kg.°K)
C38	200	7.84	440-490	600-900	18-20	~40	~440
100Cr6	210	7.81	410-470	700-900	13-27	~46	~475
M2	217	8.12				~19	~460

Les propriétés thermophysiques dépendent de la température. Par exemple, la Fig. 2.2 illustre l'évolution de la conductivité thermique de l'acier C38LTT au cours du chauffage. On remarque notamment une chute brutale de la conductivité au cours de la fusion de l'acier.

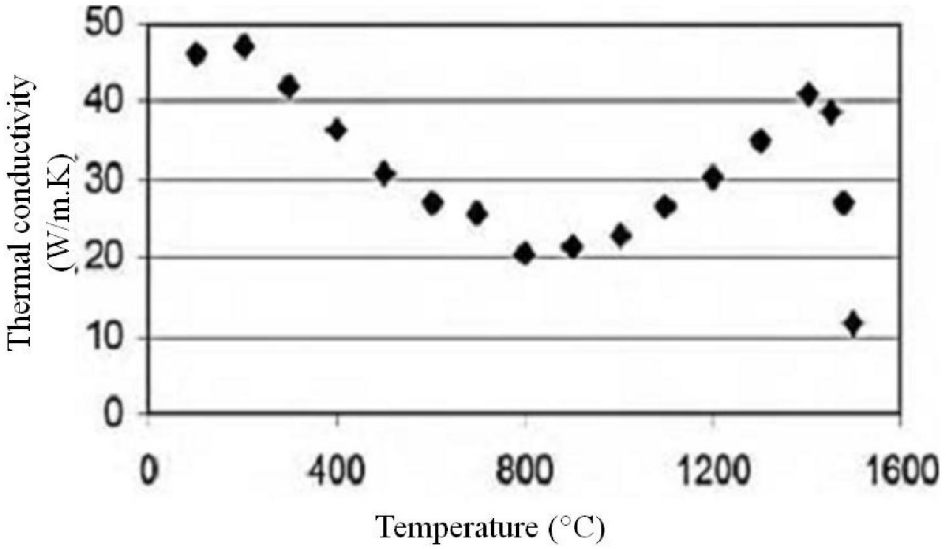

Fig. 2.2. Evolution de la conductivité thermique du C38LTT au cours du chauffage [2].

Les résultats concernant microstructure des aciers étudiés à l'état semi-solide obtenus par les techniques de caractérisation sont présentés au chapitre 3. Ce chapitre se concentre sur la caractérisation des techniques pour en établir les capacités et les limites.

3. Thixoforgeage des aciers

Différentes pièces ont été thixoforgées. La figure Fig. 2.3 illustre l'ensemble des pièces réalisées. L'étude s'est principalement concentrée sur le thixoforgeage de l'acier M2 pour lequel l'étude de la microstructure semi-solide a été menée à toutes les étapes du processus complet de mise en forme. L'influence des paramètres de thixoforgeage a été étudiée sur les pièces en 100Cr6 thixoforgées dans le cadre des travaux de thèse de Becker [5]. Des pièces en acier C38LTT thixoforgées en conditions industrielles ont également fait l'objet d'investigation concernant principalement la macro et la microstructure à froid ainsi que les propriétés mécaniques.

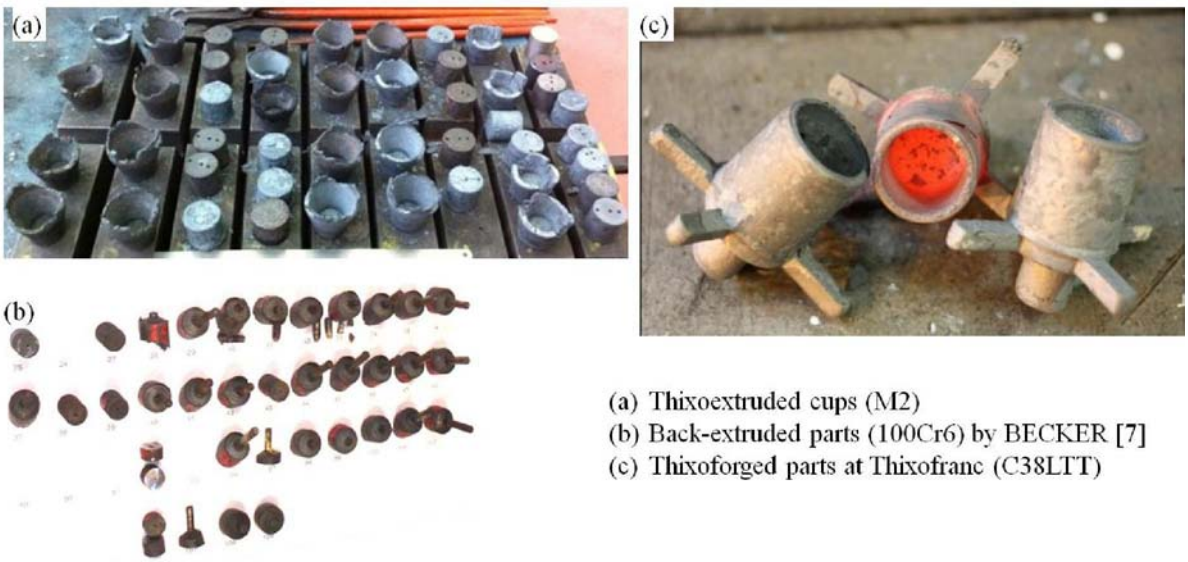

Fig. 2.3. Pièces thixoforgées ayant fait l'objet de l'étude (a) M2, (b) 100Cr6 et (c) C38LTT.

3.1. Dispositif de chauffage

Pour le thixoforgeage, il est important de porter l'alliage à l'état semi-solide avec une température la plus homogène possible dans le lopin. Ce dernier peut être chauffé en utilisant différents moyens comme le chauffage par induction, les fours à gaz, les fours électriques à résistance...

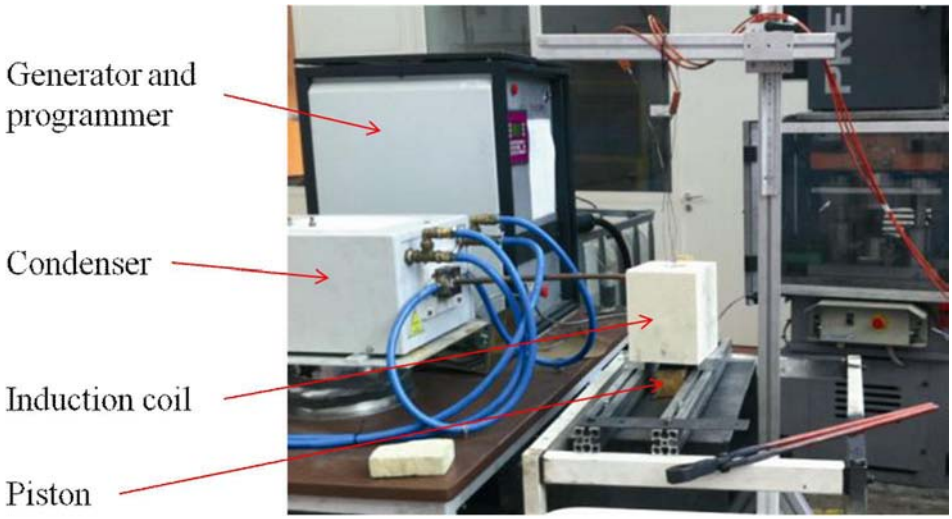

Fig. 2.4. Système de chauffage à induction au LCFC à Arts et Métiers ParisTech, METZ.

Du fait de sa grande vitesse de chauffe, de sa bonne répétabilité et de la capacité d'une chauffe sous atmosphère protectrice, le chauffage par induction est préférable en contexte

industriel aux autres techniques. La Fig. 2.4 montre le système par induction utilisé pour les essais réalisés dans le cadre de ces travaux. Ce système est constitué d'un générateur, d'un programmeur et d'un solénoïde. Le générateur (de marque **CELES**) peut fournir une puissance jusqu'à 50kW dans un intervalle de fréquence de 20 à 100 kHz. Pour obtenir une température uniforme et optimiser la chauffe, le solénoïde a été conçu à façon. Les dimensions de celui-ci ont été déterminées en fonction de la taille et du matériau du lopin ainsi que des caractéristiques du générateur.

3.1.1. Conception de l'inducteur pour un chauffage par induction uniforme dans le lopin

Au cours du chauffage par induction, l'énergie est transférée du solénoïde au lopin via un champ magnétique alternatif. Celui-ci produit dans la pièce un courant induit qui va chauffer le lopin effet Joule.

Les courants induits dans le lopin sont concentrés en surface. A partir de l'équation de Maxwell, il peut être montré que l'intensité du courant induit décroît de façon exponentielle depuis la périphérie du lopin jusqu'à son centre [6]. Pour un lopin cylindrique, la distribution de courant est donnée par l'équation Eq. 2.1 :

$$I(r) = I_0 \exp\left[(r - R)/\delta\right] \qquad \text{(Eq 2.1)}$$

où $\boldsymbol{I_0}$ est la densité de courant maximum en surface, $\boldsymbol{R}$ est le rayon du lopin et $\boldsymbol{\delta}$ est la profondeur de pénétration.

De son côté, la pénétration peut être exprimée par l'équation Eq. 2.2 :

$$\delta = 503.3\sqrt{\frac{\chi}{\mu_r f}} \qquad \text{(Eq. 2.2)}$$

où $\boldsymbol{\chi}$ et $\boldsymbol{\mu_r}$ sont la résistivité et la perméabilité magnétique relative du matériau. $\boldsymbol{f}$ est la fréquence du courant.

La loi de Joule permet de calculer la densité de puissance Eq. 2.3 :

$$P(r) = P_0 \frac{I^2}{I_0^2} = P_0 \exp[2(r - R)/\delta] \qquad \text{(Eq. 2.3)}$$

où $\mathbf{P_0}$ est la densité de puissance maximale obtenue en surface.

Les équations Eq. 2.2 et Eq. 2.3 montrent que la densité de puissance est plus importante en surface qu'au coeur du lopin. De plus, on peut noter que l'effet de concentration de la puissance en surface est plus prononcé pour les fréquences les plus élevées.

Si la fréquence du champ magnétique est trop élevée, la puissance est concentrée en surface de lopin et le cycle de chauffage devient long pour intégrer des phases d'attente pour l'homogénéisation de la température par conduction. Si la fréquence est trop basse, l'efficacité du chauffage est faible par effet d'annihilation du courant. Considérant la capacité des équipements présents au laboratoire et compte tenu des dimensions du lopin et des caractéristiques physiques du matériau, la fréquence de 28 kHz a été retenue.

En réduisant le nombre de spires ainsi que le jeu entre le lopin et le solénoïde, on peut accroître le rendement du chauffage. Toutefois, un nombre trop faible de spires peut provoquer un effet de coin sur le lopin. Le champ magnétique n'est plus uniforme sur la pièce, ceci produisant une densité de puissance hétérogène. Afin de limiter l'effet de coin, la hauteur du solénoïde est choisie trois fois supérieure à celle du lopin (Fig. 2.5).

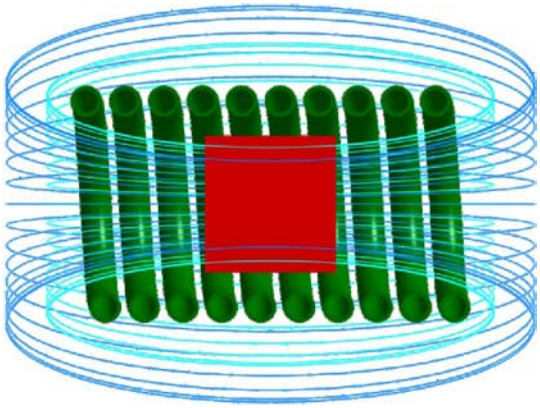

Fig. 2.5. Illustration d'une pièce dans le champ magnétique produit par un solénoïde.

Le solénoïde est constitué d'un tube enroulé qui permet le passage du fluide de refroidissement. Les dimensions du solénoïde sont établies pour un lopin de diamètre 35mm et de hauteur 34mm : elles sont données dans le tableau 2.4.

Table 2.4 Caractéristiques géométriques du solénoïde utilisé pour les essais de thixoforgeage.

Nombre de spires	10
Diamètre intérieur	45mm
Hauteur	100mm
Diamètre intérieur du tube	6mm
Épaisseur du tube	1mm

3.1.2. Cycle de chauffage

Au cours du chauffage par induction, la relation temps-température doit être maîtrisée de façon précise pour obtenir une température uniforme dans tout le lopin [7, 8]. De façon générale, la surface du lopin s'échauffe en premier du fait de la concentration de la puissance en surface. Ceci est caractérisé par la profondeur de pénétration (Eq. 2.2). L'équation Eq. 2.2 montre qu'on peut augmenter la profondeur de pénétration des courants en baissant la fréquence de l'inducteur et donc atteindre un gradient de température plus faible. Dans un contexte industriel, il est nécessaire de réduire les temps de chauffage pour accroître la productivité. Ceci nécessite l'augmentation de la puissance de chauffage, ceci se traduisant par des gradients de température plus importants. Si on ajoute à cela les échanges thermiques avec le milieu extérieur par convection et rayonnement, on se rend compte que les exigences d'une température homogène et d'une durée de chauffage faible sont antagonistes.

Les cycles de chauffage avec plusieurs étapes sont conçus pour obtenir un champ de température uniforme en un temps court. La démarche de conception de ce cycle est la suivante : un chauffage rapide avec une forte puissance est appliqué en début de cycle jusqu'à l'obtention d'une température élevée. A ce stade, la température n'est pas homogène dans le lopin. La deuxième partie du cycle consiste à chauffer le lopin avec une puissance plus faible pour compenser les pertes de chaleur par convection rayonnement et pour « alimenter » la conduction de chaleur depuis la surface vers le cœur. Différents cycles de chauffage ont été déterminés pour atteindre chaque température de mise en forme. Le critère d'acceptabilité du cycle de chauffage est basé sur la différence de température entre les trois thermocouples qui ne doit pas dépasser 10°C.

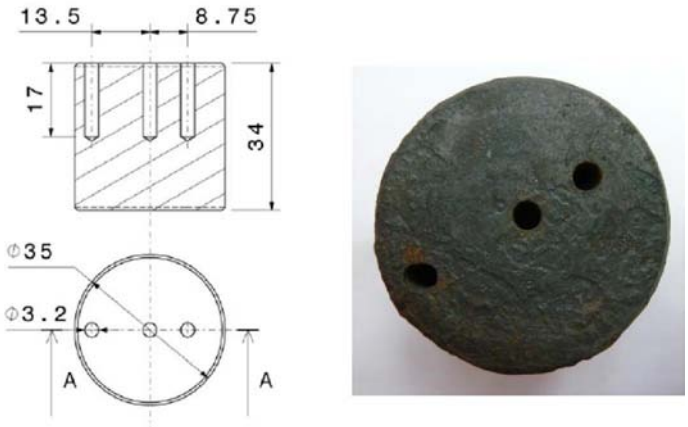

Fig. 2.6. Illustration de la position des thermocouples dans un lopin.

Pour déterminer le cycle de chauffe, des lopins sont instrumentés avec trois thermocouples (type S). Ces derniers sont placés à différents lieux du lopin pour permettre le contrôle et la mesure de la différence de température entre la surface et le cœur du lopin. Un exemple de disposition des thermocouples est présenté sur la figure Fig 2.6.

L'application d'une faible puissance en fin de cycle permet également d'éviter la fusion totale en peau. La Fig. 2.7 illustre l'évolution de la température aux différentes positions des thermocouples dans le lopin (cf fig 2.6) et de la puissance de chauffage en fonction du temps. La taille des thermocouples et leur gaine de protection en alumine nuisent à la précision et la rapidité de la mesure de température. On estime que les températures sont mesurées avec une précision de ±2.5°C.

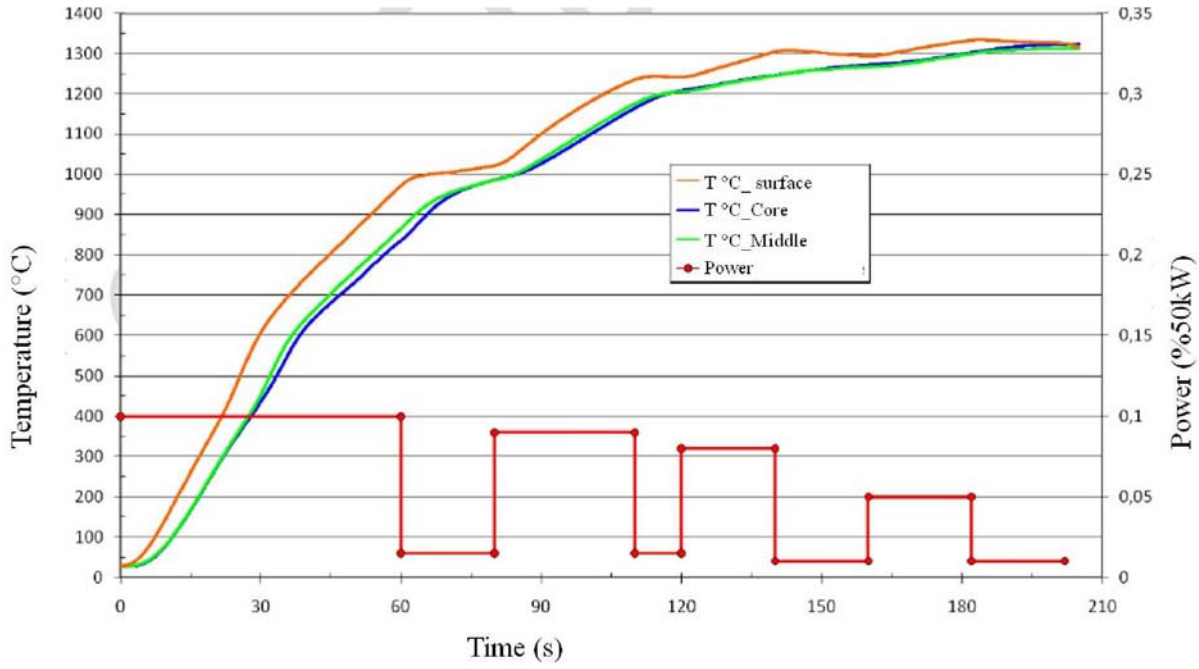

Fig. 2.7. Exemple de cycle en plusieurs étapes du chauffage d'un lopin jusqu'à un état semi-solide.

Comme stipulé par Becker [9], à l'augmentation de la température de mise en forme et associée une augmentation de la fraction liquide et une baisse de l'effort de mise en forme. En contrepartie, l'augmentation de température est limitée par le phénomène d'hétérogénéisation de l'écoulement. Il est donc nécessaire d'identifier l'intervalle de température conduisant au thixoforgeage de pièce sans défaut. L'intervalle de température est déterminé expérimentalement à travers des essais de mise en forme. Le tableau 2.5 présente des pièces thixoforgées à différentes températures.

Table. 2.5. Illustration de l'écoulement du matériau thixoforgé à différentes températures.

Pièces thixoforgées		
Ecoulement du matériau	Hétérogène	Homogène
Température max. (°C)	1340	1289

La méthode suivie (essai-erreur) pour la détermination du cycle de chauffage est longue et coûteuse. De plus, elle ne permet pas une maîtrise suffisante du chauffage qui permettrait d'extrapoler le résultat obtenu à d'autres cas, même voisins. Il serait possible pour cela d'utiliser des outils de simulation numérique comme ceux utilisés par la société CELES, fabricant du générateur.

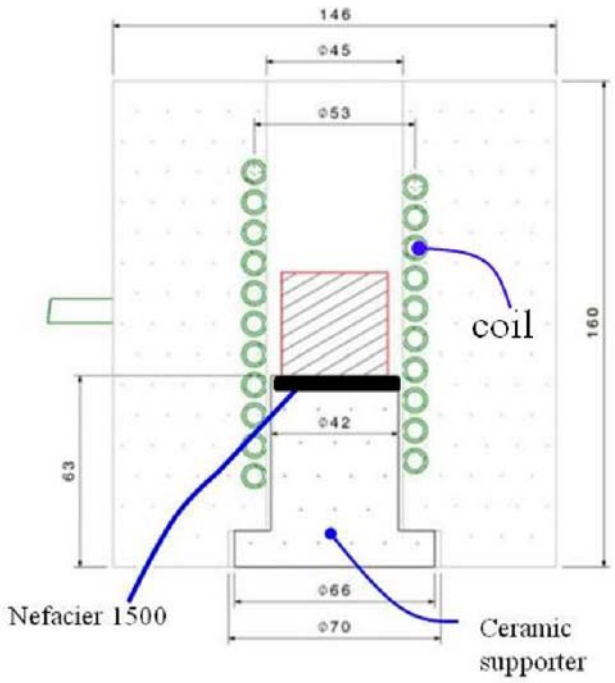

Fig. 2.8. Schéma du dispositif de chauffage des lopins.

Pour obtenir un champ de température uniforme, le lopin est placé au centre du solénoïde. Le lopin, durant la chauffe, est posé sur un support en céramique réfractaire. Celle-ci a la

propriété d'être à la fois insensible au champ magnétique et résistant à la température. De plus, entre le support en céramique et le lopin est interposée une pastille de Nefacier 1500. Ce type de pastille est constitué de fibres de céramique et va permettre d'isoler thermiquement le lopin du support pour limiter les échanges thermiques (voir Fig. 2.8). Pour éviter une dérive des conditions initiales en température en début de chauffe, le support en céramique et la pastille de Nefacier sont refroidies. Lors du transfert du lopin sous la presse, les pinces sont recouvertes de Nefacier pour limiter les échanges thermiques.

3.1.3. Difficultés rencontrées au cours du chauffage par induction

Oxydation au cours du chauffage

La plupart des métaux s'oxydent en présence de l'oxygène de l'air au cours du chauffage. Comme stipulé par nombre de chercheurs [5, 10, 11], les particules d'oxyde conduisent à une usure par abrasion rapide des outillages. Pour éviter cela, il est possible d'utiliser un gaz de protection comme l'argon. Toutefois, l'oxydation est limitée en chauffage par induction car la durée du cycle est relativement courte. Dans les essais conduits dans le cadre des travaux de thèse, aucune atmosphère protectrice n'a été mise en œuvre.

Perte de chaleur

Même avec l'utilisation de la pastille isolante de Nefacier, les échanges thermiques avec le support céramique sont plus élevés que les pertes avec l'atmosphère. Au cours du transfert du lopin vers la presse, les échanges thermiques entre le lopin et le système de manutention provoquent une chute de température dans les zones de contact. La Fig. 2.9 présente l'évolution de la température au cours du chauffage par induction et du transfert du lopin. La durée du transfert est comprise entre 6 et 12s. On note une chute de température d'environ 30°C au droit des contacts entre le lopin et les pinces.

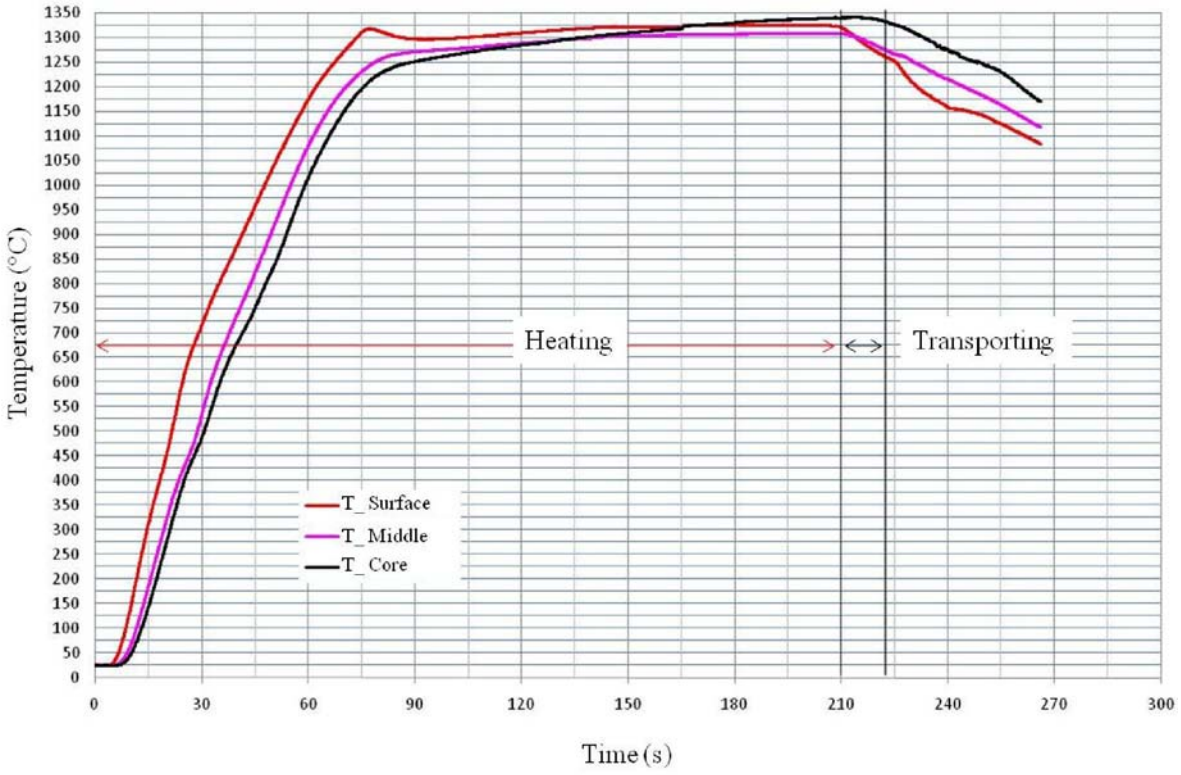

Fig. 2.9. Evolution de la température au cours du chauffage et du transfert du lopin.

3.2. La presse

L'utilisation d'une presse mécanique a été préférée à celle d'une presse hydraulique pour trois raisons :

- l'accès à de grandes vitesses de mise en forme, l'effort de mise en forme décroissant avec la vitesse de mise en forme [8, 9].
- avec de grandes vitesses de mise en forme, les temps de contact outil/matière sont réduits, limitant ainsi les échanges thermiques avec les outillages.
- la cadence de production est plus élevée et plus conforme à ce qui est attendu dans un contexte industriel.

La presse mécanique PRESSIX (Fig. 2.10) disponible au laboratoire LCFC peut fournir un effort maximum de 500kN avec une vitesse maximum 485 mm/s. Elle a été utilisée pour les essais de thixoforgeage de l'acier M2.

Fig. 2.10. Presse mécanique (PRESIX) à Arts et Métiers ParisTech, Metz.

L'outillage d'extrusion inverse (Fig. 2.11) a été utilisé pour l'extrusion d'un « godet » depuis un lopin cylindrique. Les outillages ont été réalisés en acier à outil de type X38CrMoV5.

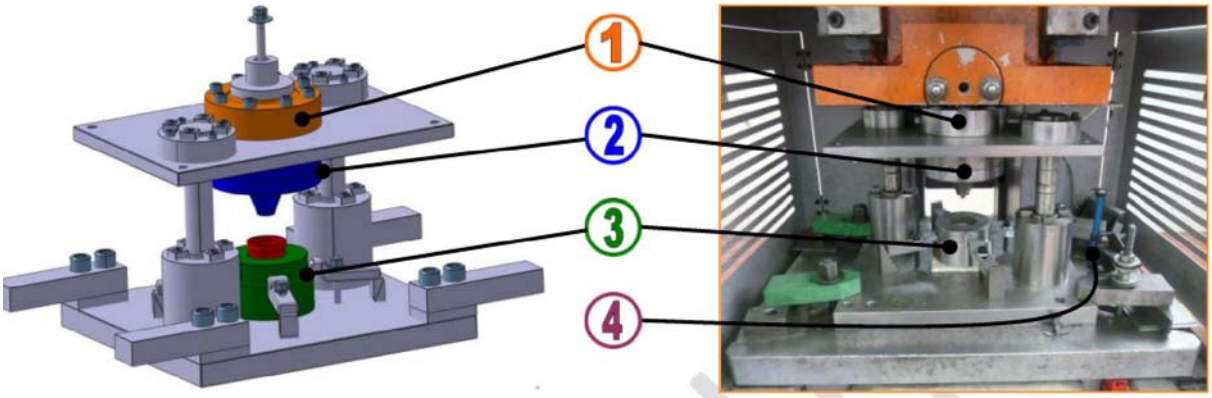

Fig. 2.11. Illustration du dispositif d'extrusion. (1) Capteur d'effort, (2) matrice supérieure, (3) matrice inférieure et (4) capteur de déplacement.

Un des paramètres de l'étude est la température de l'outillage. Celle-ci aura deux niveaux, outillage froid (température ambiante) et outillage chauffé (~350°C). Les outillages sont chauffés à la flamme avec un contrôle de température par pyromètre.

Les lopins ont un diamètre de 35mm pour une hauteur de 34mm.(voir Fig. 2.12).

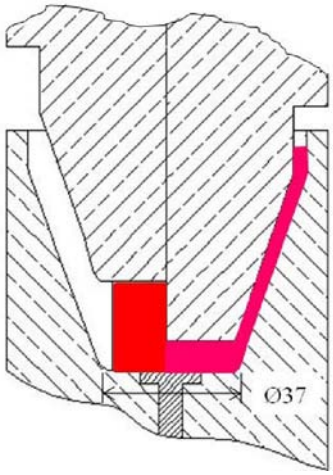

Fig. 2.12. Principe du test d'extrusion inverse.

3.3. Système d'acquisition

Au cours du thixoforgeage, plusieurs paramètres sont mesurés (température, course des outillages, effort de mise en forme…). La course des outillages et la force de mise en forme sont mesurées pour tous les essais alors que les mesures de température n'ont été utilisées que pour le calage du cycle de chauffage. Ces mesures ont été effectuées grâce à un système d'acquisition PCI6024E National Instrument disposant de huit voies (± 0.3% d'erreur sur la pleine échelle) et contrôlé par le logiciel Labview (voir figure Fig. 2.13 (a)).

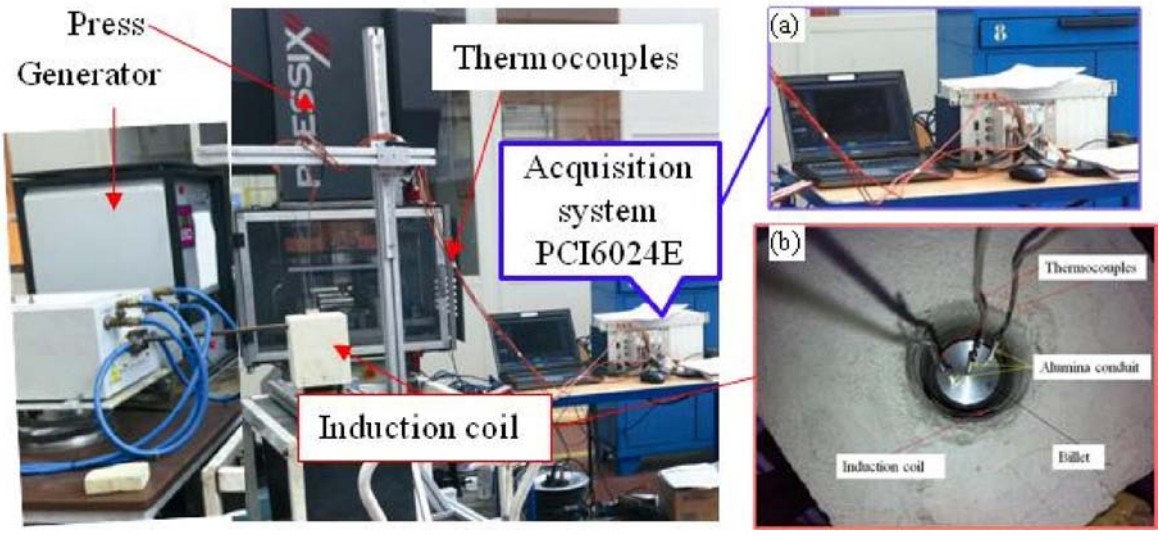

Fig. 2.13. Système d'acquisition à Arts et Métiers ParisTech, Metz.

Mesure de l'effort de mise en forme

Le capteur SCAIME (voir Fig. 2.11 (1)) peut être utilisé en traction ou compression. Sa plage d'effort maximum est de 600kN avec une erreur $\leq \pm 0.3\%$. Le principe du capteur repose sur la mesure de déformation de poutres avec des jauges d'extensométrie montées sur un pont de Wheatstone.

Mesure de la course

Le capteur mécanique (erreur ± 0.01mm) (Fig. 2.11 (4)) est constitué d'une tige reliée à un potentiomètre délivrant une tension fonction du déplacement.

Mesure de température

La mesure de température dans les lopins est réalisée par des thermocouples de type S, avec une précision de ± 2.5°C. Le signal délivré par les thermocouples est récupéré au moyen du système d'acquisition PCI6024E de National Instrument. Les thermocouples sont protégés par une gaine en alumine. La température des outillages est mesurée par pyromètre sans contact.

4. Evaluation de la fraction liquide et caractérisation de la microstructure

La fraction volumique de liquide/solide et la structure du matériau à l'état semi-solide peuvent être déterminées par différentes approches en fonction du matériau étudié et des informations recherchées. L'analyse par DSC et l'analyse métallographique du matériau après trempe depuis l'état semi-solide sont les techniques les plus utilisées. A ces méthodes peut s'ajouter l'utilisation de diagrammes thermodynamiques comme les diagrammes d'équilibre. Pour obtenir plus d'informations sur la structure liquide-solide, des méthodes plus précises peuvent être mises en œuvre. Il s'agit des techniques de caractérisation in situ ou en trois dimensions de la structure du matériau à l'état semi-solide.

4.1. Détermination directe de la fraction liquide par l'utilisation de données thermodynamiques

Lors de la fusion en conditions quasi-statiques, la fraction volumique de liquide ou solide peut être déterminée à partir du diagramme d'équilibre. Le logiciel Thermocalc, par exemple,

permet l'exploitation de diagramme d'équilibre complexe d'alliages à plusieurs éléments. La fraction massique de solide, g_s, peut être calculée à partir de l'équation Eq. 2.4 :

$$g_s = 1 - \left(\frac{T_M - T}{T_L - T_M} \right)^{-\frac{1}{1-k}} \qquad \text{(Eq.2.4)}$$

où T_M est la température de fusion du principal élément, T_L est la température du liquidus et k est le coefficient de partition de l'alliage.

Comme les masses volumiques du liquide et du solide sont différentes, la fraction volumique de solide, f_s , peut être déterminée par l'équation Eq. 2.5 :

$$fS = \frac{g_s}{g_s + (1 - f_s)\dfrac{\rho_s(C,T)}{\rho_l(C,T)}} \qquad \text{(Eq. 2.5)}$$

où ρ_s and ρ_l sont respectivement les densités des phases liquides et solide à la température T, et C est la composition.

Grâce à l'utilisation de Thermocalc, la densité des phases solide et liquide peut être calculées. Toutefois, les conditions de fusion partielle de l'alliage sont différentes de celles supposées par l'utilisation des diagrammes d'équilibre. Les transformations ne sont pas quasi-statiques et l'état initial de l'alliage provenant de son mode d'élaboration doit être pris en considération. Il est donc nécessaire de procéder à des caractérisations expérimentales dans des conditions qui doivent être les plus proches de celle rencontrées au cours du processus complet de mise en forme.

4.2. Détermination de la fraction liquide par analyse thermique

L'évaluation expérimentale de la fraction volumique de liquide est le plus souvent effectuée par analyse thermique. La DSC est la technique la plus utilisée. Cette technique consiste à mesurer la différence d'énergie nécessaire pour chauffer d'un côté l'échantillon et de l'autre côté un matériau de référence, ceci à une vitesse de chauffe fixée. L'analyse par DSC fournit des informations qualitatives et quantitatives sur les transformations physiques et chimiques exothermiques ou endothermiques dans le matériau. Pour nos travaux, un calorimètre Netzsch DSC 404C Pegasus® permettant d'atteindre des températures jusqu'à 1500°C (Fig. 2.14) a été utilisé.

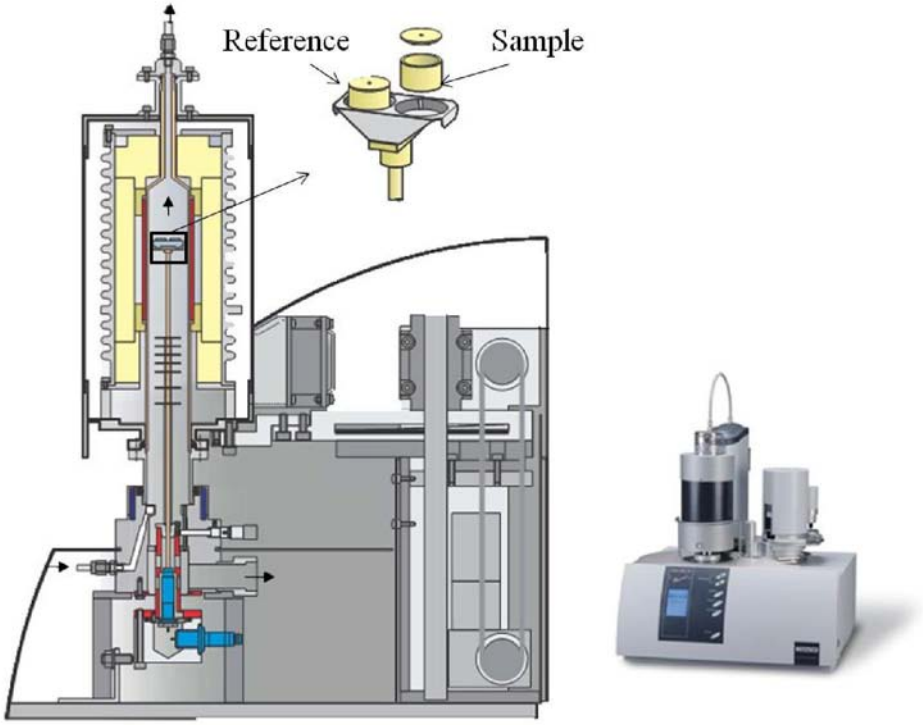

Fig. 2.14. Vue schématique du Netzsch DSC 404C Pegasus®.

Au cours de la chauffe depuis le liquide jusqu'au solide, l'échantillon subit une transformation de phase, réaction endothermique. L'énergie apportée au cours de la chauffe va contribuer à la montée en température du liquide et du solide et à la fusion. Ceci peut être traduit au travers de l'équation Eq. 2.6 :

$$\frac{dQ}{dt} = m\left(g_s C_{P,s} + (1 - g_s) C_{P,L} + \Delta H \frac{dg_s}{dT} \right) \frac{dT}{dt} \qquad \text{(Eq.2.6)}$$

où, dQ/dt est la puissance de chauffe, $\mathbf{g_s}$ est la fraction massique de solide, $\boldsymbol{C_{P,S}}$ et $\boldsymbol{C_{P,L}}$ sont les capacités thermiques massiques des deux phases, m est la masse de l'échantillon, et $\Delta\mathbf{H}$ est la chaleur latente de changement d'état.

Un traitement est nécessaire pour isoler l'énergie dédiée à la fusion du matériau. Pour cela, on utilise une courbe de base, la différence entre la courbe de base et celle correspondant au signal délivré par la DSC représente l'énergie dédiée la fusion (Fig. 2.15). Sur la figure Fig. 2.15, $\boldsymbol{T_{si}}$ et $\boldsymbol{T_{lf}}$ sont supposés être les températures de solidus et liquidus respectivement (selon l'International Conference on Thermal Analysis).

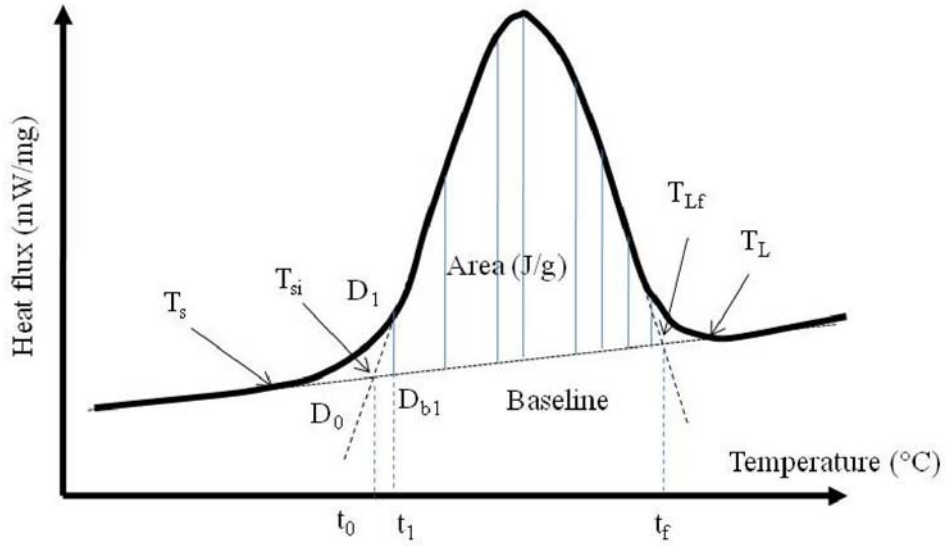

Fig. 2.15. Représentation schématique d'une courbe obtenue par DSC lors de la fusion d'un alliage.

Au cours de l'essai, l'échantillon est chauffé à une vitesse constante ($\dot{T}$). La baisse de la fraction de solide peut être calculée à partir de l'accroissement d'énergie absorbée. Ceci est décrit par l'équation Eq. 2.7 obtenue par dérivation de l'équation Eq. 2.6 :

$$dg_s = \frac{1}{\dot{T}} \int_{Ts}^{T} \frac{1}{\Delta H} \left(\frac{dQ}{dt} \right) dT \qquad \text{(Eq. 2.7)}$$

Dans cette dernière équation, il est fait l'hypothèse que la fraction liquide est proportionnelle à l'énergie absorbée. On suppose que l'énergie latente de changement d'état est constante tout au long de la fusion. En utilisant la méthode des surfaces partielles, la fraction massique de liquide peut être calculée grâce à l'équation Eq. 2.8, la fraction volumique de liquide pouvant alors être déterminée par l'équation Eq. 2.5 :

$$\begin{cases} g_s(T_i) = 1 - \dfrac{S(T_0 - T_i)}{S_{total}} \\ S(T_0 - T_i) = \displaystyle\sum_0^i \frac{t_n - t_{n-1}}{2} \bullet (D_n - D_{bn}) \bullet (D_{n-1} - D_{bn-1}) \end{cases} \qquad \text{(Eq. 2.8)}$$

Les essais ont été effectués à deux vitesses de chauffe 10°C/min et 20°/min. Les échantillons sont des disques de diamètre 3mm pour une hauteur de 1.5mm. Ils sont prélevés à différents endroits de la barre pour atténuer au maximum les effets des variations de composition chimique inhérentes au mode d'élaboration du matériau. Le protocole consiste à

chauffer l'échantillon depuis la température ambiante jusqu'à une température au-dessus du liquidus et à redescendre ensuite jusqu'à à la température ambiante. Cette méthode a plusieurs limites :

- La vitesse de chauffe maximum applicable est bien inférieure à celle obtenue en conditions industrielles lors d'un chauffage par induction (500-1000°C/min). Les conditions industrielles sont beaucoup plus éloignées de l'équilibre que celles qu'il est possible de reproduire par DSC.
- Pour la détermination de la fraction liquide, la méthode des surfaces partielles est approximative. Elle ne tient pas compte de l'effet de la composition sur la chaleur latente de fusion.

Outre ces limitations, l'analyse thermique par DSC ne donne qu'une information globale sur la fraction volumique de liquide. Il est donc nécessaire pour obtenir des informations sur la microstructure liquide solide d'associer à la DSC des techniques de caractérisation en 2D et 3D.

4.3. Evaluation de la fraction liquide par métallographie quantitative (2D et 3D)

De façon générale, la caractérisation de la microstructure à l'état semi-solide est souvent effectuée sur des échantillons chauffés dans des conditions industriellement représentatives jusqu'à l'état semi-solide, puis trempés. Outre l'étude de la fraction liquide, la caractérisation de la morphologie de la structure et de l'écoulement de la matière au cours de la mise en forme sont des objectifs. Toutefois, la trempe doit être la plus rapide possible pour figer la microstructure formée à l'état semi-solide.

Tableau 2.6. Dimensions des lopins pour le procédé de thixoforgeage.

Matériau	Dimensions (mm)
M2	Ø35mm*34mm, Ø38*30mm, Ø36*34mm, Ø1.2* 30µm
100Cr6	Ø30mm*45mm
C38LTT	Ø45mm*60mm

Au cours des essais, les échantillons ont été chauffés jusqu'à l'état semi-solide par induction. Ce mode de chauffage est rapide et représentatif des conditions industrielles. Les dimensions de l'échantillon sont données dans le tableau 2.6. Après trempe, les échantillons

sont analysés (2D et 3D) par différentes techniques : microscopie optique, microscopie électronique à balayage + EDS et la tomographie aux rayons X à haute énergie.

4.3.1. Analyse d'image en 2D

La réussite de l'analyse de la microstructure passe par l'efficacité de la trempe. Celle-ci doit pouvoir former une microstructure représentative de la structure liquide solide. On doit être capable depuis la structure observée après trempe de remonter à la structure à l'état semi-solide. Ces conditions peuvent ne pas être remplies du fait de la diffusion et des transformations de phases allotropiques. Si la structure subit des changements importants au cours de la trempe, les paramètres caractéristiques de la structure doivent être corrigés. Dans les cas les plus défavorables, ces paramètres peuvent ne pas être identifiables. Il apparaît ici qu'il est très important d'avoir un maximum de connaissances sur les mécanismes mis en jeu et ayant un impact sur les paramètres de la microstructure. Les aciers C38LTT, 100Cr6 et plus particulièrement l'acier rapide M2, ont fait l'objet d'une étude en détail de leur comportement au cours de leur fusion partielle ainsi qu'au cours de leur refroidissement. La Fig. 2.16 présente le diagramme TTT de l'acier M2 [12].

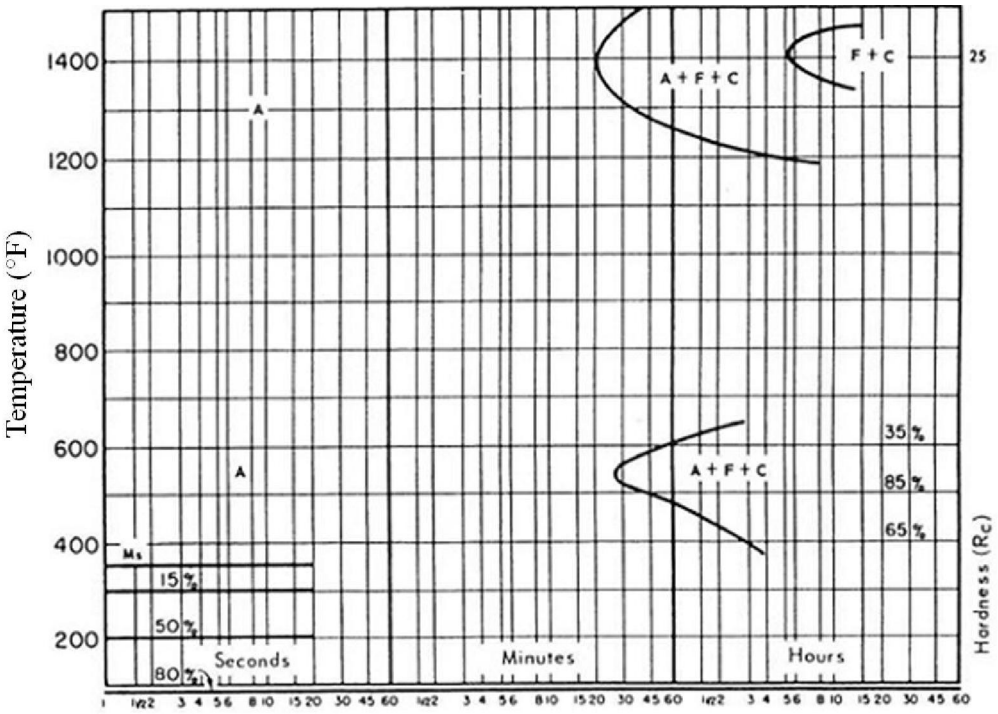

Fig. 2.16. Diagramme TTT de l'acier M2.

Les observations métallographies ont été effectuées suivant des sections longitudinales et transversales. Les échantillons étant de dimensions importantes, on ne peut pas faire l'hypothèse d'un champ de température uniforme. Plusieurs zones d'observation dans l'échantillon ont donc été définies (voir Fig. 2.17). De même, certaines pièces thixoforgées ont été trempées juste après la mise en forme (Fig. 2.18).

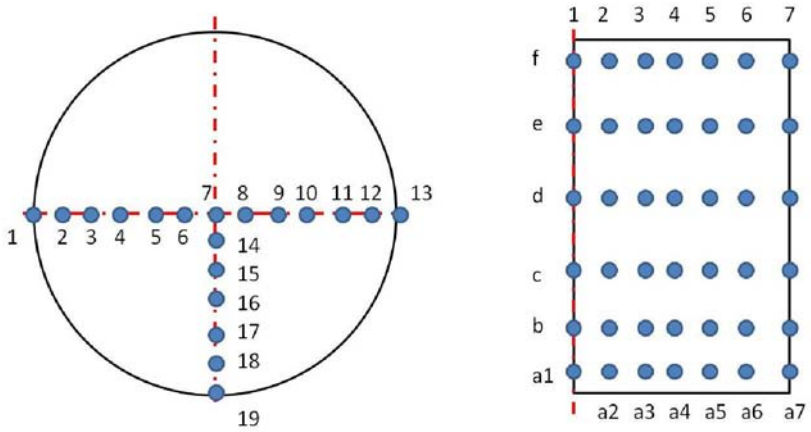

Fig. 2.17. Points d'observation sur les lopins trempés.

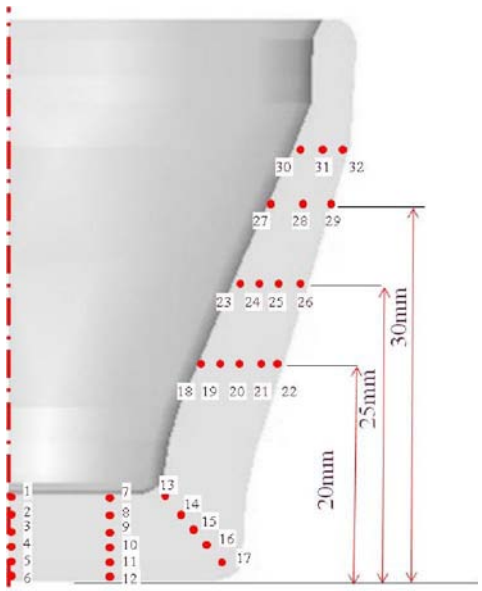

Fig. 2.18. Points d'observation sur les pièces thixoforgées.

Techniques d'observation en 2D

Selon la résolution nécessaire, différents microscopes ont été utilisées. Pour l'évaluation de la fraction de liquide, un microscope optique Olympus a été utilisé pour l'obtention de micrographies avec un faible grossissement (100 et 500 fois). Pour caractériser les particules

et les carbures, un MEB Jeol 7001 FLV a été utilisé. L'emploi d'une sonde EDS (système Oxford INCA) a permis d'étudier la distribution des différents éléments d'alliage.

Caractérisation quantitative de la microstructure

Taille de grain. Selon plusieurs travaux de recherche [13-16], la viscosité du matériau à l'état semi-solide décroît avec la diminution de la taille de grain. La taille moyenne de grain a été mesurée en utilisant la méthode d'interception linéaire moyenne telle qu'elle est décrite dans ASTM E 112-96.

Facteur de forme. Le facteur de forme joue un rôle important sur le comportement de l'alliage à l'état semi-solide, un facteur de forme proche de 1 étant recherché pour le thixoforgeage. Le facteur de forme des grains sur les micrographies 2D est calculé en utilisant l'équation Eq. 2.9 :

$$F = \frac{4\pi A}{P} \qquad \text{(Eq. 2.9)}$$

où A est la surface du grain et P sa circonférence mesurées sur la micrographie.

Fraction volumique de liquide. L'estimation de la fraction liquide est menée de façon automatique en utilisant le logiciel ImageJ sur une image codée en nuance de gris. Pour cette analyse, il est nécessaire de réaliser un compromis en termes de résolution de l'image. Les images obtenues avec un faible grossissement permettent de couvrir une surface plus grande et de « filtrer » les effets d'hétérogénéité. En contrepartie, la résolution de l'image est d'autant meilleure que le grossissement est grand. Toutefois, avec un grossissement trop important, il apparaît un problème d'identification des phases composites. Une structure eutectique provenant de la solidification de la phase liquide à haute température sera décomposée en plusieurs phases si la résolution de l'image est inférieure à la taille des phases constitutives de l'eutectique.

Le choix du grossissement dépend donc de la taille des phases et des grains dans le matériau à étudier. Dans notre cas, il semble que le même grossissement convienne à la diversité des structures à observer. Le grossissement choisi doit permettre l'analyse d'une surface représentative de la microstructure.

Table.2.7. Réactifs pour les attaques chimiques.

Attaque chimique	Composition	Concentration	Conditions	Application
Nital	Ethanol HNO3	100ml 2-4ml	Température ambiante de quelques secondes à quelques minutes	Microstructure
Groesbeck	Eau NaOH $KMnO_4$	100ml 4g 4g	à 70°C	Carbures
Béchet-Beaujard	Acide picrique solution Teepol Eau		à 70°C	Joints de grain austénitiques
HCL 50%	Acide chlorhydrique Eau distillée	50ml 50ml	à 70°C 15-25 min	Observation du fibrage

Attaques pour les observations métallographiques

Avant de procéder aux observations métallographiques, les échantillons subissent une attaque chimique avec différents réactifs suivant les objectifs. Les réactifs ainsi que les applications sont donnés dans le tableau. 2.7.

4.3.2. Observations 3D par microtomographie aux rayons X à haute énergie

L'analyse d'images en 2D ne permet pas toujours une analyse complète et pertinente de la microstructure. Une analyse en 3D peut être nécessaire. Deux techniques sont utilisées pour l'obtention la microstructure en 3D, la microtomographie et l'analyse d'image 2D prises dans des sections successives. La microtomographie est une technique non destructive et permet une meilleure résolution. La technique des sections successives est contrainte par la distance minimum entre deux plans successifs.

L'acier M2 a été analysé par tomographie aux rayons X à haute énergie à l'ESRF. L'acier M2 se prête bien à cette technique car il possède des éléments d'alliage de forte masse atomique (le tungstène et le molybdène). Par contre, les éléments d'alliage des aciers 100Cr6 et C38LTT ne permettent pas de distinguer les phases liquides et solides de l'acier par cette technique. Leur microstructure en 3D ne peut donc pas être révélée par tomographie aux rayons X.

4.3.2.1. Chauffage par induction pour l'observation de l'évolution de la microstructure

Afin d'obtenir l'évolution de la microstructure de l'acier M2 au cours du chauffage, un lopin a été partiellement porté à fusion. Lors de la chauffe, le lopin a été placé partiellement dans l'inducteur et reposait sur un support en céramique (voir Fig. 2.19).

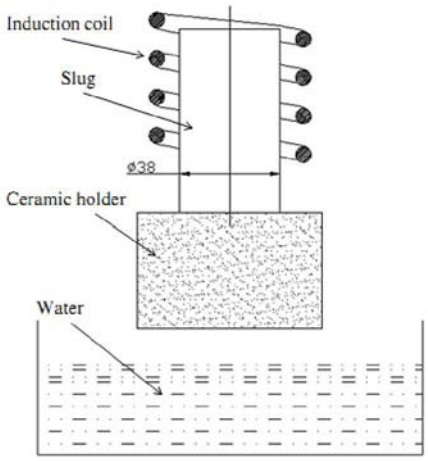

Fig. 2.19. Vue schématique du dispositif de chauffage par induction.

La température de la zone semi-solide a été mesurée par un pyromètre. Après une durée de chauffage d'environ 100s, la température de surface au point C (voir Fig. 2.20) atteint 1250°C. Le lopin est trempé à l'eau directement pour figer la structure formée à l'état semi-solide. Le chauffage a lieu sans atmosphère protectrice ; une importante couche d'oxyde s'est formée en surface. A cause de la couche d'oxyde, la température du matériau au point C est sans doute supérieure d'environ 100°C à celle mesurée avec le pyromètre. Du fait de la pénétration des courants induits, le champ de température à un profil en forme de cloche (voir Fig 2.20), la température est une fonction décroissante du rayon et de la hauteur. Le bas du lopin (près du support en céramique) est légèrement plus froid du fait des moindres courants induits dans cette zone. Celle-ci reste dans le domaine solide et pourra nous servir de référence à des fins de comparaisons.

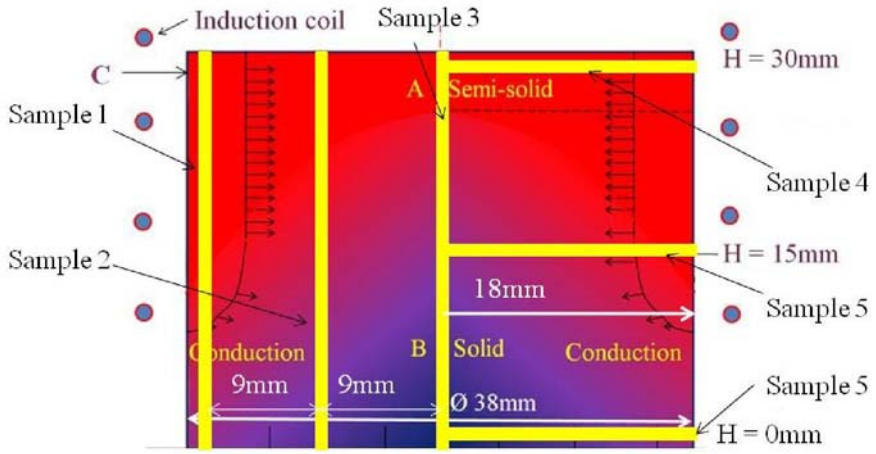

Fig. 2.20. Représentation schématique de la répartition de température au cours du chauffage par induction.

En considérant les énergies disponibles sur la ligne ID15A de l'ESRF, le diamètre des échantillons extraits du lopin pour l'analyse a été choisi à 1.2mm. Les échantillons sont découpés par électroérosion à fil. Des caractérisations par tomographie ont également été effectuées sur le matériau M2 dans son état de livraison à des fins de comparaison.

4.3.2.2. Principe de la tomographie par rayon X

Le principe de la tomographie par rayons X est basé sur celui de la radiographie X. Un faisceau de rayons X incident pénètre dans l'échantillon. Une partie du faisceau est absorbée, l'autre partie transmise est enregistrée par un détecteur CCD. Selon la loi de Beer–Lambert (Eq. 2.10), la rapport entre le nombre de photons transmis et le nombre de photons incidents est relié à l'intégrale du coefficient d'absorption du matériau μ le long du parcours du faisceau au travers de l'échantillon. Dans le domaine photoélectrique (E < 200keV), le coefficient d'absorption dépend de la densité, du numéro atomique et de l'énergie (quand le faisceau est monochromatique) suivant la fonction empirique donnée par l'équation Eq. 2.11. Si le matériau est hétérogène, l'intégrale de volume de μ (x,y, z) varie uniquement en fonction de l'orientation et de la position du faisceau (Fig. 2.21) :

$$N_1 = N_0 * \exp[-\int_{S \in ray} \mu(s) ds] \qquad \text{(Eq. 2.10)}$$

où N_1 est le nombre de photons d'énergie E transmis, N_0 est le nombre de photons incidents d'énergie E.

$$\mu(x,y,z) = K\rho\frac{Z^4}{E^3} \qquad \text{(Eq. 2.11)}$$

où K est une constante, ρ est la densité du matériau étudié, Z est le numéro atomique des éléments du matériau et E est l'énergie des photons incidents.

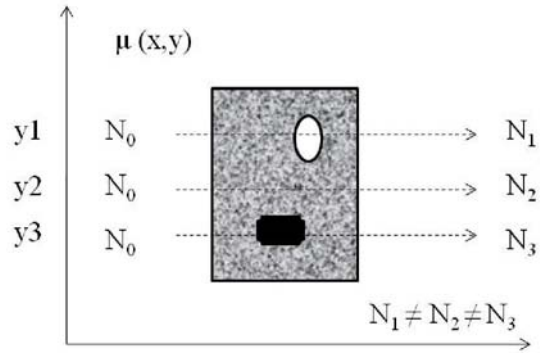

Fig. 2.21 Principe physique de la tomographie: projection dans un plan (Z=Zi). L'intensité du faisceau transmis dépend des propriétés du milieu traversé par le faisceau.

En plaçant un détecteur à l'arrière de l'échantillon, les photons transmis sont détectés et un signal fonction de leur nombre ($N_t(E)$) est traduit en nuance de gris. En plaçant un détecteur, il est possible d'obtenir une image 2D donnant la répartition de l'amplitude du faisceau sortant de l'échantillon.

Pour obtenir une vue 3D, un grand nombre de radiographies sont réalisées en faisant tourner l'échantillon entre 0° et 180° (voir Fig. 2.22). L'image est reconstruite en utilisant un algorithme de projection [17].

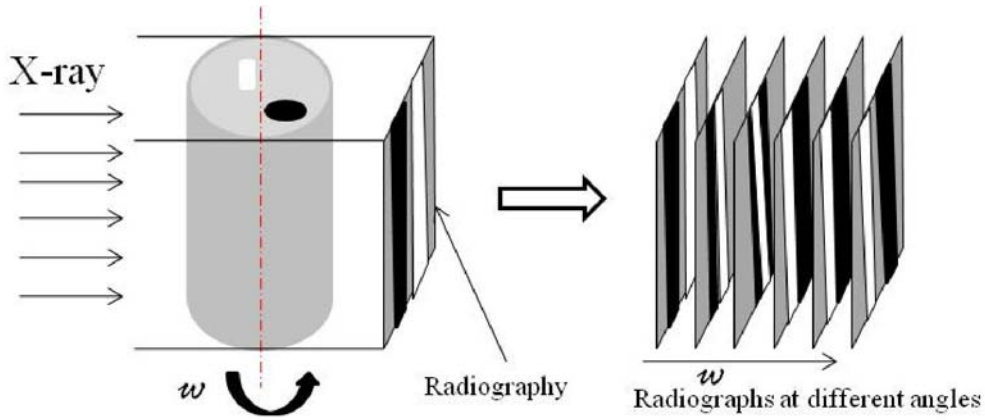

Fig. 2.22. Schéma de principe de l'acquisition par tomographie aux rayons X.

Comme abordé ci-dessus, le contraste obtenu en microtomographie peut être expliqué par la loi d'atténuation. Si les numéros atomiques des éléments de l'alliage sont proches, il sera difficile d'obtenir un bon contraste. L'acier M2 a donc été choisi pour la tomographie aux rayons X car il possède deux éléments d'alliage (W et Mo) avec des masses atomiques très supérieures à celle des autres éléments constitutifs, notamment le fer.

4.3.2.3. Mise en œuvre de la tomographie

Les caractérisations par tomographie aux rayons X ont été conduites à température ambiante sur la ligne ID15A à l'ESRF (European Synchrotron Radiation Facility) de Grenoble. L'énergie des rayons X disponible est comprise entre 50 et 100 keV. Le dispositif expérimental comprend trois parties : une source de rayons X, un support d'échantillon rotatif et un détecteur CCD (voir Fig. 2.23).

Les échantillons sont fixés sur le support rotatif. Dans un premier temps, l'échantillon est aligné avec le faisceau incident. Le faisceau incident est dirigé vers l'échantillon avec une énergie constant de 60 keV. Le faisceau transmis est récupéré par un détecteur rapide

DALSTAR Pantera 1M60 CCD dont la durée d'exposition est d'environ 25 ms. La taille des pixels est d'environ 1.2 µm et le nombre de projections est de 3600.

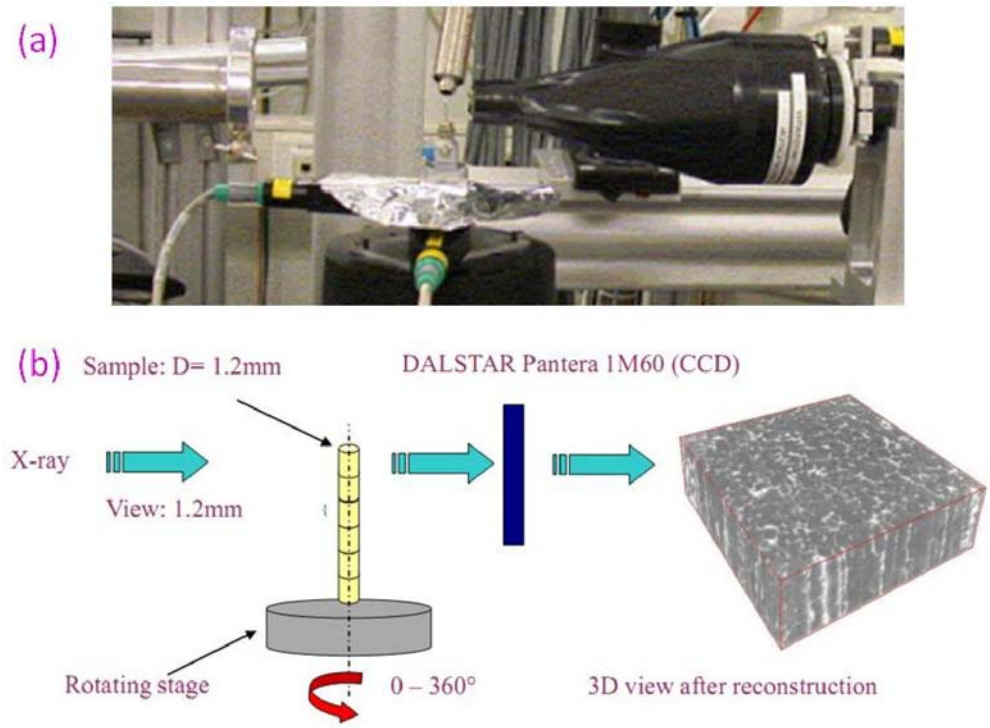

Fig. 2.23 (a) photographie du dispositif (b) vue schématique d'une microtomographie 3D.

Trois différents modes d'utilisation sont possibles pour la réalisation de tomographies : le mode contraste d'absorption, le mode contraste de phase et le mode holotomographie. En mode absorption, le contraste est donné par la différence de coefficient d'atténuation linéaire. Plus le coefficient d'absorption linéaire des éléments est différent, meilleur sera le contraste. Dans ce mode, l'échantillon doit être placé près du détecteur pour éviter l'effet des phases. Le deuxième mode tire profit de la différence de réfraction des rayons X en fonction des phases. Ce mode est utilisé lorsque les différences d'absorption entre les phases sont faibles. Le dernier mode, l'holotomographie, utilise des images saisies avec plusieurs distances entre l'échantillon et le détecteur. Dans notre cas, le mode absorption a été utilisé.

Une tomographie comporte 1024 plans ou tranches sur une hauteur de 1.2mm. Plus de 350 tomographies ont été saisies sur l'acier M2 dans son état de livraison et à l'état trempé après fusion partielle. De plus, 40 tomographies ont été réalisées sur d'autres aciers, 100Cr6, C38 et même 316L. Les plans sont ensuite assemblés pour reconstruire la microstructure 3D. Pour cela le logiciel de traitement d'image ImageJ a été utilisé.

4.3.2.4. Traitement d'image

La reconstruction volumique depuis les projections a été réalisée sur le serveur à distance de l'ESRF utilisant Matlab. L'image originale, après reconstruction, est codée en niveau de gris sur 4 bytes. Ceci conduit à une taille de fichier importante (1024^3 * 4 =4 GB de taille mémoire). Du fait de la grande taille des fichiers, il est nécessaire de reconstruire le volume en plusieurs fois. La durée totale du traitement depuis les fichiers bruts jusqu'à la reconstruction complète est de 90 minutes environ. Les volumes reconstruits peuvent être visionnés en 2D ou 3D par des logiciels comme VGStudio max, Amira ou ImageJ. C'est ImageJ qui a été utilisé dans notre étude.

La Fig. 2.24 montre la tomographie d'une tranche (acier M2 trempé depuis l'état semi-solide). L'image est d'une qualité suffisante pour une étude qualitative de la structure. Cependant, ce type d'image n'est pas propre à des analyses quantitatives directes. Il est nécessaire pour cela de procéder à un traitement préalable de l'image.

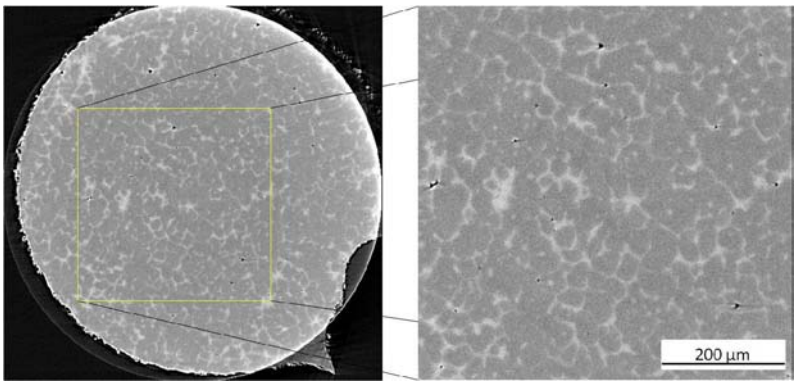

Fig. 2.24. Tomographie aux rayons X d'une tranche.

Dans notre cas, le traitement consiste à binariser l'image pour permettre la distinction entre la matrice et les carbures. Plusieurs techniques sont disponibles comme de seuillage par niveau de gris, le filtrage non-linéaire ou les opérations mathématiques morphologiques (érosion et dilation). Dans cette étude, les outils décrits ci-dessus ont été appliqués en 3D.

4.3.2.5. Microtomographie par rayons X in situ

La ligne ID15 permet la réalisation rapide de tomographies, moins de 5s pour un tour complet de l'échantillon. Ce temps est supposé inférieur à celui nécessaire à un changement important de la microstructure. L'étude de microtomographie aux rayons X in situ a été réalisée sur l'acier M2 à haute température. Au cours de l'essai, l'échantillon n'était pas

protégé d'où la présence d'oxydation. Toutefois, cette technique offre la possibilité d'observer la structure 3D et son évolution directement à haute température.

4.4. Observation in situ par CLSM

Comme évoqué plus haut, la microtomographie aux rayons X est un outil puissant pour la caractérisation en 3D de la microstructure. Toutefois, cette technique n'est pas facile d'utilisation et n'est pas aussi répandue que le MEB et les systèmess EDS. De plus, la reconstruction d'images est très coûteuse en temps pour un contexte industriel. Plus important, la technique ne peut s'appliquer qu'aux matériaux ayant des éléments chimiques constitutifs avec de grandes différences de masse atomique. Le contraste des images obtenues pour les aciers 100Cr6 et C38LTT est par conséquent trop faible pour donner des résultats exploitables. Nous avons ainsi essayé d'autres méthodes pour l'observation de l'apparition et de l'évolution de la structure liquide solide à haute température.

L'observation microscopique in situ peut être utilisée pour la caractérisation de la microstructure à haute température. Les deux techniques que sont l'ESEM (Environmental Scanning Electron Microscope) et le CLSM (Confocal Laser Scanning Microscope) ont été étudiées. Le vide est formé dans les enceintes chauffantes des deux techniques. Toutefois, vers ~400°C, de l'oxydation apparaît sur les essais réalisés sur le M2 par ESEM. De plus la vitesse de chauffe de l'ESEM ne peut dépasser les ~50°C/min. De ce fait, nous nous sommes concentrés sur les observations in situ par CLSM. Pour le CLSM, le problème de l'oxydation a été résolu en plaçant un feuillard de titane autour de l'échantillon. Cette technique de CLSM à haute température a permis l'observation de l'évolution in situ de la microstructure des trois nuances d'acier étudiées (C38LTT, 100Cr6 et M2) directement au cours de la chauffe et du refroidissement [18-21]. Outre une résolution supérieure à celle obtenue en microscopie optique classique, il est possible de scanner une surface avec différentes profondeur focale et de réaliser des observations in situ dynamiques. En particulier, il est possible d'observer les transformations de phases à haute température et l'apparition de liquide en fonction de la température.

Le CLSM utilisé dans notre étude est un Lasertec^{TM} 1LM21. Le dispositif est constitué d'une source laser, d'un capteur CCD, d'un ensemble de lentilles à longues focales et d'un four.

4.4.1. Principe du CLSM

Un schéma du dispositif utilisé est donné sur la Fig. 2.25.

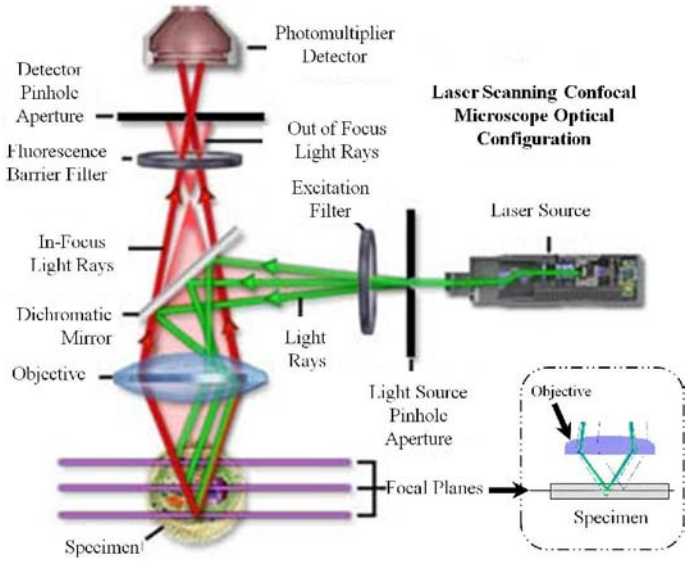

Fig. 2.25. Schéma de fonctionnement du CLSM.

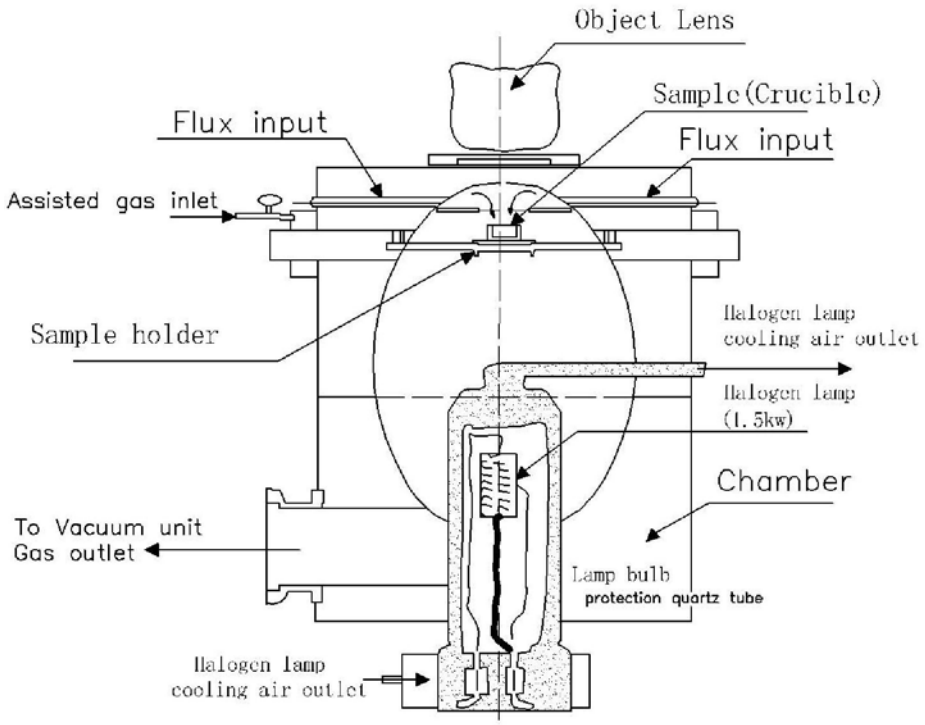

Fig. 2.26. CLSM équipé d'un four à images.

Le CLSM utilise des optiques qui permettent de visualiser la surface du matériau uniquement dans le plan focal. L'échantillon est illuminé et la lumière réfléchie est collectée par un détecteur approprié.

Observations en temps réel avec vitesse de balayage rapide

Le trajet optique du CLSM est présenté à la Fig. 2.25. Dans notre étude, le faisceau laser est réfléchi par l'échantillon qui est balayé avec une fréquence de 15.7 kHz dans la direction horizontale et 60 Hz dans la direction verticale. Le signal obtenu permet une représentation quasi topographique de la surface de l'échantillon (enregistrement de plusieurs images à différentes "profondeurs"), ce qui permet de distinguer le relief à la surface, en particulier pendant les transformations de phase.

CLSM avec four à images

Le CLSM combiné à un système de chauffage (four à images ellipsoïdal dont les parois intérieures sont revêtues d'une couche d'or) est présenté à la Fig. 2.26 : puissance de 1.5kW, lampe halogène de 100V. Il permet de réaliser des observations métallurgiques en temps réel à très haute température, et notamment de voir l'évolution de la microstructure à l'état semi-solide.

De petits échantillons (diamètre 5mm, hauteur 3mm) ont été découpés et polis jusqu'à 1µm (polissage de finition avec particules diamantées). Ils ont ensuite été placés dans un creuset en alumine sur un support en platine dans la chambre du CLSM (Fig. 2.27), sous une fenêtre en quartz et sous atmosphère d'argon. La mesure de la température s'effectue sur le creuset, ce qui induit une différence entre la valeur mesurée et la température réelle, notamment à forte vitesse de chauffe : la calibration a permis d'estimer la précision à ±15°C.

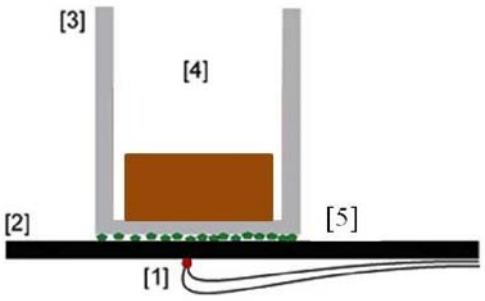

Fig. 2.27. Schéma du creuset dans lequel l'échantillon est placé. [1] Thermocouple Pt/Pt-10%Rh, [2] support en platine, [3] creuset, [4] échantillon, [5] poudre Al_2O_3 pour empêcher la soudure de pièces en platine.

4.4.2. Cycles de chauffage

Les cycles de chauffe pour plusieurs nuances d'acier sont présentés à la Fig. 2.28. Les échantillons sont chauffés à la vitesse de 1°C/s jusqu'à environ 300°C. Après 50s de maintien isotherme, les échantillons sont chauffés à une vitesse de 200°C/s jusqu'à la température désirée (état semi-solide).

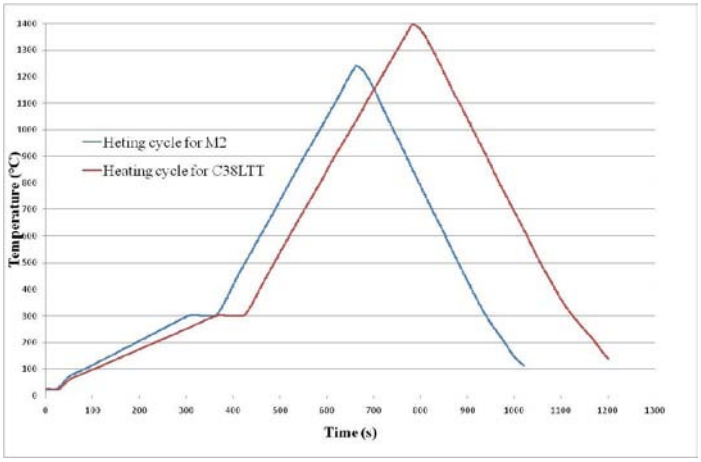

Fig. 2.28. Cycles de chauffe pour différentes nuances d'acier.

Pour les observations in situ, les échantillons ont été préalablement attaqués au Nital (2%) et validés en microscopie optique et en MEB.

5. Conclusions

L'objectif de ce chapitre était de présenter les différentes techniques utilisées pour caractériser la microstructure des aciers utilisés lors du procédé de thixoforgeage. Les outils, le système de chauffage par induction et le système d'acquisition permettent de réaliser des expériences qui garantissent la répétabilité des essais.

Plusieurs techniques ont été utilisées pour caractériser la microstructure des 3 nuances acier à chaque étape du procédé de thixoforgeage (techniques conventionnelles, mais également approches nouvelles) : elles sont résumées dans le tableau 2.8. Les nouvelles approches proposées (principalement microtomographie aux rayons X et CLSM ont nécessité la mise en place et le développement de protocoles spécifiques : ce sont des techniques qui ne sont pas faciles d'accès, mais qui ont donné des résultats très intéressants.

Les essais de thixoforgeage ont été réalisés avec des outils spécialement conçus et un système de chauffage par induction au laboratoire LCFC de l'ENSAM-Arts et Métiers ParisTech. Nous nous sommes focalisés sur les aspects suivants :

- conception d'un nouveau support pour le lopin qui permet un meilleur centrage dans l'inducteur et par conséquent un chauffage plus homogène.
- un système de transfert bien maîtrisé (temps, trajet) de telle sorte que le procédé puisse être industrialisé (robot).
- amélioration du la mesure du déplacement pour éviter les éventuelles vibrations mécaniques.

Tableau 2.8. Techniques utilisées pour la détermination de la fraction de liquide dans les aciers.

	Techniques	Objectifs	Avantages	Limitations
Méthodes conventionnelles	Thermodynamique (Thermo-Calc)	F_L vs Temp. $\rho_{L\,(T)}$, $\rho_{S\,(T)}$	Rapide, non destructif	Conditions d'équilibre
	DSC	F_L vs Temp.	Facile d'accès	Faible vitesse de chauffe
	Métallurgie quantitative	F_L vsTemp. Caractérisation de la microstructure	Conditions industrielles	Résultats en 2D, Préparation des matériaux
Nouvelles approches	Microtomographie aux rayons X	Fraction de liquide 3D Microstructure 3D	Microstructure 3D Observations in situ	Time consuming Materials selective Difficile d'accès
	CLSM	F_L vs Temp. Evolution de la microstructure	Observations in situ Vitesse de chauffe rapide	2D Résolution des images

Références

1. Püttgen W, Bleck W: **Thixoforming/semi-solid forming : DTA-measurements to determine the thixoformability of steels.** *Steel Research International* 2004, **75:**531-536.

2. Lecomte-Beckers J, Rassili A, Carton M, Robelet M, Koeune R: **Study of the liquid fraction and thermophysical properties of semi-solid steels and application to the simulation of inductive heating for thixoforming.** In *Advanced Methods in Material Forming*: Springer Berlin Heidelberg; 2005.

3. Kopp R, Kallweit J, Möller T, Seidl I: **Forming and joining of commercial steel grades in the semi-solid state.** *Journal of Materials Processing Technology* 2002, **130–131:**562-568.

4. Cézard P: **Impact des effets thermiques sur le comportement du matériau lors de la mise en forme des aciers à l'état semi-solide : Analyses expérimentale et numérique.** Thesis. L'Ecole Nationale Supériure d'Arts et Métiers, Docteur de l'Ecole National Supérieure d'Arts et Métiers; 2006.

5. Becker E: **Investigations experimentales et numeriques pour l'identification des parametres clefs du procede de thixoforgeage de l'acier sur le produit mis en forme.** Thesis. L'Ecole Nationale Supériure d'Arts et Métiers, Docteur de L'Ecole National Supérieure d'Arts et Métiers; 2008.

6. Orfeuil M: *Electric Process heating: Technologies/Equipment/Applications*. Battelle Press; 1981.

7. Jung HK, Kang CG: **Reheating process of cast and wrought aluminum alloys for thixoforging and their globularization mechanism.** *Journal of Materials Processing Technology* 2000, **104:**244-253.

8. Becker E, Favier V, Bigot R, Cezard P, Langlois L: **Impact of experimental conditions on material response during forming of steel in semi-solid state.** *Journal of Materials Processing Technology* 2010, **210:**1482-1492.

9. Becker E, Bigot R, Langlois L: **Thermal exchange effects on steel thixoforming processes.** *The International Journal of Advanced Manufacturing Technology* 2009, **48:**913-924.

10. Hirt G, Bleck W, Buhrig-Polaczek A, Shimahara H, Puttgen W, Afrath C: **Semi solid casting and forging of steel.** *Solid State Phenomena* 2006, **116-117:**34-43.

11. Atkinson H, Rassili A: **A review of the semi-solid processing of steel.** *International Journal of Material Forming* 2010, **3:**791-795.

12. **Hardening high speed steels: metallurgical benefits of salt** [http://ppunch.com/pdf/heat.pdf]

13. Bergsma SC, Tolle MC, Kassner ME, Li X, Evangelista E: **Semi-solid thermal transformations of Al−Si alloys and the resulting mechanical properties.** *Materials Science and Engineering: A* 1997, **237:**24-34.

14. Liu T, Ward P, Atkinson H, Kirkwood D: **Response of semi-solid Sn-15 pct Pb to rapid shear-rate changes.** *Metallurgical and Materials Transactions A* 2003, **34:**409-417.

15. Seo P, Kang C: **The effect of raw material fabrication process on microstructural characteristics in reheating process for semi-solid forming.** *Journal of Materials Processing Technology* 2005, **162-163:**402-409.

16. Hirt G, Kopp R (Eds.): **Thixoforming - semi-solid metal processing**. Aachen: Wiley-VCH Verlag GmbH & Co. KGaA; 2009.

17. Herman GT: *Image Reconstruction from Projections*. New York: Academic Press; 1980.

18. Heulens J, Blanpain B, Moelans N: **Analysis of the isothermal crystallization of CaSiO3 in a CaO–Al2O3–SiO2 melt through in situ observations.** *Journal of the European Ceramic Society* 2011, **31:**1873-1879.

19. Attallah MM, Terasaki H, Moat RJ, Bray SE, Komizo Y, Preuss M: **In-situ observation of primary γ′melting in Ni-base superalloy using confocal laser scanning microscopy.** *Materials Characterization* 2011, **62:**760 - 767.

20. Wang SL, Gao LW, Huang FX, Wang XH: **Confocal laser scanning microscopy and its application in metallurgy.** *Metallurgical Analysis* 2011, **31:**40 - 45.

21. Yuan F, Liang GF, Zhu GM, Wang CQ, Wu JC, Yu Y: **Confocal laser scanning microscopy and its application in in-situ observation of phase transformation of steel.** *Journal of Baosteel Technique* 2006, **6:**64 - 69.

Chapitre 3. Analyse des résultats expérimentaux concernant la caractérisation de l'évolution de la fraction liquide et de la microstructure

Les diagrammes de phase, les méthodes thermiques ainsi que les méthodes d'analyse d'image (2D et 3D) ont été décrites et appliquée pour l'évaluation de la fraction volumique de liquide en fonction de la température à l'état semi-solide. La précision et la capacité de chaque approche pour l'évaluation de la fraction liquide pour les procédés de mise en forme à l'état semi-solide industriel ont été discutées.

Les résultats des expérimentations mises en œuvre pour l'étude de l'évolution de la microstructure au cours du chauffage jusqu'à l'état semi-solide sont également présentés dans ce chapitre. La microstructure à l'état semi-solide a été analysée et caractérisée par différentes techniques appliquées sous différentes conditions.

1. Introduction

La fraction volumique de liquide en fonction de la température à l'état semi-solide de plusieurs aciers a été évaluée par plusieurs approches (utilisation de diagramme de phase, analyse thermique et les techniques de métallographie quantitative en 2D et 3D). L'acier M2 a fait l'objet d'une étude particulière. Ces résultats ont été synthétisés et compares afin de déterminer la précision, les avantages et les limitations de chaque méthode.

Le tableau 3.1 donne l'ensemble des expériences et des caractérisations qui ont été conduites pour chaque nuance d'acier étudiée.

Table 3.1 Combinassions des paramètres utilizes dans des essays différents

Nuance	Expérimentaux	intervalle de température	Vitesse de chauffe	Dimension
M2	DSC	ambiante ~ 1500°C	10°C/min 20°C/min	Ø 3* 1.5
	Tremper	1260-1350°C	~ 500°C/min	Ø35*34
	Tomographie aux rayons X	Température ambiante		Ø1.2*30
	In situ observation	ambiante ~1300°C	200°C/min	Ø5*3
C38LTT	Tremper	1410~ 1450°C	~ 500°C/min	Ø45*60
	In situ observation	ambiante ~ 1450°C	200°C/min	Ø5*3
100Cr6	Tremper	1340-1410°C	500°C/min	Ø30*45
	In situ observation	ambiante ~1420°C	200°C/min	Ø5*3

2. Evaluation de la fraction liquide par Thermo-Calc et DSC

Ces deux techniques ne permettent d'obtenir que la fraction liquide en fonction de la température. Les caractéristiques de la microstructure comme le facteur de forme des particules solides ne sont pas obtenues.

Thermo-Calc (Logiciel commercial) a été utilisé pour générer le diagramme de l'acier M2 (Fig.3.1). Le diagramme obtenu correspond à des vitesses de chauffe très faible, proche pour chaque température de l'état d'équilibre (1°C/min).

La teneur en carbone du M2 est de l'ordre de 0.85% (pourcentage massique). La température de solidus et liquidus sont de ~1240°C et ~1450°C respectivement. Selon le diagramme, la transformation eutectique n'est pas isotherme mais a lieu sur un intervalle de température où coexistent l'austénite, le liquide et des carbures. La fusion de l'acier commence donc à 1250°C avec une phase solide constituée d'austénite et de carbures. En utilisant Thermo-Calc, la fraction massique de carbures présents juste avant le début de fusion est d'environ 10% (voir Fig. 3.2).

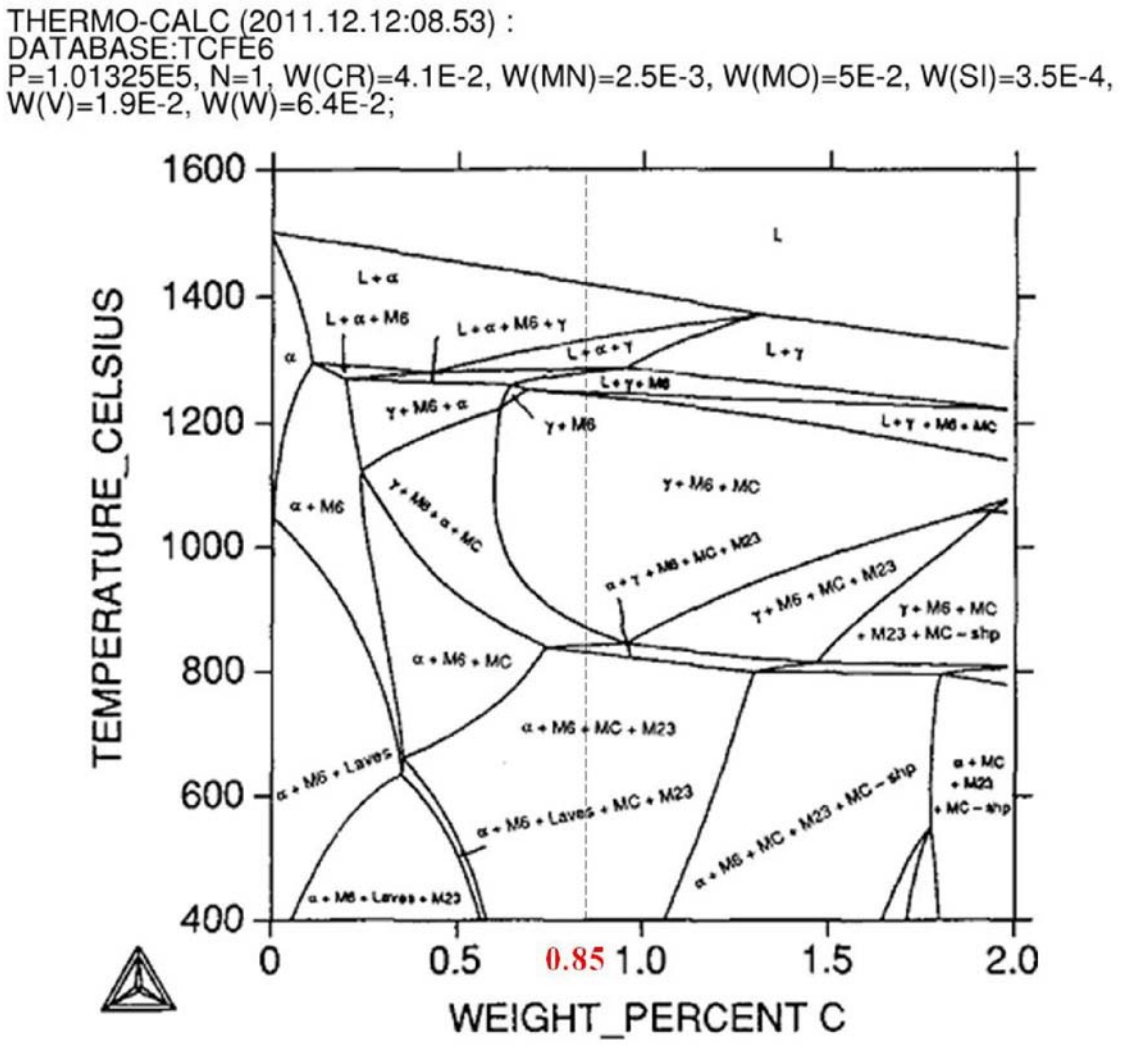

Fig. 3.1. Calculated isopleth of Fe – 4.1 wt.% Cr - 0.25 wt.% Mn – 5 wt.% Mo – 0.035 wt.% Si – 1.9 wt.% V – 6.4 wt.% W.

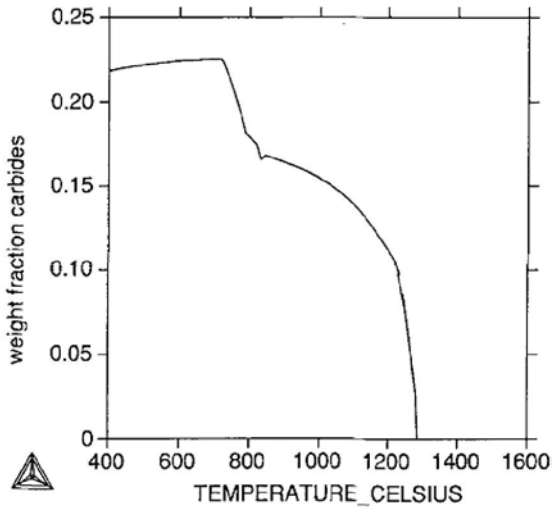

Fig. 3.2. Fraction massique de carbure en fonction de la température calculée par Thermo-Calc.

L'évolution de la fraction volumique de liquide en fonction de la température dans l'acier M2 a été calculée (voir figure 3.4).

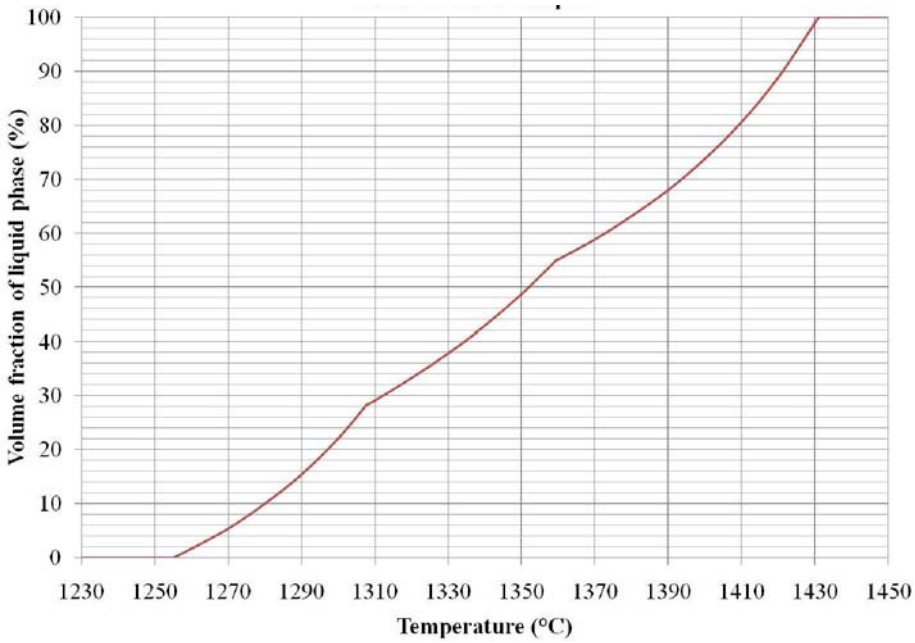

Fig. 3.4. Evolution de la fraction volumique de liquide en fonction de la température pour l'acier M2.

En conditions industrielles, le chauffage de la matière est rapide, de telle sorte que l'homogénéité ne peut être obtenue. De ce fait, l'utilisation des diagrammes de phase ne permet pas de rendre compte de la vitesse de chauffe (cinétique de diffusion des éléments d'alliage), de la structure initiale de l'acier. De même, il ne permet pas de prendre en compte les variations de composition chimique d'une même nuance d'acier.

3. Analyse de la fraction volumique de liquide par DSC

La fraction volumique de liquide dans l'acier M2 a été mesurée par DSC en utilisant un NETZSCH 404C Pegasus DSC.

Fig. 3.5 montre le résultat obtenu pour l'acier M2 et pour une vitesse de chauffe de 10°C/min. Les pics observés sont le résultat de changement de phase. Pour l'analyse de cette courbe, il est supposé que l'aire du pic est proportionnelle à la chaleur dégagée ou absorbée par la transformation. Ici, la Fig.3.5 fait apparaître cinq pics de transformation endothermique. En utilisant le diagramme de phase précédent, on peut associer à chaque pic la transformation correspondante.

Le résultat d'une DSC étant très sensible aux conditions expérimentales, plusieurs essais identiques ont été conduits. Pour tous les essais, les cinq pics ont été observés pour des niveaux de température similaires. La transformation austénitique et la température de liquidus sont de l'ordre de 815°C-825°C et 1240°C-1250°C respectivement.

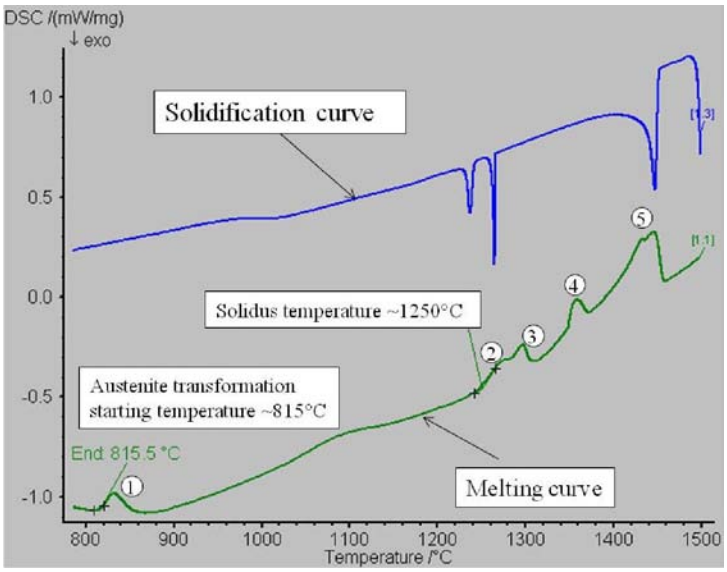

Fig. 3.5. Réponse DSC pour l'acier M2 avec une vitesse de chauffe de 10°C/min.

L'évaluation de la fraction liquide est calculée par "application of partial area intégration ».L'aire comprise entre la courbe de l'enthalpie et une "sigmoïde baseline" est calculée pour déterminer la chaleur latente de changement de phase solide-liquide de l'alliage. Fig. 3.6 illustre l'évolution du flux de chaleur et la fraction liquide en fonction de la température. La figure 3.7 donnent la fraction liquide obtenue pour deux vitesses de chauffe.

En comparant les deux courbes, on remarque qu'une augmentation de la vitesse de chauffe correspond à un décalage de la courbe sur la gauche, c'est-à-dire, à des fractions de liquide plus grandes.

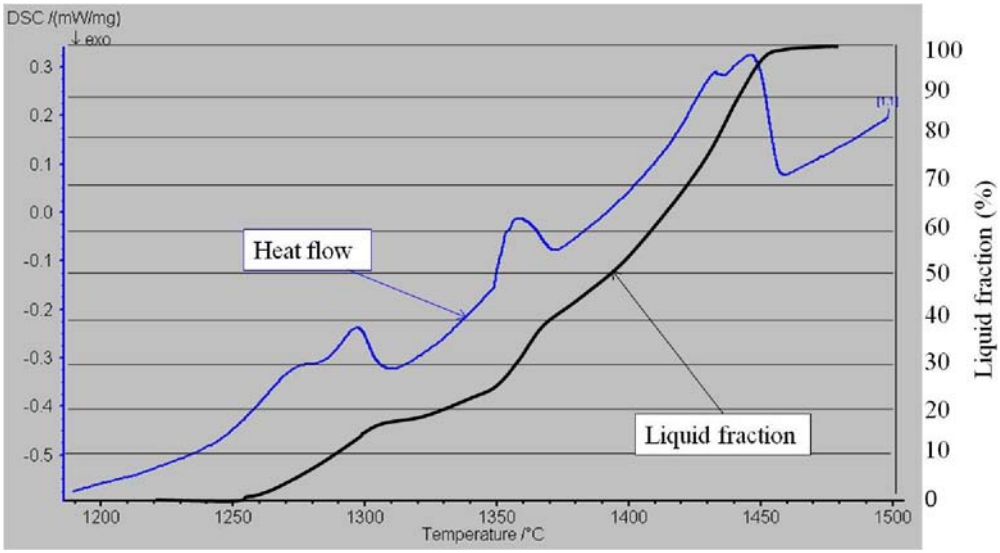

Fig. 3.6. Signal DSC et la fraction liquide en fonction de la température (vitesse de chauffe de 10°C/min).

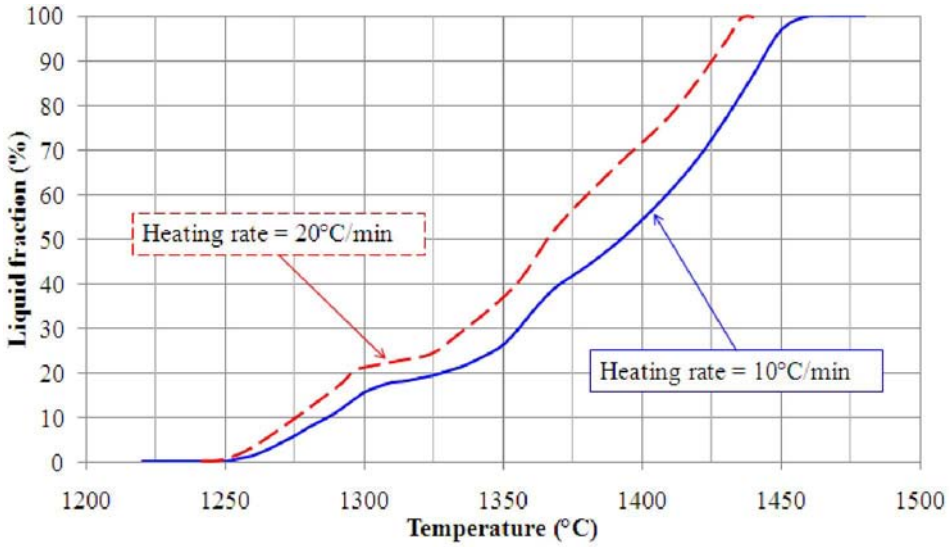

Fig. 3.7. Fraction liquide en fonction de la température à deux vitesse de chauffe, 10°C/min and 20°C/min.

Les résultats obtenus par DSC doivent être pris avec précaution en tenant compte notamment de la variation de composition chimique des échantillons testés dépendante de la présence de bande de ségrégation. La méthode de calcul de la fraction liquide est approximative. Enfin, le dispositif expérimental de DSC peut lui aussi introduire des erreurs dans l'estimation des flux de chaleur et la mesure de la température.

La figure 3.9 permet de comparer les résultats obtenus par les diagrammes de phase et par DSC à deux vitesses de chauffe. On remarque que les fractions volumiques dans l'intervalle 1250°C – 1300°C sont du même ordre de grandeur quelle que soit la méthode. Cela correspond à la fusion des carbures dans la phase liquide. Au-delà de cette température l'austénite ou la ferrite commence à fondre. La différence observée peut provenir de la différence de composition entre celle introduite dans THERMO-CALC et celle des échantillons prélevés ou les erreurs inhérentes à la méthode DSC. La différence de fraction liquide est la plus importante entre 1300°C et 1360°C, intervalle présentant le plus d'intérêt pour le thixoforgeage dans la mesure où cet intervalle correspond à celui où la fraction liquide est la moins sensible à la température.

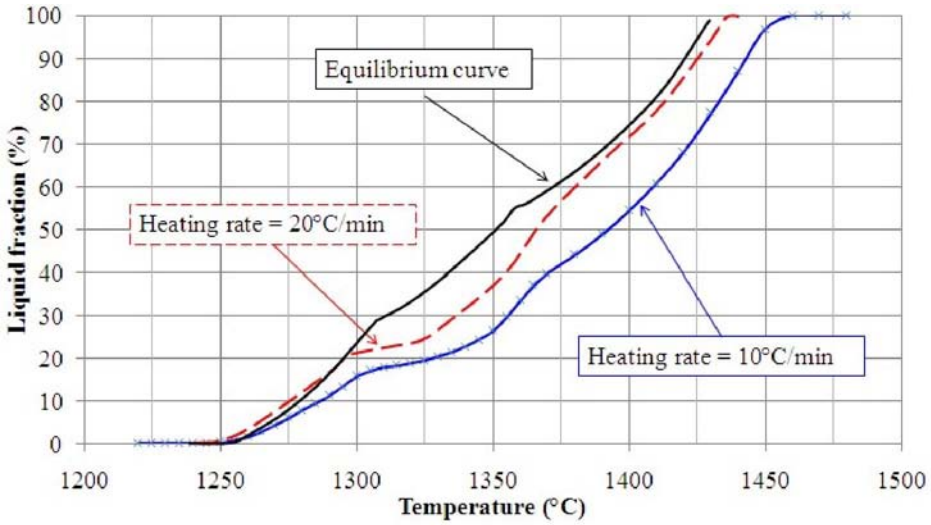

Fig. 3.9. Fraction liquide en fonction de la température obtenue par DSC et Thermo-Calc.

Même si la vitesse de chauffe utilise en DSC est bien plus faible que celle mise en œuvre en conditions industrielles, l'analyse DSC fournit des informations utilises sur la température de solidus et liquidus. L'intervalle de température pour la mise en forme, intervalle pour lequel la fraction liquide est la moins sensible à la température, est de l'ordre de 1290°C – 1340°C.

4. Analyse métallographique 2D d'un lopin trempé depuis l'état semi-solide

Un processus de thixoforgeage industriel met en œuvre des vitesses de chauffe bien supérieures à celles reproduites par DSC. Dans cette partie, des observations

métallographiques sont effectuées sur des lopins chauffés par induction jusqu'à l'état semi-solide puis trempé.

Le cycle de chauffage par induction, malgré la rapidité du chauffage, doit assurer une certaine homogénéité de la température dans le lopin. Il doit réaliser un compromis entre temps de chauffe et homogénéité de la température et de structure liquide solide associée. Pour cela, des cycles de chauffage avec plusieurs paliers de puissance ont été développés. La figure 3.10 illustre les deux types de cycle testés dans cette étude.

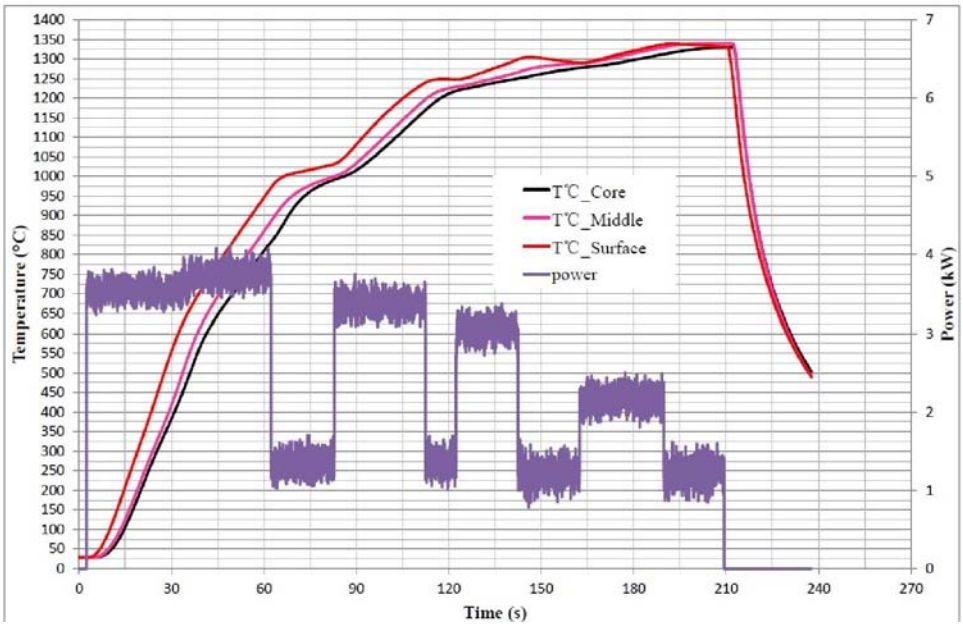

(a) **Cycle avec une "faible" vitesse de chauffe au début du chauffage.**

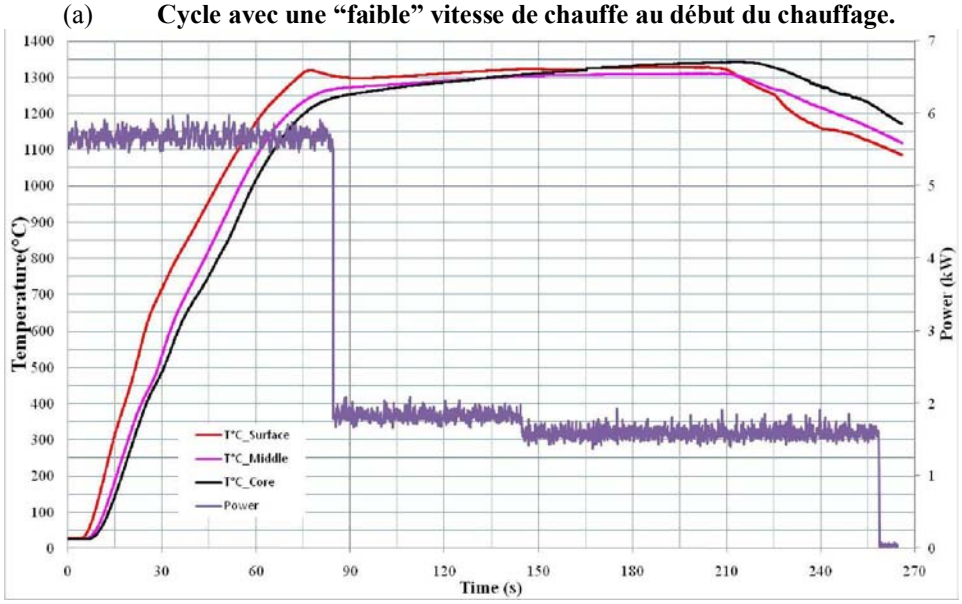

(b) Cycle avec une "forte" vitesse de chauffe au début du chauffage.

Fig. 3.10. Température dans le lopin (proche de la surface, à mi-rayon, à cœur) et la puissance de chauffe en fonction du temps.

4.1. Analyse de la microstructure

Les structures obtenues avec l'acier M2 à l'état de livraison et à l'état trempé depuis le semi-solide sont illustrées sur la figure 3.12. Les micrographies correspondantes font apparaître différents types de carbures (composition et morphologie) qui ont été identifiés par EDS (Voir Fig. 3.13).

Comme illustré sur la figure 3.12 (d), (e) et (f), les carbures sont distribués le long des joints de grain et dans la matrice. La figure 3.12 (e) met en évidence la formation de bandes par microségrégation dans le sens longitudinal du lopin, parallèlement à la direction de laminage. Les résultats obtenus par EDS confirment la présence de deux types de carbure : M_6C et MC. Les premiers sont riches en tungstène et molybdène alors que les seconds contiennent du vanadium du tungstène et du molybdène. Le tableau 3.2 donne la composition chimique des deux types de carbure.

La taille de grain moyen est de l'ordre de ~ 10µm alors que celle de la plus grande partie des carbures est inférieure au micron.

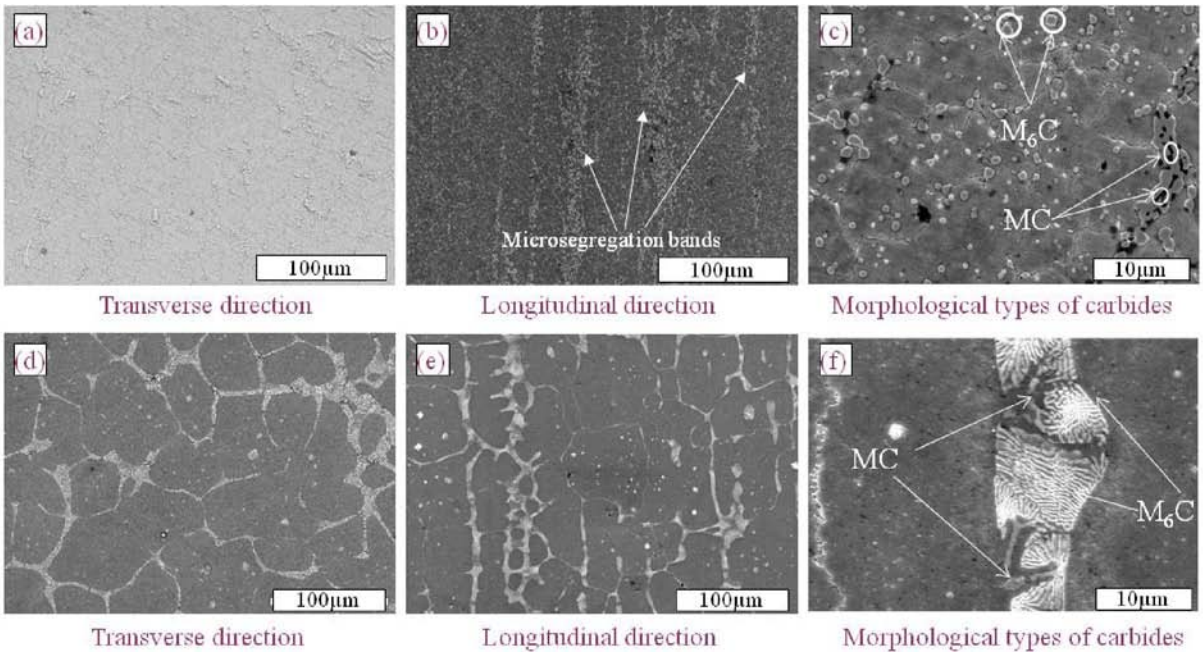

Fig. 3.12. Micrographies MEB de l'acier M2 à l'état de livraison: (a) section transversale, (b) section longitudinale, (c) morphologie type des carbures; et à l'état trempé depuis le semi-solide (d) section transversale, (e) section longitudinale et (f) morphologie type des carbures.

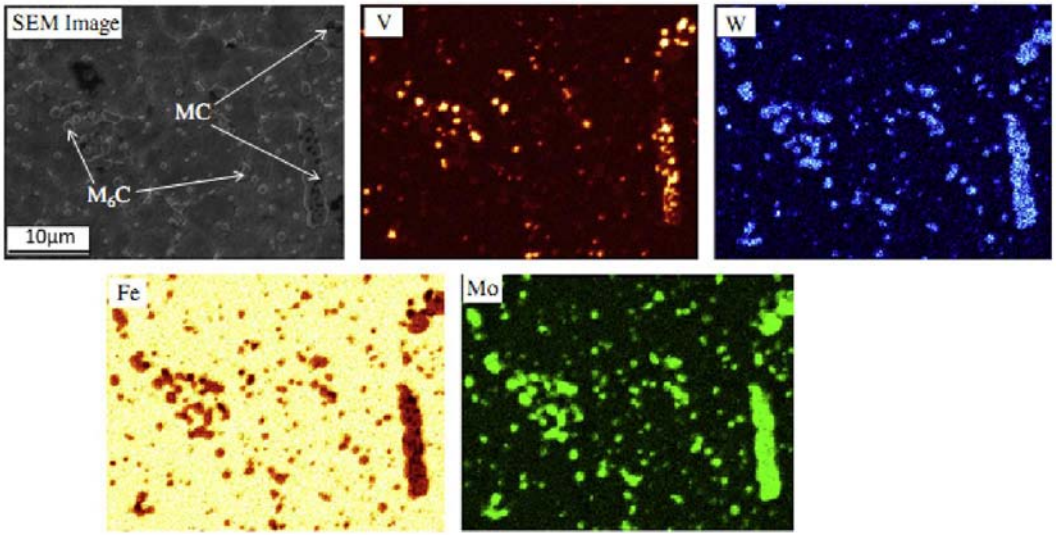

(a) Cartographie de composition MEB-EDS de l'acier M2 à l'état de livraison.

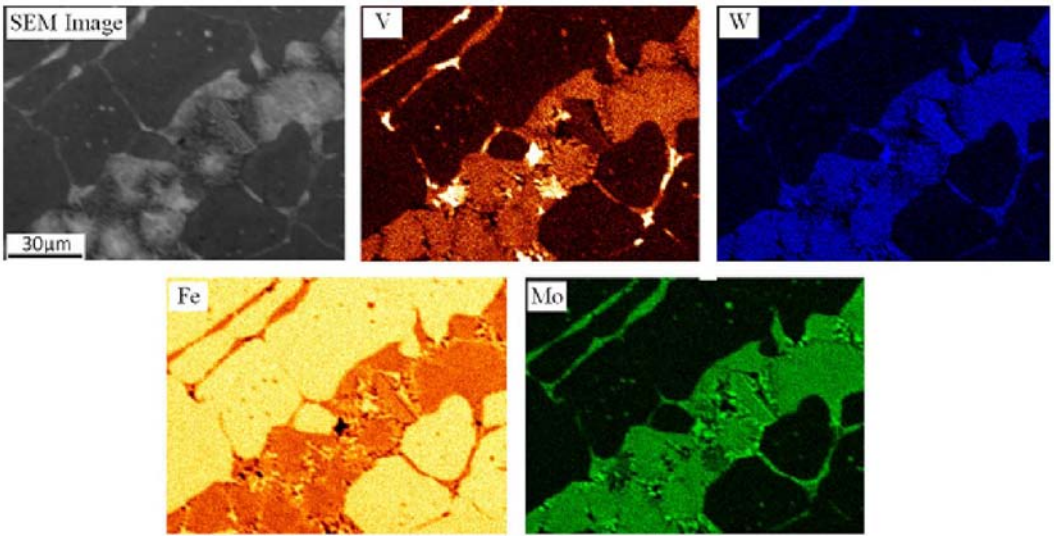

(b) Cartographie de composition MEB-EDS de l'acier M2 à l'état trempé depuis le semi-solide.

Fig. 3.13. Cartographie MEB-EDS de l'acier M2.

Tableau. 3.2. Compositions chimiques des carbures.

Carbide (weight %)					
Elements	V	Cr	Fe	Mo	W
Whiter particles	3.65	2.88	30.4	24.87	38.29
	2.55	3.19	34.2	22.37	37.69
	3.05	3.04	32.22	25.35	36.34
Darker particles	34.72	4.76	9.3	23.98	27.25
	32.7	4.61	10.43	23.67	28.6
	35.32	5.06	10.06	20.72	28.88

Les lopins sont chauffé depuis l'état de livraison jusqu'à l'état semi-solide. La trempe qui s'en suit a pour but de figer la structure obtenue à l'état semi-solide. Comparés aux carbures initiaux, la morphologie des carbures formés après trempe différent à la fois par leur taille et leur forme. Au cours du chauffage par induction, les éléments d'alliage comme le vanadium, le tungstène et le molybdène diffusent vers les zones liquides où la solubilité de ces éléments est plus grande. Les zones liquides se développent de façon privilégiée aux joints de grain et apparaissent très clairement après trempe du fait de leur forte teneur en éléments d'alliage. Ils forment un nouveau réseau de carbures interconnectés. Il peut être suppose que la microstructure du M2 était formée de liquide et solide, la trempé étant suffisamment rapide pour fixer cette structure.

La figure 3.14 montre que les microstructures observées différent suivant la direction d'observation et le type de cycle de chauffage.

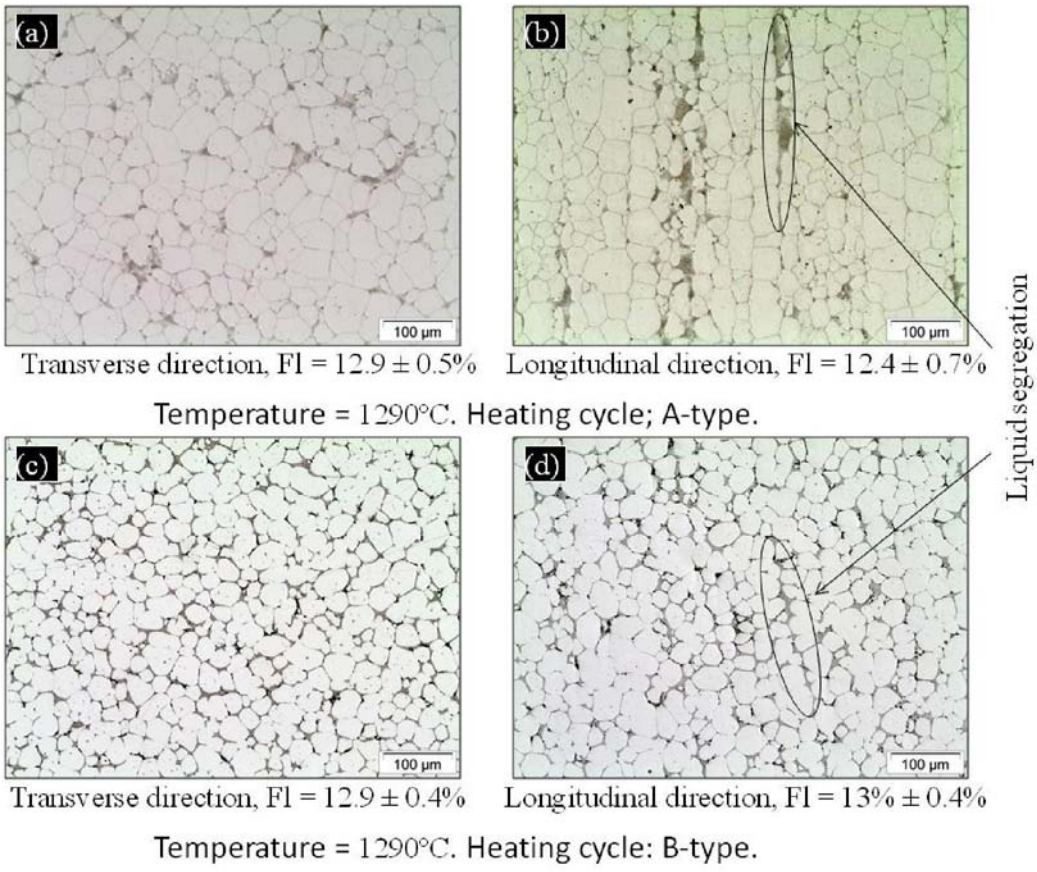

Fig. 3.14. Microhraphies de lopins trempés depuis une température de 1290°C suivant (a) une section transversale, chauffé suivant un cycle de type A, (b) section longitudinale, chauffé suivant un cycle de type A , (c)section transversale direction, chauffé suivant un cycle de type B,(d) section longitudinale, chauffé suivant un cycle de type B.

Le tableau 3.3 donne les caractéristiques de la microstructure obtenues dans les lopins chauffés à 1290°C par les deux types de cycle de chauffe. La fraction liquide obtenue avec les deux cycles de chauffe est identique. Par contre, les particules solides obtenues avec le cycle de chauffe de type B sont plus sphériques et la taille de grain est plus faible.

Table. 3.3. Microstructure paramètres.

	Cycle de chauffe: A-type		Cycle de chauffe: B-type	
Micrographies	Fig. 3.14 (a)	Fig. 3.14 (b)	Fig. 3.14 (c)	Fig. 3.14 (d)
Taille de grain	40.1 ± 3μm	43.3 ± 3μm	28.3 ± 2μm	30.2 ± 2μm
Facteur de forme	0.78 ± 0.02	0.8 ± 0.01	0.89 ± 0.005	0.89 ± 0.007
Fraction liquide	12.9 ± 0.5 %	12.4 ± 0.7%	12.9 ± 0.4 %	13 ± 0.4%

Le cycle de chauffage de type B présente un palier en température à faible vitesse de chauffe en fin de cycle. Ceci agit sans doute comme un maintien qui favorise la diffusion des éléments et donc la formation d'une structure plus globulaire.

4.2. Caractérisation de la microstructure par analyse d'image

La fraction liquide a été mesurée en fonction de la position dans un lopin chauffé entre 1306°C et 1320°C puis trempé. La figure 3.16 (a) donne les résultats obtenus le long d'un diamètre. La fraction liquide diminue avec le rayon. Ceci est sans doute dû à l'hétérogénéité du champ de température dans le lopin du fait de la concentration de la puissance de chauffe par induction en peau de pièce. Dans le sens longitudinal (figure 3.16b) on ne note pas d'évolution. La fraction liquide varie de +/- 2%. Le liquide piégé dans les particules solides peut être observé (Figure 3.17), il correspond à environ 2%.

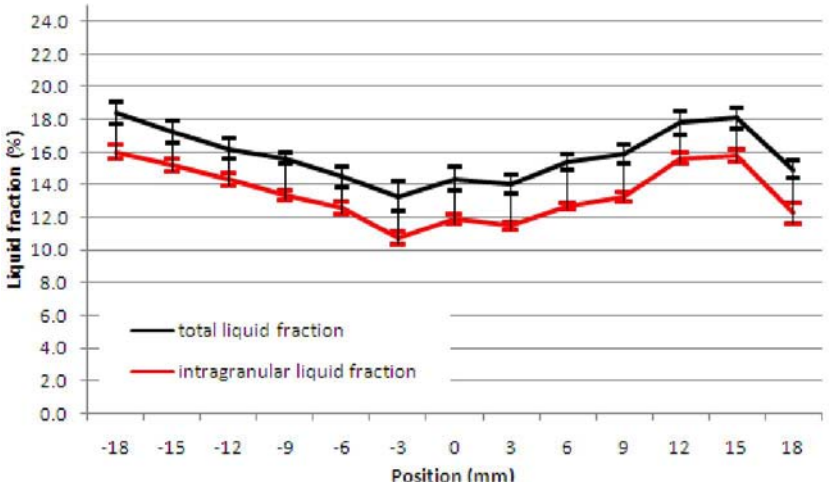

(a) Direction radiale.

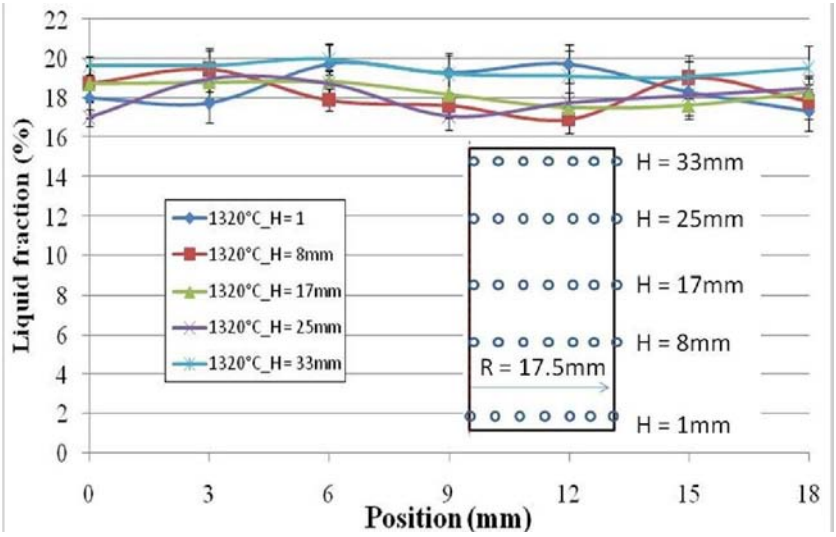

(b) Direction longitudinale.

Fig. 3.16. Variation de la fraction liquide dans un lopin trempé depuis l'état semi-solide.

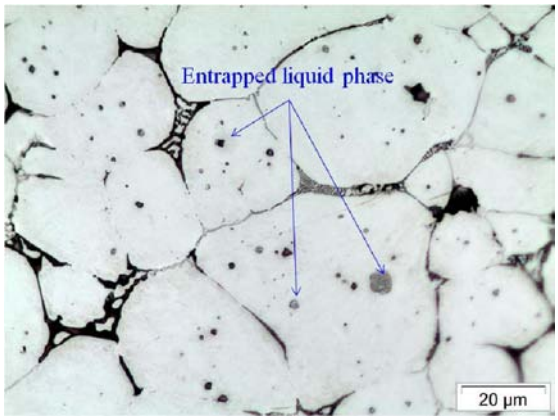

Fig. 3.17. Micrographies du matériau trempé depuis l'état semi-solide.

La technique de métallographie quantitative a été utilisée pour quantifier la distribution de la fraction liquide dans un lopin chauffé à différentes températures. La figure 3.18 montre que la fraction liquide augmente avec la température mais également que la distribution radiale est plus uniforme avec le cycle de chauffe B (celui présentant le « maintien » en fin de chauffe).

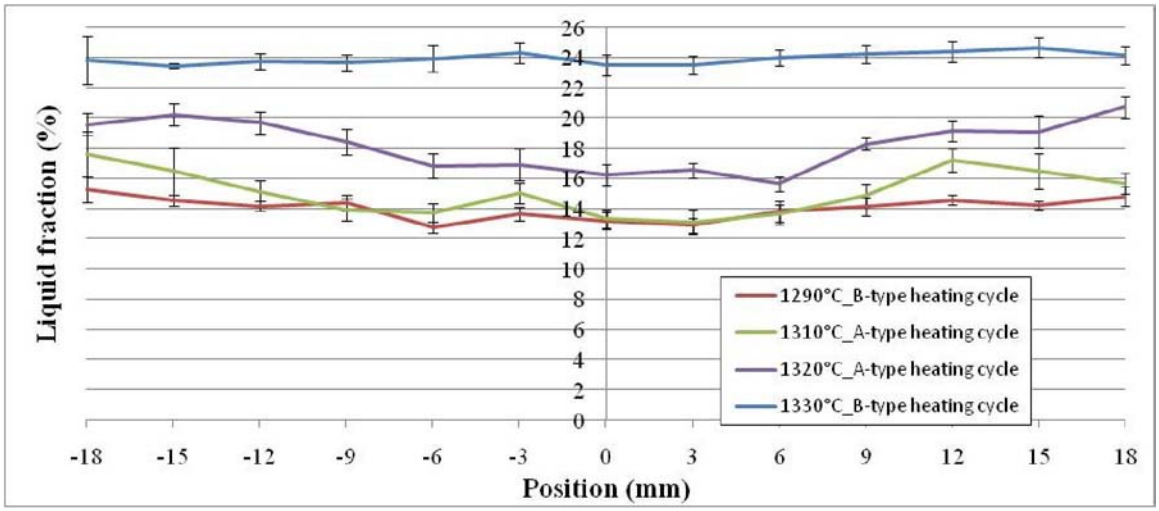

Fig. 3.18. Variation radiale de la fraction liquide d'un lopin chauffé à différentes températures.

Les mesures de tailles de grain montrent une certaine uniformité dans tout le lopin. Par contre, on constate que la taille des grains obtenus par un cycle de chauffe de type B est plus faible. A l'état solide, la taille de grain augmente avec le temps de chauffe et la température. Quel que soit le type de chauffe, les grains sont relativement petits (de l'ordre de 50 microns maximum). Ceci est sans doute dû à l'effet d'ancrage des carbures aux joints de grain.

Le facteur de forme est définie en 2D ; Il est déterminée suivant les deux directions (longitudinale et transversale).

De même que pour la fraction liquide, on peut remarquer que le facteur de forme est relativement uniforme dans un lopin (Voir Fig. 3.22 (a), (b), (c) et (d)). De même, si on compare deux lopins chauffés avec le même type de cycle de chauffage, on Remarque le facteur de forme évolue peut avec la température. Par contre, on remarque que le cycle de chauffage a un effet important sur le facteur de forme.

Les structures liquide solide des aciers C38LTT et 100Cr6 ont également été étudiées sur des lopins trempés. Les vitesses de refroidissement accessible par trempe et la faible teneur en élément d'alliage à faible vitesse de diffusion ont rendant inopérant les techniques de métallographie quantitatives.

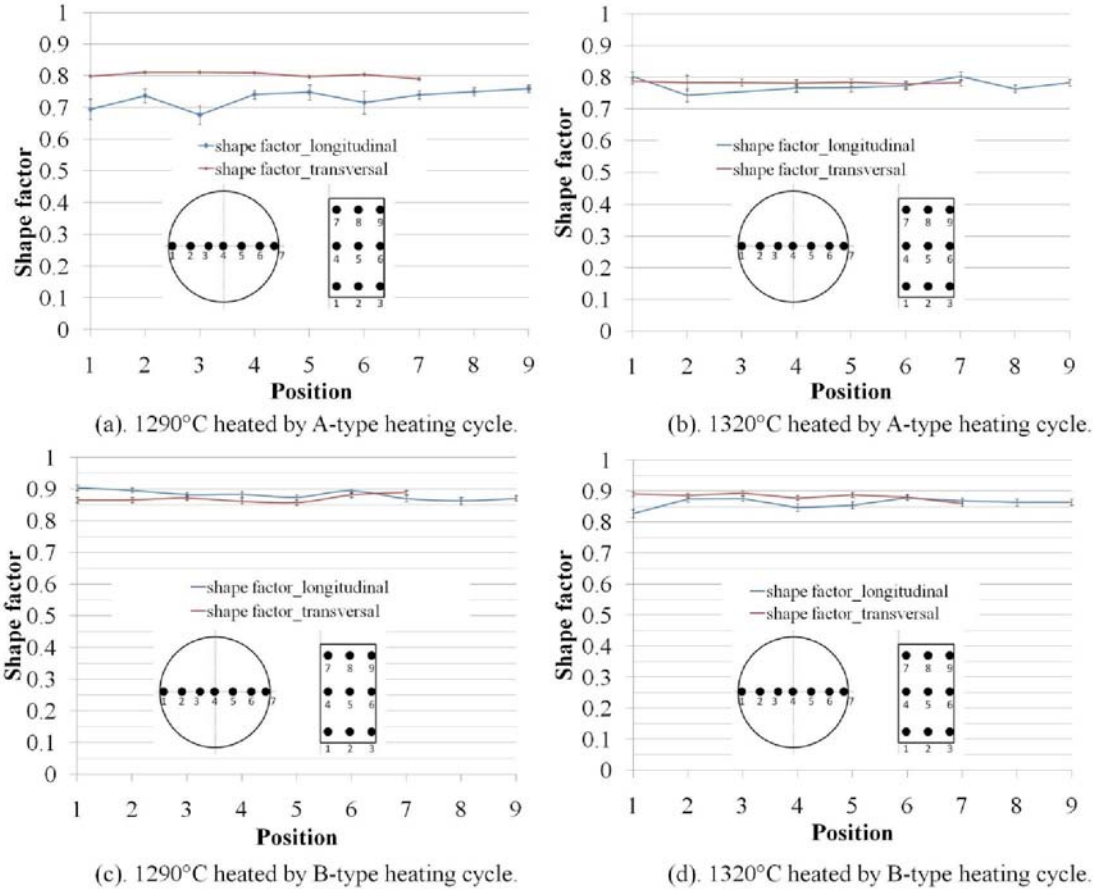

Fig. 3.22. Variation du facteur de forme dans des lopins chauffés à différentes températures par différents types de cycles.

5. Evaluation de la fraction liquide par microtomographie aux rayons X

Cette partie est consacrée essentiellement à la caractérisation 3D de la structure de l'acier M2 à l'état de livraison et à l'état semi-solide.

5.1. Etat de livraison

Des mesures par microtomographie aux rayons X ont été effectuées sur l'acier M2 dans son état initial. Grace à la présence d'éléments d'alliage lourd comme le molybdène et le tungstène, un bon contraste a été obtenu entre la matrice et les carbures (voir Fig. 3.24). Les carbures apparaissent sous la forme de zones blanches dans tous les clichés. Conformément à l'observation par MEB, leur taille est de l'ordre de quelques microns. Ils sont soit isolés soit distribués suivant des bandes.

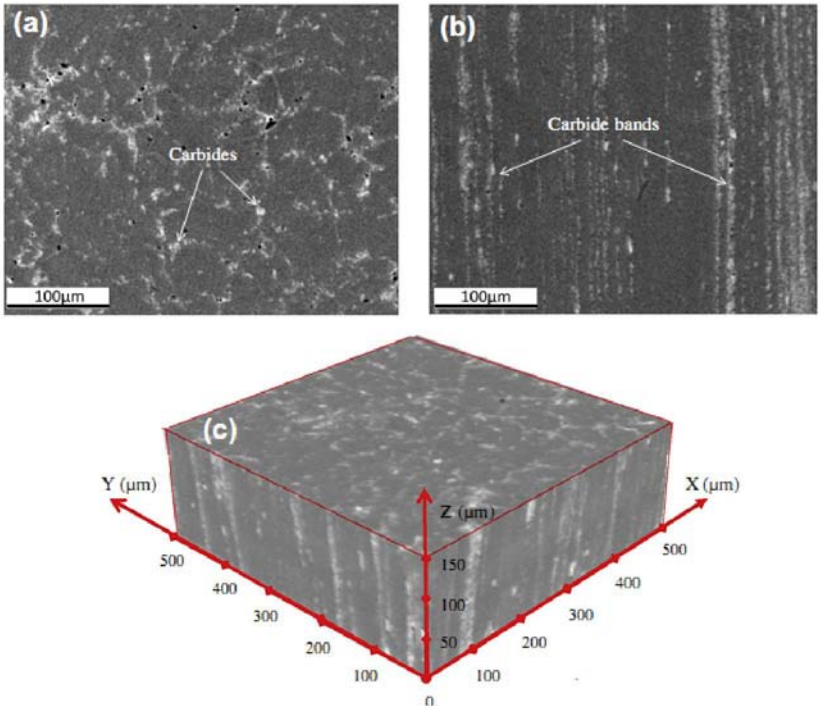

Fig. 3.24. Microtomographie aux rayons X de l'acier M2 dans son état de livraison (a) section transversale, (b) section longitudinale et (c) reconstruction 3-D.

5.2. Microstructure du matériau trempé depuis l'état semi-solide

Afin d'étudier l'évolution de microstructure liquide solide en fonction de la température, un lopin M2 a été chauffé par induction avec un cycle de chauffe formé d'un seul palier de puissance. L'état semi-solide, du fait de la concentration de la puissance en peau, n'a pas été atteint en tout point du lopin. Le champ de température obtenu est non uniforme (voire figure 3.25). La température a été mesurée au point C par un pyromètre. Le lopin a été trempé juste après que la température au point a atteint 1250°C. Durant la chauffe, le lopin est posé sur un support en céramique.

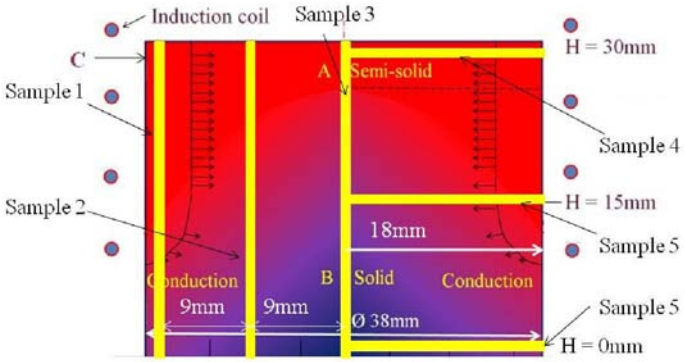

Fig. 3.25. Vue schématique de la distribution de température dans le lopin chauffé.

De ce lopin, des échantillons cylindriques de 1.2 mm de diamètre ont été prélevés par électroérosion.

Deux micrographies correspondant à des sections transversale et longitudinale et une reconstruction 3D d'un échantillon partiellement fondu sont présentées sur la figure Fig. 3.26 (a) et (b), respectivement.

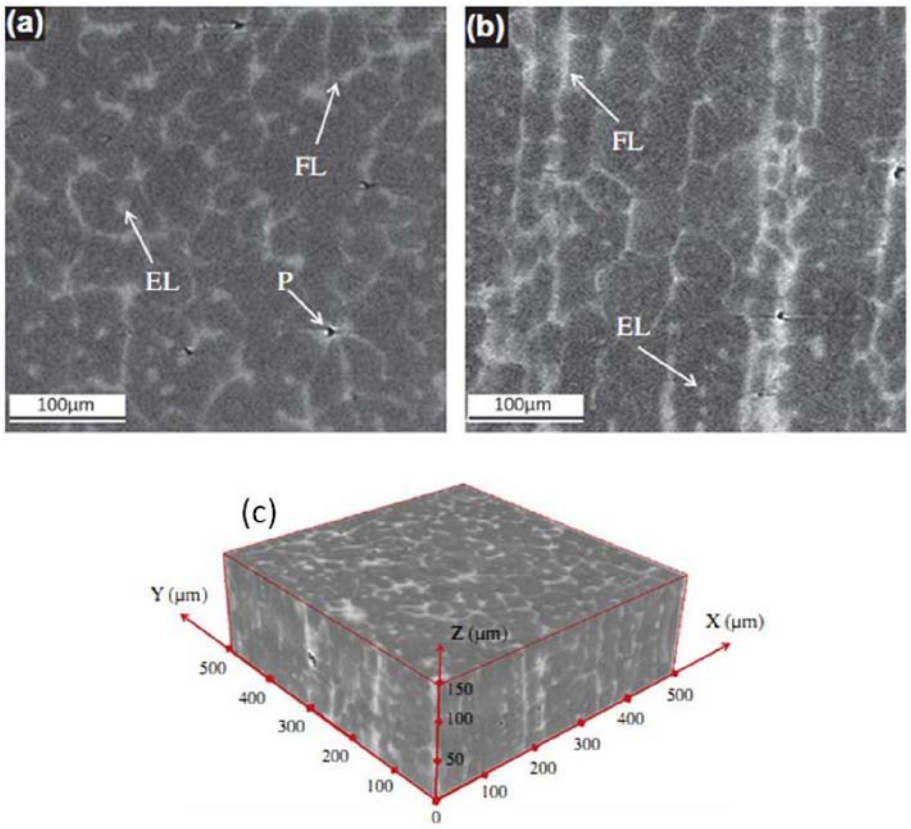

Fig. 3.26 Reconstruction d'un échantillon partiellement fondu et trempé. (a) section transversale, (b) section longitudinale (c) reconstruction 3D. FL: phase liquide; EL: liquide piégé; P: porosité.

On peut, dans un premier temps, observe les même évolutions entre l'état de livraison et l'état trempé depuis le semi-solide qu'en métallographie MEB-EDS. La microtomographie ne permet toutefois pas de connaître la composition des carbures même si le contraste atteste d'une forte teneur en éléments d'alliage lourds.

Le tableau. 3.4 permet de comparer les micrographies obtenues au MEB et celles obtenues par microtomographie aux rayons X. Les figures avec un «S » en haut à gauche correspondent à des clichés MEB. Celles avec un 'T' correspondent à des micrographies issues de tomographie.

Table. 3.4 Micrographs du MEB et de la microtomographie aux rayons X.

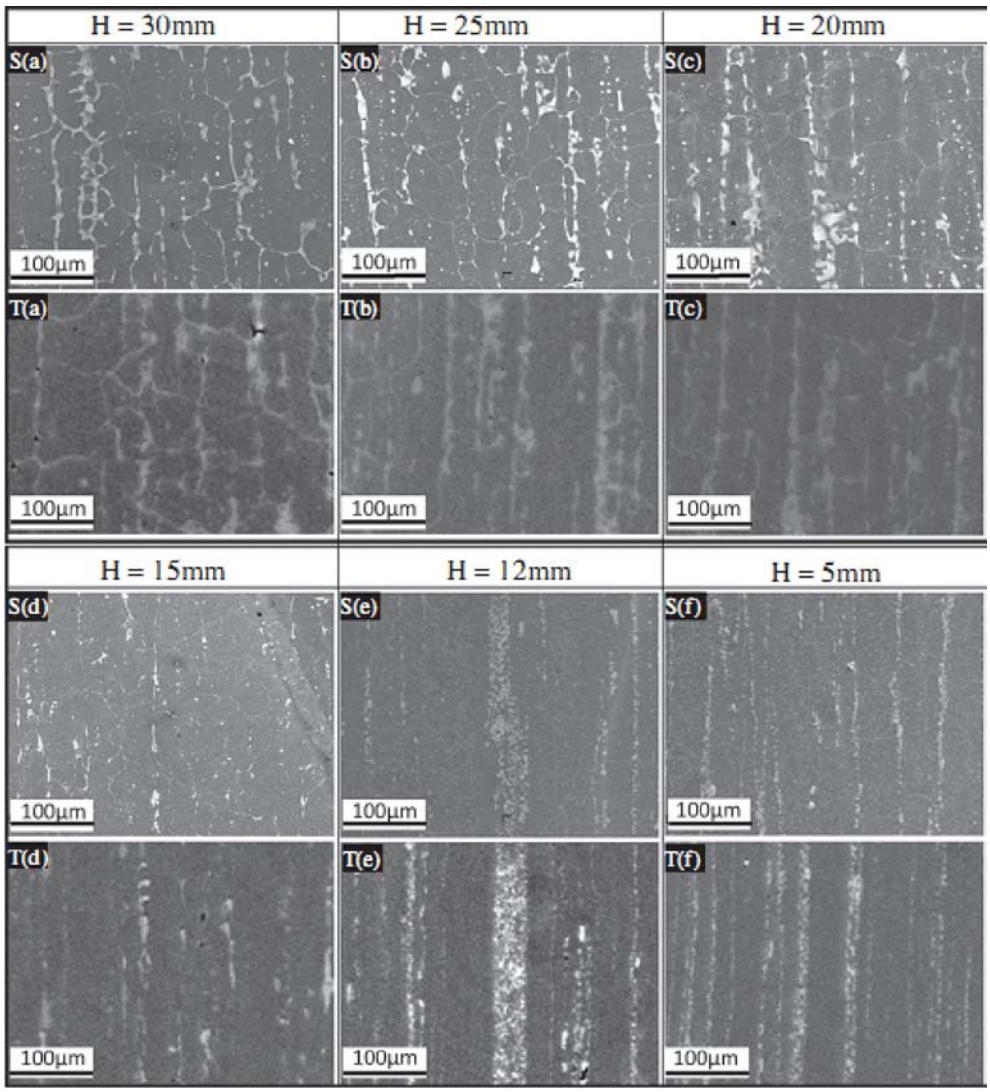

Le calcul de la fraction de liquide a été obtenu par traitement des images 3D avec le logiciel ImageJ. L'évolution de la fraction liquide en fonction de la position dans le lopin initial est donnée sur la figure Fig. 3.27. L'évolution de la fraction liquide semble suivre le profil en cloche de la température dans le lopin. La température maximale atteinte et la fraction volumique de liquide semblent correspondre.

Comme illustré sur la Fig. 3.27-a, les zones avec une fraction liquide de 11±1% montrent le même type de carbures que ceux observés sur la Fig. 3.12 (c). Les zones avec une fraction liquide supérieure à 13±1% présentent des carbures formés au cours de la trempe provenant des zones liquides (voir Fig. 3.12 (f)). Les deux types de carbure coexistent dans les zones avec une fraction liquide comprise entre 11±1% et 13±1%.

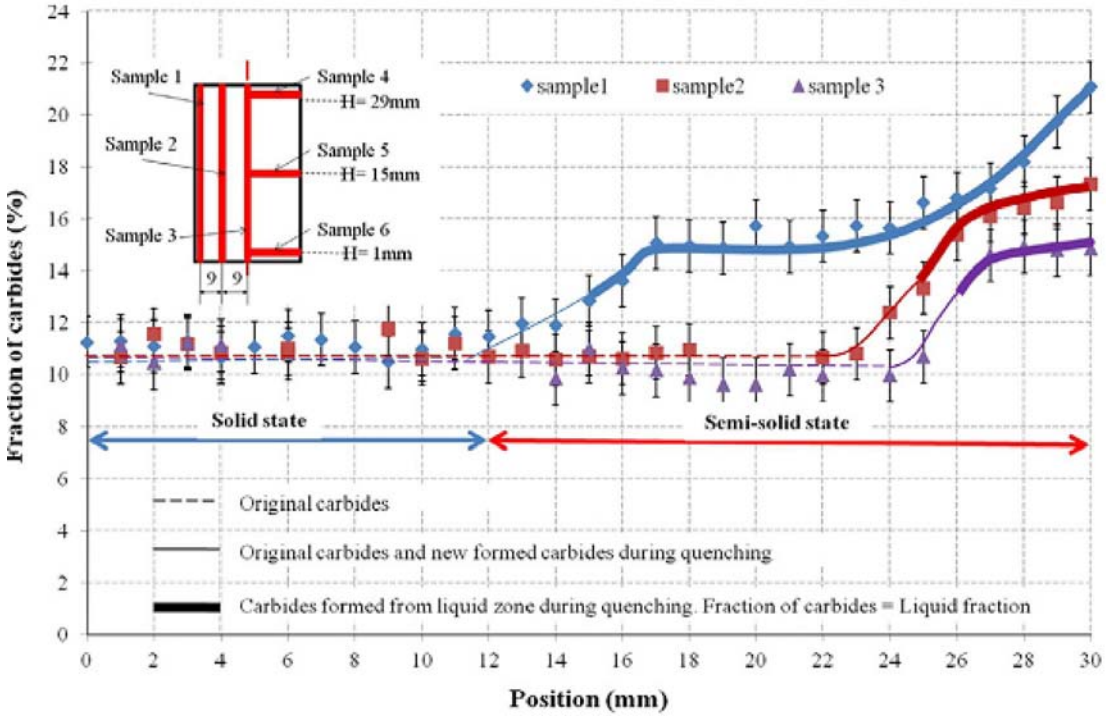

(a) **Axial direction.**

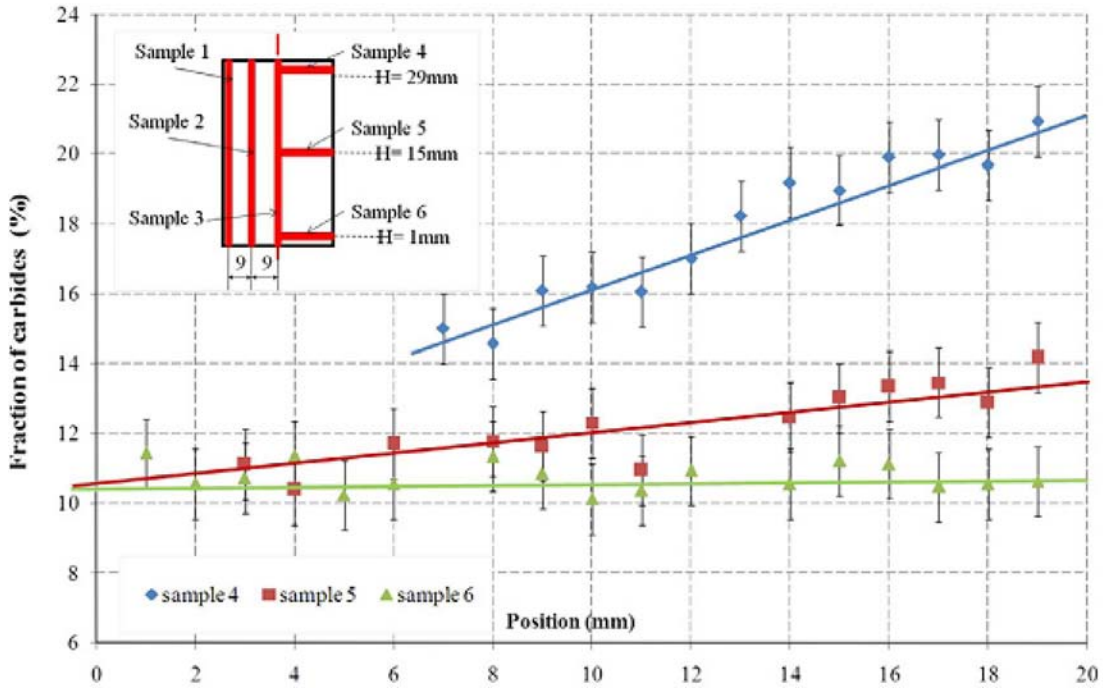

(b) **Radial direction.**

Fig. 3.27. Fraction volume du M2 chauffé et trempé en fonction de hauteur.

La fraction volumique initiale de carbure est de11±1%. C'est ce qui est observé dans la partie du lopin resté entièrement solide. Lorsque la température franchit le solidus, les

carbures de type MC fondent les premiers pour former des carbures plus gros lors de la trempe. Si la température dépasse la température de fusion des carbures M_6C, tous les carbures initiaux sont dissous et forment également de nouveaux carbures au cours de la trempe. Au-delà d'une certaine température, un réseau de zones liquides interconnectées est formé. Des petits carbures sont également observés à l'intérieur des particules solides. Ceci est dû au faible temps de maintien ne permettant pas aux éléments d'alliage de diffuser vers les zones liquides intergranulaires. Basé sur les résultats des deux techniques de mesure, une fraction de carbure au-delà de 13±1% est considérée comme étant la fraction liquide réelle.

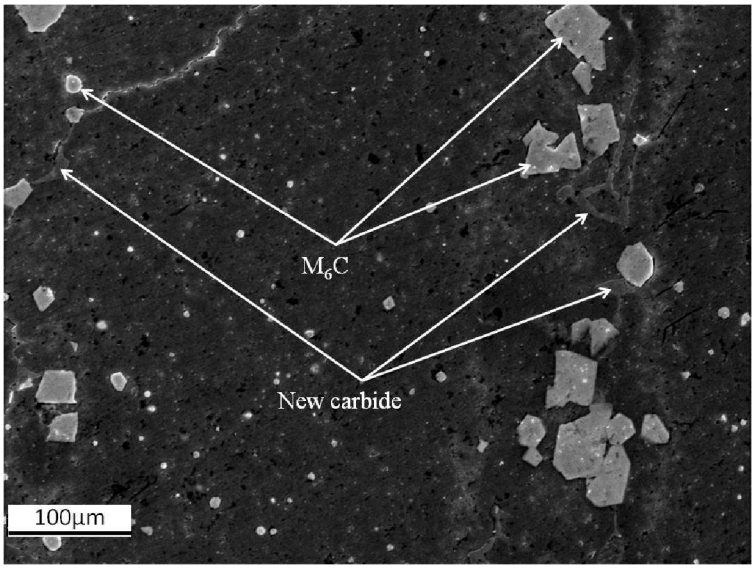

Fig. 3.28. Microstructure de l'échantillon 1 à une hauteur de 14 mm.

Table 3.5 fractions volumique de carbure à différentes positions.

Fractions of carbides in various positions.

Height (mm)	Radius (mm)	Fraction of carbides (%)					
		Sample 1	Sample 2	Sample 3	Sample 4	Sample 5	Sample 6
29	18	19.7			19.6		
29	9		16.62		16.11		
15	18	12.83				12.90	
15	9		10.97			11.66	
15	1			10.89		10.45	
1	18	11.3					10.56
1	9		11.54				10.94
1	1			11.11			10.64

Si on compare les tailles de grain, on constate que leur grossissement s'arrête lorsque des bandes de liquide interconnectées sont formées. Ceci s'explique par le rôle d'inhibiteur de grossissement de grain joué par les carbures. On constate un grossissement de grain

systématique entre l'état trempé et l'état de livraison. La taille de grain augmente avec la température et le temps de chauffe.

Comparaison entre l'analyse d'images 2D et 3D

La figure 3.29 montre la fraction de carbure mesurée en 2D et 3D. Les résultats sont très proches. La microtomographie par rayons X étant un moyen de caractérisation difficile d'accès, il est important de constater que des résultats similaires peuvent être obtenus par la technique plus accessible, notamment par les industriels, qu'est la microscopie électronique à balayage avec l'utilisation d'une sonde EDS.

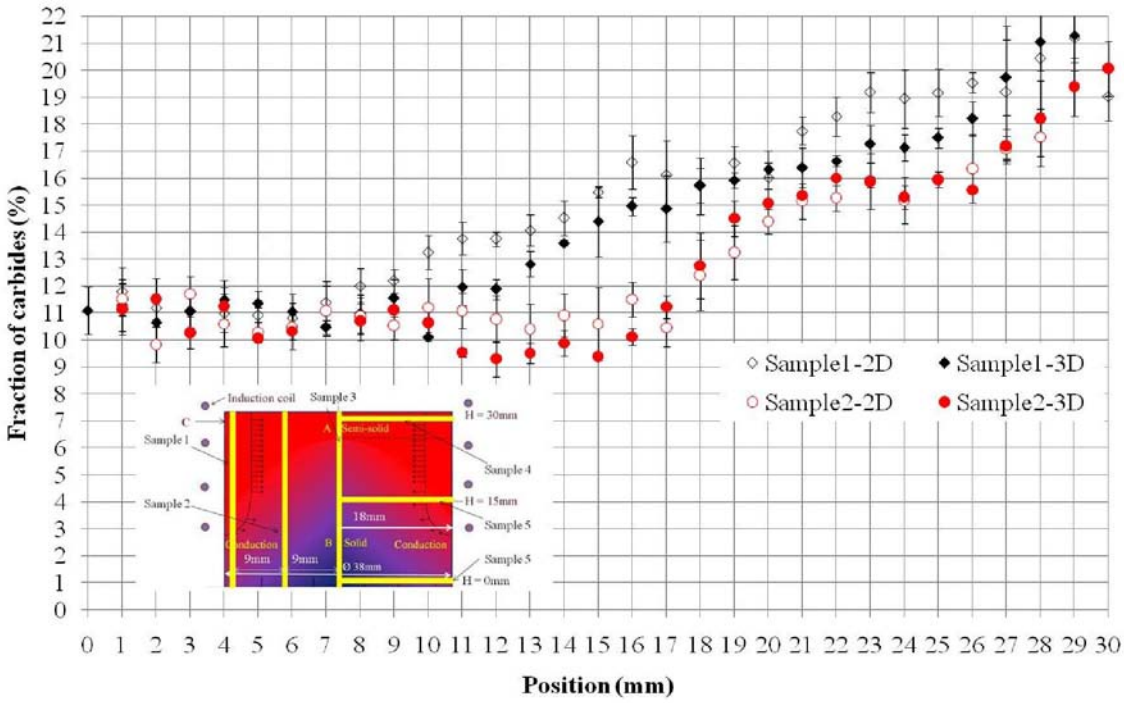

Fig. 3.29. Comparaison des fractions liquides obtenues par analyse 2D et 3D.

Des essais de microtomographie ont également été effectués sur les aciers 100Cr6 et C38LTT. Du fait de leur faible teneur en éléments d'alliage lourds, les zones fondues n'ont pu être détectées.

6. Observations in situ des aciers M2, 100Cr6 et C38LTT

La vitesse de chauffe utilisée pour les observations in situ est de 200°C/min. Ceci est plus faible que les vitesses de chauffe industrielles. Cependant, ces techniques permettent

l'observation de la structure liquide solide directement à haute température en évitant ainsi tous les problèmes liés à la diffusion des éléments d'alliage lors du refroidissement.

Des observations In situ par CLSM ont été effectuées sur l'acier M2 à différentes températures. La structure initiale de l'acier a été révélée avant la chauffe. La structure observée possède les mêmes caractéristiques que celles observes précédemment (Fig. 3.30-a). Avec l'accroissement de la température, les carbures diffusent dans la matrice avant l'apparition de la phase liquide (Fig. 3.30-b). Si la température monte encore les zones liquides s'arrondissent (Fig. 3.30-c) pour former un réseau interconnecté de cellules équiaxes (Fig. 3.30-d). On note en comparant les figures Fig. 3.30-a et Fig. 3.30-d, l'augmentation significatif de la taille de grain, entre 20µm-60µm pour une taille initiale de ~10µm.

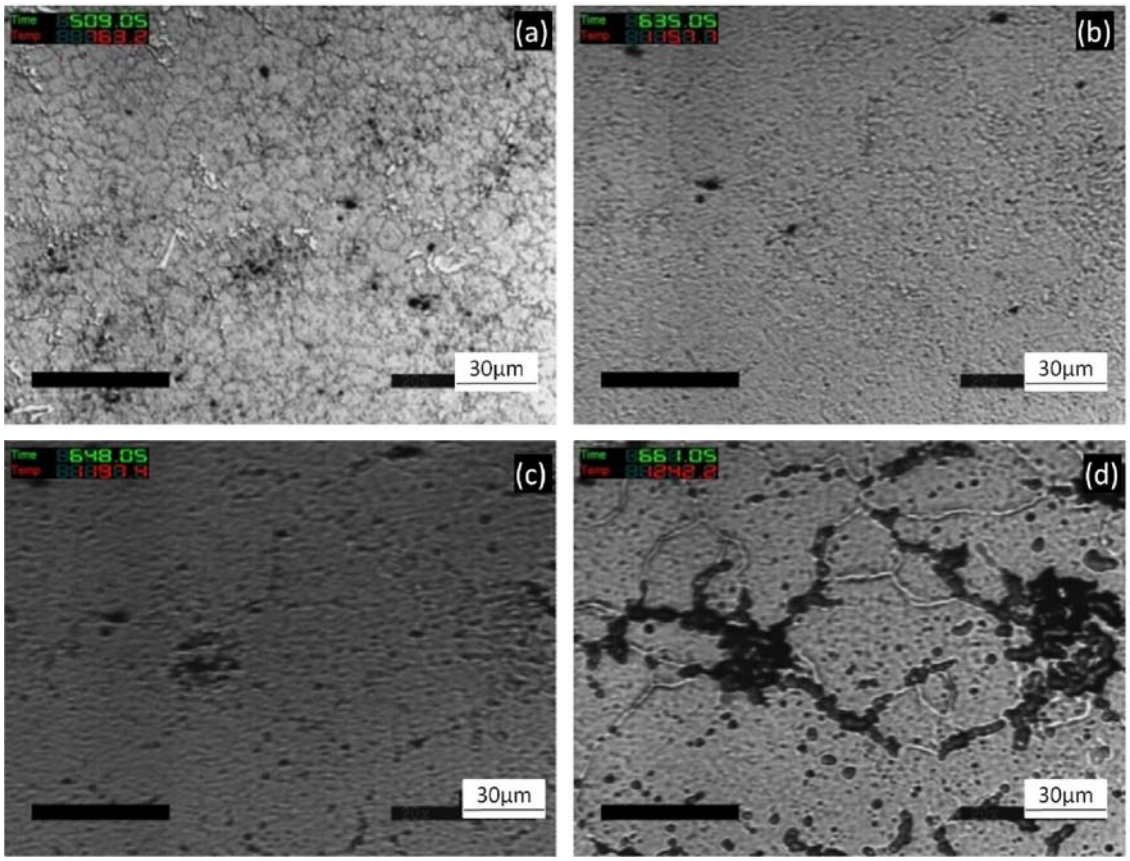

Fig. 3.30. Arrêt sur image de la séquence de chauffage (200°C/min) depuis l'état solide jusqu'à l'état semi-solide par CLSM.

Au cours du refroidissement depuis 1250°C jusqu'à la température ambiante, le réseau interconnecté de liquide est préservé et est transformé en nouveaux carbures (voir Fig. 3.31).

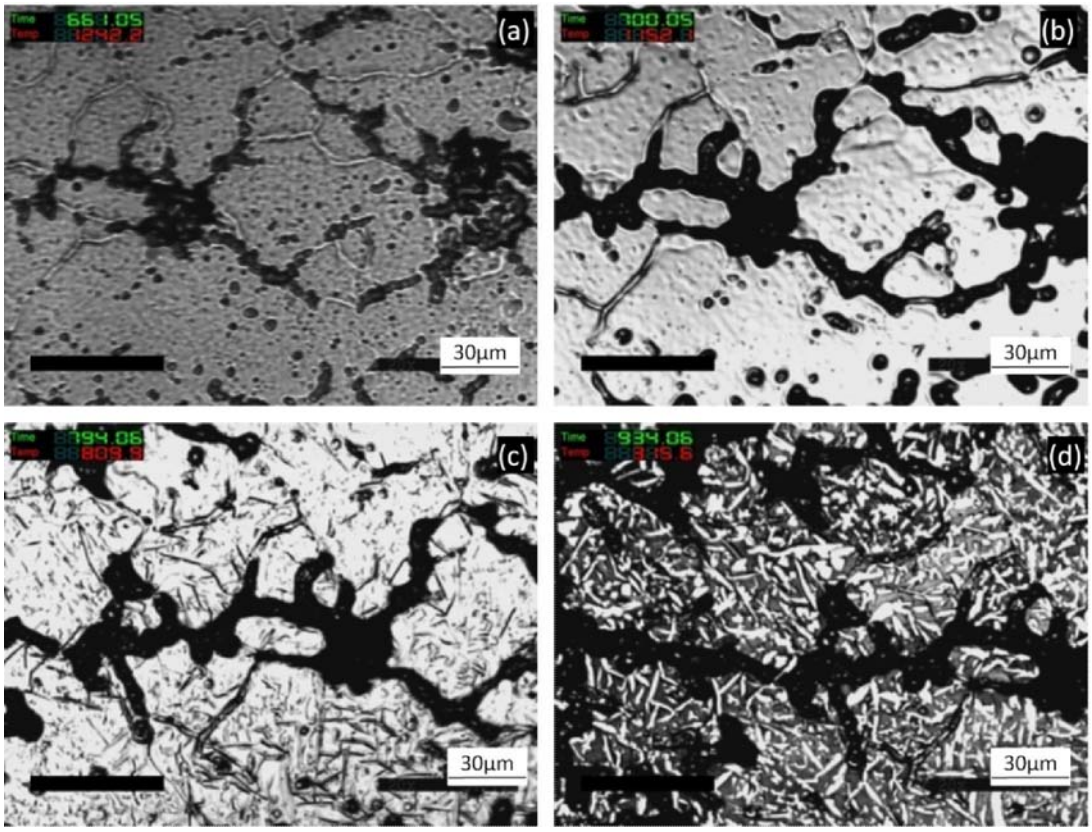

Fig. 3.31. Arrêt sur image de la séquence de refroidissement (200°C/min) depuis l'état semi-solide jusqu'à l'ambiante par CLSM.

Les résultats de ces observations montrent que les zones liquides sont conservées même pour des vitesses de refroidissement plus faibles, venant ainsi confirmer les résultats obtenus par microtomographie et MEB.

Les mêmes types d'observation ont été conduits sur l'acier 100Cr6. La microstructure de cet acier à l'état semi-solide n'a pas été clairement révélée comme le montre la figure Fig.3.32 (a): La perlite et les joints de grain n'ont pas pu être observés. Avec la montée en température, la transformation de la perlite en austénite peut être observée (Fig. 3.32 (b)). A température plus élevée, on observe le grossissement des grains austénitiques (Fig. 3.32 (c)). Quand la température devient égale au solidus, la phase liquide commence à se former depuis le joint de grain (Fig. 3.32 (d)). Cependant la phase liquide n'est pas observée à tous les joints de grain du fait soit de l'hétérogénéité de la composition chimique à cette échelle, de la non uniformité de la température, etc. (Fig. 3.32 (e)). Avec l'augmentation de la température, la quantité de liquide augmente jusqu'à couvrir la surface de l'échantillon (Fig. 3.32 (f)). Au cours de l'essai, la quantité de liquide augmente très rapidement (voir Fig. 3.32 (d) (e) et (f)).

Ceci démontre la plus fortement sensibilité de la fraction liquide à la température pour cet acier que pour l'acier M2.

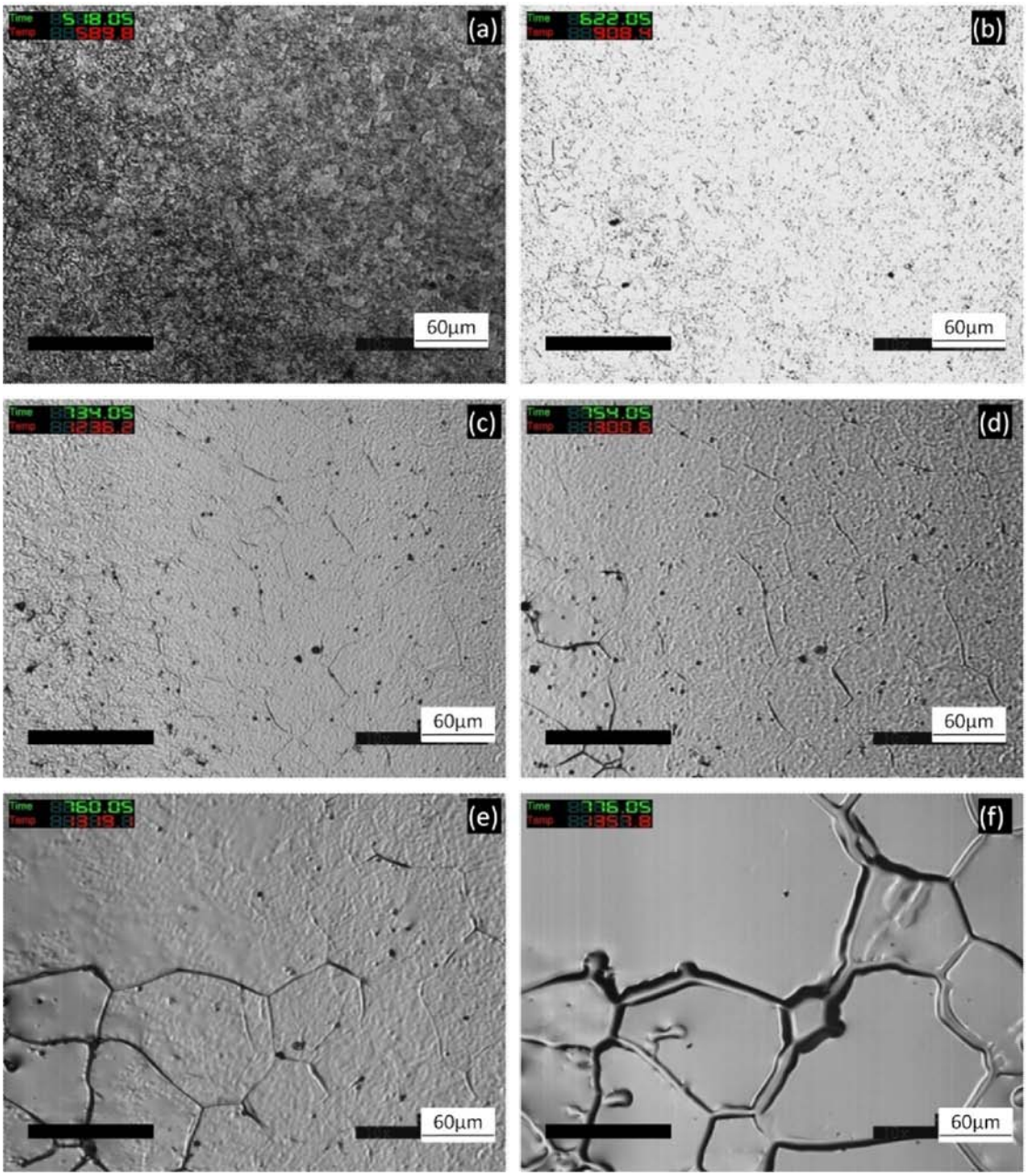

Fig. 3.32. Arrêt sur image de la séquence de chauffe de l'acier 100Cr6 jusqu'à l'état semi solide par CLSM.

Des observations micrographiques ont été conduites sur les échantillons post mortem. Il n'a pas été possible d'établir un lien entre les microstructures observées à haute température et à température ambiante après refroidissement.

La structure initiale de l'acier C38LTT, illustrée sur la figure Fig. 3.34-a et -b est constituée de ferrite, de perlite et d'inclusions non métalliques (MnS). En CLSM, la ferrite apparaît en blanc et la perlite en noir. Avec la montée en température, on peut observer la transformation de la perlite et de la ferrite en austénite (voir Fig. 3.34-c).Les premiers films liquides sont observés aux joints de grain (voir Fig. 3.34-e). En comparant les figures Fig. 3.33-e et f, on remarque que la quantité de liquide augmente rapidement sur un temps très court. De plus la distribution du liquide sur l'échantillon n'est pas uniforme. Ceci peut être dû soit à un défaut de planéité de l'échantillon ou aux hétérogénéités de composition, etc.

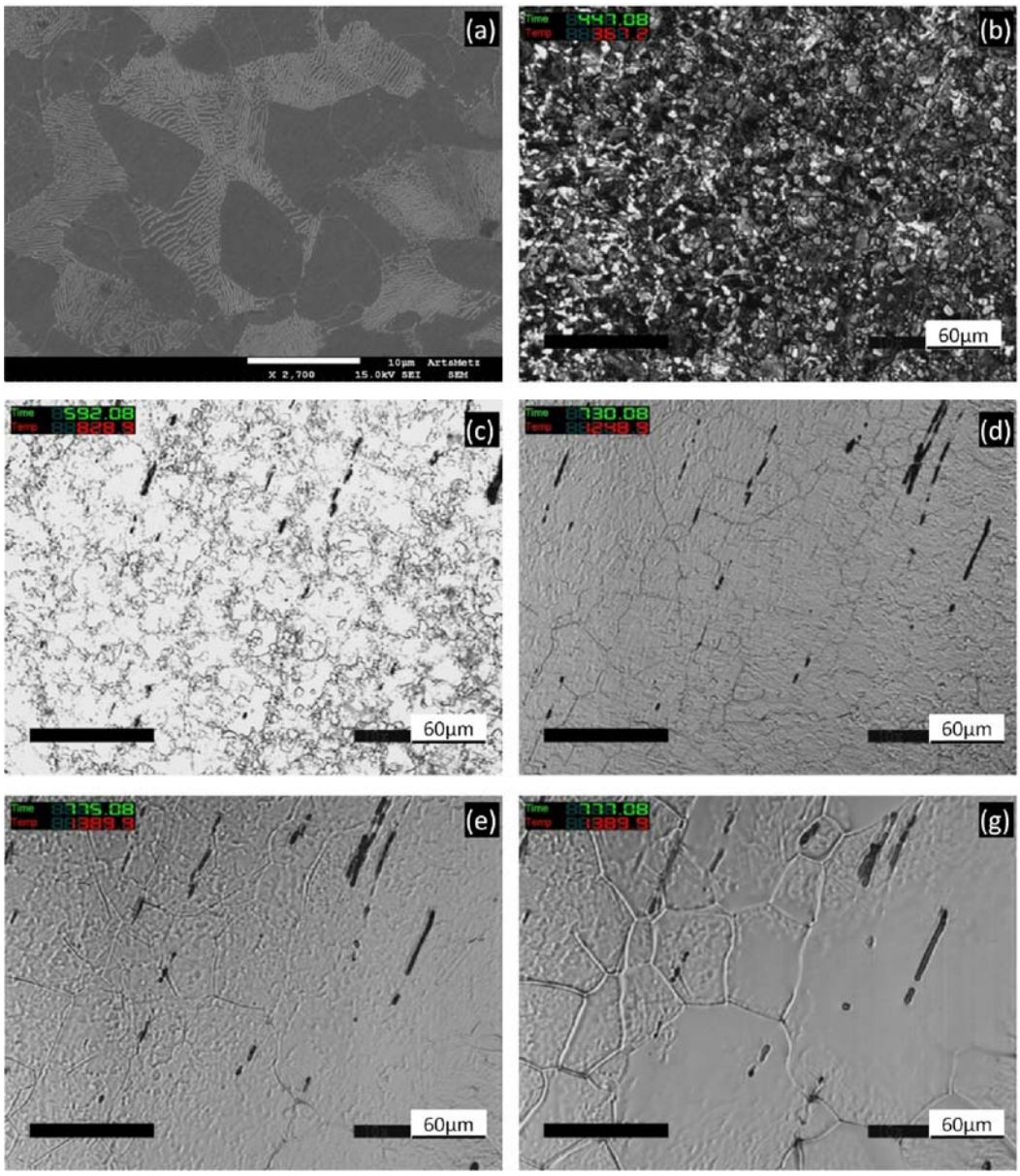

Fig. 3.34. CLSM du C38LTT à la vitesse de refroidissement à 200°C/min.

L'échantillon a été observé post mortem. La figure Fig. 3.35 compare les microstructures avant et après attaque chimique. Le film liquide de la figure Fig. 3.35 (a) est principalement présent au joint ferritique (voir Fig. 3.35 (b)).

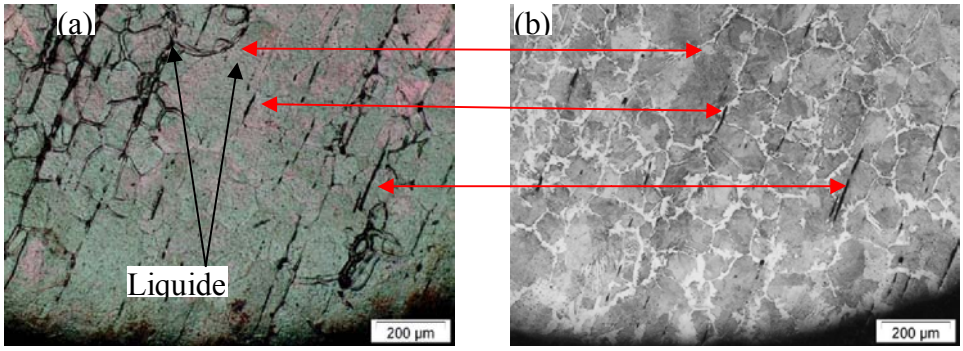

Fig. 3.35. Microstructure des échantillons après observation sin situ. (a) avant attaque, (b) après attaque.

7. Conclusion

La microstructure du matériau à l'état semi-solide est déterminante pour le procédé de thixoforgeage. Pour cela, plusieurs techniques ont été utilisées pour caractériser la microstructure au cours du chauffage depuis la température ambiante jusqu'à l'état semi-solide. Les résultats ont montré que :

(a) toutes les méthodes ont des limitations

- L'utilisation de diagramme thermodynamique peut prédire la fraction volumique de liquide en fonction de la température. Des informations supplémentaires sont nécessaires pour prendre en compte l'histoire thermique du matériau. Cette technique ne permet pas d'obtenir des informations sur la morphologie de la structure liquide solide.
- DSC est une technique simple d'utilisation pour l'évaluation de la fraction liquide. Cependant la vitesse de chauffe est très faible comparée à celle des moyens industriels. Comme les diagrammes thermodynamiques, aucune information concernant la morphologie de la structure n'est fournie.
- L'analyse d'image en 2D après trempé depuis l'état semi-solide permet d'obtenir des informations sur la fraction liquide et la morphologie de la structure liquide solide. Elle n'est toutefois opérante que lorsque la structure liquide solide peut être figée par trempe.
- La microtomographie aux rayons X fournit des informations sur la structure 3D. Elle est toutefois efficace que pour les alliages contenant des éléments chimiques lourds. La correspondance entre les résultats obtenus par analyse 2D par MEB+EDS et la microtomographie 3D prouve que les deux techniques sont aptes à caractériser les aciers fortement alliés au tungstène et molybdène à l'état semi-solide. La technique de microtomographie est difficilement accessible e comparaison avec la technique de métallographie quantitative par MEB EDS.
- CLSM permet l'observation de la microstructure à haute température. Elle a permis l'observation de la formation de la structure liquide solide du M2 mais également des deux aciers faiblement alliés 100Cr6 et C38LTT.

(b) La microstructure liquide solide du M2 peut être analysée toutes les techniques mises en œuvre. Les aciers 100Cr6 et C38LTT ne peuvent être observés que par CLSM in situ.

(c) Le thixoforgeage de l'acier M2 ne présente pas d'intérêt industriel. Toutefois, du fait de sa bonne aptitude à être observé par les techniques de caractérisation, il peut permettre de comprendre le comportement d'un matériau au cours de la mise en forme à l'état semi-solide. Il s'agit ensuite d'imaginer l' "extrapolation" à l'acier C38LTT et 100Cr6.

Chapitre 4. Etude des résultats de thixoforgeage

Ce chapitre est dédié aux expérimentations de thixoforgeage des trois nuances d'acier étudiées aux chapitres précédents. L'étude se focalise sur l'influence des paramètres du procédé sur les efforts de mise en forme, les écoulements de matière, la forme finale de la pièce, la macrostructure et les microstructures métallurgiques obtenues. Le thixoforgeage de l'acier M2 est étudié dans un premier temps dans la mesure où la caractérisation de sa structure liquide solide est envisageable avec les techniques développées au chapitre 3.

1. Thixoforgeage de l'acier M2

Le dispositif de thixoforgeage et de chauffage ont été décrits au chapitre 2.

Fig. 4.1. Pièces obtenus par thixoforgeage.

Des lopins en acier M2 de diamètre 36mm pour une hauteur de 34 mm ont été thixoforgés dans différentes conditions de mise en forme. L'intervalle de température pour lequel l'acier semble avoir la meilleure aptitude au thixoforgeage se situe entre 1290°C et 1340°C. Cet intervalle correspond à un intervalle de fraction liquide de ~16% - ~30%. La figure 4.1 présente l'ensemble des pièces chauffées et thixoforgées sous la presse mécanique SATORE du LCFC ENSAM de Metz.

Le processus de thixoforgeage est constitué d'une opération de chauffe jusqu'à l'état semi-solide suivie de l'opération de mise en forme après transfert du lopin depuis l'inducteur vers la presse. La figure 4.2 illustre les étapes de m'opération de mise en forme.

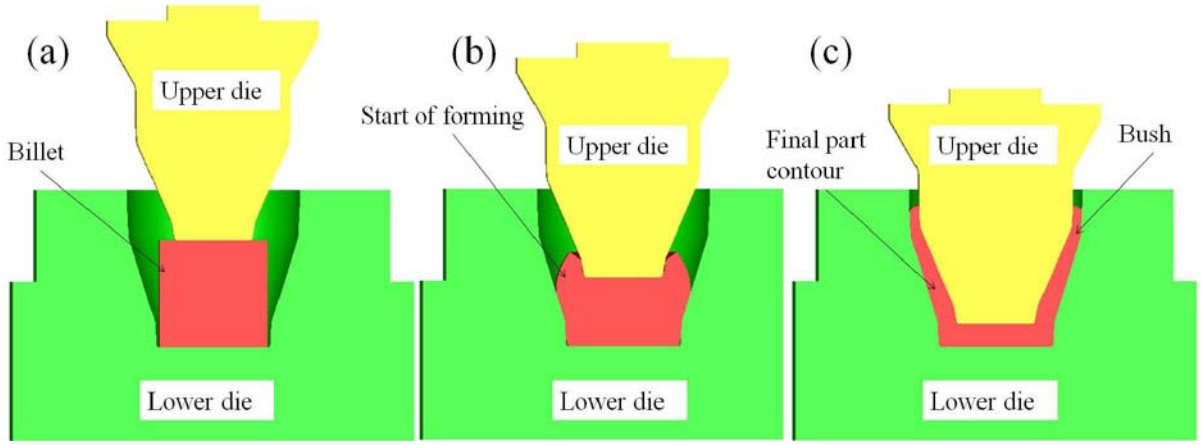

Fig. 4.2. Schéma des différentes étapes de mise en forme.

Les paramètres du processus de mise en forme sont la température du lopin, le type de cycle de chauffe ayant permis d'atteindre celle-ci et la température des outillages. L'ensemble des valeurs de ces paramètres est fourni dans le tableau 4.1.

Table. 4.1. Paramètres du processus de thixoforgeage.

Température lopin (°C)	Cycle de chauffe	Température outil
1290	A-type	Température ambiante
	B-type	Température chaude
1300	A-type	Température ambiante
	B-type	Température chaude
1310	A-type	Température ambiante
	B-type	Température chaude
1320	A-type	Température ambiante
	B-type	Température chaude
1330	A-type	Température ambiante
	B-type	Température chaude
1340	A-type	Température ambiante
	B-type	Température chaude

Fig. 4.3. présente plusieurs photos des pièces obtenues sous différentes conditions opératoires (Température de lopin de 1290°Cà1350°Cet température d'outillage ~300°C, et température ambiante).

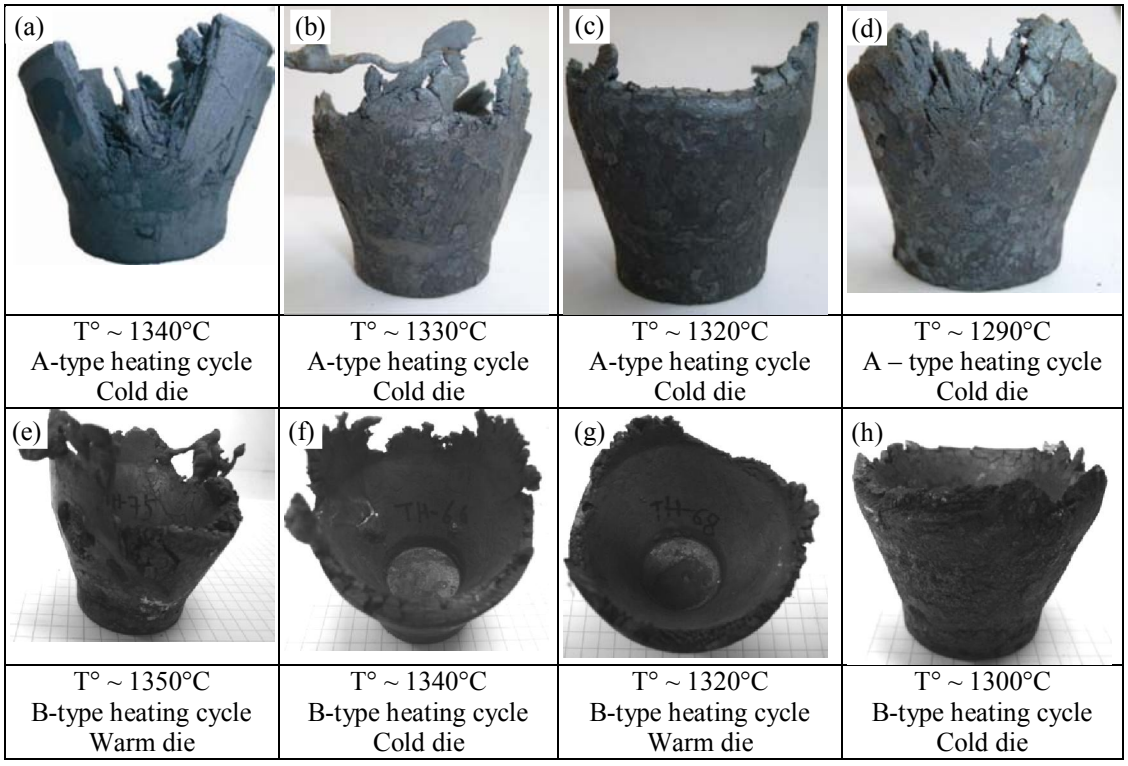

Fig. 4.3. Pièce thixoforgées sous différentes conditions opératoires.

Sur la Fig. 4.3, on peut noter que la pièce finale (appellee cup) peut être thixoforgée pour un certain intervalle de température de lopin. De façon générale, trois types de défaut sont observés : manque de remplissage (Fig. 4.3 (d)), fissuration (Fig. 4.3 (a) and (d)) éjection de liquide (Fig. 4.3 (b) and (e)).

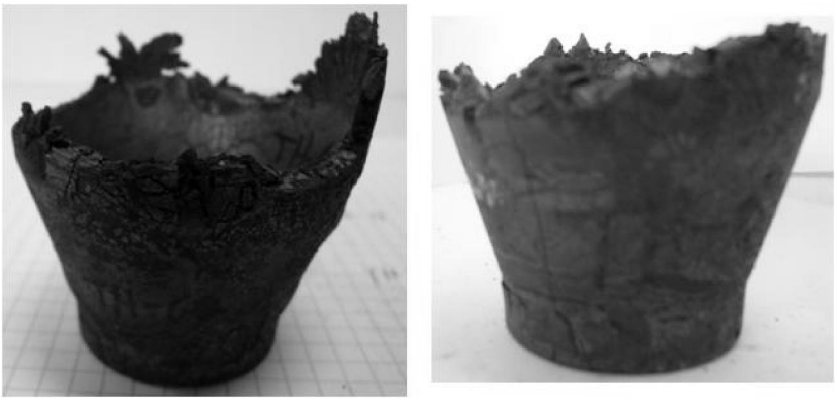

Fig. 4.4. Ecoulements non uniforme dans les pièces thixoforgées.

L'écoulement non uniforme (cup non axy-symétrique) des pièces obtenues peut provenir de la non uniformité du matériau initial, d'un défaut de position du lopin en début de mise en forme, d'un défaut de coaxialité des outils…La Fig. 4.5 illustre les épaisseurs des parois de la

"cup" dans une section contenant la hauteur maximum. On peut noter que les épaisseurs obtenues dans la plus haute paroi sont plus faibles que celles mesurées dans l'autre paroi. On note une différence moyenne de l'ordre de 0.3mm. Ce constat a été réalisé pour toutes les « cups » qui ont été coupées.

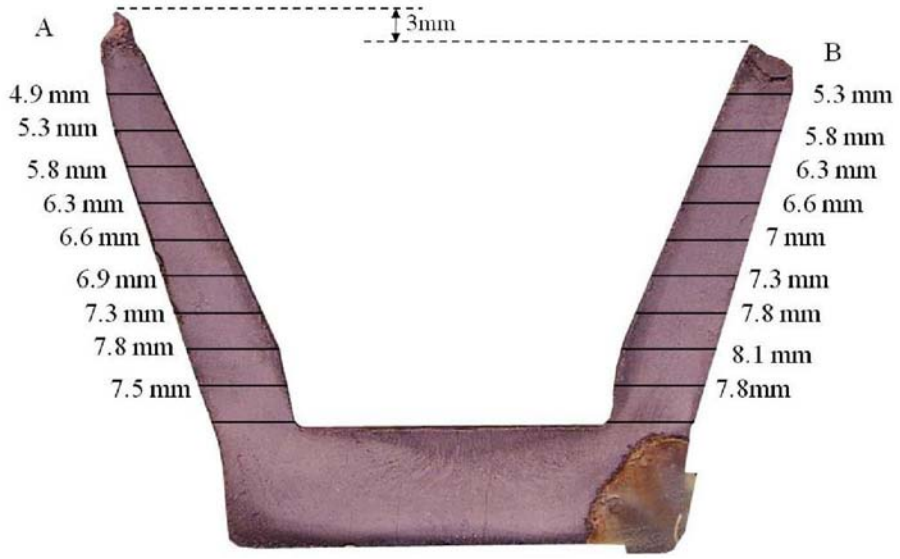

Fig. 4.5. Différence d'épaisseur de la paroi d'une "cup".

Des simulations ont été effectuées pour essayer d'expliquer ce phénomène. Les simulation effectuées avec le modèle de comportement micro-macro [1] se sont avérées infructueuses du fait de difficultés numériques. Des simulations ont été menées en forgeage à chaud en utilisant une loi de comportement thermo-visco-plastic de type Hansel-Spittel. Le but est de regarder sile lien entre l'épaisseur de la paroi de la « cup » et sa hauteur est spécifique au thixoforgeage. Des défauts de positions du lopin dans les outillages et des défauts de coaxialité des outils entre eux sont introduits dans la simulation pour en estimer les effets sur la forme de la pièce forgée. Le tableau 4.3 donne la valeur des défauts testés.

Les résultats des simulations en forgeage à chaud montre l'effet inverse. Lorsque le défaut de mise en forme génère une pièce non axy-symétrique, la paroi la plus haute est la paroi la plus épaisse. Il semblerait donc que ce phénomène soit un effet spécifique au thixoforgeage. Une des explications peut provenir de la sensibilité du comportement du matériau à l'état semi-solide à la température et à la vitesse de cisaillement. En effet, dans la partie la plus étroite la vitesse de cisaillement est la plus élevée. L'effet direct de la vitesse de cisaillement cumulé à l'effet d'échauffement de la matière par dissipation plastique peut conduire à une

chute de la contrainte d'écoulement favorisant le remplissage de la paroi la plus mince. En forgeage à chaud, la sensibilité à la température est beaucoup plus faible et la contrainte d'écoulement augmente avec la vitesse de cisaillement, ce sont donc les parois les plus épaisses qui sont les plus facile à remplir.

Tableau. 4.3. Défauts simulés en forgeage des "cups".

Matériaux	C35		316L
Position d'outil	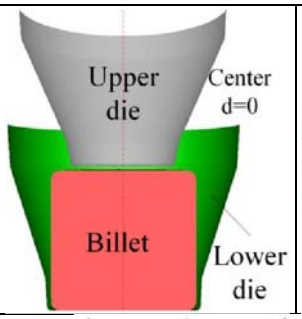	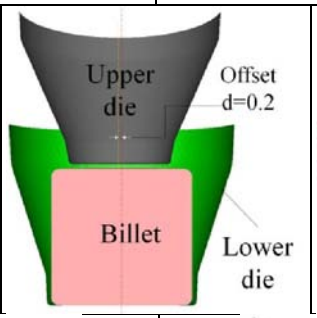	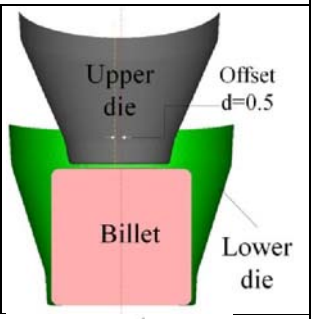
Position du lopin	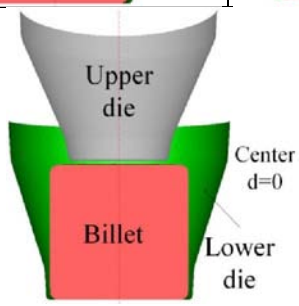		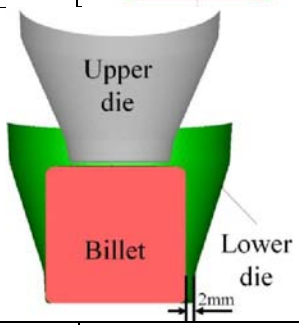
Température	1200°C	1250°C	1300°C
Frottement	0.15		0.5

Comme illustré par la Fig. 4.3, l'intervalle de température du lopin permettant le thixoforgeage est élargi quand on utilise un outillage chauffé (1290°C – 1340°C). Lorsque la température de thixoforgeage est supérieure on observe des éjections de liquide (voir Fig. 4.3 (e)).

1.1. Influence des paramètres de thixoforgeage

1.1.1. Influence de la température du lopin sur l'écoulement

On note que la qualité géométrique des pièces thixoforgées augmente lorsque la température de lopin diminue. La longueur des parois semble augmenter avec la température de lopin, ceci étant sans doute dû à l'augmentation du taux de porosité avec l'augmentation de la fraction de liquide et le phénomène d'éjection de liquide.

1.1.2. Influence de la température d'outillage

Fig. 4.11 présente la photographie de deux "cups" thixoforgées avec deux températures d'outillage, les autres conditions étant identiques par ailleurs. Les résultats constatés sont similaires. Becker [2] explique qu'une augmentation de la température de l'outillage réduit les échanges thermiques. Cette différence est sensible pour les temps de contact relativement longs et donc pour des vitesses de mise ne forme faible. Dans le cas de nos essais, la vitesse de mise en forme est supérieure à 200 mm/s, le temps de contact entre l'outil et matière est faible. On ne constate donc pas de différences significatives entre les pièces thixoforgées avec des outils chauds ou froids.

1.2. Influence des paramètres du procédé sur l'effort de mise en forme

1.2.1. Analyse d'une courbe effort déplacement

Fig. 4.12présente un courbe effort déplacement lors du thixoforgeage d'une "cup". La courbe peut être décomposée en 4 phases. La première phase à effort nul correspondant au déplacement du coulisseau avant l'accostage de l'outil sur la surface supérieur du lopin (I). Le lopin est ensuite écrasé pour remplir la partie inférieure de l'outillage avec un pic (II) suivi d'une chute d'effort (III). Une augmentation importante de l'effort est constatée en fin de mise en forme associée à l'extrusion inverse des parois de la « cups ».

Les quatre zones de la courbe d'effort peuvent s'expliquer de la façon suivante :

(I) L'effort de mise en forme comme à croître lorsque l'outil supérieur est en contact avec le lopin et commence l'écrasement.

(II) Le premier pic d'effort correspond à la résistance puis la rupture de la macrostructure et de la microstructure du lopin. Le premier concerne la peau de pièce constituée d'oxyde formé pendant la chauffe par induction. La microstructure est celle formée par les particules solides et des zones liquides comme présentée sur la figure Fig. 4.13. Le pic d'effort peut donc être également associé à l'effort nécessaire pour briser les interconnections entre les particules solides.

(III) Après la rupture de la structure, les grains sont entourés de liquide et le matériau acquière un comportement thixotrope. Ceci se traduit par une faible élévation de l'effort dû aux frictions internes entre grains solides.

(IV) L'augmentation rapide de l'effort en fin de mise en forme correspond à l'extrusion inverse des parois de la 'cup'. La surface de contact entre le lopin et les outillages augmente. De plus, en fin de mise en forme, le refroidissement de la matière en contact avec les outils conduit à un écoulement complètement solide et donc à une augmentation de la contrainte d'écoulement.

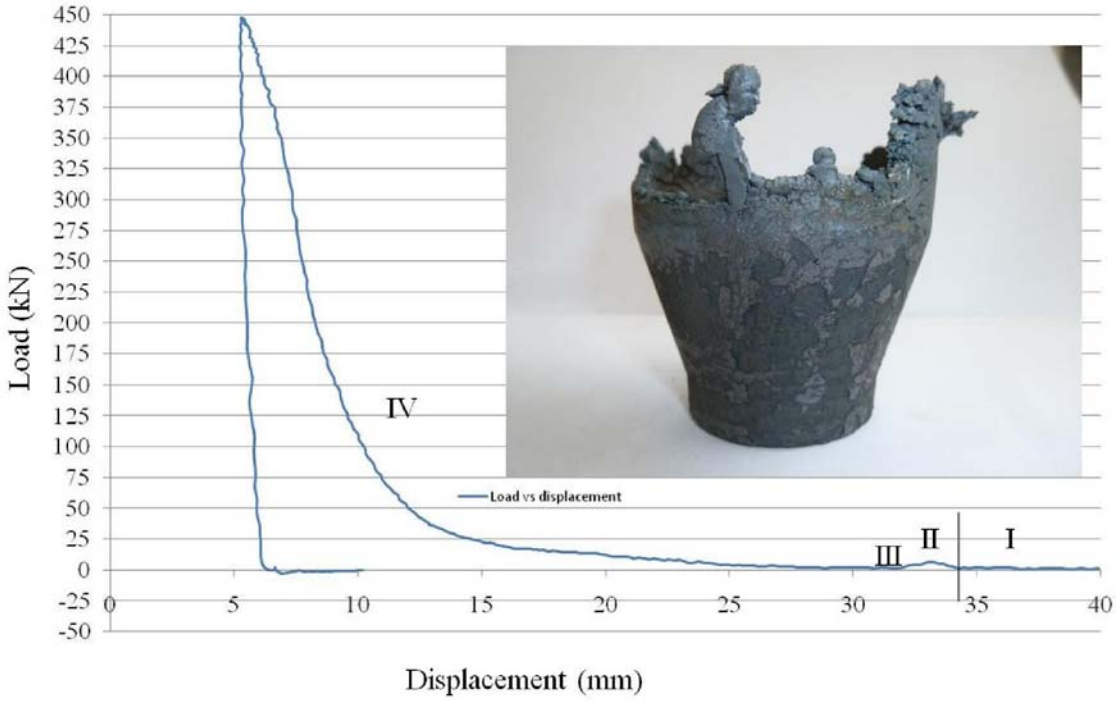

Fig. 4.12. Courbe effort – déplacement au cours du thixoforgeage.

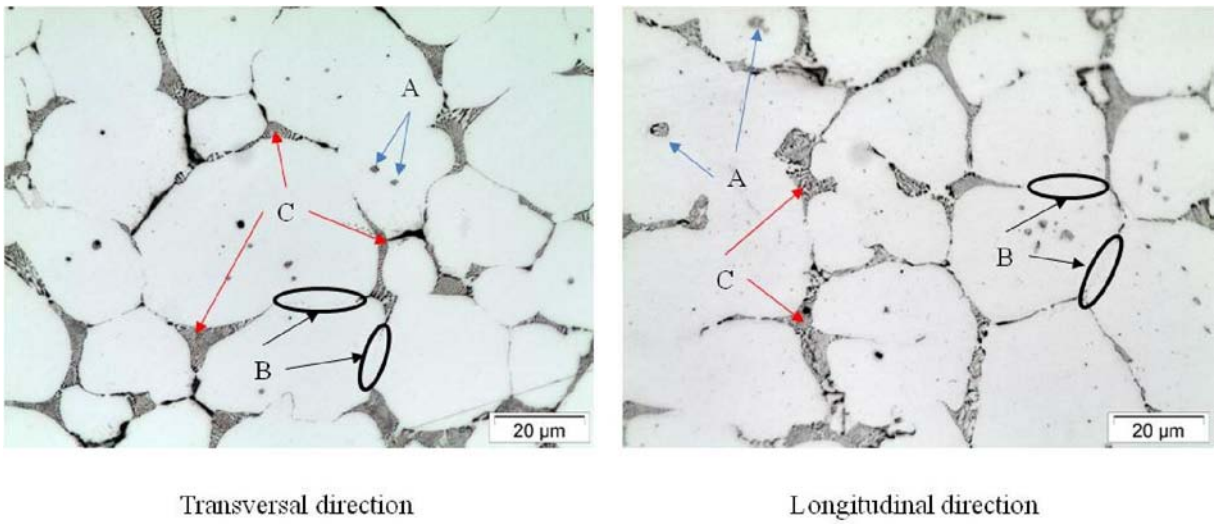

Fig. 4.13. Microstructures de l'acier M2 trempé depuis 1320°C (révélé par le réactif de Groesbeck). Zones A : liquide piégé, Zone B : joint de grain et C : liquide intergranulaire.

1.2.2. Influence de la température du lopin sur l'effort de thixoforgeage

Comme montré sur la figure Fig. 4.15 le pic d'effort apparaît pour la même course quelle que soit la valeur de la température initiale. La hauteur du pic d'effort quant à lui décroît avec l'augmentation de la température. Ceci peut s'expliquer par l'augmentation de la fraction liquide avec la température et donc la réduction des interconnections entre grains. L'effort obtenu dans la partie (III) est du même ordre de grandeur. Dans cette partie les grains sont entourés de liquide et le matériau a acquis un comportement thixotrope. Dans la partie (IV) de la courbe, l'augmentation de l'effort est d'autant plus rapide que la température est basse. L'augmentation de l'effort provient sans doute à la fois de l'augmentation de la surface lors de la formation des parois de la 'cup' et de l'écrasement de la partie basse du lopin qui par un effet de ségrégation voit sa fraction liquide diminuer. Ce phénomène est d'autant plus rapide que la fraction liquide initiale est faible, c'est-à-dire, que la température est basse.

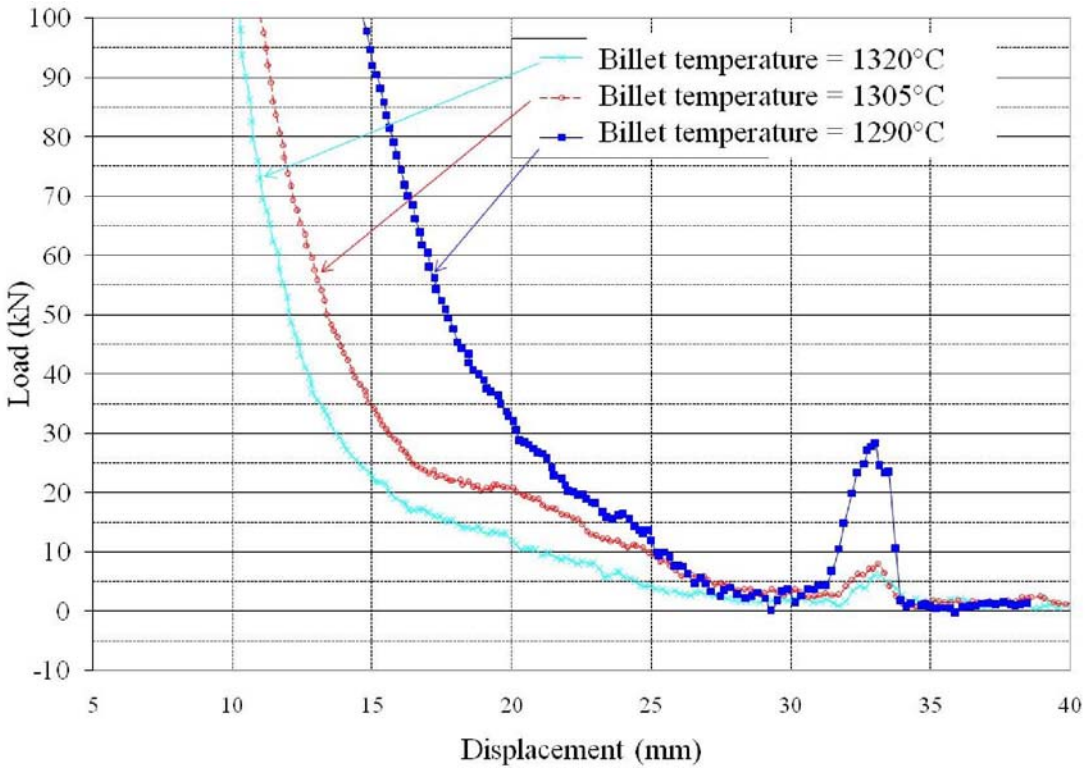

Fig. 4.15. Courbe effort déplacement pour différentes températures de lopin.

1.1.3. Influence de la température des outillages sur l'effort de mise en forme

La figure Fig. 4.17 illustre le fait qu'aucune différence d'effort significative n'a été observée en faisant varier la température de l'outillage. Ceci confirme la faible influence de la température de l'outillage constatée lors de l'étude de la forme des pièces.

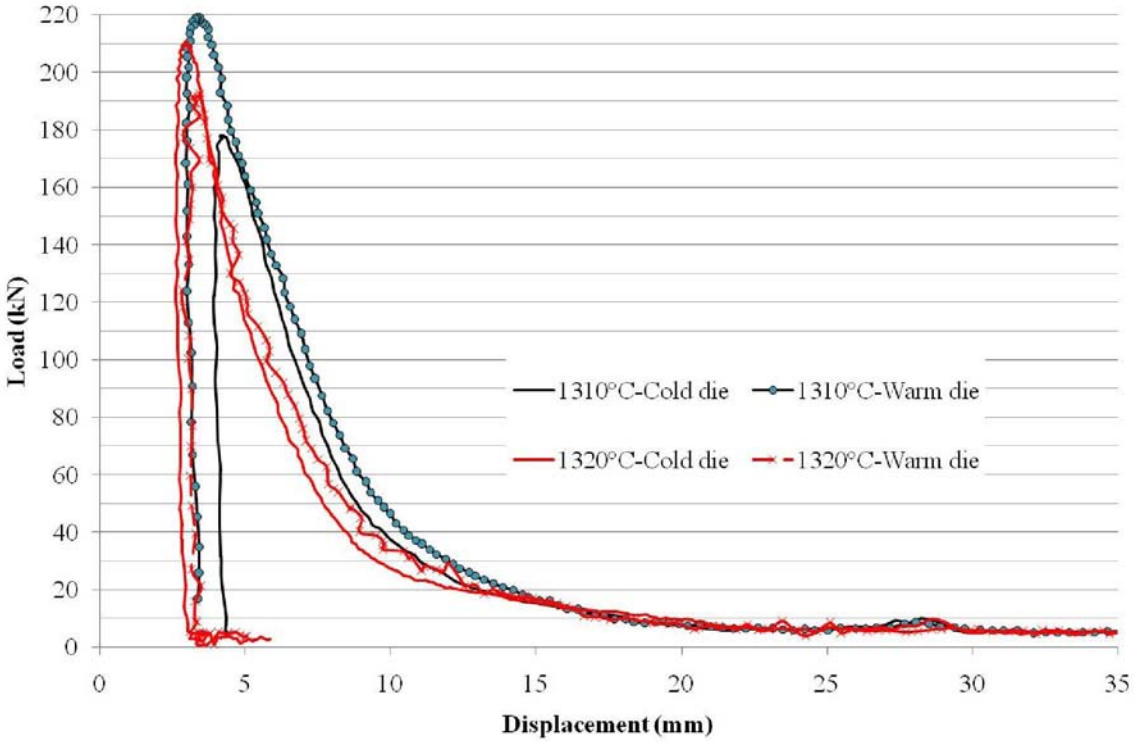

Fig. 4.17. Courbe effort déplacement pour différentes températures d'outillage.

1.3. Observations macro et microscopiques

Dans un premier temps, des observations macroscopiques des pièces thixoforgées ont été effectuées. Trois type de zones ont été observés (voir figure Fig. 4.18). Des zones à écoulement très faible (Zone A), des zones présentant des écoulements du type de ceux observés en forgeage à chaud (zone B) et des zones où l'écoulement est semi-solide (zone C). De même, deux types de fissuration sont observés. Des fissures se produisant très probablement au cours de la trempe de la pièce après thixoforgeage et des fissures apparaissant au cours de la mise en forme. Ces différents types de fissures sont observables sur la figure Fig. 4.19.

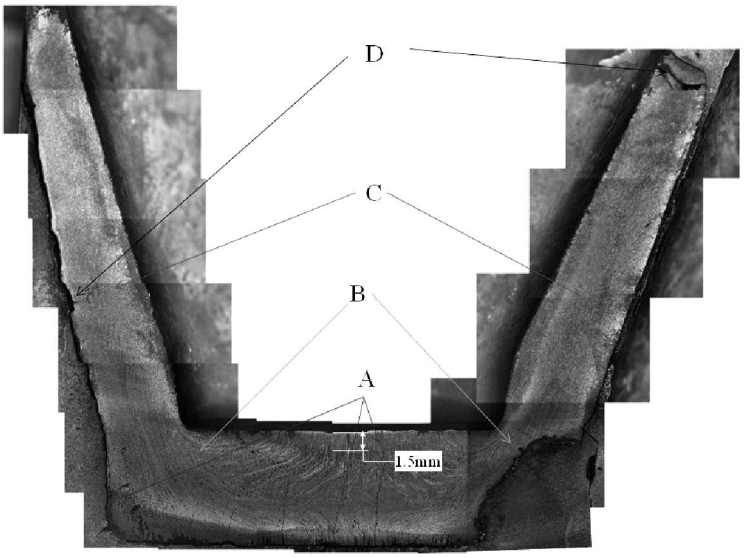

Fig. 4.18. Macrographie d'une cup thixoforgée (et trempée) (A) Zone non déformée, (B) zone forgée à chaud, (C) zone semi-solide et (D) défaut.

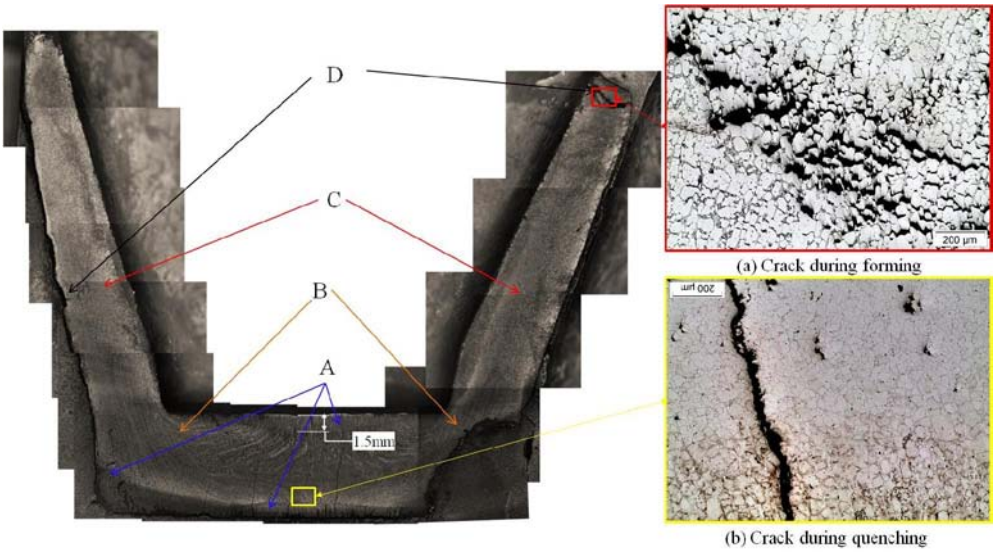

Fig. 4.19. Fissures dans une cup thixoforgée.

Des porosités peuvent également être observées dans toutes les pièces thixoforgées, principalement dans la zone plastifiée à l'état solide dans la partie inférieure de la 'cup'. Les figures Fig. 4.20 (a) et (b) présentent la zone à fort taux de porosité. Ce phénomène pourrait s'expliquer par la relative faible fraction de liquide dans cette zone pendant la mise en forme du fait de la baisse de température liée aux échanges avec les outils. La faible quantité de liquide pourrait lors de la solidification provoquer des micro-retassures du fait de la non interconnexion entre les zones liquides.

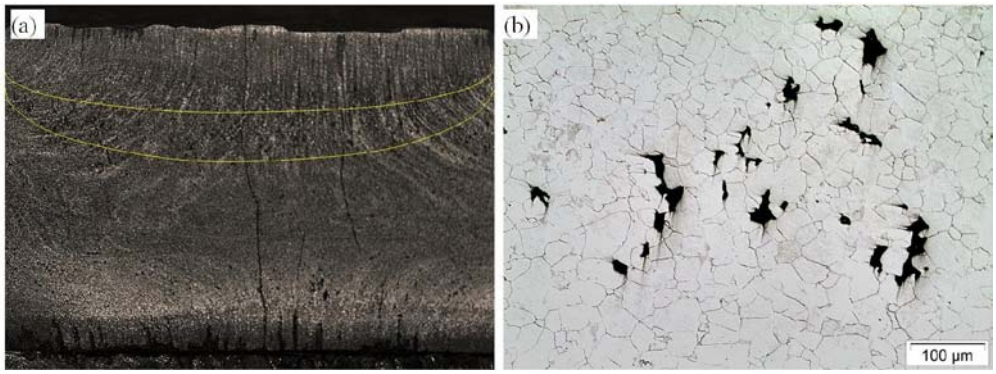

Fig. 4.20. (a) Zone à défauts internes dans les cups thixoforgées, (b) Micrographie optique des porosités.

1.3.1. La fraction de porosité.

Fig. 4.21donne les résultats concernant les mesures de porosité en différents endroits de la pièce. D'après ces résultats, on peut voir que les porosités sont principalement concentrées dans la bande observée sur la figure 4.20 (a). Cependant, des porosités sont également observables dans les autres zones de la pièce. La quantité de porosité semble diminuer avec la température du lopin. La plus grande quantité de liquide permettrait son meilleur drainage et résulterait en une diminution des porosités.

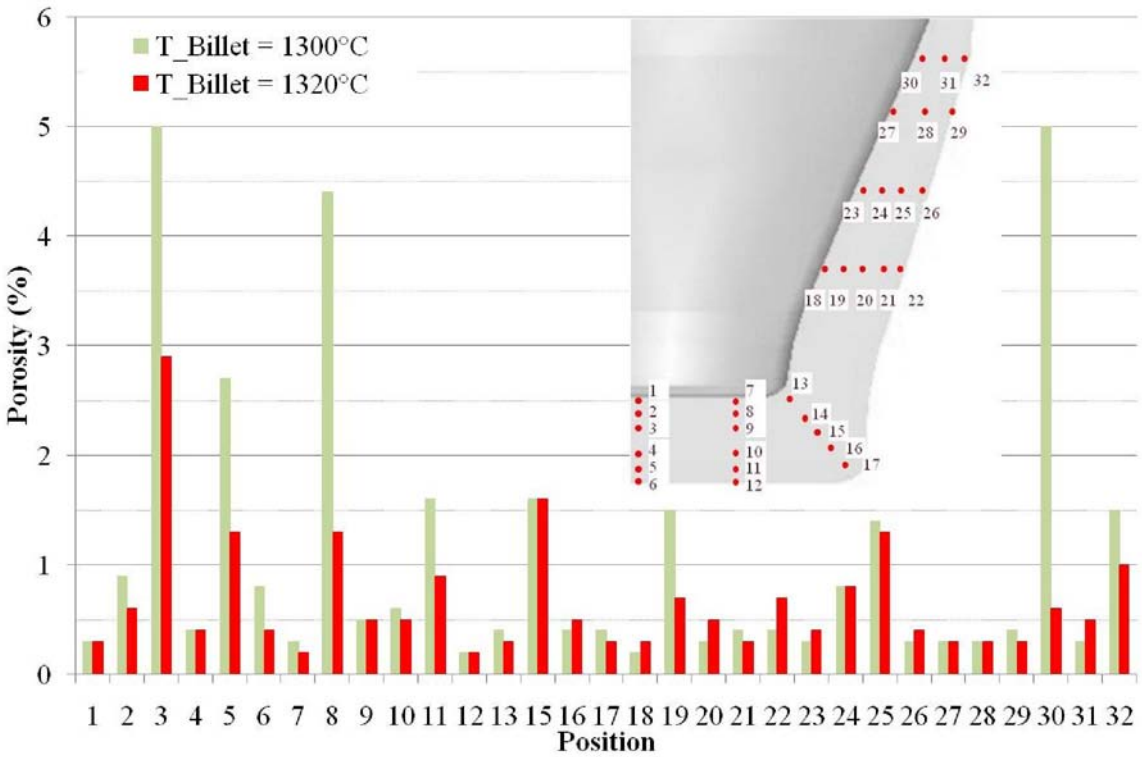

Fig. 4.21. Distribution des porosités dans des cups thixoforgées à différentes températures.

Le tableau. 4.5illustre par des micrographies dans les différentes zones, les porosités observées. Le principal résultat est que le niveau de porosité dans la zone de déformation solide plastique est plus important que dans la zone d'écoulement semi-solide. La taille moyenne des porosités est de l'ordre de 50µm. Les taux de porosité peuvent sans doute être réduits en maintenant un pression en fin de mise en forme durant la solidification comme stipulé pour les alliages d'aluminium [6]. Ceci reste toutefois à être validé dans le cas des aciers.

Table. 4.5. Structure des pièces trempées après thixoforgeage.

zones	T-billet = 1300°C	T-billet = 1320°C
3		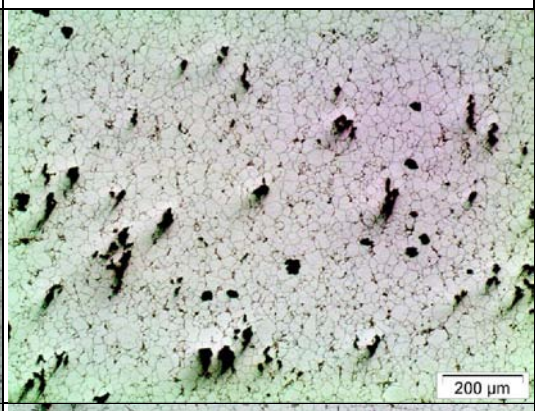
8	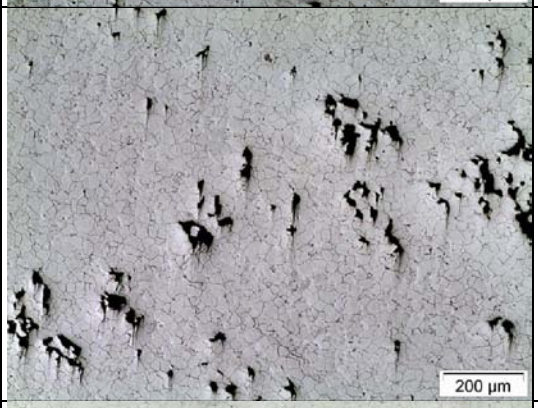	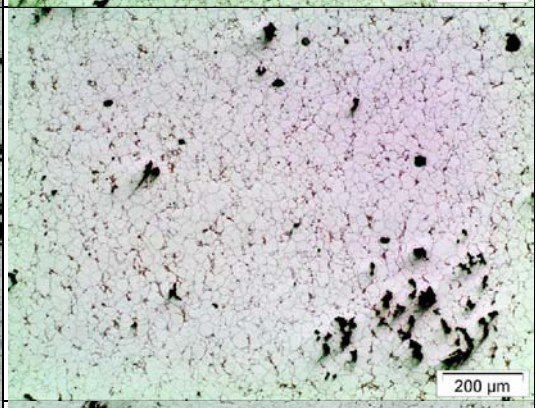
15		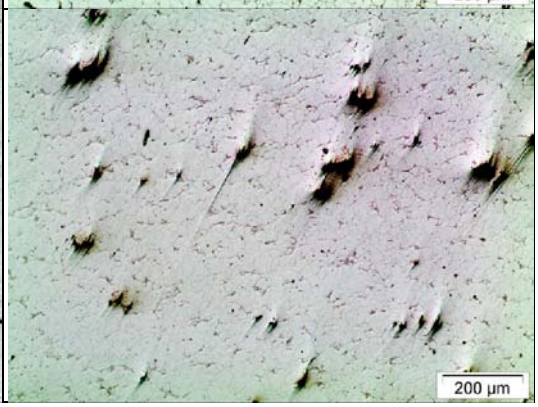

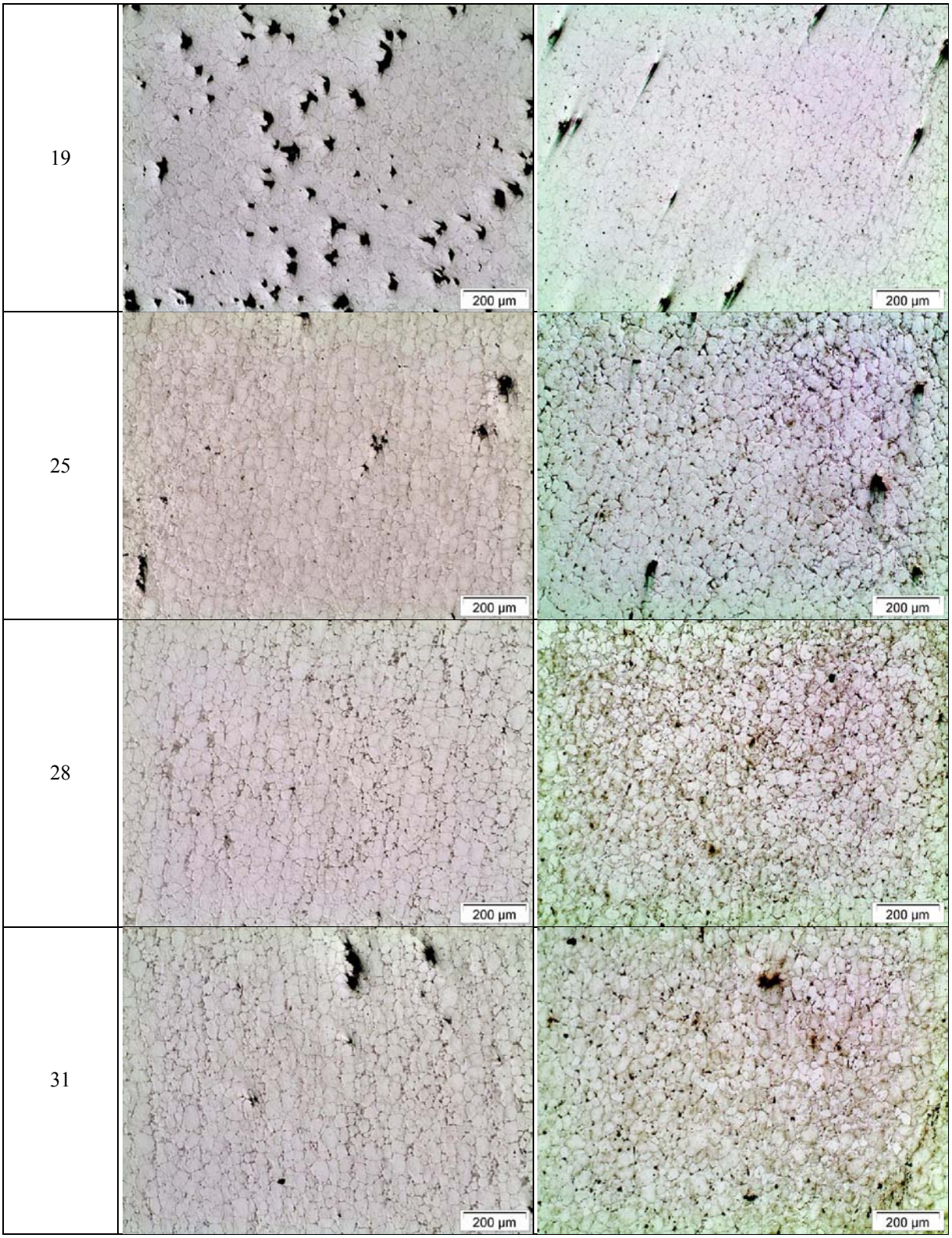

1.3.2. Caractérisation de la microstructure des pièces thixoforgées

Fig. 4.22illustre par des micrographies les microstructures obtenues dans les différentes zones de la pièce trempée après thixoforgeage. Là aussi, on observe trois types de zone de

déformation : zone à déformation nulle, zone de déformation plastique de type solide et zone de déformation thixotropique semi-solide. Selon la structure initiale du lopin et les conditions opératoires, la morphologie de la microstructure varie en termes de taille de grain et de facteur de forme.

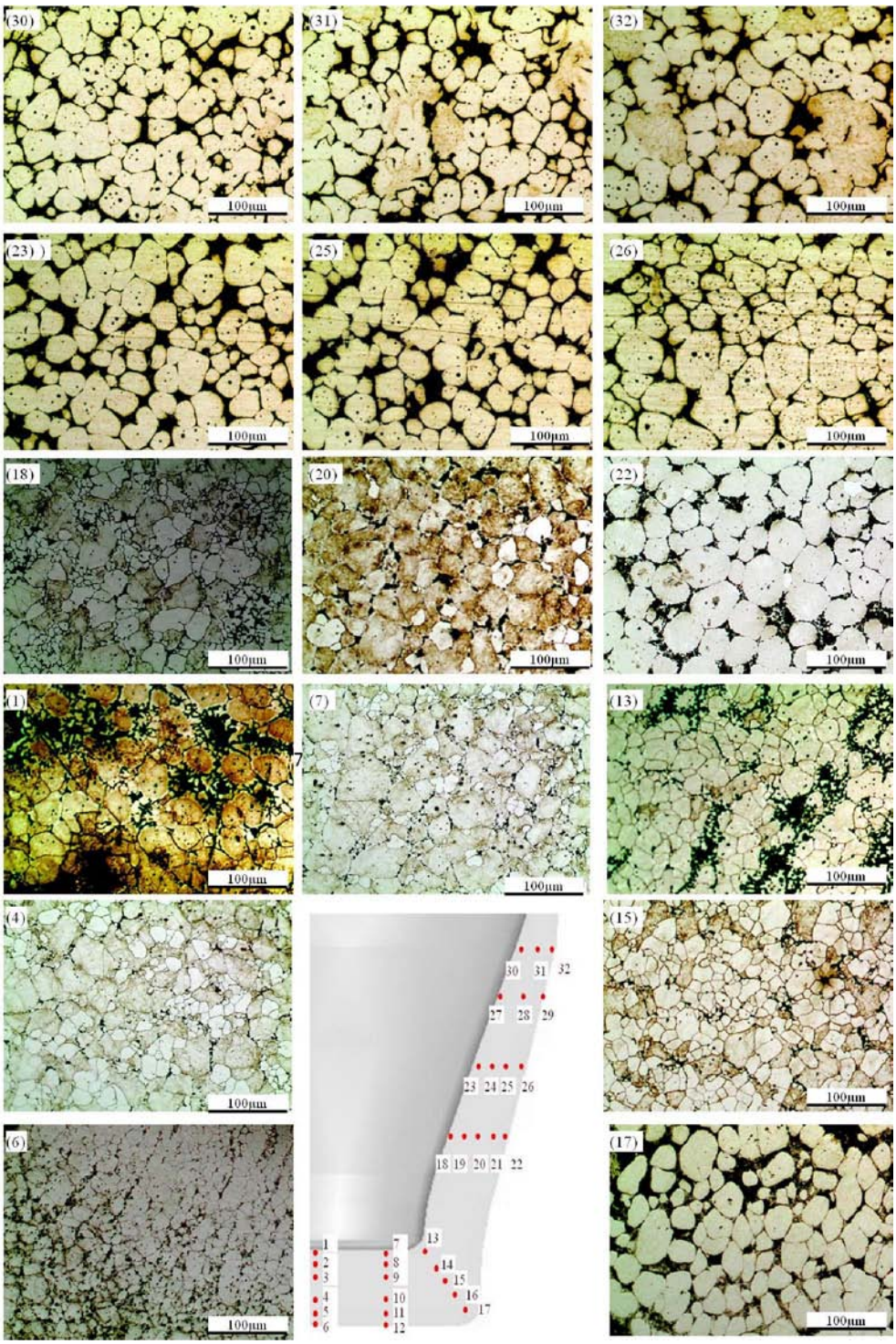

Fig. 4.22. Microstructures dans les différentes zones d'une cup thixoforgée (T lopin= 1320°C).

Par métallographie quantitative, la fraction liquide dans les différentes zones a été mesurée. Fig. 4.25 montre la variation de fraction liquide dans une cup thixoforgée à partir d'un lopin à 1320°C. On peut noter que la fraction liquide descend à 14% dans la zone à déformation plastique solide. A l'extrémité des parois, elle est maximum et atteint environ 27%.

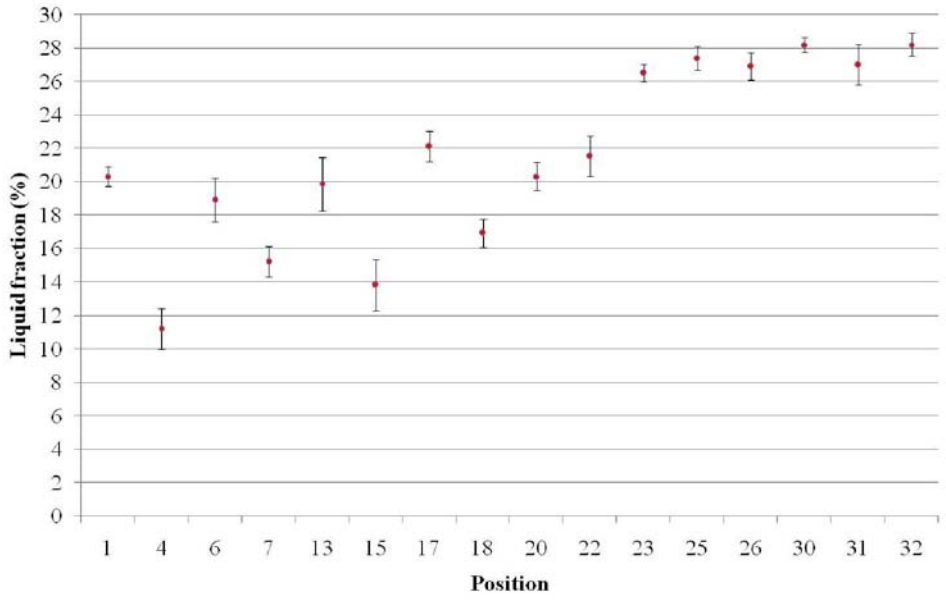

Fig. 4.25. Fraction liquide en fonction de la position dans la cup thixoforgée (T lopin= 1320°C).

Les résultats concernant la microstructure et la fraction liquide mettent en évidence la présence de ségrégation de liquide dans la pièce. De plus, cette étude fait apparaître la coexistence de différents mécanismes de déformation au cours de la mise en forme. Cinq mécanismes sont proposés :

(1) Rupture du squelette solide

(2) Ecoulement liquide

(3) Ecoulement de liquide contenant des particules solides

(4) Glissement entre particules solides

(5) Déformation plastique solide des grains

Au début de la mise en forme, le principal mécanisme de déformation correspond à la rupture du squelette solide (structure constituée des particules solides interconnectées). Ensuite, en fonction de la fraction liquide les différents mécanismes peuvent être actifs. Après la rupture du squelette solide, les grains solides disjoints se retrouvent entourés de liquide,

l'ensemble se comportant comme un liquide contenant des particules solides. Dans la partie centrale de la pièce, la fraction liquide diminue par l'effet d' « essorage » jusqu'à ce que les particules solides entrent en contact les unes avec les autres. Les mécanismes de déformation sont alors la déformation plastique solide des grains ou l'écoulement fluide avec de fortes interactions entre les grains. Dans les parois, la fraction de liquide demeure importante du fait de l'essorage, l'écoulement est de type fluide durant toute la mise en forme.

A l'augmentation de la température correspond une augmentation de la fraction liquide ; L'augmentation de la température du lopin contribue donc à repousser l'apparition des mécanismes de déformation solide plus tard lors de la mise en forme. Ceci est illustré par la figure Fig. 4.15.

2. Thixoforgeage des autres nuances d'acier (100Cr6 et C38LTT)

Des essais de thixoforgeage ont également été menés sur les deux aciers faiblement allies 100Cr6 et C38LTT. Comme indiqué par nombre de chercheurs [3, 7-12], les paramètres opératoires comme la vitesse de mise en forme, la température du lopin ou la température des outils ont une influence majeure sur les écoulements et les efforts de mise en forme. Particulièrement, les échanges thermiques entre la matière et l'outil influence l'écoulement de la matière et ont une incidence sur les propriétés mécaniques locales. Dans ce travail nous nous sommes intéressés principalement sur les propriétés mécaniques et les microstructures des pièces thixoforgées.

2.1. Résultats et conclusions

Il n'est pas possible d'observer la microstructure du matériau à l'état semi-solide par trempe pour les deux nuances d'acier testées. Les vitesses de refroidissement accessibles ainsi que la métallurgie des deux aciers ne permettent pas de figer la structure semi-solide au cours d'une trempe. Contrairement à l'acier M2, le début de la fusion des aciers 100Cr6 et C38LTT ne correspond pas à la fusion de carbure d'éléments d'alliage.

Les essais de thixo-extrusion effectués sur l'acier 100Cr6 ont mis en évidence l'hétérogénéité des écoulements. Trois zones sont observées : la première pour laquelle la déformation est faible, une deuxième où la déformation est du type de celle rencontrée en forgeage à chaud et une troisième zone à écoulement semi-solide.

La présence de ces trois zones peut être expliquée en partie par les phénomènes d'échange thermique.

- Zone de déformation du type forgeage à chaud. Au cours de la mise en forme, à l'interface entre le lopin et l'outil et le lopin et l'air, le matériau est refroidi sortant ainsi de l'état semi-solide. Cette zone subit donc une déformation du type de celle de forgeage à chaud.
- La zone de déformation faible. Du fait du refroidissement au contact des outils et de l'effet du frottement, des volumes « morts » apparaissent au cours de l'écoulement.
- La zone de déformation semi-solide. La matière « loin » de la surface du lopin et/ou située dans les zones de déformation demeurent à l'état semi-solide tout au long de la déformation.

Les essais menés sur le thixoforgeage de l'acier C38LTT (projet thixofranc) ont montré:

- la possibilité de réaliser par thixoforgeage des pièces en acier de forme complexe en une seule opération ;
- que des phénomènes de fissuration à chaud peuvent apparaître lorsque la température de mise en forme dépasse une valeur critique ;
- que l'écoulement est hétérogène du fait des effets combinés des échanges thermiques et de la déformation. Cet effet a été mis en évidence également lors du thixoforgeage des aciers M2 et 100Cr6.

L'écoulement est fortement influencé par les sources d'hétérogénéité de la température que sont les échanges thermiques et la dissipation visco-plastique. Dans les parties étroites des pièces, la puissance dissipée par frottement et par la déformation plastique peuvent conduire à une augmentation de la température conduisant elle-même à une augmentation significative de la fraction liquide. A cette évolution de la structure liquide solide du matériau est associée une chute de la contrainte d'écoulement. Ce phénomène d'adoucissement peut expliquer la capacité du thixoforgeage au remplissage de zone étroites et donc à la mise en forme de pièce complexe.

Conclusion générale

L'objectif de cette thèse était la caractérisation de la microstructure du matériau à chaque étape du processus de thixoforgeage afin de mieux comprendre l'influence des paramètres du procédé et d'identifier et caractériser les mécanismes de déformation présents au cours de la mise en forme. L'approche employée est divisée en deux parties. La première se focalise sur la caractérisation de la microstructure à l'état semi solide en utilisant plusieurs techniques. Dans la seconde partie, la caractérisation concerne la microstructure et les écoulements de matière dans les pièces thixoforgées obtenues sous différentes conditions opératoires.

La synthèse bibliographique a fait l'objet du chapitre 1. Dans un premier temps, le principe des différents procédés de mise en forme des semi-solide a été décrit en précisant leurs avantages. Ensuite, les mécanismes conduisant au comportement thixotrope ont été décrit. Des applications industrielles ont été présentées. Il a été montré, au travers de l'étude bibliographique, que la morphologie de la structure liquide-solide générée par les processus de mise en forme a un effet fondamental sur l'écoulement de la matière et les propriétés de la pièce obtenue. Il est donc nécessaire d'étudier l'évolution de la microstructure du matériau au cours du processus complet de thixoforgeage (état de livraison, étape de chauffe, étape de mise en forme, …). La première étape du travail consiste alors à caractériser la microstructure du matériau, plus particulièrement, la fraction de liquide, la taille de grain, le facteur de forme, etc.

Le chapitre 2 présente les matériaux étudiés et les différentes techniques utilisées pour la caractérisation de la microstructure depuis les techniques les plus conventionnelles jusqu'aux techniques nouvelles. Le principe, les avantages et les limites de chaque technique ont été étudiés expérimentalement. Le dispositif de thixoforgeage est également présenté de façon détaillée dans ce chapitre.

Les résultats expérimentaux ont principalement été présentés dans les chapitres 3 et 4.

Le chapitre 3 est essentiellement consacré à la caractérisation microstructurale à l'état semi-solide. Des lopins sont portés à la température semi-solide par chauffage par induction. Une microstructure constituée de particules solides sphériques peut être obtenue directement par chauffage inductif de la barre de M2 formée à chaud. Ceci laisse à penser que l'acier M2 dans cet état de livraison peut être thixoforgé directement. Des cycles de chauffe avec plusieurs stades ont été utilisés pour obtenir des champs de température homogène dans le

lopin. Il est suggéré qu'une structure plus adaptée au thixoforgeage peut être obtenue par un chauffage jusqu'à l'état solide le rapide possible suivi d'un chauffage lent jusqu'à la température visée. Un maintien prolongé peut améliorer le facteur de forme des particules solides obtenues mais na à l'encontre des contraintes de productivité industrielle. L'évolution de la fraction liquide en fonction de la température a été déterminée par différentes techniques donnant des résultats approchés. Le logiciel Thermo-Calc peut être utilisé pour prédire la variation de fraction liquide en fonction de la température. La DSC est une méthode intéressante pour l'évaluation de la fraction liquide mais ne permet pas de caractériser plus avant la microstructure. La métallographie quantitative sur les microstructures obtenues après trempe depuis l'état semi-solide permet l'obtention d'information quantitative concernant la microstructure solide liquide. La vitesse de diffusion des éléments d'alliage dépend du matériau. Pour un matériau avec peu d'éléments d'alliage (C38LTT ou 100Cr6 par exemple), il sera difficile voire impossible d'évaluer la fraction de liquide et de révéler la microstructure à l'état semi-solide par analyse d'image du matériau trempé depuis l'état semi-solide. De plus, les méthodes métallographiques ne peuvent donner que des informations 2D de la microstructure. La microtomographie aux rayons X peut donner des informations en 3D. Le contraste des images obtenues dépend de la composition chimique du matériau étudié ; si celui-ci contient des éléments chimiques lourds, un bon contraste peut être obtenu comme dans le cas de l'acier M2. Par contre, quand l'alliage ne contient pas d'éléments lourds, comme dans le cas des aciers faiblement alliés, la microstructure du matériau ne peut être obtenue par cette technique. La microtomographie aux rayons X a toutefois permit de réaliser des observations in-situ à haute température. Les résultats obtenus par la méthode de métallographique quantitative et la microtomographie sur l'acier M2 coïncident. En conséquence, lorsque la vitesse de refroidissement est suffisamment élevée pour préserver la microstructure de l'état semi-solide, la méthode de métallographie quantitative est une solution pour l'estimation de la fraction liquide et l'observation de la structure liquide solide. Ceci est important dans la mesure où même si la microtomographie est un outil puissant elle n'est pas facile à mettre en œuvre et n'est pas aussi répandue que la microscopie électronique à balayage et la techniques EDS. Pour les alliages difficiles à caractériser par trempe depuis l'état semi solide, quelle que soit la technique utilisée, il est possible d'envisager l'utilisation de la CLSM qui permet des observations in-situ à l'état semi-solide.

Les résultats des expériences de thixoforgeage sont détaillés et discutés dans le chapitre 4. Les expériences ont été réalisées pour étudier l'influence des paramètres du procédé sur la

microstructure et la géométrie finale des pièces, l'effort de mise en forme en fonction du déplacement, les écoulements de matière… Les mécanismes de déformation ont été observés. Ils peuvent être décomposés en 5 étapes majeures : rupture de la structure liquide solide interconnectée (squelette solide) ; écoulement liquide ; écoulement liquide incorporant des particules solides ; glissement des particules solides les unes sur les autres et déformation plastique des particules solides. Les deux derniers mécanismes sont prépondérants lorsque la fraction liquide diminue fortement. Deux phénomènes distinguant le thixoforgeage du forgeage à chaud ont été observés, la ségrégation de liquide et l'hétérogénéisation de l'écoulement de la matière. Le premier est lié aux mécanismes de déformation mentionnés ci-dessus. Cela peut conduire à une hétérogénéisation de la fraction liquide au cours de la mise en forme et ainsi à une hétérogénéisation de la composition chimique de la pièce thixoforgée. Les gradients thermiques inévitables dans la pièce en cours de mise en forme sont sources d'hétérogénéité de la fraction liquide et de la contrainte d'écoulement associée. Ces gradients sont dus aux échanges thermiques avec les outils et à l'énergie dissipée dans l'écoulement. La fraction de liquide maximum est obtenue « loin » des contacts avec les outils et dans les zones avec la plus grande déformation et vitesse de déformation. Ce phénomène peut conduire à la concentration de l'écoulement plastique dans des bandes ou des zones comme il a été observé dans tous les cas étudiés dans le chapitre 4. Ce phénomène peut être un avantage du thixoforgeage quand il s'agit de remplir les parties étroites d'une pièce.

Perspectives

- **Développement de plugins pour l'analyse d'images 3D**

Les travaux ont montré jusqu'ici la possibilité d'utilisation de nouvelles techniques de caractérisation des microstructures notamment lorsque des caractéristiques microstructurales en 3D sont nécessaires. Toutefois, l'analyse 3D d'images est très consommatrice de temps. Il est donc nécessaire de développer des plugins permettant le traitement automatique ou semi-automatique des images.

- **Vers l'industrialisation du thixoforgeage des aciers**

L'industrialisation du thixoforgeage nécessite de fournir à l'industrie une méthodologie pour la conception du processus complet de thixoforgeage incluant la conception des outillages, le choix du système et des paramètres de chauffage, la détermination des paramètres de conduite du thixoforgeage. L'intégration du thixoforgeage dans un processus

complet d'industrialisation comprend également le choix du matériau de la pièce et de son habillage.

La méthodologie d'industrialisation du thixoforgeage fait intervenir nécessairement la simulation. Pour cela, les modèles régissant les échanges thermiques et le comportement rhéologique du matériau doivent être suffisamment représentatif pour rendre compte des hétérogénéités apparaissant dans la pièce au cours de sa mise ne forme. De plus, le phénomène d'adoucissement important du matériau avec la montée en température et la vitesse de déformation rend difficile la convergence numérique des simulations du procédé. Le développement de la simulation numérique du thixoforgeage ne se restreint peut-être pas uniquement à obtenir des modèles plus fins mais également au développement d'algorithmes numériques intégrant, par exemple, des schémas de calcul explicites.

Les premiers résultats obtenus lors de cette thèse sont très encourageants et montrent clairement l'intérêt et le potentiel du thixoforgeage pour la réalisation de pièces en acier. Les développements futurs devront se concentrés sur les deux aspects complémentaires que sont, d'un côté, le développement de l'outil numérique pour la simulation du procédé et de l'autre côté, le développement de règles (ou méthode) de conception des outillages, le choix des nuances de matériaux des pièces et des paramètres de thixoforgeage à partir de la caractérisation des phénomènes mis en évidence et en s'aidant des techniques de caractérisation développées et éprouvées dans cette thèse.

Part II
English Version

General introduction

Economic and technological developments of recent decades have given rise to the needs of more demanding of the consumers in terms of safety, comfort, ergonomics, functionality and energy. In the aspect of materials, these requirements impose the development or improvement of new concepts and structures, especially to minimize energy consumption while optimizing mechanical properties and durability. In the aspect of manufacturing process, there is a growing demand for more efficient and economic processes to reduce production costs, increase productivity, reduce lead time and improve the product quality. Compared with casting and forging processes, the semi-solid material forming (SSM) is a new processing route, in which the process feature depends on the thixotropic structure of the feedstock, which is so called non-dendritic microstructure. The feasibility of two basic SSM processing routes, which are termed as 'rheo-route' and 'thixo-route' have been demonstrated by performing industrial trials. The rheo-route involves the preparation of an SSM slurry from liquid alloys and its transfer directly to a die or mold for component shaping. The thixo-route implies heating the solid material to the semi-solid temperature and shaping the semi-solid material into components. No matter which route employed for semi-solid forming, several advantages are obvious:

- Compared with conventional casting process, the mechanical properties of formed parts will be improved, since the porosities and shrinkage can be greatly reduced. Moreover, the process temperature is also significantly reduced which results in the prolonged tool life. Another advantage of semi-solid forming process is that less energy is required to heat the metal into the semi-solid rather than the liquid state in the casting operation.
- Compared with classical forging processes, parts with complex geometry can be obtained with less forming stages, as well as reduced forming force. In addition, the thixoformed lighter parts have good mechanical properties. Therefore, they can replace the steel components which are produced by conventional casting process.

Numerous different semi-solid forming processes have been developed. Various components of aluminium and magnesium have already been industrially produced. Apart from this, the semi-solid forming process of steel is still remaining in the research level due to many challenges, such as the higher process temperatures, the lack of understanding of the thermomechanical behaviour of materials in the given conditions, oxidation etc. Many researchers have investigated the steel semi-solid forming process, on both rheo-route and thixo-route.

Besides the selection and development of thixoformable materials, recent studies have shown that the material flow during the thixoforging process is different from that during conventional forging process. There is a significant influence of the thermal exchanges on the material flow and mechanical properties. The thixotropic effect and the thermal exchanges between the tool and the material can lead to an extremely heterogeneous macrostructure of the produced parts. The effects of process parameters have also been investigated. However, there are some scientific and technological issues that constitute an obstacle for the industrialization of the steel thixoforging process:

- Due to high process temperature, surface thermo-mechanical loadings on tools can lead to premature ageing or cracks.
- The behaviour of the semi-solid material is not controlled well enough yet.
- The influence of the forming process on microstructure and mechanical properties of thixoforged parts remains unknown.

This study mainly focuses on the last issue. Since the microstructures are at the center of materials science and engineering. They are the strategic link between materials processing and materials behaviour. Microstructure control is therefore essential for any processing activity. In order to study this issue, various experiments have been performed in various laboratories and facilities including LCFC (Laboratoire de Conception, Fabrication Commande), LEM3 (Laboratoire d'Etude des Microstructures et de Mécanique des Matériaux) and ESRF (European Synchrotron Radiation Facility)

The objective of this thesis is to characterize the microstructure of the material at each thixoforging stage in order to better understand the influence of the forming process and the mechanisms of deformation during each step. We mainly focus on the microstructure of the material in the semi-solid state, especially the liquid fraction and its evolution during the whole thixoforging process. Various techniques have been then used on three main steel grades for 3D characterization and in situ microstructure observations.

The second goal is to investigate the material flow which is affected by the process parameters and microstructure, based on the microstructure observations and the results obtained during the thixoforging process. The mechanisms of microstructure evolution and material flow involved in the deformation will be discussed especially for future modelling

development in order to better simulate and predict all the mechanisms occurring during the thixoforging process and optimize it.

Chapter 1 presents a summary of knowledge in the field of semi-solid materials. A general overview of the worldwide scientific achievements of this technology is presented in this chapter which consists of four parts: rheology, technological development, material aspects and industrial applications. This chapter will highlight the important aspects of microstructure of the material in the semi-solid state with a view to a more detailed analysis of the microstructure.

Chapter 2 presents the experimental work carried out during this thesis on three main steel grades: C38LTT, 100Cr6 and M2. The methods and techniques for microstructure characterization are illustrated and their principles are explained. Various experimental devices for thixoforging process (press, induction coil and die tools) are also presented. The experimental trials should allow highlighting the influence of various parameters, such as billet and tool temperatures, on microstructure.

Chapter 3 describes and discusses the results of the experiments for studying the microstructure evolution during heating to the semi-solid state. The microstructure in the semi-solid state has been analyzed and characterized using different techniques. If most of them are widely used, two of them are particularly new and promising for this kind of applications: high energy 3D X-ray microtomography and Confocal Laser Scanning Microscope (CLSM) in situ microstructure observations under different conditions. These parameters of the morphology in the semi-solid state are important for thixoforging process since they have an effect on the rheology of the material and therefore on the mechanical properties of the thixoforged parts.

The results of the thixoforging experiments are presented in the last chapter. The influence of the temperature of the billet on the forming load and the material flow are studied and discussed. The liquid distribution in the thixoforged parts is also investigated in order to study its influence on the final shape of the parts.

Finally, a general conclusion will synthesize the knowledge on steels in the semi-solid state in terms of microstructure and material flows for scientific research and industrial applications.

Chapter 1. Bibliography of semi-solid processing

Table of contents

1. Introduction……141

2. Semi-solid processing……142

2.1 Semi-solid processing routes ……144

2.2 Different slurry or billet preparation routes……145

2.3 Advantages of semi-solid processing……149

3. Rheology of semi-solid materials……150

3.1 Behavior of alloys at low solid fractions……151

3.2 Behavior of alloys at high solid fractions……157

4. Microstructure evolution during material preparation and forming process……161

4.1 Microstructure characterization……161

4.2 Influence of slurry preparation conditions on morphology……169

5. Alloy development for SSM processing ……178

5.1 Different technologies for SSM……178

5.2 Influence of manufacturing process on materials……180

6. Industrial applications of SSM……181

7. Conclusions……185

References……186

1. Introduction

In general, the success of a semi-solid forming process is measured by the ability to produce defect free products which result from various conditions, such as rheological behavior and material flow during forming. These conditions depend not only on the forming parameters but also on the microstructure of the material in the semi-solid state. Many parameters such as forming speed, die and billet temperature are well-known for having a great influence on the thixoforging process. They can mainly modify the thermal exchanges between billet and die which in turn affects the microstructure: liquid fraction, its distribution, viscosity and its consistency etc, therefore affects the mechanical properties of the parts [1, 2].

It has been known that the flow behavior of a fixed material in the semi-solid state depends on the volume fraction of liquid phase, size, shape and the distribution of grains. In addition, the microstructure in the semi-solid state depends on the material, its manufacture process, the thermal history and the heating method such as heating rate, holding time etc.

Fig. 1.1 illustrates the typical thixoforging route. First, the billet is machined from bars, which are obtained by different manufacturing processes. After heating up to the desired temperature, the billet is transferred to a press and is thixoforged with various process parameters.

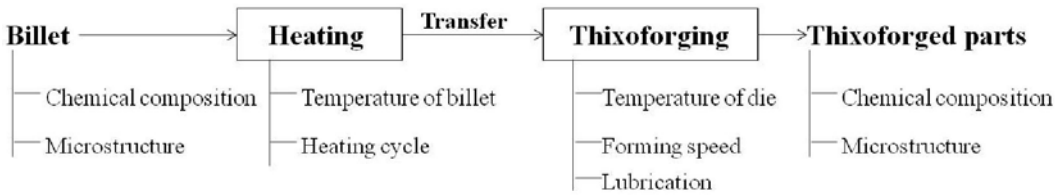

Fig. 1.1. Typical thixoforging route.

However, the influence of the forming process on the microstructure and the mechanical properties of the thixoforged parts are still not fully understood due to the complexity of the microstructure and the rheology of materials with such a unique microstructure. The objectives of this study are to gain a thorough grasp of the evolution of the microstructure during the entire thixoforging process.

- The microstructure evolution during heating from the as-received state to the semi-solid state.

- The microstructure evolution during thixoforging process and the influence of the parameters on the microstructure.
- The final microstructure and the mechanical properties of the thixoforged parts.

In order to reach the goal of this work, it is important to characterize microstructures at different stages. The worldwide achievements of the semi-solid forming technology are reviewed in this chapter which consists of four parts dealing with rheology, technological development, material aspects and industrial applications.

2. Semi-solid processing

Semi-solid forming (SSF) is a near net-shape forming process in which the metallic alloys are processed in the semi-solid state to produce complex parts with high mechanical properties, usually in a one-step process. Fig. 1.2 illustrates the typical temperatures of applicability in binary phase diagram for casting, semi-solid processing and forging, respectively. The microstructure for the semi-solid forming process is also presented in the figure. As is shown in the micrograph in Fig. 1.2, the microstructure of the material for semi-solid forming process consists of the non-dendrite solid grains which are surrounded by liquid phase.

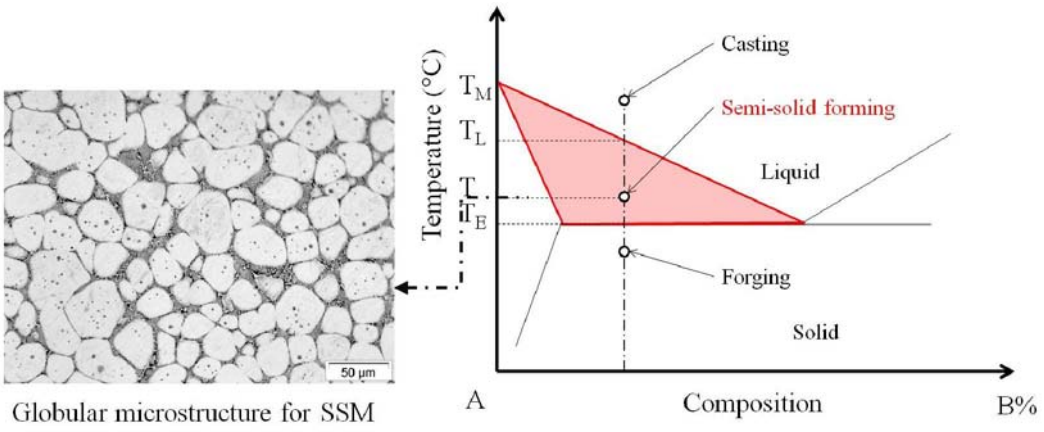

Fig. 1.2. Typical temperatures of applicability in binary phase diagram for different forming processes.

It has been 40 years since the original experiment leading to the invention of the semi-solid metal forming was performed at MIT by David Spencer [3] as a part of his doctoral research. He discovered that the agitated semi-solid alloy exhibits a thixotropic behavior (Fig. 1.3) when studying the viscosity of partially solidified Sn-15% Pb alloys by a Couette viscometer.

The viscosity increases slowly at low solid fractions ($0 < \boldsymbol{Fl} < \sim 0.5$), while increases sharply at high solid fractions ($\boldsymbol{Fl} > \sim 0.5$). The researchers immediately recognized the importance of the discovery to the metal forming process. The agitated partially solidified slurries could be formed into shapes by classical casting processes or, at a higher fraction of solid, by forging processes [4]. Further research demonstrates that after the breakdown of the dendritic microstructure, the semi-solid metal slurry which contains a globular or non-dendritic structure exhibits the thixotropic behavior (Fig. 1.4). Fig. 1.4 (a) shows dendrite bending and fracture. The uniform distributed fine round grains are shown in Fig. 1.4 (b).

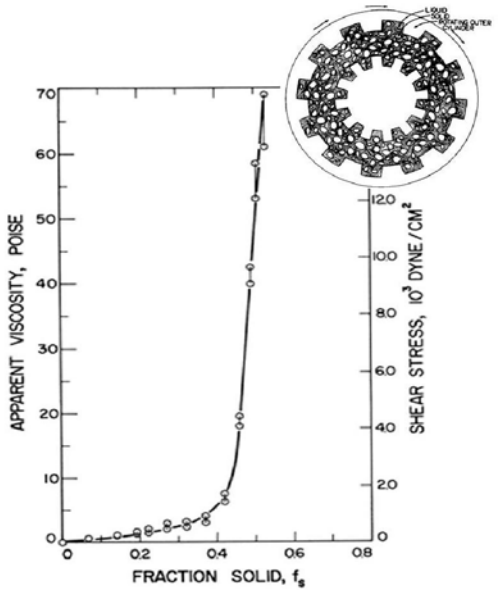

Fig. 1.3. Apparent viscosity versus solid fraction of Sn-15% Pb alloy sheared continuously and cooled at ~20°C/hour. Rotation speed 500rpm [4].

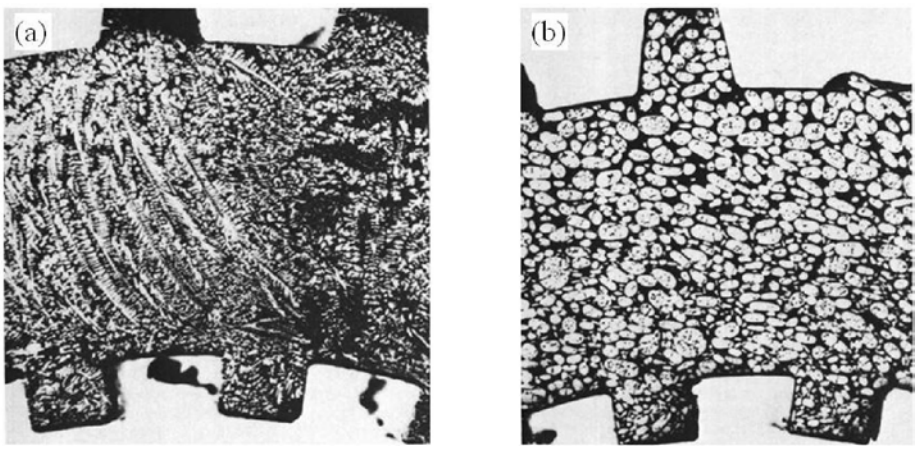

Fig. 1.4. Microstructures of Sn-15% Pb alloy in a Couette viscometer under different rotating conditions. (a) Sample cooled to 0.36 solid fraction before shearing. (b) Sample sheared continuously during cooling to 0.6 solid fraction and water quenched. Cooling rate ~20°C/hour. Rotation speed 500 rpm [4].

2.1 Semi-solid processing routes

Based on the unique rheological properties of semi-solid slurries resulting from the non-dendritic microstructures, the semi-solid metal forming process has been widely studied and partially succeeded in being applied to industrial productions.

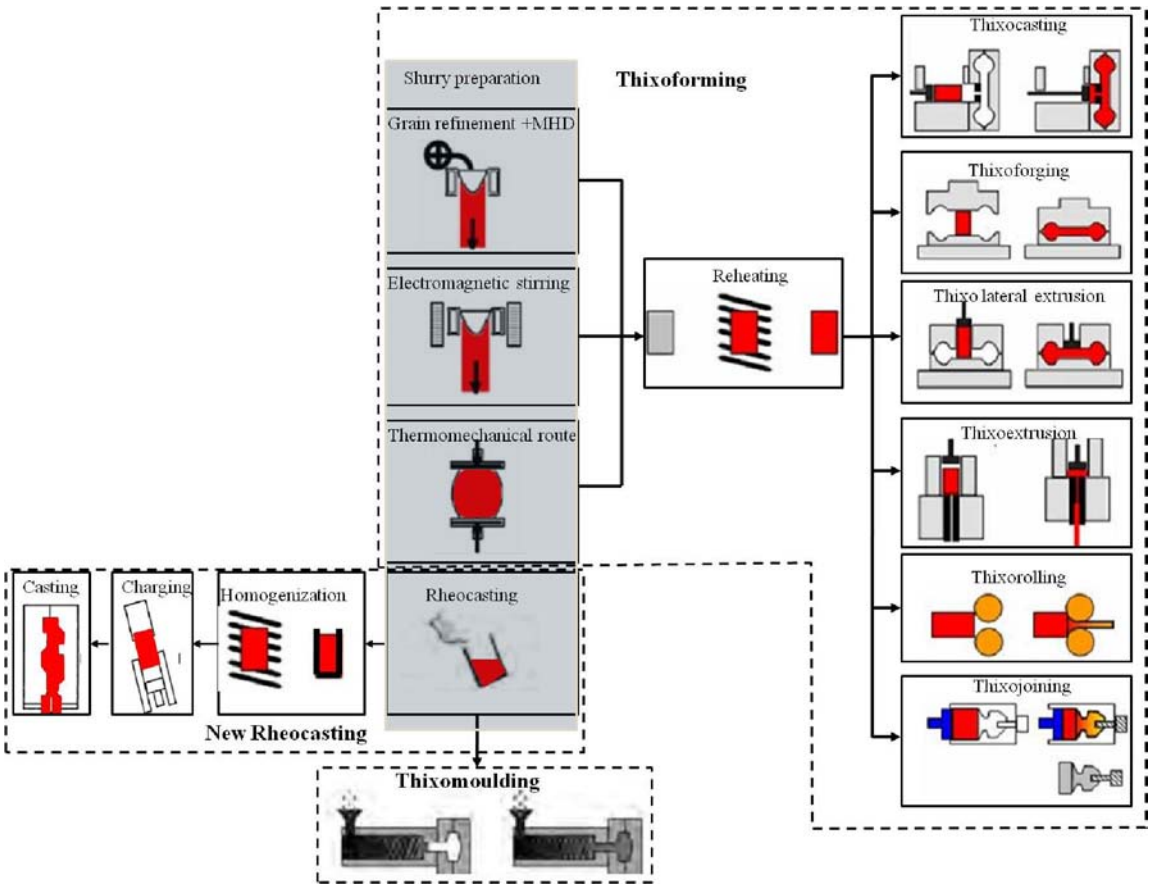

Fig. 1.5. Illustration of different SSM forming processes [1, 5].

Until now, a large number of specific process routes have been developed, most of which belong to the basic routes, termed as “thixo-route” and “rheo-route”. In brief, thixoforming begins with heating a solid material of a proper microstructure to the desired solid fraction and then form the material, while rheoforming involves the preparation of a non-denditic semi-solid slurry from liquid state and its injection into a mould to form/cast the products. Fig.1.5. illustrates various semi-solid forming routes.

Although each route has its own advantages [1, 6-9], it is still unclear which routes will be of the greatest long-term significance [10].

For each process, the slurry or billet should be in a homogeneous semi-solid state prior to the forming process. Depending on the slurry or billet preparation route, the semi-solid state can be obtained by reheating the material from solid state or by homogenizing and partially solidifying the liquid material to the semi-solid state. The well-prepared slurry or billet is then transferred to the mould or die for the forming process such as casting, forging, lateral extrusion and rolling.

2.2 Different slurry or billet preparation routes

Many rheology properties of semi-solid material depend on the globular microstructure, so that the preparation of the semi-solid slurry or billet is the key or main factor to the semi-solid forming process.

In order to obtain the desired microstructure for semi-solid forming process, various slurry or billet preparation approaches have been developed. After the first SSM slurry with a globular microstructure was prepared at MIT by mechanical stirring during solidification of the alloy, many other new slurry preparation methods have been developed, including the cooling slope, electromagnetic stirring, isothermal coarsening of solid dendritic materials, mixing of powders, passive mixing, electrical discharge through a semi-solid dendritic materials etc, almost all of which can be categorized in either dendrite breakdown technique or prohibiting the formation of dendrite technique. The obtained semi-solid material can be directly used in rheocasting or cooled to solid state as billets for further thixoforming process.

2.2.1 Slurry preparation involving agitation

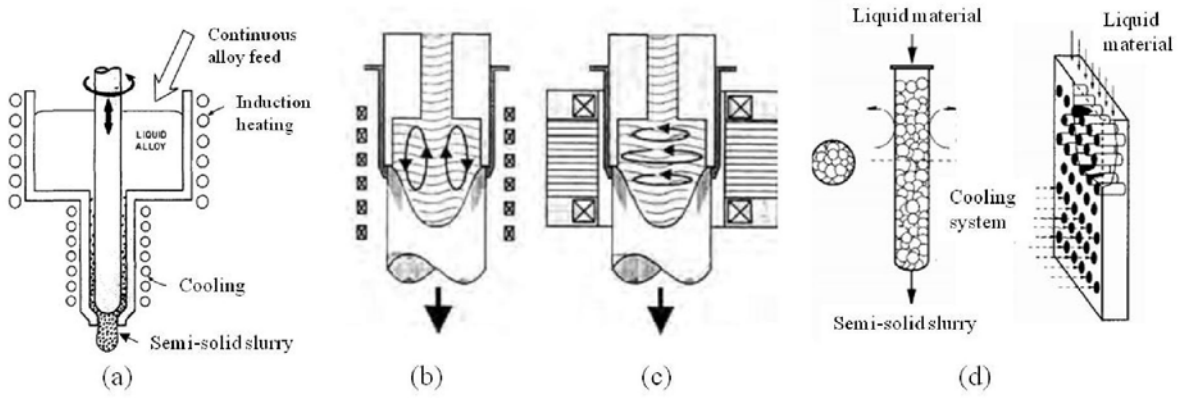

Fig. 1.6. Schematics of different techniques. (a) Mechanical stirring [11]. (b) Electromagnetic vertical stirring [12]. (c) Electromagnetic horizontal stirring [13]. (d) Passive stirring [14].

From the early observations of viscosity tests using a Couette viscometer, it is possible to produce a fine-grained globular microstructure which is required by a semi-solid forming process by vigorous agitation [3]. Following this observation, different slurry preparation methods were developed including active mechanical stirring, electromagnetic stirring and passive stirring. The schematics of each technique are shown in Fig. 1.6. These techniques are mainly based on the principal that the dendrite structures can be broken by vigorous agitation during solidification.

The mechanical stirring method originated at MIT. Basically, there are two types – batch method [15] and continuous rotating method [16]. The apparatus of the dual rotating cylinder is similar to the Couette viscometer which can produce the required semi-solid slurry and measure rheology properties simultaneously. Due to low productivity, difficulties in process parameter controlling and the low quality of the semi-solid slurry, the two routes are not appropriate for massive productions.

For the reasons mentioned above, several researchers have developed new mechanical stirring approaches based on the classical stirring methods. For example, a new method and apparatus for the injection molding of semi-solid was developed at Cornell University in 1996 [17], in which the superheated liquid metal is cooled into the semi-solid state in the barrel of a special vertical injection molding machine, with the growing dendrites being broken into small round grains by the shearing force generated by the screw or barrel. This apparatus integrates the slurry preparation, transport and casting process, which solves the difficulties in the slurry keeping and transport. The General Research Institute for Nonferrous Metals (GRINM) [18] developed two similar semi-solid slurry preparation systems which have been industrially applied to the production of aluminum alloy components by rheocasting process. Kiuchi [19] proposed a new approach for the efficient preparation of semi-solid slurries named shearing cooling rolling (SCR). In this route, the molten metal is poured between a rotating roll and a stationary cooling shoe. This gives a fine spherical microstructure by breaking the dendrites. This process provides strong mixing intensity and cooling intensity which can be used to produce high melting and high solid fraction semi-solid slurries. In 1992, Moschini [14] developed the passive stirring system in which the liquid material flows through the obstacles and is cooled to the semi-solid state by the cooling system. During flowing through the obstacles, the shear caused by forced flow prohibits the formation of large dendrites. This process has been industrially applied to the production of rails by semi-

solid casting. At CRM in Liege, Belgium, a hollow jet nozzle has been designed for continuous casting which allows powder injection and a low superheat to obtain a globular structure in the core of a continuously cast steel billet [20].

Magneto hydrodynamic (MHD) stirring method has replaced the mechanical stirring method in industrial scale, because this method is a non-touching stirring technique in which there is neither corrosion of stirring blade (or stick) nor the pollution of alloy slurry by the blade and the stick during the mechanical stirring. In addition, the determination of operation parameters is flexible and convenient for controlling the production and the quality of semi-solid slurries. Shibata et al. [21] proposed a new commercial rheocasting process by using a vertical shot unit with induction coils in order to apply strong stirring force to the melted alloy in the shot sleeve to make slurries, which creates a precedent for the non-touching rheocasting process. Then, various similar MHD apparatus have been developed and industrially applied to Al, Mg, steel semi-solid forming processes in Japan [22], Korea [23], China [24] etc.

Compared to the mechanical stirring method, the advantage of MHD method is the non-touching preparation, which improves the quality of semi-solid slurry. However, although these routes provide excellent microstructure for thixoforming, the high cost and the material losses limit their industrial applications. In order to overcome the disadvantage, several routes have been recently developed and applied.

2.2.2 Slurry preparation by controlled nucleation method

The technique for controlling the nucleation and prohibiting the formation of dendrite is to prevent the dendrite growth of the numerous nuclei which are formed in the molten metals by controlling the thermodynamic parameters during solidification process, resulting in a fine globular microstructure. In recent years, a family of processes, such as new rheocasting route (NRC) [25], cooling slope [26], semi-solid rheocasting [27], low superheating casting, low superheat pouring with a shear field (LSPSF) etc, have been developed, which create the semi-solid slurry during cooling from the molten metal. These processes share common characteristics: low superheat pouring, vigorous mixing and rapid cooling during the initial stage of solidification combined with a much slower cooling thereafter. At MIT, Martinez and Fleming [27, 28] developed a new process – SSR process in which a spinning cold rod is inserted into the molten alloy just above the liquidus (~7°C). After a short time mechanical stirring, when the temperature is a few degrees below the liquidus (~2°C), the cold rod is

removed. Very fine spherical grains can be obtained after cooling to the desired temperature. The aims of low superheat pouring, vigorous mixing and rapid cooling during the initial stage of solidification are to release the latent heat in the molten metal and isolate the numerous nuclei.

2.2.3 Billets/slurry preparation by other methods

In order to produce a homogeneous and fine globular microstructure, various chemical grain refinement methods are also developed which provide numerous nuclei by addition of particles [29]. This method can be adopted to produce the feedstock for semi-solid process which requires the non-dendritic microstructure. However, an increased alloy content can promote a more dendritic morphology which means the grain refiner addition can be very effective for some alloys but less successful in others, such as Mg (AL) alloys [30].

Apart from producing the feedstock from liquid state, there also exist solid working routes which typically consist of plastic deformation followed by recrystallization during the reheating operation. During heating to the semi-solid state by the diffusion and melting process, the liquid appears at grain boundaries which results in globular grains. This method is classified as the strain induced melt activated route (SIMA) [31]. Recrystallisation and partial melting (RAP) [32] is another commercially used billet preparation route which is limited in the billet size, since it is difficult to introduce the deformation uniformly across the billet section.

2.2.4 Billet/slurry preparation for semi-solid forming of steel

The steel slurry is mainly produced by stirring methods. Owing to the high melting point of the steel grades, corrosion of stirring blade or stick as well as the pollution of alloy slurry, the mechanical stirring is mainly used in the research level. Currently, the MHD method is particularly used in the slurry preparation. U.S. ISC (Inland Steel Company) developed several semi-solid round billet continuous casting machines for commercial work (Stainless steel: 304, 316, and 440C. Tool steel: M7, M42 and MZ. Structure steel: 434, 52100, 8720 and 1020.) and achieved encouraging results. USTB (University of Science and Technology of Beijing) has developed a MHD machine which consists of a steel slurry preparation unit and the slurry transportation system [33]. Although the MHD method has already been industrially applied to steel slurry preparation, the technique is good for producing ingots with a diameter less than 150mm.

The cooling slope method enables the molten steel to become a semi-solid slurry with a proper microstructure. By using this method, Ramadan et al. [34] studied the effect of semi-solid processing on the microstructure and the strength of gray cast iron.

The thixoformability of steel in the standard state (as-received state) was studied by many researchers. After quenching the rolled bar, cast billet and cast billet with liquid core reduction from the semi-solid state, the microstructure of 100Cr6 obtained by these manufacturing processes was compared by Bülte and Bleck [35]. No significant difference was found. Therefore it is suggested that primary as-received/as-cast billet can be used for semi-solid forming process. Omar et al. [36, 37] has performed thixoforming experiments on hot formed M2 and HP9/4/30 in the as-received state. The results demonstrated that the high alloy steel grades which are very difficult to form by other forming processes can be successfully thixoformed in the as-received state. Hirt et al. [38] thixoformed complex geometry parts in one step using the hot rolled X210CrW12. Cézard [2] and Becker [1] succeeded in performing the thixofoming process on as-received carbon steels (C38, C80 and 100Cr6).

2.3 Advantages of semi-solid processing

As demonstrated by many researchers throughout the word and the industrial successes, the semi-solid metal forming process promises several advantages.

Compared with the conventional casting processes. Owing to the laminar, viscous flow, the macroscopic turbulence during casting can be avoided, resulting in the reduced part defects. Therefore, the mechanical properties of the parts produced by semi-solid forming are improved due to the reduced part defects. Furthermore, the porosity and shrinkage are reduced as well with increased solid fraction. Moreover, the low gas content leads to microstructures which increase the weldability [39] and corrosion resistance [40]. Meanwhile, as the processing temperature of the semi-solid metal is much lower compared to the conventional die casting, the tool life can be significantly increased. Another advantage of semi-solid forming process is that less energy is required to heat the metal into the semi-solid state rather than the liquid state in the casting operation.

Compared with the conventional forging processes. Thixoforming is a near-net shape processing which gives an opportunity to produce complex geometry components. This near

net shape capability can reduce the machining operations. Moreover, during thixoforming, the forming force is decreased dramatically as compared to the conventional forging processes. In addition, the lighter parts can be produced by thixoforming process with good mechanical properties to replace the steel components produced by conventional casting processes.

Advantages of semi-solid forming process for different materials. The technical advantages of semi-solid forming apply to all metals but the benefits vary for different materials. For aluminum alloys, the benefits are mainly mechanical properties compared with casting processes, while the prolonged die life anticipated from semi-solid forming process is less important as the melting point of the aluminum alloys are relatively low. However, for high melting point metals, such as steel, casting cost can be reduced as the rapid die deterioration can probably be avoided due to the lower processing temperature. Even more interesting, the internal energy of semi-solid metals is significantly reduced as compared with the fully liquid state. Concerning the competition between steel thixoforming and conventional forging, complex geometry parts which require multi-stage forging processes can be semi-solid formed in one step. This gives the potential application of steel thixoforming for producing complex parts with reduced manufacturing cost. Semi-solid forming of low melting metals such as aluminum and magnesium has already been applied industrially; while for semi-solid forming of steels is still in the research level concerning the high processing temperature, suitable tools, process cost etc.

3. Rheology of semi-solid materials

Generally, the behavior of semi-solid metals with a globular morphology usually exhibit two unique rheological properties: thixotropy and shear thinning/pseudoplasicity [41]. The thixotropy is defined as the time dependence of transient state viscosity at a given shear rate, while pseudoplasticity or shear thinning describes the dependence of viscosity on shear rate.

According to the review articles [42-44], there are two main types of semi-solid metal slurries depending on the solid fraction: a liquid-like slurry with a low solid fraction which behaves like a fluid under external forces, and a solid-like slurry with a high solid fraction which contains an interconnected solid phase and behaves like a solid. The deformation mechanisms of these two types of slurry are fundamentally different. The behavior of the semi-solid slurries which contain a low solid fraction is described in terms of an apparent viscosity. The slurries are considered as a homogeneous medium which is always

characterized by shearing experiments. The slurry with a high solid fraction behaves like a solid due to the solid skeleton and the agglomeration phenomena, so that the behavior should be characterized by considering the two phases and their interactions. In addition, from the rheological point of view, the semi-solid alloys can be divided into three categories: the model alloys such as Sn-Pb (processing temperature ~200°C) on which the experiments are easy to be performed and the data are much more accurate for rheology modeling, the Al and Mg alloys with a low melting temperature for industrial semi-solid forming and the alloys with a high melting temperature for which the rheological tests are being studied.

Concerning the determination of the rheological behavior, the experimental techniques, findings will be presented in two parts depending on the solid fraction: low solid fraction up to 0.4 and high solid fraction.

3.1 Behavior of alloys at low solid fractions

3.1.1 Experimental techniques

Here, when talking about the behavior of alloys at low solid fractions, only the alloys with a globular morphology will be concerned. In this case, viscosity is the main parameter for the rheology of semi-solid metals and plays an important role equivalent to that of the 'fluidity' concept in liquid metals [45].

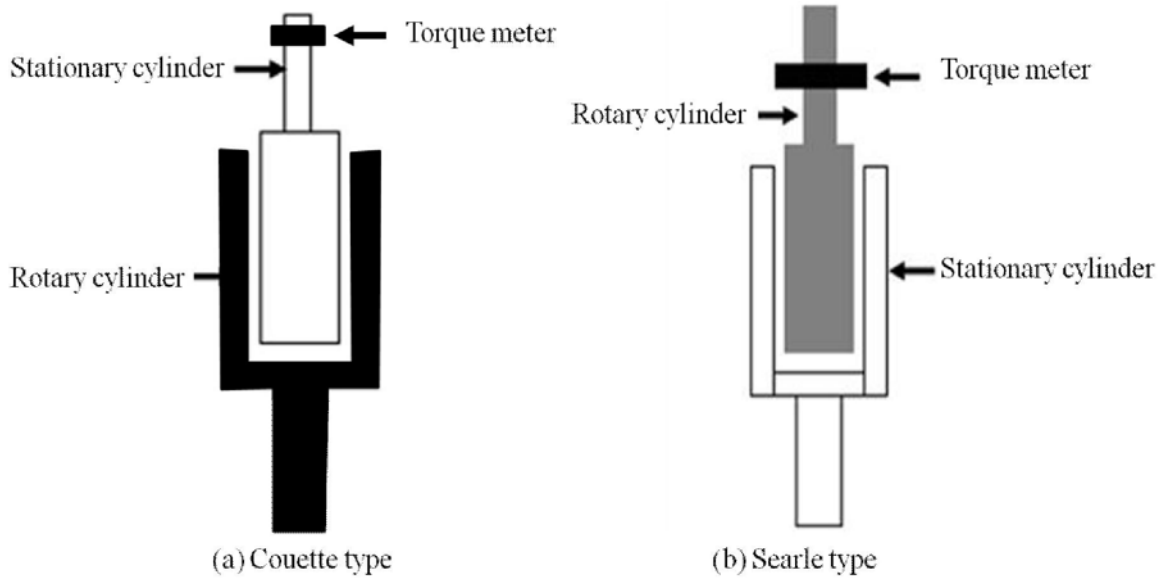

Fig. 1.7. Schematic of two types of viscometers. (a) Couette type. (b) Searle type.

There are several testing approaches to study the behavior of the semi-solid metallic slurries. The simplest methods are the methods consisting in directly measuring the induced torque in the slurries. The concentric cylinder viscometry has been used for the rheological characterization since the beginning of the research of semi-solid alloys [3, 11]. Depending on the rotation part (the cup or the bob), there are two types of viscometers, the 'Couette' and 'Searle'. The Couette type viscometer uses a rotating cup and a stationary bob to produce the shear stress on the surface of the bob. By contrast, in the Searle type viscometer, the cup is stationary and the bob or inner cylinder rotates inducing shear to the slurry. The schematic of these two types of viscometers is shown in the Fig. 1.7 [41, 46]. The shear rate and the shear stress can be deduced from the angular velocity and the torque.

By a set of equations given below, the apparent viscosity can be obtained [46].

$$\tau = \frac{T}{2\pi r^2 L} \qquad \text{(Eq. 1.1)}$$

$$\dot{\gamma} = \frac{2\omega}{r^2}\left(\frac{r_i^2 r_0^2}{r_0^2 - r_i^2}\right) \qquad \text{(Eq. 1.2)}$$

$$\eta = \frac{T}{4\pi L \omega}\left(\frac{1}{r_i^2} - \frac{1}{r_0^2}\right) \qquad \text{(Eq. 1.3)}$$

where $\boldsymbol{T}$ is the measured torque, $\boldsymbol{L}$ is the liquid altitude inside the cylinder, $\dot{\gamma}$ is the shear rate, $\boldsymbol{\omega}$ is the angular speed, $\boldsymbol{\eta}$ is the apparent viscosity, $\boldsymbol{r_i}$ is the inner cylinder radius, $\boldsymbol{r_0}$ is the outer cylinder radius and $\boldsymbol{r}$ is the actual annular gap radius.

The advantages of this technique are the possibilities to directly generate the slurry with globular morphology suitable for the forming operation and the high flexibility in terms of operating mode and well defined flow conditions. Although this technique is very simple for understanding the rheology of semi-solid slurries, there are several limitations in the materials the apparatus is made of, process controlling, solid fraction etc [47].

- Due to the aggressive behavior of atoms to particular alloys, the materials used for the apparatus should be chosen carefully. For example, the protective coatings on steels are applied in the viscometer apparatus for the rheology study of aluminum alloys in the semi-solid state.

- Generally, the viscosity depends on the solid fraction, therefore on the temperature of slurries. During testing, the thermal exchange and the viscous heating generated by shearing can lead to a heterogeneous temperature field which causes difficulties in temperature controlling.
- In order to avoid the turbulence effects and the wall slip effects, this technique is limited to low shear rates and low solid fraction.
- During testing, inertia effects can happen if the changes in shear rate are rapid which will lead to a delay in the torque recording.
- Irreversible microstructure changes may occur during such experiments which may affect the rheological properties [48].

Besides the rotation shear experiments, translation shear experiments can also be used for producing the shear by translating one part of the specimen with respect to the other. By this method, the relations between the strength of the alloy and its tendency to hot crack formation can be studied together with the rheological behavior of semi-solid alloys [49]. Fig. 1.8 shows the schematic of the translation shear test apparatus [49]. However, the exact strain is difficult to be measured by this technique.

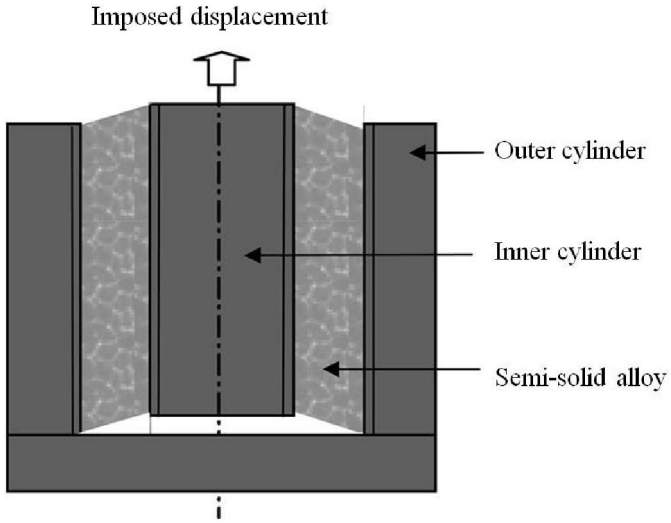

Fig. 1.8. Schematic of the translation shear test apparatus [49].

3.1.2 Phenomenology

The first investigation concerning viscosity of semi-solid alloys was performed on Sn-Pb at MIT by Spencer [3]. The viscosity of the slurry during solidification was measured by

mechanical stirring. The results indicated that the stirred semi-solid slurry at a solid fraction greater than 0.2 behaves like a non-Newtonian fluid with a much smaller viscosity than that of an unstirred dendritic slurry. The results initiated a large number of studies dealing with the rheology of the stirred semi-solid slurries. Today, although a great deal of studies have been performed on different systems trying to better understand the rheological behavior in more complex aspects, these works are still based on the findings which are demonstrated by Joly and Mehrabian [41].

The continuous cooling behavior describes the effects of solid fraction, shear rate and cooling rate on the viscosity of the semi-solid slurries. During the rotational shear experiments for the characterization of the rheological behavior, the shear rate is normally constant so that the evolution of the viscosity is caused by the change of the solid fraction.

Fig. 1.9 [41] presents the classical curves of the viscosity as a function of solid fraction. It shows that at a given shear rate and cooling rate, the viscosity increases with increasing solid fraction. The viscosity increases slowly at low solid fractions while sharply at high solid fractions. In addition, at a given solid fraction, the viscosity decreases with increasing shear rate and decreasing cooling rate. Similar results have been obtained on other semi-solid alloys [50-53].

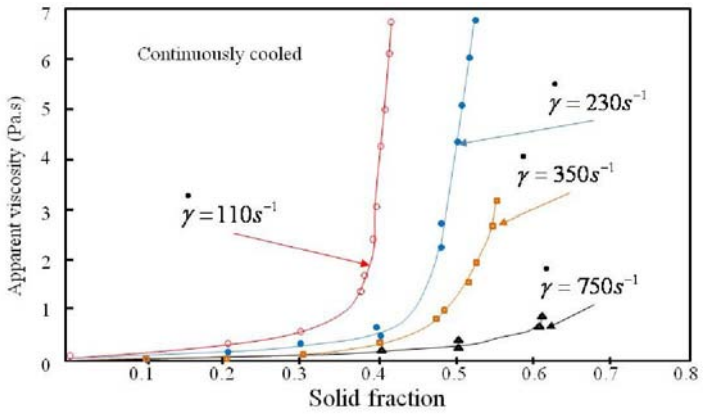

Fig. 1.9. Viscosity as a function of solid fraction of Sn-15% Pb alloy continuously sheared and cooled at 0.33K/min at different shear rates [41].

Generally, a standard model $\eta = A \exp(B f_s)$ is used to correlate the solid fraction f_s to the viscosity η. The B values for various alloys deduced from viscometer experiments are summarized in ref. [47]. It is to be pointed out that in the case of low cooling rate and isothermal holding, B value is relatively smaller.

Shear experiments during isothermal holding permit the characterization of the rheological parameters more precisely. For a given alloy at a constant temperature, that is to say the volume fraction of solid phase is constant; the steady state viscosity is defined as a function of solid fraction and shear rate in the state where the shear rate is fixed. This kind of experiment can take a long time to reach the steady state. As shown in Fig. 1.10, viscosity decreases with increasing shear rate in the steady state. In addition, depending on the solid fraction, the viscosity reaches a relatively constant value after a certain amount of shearing time. This rheological behavior is defined as shear thinning or pseudoplastic. Such behavior has also been confirmed in various alloy systems [50, 52, 54]. The shear thinning behavior can be explained by the disagglomeration of the solid grains during shearing: when shear rate increases, the solid connections (or solid skeleton) are easier to be broken down. Meanwhile, the breaking down of the solid connections results in the release of the entrapped liquid, thereby reducing the viscosity. These explanations were confirmed by metallographic observations on Al-Si alloys sheared at various shear rates. Moreover, it is also to be pointed out that high shear rates lead to a smaller volume fraction of entrapped liquid phase.

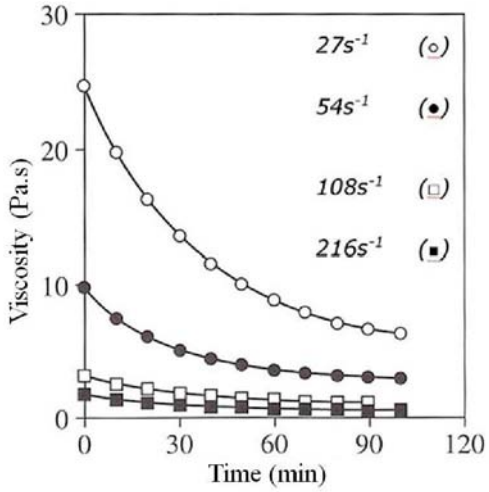

Fig. 1.10. Viscosity as a function of shearing time at 590°C of a AlSi7MG0.3 alloy (f_s = 0.35) partially solidified with different shear rates [53].

The thixotropic behavior, another rheological phenomenon in the semi-solid metallic slurries, which is first demonstrated by Joly and Mehrabian [41]. Fig. 1.11 shows the effect of the resting time on the hysteresis loops of Sn-15% Pb alloy obtained by Joly and Mehrabian. It can be seen that all the curves return to the initial point which indicates the reversible character of the microstructure. In addition, as the experiment time is relatively short, the

significant growth of the grains did not occur. It has been also found that the agglomeration process influences the shear stress more than the coarsening of the grains.

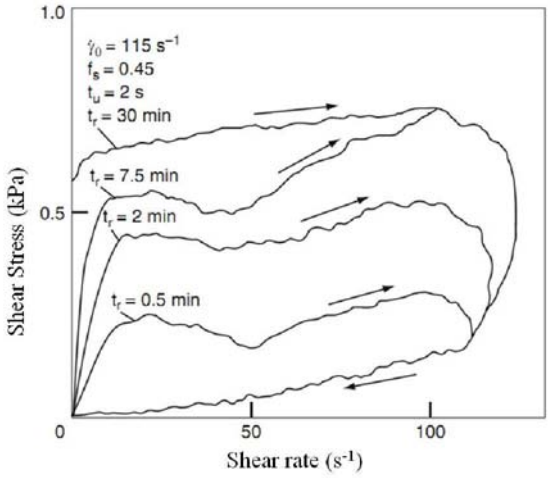

Fig. 1.11. Effect of the resting time on the hysteresis loops of a Sn-15% Pb alloy [41]. tr is the resting time. tu is the up-time to reach a maximum share rate of 115 s^{-1}.

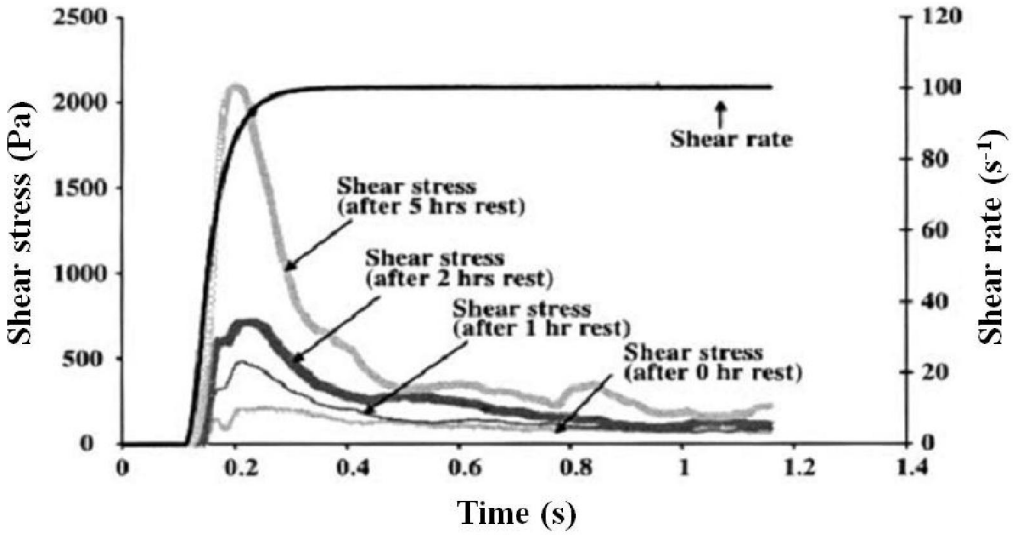

Fig. 1.12. Shear rate jumps from 0 to 100 s^{-1} after different resting times for Sn-15% Pb alloy at solid fraction of 0.36 [55].

In an industrial thixoforming process, it is also interesting to study the effect of the resting time on the shear stress. Fig. 1.12 [55] demonstrates the influence of the resting time on shear stress. The shear stress increases with increasing rest time. This can be explained by the increase of agglomeration and the grain size resulting from the increasing rest time, and therefore results in the increase in the shear stress. It can be also seen that a rapid change in shear rate occurs in less than 1 second. However, it is not always in this case. For example, in

the experiments carried out on AZ91D alloy, although the viscosity is higher at a higher solid fraction for the same resting time, it has been observed that the viscosity increases with increasing resting time at a high solid fraction (f_s = 0.4) while it decreases at a lower solid fraction as shown in Fig. 1.13 [56]. The authors explained this phenomenon by different coarsening mechanisms. At a high solid fraction, grains prefer to form larger ones resulting in greater entrapped liquid fraction. However, at a low solid fraction, the entrapped liquid could be released into the bulk liquid by Ostwald ripening.

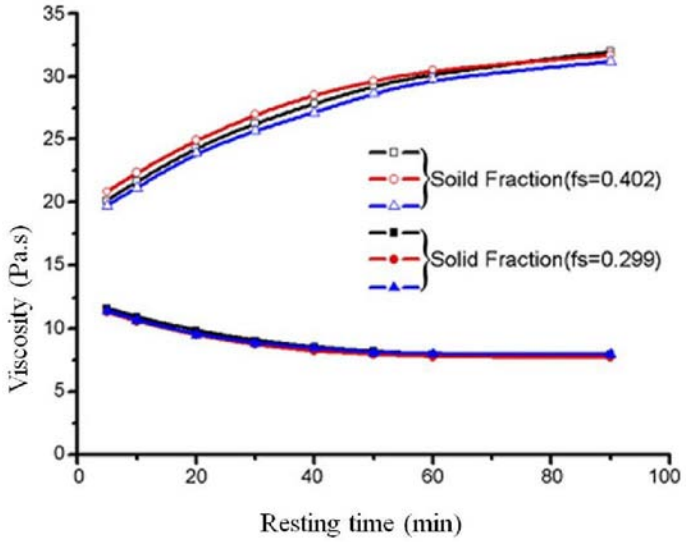

Fig. 1.13. Influence of the solid fraction and the resting time on the apparent viscosity [56].

The results presented above are mainly focused on the semi-solid alloys at a low solid fraction.

3.2 Behavior of alloys with high solid fraction

The semi-solid metallic slurries at high solid fractions behave like a solid, exhibiting a well defined yield strength due to the existence of a solid skeleton. The deformation behavior at high solid fractions has been studied experimentally and theoretically.

3.2.1 Experimental techniques

Several experimental methods have been used to characterize the behavior of high solid fraction slurries. The simplest way is parallel plate compression, and what is more, since the test is similar to an open die-forging operation, it provides useful engineering information on the deformation of the semi-solid metallic alloys. Experiments have been performed on

various alloys [57-60]. The obtained results can be further treated to characterize the rheological behavior of the tested slurries depending on different assumptions: Newtonian or non-Newtonian fluids, respectively. For a Newtonian fluid, the Stefan equation is applied to the parallel plate viscometer.

$$F = -\frac{3\mu V^2}{2\pi h^5}\left(\frac{dh}{dt}\right) \qquad \text{(Eq. 1.4)}$$

where $\boldsymbol{\mu}$ is the viscosity, $\boldsymbol{V}$ is the volume of the material, $\boldsymbol{h}$ is the instantaneous height of the sample and $\boldsymbol{t}$ is the time.

If the sample size is always smaller than the platen area, the equation (Eq. 1.4) can be obtained by integrating for $\boldsymbol{h = h_0}$ at $\boldsymbol{t = 0}$ and $\boldsymbol{h = h}$ at $\boldsymbol{t = t}$. and for the initial pressure, $P_0 = Fh_0 / V$. The viscosity-time relationship can be written as:

$$\frac{1}{h^4} - \frac{1}{h_0^4} = \frac{8\pi F t}{3\eta V^2} \qquad \text{(Eq. 1.5)}$$

$$\frac{3Vh_0}{8\pi P_0}\left(\frac{1}{h^4} - \frac{1}{h_0^4}\right) = \frac{t}{\eta} \qquad \text{(Eq. 1.6)}$$

The average shear rate of a Newtonian fluid at any instant during compression can be given by Eq. 1.7.

$$\dot{\gamma}_{av} = -\sqrt{\frac{V}{\pi}}\left(\frac{dh/dt}{2h^{2.5}}\right) \qquad \text{(Eq. 1.7)}$$

where $\dot{\gamma}_{av}$ is the average shear rate, $\boldsymbol{h}$ is the instantaneous height, $\boldsymbol{t}$ is the instantaneous time.

If the slurry is assumed to be a non-Newtonian fluid, the results are interpreted in terms of the power law, correlating shear stress ($\boldsymbol{\tau}$) to average shear rate ($\dot{\gamma}_{av}$) as $\tau = m\left(\dot{\lambda}\right)^n$, where $\boldsymbol{m}$ and $\boldsymbol{n}$ are the consistency factor and power-low index, respectively [59]. Depending on the relationship between the viscosity, shear stress and shear rate, the viscosity can be obtained as expressed in Eq. 1.8. The final results from power-low model analysis can be obtained by Eq. 1.9.

$$\eta = m\left(\dot{\lambda}\right)^{n-1} \quad \text{(Eq. 1.8)}$$

$$\frac{h_0}{h} = \left\{1 + \left(\frac{3n+5}{2n}\right) h_0^{(n+1)/n} kt\right\}^{2n/(3n+5)} \quad \text{(Eq. 1.9)}$$

$$\text{where} \qquad k = \left\{\left(\frac{2n}{2n+1}\right)^n \frac{4F}{\pi d_0^{n+3} m}(n+3)\right\}^{1/n}$$

Here, Eq. 1.8 is only valid for h << d which generally corresponds to extended time of deformation.

In order to understand the behavior of the semi-solid metallic slurry at high shear rates (the shear rates are comparable to thixoforming process), a novel compression type viscometer was developed by Yurko which can give a high shear rate up to 1000 s^{-1} [61].

Extrusion tests can also be applied to studying the viscosity of semi-solid alloys. Compared to compression tests, higher shear rates (>10 s^{-1}) can be achieved by extrusion. Furthermore, this test can also be used to identify the liquid segregation, material flow since it has similar process conditions to the semi-solid forming process [62]. Fig 1.14 presents the schematic drawings of the extrusion apparatus. In the case of direct extrusion, the semi-solid slurry is forced to flow into the mould as shown in Fig. 1.14 (a). The viscosity and the shear rate are expressed as a function of the ram speed and forming force. This test permits to determine the liquid ejection and define the liquid segregation [63]. The main drawback is the existence of friction between the piston and the container which does not allow for a precise characterization of the rheology of the semi-solid alloy. In the case of inverse extrusion, the drawback caused by friction can be avoided. During extrusion, the piston penetrates into the material, and the material flows between the container and the piston (Fig. 1.14 (b)).

Indentation test is another simple method for characterizing the behavior of semi-solid alloys which uses a tip with a given geometry to penetrate into the semi-solid material. This method was first used to evaluate the softness of the material before starting the injection. The rheology of the alloy is not easy to be obtained because of the complex stress states that are generated under and in the vicinity of the tip. Meanwhile, the geometry of the indenter influences the experimental results [64].

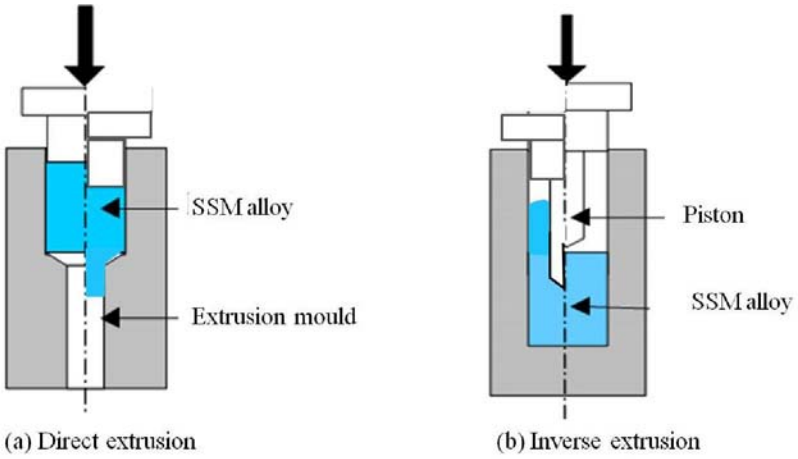

Fig. 1.14. Schematic drawings of extrusion systems. (a) Direct extrusion. (b) Inverse extrusion.

Due to the low cohesion of the material in the semi-solid state, a tensile test is not commonly used for rheological study. However, it is necessary to know the behavior of the material at any stress state for a real semi-solid forming process. This method is not suitable for the slurries at a solid fraction less than 0.85 [65].

3.2.2 Phenomenology

From the experimental results (Fig. 1.15), owing to the existence of the solid skeleton, the deformation behavior of semi-solid metallic slurries can be characterized as follows:

- A large yield stress exists during the forming process.
- Cracking of the solid skeleton and separation of liquid phase.

From the obtained load-displacement signal (Fig. 1.15 (a)), there is a rise in the load which is used for breaking down the solid skeleton. After that, the force is low due to the weak resistance of the material. At the end of the forming stage, the force rises rapidly.

For the high solid fraction materials, during forming, the solid phase bears a hydrostatic pressure caused by either grain rearrangement or by slight deformation of the grains [66]. In addition, the spatial gradient of hydrostatic pressure in the liquid phase caused by the reduction of the interstitial volume may cause phase separation [67]. Generally, the segregation phenomena can be reduced by high deformation rates or high die filling rates, low pressure gradients, low solid fractions and fine spherical grains [44].

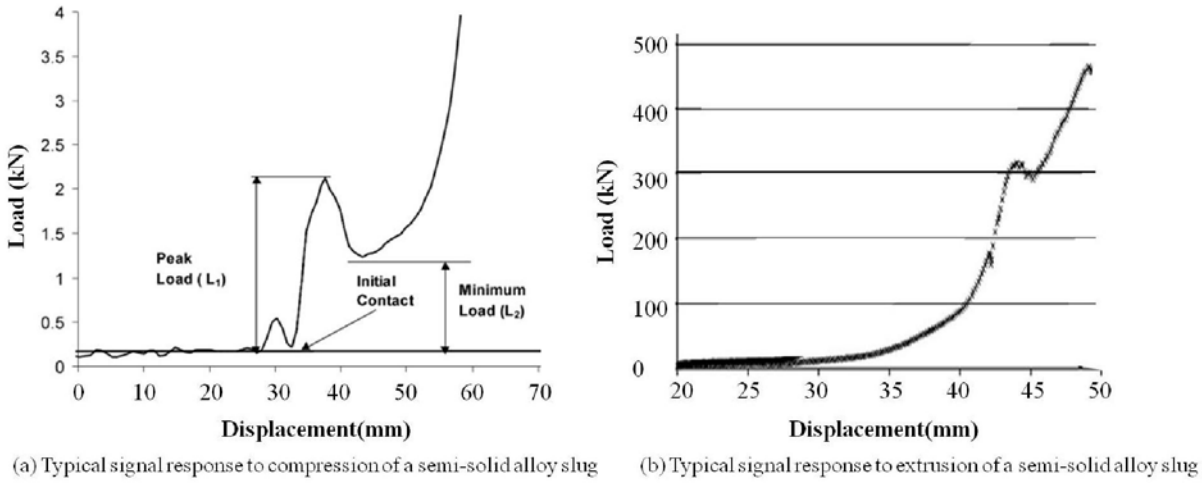

Fig. 1.15. Typical load-displacement signal during compression (a) [68] and extrusion (b) [62] of a semi-solid material at a high solid fraction.

Suery and Fleming [60] performed the compression experiment on Sn-15% Pb specimens with non-dendritic and fine dendritic microstructures. The results of the stress-strain curves performed at a constant strain rate are very different which indicates that the microstructure of the material influences the rheological behavior. Therefore, it is important to study the microstructure of the material at various processing stages to better understand the rheology and material flows.

4. Microstructure evolution during material preparation and forming process

Spencer and Fleming [3] stated that the ideal material for semi-solid forming should be processed with an accurate specified volume fraction of solid and spherical grains which are dispersed in the material uniformly. As mentioned in 1.1.2, the microstructure for a semi-solid slurry can be obtained by partial solidification of a melt or by partial remelting of a solid feedstock with a spherical microstructure which has been solidified under specific processes. The microstructure evolution during preparation will be reviewed in the following sections.

4.1 Microstructure characterization

It has been realized that the flow behavior of a fixed semi-solid metallic slurry depends on the volume fraction, size, shape, and the distribution of the grains.

Volume fraction of solid (F_s). It is critical to understand the solid fraction or liquid fraction in the semi-solid state for process controlling because it crucially influences the viscosity and therefore the flow behavior of the material. The solid fraction is related to the temperature. For a given alloy, it can be defined uniquely at a given temperature under equilibrium conditions; in any other case it depends on the thermal history. Tzimas and Zavaliangos summarized various methods for the evaluation of solid fraction for semi-solid processing [69]. To sum up, the following methods can be used for the determination of solid fraction either directly or by its effect on the physical properties:

- Evaluation by thermodynamic data, for example the equilibrium phase diagram.
- Thermal analysis techniques such as DTA, DSC.
- Quantitative metallography on microstructures quenched from the semi-solid state.
- In situ X-ray microtomography on microstructure measurements.
- Ultrasonic monitoring by measuring the propagation speed of ultrasonic waves.
- Measurement of electrical resistivity magnetic permeability.
- Measurement of mechanical properties by indentation or extrusion.

The last three methods are not usually applied because there is no unique correspondence between the measured characteristic parameter and the solid fraction due to electrical, magnetic and other physical properties.

- The first three approaches are more practically used although each one has its limitations:
- All approaches are approximate.
- The use of thermodynamic data requires additional information in order to take into account the thermal history of the alloy.
- The heating rate of the DSC is much lower than that used in industrial applications of semi-solid processing.

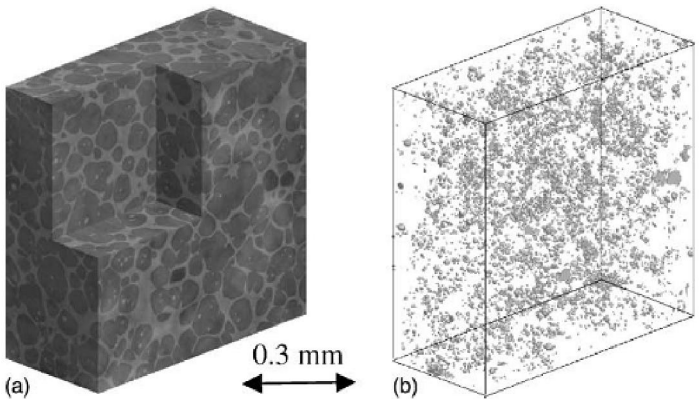

Fig. 1.16. (a) 3D visualization of Al–Si material. (b) Entrapped liquid extracted from the volume presented on (a) [70].

X-ray microtomography overcomes the limitations of all the approaches mentioned above because the 3D measurement is carried out directly in the semi-solid condition at a high heating rate. However, this technique is not easy to access.

When talking about the solid fraction or liquid fraction in the semi-solid state, the liquid phase includes the intergranular which contributes to the sliding of the solid phase during forming and intragranular liquid phase which can not contribute to the sliding of the grains. For measuring the fraction of entrapped liquid phase on 2D sections, there would be an error due to the random section. A 3D measurement can be performed by series section on quenched samples or by X-ray microtomography on quenched samples or directly on samples in the semi-solid state.

Temperature sensitivity *S.** Technically, not all the alloys can be used for semi-solid forming process. The formability for a given material can be characterized by the temperature sensitivity of the solid fraction, which can be expressed by the slope of the equilibrium solid fraction curve (Eq. 1. 10) [71].

$$S^* = -\frac{df_s^*}{dT} \qquad \text{(Eq. 1.10)}$$

where f_s^* is the solid fraction, ***T*** is the temperature.

In a real semi-solid forming process, the temperature will always be subject to an error, thus a low temperature sensitivity at a certain desired solid fraction is preferable for a stable process. In addition, a large semi-solid interval at a low processing temperature is also

desired. Regarding the width of the interval and temperature sensitivity of the solid fraction, the applicability of the Al and Mg alloys for semi-solid forming process has been confirmed, but steel alloys are much more complex. Pure iron and near eutectic alloys are restricted in their applicability for semi-solid forming because they have a specific melting point and do not show a complex melting behavior [72]. As illustrated in Fig. 1.17, high alloyed steels with a complex melting behavior exhibit a wide semi-solid interval at relatively low temperatures which are easier for semi-solid forming.

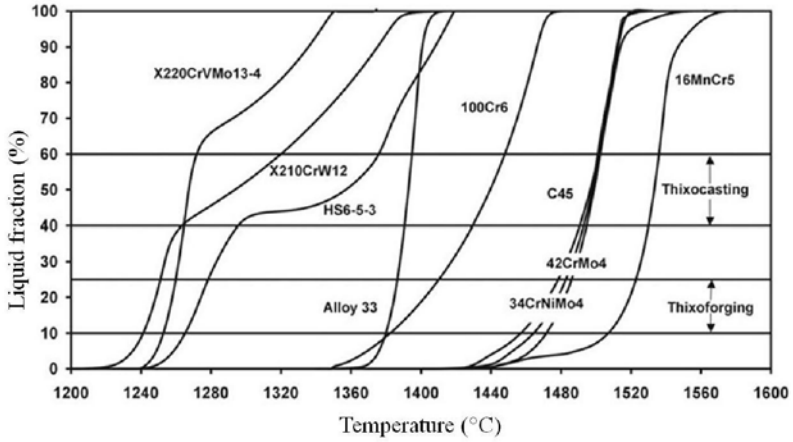

Fig. 1.17. Liquid fraction curves as a function of temperature determined by DTA at a heating rate of 10K/min for various steel grades [73].

Regarding the semi-solid interval and the temperature sensitivity, the variation of the chemical compositions should also be taken into consideration. Fig. 1.18 shows the fraction liquid curves of the steel grades 100Cr6 and 100Cr6 LTT (Low Temperature for Thixoforming) determined by DSC [2].

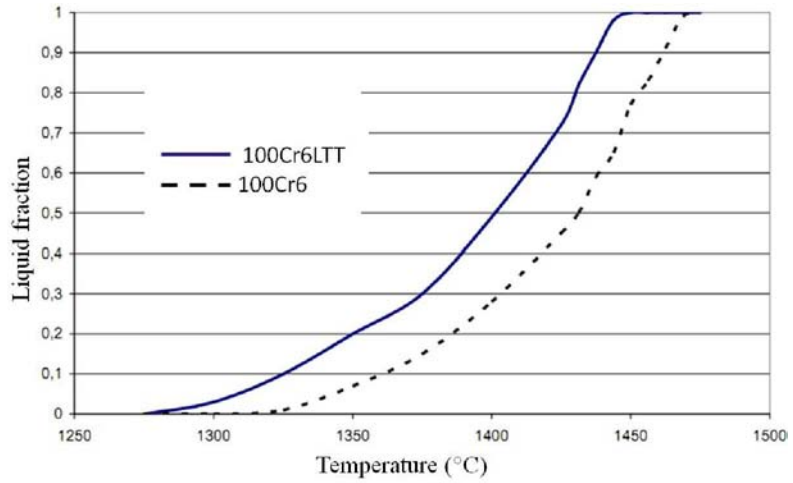

Fig. 1.18. Liquid fraction curves as a function of temperature determined by DSC [2].

It can be found that a variation of the chemical composition leads to a different melting behavior or a shifting of the temperature curve. The reason for this is a different stability of carbides caused by the amount of alloying element. The chemical compositions of these two steel grades are displayed in Table. 1.1. Therefore, for a given alloy, the melting or solidification behavior should be carefully studied.

The morphology of the microstructure is of much importance for a stable semi-solid processing. The morphology of the microstructure in the semi-solid state can be described by several metallographic parameters such as the size, shape and distribution of grains.

Table. 1.1. Chemical composition of steel grades.

Mass10-3%	C	Si	Mn	S	P	Ni	Cr	Mo	Cu	Al	Sn	As	B*	V	Ti	Nb	Ca*	N*
100Cr6LTT	1055	1215	910	11	13	176	1306	43	177	29	12	20	3	6	3	3	8	66
100Cr6	988	230	326	6	7	210	1428	82	194	31	13	10	2	4	3	1	2	109

Shape factor (F). Spherical grains in a semi-solid metallic slurry are of importance for effective semi-solid forming because they influence the flowability and the viscosity of the slurry. Therefore, it is necessary to describe quantitatively the grains. Generally, 3-dimensional structures are characterized by measurement on 2D sections. The shape factor (F) is defined by the following equation (Eq. 1.11):

$$F = \frac{4\pi A}{P^2} \qquad \text{(Eq. 1.11)}$$

where ***A*** is the area and ***P*** represents the perimeter of the grains.

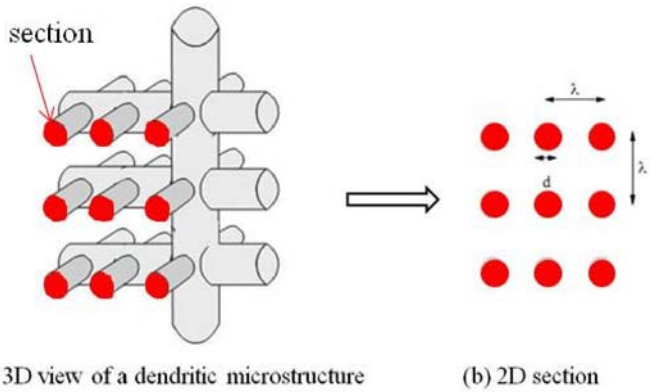

Fig. 1.19. Schematic representation of complex dendrite structure. (a) 3D view. (b) 2D section [47].

In Eq. 1.11, ***F*** varies between 0 for grains having a very elongated cross section and 1 for grains having a circular cross section. However, due to a random section, a 2D dimensional

section of a grain can give rise to several apparently isolated images. As illustrated in Fig. 1.19, a complex dendritic microstructure is reflected by several isolated spherical grains, meaning the shape factor changes greatly [47].

Loue and Suery introduced a modified dimensionless grain specific shape factor F_g which is defined by Eq. 1.12 [74].

$$F_g = \frac{1}{6\pi f_s}\frac{S_V^2}{N_A} \qquad \text{(Eq. 1.12)}$$

where S_v represents the solid-liquid interfacial area per unit volume, N_A is the number of grains per unit area, F_s is the solid fraction.

As demonstrated by the authors, F_g characterizes more accurately the grain morphology than the usually used shape factor F does. Still, the parameter N_A measured by image analysis may not reflect the true grain density due to the 2D measurement.

Grain size and Grain size distribution. Grain size has an effect on the rheological behavior in the semi-solid state and on the mechanical properties after the semi-solid forming process as shown in Fig. 1.20. The fractal dimension D is proposed by Qin and Fan [75] for describing the morphology of equiaxed dendrites.

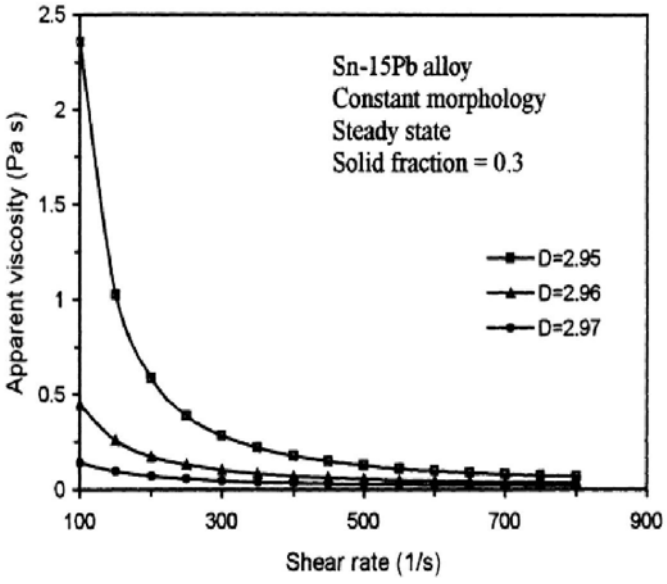

Fig. 1.20. Viscosity as a function of shear rate for Sn-15% Pb alloy with various fractal dimensions.

Liu et al. [55] pointed out that the increase in grain size and degree of agglomeration during forming would impede the movement of the grains sliding past each other, thereby

increasing the shear stress and viscosity. However, the increase of the shear stress and viscosity may be caused only by the increasing degree of agglomeration. This can be explained as follows: for a constant mass of grains, maintaining the degree of agglomeration while reducing the grain size leads to an increase in the number of grains which results in more grain interactions and therefore an increased resistance to flow. When shear rate increases, the grains are isolated, resulting in the breakdown of grain-grain interactions, causing the viscosity to decrease.

For a steady semi-solid forming process, Uggowitzer et al. [76] suggested that the average grain size should be smaller than 100μm and the shape factor be bigger than 0.5 calculated by Eq. 1.11 [5].

Contiguity and contiguity volume. For a given slurry system with a fixed solid fraction, the arrangement of the grains is of importance for the semi-solid forming process. The contiguity and the continuity can be used for characterizing the grains distribution or grain arrangement. The contiguity (***Cf_s***) characterizes the arrangement or rather the cohesion of grains and can be described by the average proportion of solid–solid and solid–liquid boundary surfaces. Eq. 1.13 is used for characterizing the contiguity:

$$Cf_s = \frac{2S_V^{ss}}{2S_V^{ss} + S_V^{sl}} \qquad \text{(Eq. 1.13)}$$

where ***Cf_s*** is the contiguity value of the solid phase, S_V^{ss} is the boundary surface of the grains, S_V^{sl} is the boundary surface of the solid and the liquid phase.

The contiguity can be determined by measuring the solid–solid and solid–liquid boundary surfaces of the obtained metallographic images. In addition, as the solid skeleton strength depends on both the contiguity and the solid fraction, the contiguity volume ***C_sF_s*** is used to describe the volume of connected phase (Eq. 1.14) [77].

$$C_s f_s = V_s Cf_s \qquad \text{(Eq. 1.14)}$$

where $C_s f_s$ is the contiguity volume, ***V_s*** is the volume fraction of the solid phase and Cf_s is the contiguity value of the solid phase.

The average number of grains in agglomerates was used by Chen and Fan [78] to describe the grain agglomeration in semi-solid slurries and also for microstructure modeling.

In reality, the contiguity is a 3D parameter which can only be determined in 3D. With the powerful X-ray microtomography technique, the connection and the distribution of the grains can be observed directly [70, 79-81]. Compared to the post quenched measurement, the evolution of liquid-solid interface area S_V is similar but much lower, as illustrated in Fig. 1.21 [79]. It also reveals that there are no free unattached grains. Grains are connected to six or seven neighbors on average, as shown in Fig. 1.22.

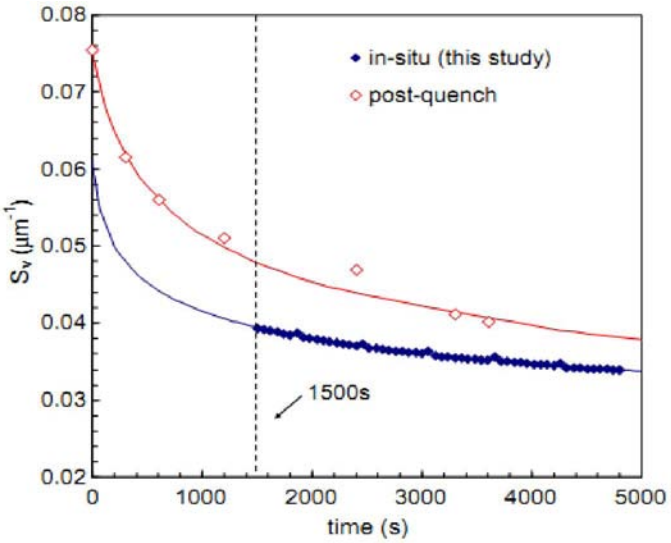

Fig. 1.21. Variation of liquid-solid interface area with time and comparison with post-quench measurements on the Al-Wt%15 Cu [79].

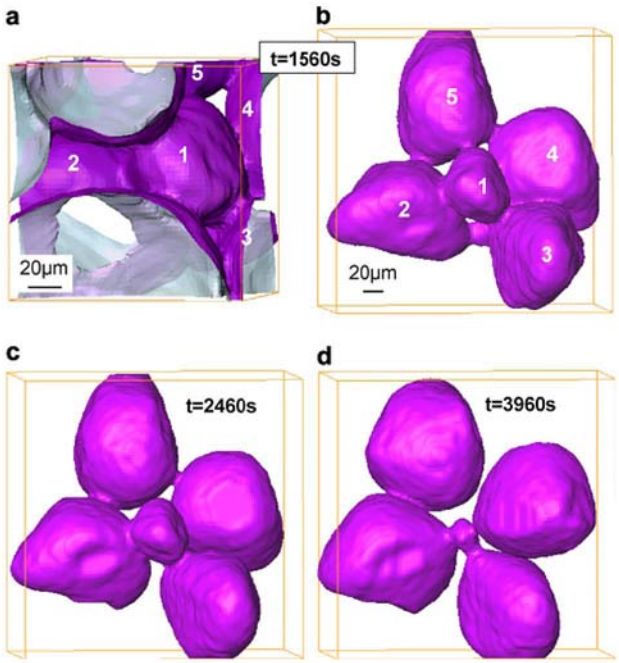

Fig. 1.22. Observations of neck representative trend with unequal grains [79].

4.2 Influence of slurry preparation conditions on morphology

As mentioned before, a semi-solid metallic slurry can be obtained either by partial solidification or by partial remelting. Depending on the preparation route, the influence will be reviewed separately.

4.2.1. Influence on morphology during slurry preparation by partial solidification

It has been concluded from experimental observations that non-dendritic structures can be produced by vigorous agitation. From the studies of different authors on various alloy systems (mainly on Sn-Pb alloy, Al alloys and Mg alloys) used for semi-solid processing, the influence on microstructure development during solidification can be summarized as follows [41, 56, 82-85]:

- With prolonged stirring time, a rosette or spherical morphology can be obtained by the destruction of the dendrite arms and the subsequent ripening or spherodization process.
- Increasing the shear rate accelerates the morphological transition from dendrtic morphology to spherical microstructure and reduces the amount of entrapped liquid inside the grains.
- Turbulent flow influences much more significantly the grain size and morphology than laminar flow does.

During the solidification with stirring, the morphology for a given alloy is mainly influenced by the shearing rate, stirring time. During their investigations on the effects of the shearing rate on viscosity of an Al-Si alloy during solidification to the semi-solid state, Yang and Tsao proposed a critical stirring time below which the grain size decreases with stirring time, while after which the grains grow with stirring time [83]. Similar results of grain size evolution as a function of shearing time were also obtained by different authors on various alloys. Fig. 1.23 presents the grain size evolution during shearing. This phenomenon can be illustrated as follows: for a partially solidified alloy with a dendritic structure, the initial dendrite arms are fragmented by shear stress, resulting in a tendency of decreasing the grain size and a high density of spherical grains during the initial stage of stirring. In the subsequent isothermal shearing, the spherical grains are not easy to be fragmented by the plastic deformation. Instead, Ostwald ripening and grains coalescence would be the predominant mechanism for the coarsening of spherical grains resulting in the growth of grains. Ji [86]

investigated the microstructure evolution of a Mg slurry which was produced by a twin-screw maker. As the initial grains were fine and spherical, there was no grain decreasing stage caused by the destruction of the dendrite arms. The increase in grain size was observed during isothermal shearing as illustrated in Fig. 1.24.

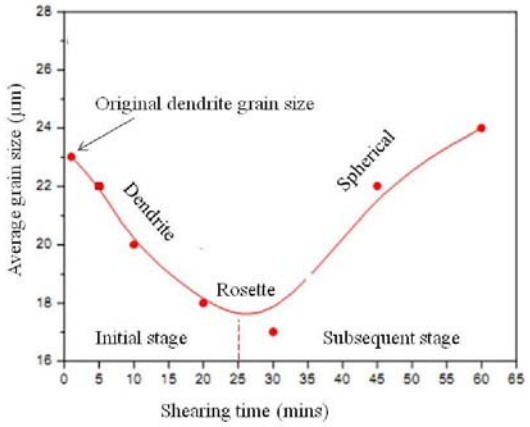

Fig. 1.23. Grain size vs shearing time of Al-5.2Si alloy at the shearing rate of 210 s^{-1} at 615°C [85].

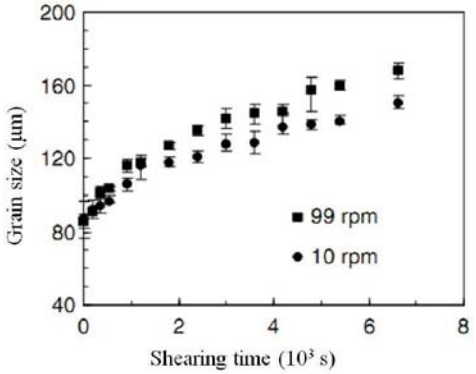

Fig. 1.24. Influence of the shearing time on grain size of AZ91D at various shear rate [86].

For a given stirring rate, shearing time not only affects the grain size, but also shape factor, solid fraction and grain density. Fig. 1.25 presents the effects of shearing time on the factors mentioned above. No significant variation in the solid fraction and the shape factor could be found during isothermal shearing. While, shearing time affects the grain size significantly; the grain density decreases with increasing shearing time. This tendency is in response to the increase of the grain size. Similar results were also obtained on various alloy systems [84].

Shear rate is another parameter which affects the morphology of the slurry, and therefore affects the rheological properties of semi-solid metallic slurries. With increasing shear rate the grain size decreases, while the grain density increases under laminar flow conditions [87]

which could be explained by an increase in initial nucleation rate with increasing shear rate. Ji and Fan also found that the formation of spherical grains could be obtained quickly under intensive turbulent flow conditions. In addition, Ji and Fan [88], Ryoo and Kim [89] also found that grain size decreased rapidly with increasing shear rate under the low shear rate region, while the grain size leveled off under the high shear rate as shown in Fig. 1.26.

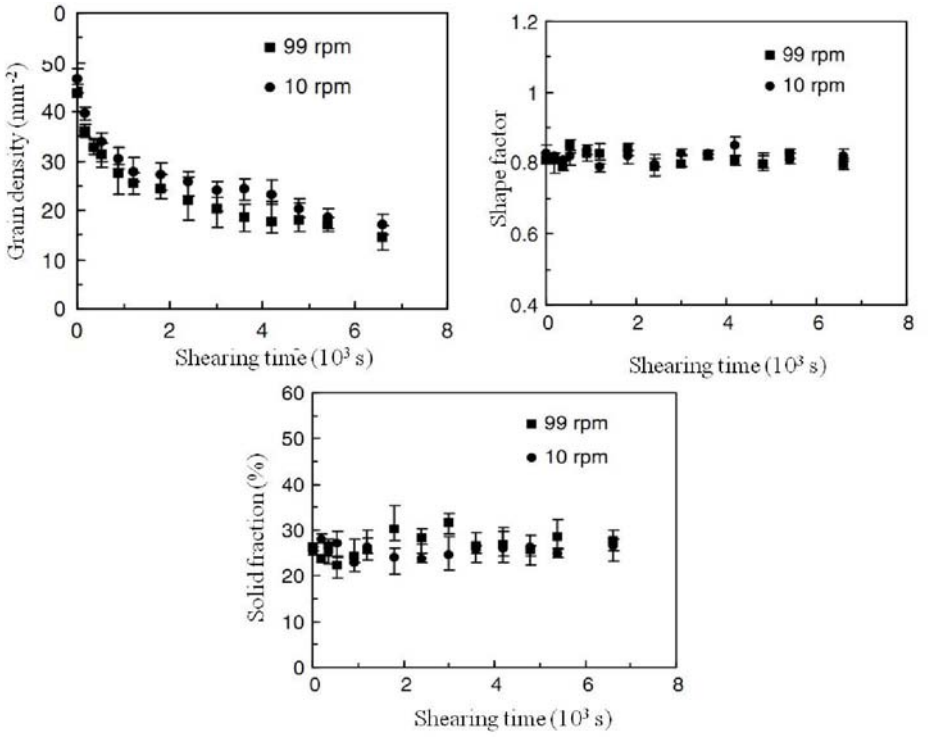

Fig. 1.25. Influence of shearing time on (a) grain density, (b) shape factor and (c) solid fraction [86, 88, 90].

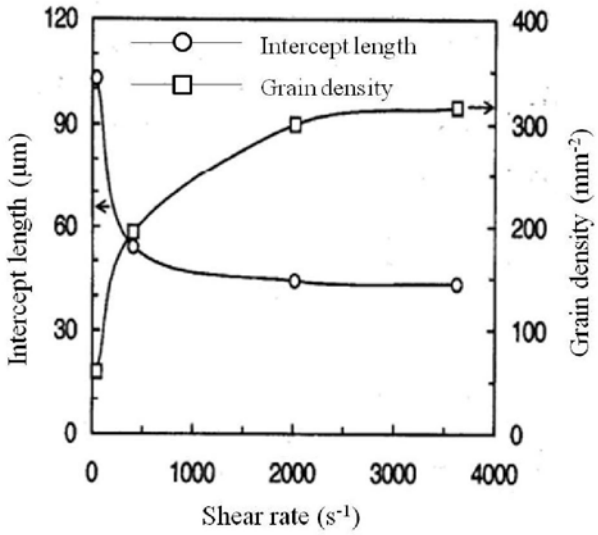

Fig. 1.26. Effect of shear rate on the grain size and density of Sn-15% Pb alloy cooled from 215°C to 205°C with a cooling rate of 0.5°C/min [88].

Another interesting result obtained by melting stirring experiments is the influence of shear rate on grain growth rate. The grain growth rate is proportional to the shear rate [86, 91]. This can be explained by Ostwald ripening and direct grain coalescence which are controlled by diffusion process. Meanwhile, the diffusivity is higher at a higher shear rate; therefore, the shear rate increases the grain growth rate.

In order to explain the evolution of grain size and morphology during partial solidification, Fig. 1.27 can be used to schematically illustrate the morphological transition from dendritic to spherical via rosette during stirring process. For a given alloy with dendrite microstructure, the dendritic grains are destroyed by shear stress and then grow into smaller spherical grains. When the slurry is continuously stirred, the smaller spherical grains will be separated by shearing and grain collision. Normally, the grain growth can be explained by two coarsening mechanisms: Ostwald ripening and grain coalescence. By the solute diffusion process, the small grains will dissolute to the larger ones. The agglomerated grains would cause grain coalescence in order to reduce the surface energy. When the agglomeration and the break down mechanisms are balanced Ostward ripening might become the prevalent mechanism.

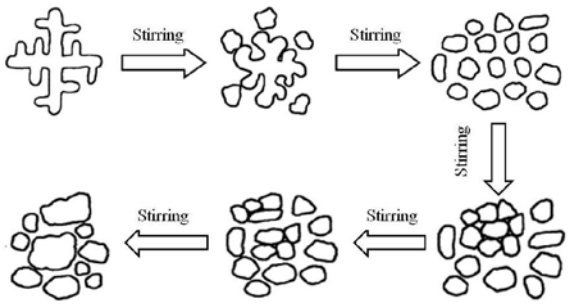

Fig. 1.27. Morphological transition during stirring process.

4.2.2. Influence on morphology during partial remelting

Remelting of a given material into the semi-solid state is important to the thixoforming process. During billet reheating, not only is the solid fraction well controlled but also a spherical morphology with fine grain size is desired. Therefore, it is necessary to understand the structure evolution for the process optimization.

Basically, microstructure evolution during reheating is controlled by diffusion process. The driving force of the transformation of the solid phase to a spherical morphology is the reduction of the interfacial energy between the solid and liquid phases. For a steady forming process, on the one hand, the heating time should be long enough in order to reach an ideal

microstructure, on the other hand, the heating time and holding time should be short to save on heating cost and to prevent excessive grain growth which is detrimental to mechanical properties of the thixoformed parts.

The microstructure evolution during partial heating depends on the initial structure of the material. Wang et al. [92] studied the microstructure evolution of different initial microstructures of an Al alloy during partial remelting. They found the final microstructure depended on the initial microstructure and the isothermal holding time. Fig. 1.28 shows the different remelting behavior of various feedstock materials heated to the same temperature and with isothermal holding time.

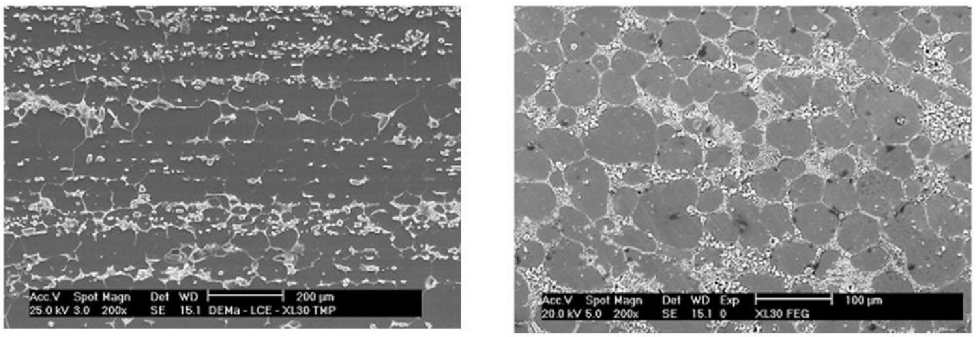

(a) Extruded feedstock (b) Rolled feedstock

Fig. 1.28. Microstructure of A356 at 575°C after isothermal holding for 2 min. (a) As extruded feedstock material. (b) Solution heat treated feedstock material [93].

Another phenomenon observed during heating to the semi-solid state is the entrapped liquid phase. For feedstock materials with a dendritic morphology, liquid will be entrapped in the grains caused by rapid coalescence of dendritic arms and grain coalescence. For the feedstock materials with an equiaxed morphology obtained by extruding or rolling, due to the self-blocking phenomenon [94], some of the liquid phase remains inside the grains during reheating and holding. In the heating and holding process, it seems that Ostwald ripening and grain coalescence affect the liquid entrapping process, but with opposite effects. The grain coalescence will cause the liquid entrapment because of the complex shaped grains. By contrast, Ostwald ripening leads to a loss of entrapped liquid, because of the dissolution of small grains to entrapped liquid. And the entrapped liquid would be released into the bulk liquid [95-97].

During isothermal holding in the semi-solid state, regardless of the initial grain morphology, the grains always evolve to a spherical morphology [92, 98, 99]. Meanwhile, the

grain size increases with increasing holding time, while there is no significant change in solid fraction. Although the total solid fraction changes a little, the volume fraction of the entrapped liquid phase decreases with increasing holding time due to the Ostwald ripening as shown in Fig. 1.29 [100].

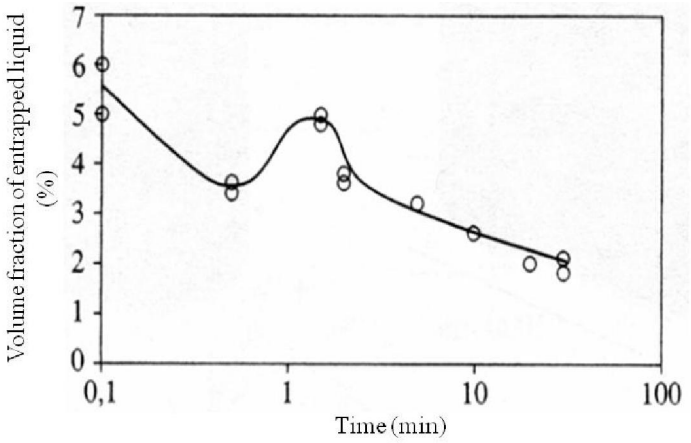

Fig. 1.29. Evolution of the entrapped liquid fraction as a function of time of AS7U3 isothermally held at 573°C [100].

The larger the initial shape factor (Eq. 1.11), the faster the kinetics for spheroidization, and the shorter holding time required for obtaining spherical grains as shown in Fig. 1.30. There are two coarsening processes occurring during the isothermal holding of dendritic or near dendritic microstructures termed as spheroidization and ripening. Normally, the former starts earlier than the latter.

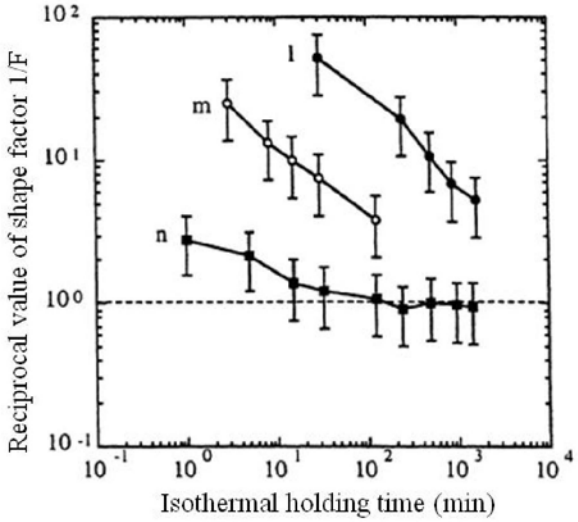

Fig. 1.30. Reciprocal value of shape factor *1/F* as a function of holding time at 580°C for Al–7Si–0·6Mg alloy obtained by classical continuous casting, without (l) and with (m) grain refining, and by MHD stirring (n) [102].

The solid fraction which depends on the temperature influences the kinetics of microstructure evolution. The coarsening rate increases with decreasing solid fraction. Based on the experimental results, Sannes et al. [101] proposed that grain growth by coalescence ripening makes a major contribution to the total microstructure coarsening, while at low solid fraction, Ostwald ripening is the dominant mechanism for structure coarsening.

Classically, the coarsening kinetic at a low solid fraction where the grains are well separated follows the Lifshitz-Slyozov-Wagner (LSW) theory [103]. The following equation gives the simple LSW law (Eq. 1.15).

$$d^3 - d_0^3 = Kt \qquad \text{(Eq. 1.15)}$$

where d is the average grain diameter at time t, d_0 is the average grain diameter at time $t=0$, K is the coarsening rate constant.

For higher fractions of solid where the grains diffusion fields are interacting, a liquid film migration model was proposed by Annavarapu and Dooherty [96] which indicates the coarsening rate should increase with increasing solid fraction. However, the experimental results for high solid fraction alloys ($F_s > 0.7$) show a decreasing coarsening rate with increasing solid fraction. Therefore, a modified liquid film migration model which takes into account the necks between the contacted solid grains was proposed by Manson-Whitton [104]. They suggest the transition value (f_{s0}) will depend on the dihedral angle between two solid grains in contact with liquid. If wetting is difficult (large dihedral angle) then the transition will occur at lower values of the fraction solid. Kim and Yoon [105] and Boettinger et al. [106] have observed that, at high solid fractions, coarsening in Mo–Ni–Fe and Al–Sn alloys is controlled by diffusion through the liquid rather than by the solid–solid contacts. In addition, grain contacts tend to lead to a decrease in grain growth rates because of the reduced solid/liquid interfacial area.

4.2.3. Influence of morphology on rheology

The effects of the morphology of the solid phase on the rheological behavior can be determined by various mechanical tests performed on semi-solid metallic slurries. The effects of morphology are always linked to the influence of experimental process parameters on the shear stress or viscosity.

Compression, extrusion and indentation tests are always applied to study the influences of the morphology of the tested alloy in the semi-solid state. Bigot et al. [64] compared the forming force used for penetrating the material with different morphology in the semi-solid state. As results show (Fig. 1.31), the force used for forming the material with a dendritic microstructure is much bigger than that used for the material with a spherical microstructure.

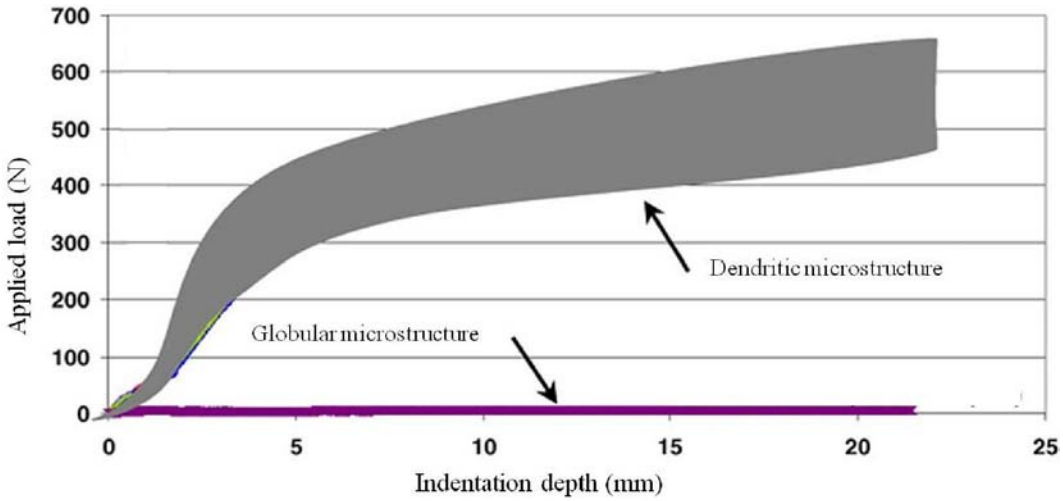

Fig. 1.31. Evolution of the forming force as a function of indentation depth at a forming speed of 1mm/s, performed on Sn-15% Pb alloy with two different microstructures [64].

The influence of the shape factor on viscosity can be investigated on different holding times by various mechanical tests. As mentioned above, during partial remelting process, the roundness of the grain (shape factor ***F*** from Eq. 1.11) increases with increasing isothermal holding time (Fig. 1.30, Fig. 1.32 (b)).

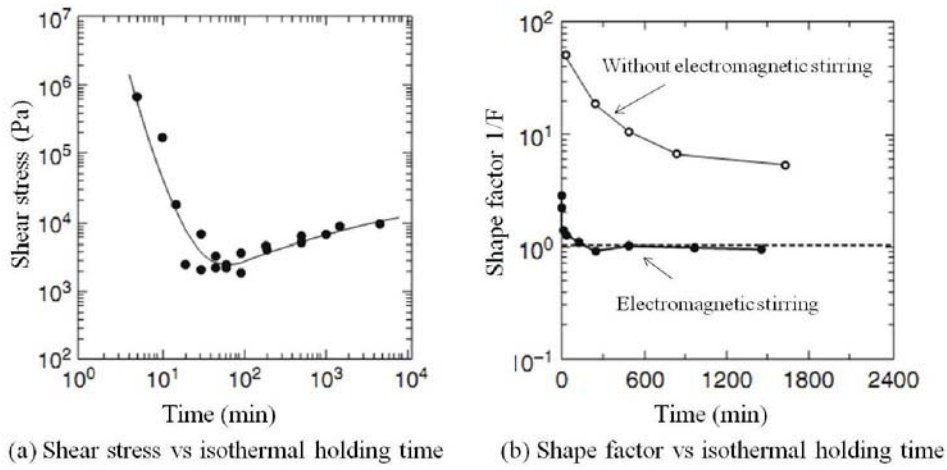

(a) Shear stress vs isothermal holding time (b) Shape factor vs isothermal holding time

Fig. 1.32. Influence of isothermal holding time on (a) shear stress and (b) shape factor.

Fig. 1.32 (a) presents the variation of shear stress deduced from a compression test performed on an A357 alloy obtained by solidification with electromagnetic stirring. The influence of the holding time on shape factor is shown in Fig. 1.32 (b). It can be found that the shear stress decreases sharply for short holding time range and then increases slightly for long holding time. The decrease of the shear stress responds to the spheroidization as shown in Fig. 1.32 (b). The increase of the viscosity can be explained by the agglomeration with long holding time.

Shear rate is another parameter which affects the morphology of the slurry, therefore affects the rheological properties of semi-solid metallic slurries. With increasing shear rate the grain size decreases, while the grain density increases under laminar flow conditions [87] which could be explained by an increase in initial nucleation rate with increasing shear rate. Ji and Fan also found that the formation of spherical grains could be obtained quickly under intensive turbulent flow conditions. In addition, Ji and Fan [88], Ryoo and Kim [89] also found that grain size decreased rapidly with increasing shear rate under the low shear rate region, while the grain size leveled off under the high shear rate (Fig. 1.26) [47, 74].

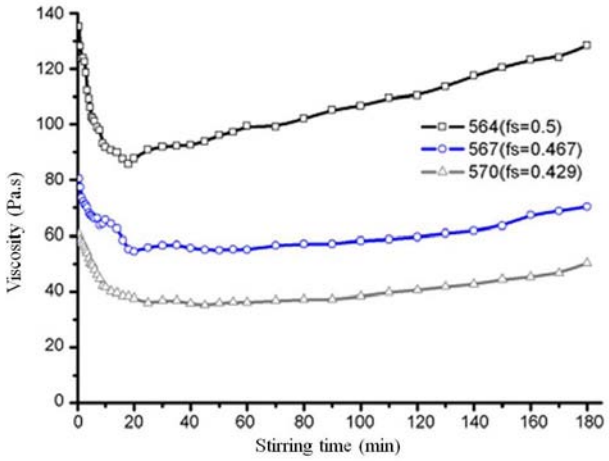

Fig. 1.33. Influence of stirring time on the apparent viscosity performed on AZ91D alloy [56].

The influence of the morphology of solid phase can also be obtained by stirring semi-solid slurry using a viscometer. Similar evolution of the viscosity as a function of stirring time is illustrated in Fig. 1.33 performed on a partially solidified AZ91D alloy. The sharp decrease in shear stress responds to the destruction of dendrite arms. Long isothermal stirring time results in the grain agglomeration and grain coarsening, therefore increases the viscosity. Meanwhile,

Loué et al. give the influence of the shape factor on viscosity. The viscosity decreases with rounder solid grains (Fig. 1.34).

As is well known, the viscosity increases with increasing liquid fraction. Here, the liquid fraction means the effective liquid fraction. The entrapped liquid inside the grains does not participate in the rearrangement of the grains during deformation. At a given temperature, increase of the entrapped liquid fraction implies a smaller effective liquid fraction, which therefore increases the viscosity.

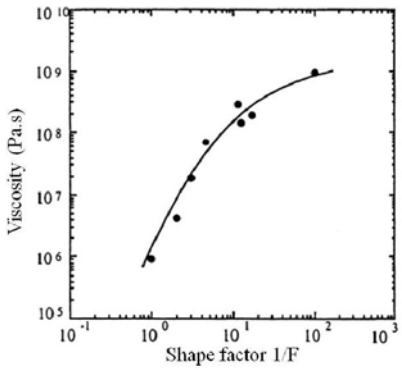

Fig. 1.34. Viscosity of Al-7Si-0.6Mg alloy with solid fraction of 0.5 as a function of grain shape factor [107].

Another important factor is the connectivity of the grains as shown from the examinations of the aluminum alloy AA6082 [108]. The author pointed out that homogeneous deformation occurs when the contiguity volume value is smaller than 0.3.

5. Alloy development for SSM processing

5.1. Different technologies for SSM

Over 40 years, the SSM processing has experienced intensive research and development. It has established itself as a scientifically sound technology for producing complex parts with improved mechanical properties and high integrity. The alloys commonly used for semi-solid metallic processing are optimized for either casting or forging process. Different from the conventional forming technologies (casting and forging processes), SSM processing shapes a metallic alloy with a non-dendritic microstructure in the semi-solid state. Due to its unique requirement, new alloys have been developed for the SSM processing. These alloys possess the properties which can improve both the SSM formability and mechanical properties, such

as low temperature sensitivity of solid fraction, wide solidification range, low solidus temperature for high melting point alloys, potential for age hardening, favorable rheological properties, stability to composition tolerance etc. Among them, the solid phase morphology, rheological properties and processability depend largely on processing conditions. Meanwhile the temperature sensitivity, solidus temperature and solidification range are sensitive to the chemical compositions. Normally, the computational thermodynamics is always applied for studying the influence of compositional variations on temperature sensitivity, solidification range and potential for age hardening for the alloy design. Liu et al. used the computational thermodynamic approach (CALPHAD) to evaluate the processability of commercial aluminum alloys [109, 110] and magnesium alloys [111]. Püttgen et al. [112] pointed out that solidus and liquidus temperatures depend on the carbon content and the dissolution of different carbides when investigating the effects of the chemical composition on the thermophysical properties of the steel grades using the software IDS (Fig. 1.35). By thermodynamic prediction, Hallstedt et al. [113] suggest the temperature ranges between 40% liquid fraction and 60% for thixocasting, and 20% - 40% for thixoforging.

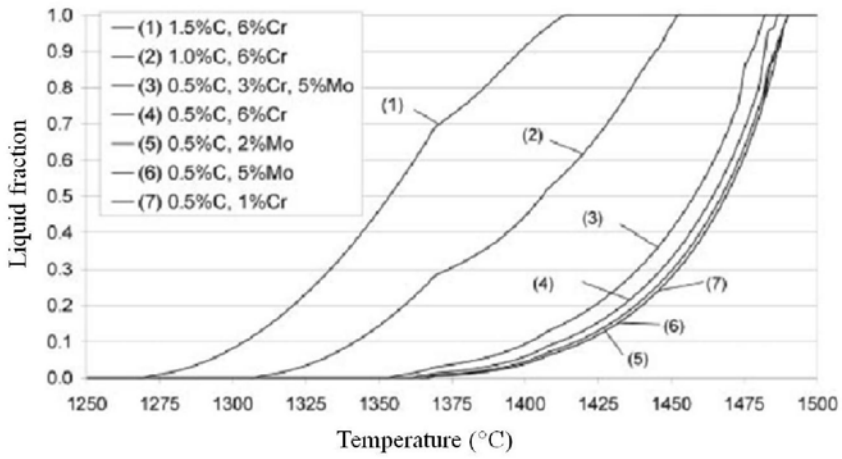

Fig. 1.35. Liquid fraction vs temperature for various compositions calculated by IDS [112].

Fig. 1.35 summaries the curves of liquid fraction against the temperature of various steel grades obtained by DTA measurements. High alloy tool steel grades X210CrW12 and HS 6-5-3 have a wide solidification range as well as bearing steel 100Cr6. In addition, ASCOMETAL developed several steel grades with lower solidus temperature and wider solidification range for semi-solid forming as shown in Fig. 1.36. Li et al. [114] argued that spheroidization will always occur in alloys with a peritectic reaction in the solid state.

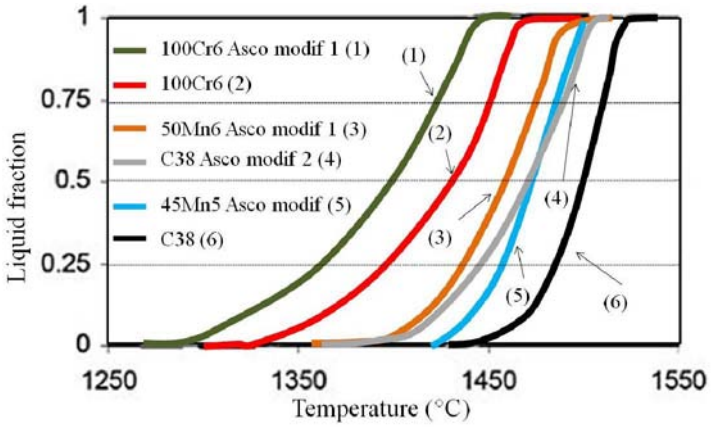

Fig. 1.36. Liquid fraction vs Temperature of various steel grades obtained by DSC [115, 116].

5.2. Influence of manufacturing process on the material

The material used for thixoforming can have various initial microstructures due to the manufacturing process such as casting, rolling, extruding etc. Due to the interplay of a variety of physical and chemical factors during cooling, the initial microstructure of the as-cast billets for the semi-solid forming process is always non-uniform, instead, three different microstructure zones can be found as shown in Fig. 1.37. However, after proper treatments on as-cast billet, when reheated into the semi-solid state it will have a spheroidal microstructure which is suitable for semi-solid forming process.

The rolled or extruded material is preferable for the thixoforming process. Because it takes less time to spheroidize the grains in the semi-solid state, owing to the refined and equiaxed initial grains.

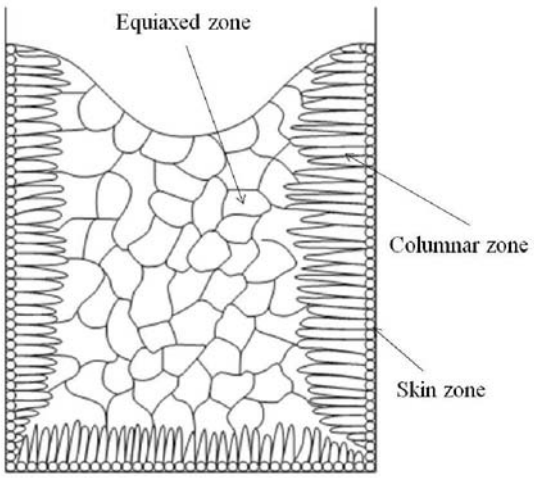

Fig. 1.37. Classical microstructure of chill-cast ingot [117].

6. Industrial applications of SSM

The SSM process of aluminum alloys has been industrialized while the steel thixoforming is being developed. Various aspects for steel thixoforming should be well understood and controlled for the development of industrial steel thixoforming.

In material aspects: the identification of the steel grades, microstructure evolution during heating.

In processing aspects: the forming speed, die temperature, billet temperature, holding time, billet heating, handling and transition systems.

In conclusion, the industrial developments mainly include: temperature measurement and induction heating, transfer and handling system, press equipment and process controlling.

As stated before, heating of the feedstock billets is not required for the rheoforming routes. In contrast, the feedstock billets for thixoforming routes are always heated by induction heating because of its high heating speed and repeatability. However, due to the skin effect, multi-step heating cycles are needed in order to obtain a uniform temperature field through the billet. In addition, the billet should maintain its shape before shaping. During induction heating, the temperature is always measured by thermocouples. However, in an industrial production environment, it is not possible to measure the temperature of each billet by thermocouples. For this reason, Becker et al. [63] suggested heating billets (without thermocouples) with predefined heating cycles obtained by extensive heating tests with thermocouples. However, this method is not robust against any changes in the production conditions. Flatness-based control approach [118] and temperature control with a pyrometer approach [119] have been applied for heating the billets into the semi-solid state without using the thermocouples.

In order to achieve high efficiency, reproducibility of transition and handling operation, industrial robots are necessary for the steel thixofoming process. After transferring the well-heated billet to the optimized position, it must be deformed with a thixofoming process which can be operated under either load or displacement control. It is suggested that the semi-solid metal should be deformed under high speed deformation either with a hydraulic or a mechanical press. A mechanical press provides high deformation while a hydraulic press presents some advantages with the possibility to use some sillies or pistons and with a very

large surface table. After forming process, the formed parts should meet the market requirements, such as the dimension, geometry, hardness and metallographic structure etc. The semi-solid forming process of low melting point alloys has been industrialized [47]. While the development of the semi-solid forming process of steel for implementation as an industrial application was slow due to technological problems. Nevertheless, various steel components have been produced by the semi-solid forming process.

The steel components are always produced by thixo-routes for their near-net shape capability. Different steel components produced by various semi-solid forming processes are shown in the following table 1.2.

Table. 1.2. Various parts produced by semi-solid forming process.

Forming route	Photos	Nuance	Ref.
Thixoforging	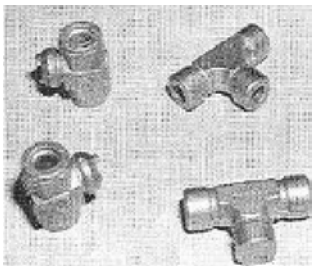	X105CrMo17, X5CrNi18-10	[120]
		M2, CoCr28MoNi	[121]
		FCD-45	[122]
		C38, C70, C80	[123]
		C38, C60, C80, HS6-5-3	[124]

	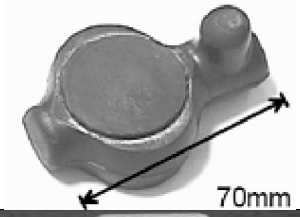	C38, C50, 100Cr6	[125]
		X210CrW12, 100Cr6	[72]
Thixocasting	 	C70, 100Cr6, HS6-5-2	[126]
	 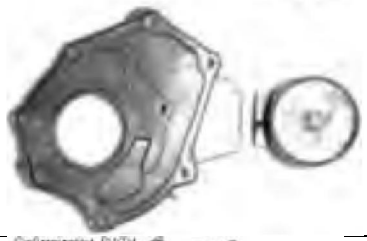	FCD450-10, Co-base alloy	[127]
		X210CrW12, X38CrMoV5-1, Laser sintered direct steel powder	[128, 129]
	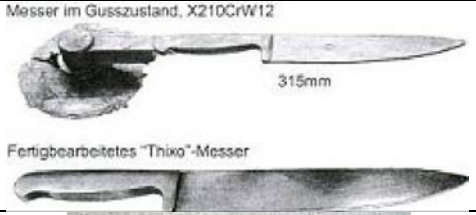	X210CrW12, X38CrMoV5-1, Laser sintered direct steel powder	[129]
Thixoextrusion		100Cr6, HS6-5-2	[112]

		HS6-5-3, X210CrW12, 100Cr6, C60	[8]
		X210CrW12	[5]
		HS6-5-3, 100Cr6	[72]
Thixojoining	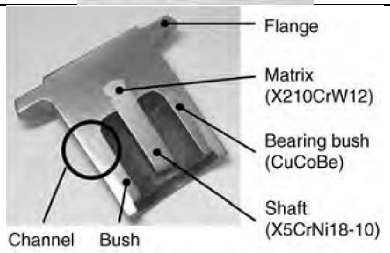	X210CrW12	[1]
		HS6-5-3, 100Cr6,	[8]
Rheoforging		X210CrW12, 100Cr6	[1]

7. Conclusions

The current status of semi-solid processing has been reviewed in this chapter.

Firstly, the thixotropic behavior of semi-solid alloys with spherical rather than dendrite microstructures has been described. The thixotropic behavior is associated with different kinetics between the aggregation and destruction of the grains. Therefore the importance of metallurgical structures was emphasized. A globular structure is the basis of the thixotropic behavior for the semi-solid forming process. Various semi-solid slurry preparation methods were introduced.

Secondly, the rheology of the semi-solid globular structure was studied. The rheology is due to the variation of the effective liquid fraction, grain size and the contiguity of the grains associated with shear rate. The influence of the process on the morphology and on rheological behavior has been introduced. Various microstructure evolution mechanisms in the semi-solid state were described. The heating time, liquid fraction and starting microstructure have a strong influence on the morphology in the semi-solid state, which in turn influence the rheology.

Finally, some examples of industrial applications have been given.

Depending on the available facilities and the earlier studies on semi-solid forming process in the LCFC (Laboratoire de Conception, Fabrication Commande), at Arts et Métiers ParisTech, Metz, the thixoforging process will be studied, mainly on the billet preparation route, microstructure characterization and the influence of the forming process on the microstructure. As for the billet preparation route, the study will focus on the thixoformability of the material in the as-received state. C38LTT, 100Cr6 and M2 steel grades will be studied for different aims. For the microstructure characterization, as stated above, the liquid fraction is important to the rheology, and thus, to thixoforging process. Therefore it is important to measure the liquid/solid fraction and characterize the microstructure during different thixoforging processes (heating, thixoforming etc). Thixoforging experiments should also be carried out with various process conditions in order to study their influence on the microstructure, mechanical properties etc.

References

1. Becker E: **Investigations experimentales et numeriques pour l'identification des parametres clefs du procede de thixoforgeage de l'acier sur le produit mis en forme.** Thesis. L'Ecole Nationale Supériure d'Arts et Métiers, Docteur de L'Ecole National Supérieure d'Arts et Métiers; 2008.

2. Cézard P: **Impact des effets thermiques sur le comportement du matériau lors de la mise en forme des aciers à l'état semi-solide : Analyses expérimentale et numérique.** Thesis. L'Ecole Nationale Supériure d'Arts et Métiers, Docteur de l'Ecole National Supérieure d'Arts et Métiers; 2006.

3. Spencer D, Mehrabian R, Flemings MC: **Rheological behavior of Sn-15 pct Pb in the crystallization range.** *Metallurgical and Materials Transactions B* 1972, **3:**1925-1932.

4. Flemings MC: **Solidification processing.** *Metallurgical and Materials Transactions B* 1974, **5:**2121-2134.

5. Hirt G, Kopp R (Eds.): **Thixoforming - semi-solid metal processing**. Aachen: Wiley-VCH Verlag GmbH & Co. KGaA; 2009.

6. Pasternak L, Carnaha RD, Decker R, Kilber R: **Semisolid production processing of Mg alloys by thixomolding** In *Proceedings of the 2nd International Conference on Semi-Solid Processing of Alloys and Composites; MIT, Cambridge, MA*. Edited by Brown SB, Flemings MC. TMS, Warrendale; 1992: 159-169.

7. Ji S, Fan Z, Bevis MJ: **Semi-solid processing of engineering alloys by a twin-screw rheomoulding process.** *Materials Science and Engineering: A* 2001, **299:**210-217.

8. Kopp R, Kallweit J, Möller T, Seidl I: **Forming and joining of commercial steel grades in the semi-solid state.** *Journal of Materials Processing Technology* 2002, **130–131:**562-568.

9. Song R, Kang Y, Zhao A: **Semi-solid rolling process of steel strips.** *Journal of Materials Processing Technology* 2008, **198:**291-299.

10. Flemings MC: **Semi-solid forming - the process and the path forward.** *Metallurgical Science and Technology* 2000, **18:**3-4.

11. Flemings MC, Riek RG, Young KP: **Rheocasting.** *Materials Science and Engineering* 1976, **25:**103-117.

12. Kenney MP, Courtois JA, Evans RD, Farrior GM, Kyonka CP, Koch AA, Young KP: **Semi-solid metal casting and forging.** In *Metal handbook. Volume* 15: ASM International; 1988: 327-338

13. Young KP: **Method of producing shaped metal parts.** 4687042 edition. US: alumax, Inc (San Mateo, CA); 1987.

14. Moschini R: **Manufacture of automotive components by semi liquid forming process.** In *Proceedings of the 2nd International Conference on Semi-Solid Processing of Alloys and Composites; MIT, Boston*. Edited by Brown SB, Flemings MC. TMS, Warrendale; 1992: 149-158.

15. Mehrabian R, flemings MC: **Metal composition and methods for preparing liquid-solid alloy metal compoitions and for casting the metal compositions.** 3951651 edition. US; 1976.

16. Flemings MC, Mehrabian R, Riek RG: **Continuous process for forming an alloy containing non-dendritic primary solids.** 3902544 edition. US: Massachusetts Institute of Technology; 1975.

17. Wang KK, Peng H, Wang N, Wang SP: **Method and apparatus for injection molding of semi-solid metals.** 5,501,266 edition. US: Cornell Research Foundation, Inc.; 1996.

18. Zhang K, Xue XX, Zhang JX, Du DC, Xu J, Shi LK: **Semi-solid slurry preparation and forming process (in Chinese).** 01134349 edition. China; 2001.

19. Kiuchi M, Sugiyama S: **A new process to manufacture semi-solid alloys.** *ISIJ International* 1995, **35:**790-797.

20. Walmag G, Naveau P, Rassili A, Sinnaeve M: **A new processing route for as-cast thixotropic steel.** *Solid State Phenomena* 2008, **Semi-Solid Processing of Alloys and Composites X:**415-420.

21. Shibata R, Kaneuchi T, Soda T: **New semi-liquid metal casting process.** In *Proceedings of the 4th International Conference on Semi-Solid Processing of Alloys and Composites; UK: University of Sheffield*. Edited by Kirkwood DH, Kapranos P. 1996: 296-300.

22. Sato S, Harada Y, Ishibashi N, Adachi M: **Effect of strontium, magnesium and iron content on mechanical properties of rheocast Al-7 mass%Si-Mg alloys.** *Materials Transactions* 2009, **50:**354-360.

23. Hong CP, Kim BM: **Development of an advanced rheocasting process and its applications.** *Solid State Phenomena* 2006, **116-117:**44-53.

24. Mao WM: **Investigation of microstructure evolution of non-dendritic AlSi7Mg alloy in semi-solid state.** Thesis. University of Science and Technology, Department of Material Science and Engineering 1999.

25. Mitsuru A, Hiroto S, Yasunori H, Tatsuo S, Atsushi Y: **Method and apparatus of shaping semisolid metals.** EP 0745694 edition. EU: UBE Industires Ltd; 1996.

26. Haga T, Suzuki S: **Casting of aluminum alloy ingots for thixoforming using a cooling slope.** *Journal of Materials Processing Technology* 2001, **118:**169-172.

27. Flemings MC, Martinez Ayers RA, De Figueredo AM, Yurko JA: **Metal alloy compositions and process.** 6645323 edition. US: Massachusetts Institute of Technology; 2003.

28. Yurko JA, Martinez RA, Flemings M: **Development of semisolid rheocasting (SSR).** In *Proceedings of the 7th International Conference on Semi-Solid processing of Alloys and Composites; Japan: National Institute of Advanced Industrial Science and Technology, Japan Society for Technology of Plasticity*. Edited by Tsutsui Y, Kiuchi M, Ichikawa K. 2002: 659-664.

29. Wang G, Witulski T, Hirt G: **Thixoforming of aluminium alloys using modified chemical grain refinement for billet production.** *La Metallurgia Italiana* 1994, **86:**29-36.

30. Wang H, Ning ZL: **Magnesium thixotropic structure produced by controlled nucleation method.** *Special Casting and Nonferrous Alloys* 2007**:**316-319.

31. Kirkwood DH, Sellars CM, Elias Boyed LG: **Thixotropic materials.** 5037489 edition. EU; 1991.

32. Young KP, Kyonka CP, Courtois JA: **Fine grained metal composition.** 4415374 edition. USA; 1983.

33. Song RB, Kang YL, Sun JL: **Microstructure evaluation of semi-solid steel materials in rolling process and the resulting mechanical properties.** *Acta Metallurgica Sinica* 2001, **14:**347-351.

34. Ramadan M, Takita M, Nomura H: **Effect of semi-solid processing on solidification microstructure and mechanical properties of gray cast iron.** *Materials Science and Engineering: A* 2006, **417:**166-173.

35. Bülte R, Bleck W: **Effects of pre-processing on thixo-formability of steel grade 100Cr6.** *Steel Research International* 2004, **75:**588-592.

36. Omar MZ, Palmiere EJ, Howe AA, Atkinson HV, Kapranos P: **Thixoforming of a high performance HP9/4/30 steel.** *Materials Science and Engineering: A* 2005, **395:**53-61.

37. Omar MZ, Atkinson HV, Howe AA, Palmiere EJ, Kapranos P, Ghazali MJ: **Solid–liquid structural break-up in M2 tool steel for semi-solid metal processing.** *Journal of Materials Science* 2008, **44:**869-874.

38. Hirt G, Bobzin K, Khizhnyakova L, Ewering M, Bagcivan N: **Semi-solid forming of non axis-symmetric parts from steel grade X210CrW12 with PVD coated tools.** *International Journal of Material Forming* 2010, **3:**731-734.

39. Gabathuler JP, Huber HJ, Erling J: **Specific properties of produced parts using the thixocasting process.** *Metallurgia Italiana* 1994, **86:**609-615.

40. Lebeau S, Decker R: **Microstructural design of thixomolded magnesium alloys.** In *5th International Conference on Semi-Solid Processing of Alloys and Composites; Colorado, USA*. Edited by Bhasin AK, Moore JJ, Young KP, Midson S. Colorado School of Mines; 1998: 217-224.

41. Joly PA, Mehrabian R: **The rheology of a partially solid alloy.** *Journal of Materials Science* 1976, **11:**1393-1418.

42. Flemings M: **Behavior of metal alloys in the semisolid state.** *Metallurgical and Materials Transactions A* 1991, **22:**957-981.

43. Kirkwood DH: **Semisolid metal processing.** *International Materials Reviews* 1994, **39:**173-189.

44. Fan Z: **Semisolid metal processing.** *International Materials Reviews* 2002, **47:**49-85.

45. Lashkari O, Ghomashchi R: **The implication of rheology in semi-solid metal processes: An overview.** *Journal of Materials Processing Technology* 2007, **182:**229-240.

46. Brabazon D, Browne DJ, Carr AJ: **Experimental investigation of the transient and steady state rheological behaviour of Al–Si alloys in the mushy state.** *Materials Science and Engineering: A* 2003, **356:**69-80.

47. Kirkwood DH, Suéry M, Kapranos P, Atkinson HV, Young KP: *Semi-solid Processing of Alloys.* Springer; 2010.

48. Modigell M, Koke J, Kopp R, Neudenberger D, Sahm P, Klaassen O: **Comparison of rheological measurement methods for semi-solid alloys.** In *6th International Conference on Semi-Solid Processing of Alloys and Composites; Turin, Italy*. Edited by Chiarmetta GL, Rosso M. 2000: 605-609.

49. Ludwig O, Drezet JM, Martin C, Suéry M: **Rheological behavior of Al-Cu alloys during solidification constitutive modeling, experimental identification, and numerical study.** *Metallurgical and Materials Transactions A* 2005, **36:**1525-1535.

50. Lehuy H, Masounave J, Blain J: **Rheological behaviour and microstructure of stir-casting zinc-aluminium alloys.** *Journal of Materials Science* 1985, **20:**105-113.

51. Nan WS, Guangji S, Hanguo Y: **Rheological study of partially solidified Tin-Lead and Aluminium-Zinc alloys for stir-casting.** *Materials Transactions* 1990, **31:**715-722.

52. Kattamis TZ, Piccone TJ: **Rheology of semisolid Al-4.5%Cu-1.5%Mg alloy.** *Materials Science and Engineering: A* 1991, **131:**265-272.

53. Loue WR, Landkroon S, Kool WH: **Rheology of partially solidified AlSi7Mg0.3 and the influence of SiC additions.** *Materials Science & Engineering A, Structural materials : properties, microstructure and processing* 1992, **151:**255-262.

54. Turng LS, Wang KK: **Rheological behaviour and modelling of semi-solid Sn-15% Pb alloy.** *Journal of Materials Science* 1991, **26:**2173-2183.

55. Liu T, Ward P, Atkinson H, Kirkwood D: **Response of semi-solid Sn-15 pct Pb to rapid shear-rate changes.** *Metallurgical and Materials Transactions A* 2003, **34:**409-417.

56. Chen H-I, Chen J-C, Liao J-J: **The influence of shearing conditions on the rheology of semi-solid magnesium alloy.** *Materials Science and Engineering: A* 2008, **487:**114-119.

57. Azzi L, Ajersch F: **Development of alumnium base alloys for forming in semi solid state.** In *TransAL Conference; Lyon, France*. 2002: 23-33.

58. Lashkari O, Ghomashchi R: **The implication of rheological principles for characterization of semi-solid Al–Si cast billets.** *Journal of Materials Science* 2006, **41:**5958-5965.

59. Laxmanan V, Flemings M: **Deformation of semi-solid Sn-15 Pct Pb alloy.** *Metallurgical and Materials Transactions A* 1980, **11:**1927-1937.

60. Suery M, Flemings M: **Effect of Strain Rate on Deformation Behavior of Semi-Solid Dendritic Alloys.** *Metallurgical and Materials Transactions A* 1982, **13:**1809-1819.

61. Yurko J, Flemings M: **Rheology and microstructure of semi-solid aluminum alloys compressed in the drop-forge viscometer.** *Metallurgical and Materials Transactions A* 2002, **33:**2737-2746.

62. Becker E, Favier V, Bigot R, Cezard P, Langlois L: **Impact of experimental conditions on material response during forming of steel in semi-solid state.** *Journal of Materials Processing Technology* 2010, **210:**1482-1492.

63. Becker E, Bigot R, Langlois L: **Thermal exchange effects on steel thixoforming processes.** *The International Journal of Advanced Manufacturing Technology* 2009, **48:**913-924.

64. Bigot R, Favier V, Rouff C: **Characterisation of semi-solid material mechanical behaviour by indentation test.** *Journal of Materials Processing Technology* 2005, **160:**43-53.

65. Ferrante M, deFreitas E, Monilha M, Sinka V: **Rheological properties and microstructural evolution of semi-solid aluminum alloys inoculated with mischmetal and with titanium.** In *5th International Conference Semisolid Processing of Alloys and Composites; Colorado, USA*. Edited by Bhasin AK, Moore JJ, Young KP, Midson S. Colorado School of Mines; 1998: 35-42.

66. Martin CL, Favier D, Suéry M: **Viscoplastic behaviour of porous metallic materials saturated with liquid part I: Constitutive equations.** *International Journal of Plasticity* 1997, **13:**215-235.

67. Suery M, Zavaliangos A: **Key problems in rheology of semi-solid alloys.** In *Proceedings of the 6th International Conference on Semi-solid Processing of Alloys and Composites; Turin*. Edited by Chiarmetta GL, Rosso M. Edimet Spa; 2000: 129-135.

68. Kapranos P, Liu TY, Atkinson HV, Kirkwood DH: **Investigation into the rapid compression of semi-solid alloy slugs.** *Journal of Materials Processing Technology* 2001, **111:**31-36.

69. Tzimas E, Zavaliangos A: **Evaluation of volume fraction of solid in alloys formed by semisolid processing.** *Journal of Materials Science* 2000, **35:**5319-5329.

70. Salvo L, Cloetens P, Maire E, Zabler S, Blandin JJ, Buffière JY, Ludwig W, Boller E, Bellet D, Josserond C: **X-ray micro-tomography an attractive characterisation technique in materials science.** *Nuclear Instruments and Methods in Physics Research Section B: Beam Interactions with Materials and Atoms* 2003, **200:**273-286.

71. Liu D, Atkinson HV, Jones H: **Thermodynamic prediction of thixoformability in alloys based on the Al–Si–Cu and Al–Si–Cu–Mg systems.** *Acta Materialia* 2005, **53:**3807-3819.

72. Püttgen W, Bleck W, Hirt G, Shimahara H: **Thixoforming of steels – A status report.** *Advanced Engineering Materials* 2007, **9:**231-245.

73. Püttgen W, Bleck W: **Thixoforming/semi-solid forming : DTA-measurements to determine the thixoformability of steels.** *Steel Research International* 2004, **75:**531-536.

74. Loue WR, Suery M: **Microstructural evolution during partial remelting of Al-Si7Mg alloys.** *Materials Science and Engineering: A* 1995, **203:**1-13.

75. Qin RS, Fan Z: **Fractal theory study on morphological dependence of viscosity of semisolid slurries.** *Materials Science and Technology* 2001, **17:**1149-1152.

76. **Metallkundliche Aspekte bei der semi-solid Formgebung von Leichtmetallen**

77. Gurland J: **A structural approach to the yield strength of two-phase alloys with coarse microstructures.** *Materials Science and Engineering* 1979, **40:**59-71.

78. Chen JY, Fan Z: **Modelling of rheological behaviour of semisolid metal slurries Part 1- Theory.** *Materials Science and Technology* 2002, **18:**237-242.

79. Limodin N, Salvo L, Suéry M, DiMichiel M: **In situ investigation by X-ray tomography of the overall and local microstructural changes occurring during partial remelting of an Al–15.8wt.% Cu alloy.** *Acta Materialia* 2007, **55:**3177-3191.

80. Zabler S, Rueda A, Rack A, Riesemeier H, Zaslansky P, Manke I, Garciamoreno F, Banhart J: **Coarsening of grain-refined semi-solid Al–Ge32 alloy: X-ray microtomography and in situ radiography.** *Acta Materialia* 2007, **55:**5045-5055.

81. Terzi S, Salvo L, Suery M, Dahle AK, Boller E: **Coarsening mechanisms in a dendritic Al–10% Cu alloy.** *Acta Materialia* 2010, **58:**20-30.

82. Kumar P, Martin C, Brown S: **Shear rate thickening flow behavior of semisolid slurries.** *Metallurgical and Materials Transactions A* 1993, **24:**1107-1116.

83. Yang Y, Tsao CY: **Viscosity and structure variations of Al–Si alloy in the semi-solid state.** *Journal of Materials Science* 1997, **32:**2087-2092.

84. Fan Z, Liu G, Hitchcock M: **Solidification behaviour under intensive forced convection.** *Materials Science and Engineering: A* 2005, **413-414:**229-235.

85. Sukumaran K, Pai BC, Chakraborty M: **The effect of isothermal mechanical stirring on an Al–Si alloy in the semisolid condition.** *Materials Science and Engineering: A* 2004, **369:**275-283.

86. Ji S, Roberts K, Fan Z: **Isothermal coarsening of fine and spherical particles in semisolid slurry of Mg– 9Al–1Zn alloy under low shear.** *Scripta Materialia* 2006, **55:**971-974.

87. Smith D, Eady J, Hogan L, Irwin D: **Crystallization of a faceted primary phase in a stirred slurry.** *Metallurgical and Materials Transactions A* 1991, **22:**575-584.

88. Ji S, Fan Z: **Solidification behaviour of Sn-15Pb alloy under high shear rate and high intensity of turbulence.** *Met Mater Trans* 2002, **33A:**3511-3520.

89. Ryoo YH, Kim DH: **Evolution of microstructure during semi-solid state processing of Mg-Al-Zn-X alloys.** In *3rd Int Conf on semisolid processing of alloys and composites; University of Tokyo, Japan*. Edited by Kiuchi M. Tokyo Institute of Industrial Science; 1994: 95-104.

90. Ji S, Das A, Fan Z: **Solidification behavior of the remnant liquid in the sheared semisolid slurry of Sn–15 wt.%Pb alloy.** *Scripta Materialia* 2002, **46:**205-210.

91. Wan G, Sahm PR: **Particle growth by coalescence and Ostwald ripening in rheocasting of PbSn.** *Acta Metallurgica et Materialia* 1990, **38:**2367-2372.

92. Wang HY, Davidson CJ, Stjohn DH: **Semisolid microstructural evolution of AlSi7Mg during partial remelting.** *Materials Science and Engineering A* 2004, **368:**159-167.

93. Kliauga AM, Ferrante M: **The influence of deformation mode on the semi-solid state microstructure of an A356 aluminium alloy.** *Jornadas SAM-Conamet* 2001**:**91-98.

94. Kleiner S, Beffort O, Uggowitzer PJ: **Microstructure evolution during reheating of an extruded Mg–Al–Zn alloy into the semisolid state.** *Scripta Materialia* 2004, **51:**405-410.

95. Secondé JF, Suéry M: **Effect of solidification conditions on deformation behaviour of semi-solid Sn-Pb alloys.** *Journal of Materials Science* 1984, **19:**3995-4006.

96. Annavarapu S, Doherty RD: **Inhibited coarsening of solid-liquid microstructures in spray casting at high volume fractions of solid.** *Acta Metallurgica et Materialia* 1995, **43:**3207-3230.

97. Chen TJ, Hao Y, Sun J, Li YD: **Phenomenological observations on thixoformability of a zinc alloy ZA27 and the resulting microstructures.** *Materials Science and Engineering: A* 2005, **396:**213-222.

98. Chen TJ, Hao Y, Sun J, Li YD: **Effects of Mg and RE additions on the semi-solid microstructure of a zinc alloy ZA27.** *Science and Technology of Advanced Materials* 2003, **4:**495-502.

99. Amin-Ahmadi B, Aashuri H: **Globular Structure of M2 High Speed Steel by Thermomechanical Treatment in the Semisolid State.** *Steel Research International* 2010, **81:**381-386.

100. Suery M: *Mise en forme des alliages métalliques à l'état semi-solide.* Paris: Hemès Science Publications; 2002.

101. Laukli H, Lohne O, Sannes S, Gjestland H, Arnberg L: **Grain size distribution in a complex AM60 magesium alloy die casting.** *Int J Cast Metals Research* 2003, **6:**515-521.

102. Blais S, Loue WR, Pluchon C: **Structure control by electromagnetic stirring and reheating at semi-solid state.** In *Proceedings of 4th International Conference on Semi-solid Processing of Alloys and Components; Sheffield, UK*. Edited by Kirkwood DH, Kapranos P. University of Sheffield; 1996: 187-192.

103. Lifshitz IM, Slyozov VV: **The kinetics of precipitation from supersaturated solid solutions.** *J Chem Phys Solids* 1961, **19:**35-50.

104. Manson-Whitton ED, Stone IC, Jones JR, Grant PS, Cantor B: **Isothermal grain coarsening of spray formed alloys in the semi-solid state.** *Acta Materialia* 2002, **50:**2517-2535.

105. Kim K, Yoon DN: **Coarsening behaviour of Mo grains dispersed in liquid matrix.** *Acta Metallurgica* 1983, **31:**1151-1157.

106. Boettinger W, Voorhees P, Dobbyn R, Burdette H: **A study of the coarsening of liquid-solid mixtures using synchrotron radiation microradiography.** *Metallurgical and Materials Transactions A* 1987, **18:**487-490.

107. Loue WR, Suery M, Querbes JL: **Microstructure and rheology of partially remelted AlSi-alloys.** In *Proc 2nd Int Conf on the Processing of Semi-Solid Alloys and Composites; Cambridge, USA*. Edited by Brown SB, Flemings MC. TMS, Warrendale; 1992: 266.

108. Gullo GC, Steinhoff K, Uggowitzer PJ: **Microstructural changes during reheating of semi-solid alloy AA 6082.** In *6th International Conference Semi-Solid Processing of Alloys and Composites; Turin*. Edited by Chiarmetta GL, Rosso M. Edimet Spa; 2000: 367-372.

109. Liu YQ, Fan Z, Patel J: **Thermodynamic approach to aluminium alloy design for semisolid metal** In *7th S2P on Advanced Semi-Solid Processing of Alloys and Composites; Tokyo, Japan*. Edited by Tsutsui Y, Kiuchi M, Ichikawa K. National Institute of Advanced Industrial Science and Technology and the Japan Society for Technology of Plasticity; 2002: 599-604.

110. Patel JB, Liu YQ, Shao G, Fan Z: **Rheo-processing of an alloy specifically designed for semi-solid metal processing based on the Al–Mg–Si system.** *Materials Science and Engineering: A* 2008, **476:**341-349.

111. Liu YQ, Fan Z: **Magnesium alloy selections for semisolid metal processing.** In *7th S2P International Conference on Semi-solid Processing of Alloys and Composites; Tokyo, Japan*. Edited by Tsutsui Y, Kiuchi M, Ichikawa K. National Institute of Advanced Industrial Science and Technology and the Japan Society for Technology of Plasticity; 2002: 587-592.

112. Püttgen W, Bleck W, Seidl I, Kopp R, Bertrand C: **Thixoforged damper brackets made of the steel grades HS6-5-3 and 100Cr6.** *Advanced Engineering Materials* 2005, **7:**726-735.

113. Hallstedt B, Baltichev E, Shimahara H, Neuschutz D: **Semi-solid processing of alloys: principles, thermodynamic selection criteria, applicability.** *ISIJ International* 2006, **46:**1852-1857.

114. Li J, Sugiyama S, Yanagimoto J, Chen Y, Fan G: **Effect of inverse peritectic reaction on microstructural spheroidization in semi-solid state.** *Journal of Materials Processing Technology* 2008, **208:**165-170.

115. Robelet M, Rassili A, Fischer D: **Steel grades adapted to the thixoforging process: metallurgical structures and mechanical properties.** *Solid State Phenomena* 2006, **Semi-Solid Processing of Alloys and Composites,116-117:**712-716.

116. Lecomte-Beckers J, Rassili A, Carton M, Robelet M, Koeune R: **Study of the liquid fraction and thermophysical properties of semi-solid steels and application to the simulation of inductive heating for thixoforming.** In *Advanced Methods in Material Forming*: Springer Berlin Heidelberg; 2005.

117. Smallman RE, Ngan AHW: *Physical Metallurgy and Advanced Materials.* Elsevier; 2007.

118. Gasper R, Schönbohm A, Enning M, Abel D: **Flatness Based Control of Inductive Heating of X210CrW12 into the Semi Solid State.** *Semi-Solid Processing of Alloys and Composites X* 2008, **141-143:**127-132.

119. Schönbohm A, Gasper R, Abel D: **Inductive Reheating of Steel Billets into the Semi-Solid State Based on Pyrometer Measurements.** *Solid State Phenomena* 2006, **Semi-Solid Processing of Alloys and Composites (116-117):**734-737.

120. Midson SP, Nicholas NH, Nichting RA, Young KP: **Semi-solid forming high temperature alloys. .** In *the 2nd International Conference on the Processing of Semi-Solid Alloys and Composites; Cambridge, MA, USA*. Edited by Brown SB, Flemings MC. TMS, Warrendale; 1992: 140-148.

121. Kapranos P, Kirkwood DH, Sellars CM: **Semi-solid processing of tool steel.** *Le Journal de Physique IV* 1993, **3:**835-840.

122. Kiuchi M, Sugiyama S, Arai M: **Experimental study on mushy metal forming.** *Journal of the Japan Society for Technology of Plasticity* 1996, **37:**1219-1224.

123. Rassili A, Fischer D, Robelet M, Dermurger J, Cucatto A, Klemn H, Walkin B, Kalsson M, Flüß A: **Improvement of materials and tools for thixoforming of steels.** In *8th International Conference on Semi-Solid Processing of Alloys and Composites* (Alexandrou GG, Jorstad J, Makhlouf M eds.). pp. 533-543. Limassol, Cyprus: NADCA (North American Die Casting Association); 2004:533-543.

124. Behrens B, Haller B, Fischer D: **Thixoforming/semi-solid forming : Thixoforging of steel using ceramic tool materials.** *Steel Research International* 2004, **75:**561-568.

125. Behrens B, Fischer D, Haller B, Rassili A, Jean-Christophe P, klemm H, Studinski A, Walkin B, Kalsson M, Robelet M, et al: **Series Production of Thixoformed Steel Parts.** *Solid State Phenomena* 2006, **Semi-Solid Processing of Alloys and Composites:**686-689.

126. Nohm B, Morjan U, Hartmann D: **Thixoforming of steel.** In *6th Inter Conf on Semi-solid Processing of Alloys and Composites; Turin, Italy*. Edited by Chiarmetta GL, Rosso M. Edimet Spa; 2000

127. Tsuchiya M, Ueno H, Takagi I: **Research of semi solid casting of iron.** *JSAE Review* 2003, **24:**205-214.

128. Bramann H, Fehlbier M, Sahm P, Buhrig-polaczek A: **Casting of a cold work steel alloy in semi-solid state.** *Journal of Materials Processing Technology* 2004**:**1357-1364.

129. Hirt G, Bleck W, Buhrig-Polaczek A, Shimahara H, Puttgen W, Afrath C: **Semi solid casting and forging of steel.** *Solid State Phenomena* 2006, **116-117:**34-43.

Chapter 2. Methodology of microstructure characterization and steel thixoforging

Table of contents

1. Introduction……197

2. Materials……198

2.1 Material selection……199

2.2 Chemical compositions……199

2.3 Evaluation of liquid fraction in the semi-solid state……199

2.4 Physical properties……200

3. Steel thixoforging……202

3.1 Heating system……202

3.2 The press……210

3.3 Acquisition systems……212

4. Evaluation of liquid fraction and microstructure characterization……213

4.1 Direct evaluation of the liquid fraction using thermodynamic data……214

4.2 Determination of volume fraction of liquid by thermal analysis……215

4.3 Evaluation of liquid fraction by quantitative metallography in 2D and 3D……217

4.4 In situ observations with CLSM……229

5. Conclusions……233

References……235

1. Introduction

As mentioned in Chapter 1, the accurate evaluation of the volume fraction of liquid, its location, size and shape are needed for the semi-solid forming process, since they directly influence the microstructure development, forming process and rheology behavior. Therefore, this chapter presents the materials studied, the different techniques used for microstructure characterization from the most conventional to the newest methods (fraction of liquid, grain size etc) as well as the experimental devices for thixoforming process.

The material should fulfill several requirements for a successful thixoforming process, such as a large melting interval ($\Delta T = T_l - T_s$), low sensitivity of liquid fraction to the forming temperature and a suitable microstructure [1, 2]. Three steel grades were chosen in this study: low carbon steel C38LTT, hypereutectic steel 100Cr6 and high speed tool steel M2. C38LTT and 100Cr6 were used for the study of industrial application, while M2 was chosen for the study of material flow and microstructure characterization.

In metallurgical aspects, it is crucial to study the microstructure in the semi-solid state to improve the understanding of the thixoforging process since the material behavior strongly depends on main parameters: the liquid fraction, its distribution as well as the coherence of the solid skeleton. In order to study the microstructure evolution during thixoforging process, various characterization techniques, such as DSC (Differential Scanning Calorometry), OM (Optical microscopy), SEM-EDS (Scanning Electron Microscope and Energy Dispersive Spectrometry), high energy X-ray microtomography, CLSM (Confocal Laser Scanning Microscopy) etc have been studied for their potential application for the thixoforging process. Table 2.1 illustrates different studies with various techniques on different steel grades.

As stated by many researchers, the parameters (process conditions and material) are important as they influence the properties of thixoformed parts, especially for thixoforging materials with a high melting point such as steel grades. Becker [3] has pointed out that the process parameters, such as forming speed, die and billet temperature have a great influence on the thixoforging process. They can mainly affect the thermal exchanges between billet and die, and between billet core and skin, which in turn has an effect on the liquid ratio and the microstructure, therefore on the viscosity and the consistency, and finally on the mechanical properties. Our thixoforming experiments on steel grades (C38LTT, 100Cr6 and M2) were performed under industrial conditions with various process parameters in order to study the

material flow and the influence of the main parameters on the final mechanical properties of the thixoforged parts. The properties of each steel grade were first investigated for understanding their suitability for thixoforming process. The main advantages and limitations of each technique for microstructure characterization are introduced and discussed in detail, followed with the experimental devices for thixoforging experiments performed on the steel grades.

Table. 2.1. Various techniques applied for the study of thixoforging process.

Grades / Forming stages	M2	100Cr6	C38LTT	C38
As-received state	OM. SED-EDS. Microtomography	OM. SED-EDS. Microtomography	OM. SED-EDS. Microtomography	OM. SED-EDS. Microtomography
Semi-solid state	DSC. OM. SEM-EDS. CLSM. Microtomography	OM. SEM-EDS. CLSM. Microtomography	OM. SEM-EDS. CLSM. Microtomography	OM. SEM-EDS. CLSM. Microtomography
Thixoforging	Thixoforging tests. OM. SED-EDS	No	Thixoforging tests. OM. SEM-EDS	No

2. Materials

Steel is the most widely used and most recycled metallic material on Earth. With varying combinations of alloying elements, different steel grades offer various properties to meet a wide range of applications. Compared with the conventional steel forming process, semi-solid forming or thixoforming provides an opportunity to produce products with complex geometry with fewer forming operations. However, the industrial application of steel thixoforming has been constrained by the high processing temperature and a lack of understanding of the material's thermo-mechanical behavior in those conditions: especially location, volume fraction, size and shape of the liquid zones etc. Therefore, steel thixoforming requires more investigations regarding both the materials and the technical tools dedicated to the elaboration of the process. When choosing a steel grade for thixoforming process, various parameters have to be taken into account. The adjustment of the liquid fraction content is of crucial importance for the thixoformability of steels. Therefore, a steel grade with a low temperature sensitivity at a certain temperature and a large solidification range at a low process temperature is preferable.

2.1. Material selection

The low carbon steel C38LTT (Low Temperature for Thixoforming) manufactured by ASCOMETAL specifically for thixoforming process and an hypereutectic steel 100Cr6 were first selected in this study as they are widely used in many industrial applications. Another reason for choosing these two grades is their thixoformability [4, 5]. However, due to their low content of elements and high diffusion rate, it is difficult to study the microstructure evolution during heating up to the semi-solid state by classical ways, for example after quenching the material from the semi-solid state. Thus, the high speed tool steel M2 which contains a high amount of heavy elements (V, W, Mo, Cr) was mainly investigated for extensive trials in this work. Thereby, as a 'model', M2 may help to predict the behavior of other two grades which are mainly industrially used. All these three grades are manufactured by rolling process.

2.2. Chemical compositions

As is well-known, steel grades are not always of the same precise composition. This variation in the chemical composition can lead to different melting behaviors and different microstructure evolutions. Therefore, it is necessary to precisely identify the chemical compositions of the materials for a precise liquid fraction evaluation. The chemical compositions of each grade are given in Table 2.2 provided by suppliers.

Table. 2.2. Chemical composition of different steel grades.

	Chemical composition (wt 10^{-3}%)																		
	C	**Si**	**Mn**	**S**	**P**	**Ni**	**Cr**	**Mo**	**Cu**	**Al**	**Sn**	**As**	**B***	**V**	**Ti**	**Nb**	**Ca***	**N***	**W**
C38	372	209	757	27	15	144	205	47	212	21	17	13	2	2	1	2	6	67	0
C38LTT	399	596	1424	83	77	91	130	29	114	3	9	9	4	89	15	0	10		0
100C6	988	230	326	6	7	210	1428	82	194	31	13	10	2	4	3	1	2	109	0
M2	850	35	250	≤40	≤40	200	4100	5000	100					1900					6400

2.3. Evaluation of liquid fraction in the semi-solid state

Fig. 2.1 presents the evolution of liquid volume fraction as a function of temperature obtained by DSC/DTA. As shown in Fig. 2.1, this technique provides the approximate solidus

and liquidus temperatures of each grade. By comparing these curves, the high carbon composition steel grade (M2) has a wide solidus-liquidus range. This is due to the dissolution of a big amount of carbides during heating. The solidus-liquidus interval of 100Cr6 is also relatively large, meaning it is suitable for thixoforging process. A lower solidus temperature and a larger solidus-liquidus temperature interval can be obtained by modifying the chemical elements (Fig. 2.1). Meanwhile, the slope of these curves at liquid fraction 10% and 30% is relatively low, giving a small sensitivity of liquid fraction to temperature, suggesting the suitability of each grade.

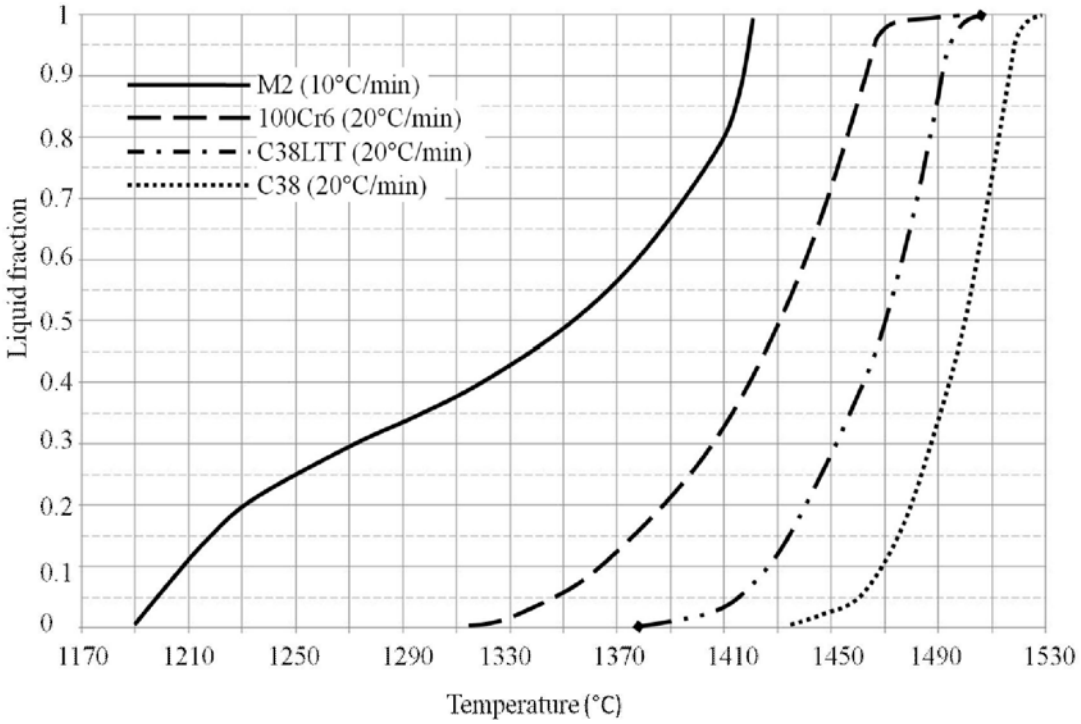

Fig. 2.1. Liquid fraction curves for different steel grades as a function of temperature by means of DSC/DTA measurements obtained by different researchers [5-8].

2.4. Physical properties

In industrial thixoforging processes, the billets are always heated up to the semi-solid state by induction heating. Due to the penetration depth during heating, the homogeneous temperature field of the billet is always obtained by a multi-step heating process. The thermal properties of the materials are helpful, on the one hand, for studying and optimizing the material behavior in the semi-solid state, and on the other hand, for obtaining parameters to be

implemented in numerical models. The physical properties of each grade at room temperature provided by suppliers are given in Table. 2.3.

Table. 2.3. Physical properties of different steel grades at room temperature.

Grade	Elastic modulus	Density	Yield strength	Ultimate strength	Elongation	Thermal conductivity	Specific heat capacity
	E (GPa)	ρ (g/cm^3)	σ_s (MPa)	σ_b (MPa)	A (%)	λ (W/m.°K)	Cp (J/kg.°K)
C38	200	7.84	440-490	600-900	18-20	~40	~440
100Cr6	210	7.81	410-470	700-900	13-27	~46	~475
M2	217	8.12				~19	~460

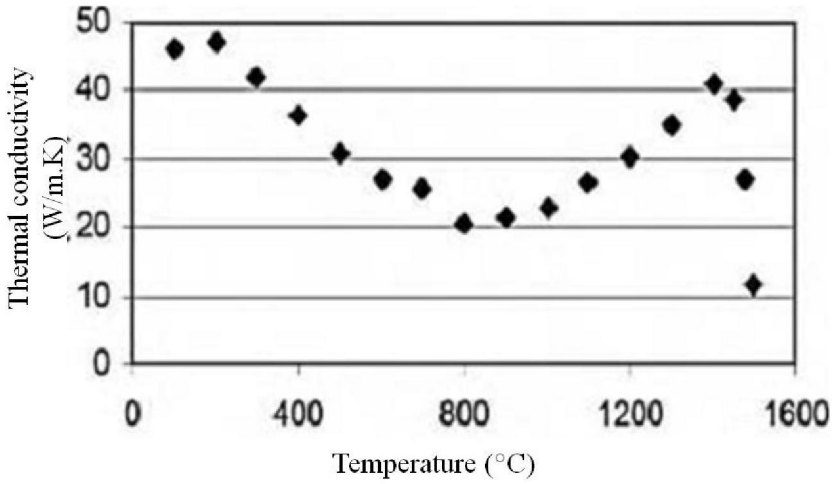

Fig. 2.2. Evolution of the thermal conductivity of C38LTT during heating [5].

The thermal physical properties of a material are different from those at room temperature. For example, Fig. 2.2 illustrates the evolution of thermal conductivity of C38LTT during heating. After decreasing to 750°C, the thermal conductivity increases until the beginning of melting. There is a dramatic decrease in thermal conductivity during melting process. The thermal properties are useful for temperature controlling during heating, especially for simulation which is used to optimize the electrical and geometrical parameters for the induction heating.

In conclusion, for a successful thixoforming process, various process parameters as well as the material properties should be well-understood and controlled. From the curves of the liquid fraction as a function of temperature, the steel grades were thixoforged at the

temperature where the liquid fraction sensitivity to temperature is low. By different liquid fraction evaluation methods, the liquid fractions as a function of temperature of our materials are obtained, detailed in Chapter 3.

3. Steel thixoforging

Different parts with various geometries have been thixoforged for various studies in LCFC at Arts et Métiers ParisTech, Metz. Fig 2.3 shows the investigated thixoforged parts. In my study, M2 steel was mainly studied. M2 parts were investigated for microstructure characterization during the entire thixoforging process, especially for studying the distribution of the liquid phase and the microstructure evolution. The influence of thermal exchange on the material flow and the mechanical properties were also investigated on the parts (100Cr6) thixoextruded by BECKER [8]. Some industrial parts (C38LTT) which were thixoforged for Thixofranc project at various billet temperatures with a cold die were also studied, mainly on the microstructure, mechanical properties, for further industrial applications of steel thixoforging process.

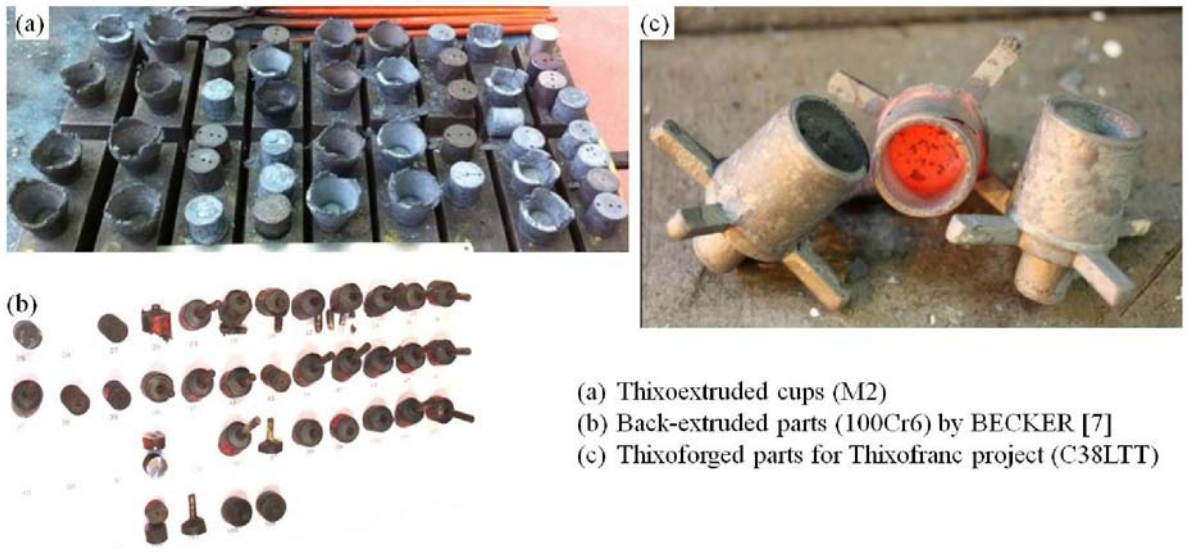

Fig. 2.3. Investigated thixoforged parts of (a) M2, (b) 100Cr6 and (c) C38LTT.

3.1. Heating system

For the thixoforging process, especially for thixoforging high melting point alloys, it is extremely important to heat the material to the semi-solid state with a uniform temperature

distribution throughout the billets prior to the thixoforging operation. The billets can be heated in many ways, including the use of induction system, gas-fired furnaces, infrared heaters, electrical resistance furnace etc. Compared to other heat sources, induction heating offers several attractive features, such as a noticeable reduction of scale, energy efficiency etc. For example, Neag [9] compared the shape factor of an aluminum alloy heated by electrical resistance furnace and induction heating coil. The results showed that more spherical solid particles could be obtained in a shorter heating time by induction heating than by electrical resistance furnace heating.

Thanks to its high heating speed, repeatability and its ability to heat in a protective atmosphere, the induction heating approach is preferable used in an industrial thixoforging process. Therefore, an induction heating system was applied in my study. Fig. 2.4 shows the induction system which is used for heating the billets. This system consists of an induction generator, a programmer and induction coils. The generator (brand **CELES**) can provide a power of 50kW in a frequency interval, ranging from 20 to 100kHz. In order to have a uniform temperature distribution throughout the billets, the induction coil was purpose made, considering the billet dimension and material properties as well as the capacity of the induction generator.

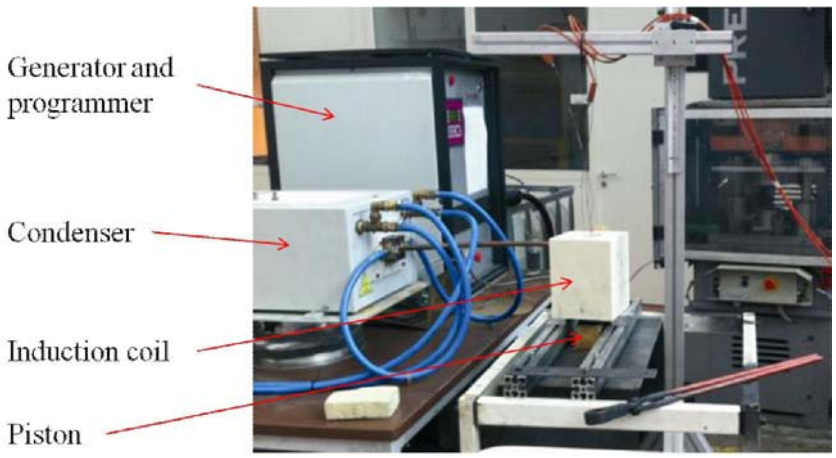

Fig. 2.4. Induction heating system in LCFC at Arts et Métiers ParisTech, Metz.

3.1.1. Coil design for uniform induction heating

During the induction heating process, energy is transferred from a coil to the workpiece via an alternating magnetic field which produces a circulating current in the billet by the induced electro-magnetic force. In order to heat the billets into the semi-solid state quickly and

homogeneously, it is important to use a proper induction coil, which means the design of the coil is important. A well designed coil maintains the proper heating pattern and production rate and improves the efficiency of the induction heating power as well. Meanwhile, the shape of an induction coil is of importance for the heating process. In addition, selection of power, frequency in induction billet heating applications is highly subjective, depending on the material, the temperature homogeneity, billet size etc.

Derived from Maxwell equations, it can be found that the induced current density decreases at an exponential rate from the periphery of the billet towards the center [10]. For a cylinder billet, the distribution of current density is of the form, expressed in Eq. 2.1.

$$I(r) = I_0 \exp\left[\left(r - R\right)/\delta\right] \quad \text{(Eq. 2.1)}$$

where $\boldsymbol{I_0}$ is the maximum eddy current on the surface, $\boldsymbol{R}$ is the radius of the billet and $\boldsymbol{\delta}$ is the penetration depth.

Meanwhile, penetration depth δ can be expressed in Eq. 2.2.

$$\delta = 503.3\sqrt{\frac{\chi}{\mu_r f}} \quad \text{(Eq. 2.2)}$$

where, $\boldsymbol{\chi}$ is the resistivity of the material, $\boldsymbol{\mu_r}$ is the relative magnetic permeability and f is the current frequency.

From Joule's law, the radial power density distribution is expressed by Eq. 2.3.

$$P(r) = P_0 \frac{I^2}{I_0^2} = P_0 \exp[2(r - R)/\delta] \quad \text{(Eq. 2.3)}$$

where $\boldsymbol{P_0}$ is the maximum power density on the billet surface.

Therefore, during the induction heating process, the core of the billet is heated slower than the surface. The reason for the heat deficit in the core of the billet is the skin effect which depends on the material's electro-magnetic properties and frequency. If the frequency is too low, an eddy current cancellation in the billet can occur resulting in poor coil efficiency. On the contrary, when the frequency is too high, only a fine surface layer can be heated, which means a long heating time will be required in order to get a uniform temperature in the billet. The prolonged heating time is not intended for the thixoforging process. Considering the

capability of the equipment in LCFC at Arts et Métiers ParisTech, the frequency of 28kHz was applied for heating the billets.

Decreasing the number of the spiral turns as well as the gap between the billet surface and inner coil will increase the heating efficiency. However, an induction coil with a small number of turns may cause the edge effect on the billet during heating caused by the non-uniform magnetic field. In order to minimize or eliminate the edge effect, the height of induction coil is chosen three times bigger than billet height during the coil design (Fig. 2.5). Owing to the capacity of the heating system (high frequency), the air gap between the billet surface and the coil should be small for homogeneous heating.

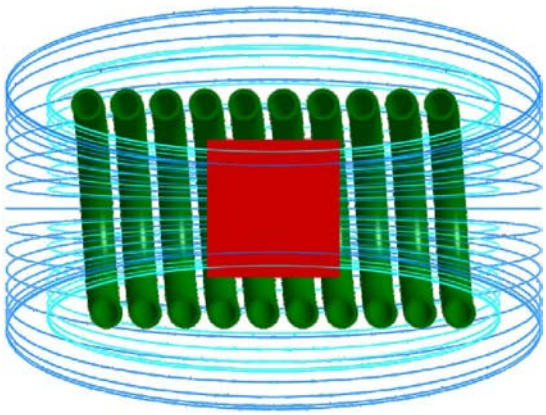

Fig. 2.5. Illustration of the magnetic field during induction heating.

A cooling system equipped with a pump and a tank of $1m^3$ is critical for an induction heating system, since it cools the generator and the solenoid. To ensure the water flow rate (26 l/min), a copper tube with an external diameter of 8mm and 6mm in internal diameter was selected.

Taking into consideration the specificities mentioned above, an induction coil is designed to be adapted to heat a billet with a diameter of 35mm and 34mm in height. The parameters are given in Table 2.4.

Table. 2.4. Characteristics of the induction coil used for thixoforging process.

Number of spiral turns	10
Inner diameter of coil	45mm
Height of the coil	100mm
Inner diameter of copper tube	6mm
Thickness of the copper tube	1mm

3.1.2. Heating cycle

During the induction heating process, the relationship between time and temperature must be precisely controlled to obtain a uniform temperature distribution over entire cross sections [3, 11]. Generally, the surface of the billet heats up first due to the higher power density near the billet surface, while the inside of the billet lags behind. This is characterized as penetration depth. However, from Eq. 2.2, it can be deduced that for a given billet, the penetration depth can be increased by decreasing the frequency of the current. This suggests that the homogeneity of the temperature distribution can be increased by using a lower frequency heating. On the other hand, in the industry, the heating time should also be considered. Fast heating requires a high power which results in a significant temperature gradient. In addition, during heating, heat losses by convection and radiation from the billet surface and the heat transfer to the inside of the billet lead to a difference between the temperature of the core and that of the surface of billet. From the discussion mentioned above, the requirements of homogeneous heating and fast heating to the semi-solid state are contradictory.

Therefore, multi-step heating cycles were designed for uniform heating with a short heating time. High power was applied at the beginning of the heating process for rapid heating to a high temperature. The lower power was used for compensating heat losses and for homogenizing the temperature of the billet. Different heating cycles were designed for reaching various processing temperatures.

Three thermocouples (S-type) were placed in different positions for monitoring or recording the temperature of the billet. This approach can be used to quantify the temperature heterogeneity of the billet. Fig 2.6 shows an example of thermocouple positions.

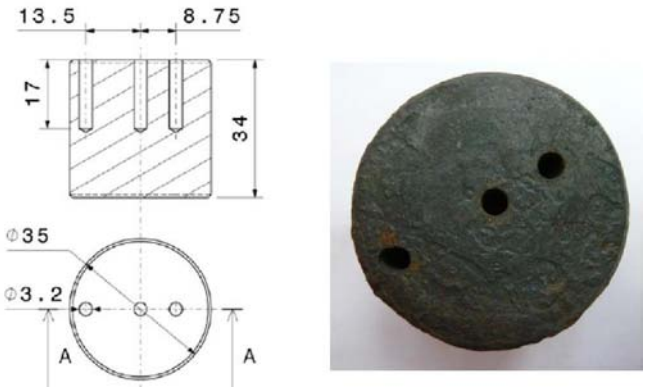

Fig. 2.6. Illustration of the positions for thermocouples.

During heating, high power is first used in order to bring the billet to a high temperature quickly followed with low power heating for thermal conduction from the surface to the center of the billet. Meanwhile, low power heating at the end of the heating process prevents melting of billet skin. Fig. 2.7 illustrates the temperature evolution of the billet during induction heating at different positions. The heating curves show that the surface of the billet heats up quickly due to the skin effect phenomenon, while the temperature of the inside of the billet increases slowly by thermal conduction from the surface of the billet. Meanwhile, the temperature difference between the core and middle of the billet is relatively small. The heating curves also indicate that the temperature of the billet increases rapidly with a higher heating power.

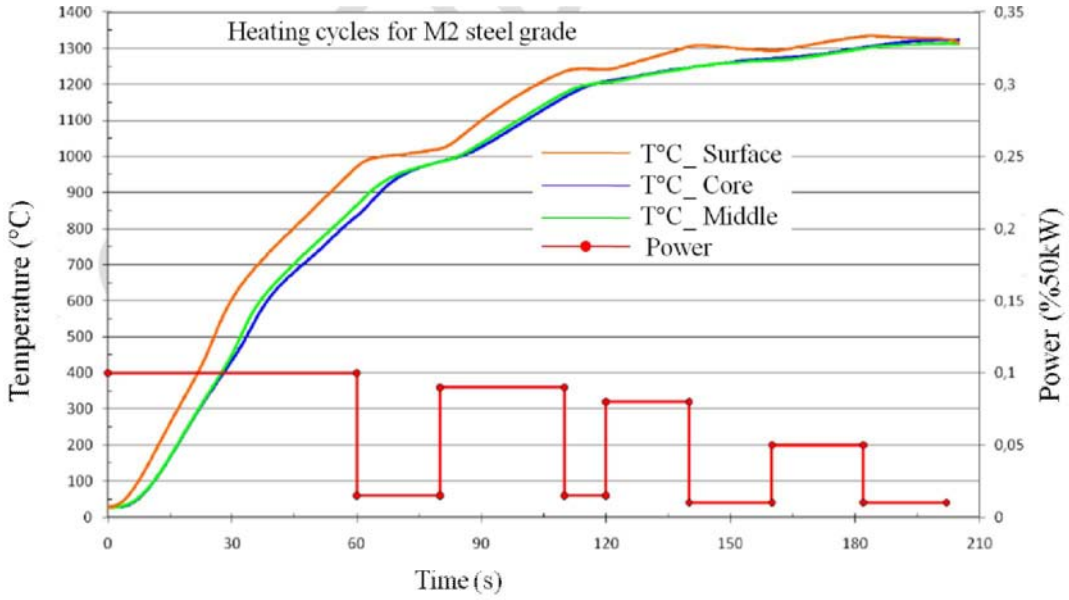

Fig. 2.7. Example of a multi-step heating cycle for heating the billet (M2) to the semi-solid state.

In order to protect the thermocouples during heating, each thermocouple was inserted into an alumina conduit which was in contact with the material. The thermocouples were held to ensure that the temperature of measuring points can be recorded. Even so, it is quite challenging to obtain the precise billet temperature because on the one hand, the accuracy of the thermal couples is ± ~2.5°C; on the other hand, the temperature obtained was not that of the real material, but that of alumina conduits. There is a temperature difference between the alumina conduit and the material.

As stated by Becker [12], increasing billet temperature results in a reduction of solid fraction, therefore reduces the forming load. However, the increase in billet temperature is limited by a heterogeneous material flow. Thus, it is necessary to find a temperature range for a successful thixoforging process. The temperature range was determined by experimental trials. Table. 2.5 illustrates the parts thixoforged at various temperatures.

Table. 2.5. Illustration of the material flow thixoforged at various temperatures.

Thixoforged parts		
Material flow	Heterogeneous	Homogeneous
Max temperature (°C)	1340	1289

In order to have a homogeneous temperature distribution throughout the billet, it is necessary to design proper heating cycles. In our study, heating cycles for various target billet temperatures were designed based on the experience and trial-error process. For one target temperature, several heating cycles were tried in order to reach a relatively homogeneous temperature (the temperature difference among the three temperature measuring points should be less than 10°C.). In the study of repeatability of the heating cycles, the same thermocouples were applied in the same measuring point. Similar procedures were used for obtaining the heating cycles for different target billet temperatures. When designing the heating cycles, we mainly followed one strategy, which is heating the material as homogeneously as possible in a shorter heating time.

The method for induction coil and heating cycle design is time-consuming and expensive. In addition, another limitation of this method is that it does not provide much information for future process design. In our study, the numerical simulation was utilized for obtaining proper frequency, mainly performed at CELES.

For obtaining a uniform temperature field, the billet was placed in the center of the induction coil. In addition, a high temperature refractory ceramic support was selected, since ceramic is not sensitive to magnetic fields or large temperature variation. During induction heating, a piece of Nefacier 1500 disc (based on ceramic fibers with low content of non-fibrous ceramic particles) was placed between the billet and the ceramic supporter to reduce the heat losses (Fig. 2.8). The time between two heating experiments varies a lot since the heating experiments were carried out under laboratory condition: the heated billet is transferred manually but not by a robot. That may leads to a big temperature difference of the Nefacier 1500 disc between two tests, therefore changing the initial billet temperature. To avoid this problem, both the supporter and the Nefacier 1500 disc were cooled by a sprayer pistol. During the billet transportation stage, the clamps were also covered by the Nefacier 1500 disc to decrease the thermal exchange between the billet and the clamps.

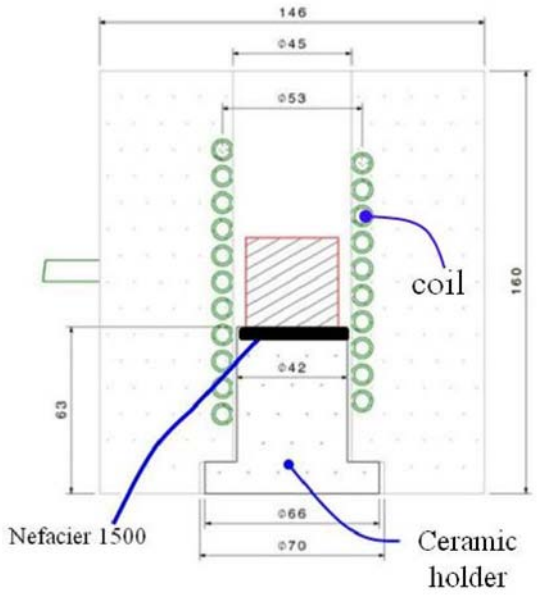

Fig. 2.8. The position of the billet in the induction coil.

3.1.3. Difficulties during induction heating

Oxidation during heating

Almost all of metals are oxidized by the oxygen in the air during heating. As stated by many researchers [2, 8, 13], the oxide scale leads to a fast wear of die tools and degradation of mechanical properties of the thixoforged parts. The oxidation phenomenon can be minimized or eliminated by protective gas, such as argon. However, the oxidation can be limited by

induction heating as the heating rate is high. In the thixoforging experiments, protective gas was not applied.

Heat loss

During induction heating, as the billet is placed on a ceramic supporter, the thermal exchange on this surface is not the same as others which are in contact with the air. When the billet is homogeneously heated to the desired temperature, it is manually transported to the die with a gripper. During transport, the temperature of the surface decreases due to the thermal exchange between the billet and the clamp. Fig. 2.9 shows the temperature evolution during induction heating and transferring to the press. The transportation time ranges from 6 to 12s. There is a ~30°C decrease in temperature near surface during transportation procedure.

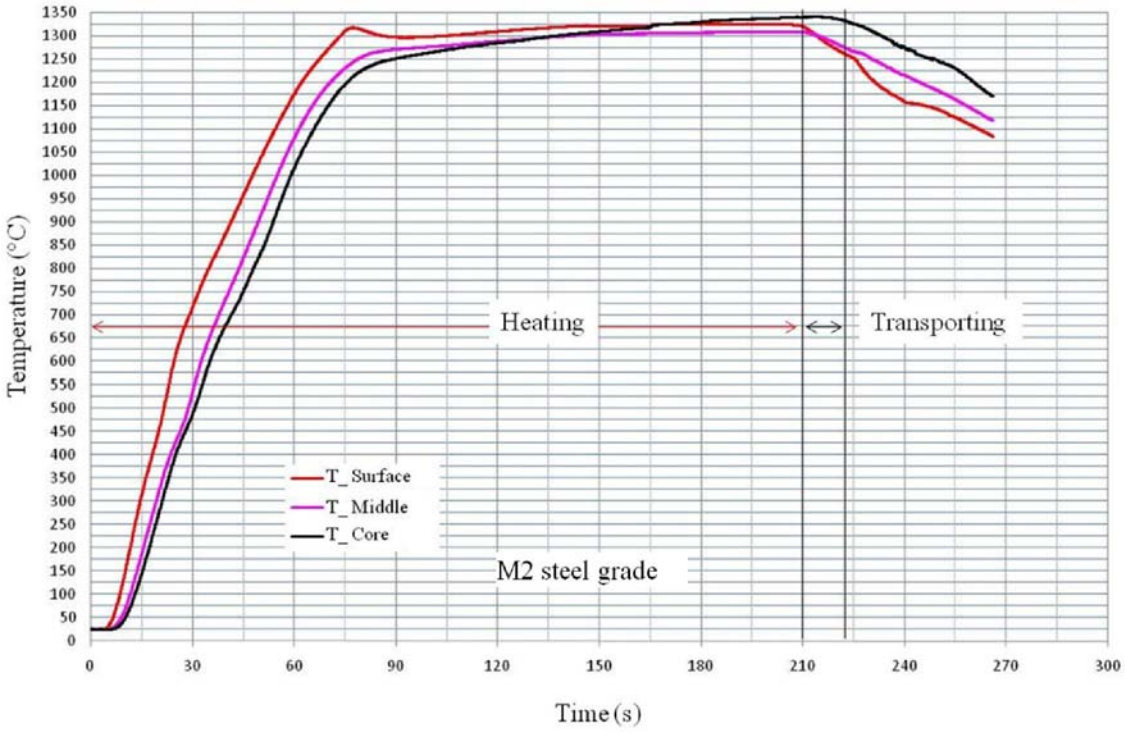

Fig. 2.9. Temperature evolution of M2 billet at the heating and transportation stage.

3.2. The press

Compared with the hydraulic press, a mechanical press was used for thixoforging process for three reasons:

– High forming speed leads to a decrease in forming load [3, 12].

- High forming speed can also reduce the contact time of the billet and die tools during thixoforging process, therefore reduces the heat loss.
- High production rate which meets the industrial requirements.

The mechanical press PRESSIX (Fig. 2.10) which can provide a maximum load of 500kN with a maximum forming speed of 485 mm/s was used for thixoforging the M2 parts.

Fig. 2.10. The mechanical press (PRESIX) at Arts et Métiers ParisTech, Metz.

The back-extrusion set up (Fig. 2.11) was employed for extruding a cylinder billet to a cup-shape part. The dies were made of tool steel X38CrMoV5.

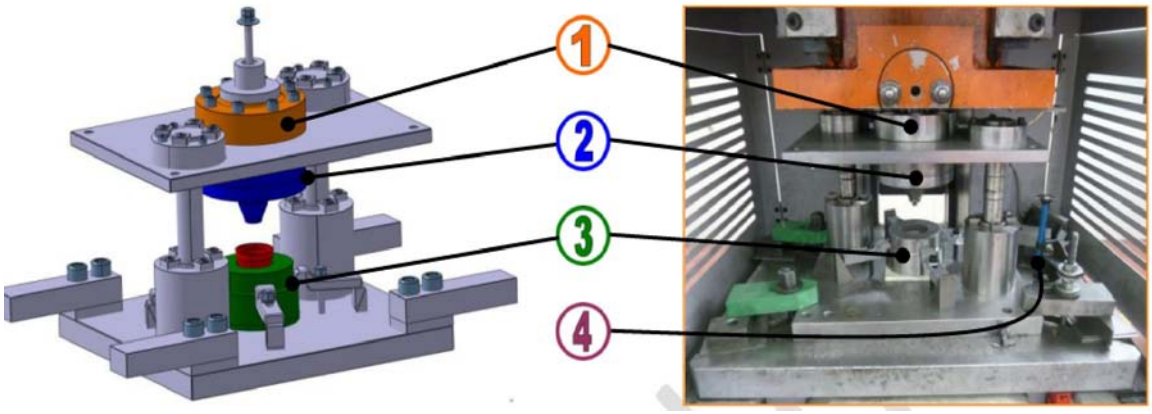

Fig. 2.11. Illustration of the extrusion set up. (1) Load sensor. (2) Upper die. (3) Lower die. (4) Displacement sensor.

As shown in Fig. 2.11, the extrusion set-up is composed of two sliding columns. The lower die (3) is fixed on the table of the press, while the upper die which is connected to the load sensor is mounted with the press.

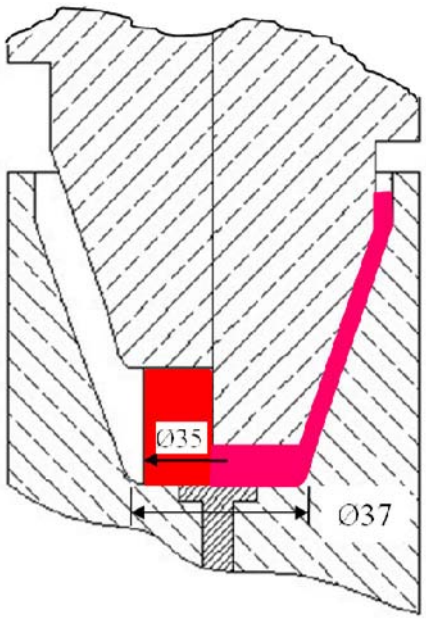

Fig. 2.12. Principle of backward extrusion test.

In order to study the influence of the die temperature on the material flow, the thixo-extrusion experiments were performed under the same process conditions except the die temperature – cold die (room temperature) and warm die (~350°C). When performing the thixo-extrusion experiments with a warm die, the die was gas-fire heated. During heating, the die temperature was monitored by a pyrometer.

During thixoforging, a cup-shaped part was backward extruded from the cylindrical billet with a diameter of 35mm and a height of 34mm (Fig. 2.12).

3.3. Acquisition systems

During the thixoforging process, several parameters (temperature, displacement of die, forming load etc.) were measured and controlled. The displacement and the force were measured for all the thixoforging tests, while the measurements of billet and die temperature were performed to verify the homogeneity of billet temperature and warm die temperature. In order to obtain these measurements, an 8-channel acquisition system PCI6024E National Instrument (± 0.3% error at full scale) was used, as shown in Fig. 2.13 (a).

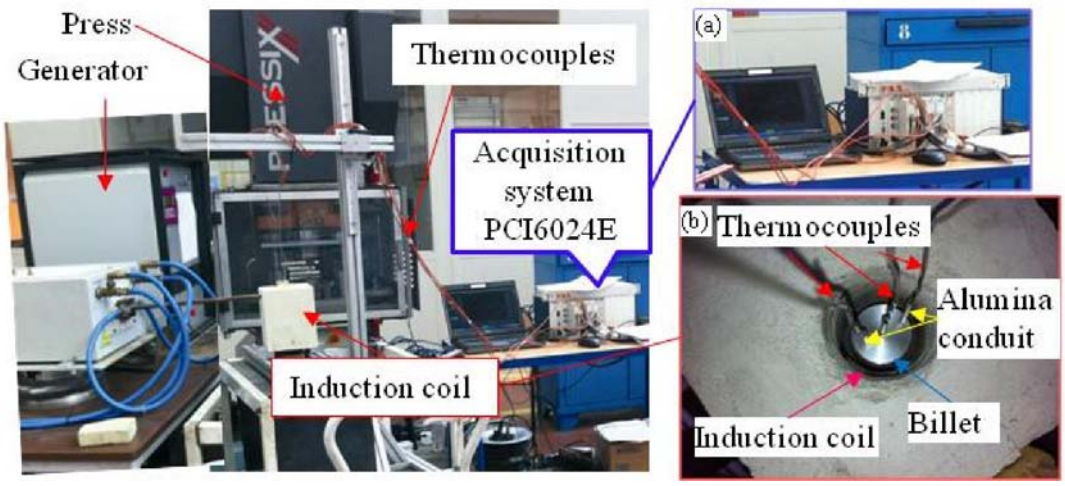

Fig. 2.13. Acquisition system at Arts et Métiers ParisTech, Metz.

Measurement of forming load. The stainless steel sensor (Fig. 2.11 (1)) can be used for tensile/compression tests. Its maximum operating stress is 600kN with an error $\leq \pm 0.3\%$.

Measurement of displacement. The mechanical sensor (error ± 0.01mm) (Fig. 2.11 (4)) comprises a rod which is linked to a potentiometer that varies the output voltage as a function of its position.

Temperature measurement. The billet temperature before thixoforming was measured by S-type thermocouples (error ± 2.5°C) and recorded by the Acquisition system PCI6024E National Instrument. During the measurement, the thermocouples were protected by the alumina conduit (Fig. 2.13 (b)). While the warm die temperature was measured by the pyrometer.

4. Evaluation of liquid fraction and microstructure characterization

For a certain material, the volume fraction of liquid/solid is defined as a function of temperature. Depending on the prior thermal history, heating process etc, the volume fraction of liquid/solid can be determined by various approaches. The thermal analysis (Differential Scanning Calorimetry (DSC)) and quantitative metallography on microstructures of the material quenched from the semi-solid state are mostly performed for the evaluation of the volume fraction of liquid/solid in the semi-solid state. In addition, thermodynamic data provides the information of the liquid content under the equilibrium conditions. However,

these three methods are approximate. The in situ and 3-dimensional microstructure observations are of interest regarding the microstructure evolution and evaluation of the liquid fraction of alloys in the semi-solid state.

4.1. Direct evaluation of the liquid fraction using thermodynamic data

During melting or solidification under equilibrium condition, the volume fraction of liquid/solid of an alloy can be calculated based on the phase diagram. The thermodynamic database software, Thermo-Calc gives equilibrium diagrams of complex multi-component alloys. Furthermore, it provides useful information for proper equipment selection, for example the liquidus temperature should not exceed the capacity of DSC equipment. The weight fraction of solid can be calculated by Eq. 2.4.

$$g_s = 1 - \left(\frac{T_M - T}{T_L - T_M} \right)^{-\frac{1}{1-k}} \qquad \text{(Eq.2.4)}$$

where g_s is the weight fraction of solid, T_M is the melting point of the pure solvent, T_L is the liquidus temperature and k is the partition coefficient of the alloy.

As the densities of solid and liquid phases in the semi-solid state are different, the volume fraction of solid can be determined by Eq. 2.5.

$$fS = \frac{g_s}{g_s + (1 - f_s)\dfrac{\rho_s(C,T)}{\rho_l(C,T)}} \qquad \text{(Eq. 2.5)}$$

where f_s is the volume fraction of solid, ρ_s and ρ_l are the densities of the solid and liquid phases at a given temperature T, respectively, and C is the composition.

Using the software Thermo-Calc, the densities of solid and liquid phases can be predicted for the volume fraction of solid evaluation. However, when taking into account of the prior thermal history, the microstructure and the industrial conditions, there will be an error in determining precisely the liquid fraction by the thermodynamic data. Therefore, there is a need for experimental methods which determine the volume fraction of liquid under the conditions similar to those employed in industrial thixoforming processes.

4.2. Determination of volume fraction of liquid by thermal analysis

The experimental evaluation of the volume fraction is traditionally done by thermal analysis techniques. Differential Scanning Calorimetry (DSC) is one of the most used thermal analysis techniques in which the difference in energy input between a substance and a reference material is measured as a function of temperature, while the substance and reference material are subjected to a controlled temperature program. It provides quantitative and qualitative information about physical and chemical changes which involve endothermic or exothermic processes. In our study, a Netzsch DSC 404C Pegasus® which permits measurements with temperatures up to 1500°C (Fig. 2.14) was used to study the evolution of the liquid fraction as a function of temperature.

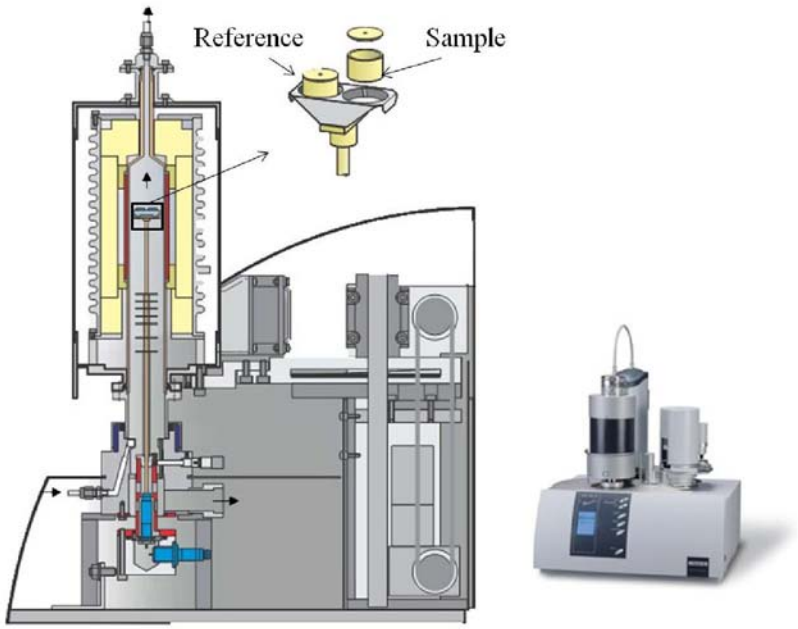

Fig. 2.14. Schematic view of Netzsch DSC 404C Pegasus®.

During heating from solid to liquid, the sample undergoes a phase transformation which absorbs energy. The energy absorbed during heating contributes to the change of the heat of solid and liquid phases and the heat of melting, as expressed in Eq. 2.6.

$$\frac{dQ}{dt} = m\left(g_s C_{P,s} + (1 - g_s) C_{P,L} + \Delta H \frac{dg_s}{dT} \right) \frac{dT}{dt} \qquad \text{(Eq. 2.6)}$$

where, dQ/dt is the rate of heat flow, g_s is the weight fraction of solid, $C_{P,S}$ and $C_{P,L}$ are the heat capacities of the solid and liquid phases, respectively, m is the mass of the sample, and ΔH is the heat of melting.

A sigmoidal baseline is defined in order to isolate the energy which corresponds to the heat for melting the solid phase. The area between the DSC signal curve and the baseline corresponds to the energy for melting the sample (Fig. 2.15). The T_{si} and T_{lf} are considered to be the solidus temperature and liquidus temperature, respectively, according to ICTA (International Conference on Thermal Analysis).

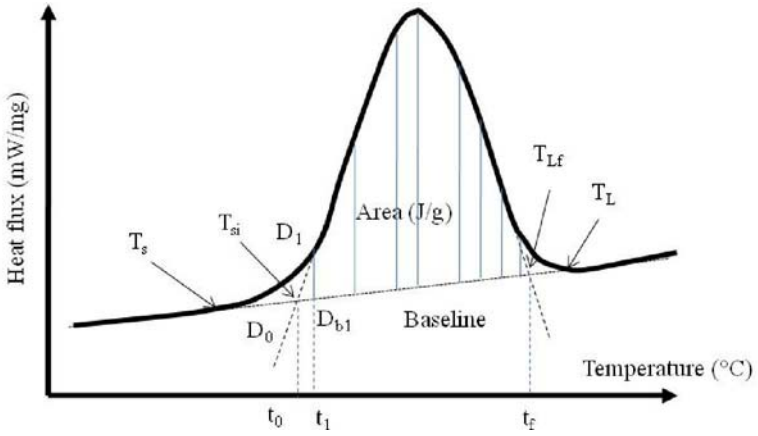

Fig. 2.15. Solid-liquid transformation curve obtained by DSC for the determination of liquid fraction as a function of temperature.

During experiments, the samples are heated at a constant heating rate ($\dot{T}$), the decrease of the weight fraction of solid can be calculated from the increase of the absorbed energy. Eq. 2.6 can be derived to Eq. 2.7.

$$dg_s = \frac{1}{\dot{T}} \int_{Ts}^{T} \frac{1}{\Delta H} \left(\frac{dQ}{dt} \right) dT \qquad \text{(Eq. 2.7)}$$

Here, we assume that the liquid fraction is proportional to the absorbed energy during the transformation. Using the method of partial areas, the weight fraction of liquid can be calculated with Eq. 2.8. Then, the volume fraction of liquid can be obtained by Eq. 2.5.

$$\begin{cases} g_s(T_i) = 1 - \dfrac{S(T_0 - T_i)}{S_{total}} \\ S(T_0 - T_i) = \sum_0^i \dfrac{t_n - t_{n-1}}{2} \bullet (D_n - D_{bn}) \bullet (D_{n-1} - D_{bn-1}) \end{cases} \qquad \text{(Eq. 2.8)}$$

The experiments were performed with two heating rates of 10°C/min and 20°C/min, respectively. Small samples (Ø3*1.5mm) were taken from various positions to minimize the possibility of getting non-representative results due to local compositional variations caused by segregation. These samples were heated from 100% solid to a temperature above the liquidus temperature and then cooled down to room temperature. This method is always used due to the specimen preparation and experimental performance. However, there are some limitations to this method:

- The heating rate of DSC is much lower than that used in industrial applications (500-1000°C/min). Due to this limitation, the results of DSC make it impossible to fully simulate the industrial conditions, because the homogenization will be enhanced during thermal analysis; this therefore induces an error on the results of the material with different thermal histories.
- During the liquid fraction determination, the partial areas method is approximate, as it does not take into account of the effects of the composition on the heat of melting.

To overcome these limitations, the liquid fraction measurements should be performed under industrial conditions. Generally, this can be done by image analysis on the micrographs of the quenched material or on the images of the material in the semi-solid state. 2-dimensional evaluation of volume fraction of liquid is carried out on the microstructures of material quenched from semi-solid state.

4.3. Evaluation of liquid fraction by quantitative metallography in 2D and 3D

In general, the characterization of the microstructure in the partial liquid state is often carried out on quenched samples which were heated under industrial conditions. Besides the study of the liquid fraction, the morphology of the liquid phase and the material flow during forming are also of interest. Therefore, the samples have to be quenched quickly in order to preserve the former microstructure in the semi-solid state.

During the experiments, samples were induction heated to the semi-solid state. The induction heating approach was chosen for its high heating rate and its high repeatability. The dimensions of the samples are given in Table. 2.6.

By controlling the induction heating parameters and the positions of the samples in the induction coil, the temperature of the samples could be obtained as desired. After water quenching, the samples were 2D and 3D analyzed with various techniques such as Optical microscope, Scanning Electron Microscope (SEM), Energy Dispersive Spectrometry (EDS) and high energy X-ray microtomography.

Table. 2.6. Billet dimensions for thixforging process.

Material	Dimensions (mm)
M2	Ø35mm*34mm, Ø38*30mm, Ø36*34mm, Ø1.2*30µm
100Cr6	Ø30mm*45mm
C38LTT	Ø45mm*60mm

4.3.1. 2D image analysis

The microstructure in the semi-solid state is of great importance for the thixoforging process. Therefore, the samples have to be quenched quickly so that the microstructure at room temperature reflects the partial liquid state. Due to diffusion processes and phase transformations, this can be unsuccessful; therefore the microstructure changes caused by quenching have to be considered. However, the diffusion process for M2 steel in the semi-solid state is relatively low, which was verified by CLSM in situ observations. The results will be detailed in Chapter 3. If the structure was changed much during quenching, the determined structural parameters have to be corrected or can possibly not be determined at all. Therefore, exact knowledge and examinations of the mechanisms that occur and their effects on the structural parameters are of special importance. Due to extremely large changes during quenching, error-tolerance ranges have to be prepared. Within the scope of the examinations, C38LTT, 100Cr6 and especially the high speed tool steel M2 used for thixoforming were observed in detail to evaluate the behavior of a complex melting during heating up to the semi-solid state.

Fig. 2.16 is the typical time, temperature and transformation (TTT) diagram for M2 high speed steel [14].

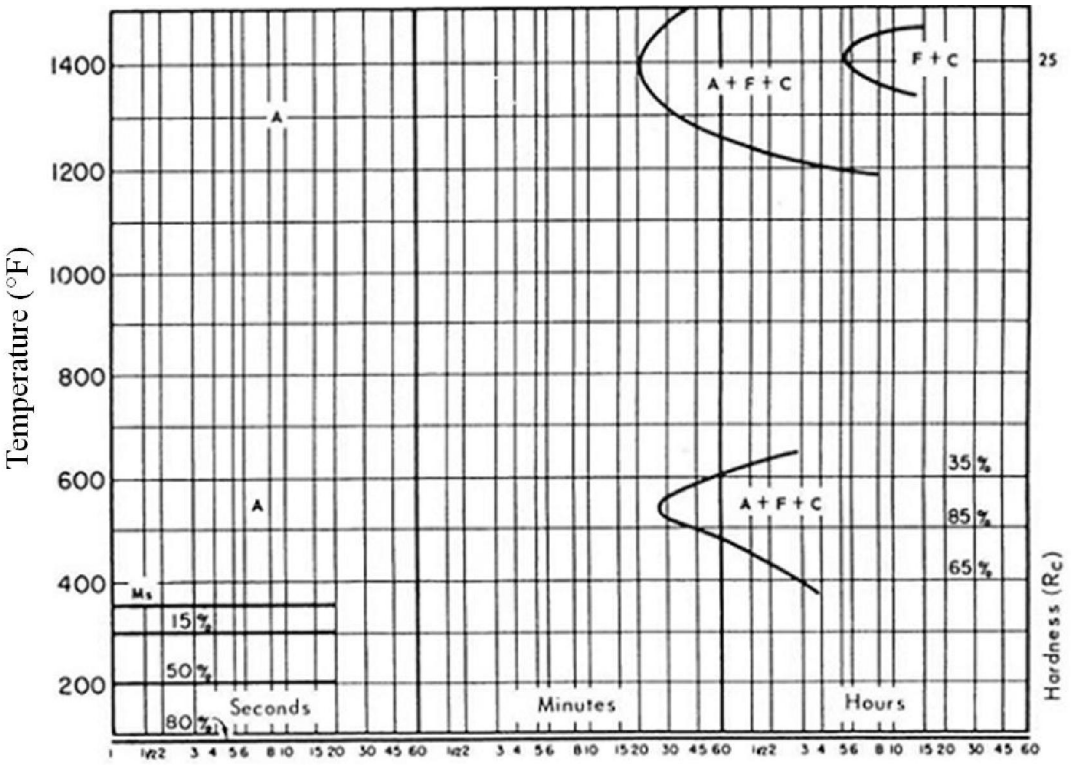

Fig. 2.16. TTT diagram for M2 steel.

During the metallurgical observations, the heated and quenched billets were observed in both longitudinal and cross sectional directions. As the billets are of big dimension, the temperature of the billet is not perfectly homogeneous; therefore the microstructure at various positions may not be the same. Thus, it is necessary to define the observation zones as shown in Fig. 2.17.

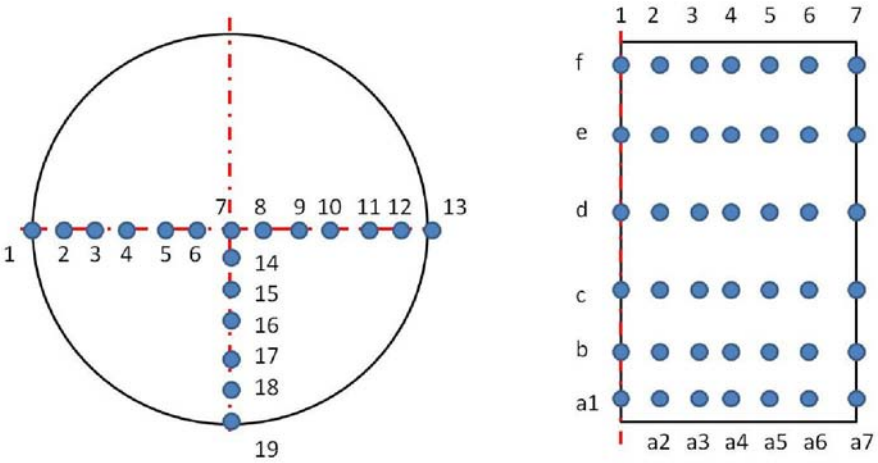

Fig. 2.17. Observation points on the quenched billets.

Some of the thixoforged parts were also quenched in the water tank after the thixoforging process (transportation time is around 15s) in order to study the material flow and the distribution of liquid phase. The observation zones on the thixoforged parts are illustrated in Fig. 2.18.

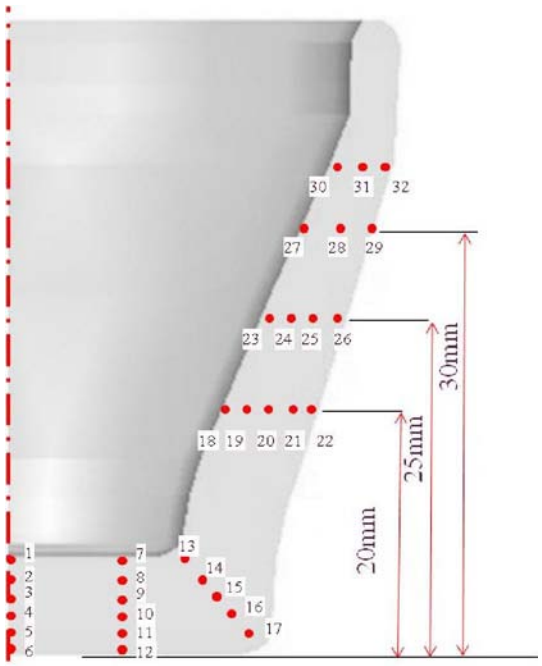

Fig. 2.18. Observation points on the thixoforged part.

2D Observation techniques

According to the desired resolution, the microstructures of different parts were observed using different microscopes. For the liquid fraction evaluation and microstructure phase determination, an Olympus optical microscope was used for obtaining images with small magnifications (100 times – 500 times). In order to characterize the small particles and carbides types, a Jeol 7001 FLV Scanning Electron Microscope (SEM) was used and the Energy Dispersive Spectrometry (EDS) analyses were finally done with an Oxford INCA system to study the distribution of the different alloying elements.

Quantitative characterization of microstructure

Grain size. Concluded from other researches [15-18], the viscosity of the material in the semi-solid state is reduced with a finer grain size. During the image analysis of the microstructure, the mean grain size was measured using the mean lineal intercept method as explained in ASTM E 112-96 standard.

Shape factor. For a successful thixoforging process, solid particles should exhibit a relative round or equiaxed shape. Shape factor for the simulated grains in 2D micrographs was calculated by Eq. 2.9.

$$F = \frac{4\pi A}{P} \qquad \text{(Eq. 2.9)}$$

where ***A*** is the area and ***P*** the circumference of a grain.

Liquid fraction. The estimation of volume fraction of liquid was carried out adopting automatic image analysis using ImageJ. During the image analysis, we made a compromise in magnification. Indeed, an image taken with a low magnification can cover a bigger area, thus reducing the error caused by the inhomogeneity of the micrograph. However, the resolution of the image at a low magnification is lower than that of the image taken at a high magnification. By contrast, the high magnification can increase the resolution, but reduce the area. When analyzing the high magnification image, instead of considering the eutectic as liquid phase, it will be separated by thresholding. The magnification selection depends on the grain size, phase distribution etc. In our case, there were no significant changes in the grain size, phase distribution at different temperatures and at different positions. Therefore, the same magnification was applied for liquid fraction evaluation. The determination of the magnification followed the strategy: the micrographs with a proper resolution should cover a certain area in which the microstructure is representative.

Etchants

Before the observation and analysis, the samples were chemically etched with different etchants for different aims. The etchants are given in Table. 2.7.

Table. 2.7. Chemical etchants used in the study.

Etchant	Composition	Quantity	Conditions	Application
Nital	Ethanol HNO3	100ml 2-4ml	Room temperature Seconds to minutes	Microstructure
Groesbeck	Water NaOH $KMnO_4$	100ml 4g 4g	At 70°C	To reveal carbides
Béchet-Beaujard	Picric acid solution Teepol Water	1.5g 20ml 100ml	At 70°C	Prior-austenite grain boundaries
HCL 50%	Hydrochloric acid Distilled water	50ml 50ml	At 70°C 15-25 min	To observe the ‘fibering’

4.3.2. 3D observations by high energy X-ray microtomography

As the 2D image analysis may not give a complete image of the structure and can sometimes lead to invalid conclusions. 3D analysis is often required. Both X-ray microtomography and serial section can be used to obtain 3-dimensional microstructures. Compared with the X-ray microtomography, serial section is a destructive technique which gives lower spatial resolution.

M2 grade was investigated using high energy X-ray microtomography at ESRF, because of high difference in X-ray absorption among its high content of alloying elements (especially tungsten and molybdenum) and iron. However, due to the content of alloying elements in 100Cr6 and C38LTT, the liquid phase in the semi-solid state is not easy to identify by this technique; therefore, the microstructure information was not obtained.

4.3.2.1. Induction heating for microstructure evolution observation

In order to study the microstructure evolution of M2 during heating, a billet was partially heated to the semi-solid state by a direct induction heating route. During the induction heating process, the slug was partially inserted into the induction coil with a part sitting on a ceramic holder, to ensure the coexistence of solid and semi-solid state, as illustrated in Fig. 2.19.

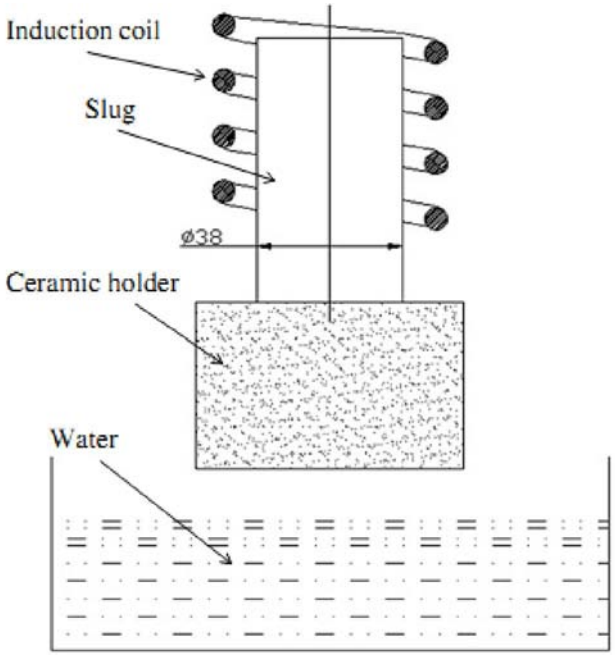

Fig. 2.19. Schematic view of the set-up for induction heating experiments.

The temperature of the semi-solid zone was measured by a pyrometer. After heating for ~120s, the temperature at the point **C** reached 1250°C and the billet was directly quenched in order to preserve the former structure in the semi-solid state. During heating, the protective gas was not used, so oxide scale was obtained on the billet surface. Owing to the oxide scale, the real material temperature is about 100°C higher than the measured value. Due to the effect of penetration depth, a typical bell-shaped temperature profile was obtained; temperature decreased with decreasing radius and height. The bottom of the billet was slightly colder due to a deficit of heat source in this area: it remained in the solid state during induction heating (Fig. 2.20). Therefore, the microstructure in the solid zone can be used for comparing to the one in the semi-solid state.

Considering the material and the available energy at the Beamline 15A at ESRF, the cylindrical samples 1.2 mm in diameter were electrodischarge-machined from the quenched billet in various directions (Fig. 2.20) for the high energy X-ray microtomography experiments. Meanwhile, the tomography experiments were also performed on the material in the as-received state in order to make a complete comparison between the two states.

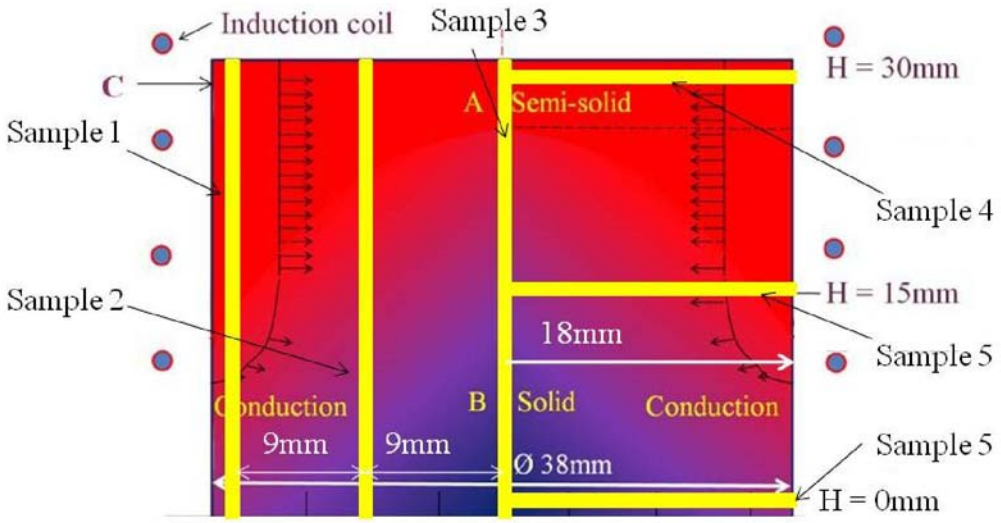

Fig. 2.20. Schematic view of temperature distribution during induction heating.

4.3.2.2. Principle of X-ray tomography

The basis of X-ray tomography is X-ray radiography: an X-ray beam is sent on a sample and the transmitted beam is recorded on a CCD (Charge Coupled Device) detector. According to Beer–Lambert law (Eq. 2.10), the ratio of the number of transmitted to incident photons is related to the integral of the absorption coefficient of the material μ along the path that the

photons follow through the sample. In the domain of the photoelectric effect (E < 200keV), the absorption coefficient μ depends on the density, the atomic number and the energy (when the beam is monochromatic) by using an empirical law as expressed in Eq. 2.11. If the material is heterogeneous, the integral volume of μ (x, y, z) varies also with the beam orientation, in particular x, y and z (Fig. 2.21).

$$N_1 = N_0 * \exp[-\int_{S \in ray} \mu(s) ds] \quad \text{(Eq. 2.10)}$$

where N_1 is the number of transmitted photons of energy E, N_0 is the number of incident photons of energy E.

$$\mu(x, y, z) = K\rho \frac{Z^4}{E^3} \quad \text{(Eq. 2.11)}$$

where K is a constant, ρ is the density of the investigated material, Z is the atomic number of the material and E is the energy of the incident photons.

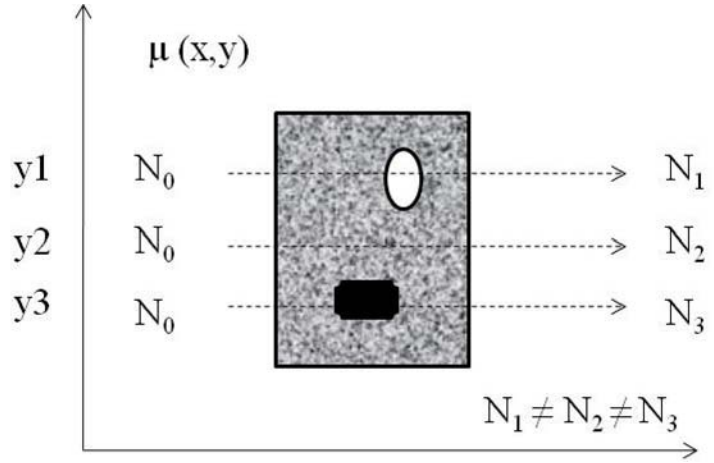

Fig. 2.21. The physical principle of the tomography: transmission in a section in a plan (Z = Zi). The intensity of the transmitted photons depends on the properties of the crossing portion of material.

By placing a photon detector behind the sample, the photons are detected and the transmitted information is digitally transcribed into a gray level proportional to N_t **(E).** If the detector is a plane, the resulting image (radiograph) is the projection of all sections of the radiographed volume parallel to the detector on the same plane. In order to obtain the 3D information, the classical way is to perform a large number of radiographs while rotating the

sample between 0° and 180° as shown in Fig. 2.22. The images were reconstructed using an algorithm of filtered back projection [19].

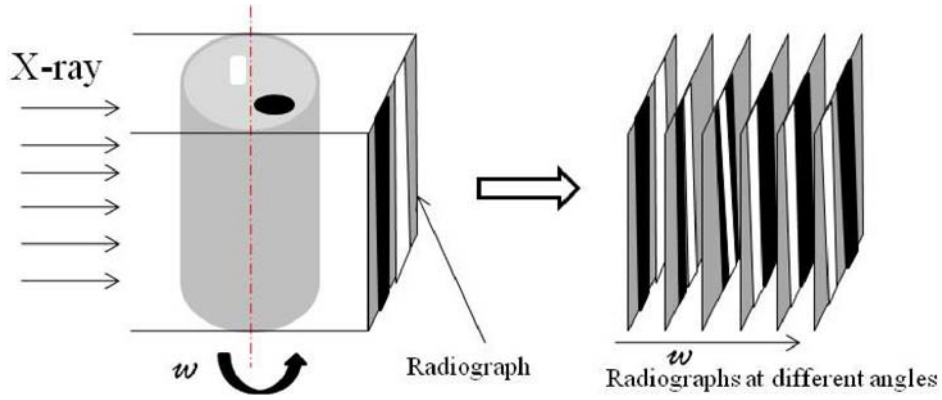

Fig. 2.22. Schematic diagram of the principle of projection acquisition of X-ray tomography.

As mentioned above, the contrast of a material observed in the X-ray microtomography can be explained by the attenuation law. If the atomic numbers of the alloying elements are similar, a good contrast can not be obtained. Therefore, the M2 was chosen for the X-ray microtomography experiments, because it contains a big amount of alloying elements which are placed far away from the iron in the periodic table, such as Mo and W.

4.3.2.3. Tomography set-up

Our X-ray microtomography experiments were carried out at room temperature on the high-energy ID15A beamline at ESRF (European Synchrotron Radiation Facility) in Grenoble, France, where the X-ray energy ranges from 50 to 100keV. The tomography device consists of three parts: an X-ray source, a rotation stage on which the samples are fixed and a CCD detector (Fig. 2.23).

Samples were electrodischarge-machined from the different bars (as-received bar and quenched from semi-solid state bar) for the microtomography experiments. In these experiments, each sample was mounted on translation and rotation stages in order to achieve a good alignment with the X-ray beam before the measurement and a 360° rotation for 3-D observation. In the tests, a 15µm thick LuAG:Ce scintillator was used to convert the X-ray light into visible light. The incident X-ray beam was directed onto the rotating samples with a constant energy of 60keV. The transmitted beam was recorded using a fast DALSTAR

Pantera 1M60 CCD detector, with an exposure time of ~25ms. The effective pixel size was ~1.2µm and 3600 projections were captured.

Three different modes are available to perform tomography: the absorption mode, the phase contrast mode and the holotomography mode. With the absorption mode, the contrast is given by the difference between the linear attenuation coefficients $\boldsymbol{\mu_1}$ and $\boldsymbol{\mu}$, so that the larger the difference of element, the better the contrast and the easier the subsequent image analysis. Using this mode, the sample should be placed close to the detector in the synchrotron radiation source in order to avoid phase effects caused by the propagation from sample to detector. The contrast mode takes advantage of the difference in refraction of the various phases of the material. It is mostly used in cases where the difference in absorption between two phases is low and thus better detects the interface between these two phases. The holotomography mode uses images taken at several sample-to-detector distances. In our case, the contrast mode was used for taking images.

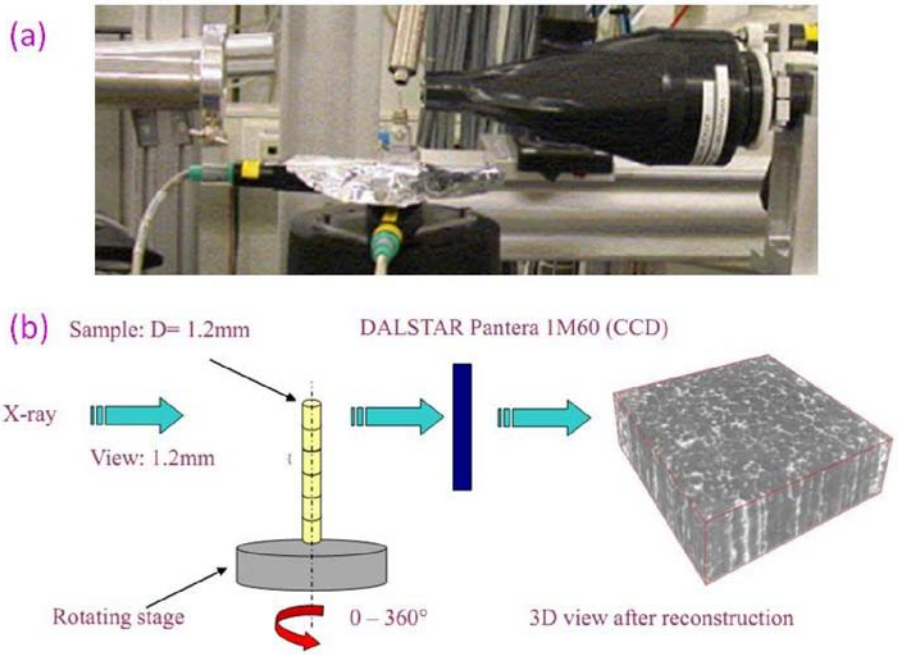

Fig. 2.23. (a) Set-up and (b) schematic view of 3D X-ray microtomography.

During the experiments, for one tomographic scan, 1024 slices would be generated, covering the sample length of 1.2mm. More than 350 tomographic scans were carried out on M2 steel grade in both as-received state and quenched from the semi-solid state. Besides, more than 40 scans were performed on other grades, such as 100Cr6, C38, 316L etc. The

slices were then reconstructed and the obtained stacks were processed and analyzed with the image analysis software ImageJ.

4.3.2.4. Image processing

The reconstruction of the volumes from the projections has been performed on the remote cluster (at ESRF) using Matlab. The obtained original images after reconstruction are coded in gray levels in four bytes, which is a very large volume data (1024^3 * 4 =4 GB of memory size). In fact, for one tomographic scan, there are 1024 slices in total. But due to the capacity of memory, 60 slices can be reconstructed at a time, which means there are 17 small stacks. Subsequently, the 17 small stacks were combined into a new stack of 1024 slices. For a stable network connection, it takes around 90 minutes to reconstruct 1024 slices as one stack. These reconstructed images can be visualized either in 3D or 2D sectional thanks to softwares such as VGStudio max, Amira and ImageJ. ImageJ was applied in our study for image analysis. ImageJ is a public domain, Java-based image processing program which can display, edit, analyze, and process images in different formats. After reconstruction, the images are cropped to a final size in order to be able to perform 3D calculations with a classical computer or on a remote cluster. In general, it takes about 45 minutes for one calculation.

Fig. 2.24 shows one local tomographic slice of quenched M2. It presents the uniform noise which is distributed over the entire image. The image is of good quality for the structure qualification and description (the forms of grains). However, the image is not appropriate in the current description for a direct quantitative analysis. Therefore, it is necessary to perform a prior image processing.

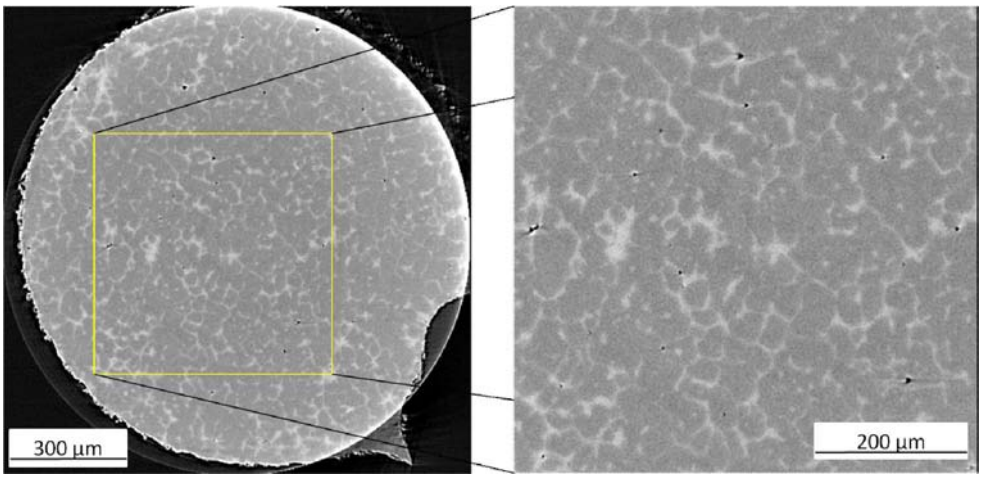

Fig. 2.24. X-ray tomography slice.

The purpose of this treatment is to binarize images to numerically distinguish the matrix and carbides. Several techniques are used, such as gray level thresholding, region growing, nonlinear filtering and mathematical morphology operations (erosion and dilation). In this study, the tools described above were applied in 3D.

The non-linear diffusion filter can effectively remove noise and preserve the boundaries. Meanwhile, it eliminates the noise by increasing the contrast spot near the edges. (3D implementation in ImageJ)

Thresholding allows selecting the pixels from their gray level. After thresholding, the selected parts have been changed to white while the rest is in black. This operation is sufficient to separate two phases which have a good contrast. However, the threshold has to be done by eyes and is difficult to run automatically. To get an error bar for the final data, the operation was repeated several times by adjusting the threshold values.

The image processing steps are indicated as follows (Fig. 2.25):

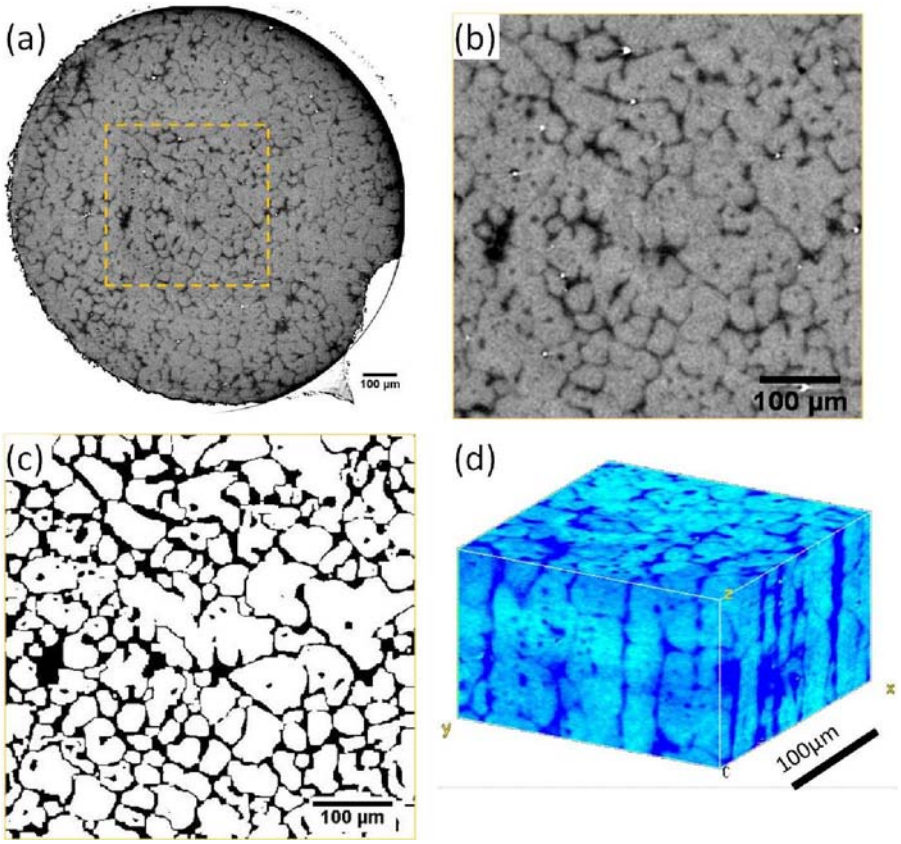

Fig. 2.25. Examples of 3D image processing with 2D slice in the cylindrical specimen: (a) grey-scale original image (liquid is in dark grey), (b) crop of the zone in (a), (c) segmentation of liquid and solid phase and (4) an example of reconstructed 3D stack (liquid is in blue).

- A 3D non-linear filter (Kuwahara filter) was applied to reduce the noise.
- Make a 3D binary stack.
- In the grayscale image, the solid and liquid phases were segmented.
- Calculation (different parameters).

4.3.2.5. In situ X-ray microtomography

The beam line ID 15 allows a fast tomography scan, since the scan time over a total rotation is smaller than 5s, which is assumed to be less than the time required for great microstructure changes. The in situ X-ray microtomography experiments were carried out on M2 steel grade at high temperature. During testing, the samples were not protected by argon, resulting in some oxidation. However, this technique offers a possibility to obtain 3D information and retrieve microstructure evolution locally.

4.4. In situ observations with CLSM

As mentioned above, the X-ray microtomography is a powerful tool for 3D microstructure characterization. However, it is not as easy to use, nor as ubiquitous as SEM and EDS techniques that are more readily accessible in laboratories. In addition, the reconstruction and image analysis are time-consuming for industrial applications. More importantly, this technique is selective in material. As explained before, it is difficult to obtain good microtomography images with good contrast because of less heavy elements such as 100Cr6 and C38LTT. Thereby, we tried other ways to see where the liquid appears and try to see what the volume fraction is at a certain temperature.

The in situ observation can be used for the characterization of the microstructure at high temperature. Both ESEM (Environmental Scanning Electron Microscope) and CLSM (Confocal Laser Scanning Microscope) were applied. During the tests, the heating chambers of ESEM and CLSM were vacuumed and purged several times by Argon. During heating, the Argon was charged. However, the oxidation phenomenon occurred at ~400°C during the tests performed on M2 by ESEM. In addition, the heating rate of ESEM can not exceed ~50°C/min. Thus, we mainly focused on the in situ observation by CLSM. During the observation by CLSM, the oxidation phenomenon was solved by placing a Titanium foil around the specimen to absorb the oxygen. This High Temperature Confocal Laser Scanning

Microscopy (HT – CLSM) permits in situ observations of microstructure evolution of these thixoformable grades (C38LTT, 100Cr6 and M2) directly during heating and cooling [20-23]. Besides higher resolution than general optics microscopy, it can also scan a surface at various focal depths and realize dynamic in situ observation. In particular, it is possible to observe at high temperature the phase transformation and liquid appearance as a function of temperature.

A Lasertec^{TM} 1LM21 confocal laser scanning microscopy system was used in our study. The CLSM set on a desktop vibration absorber consists of a laser source, a CCD sensor, a set of microscope lenses with long focal length, and a heating furnace as schematically shown in Fig. 2.26.

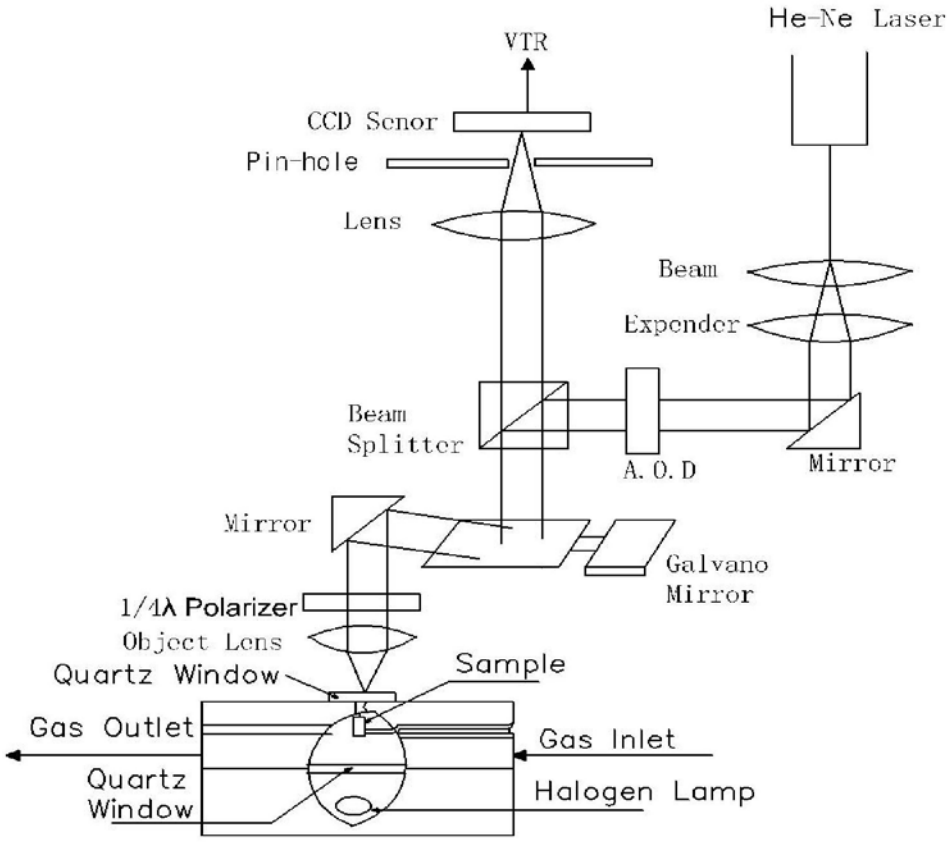

Fig. 2.26. Schematic view of CLSM with infrared image furnace.

4.4.1. Principle of CLSM

Generally, the CLSM employs the confocal optics which gathers information only from the focus plane. In the confocal optics, a sample is illuminated with a point light and the reflected light is collected on a point light detector. Therefore, accumulation of obtained images in the image memory while moving a focal point allows a clear image.

Real time observation with high speed scanning

The laser beam is scanned by an acousto-optic (AO) deflector in the horizontal direction and by a servo galvano mirror in the vertical direction. The reflected light is detected with a CCD image sensor. The AO deflector leads to high speed scanning because it has no mechanically movable part, allowing real time observations at a video rate. The optical path diagram of CLSM is schematically shown in Fig. 2.26. In our study, the laser beam is reflected by the specimen and scanned at a rate of 15.7kHz by an AO deflector in the horizontal direction, and by a galvano-mirror in the vertical direction at 60Hz. The obtained signal represents a quasi-topographical representation of the specimen surface through recording several captures at different depths, making it possible to distinguish the surface relief during phase transformations.

CLSM with a heating furnace

The CLSM combined with a heating stage mounted at the focal point of an ellipsoidal gold-plated infrared image furnace (IIF) powered by a 1.5kW, 100V halogen lamp, enables us to make in situ real time metallurgy observations at high temperature (Fig. 2.27).

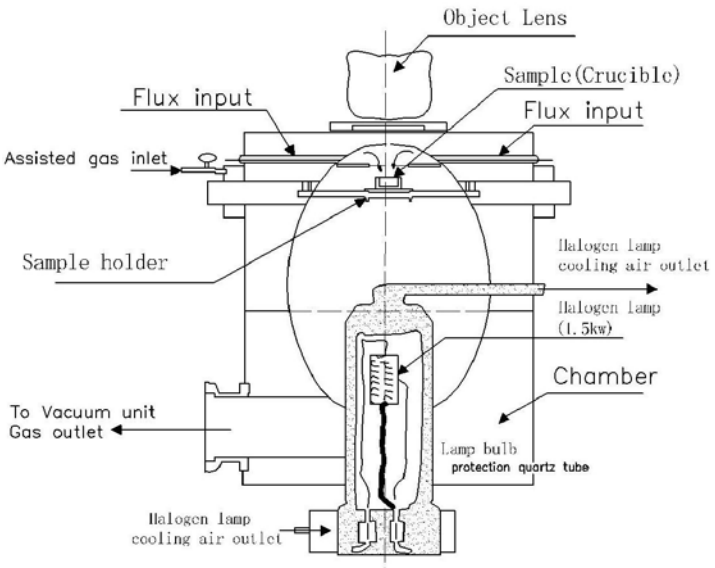

Fig. 2.27. Schematic view of CLSM heating system.

Small specimens (Ø5mm, 3mm height) were sectioned, ground and mechanically polished to 1µm. Each specimen was placed in an alumina crucible placed on the Pt stage in the CLSM enclosure (Fig. 2.28), below a quartz viewing window, and in a high purity Argon

atmosphere. Due to the nature of the temperature measuring and controlling, there is a difference in temperature between the real and measured temperatures during rapid heating. The thermal calibration shows that the temperature difference between the specimen surface and the recorded thermocouple temperature does not exceed ±15°C. During heating, Titanium foil was placed near the specimens to prevent the oxidation phenomenon.

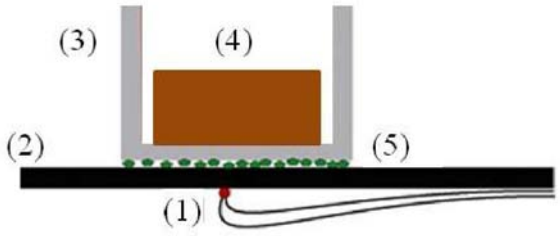

Fig. 2.28. Schematic drawing of the sample crucible. [1] Pt/Pt-10%Rh thermocouple. [2] Platinum sample holder. [3] Crucible. [4] Sample. [5] Al_2O_3 powder to prevent welding of the platinum parts.

4.4.2. Heating cycles

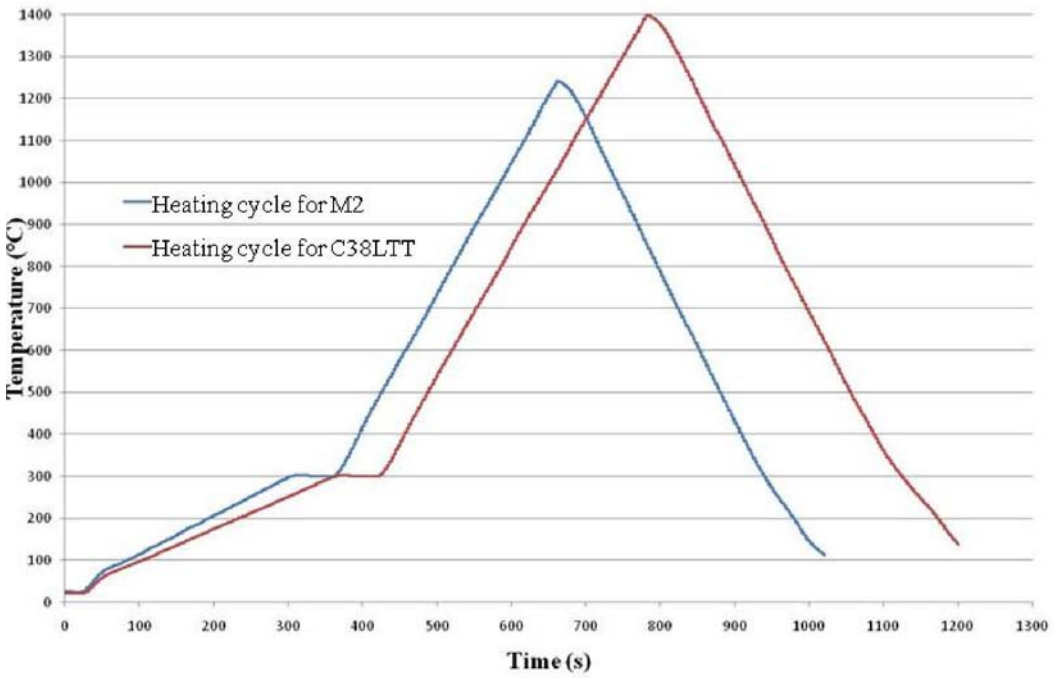

Fig. 2.29. Heating cycles for different steel grades.

The heating cycles for various steel grades are shown in Fig. 2.29. The samples were heated at a heating rate of 1°C/s until a plateau was reached at about 300°C. After 50s

isothermal holding, the samples were heated at a heating rate of 200°C/min to the predetermined temperature.

Following the in situ observations, the specimens were prepared for microstructural characterization at room temperature, by grinding, polishing and Nital(2%) etching. The specimens were examined in optical microscope and SEM.

5. Conclusions

This chapter has aimed to present various approaches for the characterization of microstructure of the material at different stages of a thixoforging process. The designed die tools, coils for induction heating system and the acquisition systems allow to perform the experiments which ensure the repeatability of experimental results.

Various techniques for microstructure characterization during each stage of metallic thixoforging process have already been summarized from conventional to new approaches (Table. 2.8). Especially for new techniques, although these techniques are complicated, high-technology, and difficult to access, it is possible to obtain interesting results for thixoforging research.

Table. 2.8. Summaries liquid fraction evaluation techniques.

	Techniques	Aims	Advantages	Limitations
Conventional methods	Thermodynamic (Thermo-calc)	F_L VS Temp. $\rho_{L(T)}$, $\rho_{S(T)}$	Fast. No materials consumption	Equilibrium conditions
	Thermal analysis (DSC)	F_L VS Temp.	Easy access	Low heating speed
	Quantitative metallography	F_L VS Temp. Microstructure characterization	Industrial conditions	2D results. Materials preparation
New developed approaches	X-ray microtomography	3D liquid fraction. 3D microstructure	3D Microstructure information. Capable of in situ observations	Time consuming. Materials selective. Difficult to access
	CLSM	F_L VS Temp. Microstructure evolution	In situ observations. High heating rate	2D. Images resolution

The characterized microstructures and macrostructures can be used to study the influence of the thixoforging process and process control.

The thixoforging experiments can be performed with the designed die tools, coils for induction heating system and the acquisition systems under a laboratory condition. The industrial thixoforging experiments can be concentrated on the aspects as follows:

- A new design of a billet holder which allows a better centering of the billet in the coil for a better induction heating repeatability.
- A transferring system with a controlled transferring time and path, such as a robot which can be used for a real industrial thixoforging process.
- Improvement of displacement measuring system which can avoid mechanical vibration phenomena.

References

1. Kazakov AA, Luong NH: **Characterization of semisolid materials structure.** *Materials Characterization* 2001, **46:**155-161.

2. Atkinson H, Rassili A: **A review of the semi-solid processing of steel.** *International Journal of Material Forming* 2010, **3:**791-795.

3. Becker E, Favier V, Bigot R, Cezard P, Langlois L: **Impact of experimental conditions on material response during forming of steel in semi-solid state.** *Journal of Materials Processing Technology* 2010, **210:**1482-1492.

4. Püttgen W, Bleck W: **Thixoforming/semi-solid forming : DTA-measurements to determine the thixoformability of steels.** *Steel Research International* 2004, **75:**531-536.

5. Lecomte-Beckers J, Rassili A, Carton M, Robelet M, Koeune R: **Study of the liquid fraction and thermophysical properties of semi-solid steels and application to the simulation of inductive heating for thixoforming.** In *Advanced Methods in Material Forming*: Springer Berlin Heidelberg; 2005.

6. Kopp R, Kallweit J, Möller T, Seidl I: **Forming and joining of commercial steel grades in the semi-solid state.** *Journal of Materials Processing Technology* 2002, **130–131:**562-568.

7. Cézard P: **Impact des effets thermiques sur le comportement du matériau lors de la mise en forme des aciers à l'état semi-solide : Analyses expérimentale et numérique.** Thesis. L'Ecole Nationale Supériure d'Arts et Métiers, Docteur de l'Ecole National Supérieure d'Arts et Métiers; 2006.

8. Becker E: **Investigations experimentales et numeriques pour l'identification des parametres clefs du procede de thixoforgeage de l'acier sur le produit mis en forme.** Thesis. L'Ecole Nationale Supériure d'Arts et Métiers, Docteur de L'Ecole National Supérieure d'Arts et Métiers; 2008.

9. Neag A, Favier V, Bigot R, Pop M: **Microstructure and flow behaviour during backward extrusion of semi-solid 7075 aluminium alloy.** *Journal of Materials Processing Technology* 2012, **212:**1472-1480.

10. Orfeuil M: *Electric Process heating: Technologies/Equipment/Applications.* Battelle Press; 1981.

11. Jung HK, Kang CG: **Reheating process of cast and wrought aluminum alloys for thixoforging and their globularization mechanism.** *Journal of Materials Processing Technology* 2000, **104:**244-253.

12. Becker E, Bigot R, Langlois L: **Thermal exchange effects on steel thixoforming processes.** *The International Journal of Advanced Manufacturing Technology* 2009, **48:**913-924.

13. Hirt G, Bleck W, Buhrig-Polaczek A, Shimahara H, Puttgen W, Afrath C: **Semi solid casting and forging of steel.** *Solid State Phenomena* 2006, **116-117:**34-43.

14. **Hardening high speed steels: metallurgical benefits of salt** [http://ppunch.com/pdf/heat.pdf]

15. Bergsma SC, Tolle MC, Kassner ME, Li X, Evangelista E: **Semi-solid thermal transformations of Al–Si alloys and the resulting mechanical properties.** *Materials Science and Engineering: A* 1997, **237:**24-34.

16. Liu T, Ward P, Atkinson H, Kirkwood D: **Response of semi-solid Sn-15 pct Pb to rapid shear-rate changes.** *Metallurgical and Materials Transactions A* 2003, **34:**409-417.

17. Seo P, Kang C: **The effect of raw material fabrication process on microstructural characteristics in reheating process for semi-solid forming.** *Journal of Materials Processing Technology* 2005, **162-163:**402-409.

18. Hirt G, Kopp R (Eds.): **Thixoforming - semi-solid metal processing**. Aachen: Wiley-VCH Verlag GmbH & Co. KGaA; 2009.

19. Herman GT: *Image Reconstruction from Projections.* New York: Academic Press; 1980.

20. Heulens J, Blanpain B, Moelans N: **Analysis of the isothermal crystallization of CaSiO3 in a CaO–Al2O3–SiO2 melt through in situ observations.** *Journal of the European Ceramic Society* 2011, **31:**1873-1879.

21. Attallah MM, Terasaki H, Moat RJ, Bray SE, Komizo Y, Preuss M: **In-situ observation of primary γ′melting in Ni-base superalloy using confocal laser scanning microscopy.** *Materials Characterization* 2011, **62:**760 - 767.

22. Wang SL, Gao LW, Huang FX, Wang XH: **Confocal laser scanning microscopy and its application in metallurgy.** *Metallurgical Analysis* 2011, **31:**40 - 45.

23. Yuan F, Liang GF, Zhu GM, Wang CQ, Wu JC, Yu Y: **Confocal laser scanning microscopy and its application in in-situ observation of phase transformation of steel.** *Journal of Baosteel Technique* 2006, **6:**64 - 69.

Chapter 3. Liquid fraction evaluation and microstructure characterization

Table of contents

1. Introduction……239

2. Liquid fraction evaluation by Thermo-Calc……240

3. DSC analysis of liquid volume fraction……243

3.1 DSC curves……243

3.2 Liquid fraction obtained by partial area integration……244

3.3 Comparison between the DSC and equilibrium results……247

4. 2-Dimentional image analysis on the billet quenched from the semi-solid state……247

4.1 Heating cycle……248

4.2 Microstructure analysis……250

4.3 Microstructure characterization by image analysis……255

4.4 Microstructure characterization on C38LTT and 100Cr6……261

4.5 Summary……261

5. Evaluation of liquid fraction by X-ray microtomography……261

5.1 As-received state……262

5.2 Microstructure of M2 quenched from the semi-solid state……263

5.3 X-ray tomography on other steel grades……270

5.4 Summary……270

6. In situ observation on M2, 100Cr6 and C38LTT……270

6.1 Heating cycles for the grades……270

6.2 Microstructure evolution of M2……271

6.3 Microstructure evolution of 100Cr6……273

6.4 Microstructure evolution of C38LTT……275

6.5 Summary……276

7. Conclusions……277

References……279

Phase diagrams, thermal analysis and image analysis (2D and 3D) have been described and applied for the evaluation of the volume fraction of liquid/solid as a function of temperature in the semi-solid state. The accuracy and abilities of each approach to the evaluation of the volume fraction for industrial semi-solid processing was discussed. We evaluated the volume fraction of liquid in various steel grades which have been produced by different manufacturing methods for obtaining near equiaxed microstructure which is essential for subsequent semi-solid processing.

The results of the experiments for studying the microstructure evolution during heating to the semi-solid state are also presented in this chapter. The microstructure in the semi-solid state has been analyzed and characterized by various techniques performed under different conditions. These parameters of the morphology in the semi-solid state are important as they have an effect on the rheology of the material and therefore on the mechanical properties of the thixoforged parts.

1. Introduction

The volume fractions of liquid or solid as a function of temperature in the semi-solid state of various grades have been evaluated by various approaches (phase diagrams, thermal analysis techniques and quantitative metallography analysis on microstructures in 2D and 3D), especially for the high speed tool steel M2. These results have been synthesized and compared in order to define the accuracy, advantages and limitations of each method for the determination of the liquid fraction and microstructure evolution.

Various experiments have been performed on different steel grades under different process conditions in order to evaluate the liquid fraction and study the evolution of the microstructure during heating to the semi-solid state. Table 3.1 presents the parameters of various approaches used for the microstructure characterization and the evaluation of the liquid fraction as a function of temperature.

Depending on the equipment and the temperature measurement method, the temperature of the sample given in the table is approximate.

Table. 3.1. Combination of the parameters used in various experimental approaches.

Grade	Experiment approaches	Temperature range	Heating rate	Dimensions of samples
M2	DSC	Room ~ 1500°C	10°C/min 20°C/min	Ø 3*1.5
	Quenching	1260-1350°C	~ 500°C/min	Ø35*34
	X-ray tomography	Room temperature		Ø1.2*30
	In situ observation	Room ~1300°C	200°C/min	Ø5*3
	Thixoforging	1290 ~ 1350°C	~ 500°C/min	Ø35*34
C38LTT	Quenching	1410~ 1450°C	~ 500°C/min	Ø45*60
	In situ observation	Room ~ 1450°C	200°C/min	Ø5*3
	Thixoforging	1410~ 1450°C	~ 500°C/min	Ø45*60
100Cr6	Quenching	1340-1410°C	500°C/min	Ø30*45
	In situ observation	Room ~1420°C	200°C/min	Ø5*3
	Thixoforging	1340-1410°C	500°C/min	Ø30*45

2. Liquid fraction evaluation by Thermo-Calc

Thermo-Calc commercial software was used to generate the phase diagram for the M2 steel grade in the work. The calculation was performed under the consideration which involves five major constituents and two minor ones in addition to the number of phases of which most are solid solutions as shown in the general diagram (Fig. 3.1). In the thermodynamic calculations, the low heat transfer rate was considered, close to equilibrium conditions (1°C/min).

The carbon content of M2 is about 0.85% wt.%, and for this carbon content, the ferrite is not stable above 850°C. The solidus and the liquidus temperatures are ~1240°C and ~1450°C, respectively. The obtained liquidus temperature is used for selecting proper DSC equipment and conditions (maximum working temperature). As illustrated in the diagram, the eutectic transformation is not isothermal but takes place in a range of temperatures, where the austenite, liquid and carbides coexist. From the diagram, it can also find that there are three types of carbides: MC, M_6C and $M_{23}C_6$. Normally, $M_{23}C_6$ is not stable at high temperature. Moreover, as the content of chemical elements is very high, even at very low heating rate it is impossible to dissolve all of these carbides before melting starts. As shown in Fig. 3.1, at around 1250°C where melting starts, some MC and M_6C carbides coexist with liquid phase. Using the Thermo-Calc, the weight fraction of remained carbides before melting starts is ~10 wt.% (Fig. 3.2).

As illustrated in Chapter 2, for a phase volume fraction evaluation, it is necessary to know the composition of the solid and liquid phases as well as their densities $\boldsymbol{\rho_s}$ and $\boldsymbol{\rho_L}$ as a function of temperature. These densities are illustrated for M2 in Fig. 3.3.

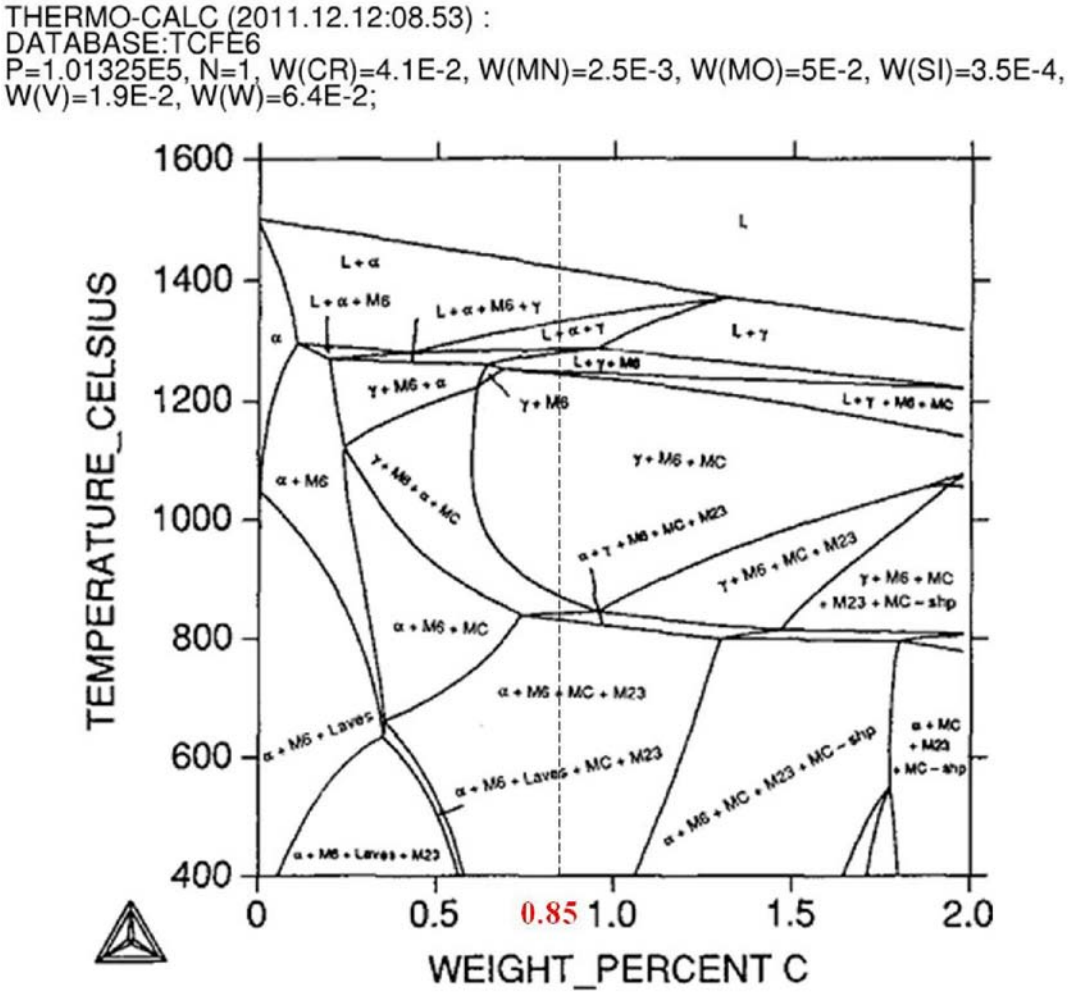

Fig. 3.1. Calculated isopleth of Fe – 4.1 wt.% Cr - 0.25 wt.% Mn – 5 wt.% Mo – 0.035 wt.% Si – 1.9 wt.% V – 6.4 wt.% W.

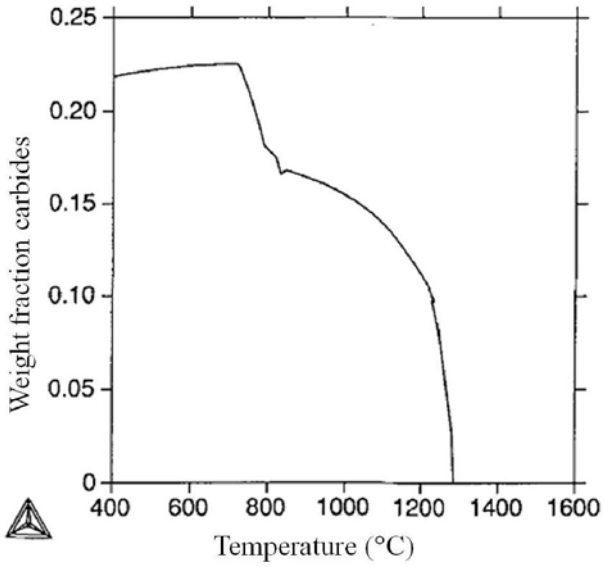

Fig. 3.2. Calculated weight fraction of carbides as a function of temperature.

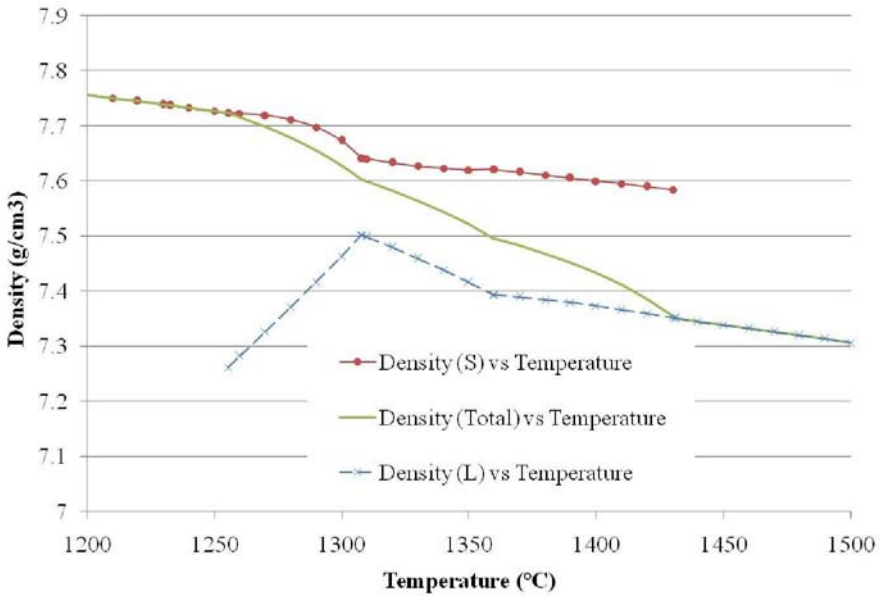

Fig. 3.3. Densities of solid and liquid phases of M2 as a function of temperature.

Finally, the evolution of volume fraction of liquid with temperature in the M2 steel has been calculated as shown in Fig. 3.4. It can be seen from this figure that the slope of the curve becomes less steep between the liquid fraction of 25% and 55%. That means that the liquid fraction sensitivity is reduced in this range. The liquid fraction sensitivity is important to the semi-solid forming process, because if the sensitivity is high, some zones may reach a high liquid fraction while others stay at a lower liquid fraction or even in the solid state, which is not preferred for thixoforging process.

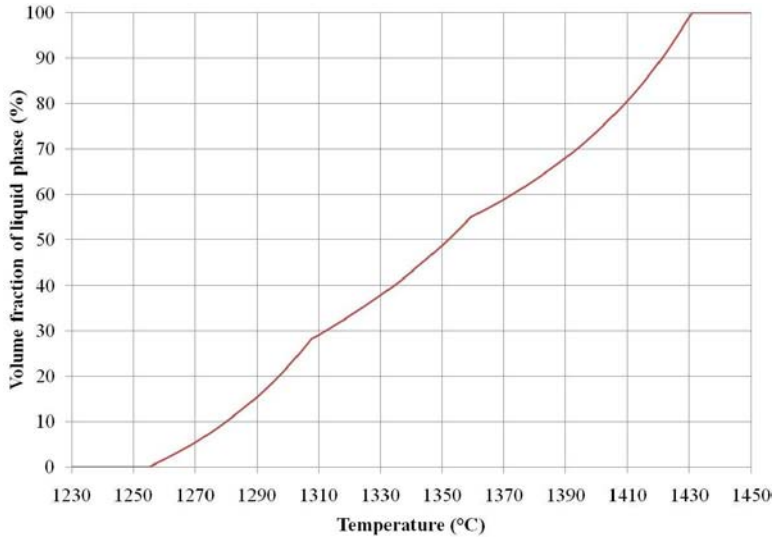

Fig. 3.4. Evolution of volume fraction of liquid with temperature of M2 steel.

Industrial thixoforming conditions involve a rapid heating stage. The heating rate is so high that homogenization of the material can not be obtained. In this case, the microsegregation changes a little, the carbides remain undissolved. As a result, non-equilibrium liquid is formed as soon as the temperature reaches to the non-equilibrium eutectic temperature.

The thermodynamic database can be used to establish the evolution of the liquid fraction during heating under equilibrium condition. However, microsegregation bands have been observed, which is normal for commercial hot formed steel grades such as M2. As the thermodynamic calculation does not take into account of the thermal history of M2, there is a need for experimental methods to evaluate the liquid fraction during heating.

DSC analysis and quantitative metallurgy were used for the characterization of the liquid volume fraction.

3. DSC analysis of liquid volume fraction

3.1. DSC curves

Fig. 3.5 shows the result of thermal analysis of the M2 performed at the heating rate of 10°C/min. In the DSC curves, the reaction peaks reflect the specific phase changes. In the study, an assumption has been made: 'the peak area is proportional to the heat of reaction associated with the phase transformation'. As shown in Fig. 3.5, there are five endothermic

peaks for this grade. Based on the equilibrium diagram, peak 1 corresponds to the austenite phase transformation; peak 2 and 3 are associated with the melting of carbides; peak 4 represents the delta ferrite transformation and peak 5 indicates the inverse peritectic reaction.

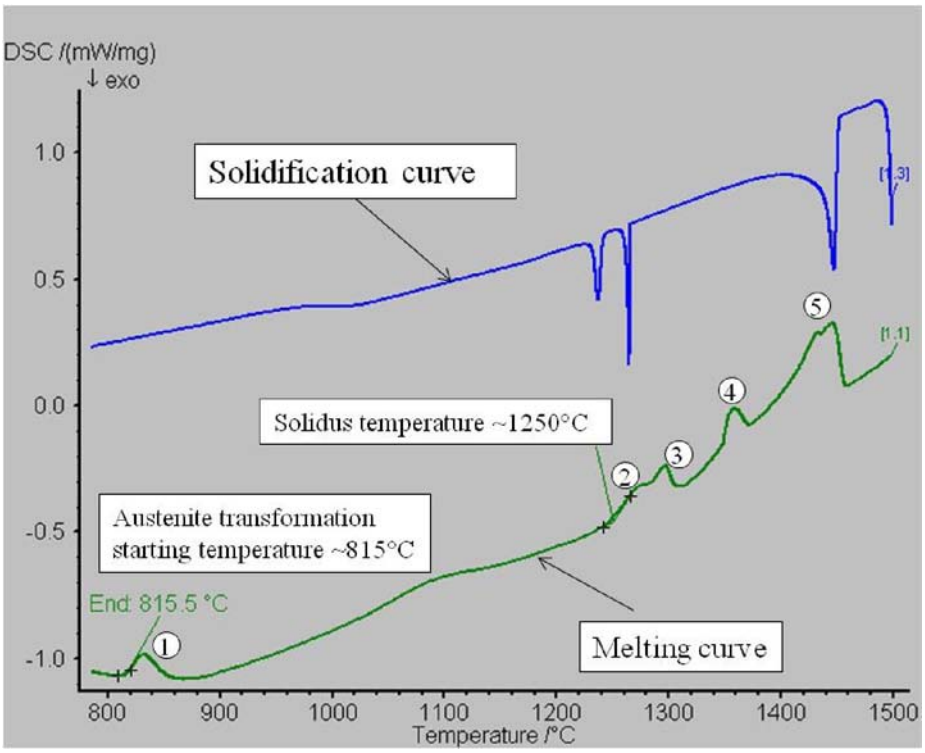

Fig. 3.5. DSC signal for M2 steel grade. Heating rate: 10°C/min.

Several experiments have been performed in the same test conditions to make the results more reliable, as DSC is very sensitive to experimental conditions such as sample mass, heating rate, contact of the material with crucible etc. A similar behavior was observed from the DSC tests: 5 reaction peaks have been obtained in the heating process, the austenite transformation starting temperature and solidus temperature are around 815°C-825°C and 1240°C-1250°C, respectively obtained by the tangent method.

3.2. Liquid fraction obtained by partial area integration

The evaluation of the liquid phase distribution is carried out by the application of a peak partial area integration. The total area between the enthalpy area curve and a created sigmoidal baseline is used to determine the melting enthalpy of the material.

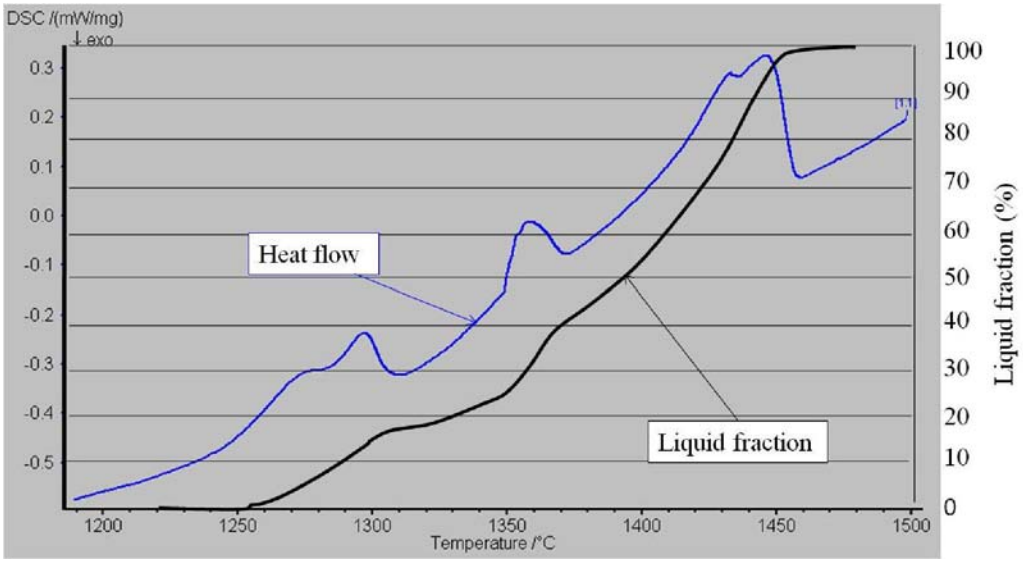

Fig. 3.6. DSC curve and the liquid fraction as a function of temperature (Heating rate: 10°C/min).

Fig. 3.6 gives the evolution of heat flow with temperature and the liquid fraction as a function of temperature. Moreover, curves of liquid fraction as a function of the temperature obtained at two heating rates are shown in Fig. 3.7. Comparing these two curves, it can be noted that when the heating rate is high, the liquid fraction curve as a function of temperature shifts to the left, meaning the solidus temperature is lower. Similar results have been observed by other researchers on other alloys [1-3]. However, it is well known that the increased heating rate may lead to an increase in solidus temperature because of the latent heat. The obtained DSC results can be discussed in several aspects: the heterogeneity of the material, the DSC device and the liquid fraction calculation method.

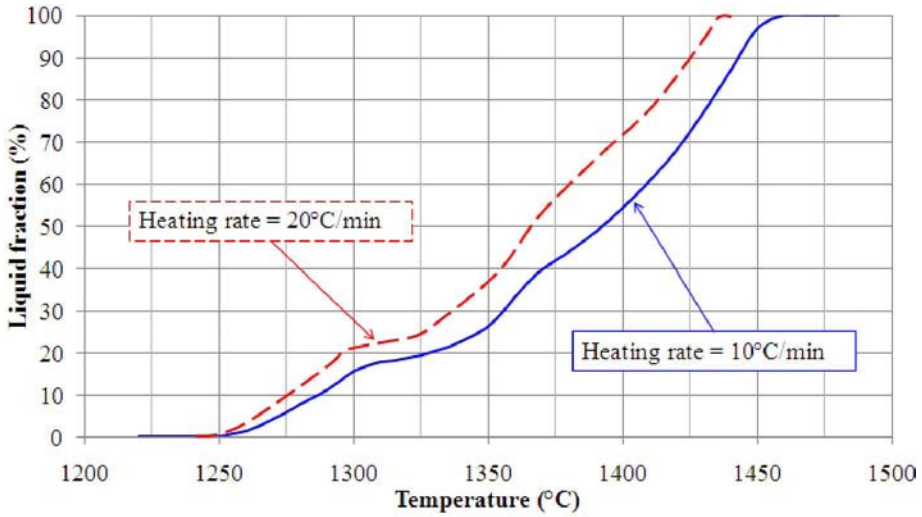

Fig. 3.7. Liquid fraction as a function of temperature at two heating rates, 10°C/min and 20°C/min.

The samples tested by DSC were sectioned from a rolled bar with microsegregation bands. The small sample dimensions (Ø3*1.5mm) may cause a change of percentage in chemical elements, and the alloying elements can influence the liquid fraction as a function of temperature [4, 5]. During heating, the composition affects the energy required to transfer the atoms from solid phase to the liquid phase via the solid/liquid interface, since it depends on the type of atoms, their concentration and the distribution.

It is also important to consider the design of the DSC equipment when studying the temperature obtained. In the DSC tests, the sample is placed in a crucible. During heating, the temperature measured by the thermocouple is that of the crucible which always causes a temperature lag between the sample and the thermocouple as shown in Fig. 3.8. Moreover, the temperature lag increases with increasing heat flux and thermal resistance between sample and thermocouple. In addition, heating rate influences the temperature distribution through the sample; the temperature difference between the end and the surface of the sample increases with increasing heating rate.

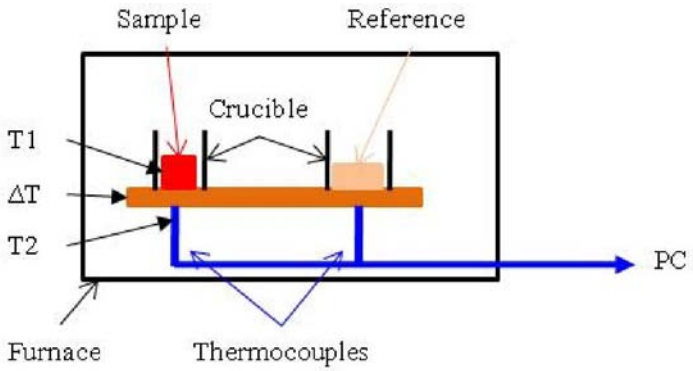

Fig. 3.8. Schematic diagram of temperature acquisition of DSC.

The calculation method of partial areas is approximate, since the calculation was made under an assumption: 'the heat of melting does not depend on the temperature and the composition of the solid phase.' As the temperature increases, the composition of the solid phase changes to maintain a local equilibrium at the solid-liquid interface following the equilibrium phase diagram. Based on thermodynamics principle, Tzimas and Zavaliangos quantified the effect of composition on the heat of solidification/melting and found that there was a significant error in the results obtained by the partial areas method, particularly when there is a big difference between the heat for melting of the alloy and the latent heat of the solvent metal [6].

3.3. Comparison between the DSC and equilibrium results

The curves of liquid fraction as a function of temperature obtained by Thermo-Calc and DSC are shown in Fig. 3.9. It can be observed that the liquid fraction in the temperature range of 1250°C – 1300°C is similar and corresponds to the dissolution of the carbides into the liquid phase. Then austenite or ferrite began to melt with increasing temperature. The difference may be due to several factors: the difference in chemical compositions between Thermo-Calc and the alloys used for DSC experiments, the influence of the heating rate, the precision in temperature measurement etc. More importantly, the difference of liquid fraction increases at a temperature interval (1300°C ~ 1360°C), which is the range of interest for thixoforging M2 because the liquid fraction does not vary a lot with temperature in this range.

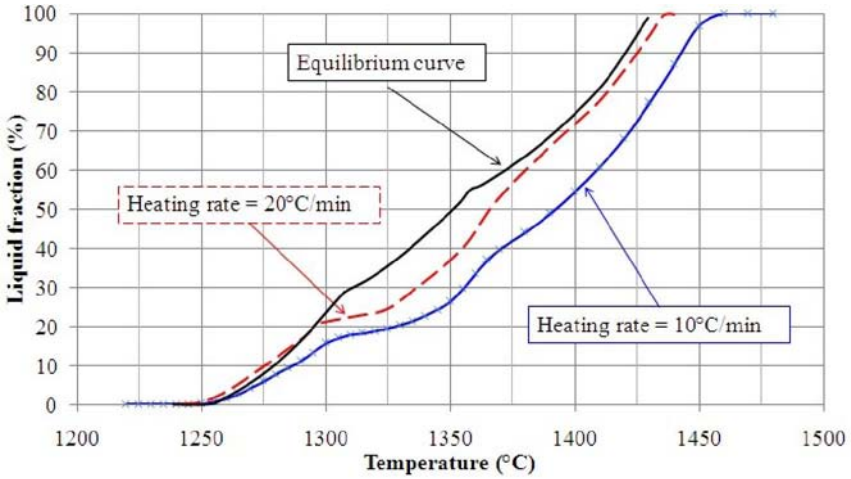

Fig. 3.9. Liquid fraction as a function of temperature obtained by DSC and Thermo-Calc.

Although the heating rate used in the DSC tests is much lower than that used in the thixoforming process, it can provide useful information on the solidus and liquidus temperatures. For an easier thixoforging process control, the liquid fraction should not change dramatically with temperature. Therefore, the processing temperature for thixoforging was chosen in the range of 1290°C ~ 1340°C based on the liquid fraction obtained by DSC.

4. 2-Dimensional image analysis on the billet quenched from the semi-solid state

For an industrial thixoforming process, the heating rate is much higher than that used in the DSC tests. In order to evaluate the liquid fraction and the microstructure in a billet in the

semi-solid state, quenching experiments were performed on the billet heated by multi-step heating cycles.

4.1. Heating cycle

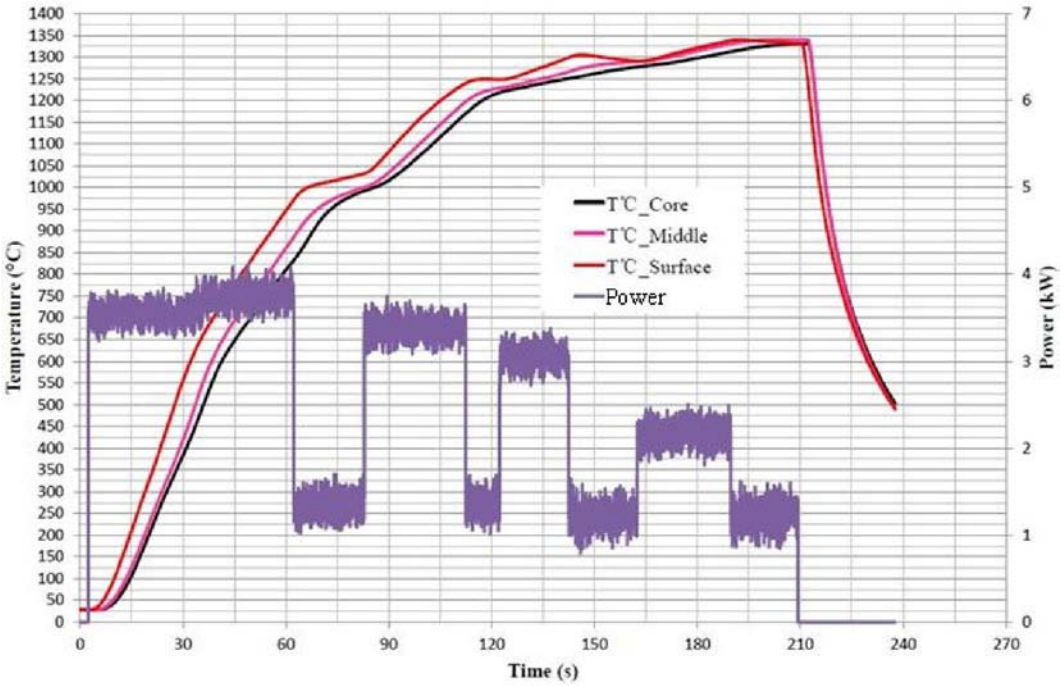

(a) Heating cycle with a lower heating rate at the beginning of the heating process.

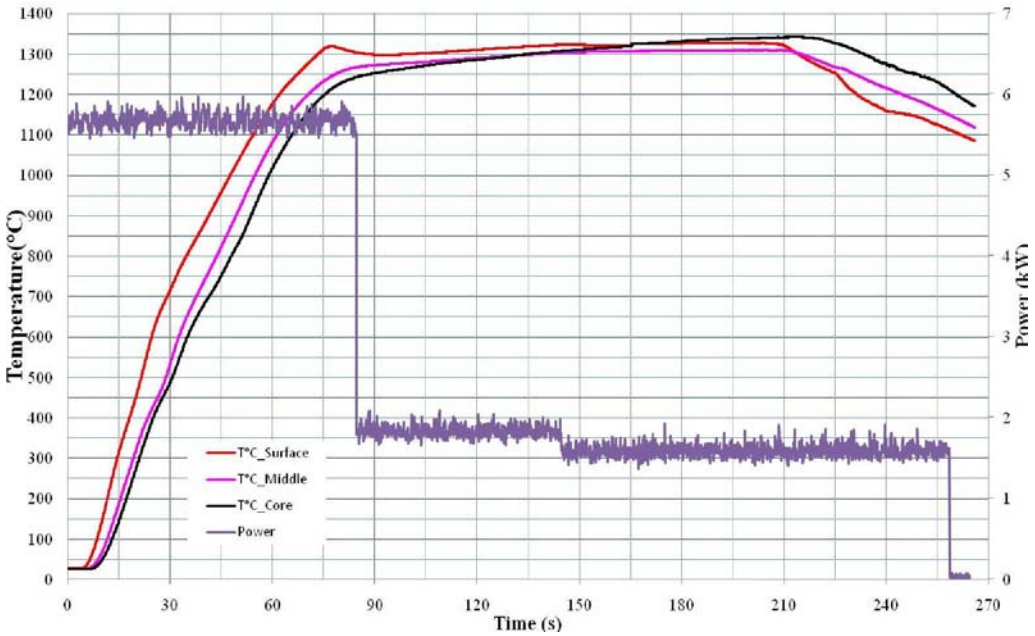

(b) Heating cycle with a higher heating rate at the beginning of the heating process.

Fig. 3.10. Temperature distribution in the billet and the heating power.

Following the requirements of industrial thixoforming process (high heating rate, homogeneous temperature across the billet, near-spherical solid grains), two types of heating cycles were designed for heating the billets as shown in Fig. 3.10 ((a): A-type, (b): B-type).

The difference of these two strategies of heating cycles lies on the average heating rate at the beginning of the heating process. A rapid rise of temperature can be obtained with a higher heating power. Compared with the A-type heating cycle, B-type heating cycle (4 steps) applies a higher heating power at the beginning of the heating process in order to reach a higher temperature with less heating time. The reduced heating power leads to a slower and a smaller temperature difference at various positions. During heating, the billets were heterogeneously heated to a high temperature. The temperature profiles show that the surface of the billet is heated first due to the skin effect phenomenon. The inside of the billet is heated slowly by thermal conduction from the surface. At the end of the heating period, the billets were heated slowly to the required temperature with a lower heating power. During the slow heating process, a relative homogeneous billet temperature field can be achieved by thermal convection and conduction. Meanwhile, the spherodization of the solid phase which is important to the thixotropic behavior can be promoted in this slow heating stage.

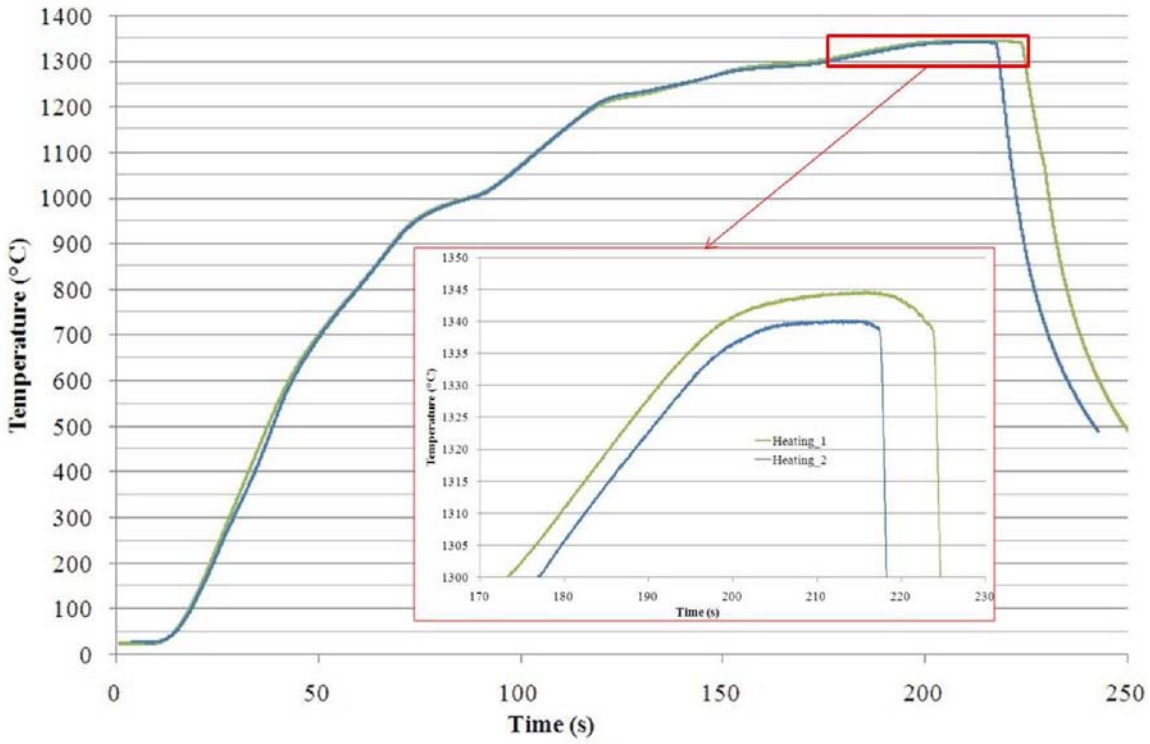

Fig. 3.11. Temperature vs time curves (at the center of billets) showing the repeatability of the heating cycle.

Several issues associated with temperature measurement and control during the heating process are needed to be solved in the future. The first is the accuracy of the temperature measurement. The accuracy of S-type thermocouples is around ±2.5°C. The second issue is that the temperature of the billet is not directly measured by thermocouples, because they are protected by alumina conduits. The thermocouples do not measure the temperature of the billet but that of the alumina conduits. The third issue is the repeatability of a temperature curve. Fig. 3.11 shows two curves with the same power sequence. The temperature difference is around 4°C. The issue of temperature control has proved to be quite a challenge.

4.2. Microstructure analysis

The billets were heated to various desired temperatures by various heating cycles. Typical microstructure of quenched material from the semi-solid state is shown in Fig. 3.12 (d) (e) and (f); while (a) (b) and (c) present the as-received microstructure of M2. Meanwhile, different types of carbides with different morphologies were identified using EDS. Fig. 3.13 illustrates the EDS results for carbides in both the as-received state (c) and the quenched from the semi-solid state (f).

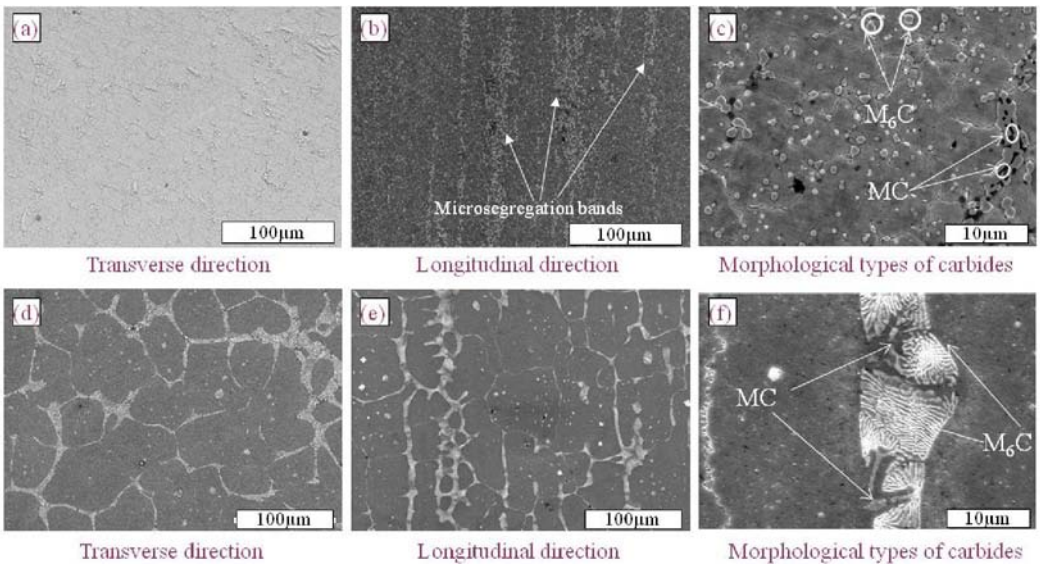

Fig. 3.12. SEM micrographs of the M2 steel in the as received state (a) transversal direction, (b) longitudinal direction, (c) typical morphology of carbides; and in the quenched from the semi-solid state (d) transversal direction, (e) longitudinal direction and (f) typical morphology of carbides.

As presented in the SEM micrographs of the as-received M2 steel on transverse and longitudinal directions (Fig. 3.12 (d) (e) and (f)), the carbides particles are distributed along

the grain boundaries and in the matrix. The longitudinal surface (Fig. 3.12 (e)) bears evidence of microsegregation banding along the longitudinal direction of the billet. The microsegregation bands are parallel to the rolling direction. These phenomena are typical for the commercially produced high speed tool steels which contain a high amount of slowly diffusing elements [7]. In addition, two different types of carbides present in the material were confirmed by EDS (Fig. 3.13 (a)): the whiter particles are M_6C type carbides, rich in tungsten and molybdenum, while the darker ones are MC-type carbides rich in vanadium, tungsten and molybdenum. Table 3.2 gives the chemical composition (wt.%) of these two types of carbides obtained by EDS. The microstructure of the as-received material consists of retained austenite in martensitic matrix. The average grain size is ~10μm. The size of many carbides particles in the as-received state is smaller than 1μm.

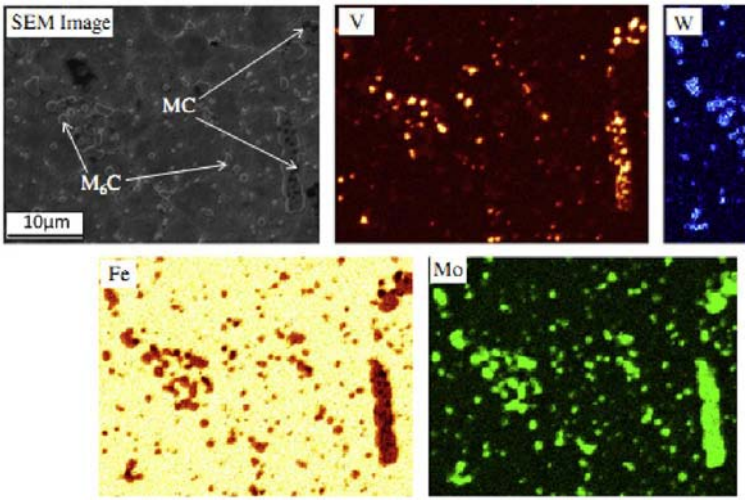

(a) SEM-EDS mapping of M2 in the as-received state.

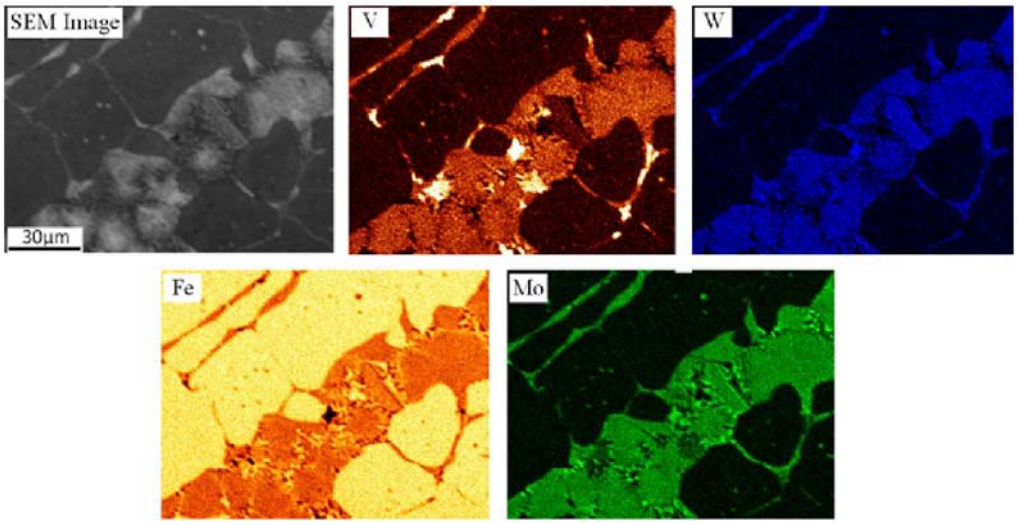

(b) SEM-EDS mapping of M2 quenched from semi-solid state.

Fig. 3.13. SEM-EDS mapping of M2 in two different states. (a) As-received state. (b) Quenched from the semi-solid state.

Table. 3.2. The characteristic chemical compositions of the large and fine carbides.

	Carbides (weight %)				
Elements	V	Cr	Fe	Mo	W
Whiter particles	3.65	2.88	30.4	24.87	38.29
	2.55	3.19	34.2	22.37	37.69
	3.05	3.04	32.22	25.35	36.34
Darker particles	34.72	4.76	9.3	23.98	27.25
	32.7	4.61	10.43	23.67	28.6
	35.32	5.06	10.06	20.72	28.88

After induction heating from its as-received state to semi-solid state, the billets were then quenched to preserve the microstructure presented in the semi-solid state. The microstructure of the material quenched from the semi-solid state differs from that in the as-received state in grain size, distribution of carbides and morphology. The grains are bigger in size compared to that in the as-received state. Compared to the original carbides particles, the morphology of new formed carbides is different in both their dimensions and localization. During induction heating, as the temperature rises, alloying elements, such as vanadium, tungsten and molybdenum among others, diffuse to the liquid zones where the solubility is higher. These liquid zones, preferably developing from the grain boundaries, appear very clearly after quenching because of their high content in alloying elements. They form new interconnected carbide networks that make the definition of the new grain size obvious. It can be conjectured that the microstructure of M2 steel combines both solid and liquid phases before quenching. During quenching, the cooling speed was efficient to preserve the microstructure in the semi-solid state.

When comparing the microstructure of M2 quenched from semi-solid state, the structure on the transversal surface differs from the one on the longitudinal surface. In addition, the microstructure of the material heated to the same temperature by different heating cycle types is also different in grain size and carbides or liquid phase distribution as presented in Fig 3.14: the transversal ((a), (c)) and longitudinal ((b), (d)) microstructures of the billets quenched from 1290°C. The billets were heated by two different heating cycles.

The micrographs on transversal section (Fig. 3.14 (a) and (c)) show equiaxed or spherical grains. The solid phase is surrounded by the liquid phase (dark zones). The grain boundaries are smooth. Contrary to the microstructure on the transversal surface, the microstructure on

the longitudinal surface (Fig. 3.14 (b)) shows some distinct polygonal grains. The segregated bands are observed on the longitudinal surface (Fig. 3.14 (b) and (d)).

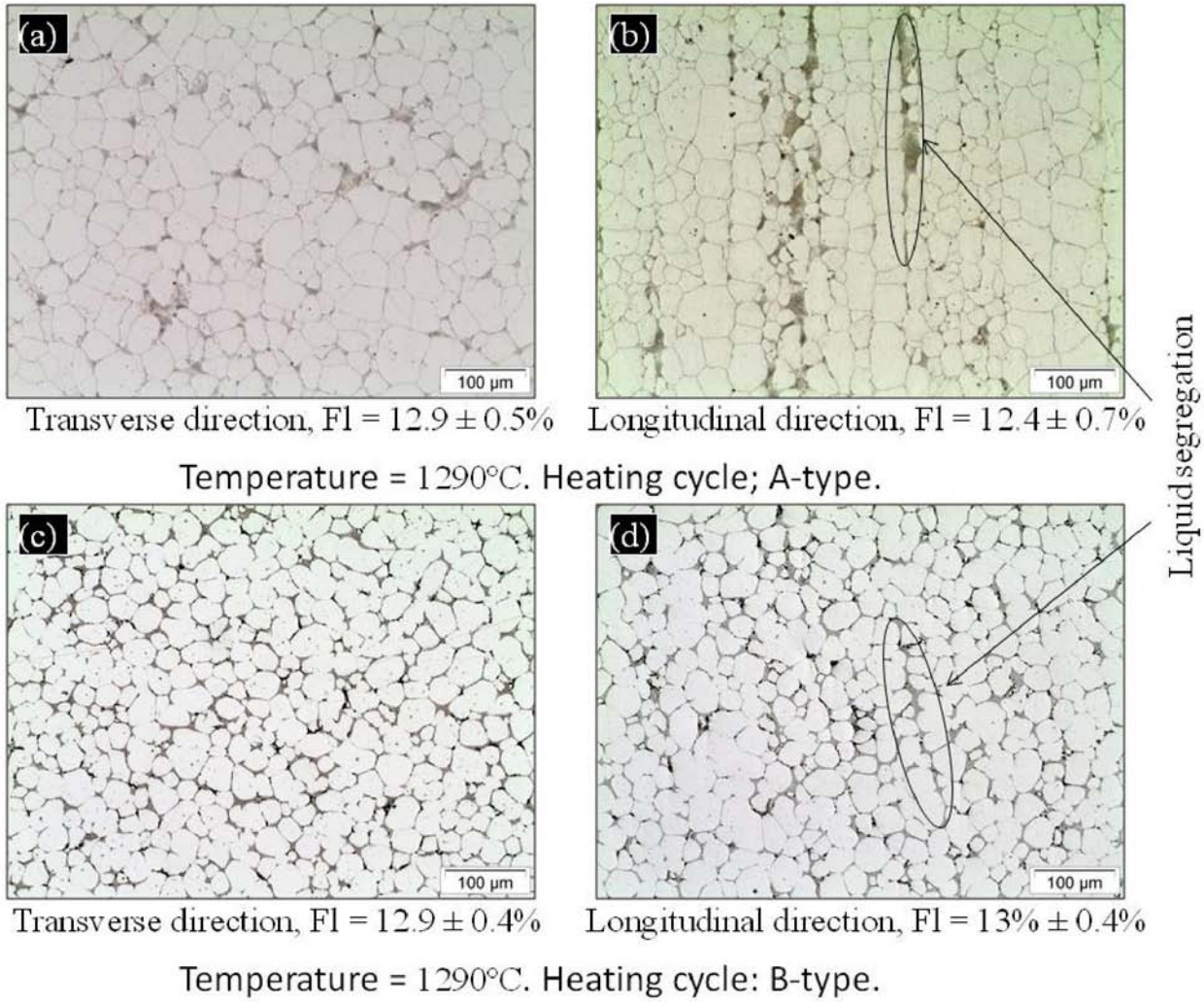

Fig. 3.14. Micrographs of billets quenched from 1290°C on (a) transversal direction, heated by A-type heating cycle, (b) longitudinal direction, heated by A-type heating cycle, (c) transversal direction, heated by B-type heating cycle and (d) longitudinal direction, heated by B-type heating cycle.

Table 3.3 gives the values of microstructure parameters of the billets at 1290°C heated by different heating cycles. At the same temperature, the liquid fractions of the billets heated by different heating cycles are similar. However, the microstructures of these billets are not the same. For example the grains of the billet heated by B-type heating cycle are more spherical than those heated by A-type heating cycle. The average grain size in Fig. 3.14 (c) and (d) is smaller than that in Fig. 3.14 (a) and (b). Moreover, the grains in Fig 3.14 (c), (d) are much wetted by the liquid phase compared to those shown in Fig. 3.14 (a), (b).

Table. 3.3. Microstructure parameters.

	Heating cycle: A-type		Heating cycle: B-type	
Micrographs	Fig. 3.14 (a)	Fig. 3.14 (b)	Fig. 3.14 (c)	Fig. 3.14 (d)
Grain size	40.1 ± 3µm	43.3 ± 3µm	28.3 ± 2µm	30.2 ± 2µm
Shape factor	0.78 ± 0.02	0.8 ± 0.01	0.89 ± 0.005	0.89 ± 0.007
Liquid fraction	12.9 ± 0.5 %	12.4 ± 0.7%	12.9 ± 0.4 %	13 ± 0.4%

The differences of microstructure in the semi-solid can be related to the thermal history and various heating cycles. In order to measure the temperature during heating, the as-received billets were annealed to reduce the hardness for drilling holes for the thermocouples. The manufacturing route is as follows: the steel which was hot formed at a temperature approximately 1150°C, was tempered at 650°C-750°C for about 4h, and then annealed before being furnace cooled to room temperature. The microstructure prior to the thixoforging process is shown in Fig. 3.15. Carbide particles in the ferrite matrix contained in bands are parallel to the working direction along the billet.

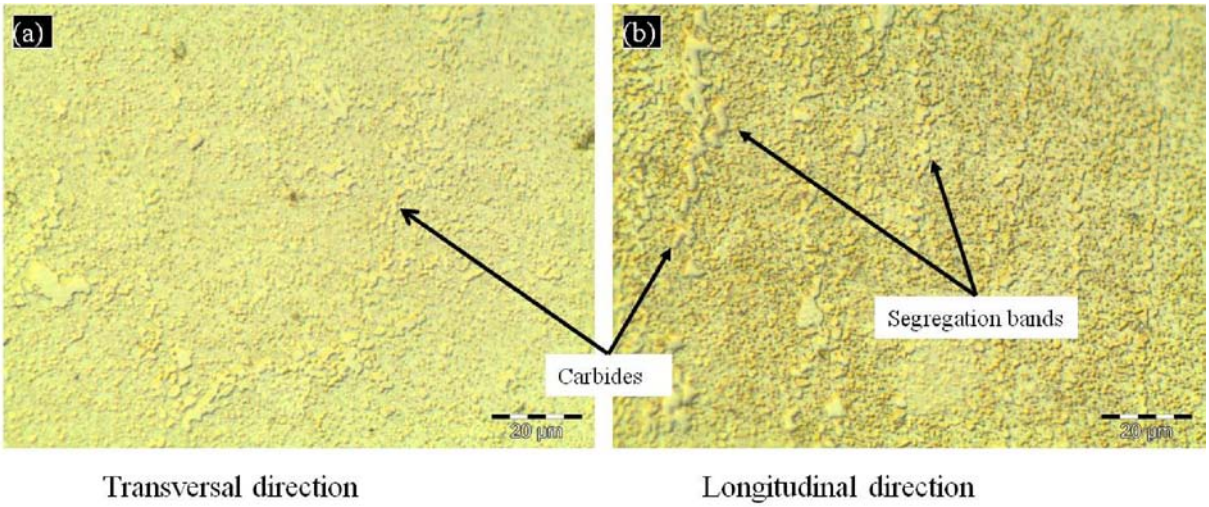

Fig. 3.15. Microstructure of the billet prior to the partial melting obtained by an optical microscope.

The difference in the morphology of the billets in the semi-solid state may have resulted from the heating cycles. Comparing these two types of heating profile, it takes longer time to heat the billet from the room temperature to the solidus temperature (around 1250°C) by A-type heating cycle (Fig. 3.10 (a)). As is well known, the grain grows with heating time, thereby resulting in a bigger grain size in the billet heated by A-type heating cycle. For B-type heating cycle, the longer time for material staying in the semi-solid state allows homogenizing

the material and relatively uniform heating which results in a uniform liquid distribution and more spherical grains.

4.3. Microstructure characterization by image analysis

The structure in the semi-solid state was characterized on the quenched billet. As the diffusion rate of the alloying elements is low, the former liquid phase can be preserved in the quenched billet (this will be detailed in the in situ observations by CLSM).

Fig. 3.16 (a) illustrates the liquid fraction at different positions of the billet (temperature = 1306 - 1320°C) measured on the transversal direction.

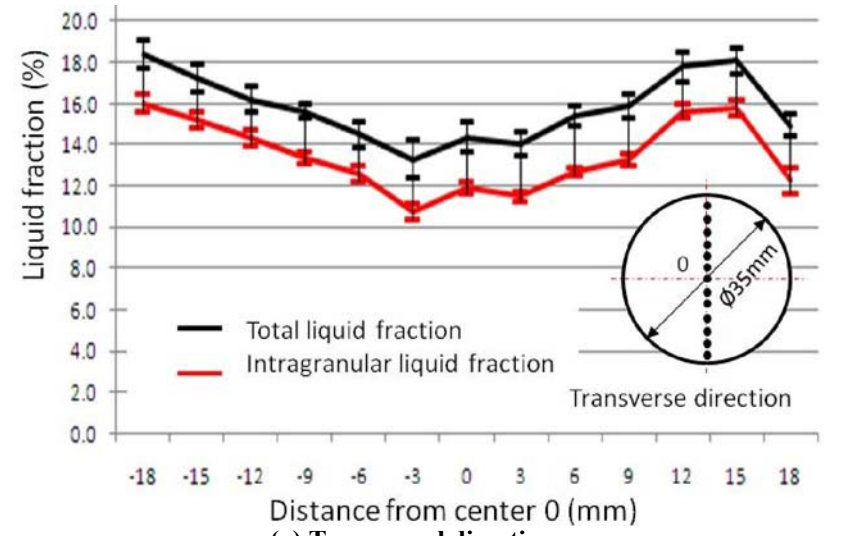

(a) Transversal direction.

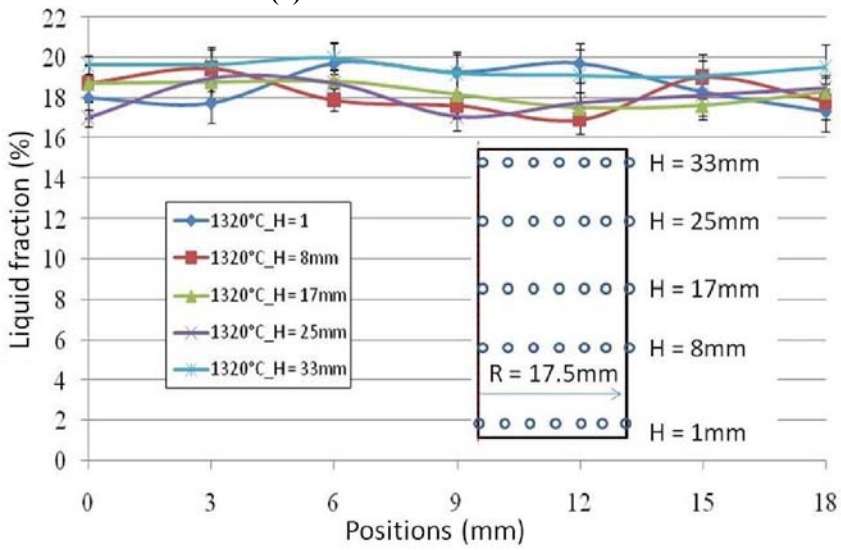

(b) Longitudinal direction.

Fig. 3.16. Variation of the liquid fraction at different positions on (a) cross sectional and (b) longitudinal directions.

The liquid fraction decreases closer to the center, because a perfect homogeneous temperature field across the billet can not be obtained due to the heating process and the initial microstructure of the material. However, the variation of the liquid fraction measured on the longitudinal direction does not have the same trend as that measured on the transverse section as shown in Fig. 3.16 (b). The liquid fraction on the longitudinal section varies between ~18% - ~ 20%. This is due to a heterogeneous distribution of phases in the longitudinal section. During heating process, the homogenization of the microstructure could not be completed due to short heating time. The entrapped liquid was also observed as shown in the Fig. 3.17; the liquid fraction of the entrapped liquid is around 2.2%.

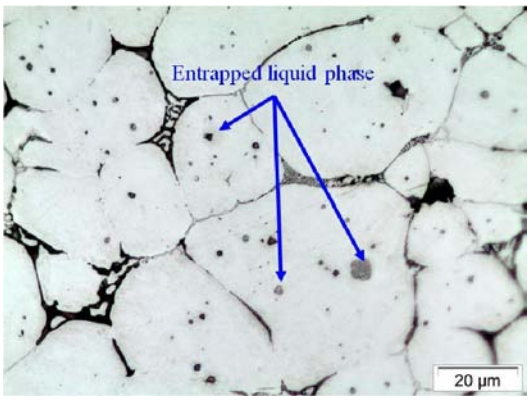

Fig. 3.17. Micrographs of the quenched material.

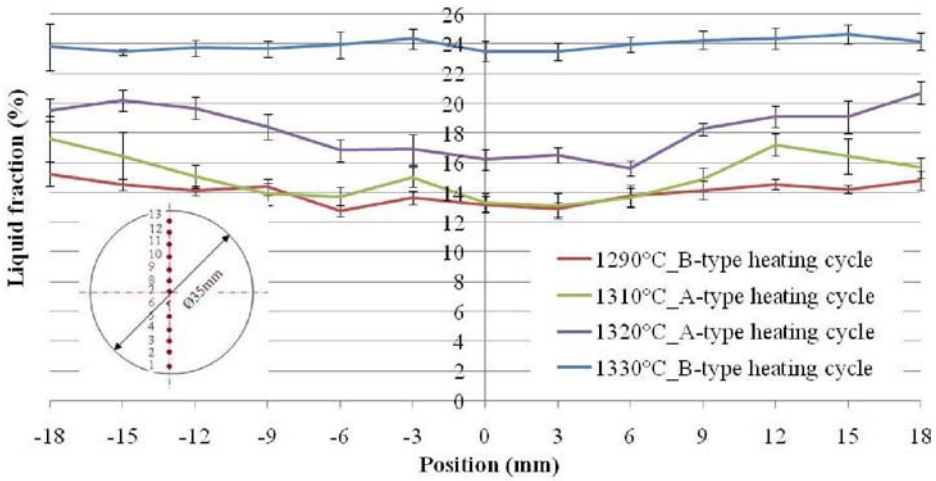

Fig. 3.18. Variation of liquid fraction through the cross section of the billets heated at different temperatures.

Quantitative metallography was used to quantify the distribution of the liquid fraction in the billets heated to various temperatures. The liquid fractions on the transversal sections of

the billets are shown in Fig. 3.18. The liquid fraction increases with increasing temperature. In addition, compared to the variation of the liquid fraction across the billets heated by A-type heating cycle, a more uniform distribution of the liquid fraction across the billets can be obtained with B-type heating cycle.

Grain size vs position.

Fig. 3.19 shows the variation of the mean grain size at different positions.

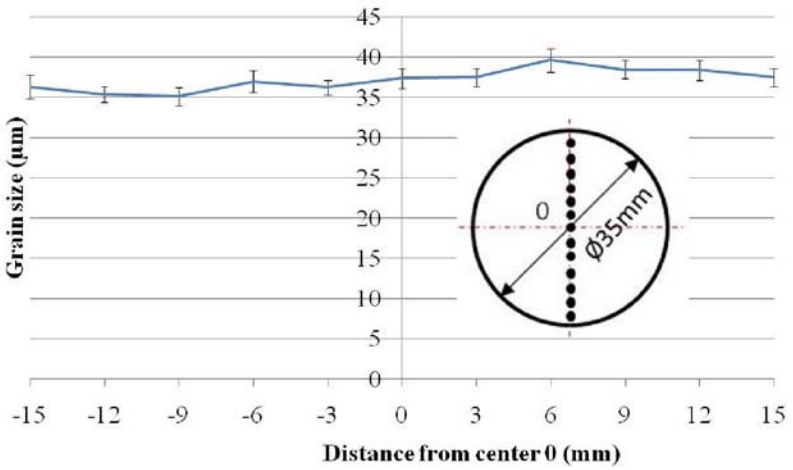

(a) Grain size vs position on transversal section.

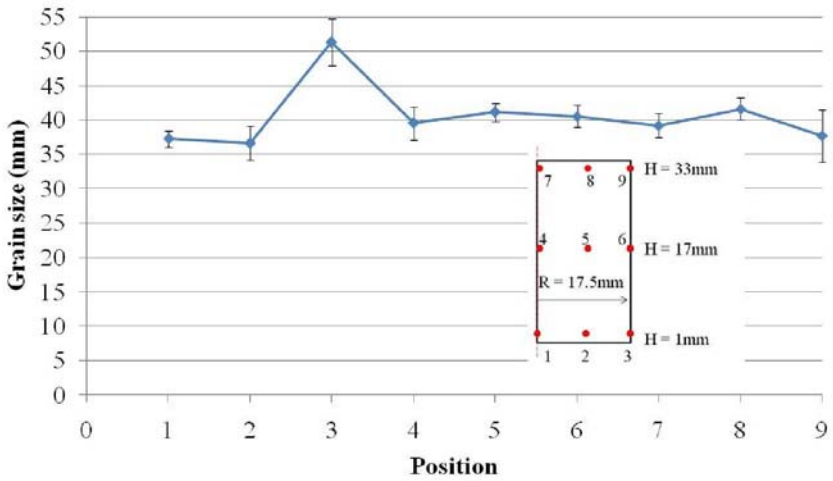

(b) Grain size vs position on longitudinal section.

Fig. 3.19. Variation of the mean grain size at different positions.

The results indicate that the mean grain size has a relative uniform distribution throughout the entire cross section of the billet. Only a slightly bigger mean grain size is observed at the bottom billet surface (point 3 on longitudinal direction); it may be due to the coalescence of the grains caused by the weight effect during heating as shown in Fig. 3.20 which compares

the microstructures at various points. Meanwhile, the billet edge collapsed by the weight effect was observed at high billet temperature as shown in Fig. 3.21.

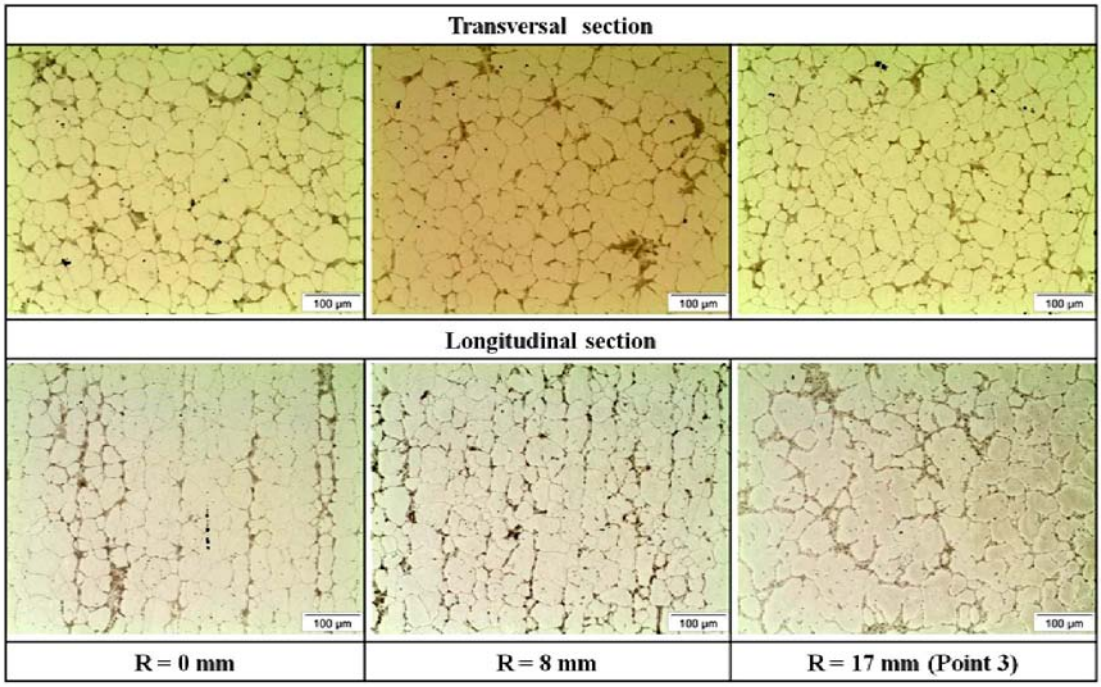

Fig. 3.20. Micrographs at various positions.

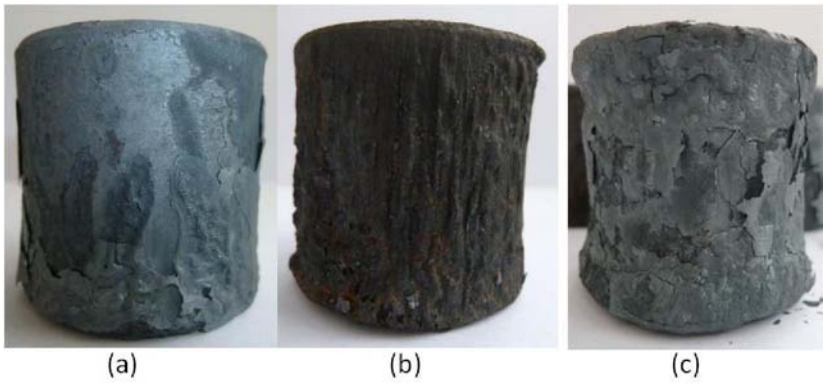

Fig. 3.21. The billet deformation shape according to the billet temperature throughout heating process with M2: (a) 1300°C (~ Fl = 17%), (b) 1320°C (~ Fl = 22%), (c) 1350°C (~ Fl = 28%).

Table 3.4 gives the grain size as a function of temperature. The results show that the mean grain size does not vary a lot at various billet temperature heated by the same type heating cycle. In addition, the mean grain size heated by B-type heating cycle is smaller than the one heated by A-type heating cycle, because the heating time of A-type heating cycle from the room temperature to the solidus temperature is longer as compared to that heated by B-type heating cycle. At the solid state, the grain grows with heating time and temperature. However,

the grain size is relatively small (< 50µm). This is thought to result from the carbide pinning of grain boundaries. As shown in Fig. 3.15, a large amount of undissolved fine carbides are distributed in the material prior to the heating process. These carbides have an effect on the grain growth [8-10]. The vanadium-rich carbides have a strong pinning effect on grain growth; the tungsten-molybdenum-rich carbides also restrict the grain growth during heating.

Table. 3.4. Mean grain size at various billet temperatures.

Grain size				
Temperature	A-type heating cycle	Heating time	B-type heating cycle	Heating time
1290°C	39.5 ± 2.4 µm	182 s	30.1 ± 1.1 µm	194 s
1310°C	41.6 ± 1.6µm	189 s	32.6 ± 1.5µm	228 s
1320°C	41.4 ± 1µm	245 s	31.6 ± 1µm	185 s
1330°C	40.4 ± 0.8µm	252 s	32.4 ±1.4µm	193 s

Shape factor vs position.

The shape factor is always characterized in 2D view. Considering the manufacturing process of the M2 steel, it is interesting to know the shape factor measured in both longitudinal and transversal sections.

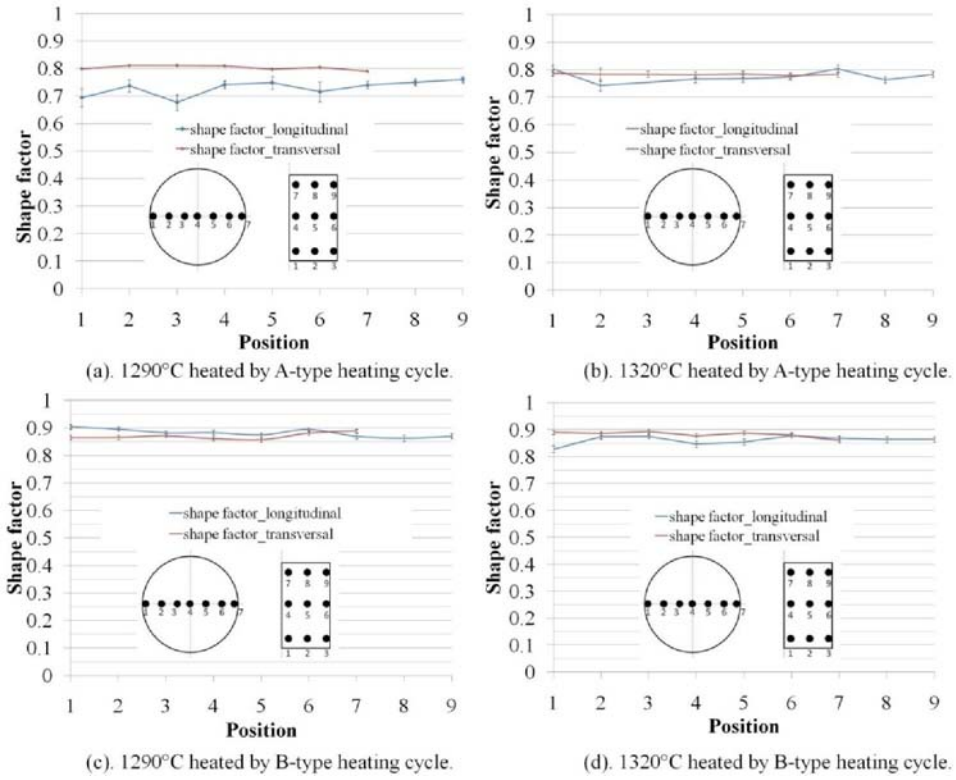

Fig. 3.22. The variation of shape factor in the billets at different temperatures heated by different heating cycles.

Fig. 3.22 illustrates the variation of shape factor in the billets at different temperatures heated by various heating cycles. From the curves, it can be concluded that in a billet the shape factor at various positions is relative uniform. When comparing the shape factor of different billets at different temperatures heated by the same heating cycle (for example, Fig. 3.22 (a) and Fig. 3.22 (b)), the value changes a little which means that the temperature does not have a big effect on the shape factor. When comparing Fig. 3.22 (a) and (c) or Fig. 3.22 (b) and (d), the value of shape factor is increased from ~0.8 to ~0.9 using B-type heating cycle. From these results, it can be recognized that the heating time is probably the essential parameter influencing the shape factor. The frequency distribution of shape factor at different temperatures heated by various heating cycles is then illustrated in the Fig. 3.23. The higher value of shape factor indicates probably higher thixoformability.

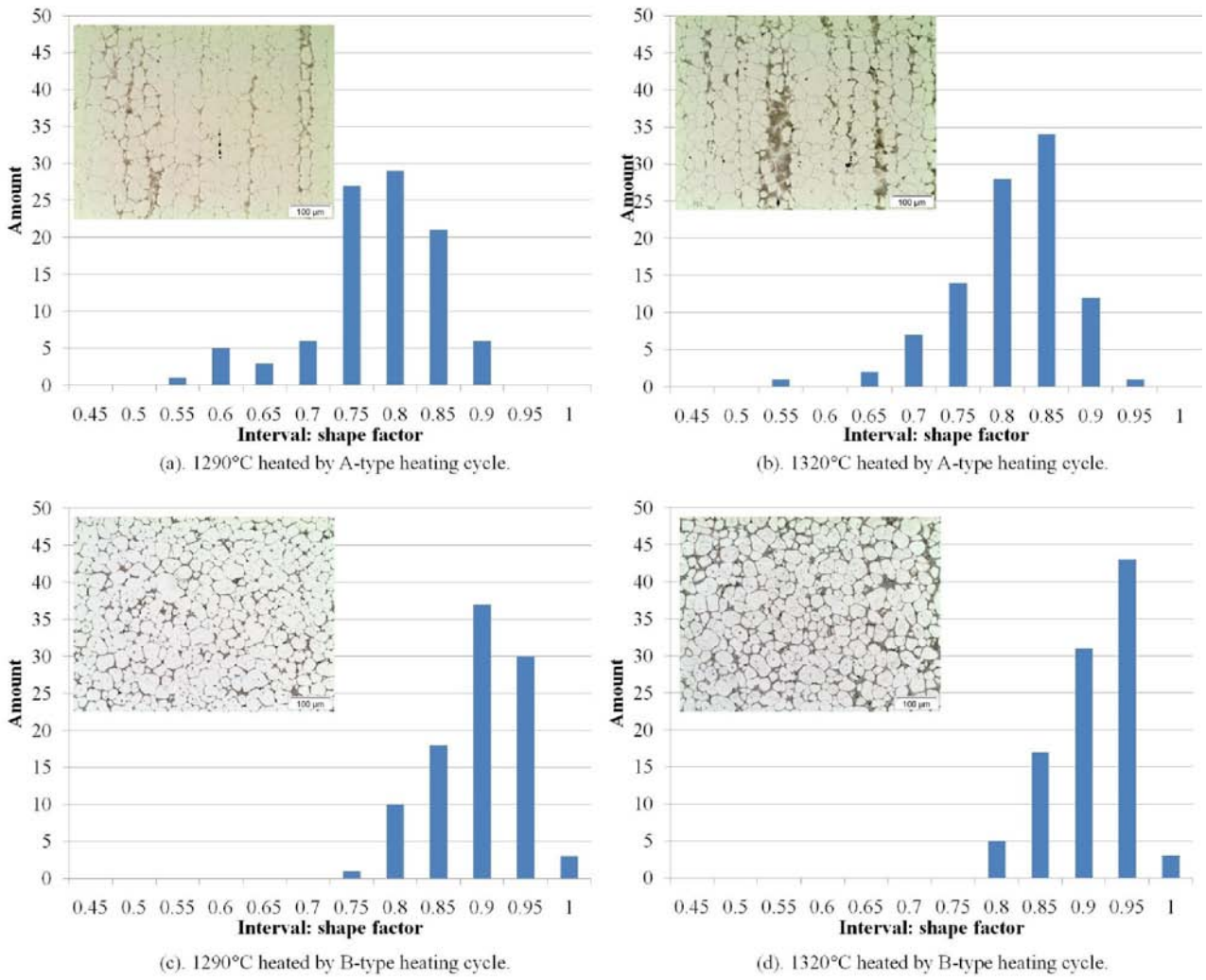

Fig. 3.23. The typical profiles of frequency distribution of the shape factor at various temperatures heated by different heating cycles.

4.4. Microstructure characterization on C38LTT and 100Cr6

The microstructures of C38LTT and of 100Cr6 in the semi-solid state were also studied on quenched billets. However, due to the inefficiency cooling rate, the liquid phase in the semi-solid state was not preserved. During cooling stage, a liquid to solid transformation occurred.

4.5. Summary

Typically, induction heating is used in the thixoforming process due to its advantages: it allows fast heating and process controlling. However, due to the skin effect, it is necessary to design a suitable heating cycle in order to reach the requirements of thixoforming process such as less heating time, homogeneous temperature distribution in the billet and the repeatability of the heating process to the desired temperature. In the study, two types of heating cycles were studied which meet the requirements of the thixoforging process. By studying the microstructure obtained by the two types of heating cycle, it suggests that with a higher power for rapid heating until the appearance of liquid phase, the microstructure more suitable for thixoforging process can be obtained. Consequently, with a lower power, the homogeneity of the temperature distribution will increase the shape factor and lead to a homogeneous microstructure of the billet.

As compared to other methods such as DSC, thermodata, image analysis offers significant advantages, as it can not only study the volume fraction of liquid, but also characterize the microstructure in the semi-solid state such as grain size and shape factor. However, the microstructure at a low liquid fraction for several steel alloys was impossible to characterize using image analysis. This may be attributed to an insufficient cooling rate.

The characterization of microstructure was performed on 2D metallographic sections obtained after quenching from the semi-solid state. However, the method only gives information on surface values; 3D information will give better understanding of the microstructure evolution.

5. Evaluation of liquid fraction by X-ray microtomography

This part will focus on the 3D characterization of the microstructure of M2 steel grade in the as-received and semi-solid state.

5.1. As-received state

High energy X-ray microtomography experiments were carried out on as-received samples. Thanks to the high content of heavy alloying elements, especially W and Mo, a good contrast between the matrix and carbides could be obtained. Fig. 3.24 shows two tomographic slices and a reconstructed stack of a cylindrical sample of as-received M2 steel. The carbide particles are present as white zones in all images; they are relatively small (a few micrometers) and are observed to be either isolated or distributed in bands. This is in good agreement with the SEM - EDS observations (Fig 3.12 (a), (b), (c) and Fig. 3.13 (a)).

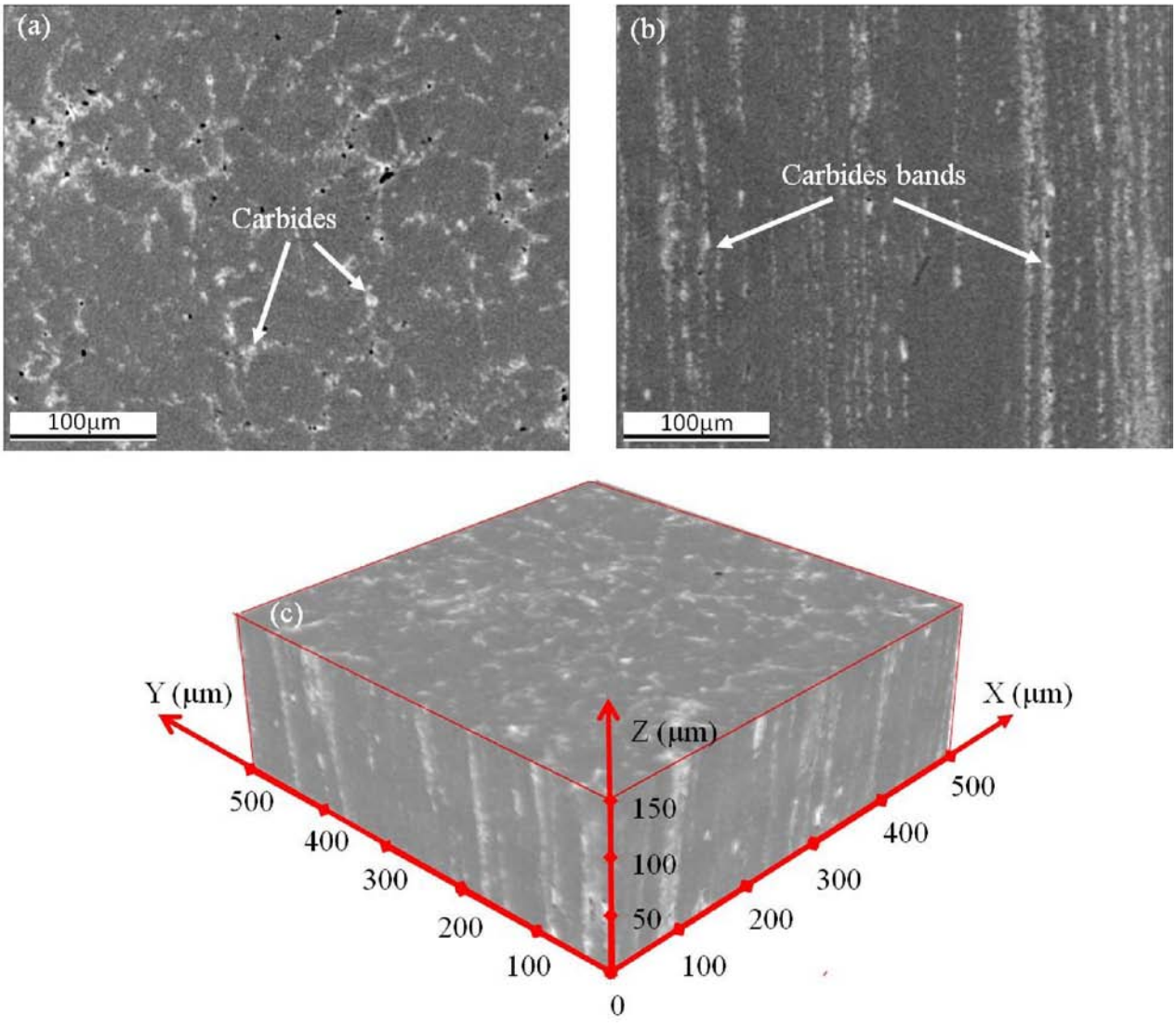

Fig. 3.24. X-ray microtomographic results of as-received M2 steel. Carbides are shown as white zones in (a) transversal section, (b) longitudinal section and (c) reconstructed 3-D stack.

5.2. Microstructure of M2 quenched from the semi-solid state

In order to study the microstructure evolution, the M2 slug was partially induction heated to the semi-solid state by a direct remelting route. Due to the skin effect, the temperature field was not uniform in the slug, meaning that some zones were in the semi-solid state at high temperature while others remained totally solid, similar to the as-received state as shown in Fig. 3.25. During heating, the temperature was measured by a pyrometer. After heating for 120s, the temperature at point C reached ~1250°C and the slug was directly quenched in the water in order to preserve the former structure in the semi-solid state. The cylindrical samples with a diameter of 1.2mm were electrodischarge-machined from the quenched slug in different directions for the X-ray microtomography experiments.

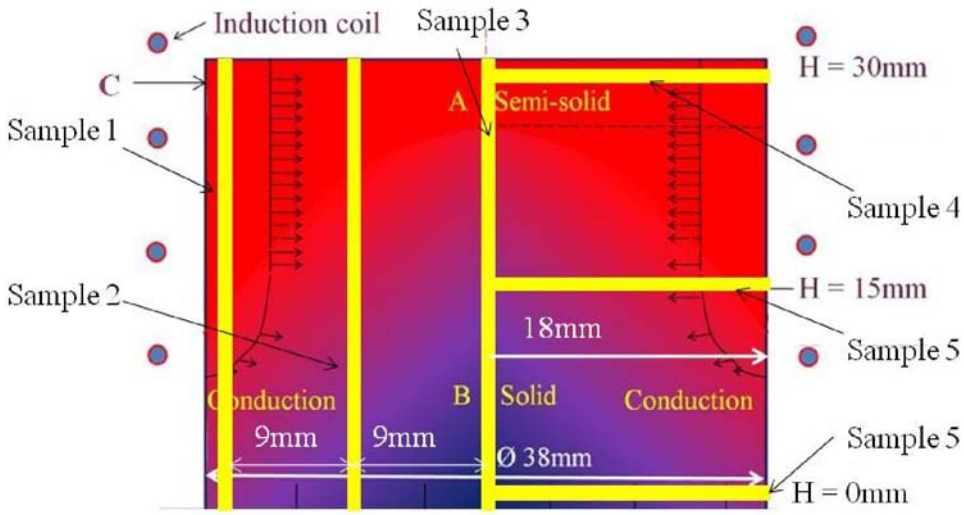

Fig. 3.25. Schematic view of temperature distribution during induction heating.

X-ray microtomography images were successively recorded in parallel after quenching at room temperature.

Two reconstructed slices representing the transverse and longitudinal sections of the partial remelted sample are presented in Fig. 3.26 (a) and (b), respectively. Compared to the SEM micrographs, the similarities of the structures are clear.

It is well observed that the material evolves dramically during partial remelting. The morphology of these reformed carbides is different in both dimensions and localization. During induction heating, as the temperature rises, alloying elements, such as vanadium, tungsten and molybdenum among others, diffuse to the liquid zones where the solubility is

higher. These liquid zones, preferably developing from the grain boundaries, appear very clearly after quenching because of their high content of alloying elements. They form new interconnected carbide networks that make the definition of the new grain size obvious.

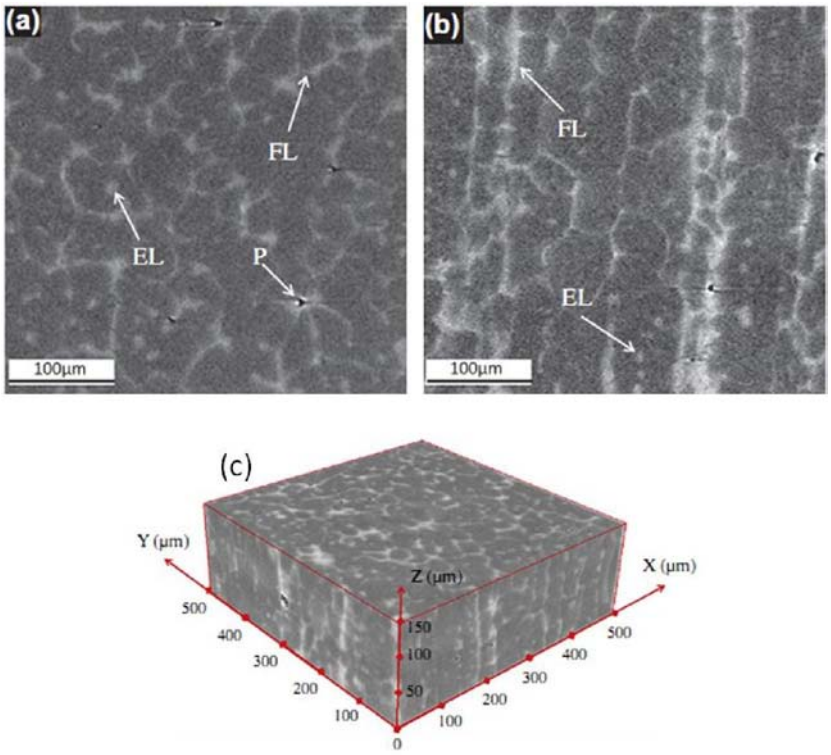

Fig. 3.26. Reconstructions of partial remelted and quenched sample. (a) Transverse. (b) Longitudinal sections. (c) 3D reconstructed stack. FL: former liquid phase; EL: entrapped liquid; P: porosity.

Table. 3.5 compares the SEM micrographs and X-ray microtomography slices. Figures marked with 'S' are SEM micrographs while the ones marked with 'T' come from X-ray microtomography images. As the agreement between 2D SEM observations and X-ray microtomography results is good, the real volume fraction of liquid can be obtained by the image analyses on reconstructed stacks.

With the image processing software ImageJ, the total volume fraction of carbides as a function of height and diameter of samples taken from the quenched slug are shown in Fig. 3.27. First, it can be seen that the fraction of carbides increases with height and radius, Fig. 3.27-a and Fig. 3.27-b, but at different rates. As illustrated in Fig.3.27-a, for sample 1, this fraction remains stable from the bottom up to the height of 12mm, around 11±1%. Then, it grows rapidly from 11±1% to 15±1% from 12mm to 17mm in height, and seems to remain constant until 24mm in height. Finally, it increases until the value of 21±1%. The evolution of

carbide fraction in sample 2 and in sample 3 is quite similar to that of sample 1, but with a discrepancy of about 10mm and 14mm in height, respectively. The expected bell-shaped profile is here confirmed. Moreover, at the same height (> 23mm), the fractions of carbides in sample 3 are smaller than those in sample 2 by 2%. In Fig.3.27-b, the fraction in sample 4 increases with radius, while the one of sample 6 remains relatively constant. For sample 5, it increases to 14±1% after maintaining at 11±1% from the core until the radius of 11mm. In addition, for the same radius, the fraction of carbides increases with height in these 3 samples.

Table. 3.5. SEM micrographs and X-ray microtomography slices.

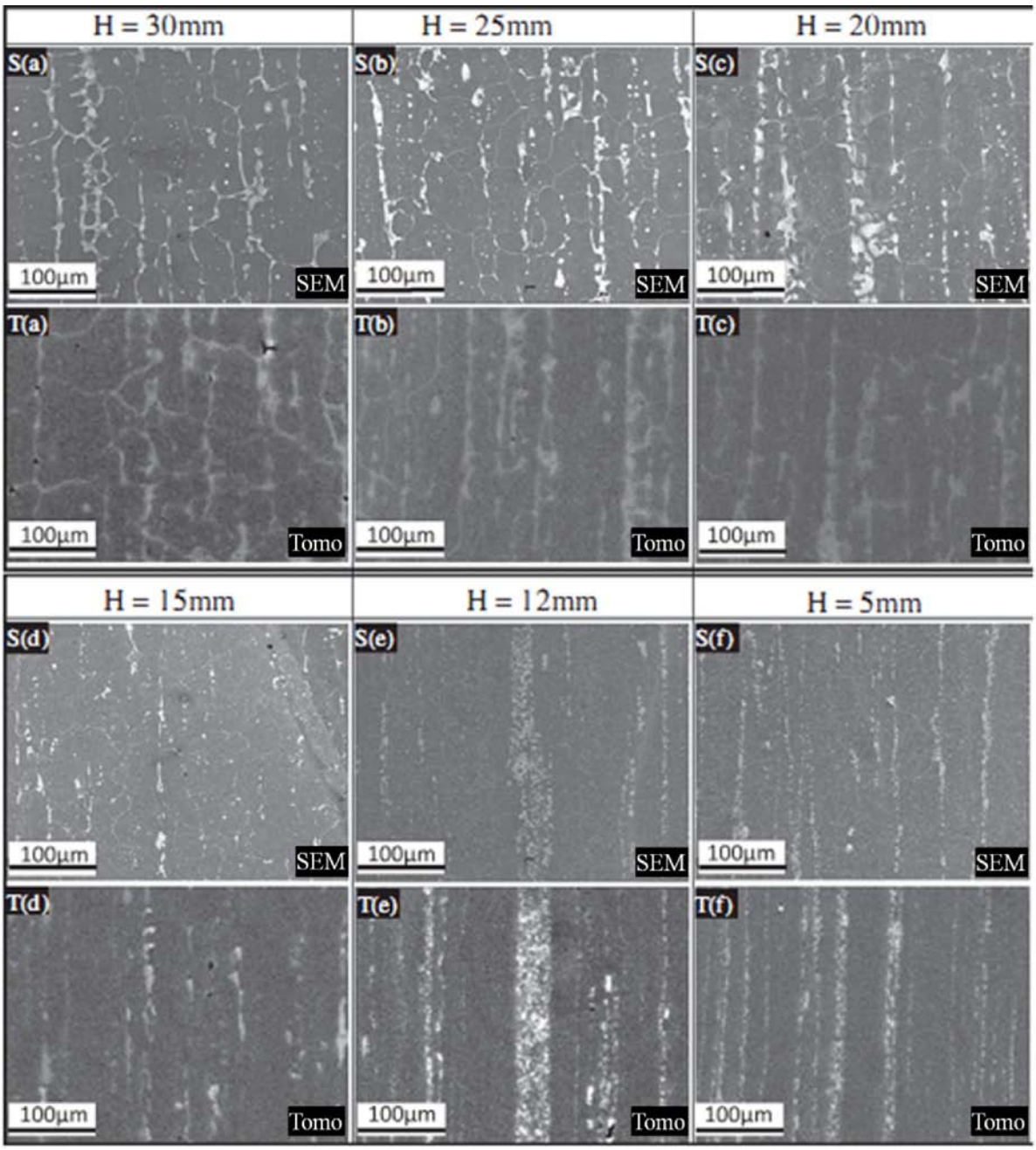

Furthermore, as illustrated in Fig. 3.27-a, the zones with a fraction of carbides of 11±1% in sample 1, 2 and 3 exhibit the kind of carbides seen in Fig. 3.12 (c), while the ones with a fraction of carbides more than 13±1% show the newly formed carbides during quenching from liquid state as presented in Fig. 3.12 (f). Finally, initial carbides and new ones coexist in the zones with a fraction of carbides between 11±1% and 13±1%.

With increasing temperature, most of the original carbides particles are dissolved and the alloying elements in carbides along the microsegregation bands start diffusing to the liquid zones; new carbides are being created at the grain boundaries after quenching, as illustrated by the microstructure at the height of 15mm. At the same time, the grains are growing. Then, higher in the sample, for instance at the height of 20mm, the process is enhanced with the development of still larger interconnected liquid zones and grains. Finally, at the height of 25mm and 30mm, the original carbides are completely dissolved, with the diffusion of the alloying elements to the liquid zones, forming very large new carbides after quenching because the fraction of liquid is about 21%. Small carbides can also be present inside the grains, corresponding to the entrapped liquid zones at high temperature which represent around 7% of total liquid, using image analysis. In addition, the SEM micrographs and X-ray microtomography results are in quite good agreement, when taking into account the resolution of the two techniques.

For the same position, fractions of carbides of different samples are compared in Table 3.5. By comparing these values, the axisymmerical temperature field in the heated bar is confirmed.

During heating, the typical bell-shaped temperature profile marks the boundary between the semi-solid zone and pure solid zone; the initial carbides are shown in solid zone with a fraction of 11±1%. When they reach the solidus temperature, alloying elements in the original carbide MC first diffuse into the liquid zone and form large new carbides when quenched as presented in Fig. 3.28: microstructure of sample 1 at the height of 14mm. With increasing temperature above the melting point of M_6C, all original carbides at the grain boundary are dissolved and new carbides are created during the following quenching process as shown in Table 3.5-S(d). As the temperature increases with height, the diffusion process is enhanced with the development of interconnected liquid zones in higher positions. Small carbides are also observed inside the grains, corresponding to the entrapped liquid zones at high temperature. This is due to the high heating speed and the short holding time that prevent all

the alloying elements from diffusing completely to the liquid zones. Here, due to the resolution of X-ray tomography, few carbides allocated in grains are detected when comparing the images presented in Table 3.5 obtained by two techniques. Thus, based on the X-ray microtomography results, the fraction of carbides of 13±1% is considered to be the real liquid fraction.

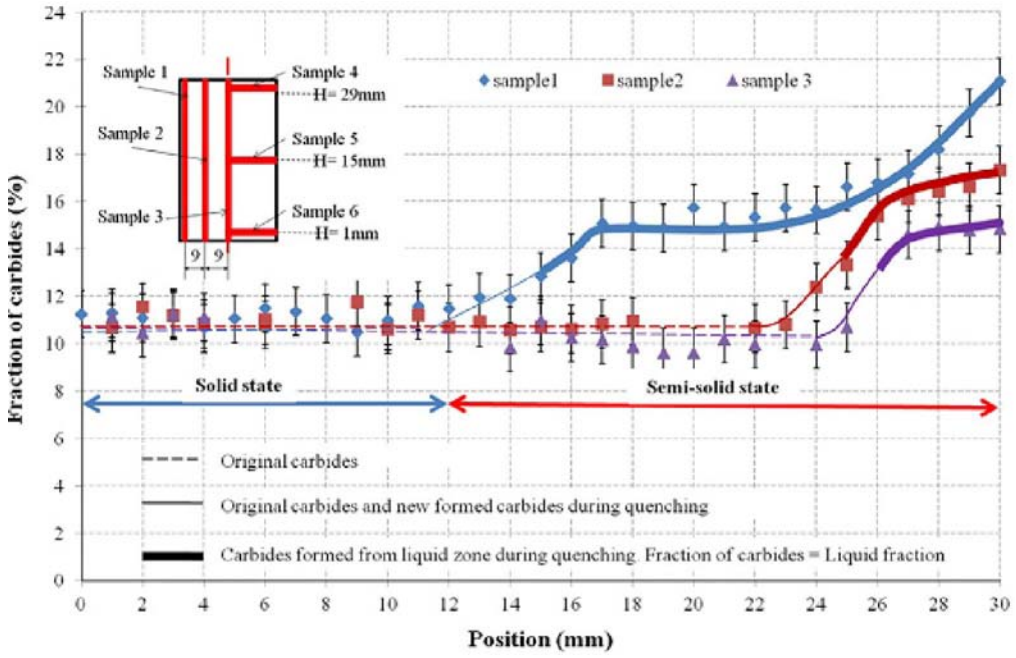

(a) Axial direction.

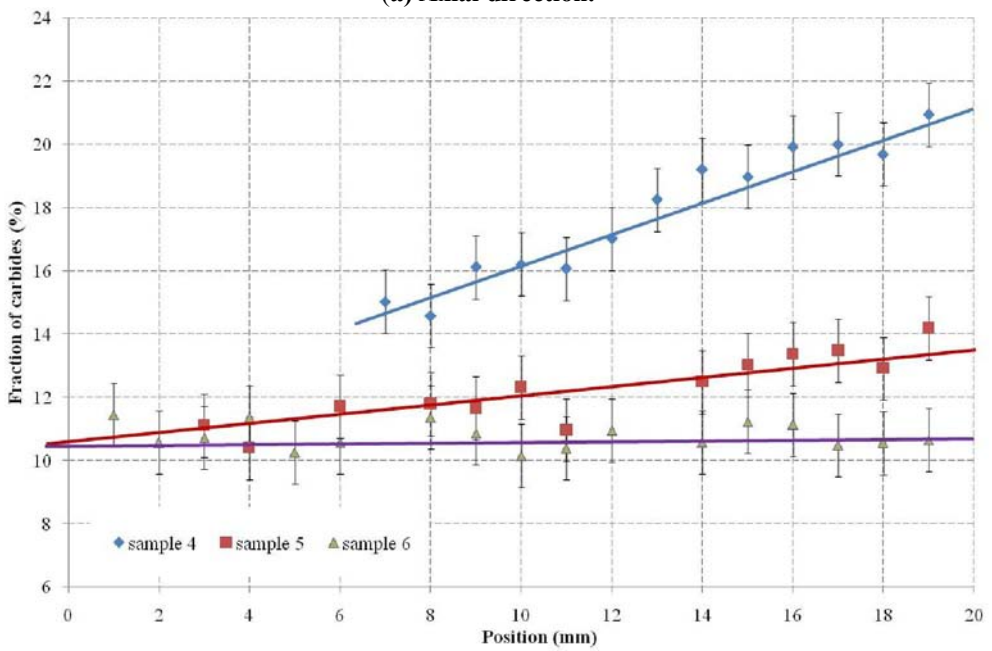

(b) Radial direction.

Fig. 3.27. Volume fraction of liquid as a function of the height of partial remelted and quenched M2 steel.

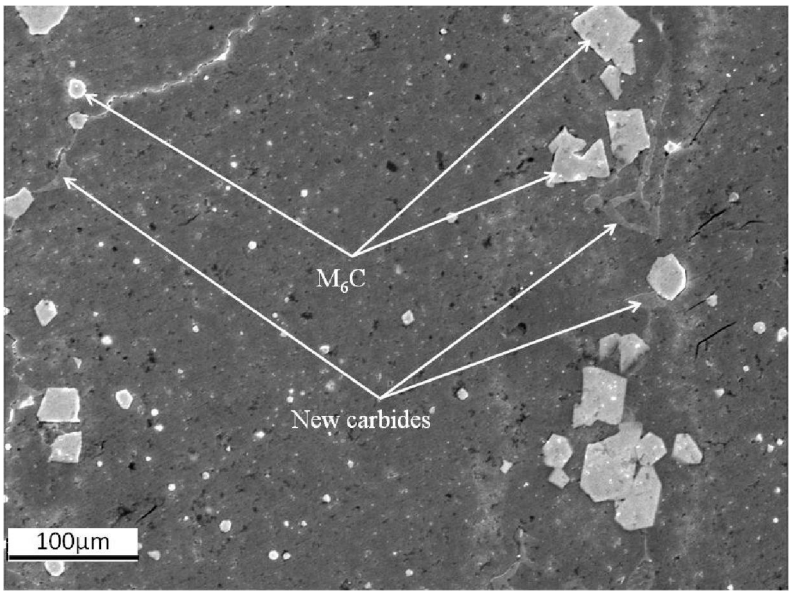

Fig. 3.28. Microstructure of sample 1 at the height of 14 mm.

Since sample 6 was taken from solid zone, the fraction of carbides is relatively constant which means that the distribution of original carbides is homogeneous. Indeed, the temperature distribution in the radial direction is similar to that in the axial direction: temperature increases with increasing radius, the evolution of microstructure in the radial direction is similar to that in the axial direction. Fractions of carbides of sample 4 and 5 in semi-solid zone increase with the radius, with higher values on the surface than in the core of the slug. Meanwhile, temperature is also height-dependent: the higher the position, the higher the temperature. For the same position, fractions of carbides of different samples are compared in table 3.6. By comparing these values, the axisymmetrical temperature field in the heated bar is confirmed.

Table. 3.6. Fractions of carbides in various positions.

Fractions of carbides in various positions.

Height (mm)	Radius (mm)	Fraction of carbides (%)					
		Sample 1	Sample 2	Sample 3	Sample 4	Sample 5	Sample 6
29	18	19.7			19.6		
29	9		16.62		16.11		
15	18	12.83				12.90	
15	9		10.97			11.66	
15	1			10.89		10.45	
1	18	11.3					10.56
1	9		11.54				10.94
1	1			11.11			10.64

When comparing the grain size at various heights, it is noted that the grains stop growing when large connected liquid bands are formed, which may be related to the carbide pinning of grain boundaries[8]. There is a significant grain growth during reheating when comparing the grain size of as-received state and of quenched from semi-solid state. In general, the grain grows with increasing temperature and holding time. It is important to study the grain growth during reheating, as large grains cannot flow into thin sections as easily as those of a finer size. Furthermore, the mechanical properties of the part will be weakened if the grain size is larger. One explanation for the grain growth was proposed by Omar et al[7]: the grain growth and diffusion process are thermally activated. They are also related to the liquid fraction, because liquid provides a much faster diffusion path than solid, and once a continuous liquid path is present around the solid phase, coarsening can accelerate which results in the grain growth. In addition, grain coalescence is also thought to be an important factor to the grain growth as stated by Tzimas and Zavaliangos[6].

Comparison with 2D image analysis

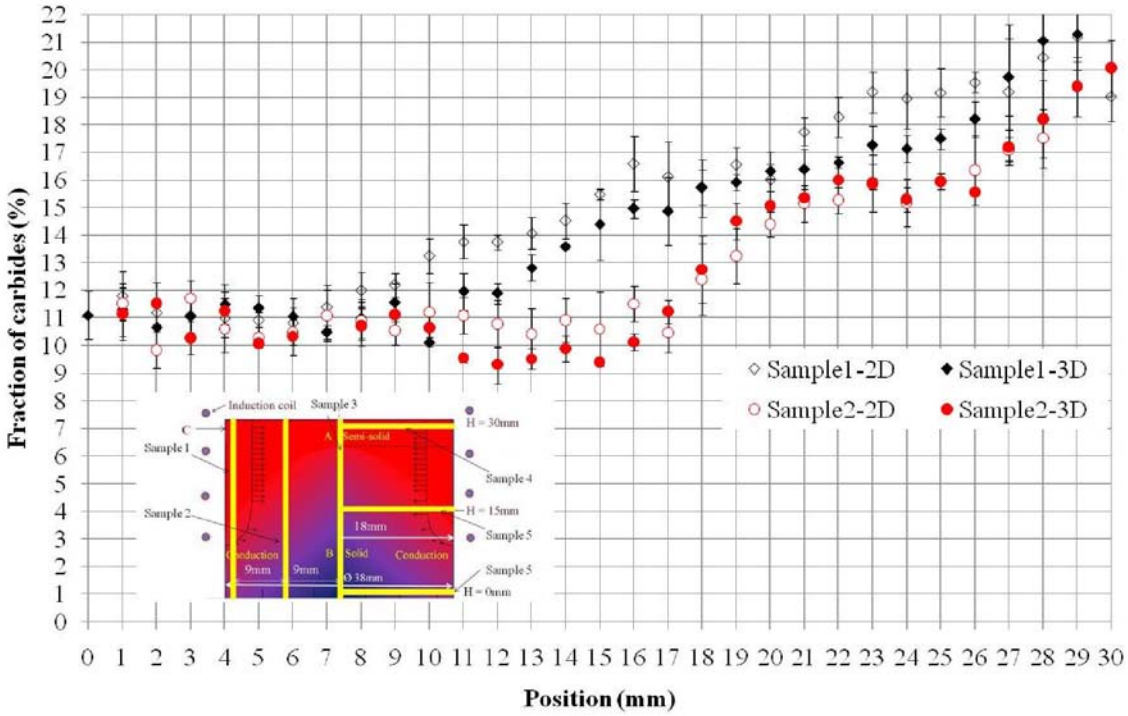

Fig. 3.29. Comparison of carbides fraction in 2D and 3D.

The fraction of carbides measured in 2D and 3D were compared in Fig. 3.29. It can be seen from the figure that the variations measured in 2D and 3D are similar. But to the high

energy X-ray microtomography has been proven to be a powerful tool, it is not easy to access to this technique. As the 2D image analysis is much utilized and applied in laboratories and industries, it can be more used for the liquid fraction evaluation.

5.3. X-ray tomography on other steel grades

The X-ray microtomography experiments were also performed on 100Cr6 and C38LTT. Due to less chemical elements in these grades, the liquid fraction in the semi-solid state was not detected by X-ray tomography.

5.4. Summary

After being induction-heated and water-quenched, the microstructure evolution of the M2 steel was monitored and examined with various 2D and 3D techniques. The good agreement between 2D SEM-EDS microstructures and 3D X-ray microtomography results proves that both kinds of techniques are just as efficient in characterizing high-alloyed steels in the semi-solid state. Considering the good agreement between 2D and 3D results and the difficulty in access to the X-ray microtomography, the 2D microstructure characterization method can be applied for industrial characterization of microstructure. As the X-ray microtomgraphy is a non-destructive technique, it can be used for studying the evolution of microstructure by performing in situ experiments directly at high temperature. However, the X-ray microtomography has its limitation as the technique is element-dependent which makes this technique limited only to some high alloyed steels. In order to study the distribution of liquid phase during heating two other steel grades for which the 2D and 3D techniques can not be used, in situ observation was carried out using a CLSM system in Louvain, Belgium.

6. In situ observation on M2, 100Cr6 and C38LTT

6.1. Heating cycles for the grades

The heating rate used for the in situ microstructure observation was 200°C/min (see chapter 2 Fig. 2.30) which is lower than the heating rate of industrial thixoforging process. However, it allows observing the microstructure directly at high temperature using a CSLM. This technique can avoid the effect of the cooling rate on the microstructure evolution or phase transformation.

6.2. Microstructure evolution of M2

In situ CLSM snapshots were taken at different temperatures in the attempted heating cycles. Prior to perform the rapid heating at 200°C/min, the specimen surface was etched in order to reveal the microstructure, define the observation field and determine the optimized magnification.

The specimen surface reveals the microstructure in the solid state (Fig. 3.30-a), showing the grain boundaries and a distribution of particles. These particles were identified as carbides due to their morphology, location at the grain boundaries and distribution. With increasing temperature, the carbides diffuse to the matrix prior to the appearance of the liquid phase (Fig. 3.30-b). Then, the liquid phase started bulging out of the grain boundaries and the retained carbides particles were also observed (Fig. 3.30-c). With increasing temperature, the liquid phase started to form interconnected networks of equiaxed cells (Fig. 3.30-d). Comparing Fig. 3.30-a and Fig. 3.30-d, it was found that the heating process led to a significantly grain growth, between 20µm-60µm, compared to that in the initial conditions (~10µm).

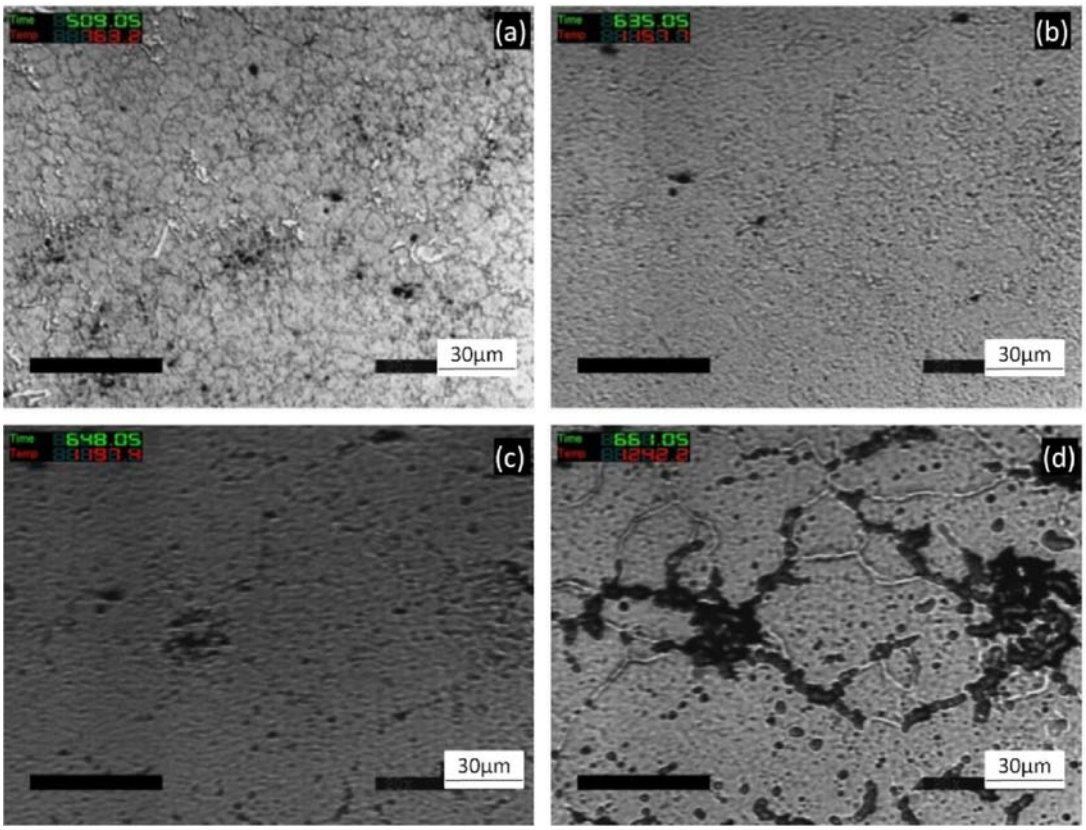

Fig. 3.30. CLSM snapshots for the sequence of melting during heating at 200°C/min to the temperature of 1250°C. Microstructure evolution of M2 during heating to the semi-solid state.

During cooling from 1250°C to room temperature at the cooling rate of 200°C/min, the liquid networks were preserved and transformed to new carbides (black zones), as shown in Fig. 3.31. The phase transformations were also directly observed (Fig. 3.31-c, and -d).

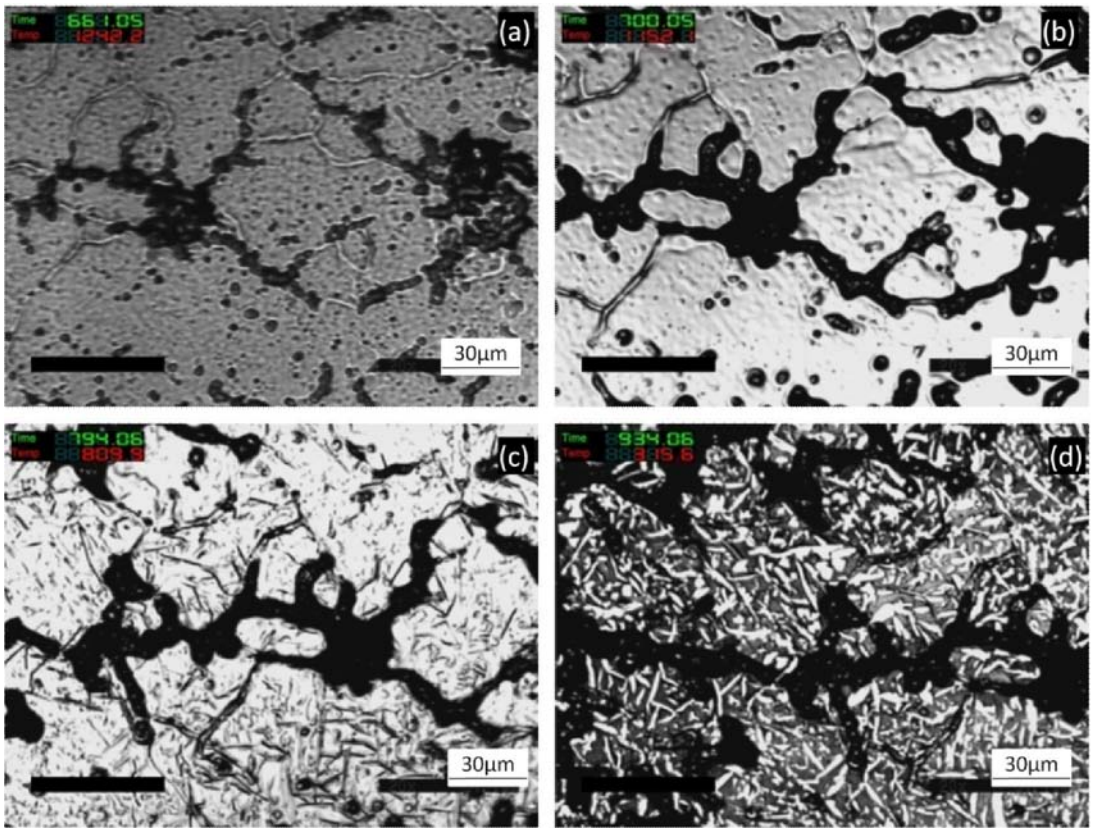

Fig. 3.31. CLSM snapshots for the sequence of solidifying during cooling at 200°C/min to the room temperature.

In this investigation, it can be found that the former liquid zones were preserved even at a lower cooling rate. This verified the previous results of 2D image analysis and 3D X-ray microtomography on M2 steel. The diffusion of alloying elements during cooling is not visible.

The evolution of isothermal heating was not studied for the reason that the oxidation may occur during the observation. In the semi-solid state, the grains stop growing due to the pinning effect. A spheroidization may occur during isothermal heating which makes the grains more spherical.

6.3. Microstructure evolution of 100Cr6

The in situ experiments were also carried out on 100Cr6, aiming at studying the microstructure evolution during heating from the solid state to the semi-solid state, the distribution of liquid etc.

The microstructure of 100Cr6 in the solid state was not clearly revealed, as shown in Fig.3.32 (a): the pearlite and grain boundaries which have been observed using SEM could not be determined using CSLM.

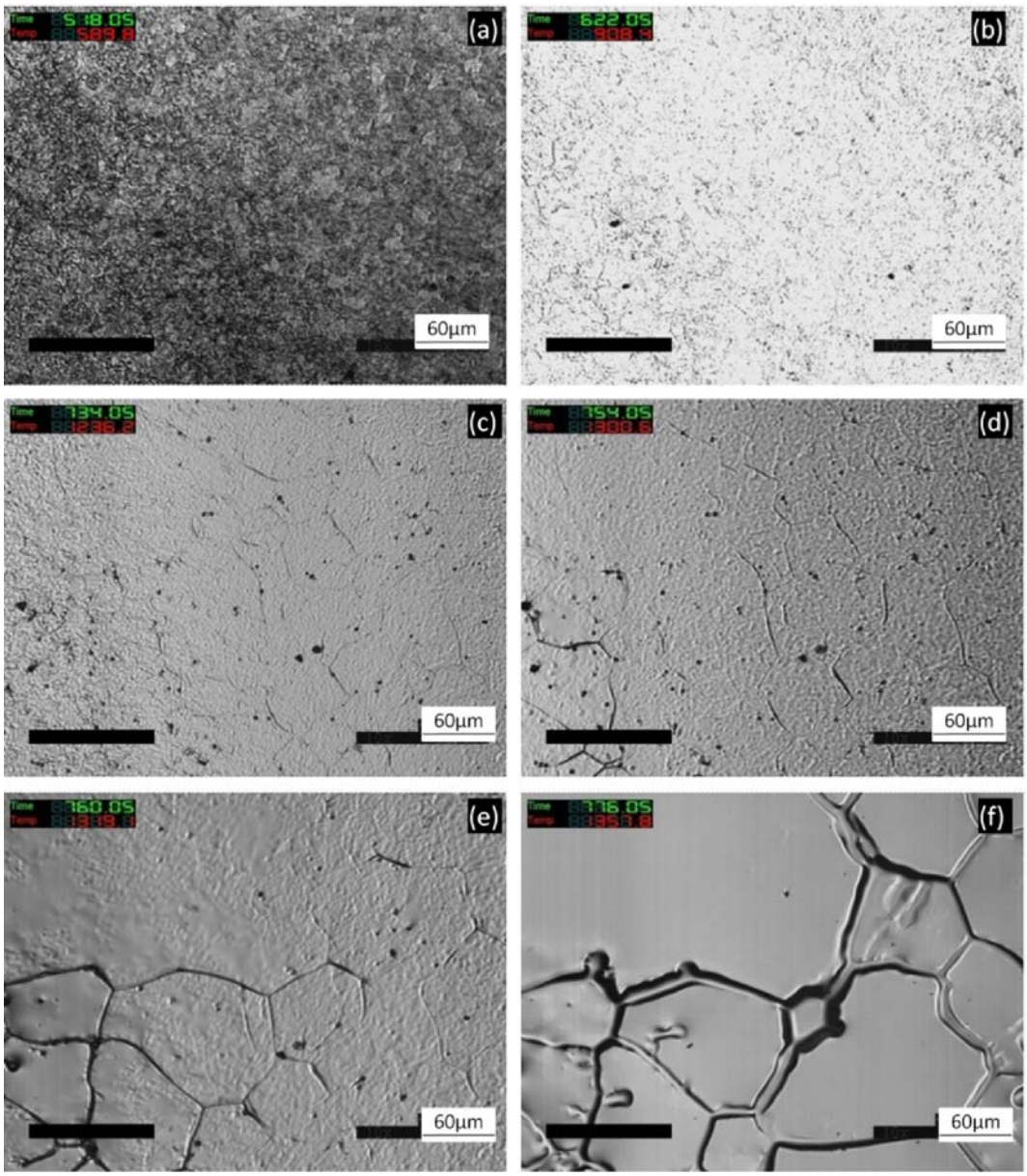

Fig. 3.32. CLSM snapshots of 100Cr6 for the sequence of solidifying during cooling at 200°C/min to the room temperature.

With increasing temperature, the pearlite to austenite phase transformation occurred (Fig. 3.32 (b)). At higher temperature, big austenite grains and grain boundaries were clearly revealed as well as the retained inclusions (Fig. 3.32 (c)). When the temperature of the sample reaches the liquidus temperature, the liquid phase started to form from the grain boundaries (Fig. 3.32 (d)). However, the liquid films were not observed in all grain boundaries owing to the heterogeneity of the alloying distribution or the nonuniform temperature distribution throughout the sample (Fig. 3.32 (e)). With increasing temperature, the quantity of liquid phase increased. As a result, extra liquid phase bulged out of the grain boundaries and covered the surface of the sample (Fig. 3.32 (f)). The flatness of the sample surface could also lead to this phenomenon. During heating, the liquid content increased a lot in a very short time, Fig. 3.32 (d) (e) and (f). This means that during reheating stage of thixoforging process, the temperature of the billet and heating time should be precisely controlled. The austenite grain size in the semi-solid state is much bigger than that of M2 steel grade.

The same samples were also investigated post mortem, after cooling. Fig. 3. 33 presents the micrographs of the surface before and after etching. The oxidation of the sample surface is observed, as shown in Fig. 3.33 (a). The boundaries shown in Fig. 3.33 (a) may be related to the austenite grain boundaries, since they are deeper than the surface in the semi-solid state, as illustrated in Fig. 3.32 (f). After etching, some pearlite is observed in the sample; the primary austenite grain boundaries could not be revealed using Béchet-Beaujard etchant. Thereby, with such a cooling rate, it is difficult to find a correlation between the final microstructure at room temperature and that in the semi-solid state.

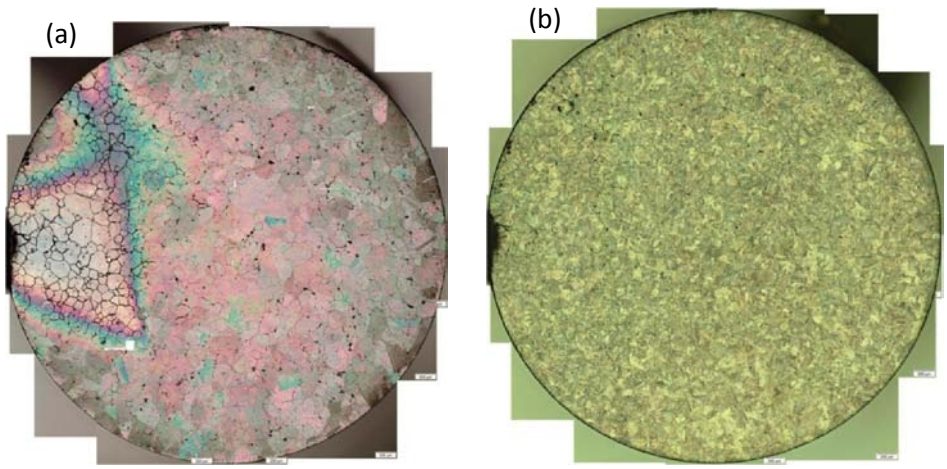

Fig. 3.33. Micrographs of in situ tested samples. (a) Without etching. (b) Etched with Nital (2%).

6.4. Microstructure evolution of C38LTT

During heating the specimen from room temperature to the austenization temperature, the microstructure of C38LTT, first consists in ferrite, pearlite and non-metallic inclusions (MnS which is identified by EDS) as shown in Fig. 3.34-a and -b. The color of the different phases is different in comparison with SEM images; in CSLM images, ferrite is white and pearlite is black.

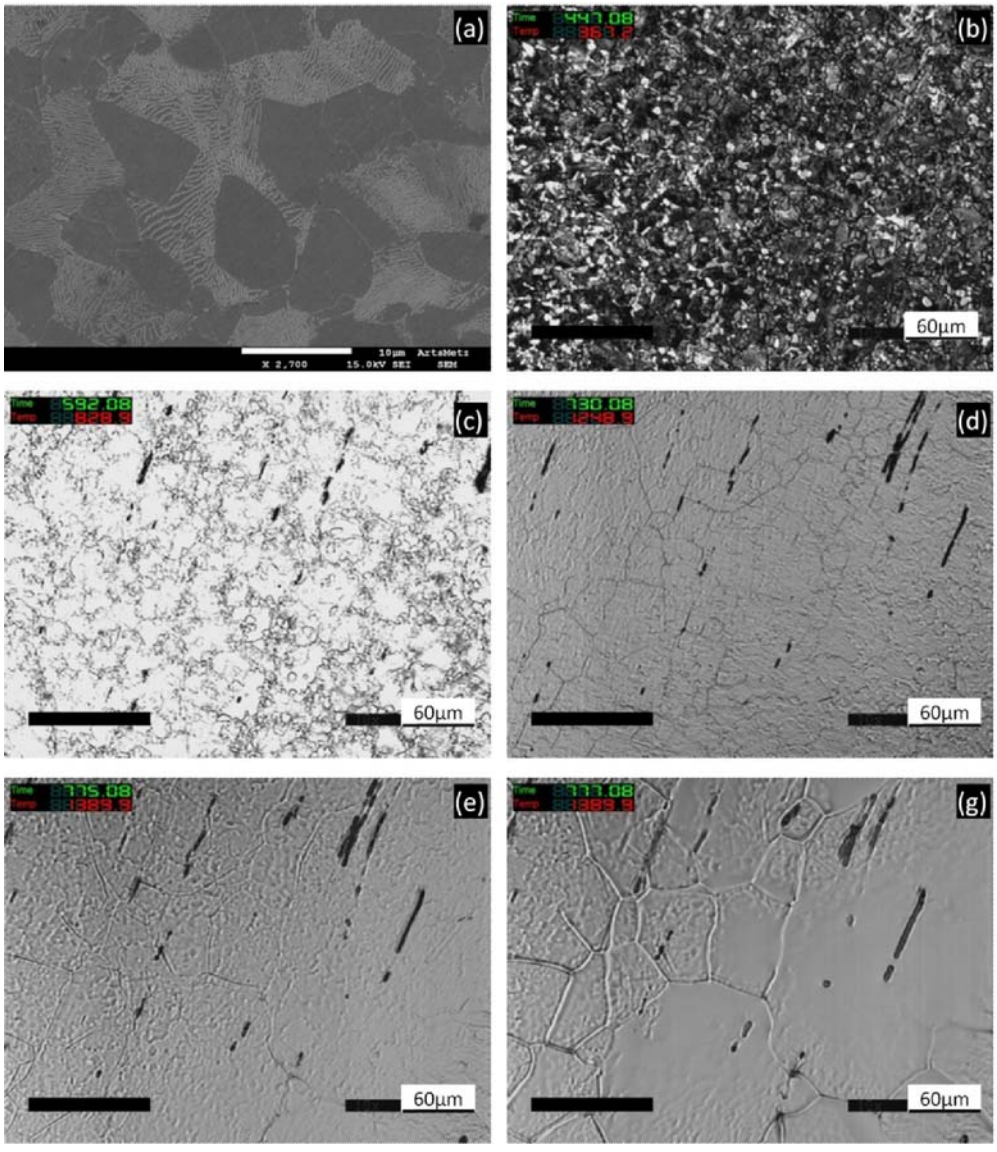

Fig. 3.34. CLSM snapshots of C38LTT for the sequence of solidifying during cooling at 200°C/min to the room temperature.

Then, when the austenization temperature is reached, ferrite and pearlite are transformed into austenite as shown in Fig. 3.34-c. The sample was etched before in situ observations

which leads to a rugged surface; since CSLM is sensitive to the relief, as a result, the grain boundaries could be observed. With increasing temperature, thermal etching started to reveal the austenite grain boundaries (Fig. 3.34-d). The liquid films were first observed along the grain boundaries as shown in Fig. 3.34-e. However, when comparing Fig. 3.33-e and f, it is found that the liquid content increases a lot during a very short time. Moreover, the liquid distribution on the sample surface is not uniform. These phenomena can result from the flatness of the sample surface or the heterogeneity of the material.

After in situ observations, the samples were etched by Nital 2%. Fig. 3.35 compares the microstructures before and after etching. Ferrite in white, pearlite in gray and MnS inclusions in black are observed in Fig. 3.35 (b). The liquid films shown in Fig. 3.35 (a) are mainly located at the ferrite grain boundaries shown in Fig. 3.35 (b).

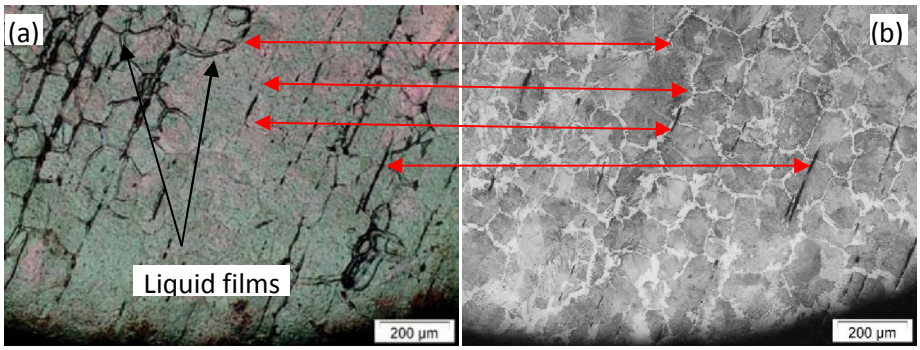

Fig. 3.35. Microstructure of the samples after in situ observations. (a) Before etching. (b) After etching.

6.5. Summary

As stated before, it is impossible to recognize the semi-solid microstructure of 100Cr6 and C38LTT with a low liquid fraction after quenching. Contrary to M2, it is impossible to reveal the liquid zones, even using EDS with long exposure time and 'tracking' alloying elements such as Mn and Cr. The CSLM technique permits to study the microstructure directly at high temperature: observations of phase transformations, grain growth, liquid appearance etc. It is noted that the diffusion rate of the alloying elements during cooling M2 steel grade is very low. This confirms that image analysis and X-ray microtomography can be used to evaluate the liquid fraction in the semi-solid state from the quenched M2 specimens. Although it is possible to observe the microstructure evolution of 100Cr6 and C38LTT at high temperature, it is impossible to identify the liquid zones after cooling from the semi-solid state.

7. Conclusions

The microstructure of the material in the semi-solid state is very important for the thixforging process. In order to study the microstructure of the material in the semi-solid state, various techniques were used to characterize the microstructure during heating process from the room temperature to the semi-solid state. The results showed that:

All methods can have some limitations.

- The use of thermodynamic data can predict the volume fraction of liquid as a function of temperature. Additional information is needed to predict the liquid fraction when taking into account of the thermal history of the material.
- DSC is an attractive method for the liquid fraction evaluation. However, the heating rate used in DSC is much lower as compared to the one used in industrial thixoforging process. Another restriction is that the morphology of the material can not be characterized.
- 2D image analysis after quenching provides useful information (liquid fraction, morphology of the material etc) when considering high-alloy steels.
- X-ray microtomography provides 3D information about the microstructure. This technique works well with a steel containing heavy elements. The good agreement between 2D SEM - EDS microstructures and 3D X-ray microtomography results proves that both kinds of techniques are efficient in characterizing high-alloyed steels in the semi-solid state. High-energy X-ray microtomography has proven to be a powerful tool, but it is not as easy to use (proposals are necessary), nor as ubiquitous, as SEM and EDS techniques that are more readily accessible in laboratories and well-adapted the microstructure characterization.
- CLSM provides the opportunity to study the microstructure at high temperature. It confirmed that the diffusion rate of alloying elements in M2 steel is quite low. It also permits to study the microstructure directly at high temperature: observations of phase transformations, grain growth, liquid appearance etc.

The microstructure of M2 steel grade in the semi-solid state can be studied either at room temperature using image analysis and X-ray microtomography or in semi-solid state by CSLM. For the microstructures of 100Cr6 and C38LTT in the semi-solid state, they can only be revealed by CSLM at high temperature.

(1) Although the thixoforging of M2 does not show a great industrial interest, it is interesting to perform the thixoforging experiments on M2 in order to study behavior of this steel and imagine a 'transposition' to C38LTT and 100Cr6 steels.

(2) Two types of heating cycle were designed for thixoforging process on M2. The mean grain size can be reduced with a fast heating rate from room temperature to solidus temperature. More spherical grains can be obtained with prolonged heating time.

(3) Although the microstructures of 100Cr6 and C38LTT in the semi-solid state can not be observed at room temperature, it is necessary to carry out the thixoforging experiments on these two steel grades, since they are more preferred in industrial applications.

References

1. Atkinson H, Rassili A: **A review of the semi-solid processing of steel.** *International Journal of Material Forming* 2010, **3:**791-795.

2. Lecomte-Beckers J, Rassili A, Carton M, Robelet M, Koeune R: **Study of the liquid fraction and thermophysical properties of semi-solid steels and application to the simulation of inductive heating for thixoforming.** In *Advanced Methods in Material Forming*: Springer Berlin Heidelberg; 2005.

3. Becker E: **Investigations experimentales et numeriques pour l'identification des parametres clefs du procede de thixoforgeage de l'acier sur le produit mis en forme.** Thesis. L'Ecole Nationale Supériure d'Arts et Métiers, Docteur de L'Ecole National Supérieure d'Arts et Métiers; 2008.

4. Fraipont C, Lecomte-Beckers J: **Alloy Characterization to Adapt Steels to Thixoforming: Study of a High Chromium High Carbon Steel.** *Solid State Phenomena* 2008, **141-143:**523-527.

5. Püttgen W, Bleck W, Seidl I, Kopp R, Bertrand C: **Thixoforged damper brackets made of the steel grades HS6-5-3 and 100Cr6.** *Advanced Engineering Materials* 2005, **7:**726-735.

6. Tzimas E, Zavaliangos A: **Evaluation of volume fraction of solid in alloys formed by semisolid processing.** *Journal of Materials Science* 2000, **35:**5319-5329.

7. Omar MZ, Palmiere EJ, Howe AA, Atkinson HV, Kapranos P: **Thixoforming of a high performance HP9/4/30 steel.** *Materials Science and Engineering: A* 2005, **395:**53-61.

8. Omar MZ, Atkinson HV, Howe AA, Palmiere EJ, Kapranos P, Ghazali MJ: **Solid–liquid structural break-up in M2 tool steel for semi-solid metal processing.** *Journal of Materials Science* 2008, **44:**869-874.

9. Roberts GA, Krauss G, Kennedy R, Kennedy RL: *Tool steels.* ASM International; 1998.

10. Honeycombe R, Bhadeshia H, Bhadeshia H (Eds.): **Steels: Microstructure And Properties**: Butterworth-Heinemann; 2006.

Chapter 4. Thixoforging - experimental results

Table of contents

1. Thixoforging of M2……..283

1.1 Introduction of the thixoforging process……283

1.2 Final geometry of the thixoforged parts……285

1.3 Influence of process parameters on final part shape……293

1.4 Influence of the process parameters on the forming load……295

1.5. Macroscopic & microscopic observations……301

1.6 Conclusions……311

2. Thixoforming of other steel grades……312

2.1 Thixoforged parts of 100Cr6 steel grade……313

2.2 Thixoforged parts of C38LTT steel grade……317

2.3 Conclusions……324

3. Conclusions……326

References……328

The results of the thixoforging experiments on different parts with different geometries are presented in this chapter. The influence of the process parameters on the forming load, the material flow and the microstructure has been studied. The liquid distribution on the thixoforged parts (M2 steel grade) has also been investigated in order to study the influence of the parameters on the final shape of the thixoforged parts. During the thixoforging process, the solid grains at different zones have different behaviors.

1. Thixoforging of M2

1.1. Introduction of the thixoforging process

The device and the heating cycles have been introduced in the chapter 2 and 3. This chapter mainly focuses on the results of thixoforging experiments.

Fig. 4.1. M2 parts obtained by thixoforging process.

M2 billets with a diameter of 36mm and 34mm in height were thixoforged under various process conditions. From the results of the partial remelting experiments, the suitable temperature for thixoforming M2 grade appears to be in the temperature range of 1290°C – 1340°C which corresponds to the liquid fraction range of ~16% - ~30%.

Fig. 4.1 presents the thixoforged parts which were thixoforged on the SATORE mechanical press with various process parameters in the LCFC laboratory, Arts et Méteirs

ParisTech Metz. During the thixoforging process, the billet was first induction heated up to the semi-solid state and then transferred to the lower die for subsequent thixoforging process. After the insertion of the billet, the upper die moves forward to the billet, carrying out the forming operation. Finally, the part is ejected by raising the ejecting rod, which is assembled with the lower die. Fig. 4.2 presents the schematic view of the thixoforging step. The given part geometry is characterized by a long flow length in the bush in cross section in Fig. 4.2 (c).

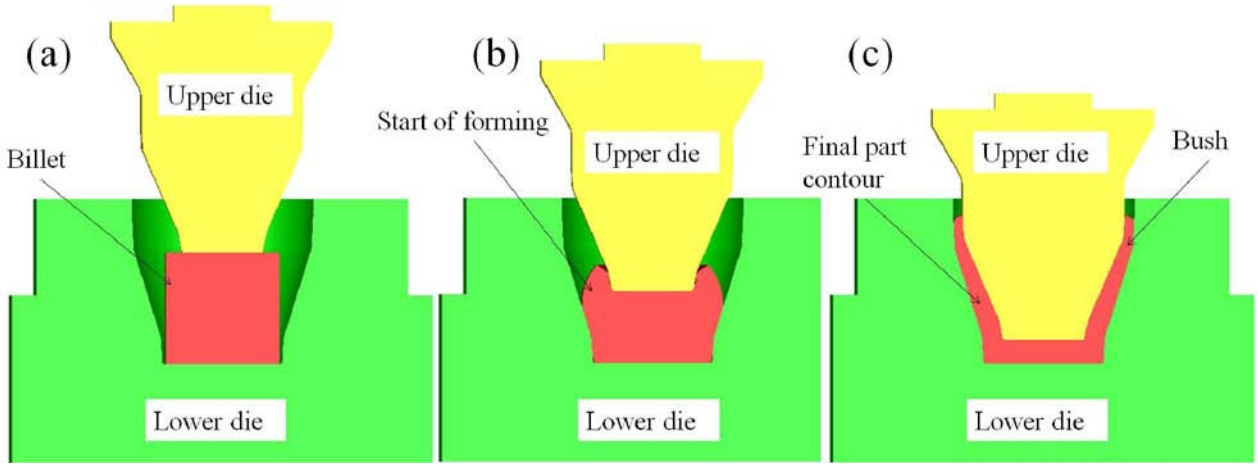

Fig. 4.2. Schematic view of forming steps.

The adjustable parameters are the billet temperature, heating cycles for billet temperature and the tool temperature. Table. 4.1 gives the various parameters used for the thixoforging experiments.

Table. 4.1. Different process parameters for the thixoforging process.

Billet temperature (°C)	Heating cycle	Die temperature
1290	A-type	Room temperature
	B-type	Warm temperature
1300	A-type	Room temperature
	B-type	Warm temperature
1310	A-type	Room temperature
	B-type	Warm temperature
1320	A-type	Room temperature
	B-type	Warm temperature
1330	A-type	Room temperature
	B-type	Warm temperature
1340	A-type	Room temperature
	B-type	Warm temperature

1.2. Final geometry of the thixoforged parts

Fig. 4.3. presents the cups which were thixoforged at a high ram speed, at different temperatures (from 1290°C to 1350°C) and with various die temperatures (warm die ~350°C, cold die ~ room temperature).

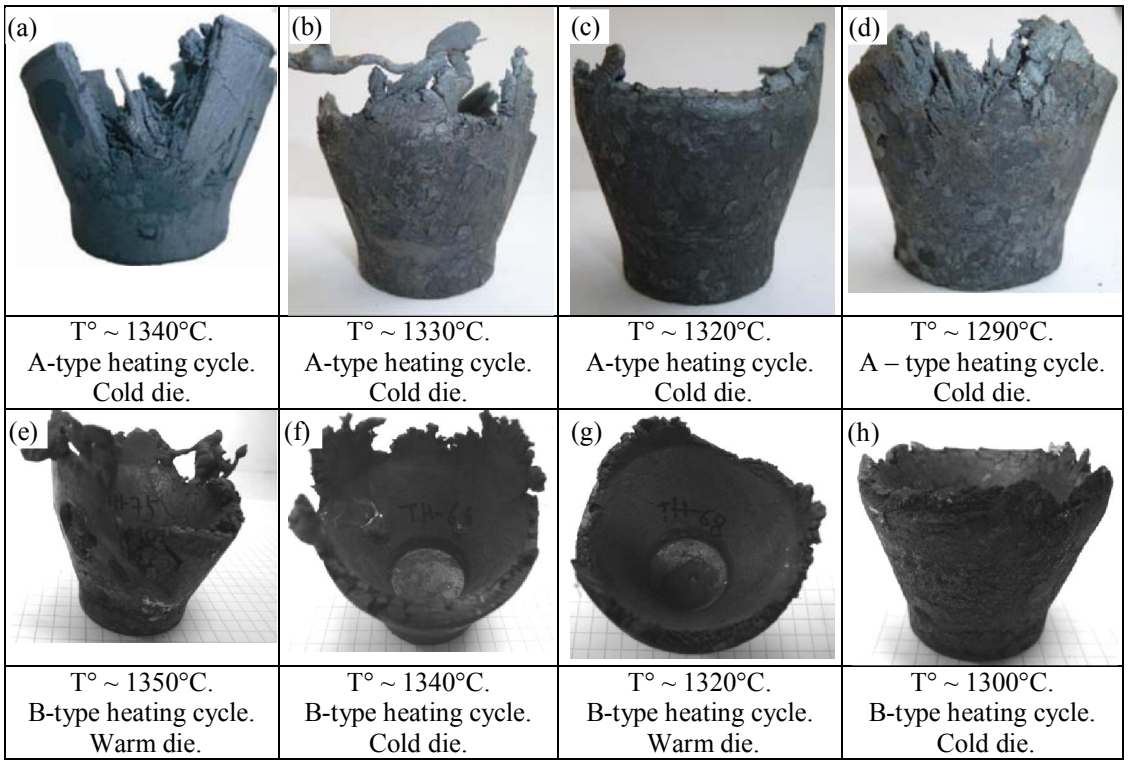

Fig. 4.3. Cups thixoforged under various process parameters.

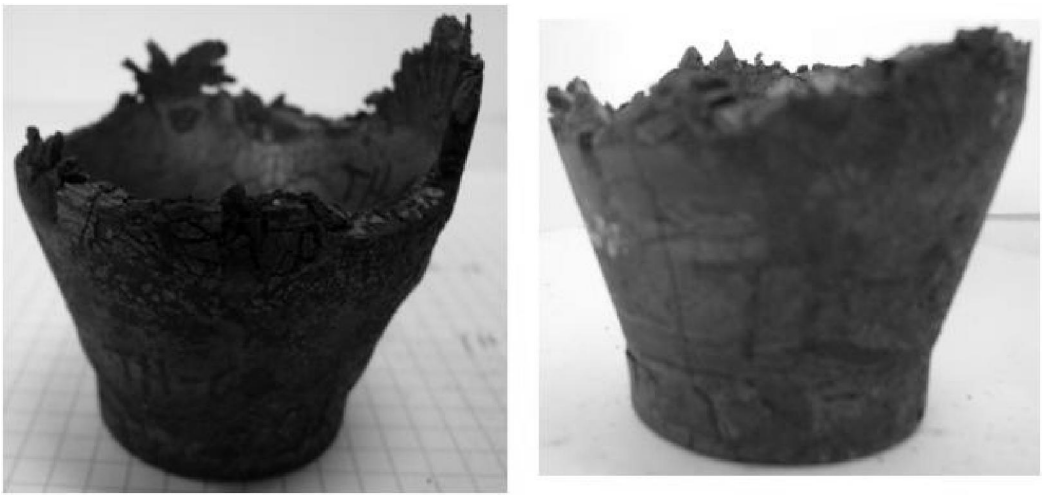

Fig. 4.4. Heterogeneous material flows of thixoforged parts.

The heterogeneous material flow behavior may be resulted from several points, such as the heterogeneous microstructure which influences the material behavior, the positions of the billet during forming and the geometry of the billet etc. Fig. 4.5 compares the distances between interior and exterior surfaces at the same height on both sides (A and B). It can be found that the distance on the left (A) is smaller than that on the right (B). The difference in distance is ~ 0.3mm. After measuring all the cut thixoforged cups, we noted that the smaller distance between the interior and exterior cup surfaces, the longer the bush length, which is similar to that shown in Fig. 4.5.

Fig. 4.5. Width comparison at the same height.

In order to understand the specific phenomenon described above, it will be helpful to perform the simulations with an appropriate material rheology and boundary conditions. However, the simulations of the thixoforming process with the micro-macro model [1] were unsuccessful due to numerical problems. Therefore, hot forging simulations were performed with Forge 2011® in order to see the difference of material behavior under hot forming process (numerical) and that under thixoforging process (experimental). The hot forging experiments were not performed because of the limited press capacities. The influence of the die and billet positions, the friction as well as the material rheology on the material flow during hot forming was studied.

Table. 4.2. Coefficient values for different steel grades.

	A	m_1	m_2	m_3	m_4	$m_5=m_7=m_8=m_9$
C35	1498.8708	-0.00269	-0.12651	0.14542	-0.05957	0
316L	8905.34	-0.00383	0.01248	0.09912	-0.02413	0

Table. 4.3. Variable parameters for the simulations.

Material	C35		316L	
Die position	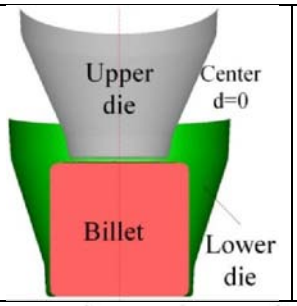	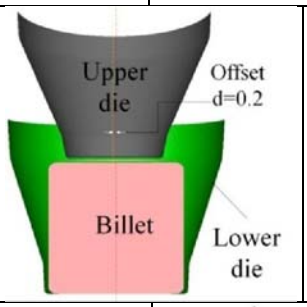	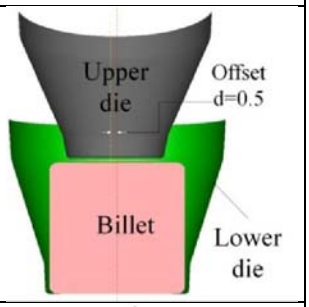	
Billet position	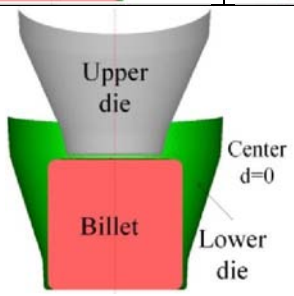		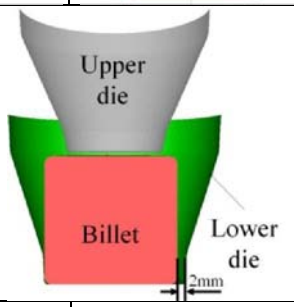	
Temperature	1200°C	1250°C		1300°C
Friction	0.15		0.5	

Regarding the influence of billet position in the die, a billet of 35mm in diameter and 34mm in height, which was not center placed but touching the die surface (Table. 4.3 – billet position) was used in the hot forging simulations. The simulation for a half section was performed, since the specimen is symmetric; rigid dies were considered. The mechanical press was used for the forging process. Two different friction factors (Coulomb) at the interface of the die and billet were used in order to study the influence of the friction on material flow. The die temperature was defined to be 350°C which is used in the thixoforging experiments. The heat transfer of 10000°K^{-1} was used to simulate the thermal exchange between the material and die. Two steel grades, C35 and 316L, following Spittel's law (Eq. 4.1) were used in the simulations.

$$\sigma_f = A e^{m_1 T} T^{m_9} \varepsilon^{m_2} e^{m_4/\varepsilon} (1+\varepsilon)^{m_5 T} e^{m_7 \varepsilon} \dot{\varepsilon}^{m_3} \dot{\varepsilon}^{m_8 T} \qquad \text{(Eq. 4.1)}$$

Table. 4.2 gives the coefficient values of the material rehology. Table. 4.3 presents various parameters for the simulations. The variation of the material geometry is shown in Table. 4.4. For all the cases described in Table. 4.3, the material is first compressed with the penetration of the upper die and flows up freely without touching the upper die until to the punch

displacement of ~12mm. When the displacement exceeds 12mm, the back-extrusion starts, as shown in Table. 4.4.

Table. 4.4. Material flows during hot forging.

	Center billet - Center die	Offset billet - Center die	Center billet - Offset die
Displacement = 0	(a) 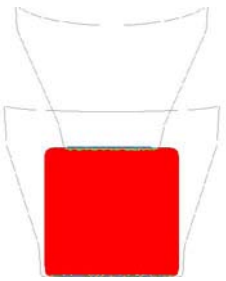	(b) 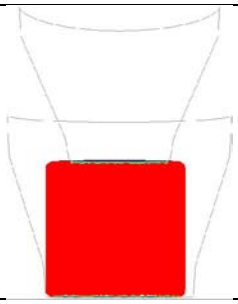	(c) 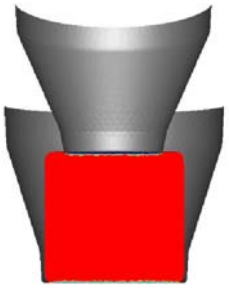
Displacement = 13	(d) 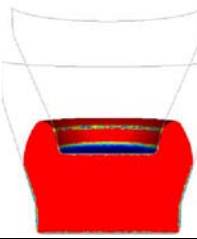	(e) 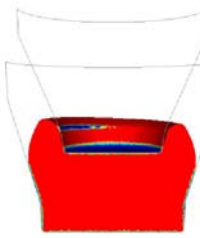	(f) 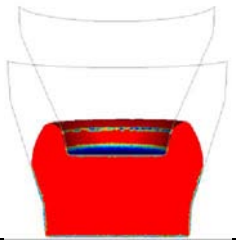
Displacement = 15	(g) 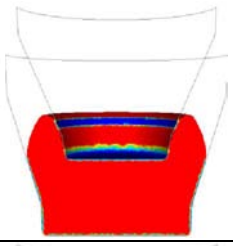	(h) 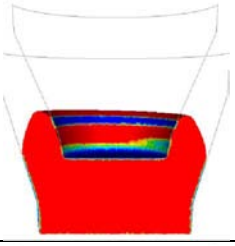	(i) 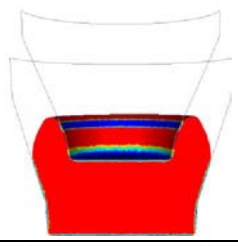
Displacement = 17	(j) 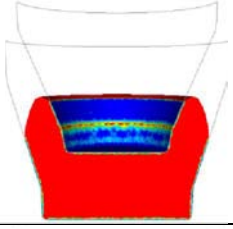	(k) 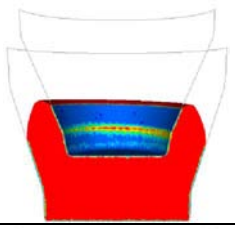	(l) 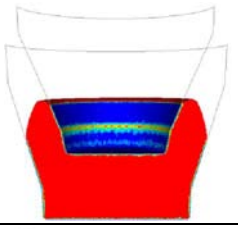
Displacement = 19	(m) 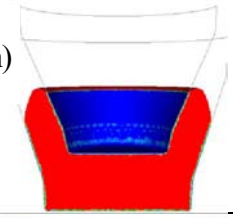	(n) 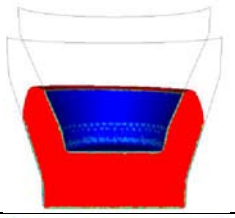	(o) 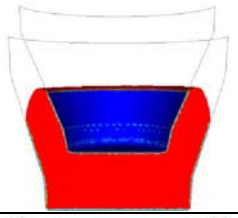
Displacement = 27	(p) 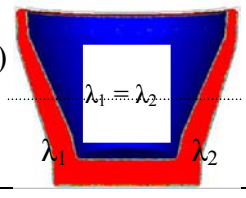	(q) 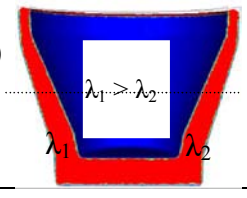	(r) 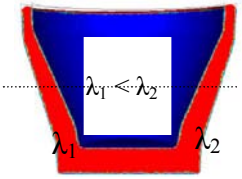

As for the simulation results, we mainly focus on the height difference of the bush on both sides (Fig. 4.6 (a)). Fig. 4.6 illustrates the influence of the billet temperature (Fig. 4.6 (b)),

billet position (Fig. 4.6 (c) and (d)) and die position (Fig. 4.6 (e) and (f)). Here, the height difference between A and B is a value which is calculated by the method: at the same punch displacement, the maximum bush length on the left side (A) minus that on the right side (B).

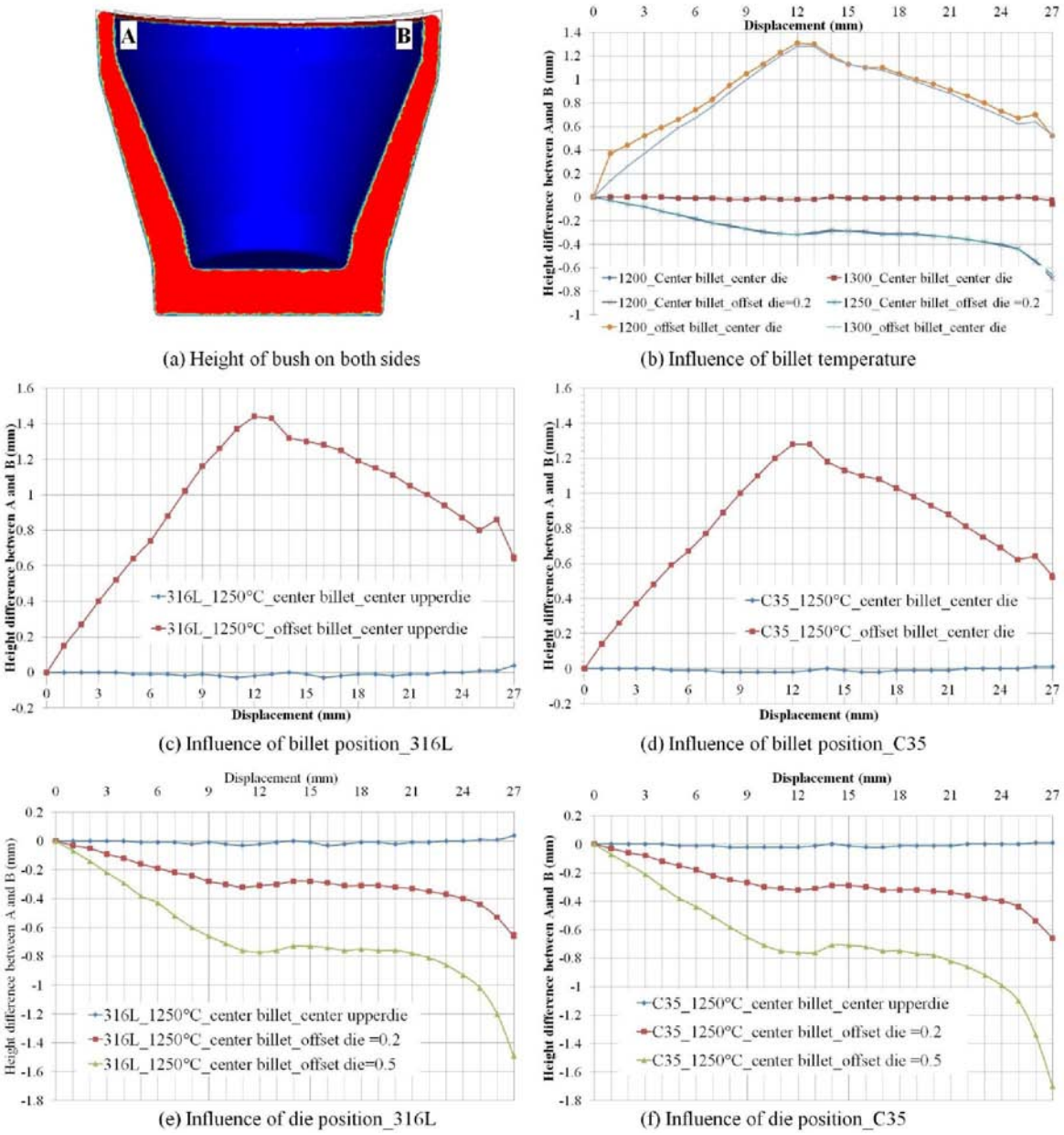

Fig. 4.6. Influence of various parameters on bush height.

From the curves shown in Fig. 4.6, it can be noted that when the displacement is less than ~12mm:

– In the case of shifting the billet, the height difference increases with increasing

displacement. That is to say, the bush height on the left side (A) is bigger than that on the right side (B).

- In the case of shifting the upper die, the absolute height difference also increases with increasing displacement. In this case, the bush height on the left side (A) is smaller than that on the right side (B).

When the insertion depth exceeds ~12 mm, the material starts getting contact with upper die shown in Table. 4.4.

- In the case of shifting the billet, the height difference decreases with increasing displacement. However, the increase in height difference appears in the displacement interval [25mm, 26mm], that is caused by the die geometry. Still, the bush height on the left side (A) is bigger than that on the right side (B).
- In the case of shifting the upper die, the absolute height decreases with increasing displacement from 12mm to 14mm, followed by a smooth increase in height difference from 14mm to 21 mm and a sharp increase from 21mm to 27mm.

Fig. 4.6 (c) and (d) show that for 2 different steel grades, the values of height difference are different, but the influence of billet position on the bush height difference is similar. Moreover, the comparison of the influence of the die position shown in Fig. 4. 6 (e) and (f) also reflects that the material rheology at high temperature (in the solid state) has less effect on the variation of height difference. Therefore, we can study the influence of the billet, die position and billet temperature by focusing on one material: for example on C35. In addition, during hot forming process, if the billet and die are in the ideal positions (both billet and die are well centered), there is no big difference in bush height as shown in Fig. 4.6 (b) – (f).

It is also interesting to study the influence of the friction on the height difference. As compared in Fig. 4.7, there is no big change in the height difference when using two different friction coefficients ($\mu_1 = 0.15$ and $\mu_2 = 0.5$).

Another situation which may also lead to a bush height difference is forging a billet which is not in good geometry; the top surface is not parallel to the bottom, as shown in Fig. 4.8 (a). In the simulation, the billet and the upper die are center placed. Fig. 4.8 (b) shows the variation of the height difference during the forging process. It covers ~ 12mm in

displacement to increase the height difference from 0.4mm to ~ 0.6mm. After that, the height difference decreases with increasing the displacement.

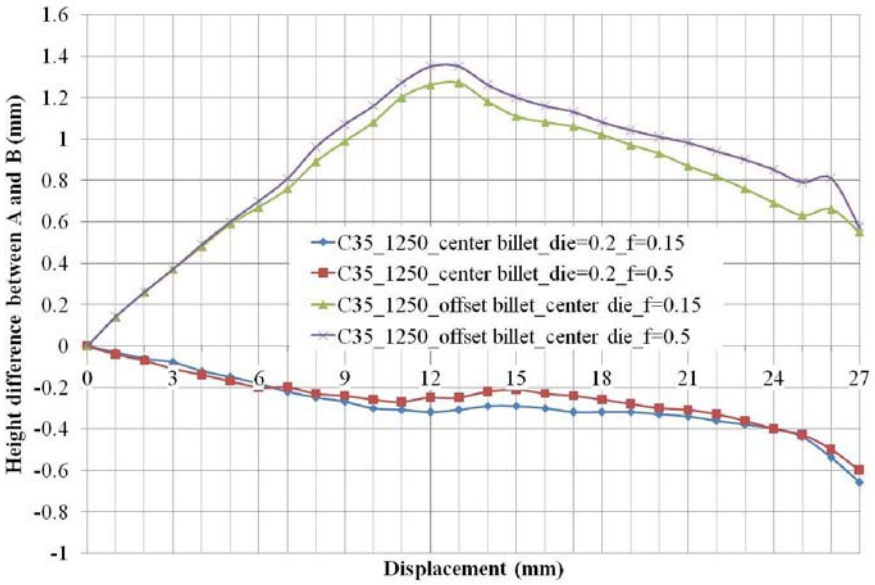

Fig. 4.7. Influence of the friction on the height difference.

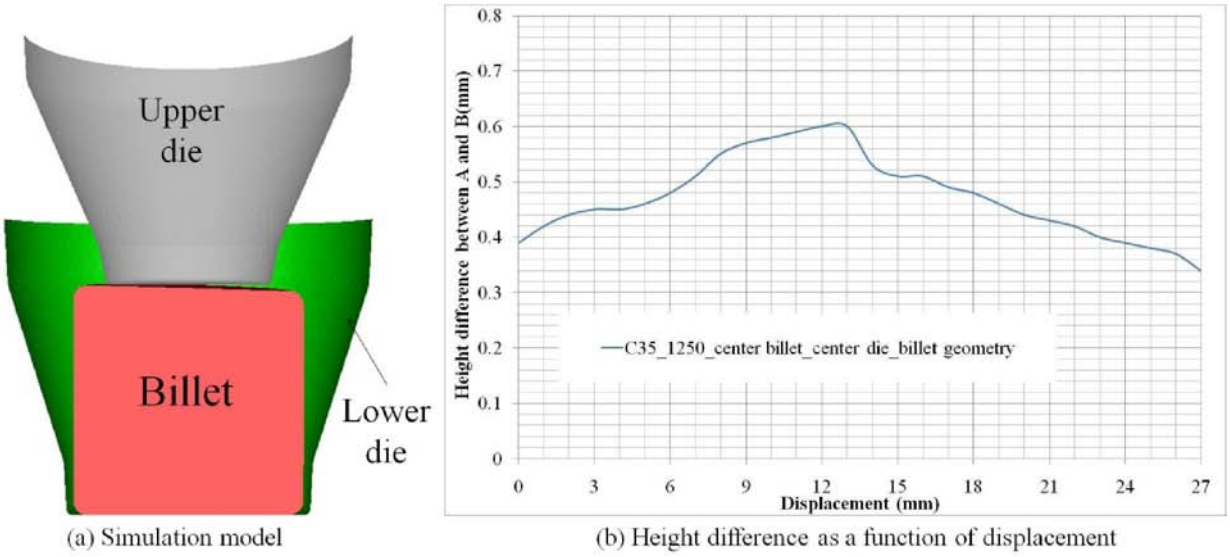

Fig. 4.8. Influence of billet geometry on the height difference.

To sum up, from Fig. 4.6, Fig. 4.7 and Fig. 4.8, the parameters (billet, die positions, billet temperature, friction coefficient and billet geometry) influence the height difference. However, the influence of the billet temperature and the friction coefficient is relatively smaller than the influence of others. During forging process, the shift of the billet, die

positions and unideal billet geometry parameters affect the strain, strain rate distribution, which in turn influence the material flow.

Compared to the numerical results, the thixoforging experimental results show an inverse effect on the height difference: the smaller distance between the interior and exterior cup surfaces, the longer the bush length (Fig. 4.5). The different phenomena may result from the unique thixotropic behavior of the semi-solid material: the viscosity decreases with increasing shear rate. For a material in the solid state, the stress increases with increasing shear rate. However, the semi-solid material exhibits the behavior that the viscosity decreases with increasing shear rate.

Fig. 4.9 presents the macrograph of one thixoforged part. The material flows in zone A and B are similar: the material flow is similar to that of classical hot forging. The differences are mainly related to the microstructure such as the liquid fraction, its distribution, the contiguity etc.

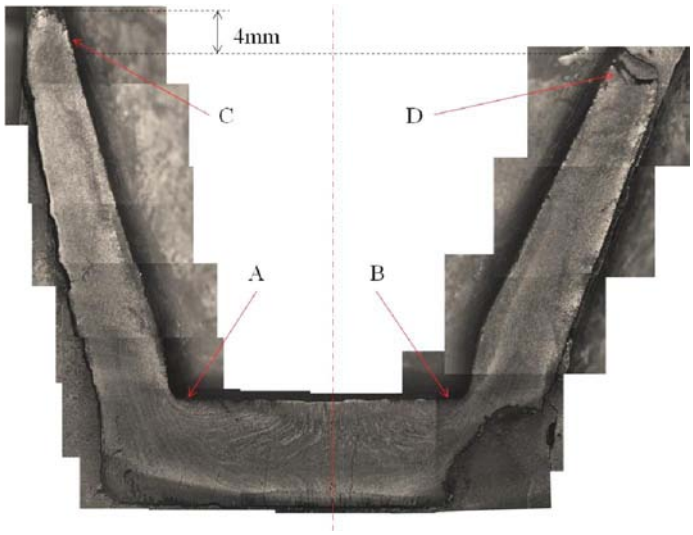

Fig. 4.9. Macroscopic view of material flow of the thixoforged part.

As illustrated in Fig. 4.3, the billet temperature range for obtaining a good final part shape is widen (1290°C – 1340°C) by using a warm die. When the billet was thixoforged at 1350°C with a warm die, the phenomenon of liquid ejection was observed as shown in Fig. 4.3 (e). Because of the better flexibility of the liquid phase, it was pressed out and separated from the semi-solid bulk material which results in a heterogeneous phase distribution.

The material flows during the thixoforging process depend on the process conditions, such as billet temperature, die temperature and also microstructure [2].

1.3. Influence of process parameters on final part shape

1.3.1. Influence of the billet temperature on material flow

When comparing the material flow of the thixoforged cups formed at the same die temperature but at various billet temperatures (Fig. 4.3 (a), (b) and (c)), in the billet temperature interval (1290°C – 1350°C), the reduction of the billet temperature improves the quality of final part shape. The bush length maybe increases with increasing temperature. The apparent volume of the bush may be larger than that of the material, because of the voids or porosities. The increase of temperature leads to an increase in liquid fraction which improves the fluidity of the material. The liquid ejection at a high liquid fraction may lead to an increase in bush length.

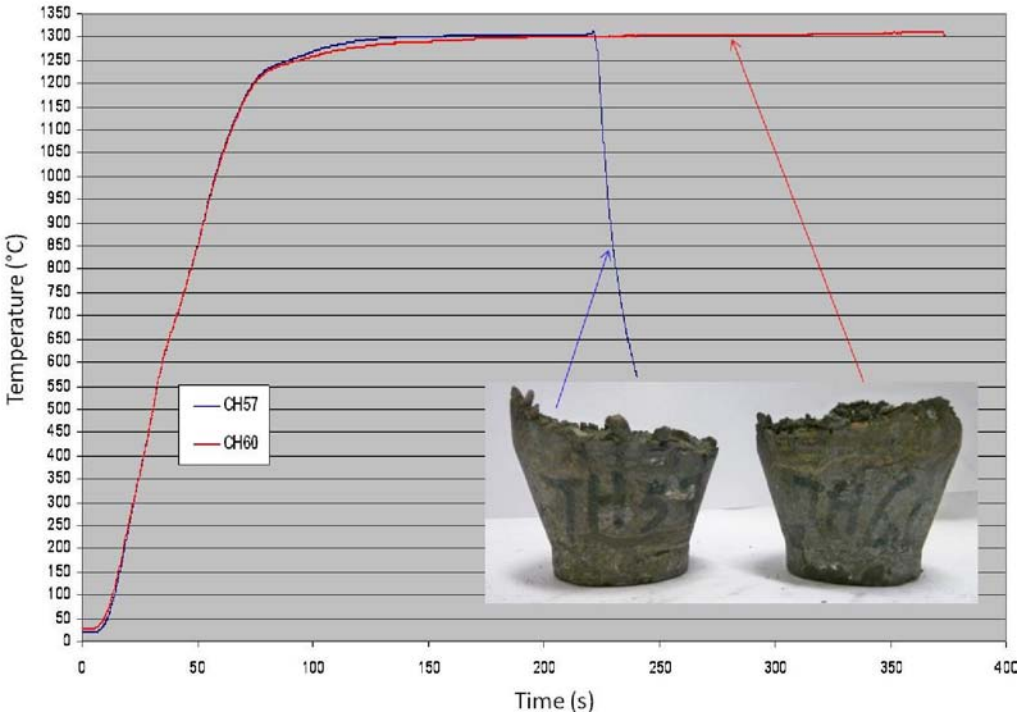

Fig. 4.10. Heating curves of temperature as a function of time.

In addition, for a constant billet temperature and different heating times, the material flow behavior may be also different. Fig. 4.10 presents two heating cycles for the billet temperature of ~1305°C with different heating time. From the figure, it can be observed that the material flows of the thixoforged part (TH-60) heated by the heating cycle CH-60 is more homogeneous than the other (TH-57, heated by the heating cycle CH57). The homogeneous material flow may result from the homogenous microstructure in the aspects of liquid

fraction, its distribution, grain size etc. In the heating stage, with prolonged heating time in the semi-solid state, the microstructure of the billet may be homogeneous with more spherical solid grains and more homogeneous liquid fraction distribution. During forming, the material flows much more homogeneously with a homogeneous microstructure. As presented in Chapter 3, more spherical grains can be obtained by increasing the holding time. However, different heating time may not influence the material behavior greatly.

1.3.2. Influence of the die temperature on final geometry

Fig. 4.11 illustrates the two cups thixoformed with a cold die (TH57) and with a warm die (TH68). Similar results were obtained. Heterogeneous material flows were observed on both thixoforged cups (Fig. 4.11). The main difference in the material flow between the two thixoforged cups was the length of the bush. Becker [3] stated that the increase in die temperature reduces the heat exchange between billet and die, and therefore improves the fluidity of the material because of the higher liquid fraction. However, in our case, the forming speed is high (> 200mm/s), which means that the thixoforming process time is short. In addition, the thermal conductivity of M2 steel is low. During thixoforming, the heat loss of the billet forging with a cold die and that with a warm die is similar. Therefore, the material flow is similar when thixoforming the billets at the same billet temperature but with different die temperatures.

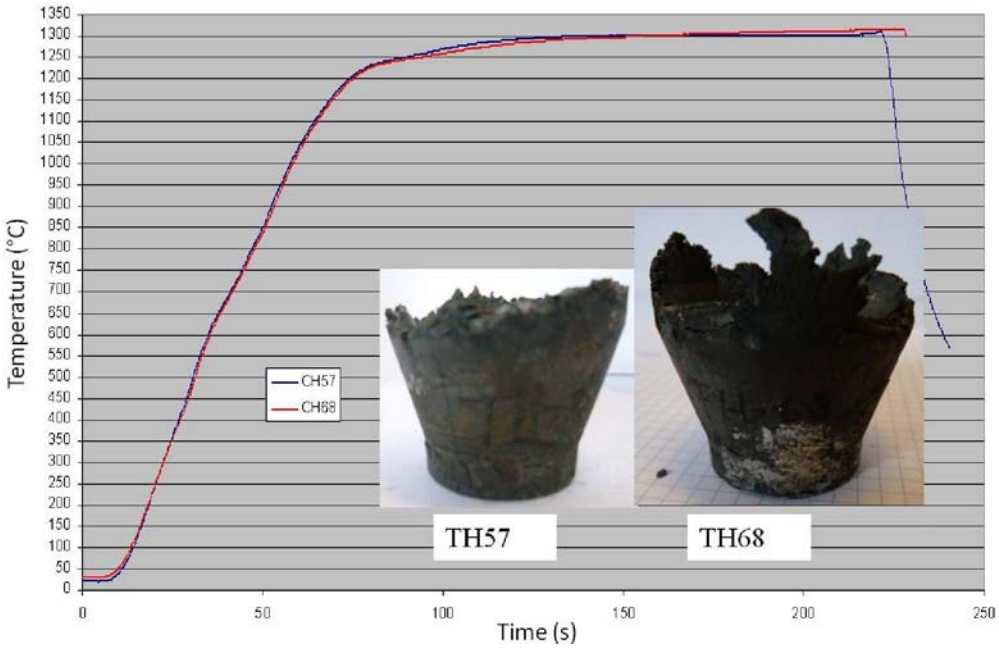

Fig. 4.11. Temperature evolution as a function of time for thixoforging with different die temperatures.

1.4. Influence of the process parameters on the forming load

1.4.1. Analysis of the load-displacement curves

Fig. 4.12 presents a load-displacement signal curve of the thixoforged cups. The curve shows the stroke length of the ram just after that the upper die first impacts the top of the billet denoted on the ram displacement axis. The height of the billet is 34mm. The curve can be divided into four distinct zones. The first zone associated with zero force corresponds to the motion of the upper die until it touches the top surface of the billet (I). Then, the billet is compressed and fills the lower die with a peak load (II). Followed by a drop in load (III), a significant increase of the load (IV) which is related to the backward extrusion and the filling of the cup was observed. Generally, the load-displacement curves of thixoforging process for various process conditions exhibit similar patterns.

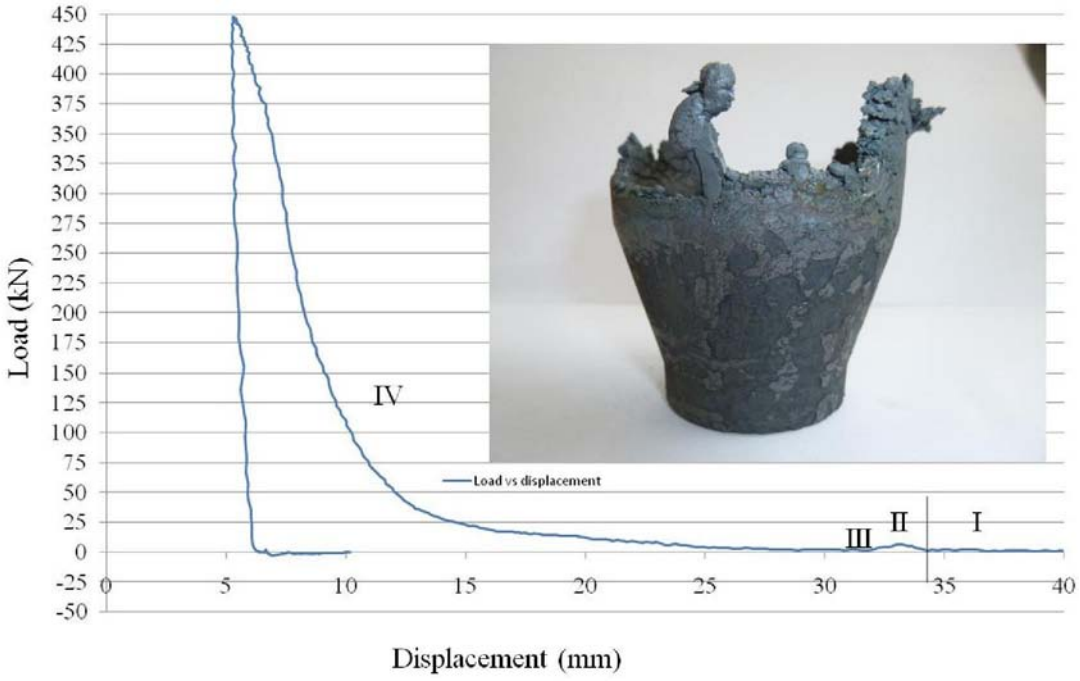

Fig. 4.12. Load – displacement curve during thixoforging process.

The four zones of load-displacement curves studied in this work can be explained as follows.

(I) Before reaching the billet, no load signal was collected from the load cell which was at the back of the die. Therefore, the load is equal to ~ 0.

(II) The first peak load corresponds to the breakdown of structure. Here, the structure consists in both microstructure and macrostructure. During thixoforging, the billets were not protected by a protective gas, resulting in the oxidization skin. During forming, the rupture of the oxidization skin may result in the first peak of the load. Meanwhile, in the microstructure scale, as presented in the Fig. 4. 13, the M2 steel in the semi-solid state is partially interconnected by unwetted grain boundaries. The load represents the one required for decohesion of insufficiently wetted grain boundaries and segregation bands to allow solid grains to move freely and rearrange the solid grains. Moreover, for cohesionless granular grains, the load is also used to overcome the resistance of shear which comes from the relative motion of grains (termed as 'internal friction' by Tzimas and zavaliangos [4]).

(III) After breaking down of the structure, the solid grains are surrounded by liquid and the material shows a thixotropic flow behavior, resulting in a relatively plateau or a very low rise of load caused by the internal friction.

(IV) Rapid increase in the forming load that is related to the backward extrusion and the filling of the cup. During this stage, the contact area between the billet and die increases. In extreme, as the thickness of the cup wall is thin, the part of material solidifies resulting nearly no liquid phase, and there is no room for the solid grains to slide by each other. As a result, the load increases sharply due to the increasing friction [5] and plastic deformation of solid grains.

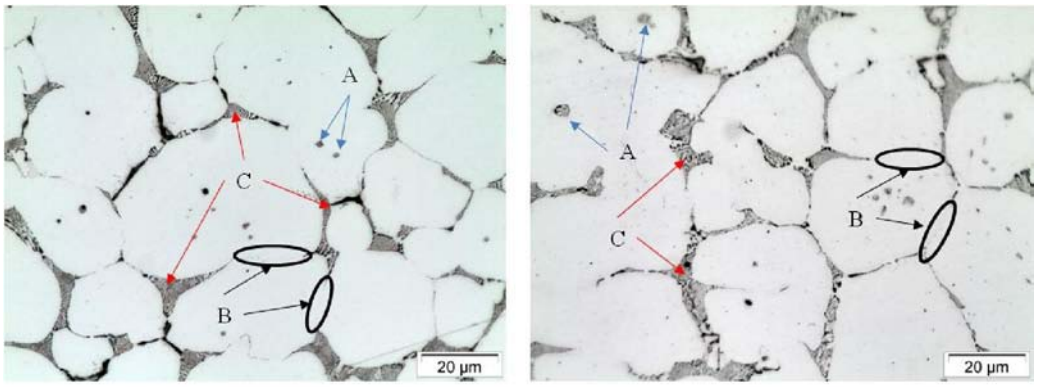

Fig. 4.13. Microstructures of the quenched M2 steel grade from 1320°C (etched by Groesbeck). Area A presents the entrapped liquid, area B refers to the grain boundaries and area C is the intergranular liquid.

Repeatability of the thixoforging process

In order to study the stability of the thixoforging process, the experiments with various process parameters were repeated several times. The load-displacement curves shown in Fig. 4.14 are similar. However, due to the difficulties in billet temperature controlling at the induction heating stage, there are some differences in billet temperature for various billets which result in different microstructures (liquid fraction, its distribution and etc.) and therefore in different load-displacement curves and final part shapes. Nevertheless, the maximum deviation of the loads obtained from the experiments under the same process conditions is less than 10%. Here, we consider that the repeatability of the experiments is good and the results can be used for further study.

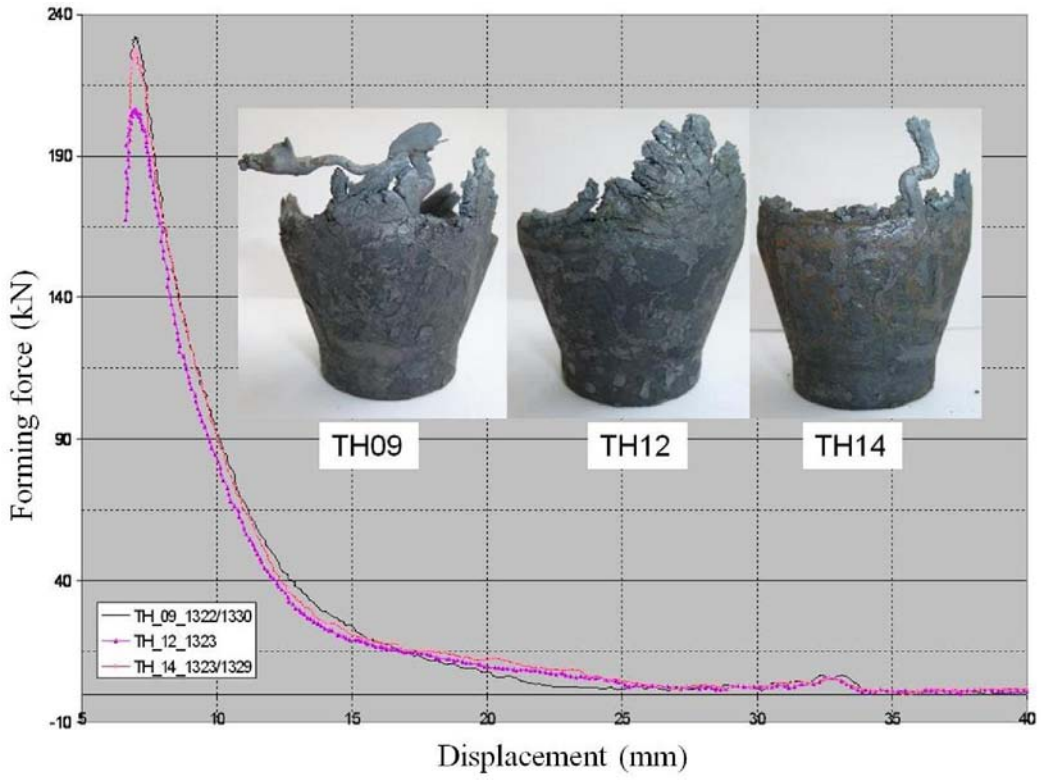

Fig. 4.14. Load-displacement curves and final parts thixoforged under the same process conditions.

1.4.2. Influence of the billet temperature on the forming load

As shown in Fig. 4.15, the peak load and subsequent decrease to the plateau or very low rise of load happened in a small displacement (~3mm). The 3-mm breakdown displacement may suggest that the solid skeleton is brittle. It can be also concluded from the figure that the influence of the billet temperature on the structural breakdown displacement is not big (3mm

for various billet temperatures). In addition, the peak load decreases with increasing temperature, for example, the peak load of around 29 kN at 1290°C (F_L ~ 11%) is more than three times the peak load at 1320°C (F_L ~ 25%). The increase in material temperature leads to an increase in liquid fraction. As a result, there is an increase in the wetted grain boundaries and the liquid film thickness increases. As presented in Chapter 3, the temperature does not significantly influence the shape factor of the solid grains. However, for the material with a low liquid fraction, the grains are difficult to shear and pass each other due to the thin liquid layer between the grains. Hence, a large load is required for breaking down of insufficiently wetted grain and for the sliding of solid grains. By comparing the peak loads at 1305°C and 1320°C, there is no big difference. It may be explained as follows.

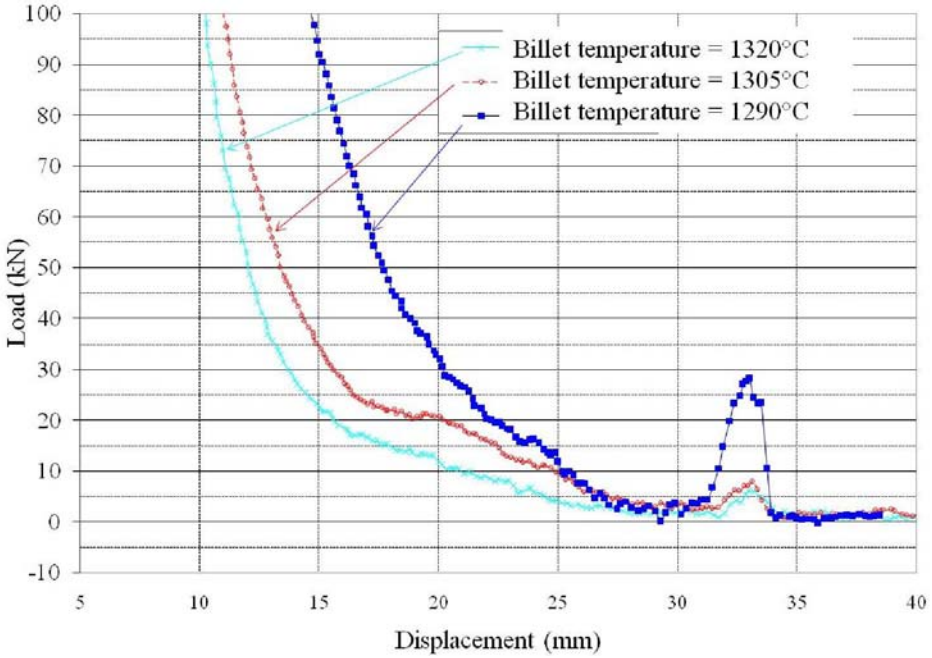

Fig. 4.15. Load-displacement curves during thixoforging experiments.

With increasing temperature, the liquid fraction increases, resulting in the augmentation of the amount of liquid at the grain boundaries and the thickness of the liquid film. The amount of liquid reaches a certain level where the solid grain boundaries can be wetted with a sufficient liquid film for grains sliding; however, due to high heating rate, the liquid phase can not wet all grain boundaries, leading to a proportion of insufficient wetted grain boundaries. The magnitude of the load peaks can be used to indicate the contribution of insufficient wetted grain boundaries under various the process conditions.

After the solid skeleton was broken down, the solid grains are surrounded by a liquid phase, the strength of the material decreases and the forming load decreases to a low value (relative plateau or low rise of load). The material shows the thixotropic behavior. In the incipience of this stage, the deformation is achieved by a cooperative movement of the solid grains and liquid phase. A forming load as low as around 3 kN was achieved when processing at different temperatures. The resistance to the grain rearrangement may contribute to the low forming load. With increasing forming displacement, there may be a solid grain segregation phenomenon resulting from the liquid segregation during forming. As a result, the forming load starts increasing slowly with various increasing rates for different temperatures. The load may be used to overcome the friction generated from the sliding between solid grains and also the restriction of the solid grain movement due to the spatial constraint imposed by the surrounding grains. Finally, the deformation is completed by the plastic deformation of the solid grains at the bottom of the thixoforged cups as shown in the Fig. 4.16. This figure presents the microstructures of the bottom zones in the cups thixoforged at various processing temperature. The grains in this zone are deformed and the liquid fraction is smaller as compared to that in the semi-solid state before forming process. In this stage, the load is mainly to overcome the yield strength of the grains. Meanwhile, the load is also used for solid grains sliding and rotating between each other. At the same displacement, the load increases with decreasing billet temperature. However, the increasing rate of the loads is similar for various billet temperatures, but with a discrepancy which is resulted from the thixotropic stage.

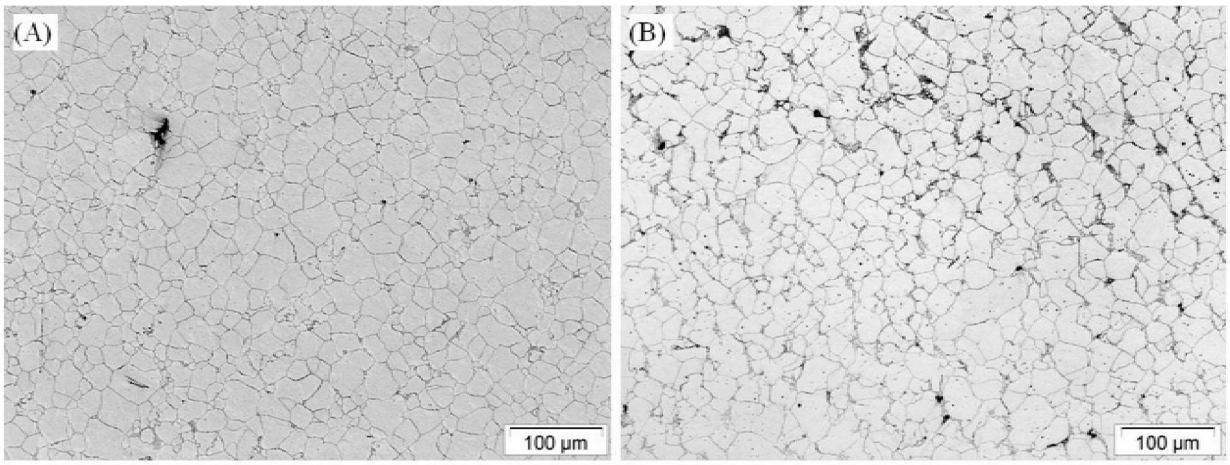

T°C billet= 1300°C. Shape factor (F) = 0.67 T°C billet = 1320°C, Shape factor (F) = 0.71

Fig. 4.16. Micrographs showing the plastic deformation of solid grains processed at various temperatures.

1.4.3. Influence of the die temperature on the forming load

As expected, the loads are almost the same. When comparing the load curve obtained with the same billet temperature at various die temperatures, there is no big difference in the load value. The obtained results differ from the ones performed on aluminum alloys (the same press, the same die speed and the same part geometry). A good final shape and a low forming load were obtained when thixoforging the aluminum alloy cups. During the thixoforming on aluminum alloys with a warm die [Neag 2012], the thermal exchange between the billet and die are lower, because the processing billet temperature is relatively low (~ 600°C). The die temperature was ~300°C. In addition, the thermal conductivity of the aluminum alloy is big. Therefore, the heat loss was reduced and resulted in a prolonged thixotropic flow stage. While, for M2 steel grade, the heat losses during forming with a cold die and a warm die are similar because of the low thermal conductivity (one order of magnitude less than the one of aluminum) and short forming time (~0.13s). For the steel thixoforming, a die temperature of ~ 300°C has little impact on the final part geometry and forming load. A lower forming load may be obtained by using a warmer die of 600°C. However, the experiments with a warmer die of 600°C were not performed due to the insufficient die heating method and die design.

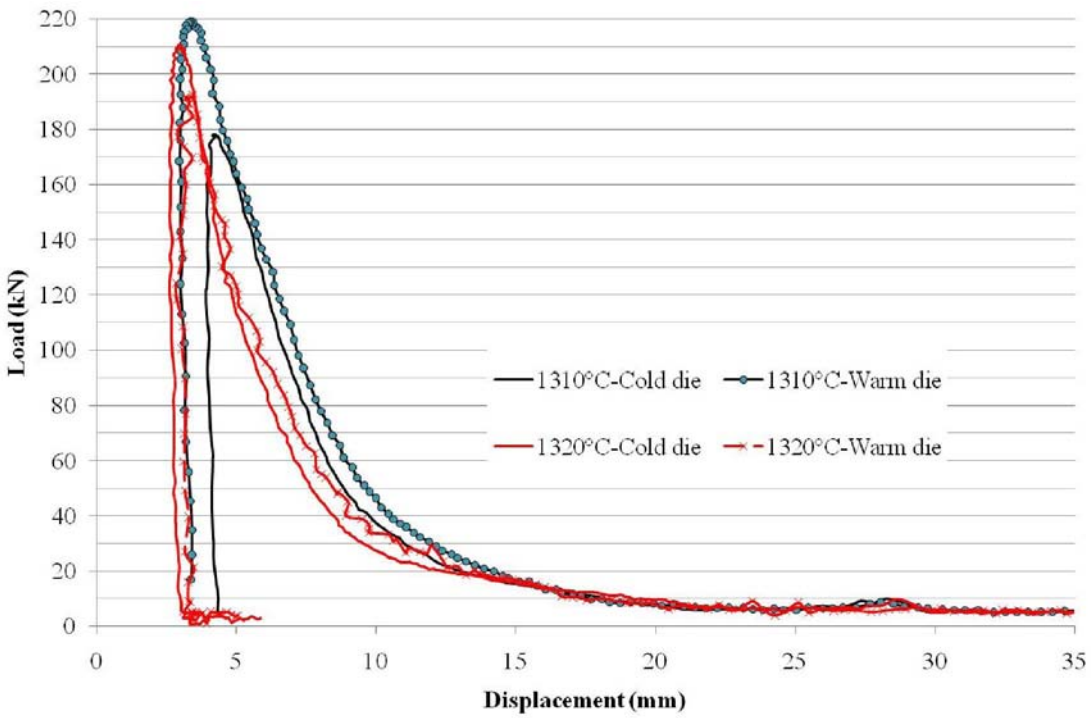

Fig. 4.17. Load-displacement curves of the thixoforging process at the same billet temperature but with various die temperatures.

Summary

A homogeneous microstructure of the billet is better for a good material flow which requires a homogenizing heating cycle. A proper heating time should be considered for the microstructure homogeneity and the industrial application as well.

For the same heating cycle, a warm die temperature may result in a good material flow during thixoforging process. Here, the die temperature below 350°C has a small influence on the material flow.

Load-displacement curves can be divided into four distinct stages of deformation, the flow resistance of the material with a high solid fraction accounts for:

- Breakdown of the cohesive bands between solid grains.
- Resistance to the grain rearrangement and to the flow of liquid relative to the solid.
- The friction of sliding between the solid grains.
- Plastic deformation of the grains.

The first peak load and the load for forming the cups decrease with increasing initial billet temperature. Meanwhile, the thixotropic stage is prolonged by increasing initial billet temperature. However, there is no big difference in the load-displacement curves during thixoforging with various die temperatures.

Under a critical temperature (1350°C for M2 steel grade), the material flow quality was improved with increasing the billet temperature.

In conclusion, in order to obtain a good quality thixoforged part with a lower forming load, it is suggested to heat the material to a higher temperature with a proper heating cycle for obtaining a more homogeneous microstructure and avoid the liquid ejection.

1.5. Macroscopic & microscopic observations

For the characterization of the material flow during the thixoforging process, a macroscopic observation was performed. The extruded cup was sectioned along the vertical axis for metallographic observations. Fig. 4.18 shows a macrograph etched by HCL. There are 3 different zones showing different material flows. The material in zone A does not flow or exhibits a weak flow, and the material remains in contact with the tool and is cooled quickly

during the forming process. The maximum thickness of this zone is ~1.5mm. Zone B exhibits a material flow behavior similar to the classical forging process. While zone C contains an amount of semi-solid metal which is useful to feed the whole die cavity. There are mainly two kinds of cracks which are observed on the parts. The quench cracking is featured with intergranular failure (as shown in Fig. 4.19 (b)). During quenching, as the temperature decreases, the quenching stresses induced by thermal contraction increase, which results in cracks that propagate along the grain boundaries. The other type of crack may result from the material flow during the forming process. The heterogeneity in local geometry and strength results in strain localization which may lead to the material tearing.

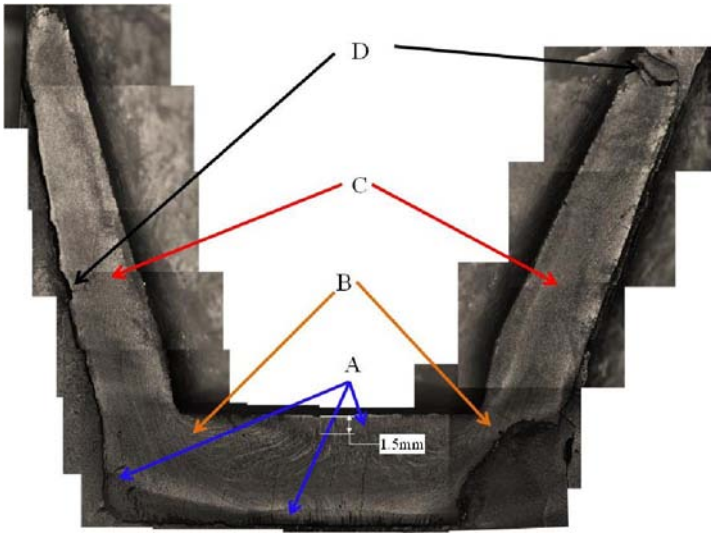

Fig. 4.18. Macrograph of the thixoforged cup (quenched). (A) non-deformed zone, (B) zone equivalent to classical forging, (C) semi-solid zone and (D) defects.

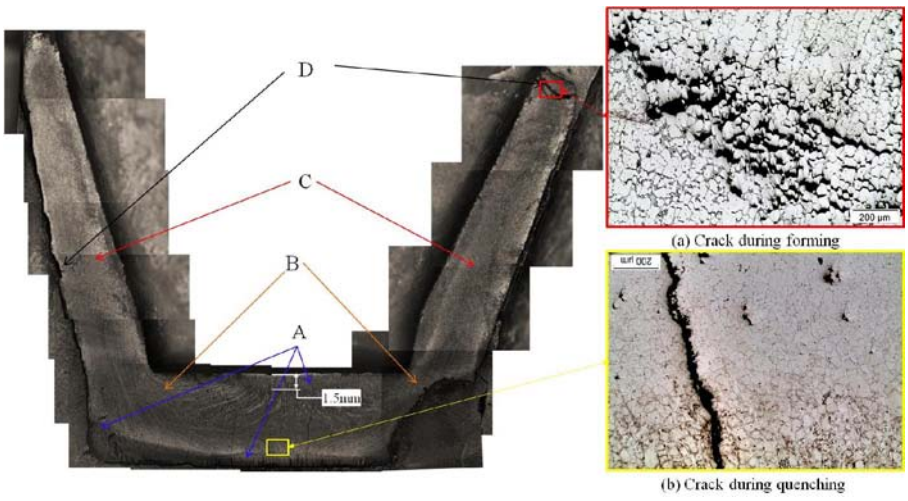

Fig. 4.19. Cracks on the thixoforged cup.

During solidification of material, the cracks may result from the coalescence of the voids as shown in Fig. 4.19 (a). From figure 4.19 (a), it can also be found that the material flow involves not only single grains but also groups of agglomerated grains which still hold together. This may cause more damage in the thixoforged cups.

Internal damage in the form of porosity was also observed in all thixoforged cups, mainly in the solid plastic deformation zones (the bottom of cups). Metallographic observation on the sections along the vertical axis reveals the zones with increased porosity parallel to the loading direction. Fig. 4.20 (a) shows the bands of the internal damage on the M2 cup thixoforged at 1300°C. These bands are symmetrically positioned around the vertical axis of the cup. A typical porosity surface is shown in Fig. 4.20 (b). The thixoforging process with a high solid fraction may be accommodated with several deformation mechanisms: breaking down of the solid skeleton, grain rearrangement and the plastic deformation. With a high forming speed (> 200mm/s), after the breakdown of the solid skeleton, the liquid does not have enough time to flow sufficiently, resulting in undrained zones. During solidification, these liquid zones shrink and form the shrinkage voids.

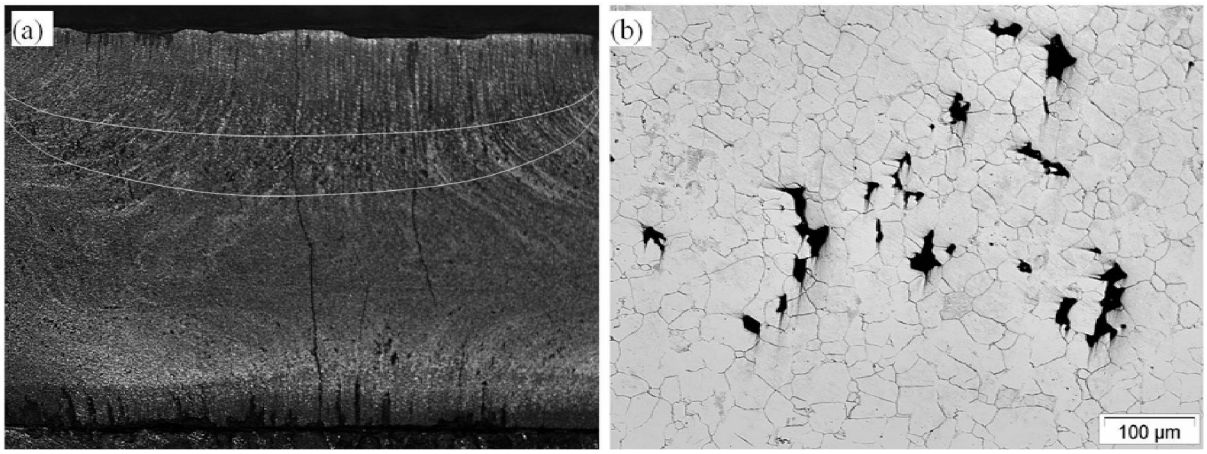

Fig. 4.20. (a) Internal damage zones (shear bands) in M2 thixoforged cup. (b) Optical micrograph of the porosity.

1.5.1. The porosity fraction

Fig. 4.21 summarizes the porosity measurements performed in different regions of the thixoforged cups with different billet temperatures. From the figure, it can be concluded that the pororisity (shrinkage voids) is mainly concentrated at the shear bands. Meanwhile, shrinkage voids can also be observed in the zones where solid plastic deformation occurs. In

addition, the degree of damage decreases with increasing billet temperature. During forming, with increasing liquid fraction, liquid flow paths are easier to be formed which results in less undrained liquid and therefore, in reduced porosities in the cups.

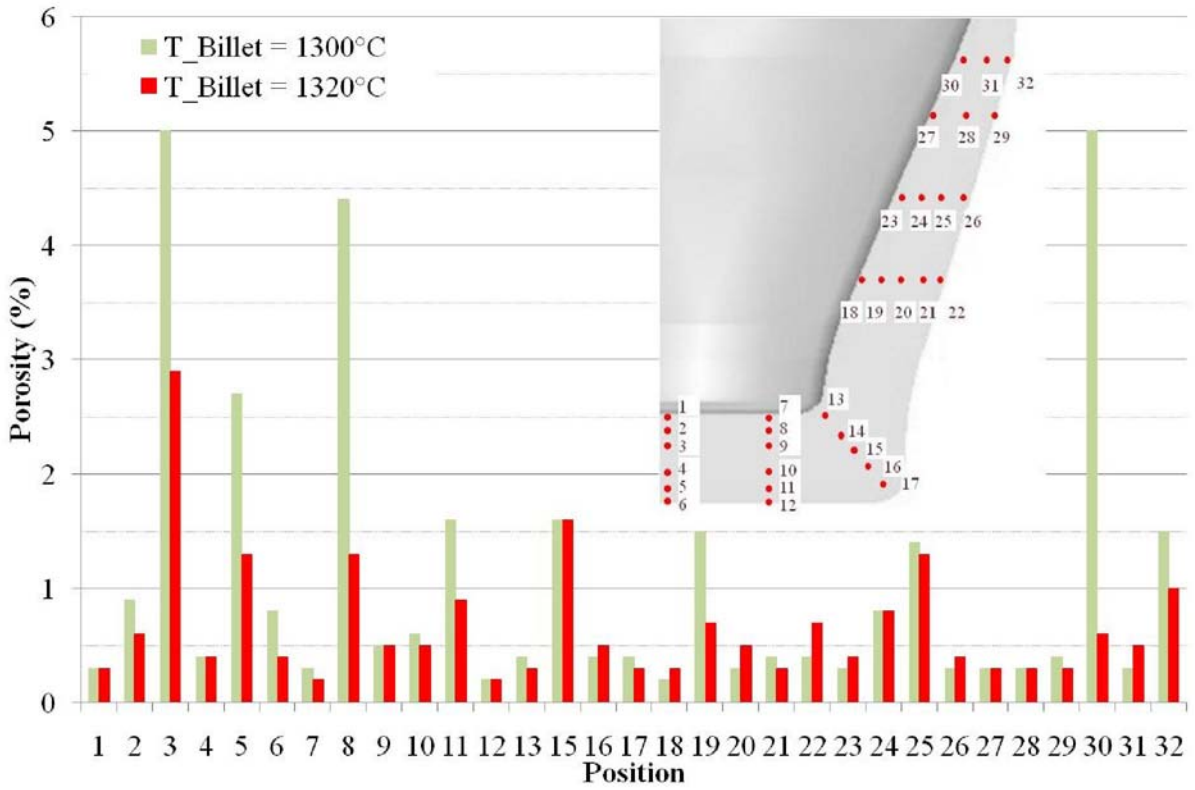

Fig. 4.21. Porosity distribution in the cups thixoforged with various billet temperatures.

Table. 4.5 gives the micrographs in different zones showing the porosities. The general observation is that the porosity level is higher in the solid plastic deformation zones than in the thixotropic flow zone. Another observation considering the pore size is that the average diameter is around 50µm. The porosity can probably be eliminated by maintaining the pressure on the parts during solidification as stated in the experiments of aluminum alloy [6]. We did not perform similar experiments on M2 steel, therefore it is difficult to state the influence of the maintained pressure on the porosity of the thixoforged parts.

Table. 4.5. Quenched microstructure of the thixoforged parts.

Zones	T-billet = 1300°C	T-billet = 1320°C
3	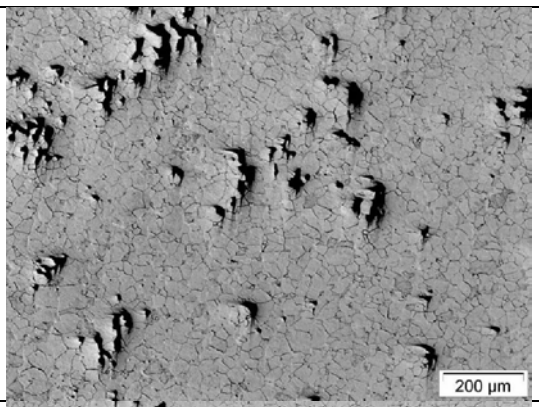	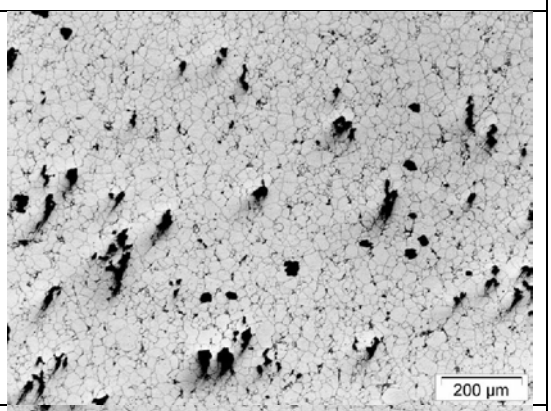
8	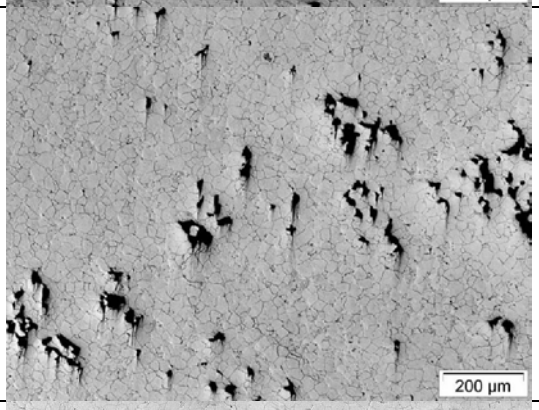	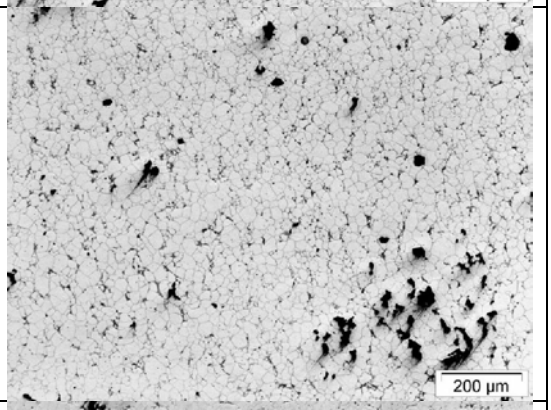
15	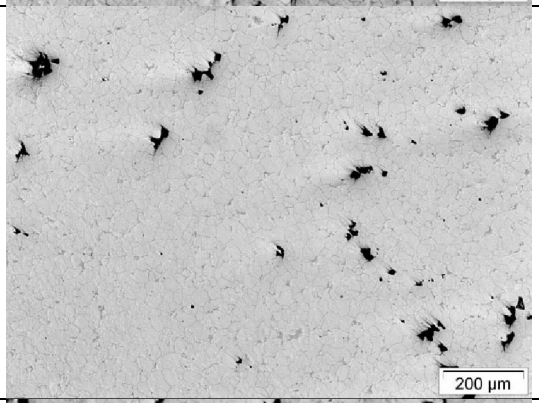	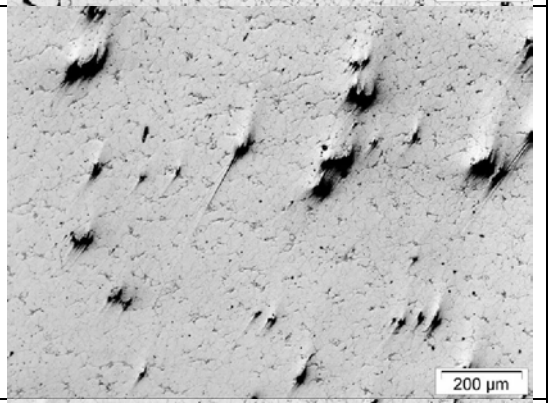
19	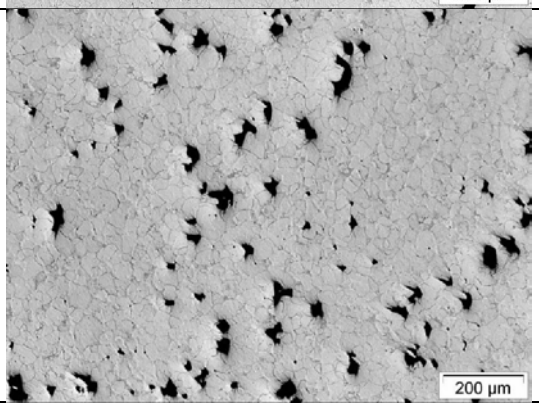	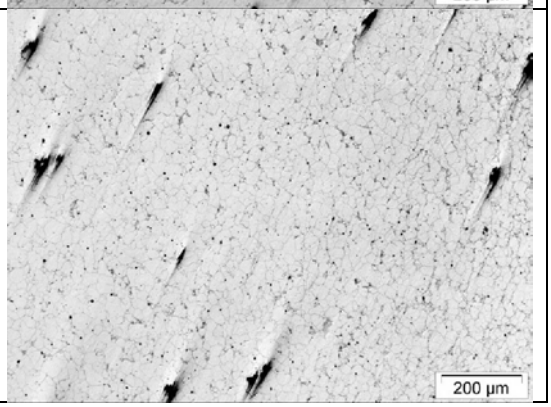

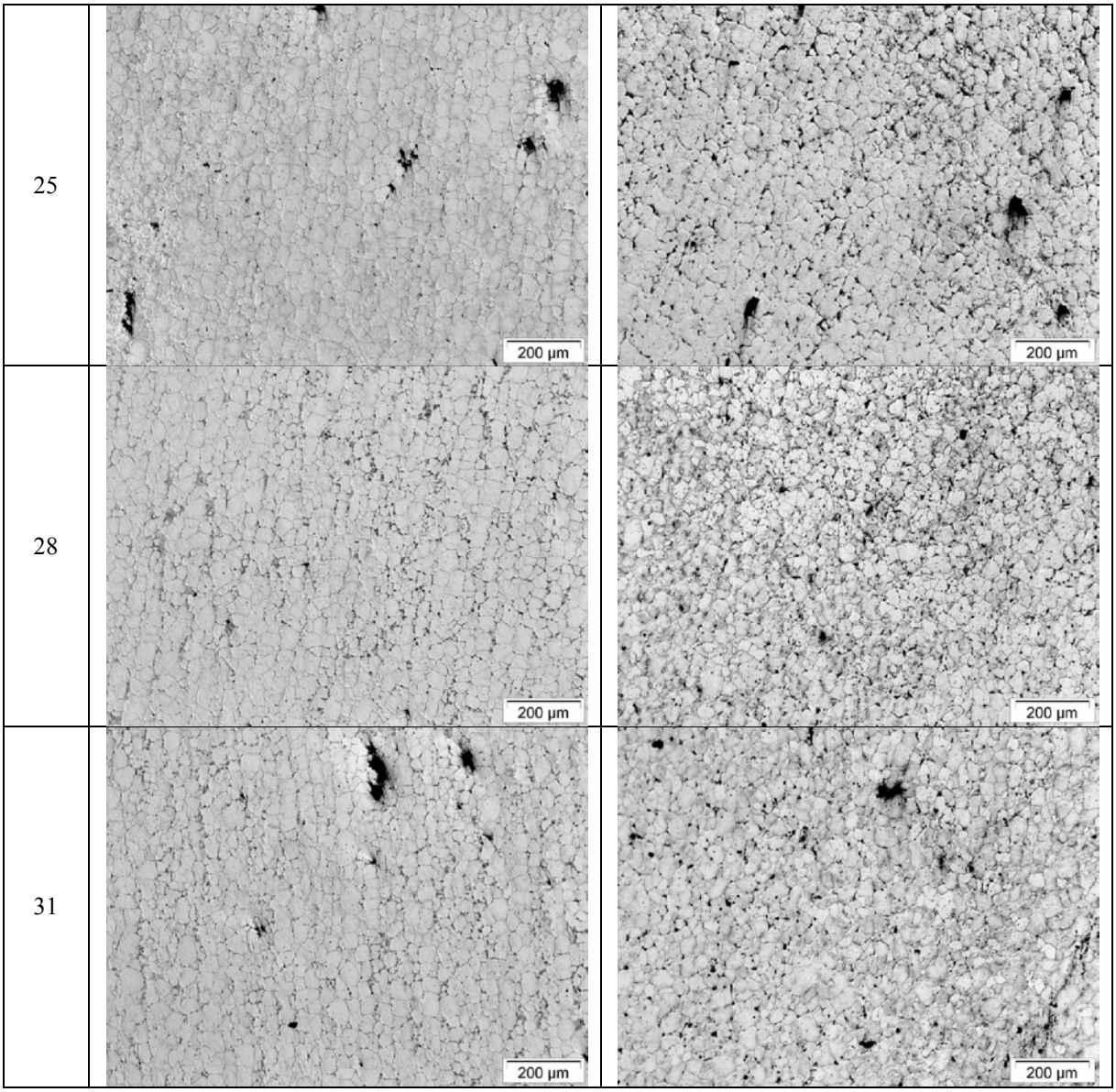

1.5.2. Microstructure characterization on thixoforged parts

Fig. 4.22 shows the typical microstructure in different zones of the quenched thixoforged parts. Different microstructures were observed in various zones. As mentioned before, there are three main different material flow zones on the parts: non-deformed material zone, thixotropic flow zone and solid plastic deformation zone. Depending on the microstructure prior to the thixoforging process and the process conditions, the morphologies at various positions are different in grain size and shape factor.

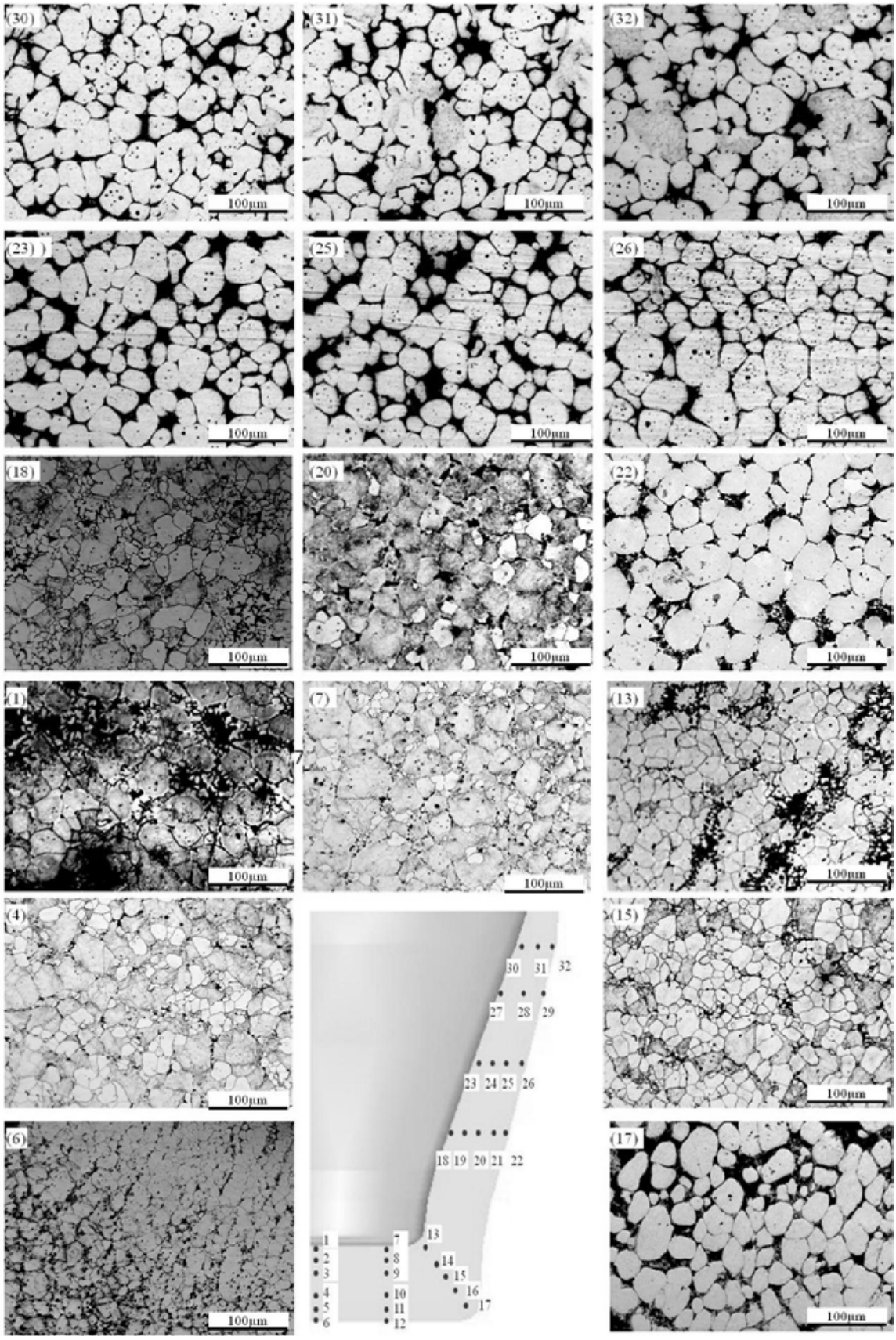

Fig. 4.22. Microstructures of quenched thixoforged cup (T billet = 1320°C).

Combining the results of shape factor shown in Fig. 4.23, there are three main types of microstructure: globular microstructure of solid grains which is similar to the microstructure observed in the billet in the semi-solid state prior to the thixoforging process (in zones 1, 6); microstructure of plastic deformed grains (in zones 4, 7, 13, 15, 18) and the microstructure with globular grains which are surrounded by liquid phase (in zones 22-32). Here, we should also keep in mind the edge effect during induction heating. In the heating process, due to the edge effect, the edge (zone 17) of some billets were over-heated, resulting in the coalescence of grains as shown in Fig. 4.24. During thixoforging, the material in this zone was not deformed, meaning the microstructure stayed the same as the one prior to the thixoforging process.

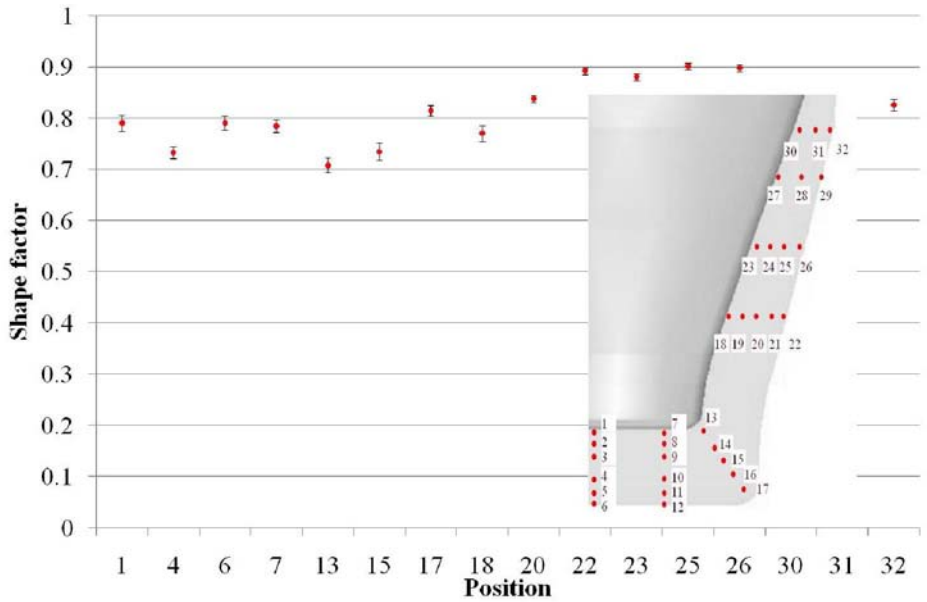

Fig. 4.23. Shape factor of solid grains in different zones.

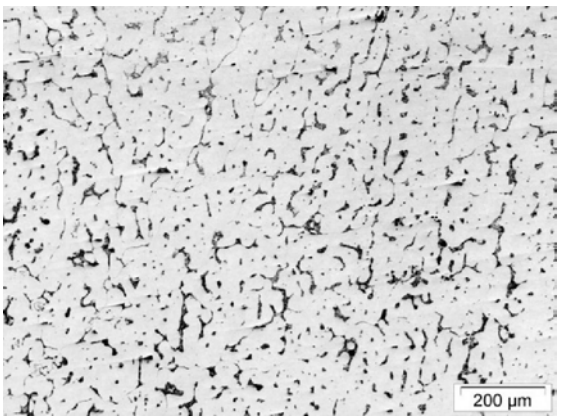

Fig. 4.24. Microstructure in zone 17 (the material in the zone is over-heated).

By quantitative image analysis, the liquid fraction in various zones was obtained. Fig. 4.25 shows the variation of the liquid fraction in different zones of the cup thixoforged at ~1320°C (*Fl* = ~ 21%). It can be found that the liquid fraction in the plastic deformation zones decreases to about 14% while it increases to around 27% in the upper portion of the cup. In addition, the liquid fraction of the zones (1, 6, 7, 13, 17, 18 and 22) which get contact with the dies does not vary a lot. As observed in chapter 3, the former liquid zones could be preserved at a low cooling rate. During the thixoforging process, the liquid zones would be solidified due to the thermal exchange between the material and die.

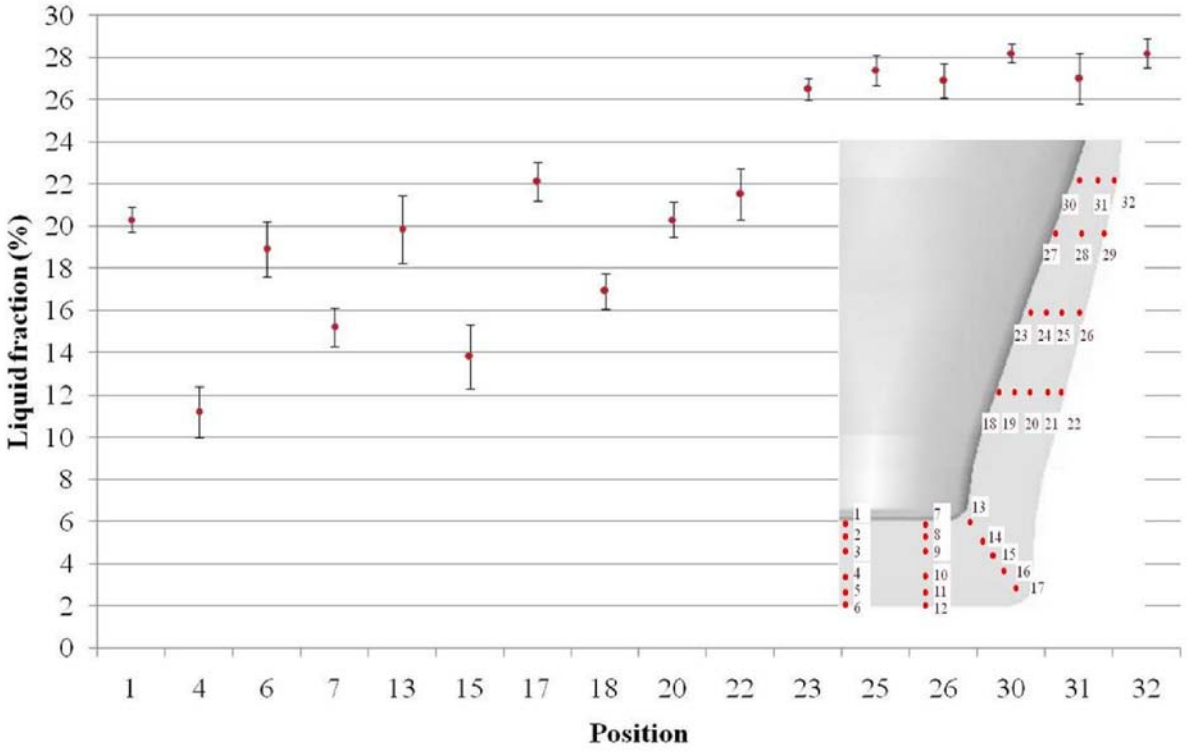

Fig. 4.25. Liquid fraction vs position of the thixoforged part (T billet = 1320°C).

The study of the microstructure results and the liquid fraction in different zones, reveals the presence of the segregations of liquid (mainly in zone 13) and solid (mainly in plastic deformation zone) in the parts. In addition, the results also indicate the coexistence of different deformation mechanisms during thixoforging. Here, we propose five deformation mechanisms which are controlling the deformation of the alloy in the semi-solid state: (1) breaking down of solid skeleton (BS); (2) liquid flow mechanisms (LF); (3) the flow of solid combining with the liquid phase (SLF); (4) sliding among solid grains (SS) and (5) plastic deformation of solid grains mechanisms (PDS).

At the very beginning of the process, due to the low liquid fraction, amounts of unwetted grain boundaries and segregation bands exist in the billet. The dominant deformation mechanism is the breakdown of the solid skeleton mechanism (BS) since the deformation force required for decohesion and overcoming the resistance to shear the broken down structure. As a result, the weakly connected grains are broken. Most of the grain boundaries are wetted by the liquid phase. As the deformation proceeds, the liquid flow is the dominating deformation mechanism (LF) since the forming load is the minimum as shown in Fig. 4.15. The liquid phase is pressed to the edge (like water out of a sponge) resulting in a decrease of the liquid fraction in the center portion. With increasing deformation, the liquid fraction in the center portion of the part decreases. While in the filling portion, the liquid fraction is relatively big. Therefore, in the course of filling, the material flow in the filling portion is mainly driven by the liquid flow combining with the rearrangement of solid grains (SLF). Meanwhile, the flow front area is rich in liquid phase, leading to an increase in liquid fraction (see Fig. 4.22 and Fig. 4.25). Such an increase is related to the cup geometry. The flow front surface area increases with the increasing diameter of the cup. During the filling, the increase can be easily accommodated by the liquid phase, since the liquid is much more fluid than the solid [5]. The liquid segregations are observed in zone 13. During the deformation, the solid grains could come into contact with each other, blocking the flow of the liquid phase. Consequently, the segregation of liquid phase becomes evident. However, the segregation phenomenon remains small because of the low quantity of liquid. The liquid fraction of the center portion decreases with increasing deformation. When the solid grains start coming into contact with each other, the SS and PDS mechanisms prevail. From the curves of forming load as a function of displacement, it can also be concluded that the forming load for plastic deformation of grains is much higher than for grains sliding and liquid flow. At the end of deformation, the plastic deformation is the prevailing mechanism in the center portion as shown in Fig. 4. 23. The deformed grains are observed in the center portion (at the bottom of the cups).

The influence of the liquid fraction or the billet temperature on the distribution of the dominance of each deformation mechanism can be deduced from Fig. 4.15. All the five deformation mechanisms appear in sequence as the deformation strain increases, even at the highest billet temperature, which is not shown in Fig. 4.15. At the beginning of the deformation, the prevailing mechanism is always the BS mechanism. In addition, the BS

mechanism dominates a relatively similar amount of deformation regardless of the liquid fraction. The difference in this stage lies in the values of the forming force. Once the solid skeleton is broken down, the solid grains are surrounded by liquid: the dominant mechanisms are then LF and SS mechanisms. At a higher billet temperature or a higher liquid fraction, the LF and SS mechanisms prevail on a relatively larger amount of deformation and are followed with the PDS mechanisms as the dominant mechanism.

1.6. Conclusions

The thixoforging experiments are carried out under various process conditions, mainly at different billet and die temperatures. The material is successfully thixoforged in the semi-solid state at the processing temperature interval, ranging from 1290-1340°C. It seems that the influence of the die temperature (below 350°C) on the material flow is not significant.

The forming load can be reduced with increasing billet temperature. By analyzing the curves of thixoforming load as a function of displacement, it can be indicated that there are several deformation mechanisms: (1) breakdown of solid skeletons at the beginning of the forming; (2) Liquid-like flow; (3) liquid-like flow combining with sliding and rotating of solid grains (4) grains sliding and rotating between each other and (5) plastic deformation of grains. In order to achieve complete die filling with a relatively low forming load, it would be desirable to have a low structure breaking down load and a larger thixotropic flow deformation with a relatively constant thixotropic flow load. When comparing the numerical results of hot forging process and the experimental results of the thixoforging process, there is a big difference in material flow, since the semi-solid material has a unique thixotropic behavior: the viscosity decreases with increasing shear rate.

As it is possible to preserve the microstructure of M2 in the semi-solid state by water quenching, the material flow and microstructure evolutions during the thixoforging process can be studied.

- The heterogeneous flow during thixoforging has been observed. There are several possibilities which may lead to the heterogeneous flow. First, a perfect homogeneous temperature distribution throughout the billet is not obtained in the induction heating state. Combined with the impact of the manufacturing process (rolling process), which leads to the segregation of carbides bands in the material, a heterogeneous liquid

fraction distribution or a heterogeneous microstructure can be obtained. The difference in liquid fraction may lead to a big influence on the material behavior, resulting in a heterogeneous flow. Secondly, during the transferring and thixoforging stages, the material which is in contact with the die solidifies quickly due to the thermal exchange. In these zones, a material flow which is similar to that obtained in classical forging process can be obtained. Thirdly, owing to the heterogeneous distribution of liquid phase throughout the billet, the die geometry and the processing diameter etc, the liquid segregation or liquid ejection has been observed in the thixoforged parts. The segregations or liquid ejections may indicate that the local microstructure influences the local material behavior greatly, which in turn affects the material flow.

- The microstructure evolution during processing can also be analyzed thanks to the efficient cooling rate for preserving the microstructure of the material in the semi-solid. The microstructures (grain size, shape factor, liquid fraction etc) at various positions are different, which is affected by the process parameters. According to the difference in the microstructure in various positions, the semi-solid deformation mechanisms are proposed to be five major mechanisms: (1) breakdown of solid skeletons (BS); (2) liquid flow (LF); (3) the flow of solid combining the liquid phase (SLF); (4) sliding among solid grains (SS) and (5) plastic deformation of solid grains (PDS). Here, the mechanisms mentioned above may not occur everywhere in the billet during forming. However, they may exist during the whole forming process, but the dominated prevailing change during the thixoforging process, depending on the liquid fraction and deformation state.

2. Thixoforming of other steel grades

The thixoforging experiments were also performed on other steel grades (100Cr6, C38LTT) to produce different parts with various geometries. As stated by many researchers [2, 7-12] that the process parameters, such as the forming speed, the billet temperature and the die temperature have a major influence on the flow and the load. Particularly, thermal exchanges influence the material flows and local mechanical properties. Here, we mainly focus on the effects of thermal exchange on the microstructure and mechanical properties and on understanding the relation between the mechanical properties and microstructure.

2.1. Thixoforged parts of 100Cr6 steel grade

A rolled 100Cr6 bar of 30mm in diameter was extruded under various process conditions with an extrusion set-up shown in Fig. 4.26 [2]. The extrusion die was axisymmetric. The container was 40mm in diameter. The extrusion is 12mm in diameter (extrusion ratio = 0.3). The cone angle is 30◦. The slug was placed on an Inconel piston. A Nefacier1500 disc (based on ceramic fibrous with low content of non-fibrous ceramic grains) was placed between the piston and the slug to reduce heat losses during the induction step. The material of the die was Inconeland the container was X38CrMoV5 tool steel.

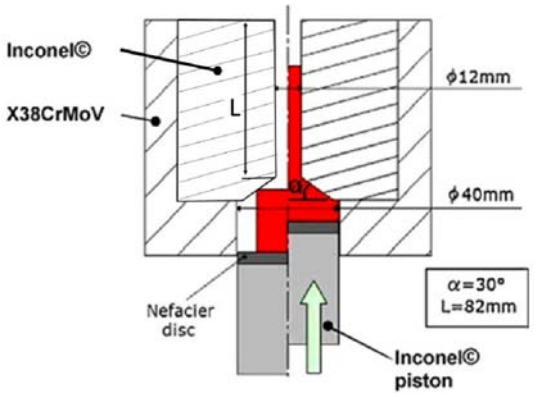

Fig. 4.26. Principle of the extrusion experiments.

The experiments were performed under various process conditions. Table. 4.6 gives the various process parameters used for extrusion.

Table. 4.6. Experimental conditions.

Punch speed (mm/s)	Die temperature (°C)	Billet temperature(°C)
200	30-400	1240-1276

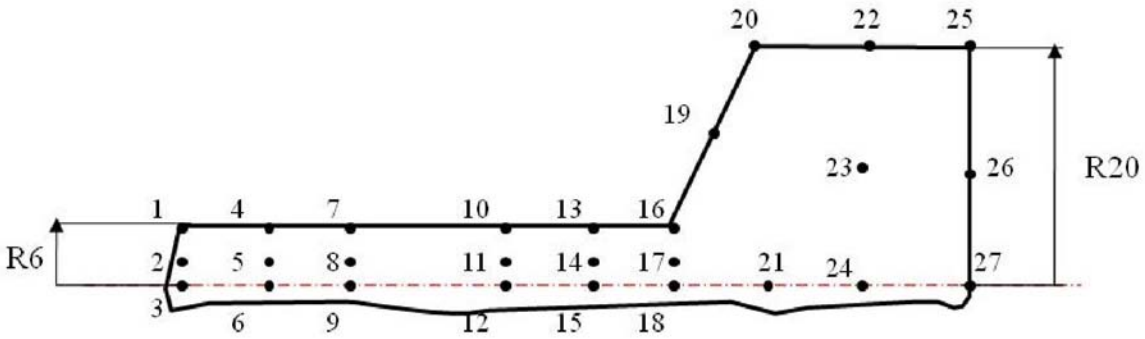

Fig. 4.27. Location of studied points of extruded parts.

Fig. 4.27 presents the positions which are defined by numbers for hardness and microstructure studies.

2.1.1. Material flow

Fig. 4.28 shows the macrographs obtained by HCL etching of two parts formed under various conditions: both parts were formed at a punch speed of 200mm/s. However, Part 1 was formed at 1240°C with a cold die and Part 2 was formed at 1276°C with a die temperature of 400°C.

Three different zones (termed as A, B and C in Fig. 4.28) were observed on the parts. Zone A exhibits a weak flow. The material is still in contact with the die. Zone B presents a material flow which is similar to that of semi-solid forming. In this zone, the fibers are not observed but material waves are. Area C illustrates an axial flow which is similar to that of the classical extrusion.

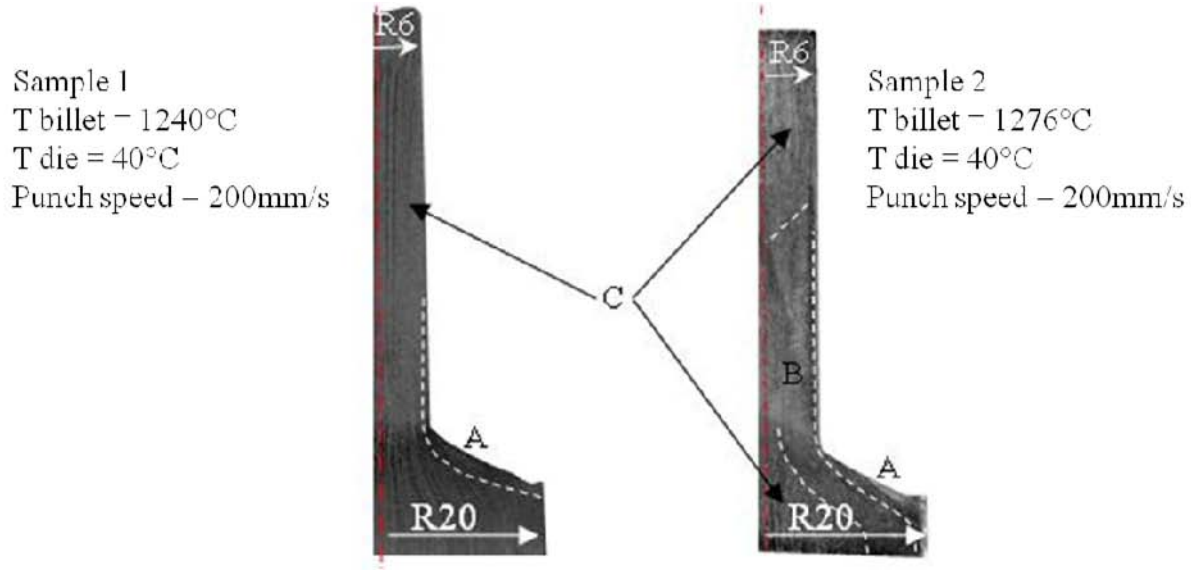

Fig. 4.28. Material flows of extruded parts.

During the extrusion, the billet temperature of Part 1 was 1240°C which is under the solidus temperature of 100Cr6. Therefore, the axial flow was observed in the part. For Part 2, the axial flow was also observed but not through the whole part. Zone B exhibits radial undulations which correspond to a semi-solid material which is useful to feed the whole shape. The axial flow in Part 2 is caused by the thermal exchange between die/piston and billet. Prior to the extrusion process, the material was aimed to be heated to the semi-solid state. However, due to the thermal exchange between the billet and the piston, the material

which is in contact with the piston remains in the solid state. During extrusion, the semi-solid material which is in contact with the die surface was solidified quickly and extruded in the solid state. Therefore, the classical extrusion flow was observed at the end of Part 2 (Zone C).

By comparing the material flows of these two parts, the thickness of zone A is not significant. Becker [2] has numerically and experimentally compared the thickness of Zone A of two thixoextruded parts under various die temperatures. It has been stated that the thermal exchange greatly influences the thickness of Zone A. During forming, the higher level of thermal exchange between die and billet results in a larger amount of solidified material in Zone A. Since the semi-solid material is much more fluid than the solid material. Hence, a thicker Zone A can be obtained when forming with a cold die. Here, in our case, the thixoextruded part has similar material flows to that in Ref. [12]. The thickness of Zone A in Part 2 is small due to a small thermal exchange between the material and die.

2.1.2. Microscopic analysis of the extruded parts

The parts were sectioned in half. The microstructures in different points of these two thixoforged parts are shown in Table. 4.7.

Due to the insufficient cooling rate after extrusion, the microstructure in the semi-solid state can not be preserved. There were liquid/solid and solid/solid phase transformations. Because of thermal exchange between the material and die during extrusion process, the cooling rate varies at different positions. Hence, different structures are observed at different positions. When observing Part 1, which is formed with a cold die, martensitic structure (positions 4-12) is observed at the top, which is due to high cooling rate; whereas during forming, the heat induced by friction and metal forming, slows the cooling rate. With an average or a low cooling rate, the structure mainly consists of pearlite and cementite outlining the grain boundaries. Part 2 was formed with a warm die. During extrusion, the thermal exchange is relatively low, which results in a relatively smaller martensite zone.

Table. 4.7. Micrographs for two extruded parts at various positions.

Position	Part 1 T billet = 1240°C, T die = 40°C		Part 2 T billet = 1240°C, T die = 40°C	
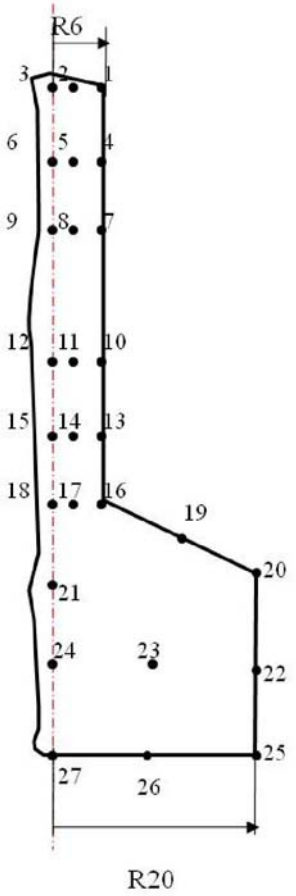	(4) 40µm	(6)	(4)	(6)
	(7)	(9)	(7)	(9)
	(10)	(12)	(10)	(12)
	(13)	(15)	(13)	(15)
	(16)	(18)	(16)	(18)
	(19)	(20)	(19)	(20)
	(22)	(24)	(22)	(24)

Hardness of extruded parts

The hardness of extruded parts was analyzed by Vickers hardness tests under a 1 kg load. Fig.4.29 sums up the variation of the hardness through the parts. The hardness at the top the parts is higher than that at the bottom.

By comparing the hardness of the parts extruded with a warm die (400°C) and a cold die (40°C). The values of hardness at different zones of the parts extruded under various process conditions vary greatly.

The hardness of the part extruded with a warm die is relatively smaller and uniform, because the thermal exchange between material and die is relatively small. Meanwhile, it can also be concluded that the hardness decreases with decreasing cooling rate. In the center of the parts, the material remains at high temperature for a long time, the cooling rate is the lowest. The structures of various points (Table. 4.7) agree with the hardness results.

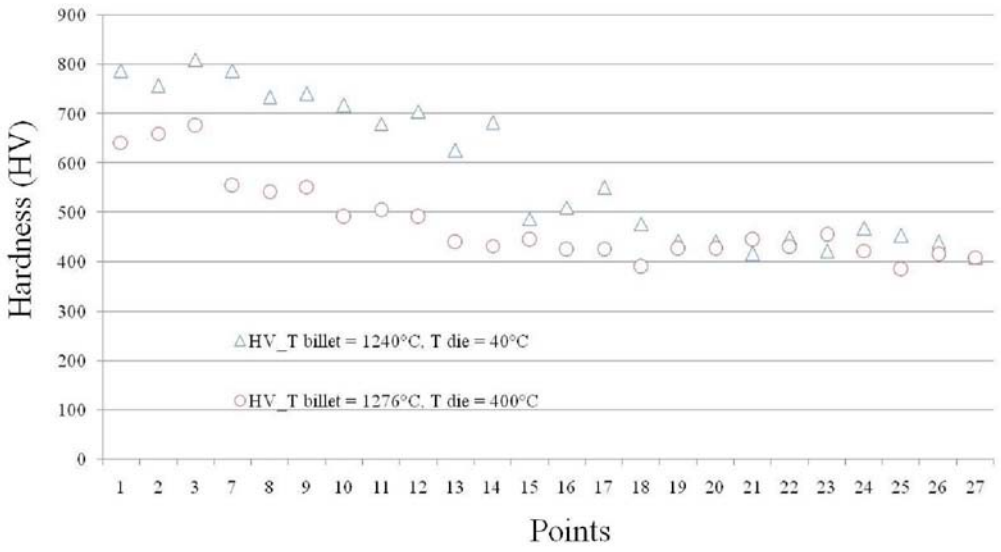

Fig. 4.29. Variation of Vickers hardness of the parts extruded under various conditions.

2.2. Thixoforged parts of C38LTT steel grade

C38LTT was studied for the purpose of industrial application of the thixoforging process. Here, the C38LTT was thixoforged at Thixofranc in the temperature range of 1410°C-1450°C. Depending on the billet temperature, a good final part shape could be obtained when formed in the billet temperature interval of 1410°C-1430°C. Several thixoforged parts were studied, trying to characterize the microstructure and mechanical properties.

The geometry of the part was not symmetric; therefore, the parts were longitudinally sectioned in two different directions as shown in Fig. 4.30.

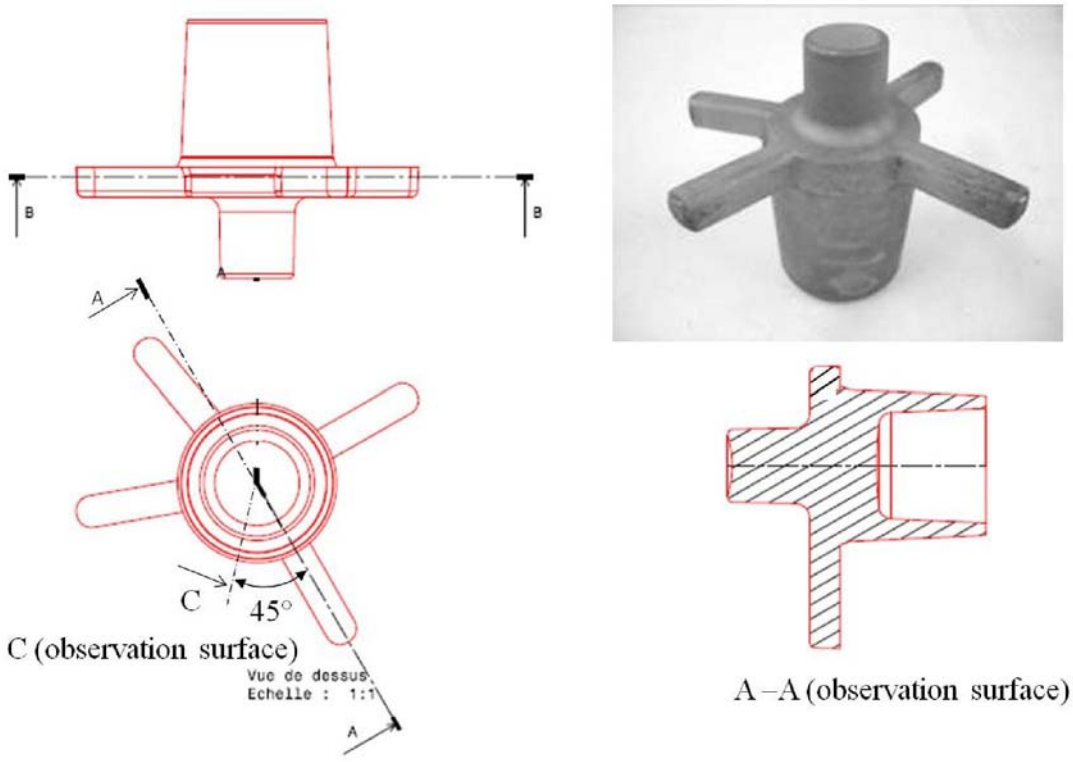

Fig. 4.30. Observation surfaces for micro-macro structure characterization.

2.2.1. Macrographic analysis

Fig. 4.31 presents the macrographs of two parts which are thixoforged under different billet temperatures. The macrostructures are revealed by HCL etching at ~70°C. By comparing the macrographs, it can be easily seen that there are two different material flows across the thixoforged parts. The segregated bands which correspond to the original state of the rolled bar were observed in Fig. 4.31 (a). The semi-solid material flow was presented in the center of the part when forming at a higher billet temperature (Fig. 4.31 (b)). In addition, the cracks were also observed in Fig. 4.31 (b).

For the part thixoforged at 1420°C, the semi-solid zone could not be detected on macrographs as shown in Fig. 4.31 (a). Due to the insufficient cooling rate, the liquid phase can not be determined on quenched parts. However, from the DSC curve of the C38LTT, the liquid fraction is around 8% at 1420°C. When forming the material at 1420°C, the liquid phase may not be sufficient for the arrangement of solid grains during the process, resulting in the material flow which is similar to that of classical forging process. For the part formed at

1450°C, the cracks were observed in the semi-solid zone, mainly located at the interface of the semi-solid zone/ the weak material flow zone, and the center part of the semi-solid zone.

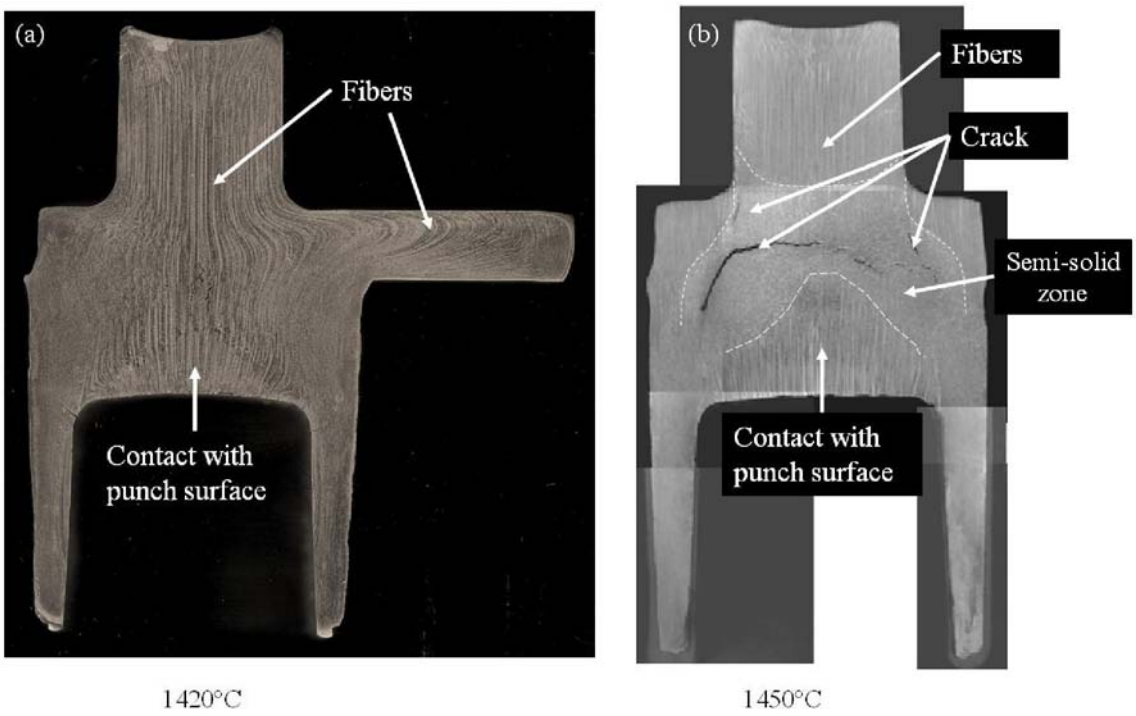

Fig. 4.31. Macrographs of the parts thixoforged under different billet temperatures (a) T billet = 1420°C and (b) T billet = 1450°C.

As shown in Fig. 4.32 (a), the fluidity of the semi-solid material is much better than that of the solid zone, during the forming process, the material may be torn up at the interface of the semi-solid zone and the solid zone. The cracks in the center of the semi-solid zone may result from the segregation of liquid phase [13] and the thermal contraction stress associated with the solidification shrinkage .

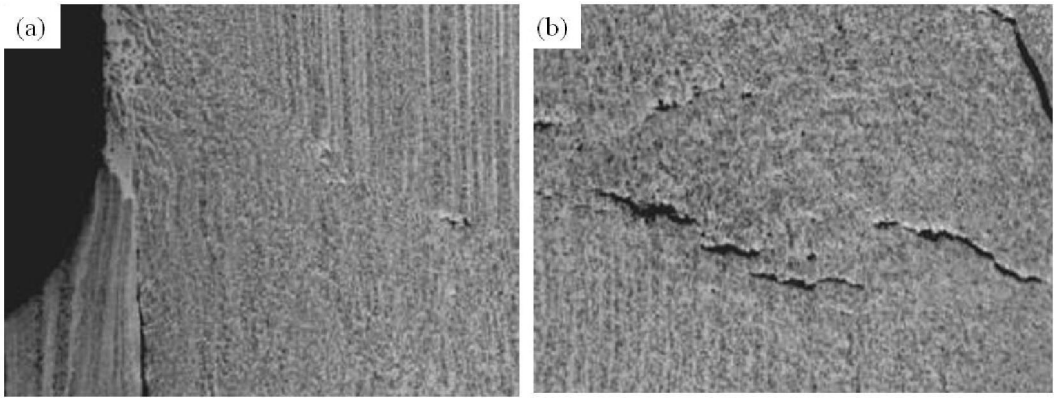

Fig. 4.32. Macrographs of the semi-solid zone in the part formed at temperature 1450°C.

2.2.2. Microstructure analysis

The microstructure was analyzed at various positions on the thixoforged parts under different conditions (by air cooling and quenching), shown in Fig. 4.33. Due to the special chemical elements in the material, elongated MnS inclusions were observed and confirmed by the EDS. Both non-deformed and deformed inclusions were observed as presented in Fig. 4.34.

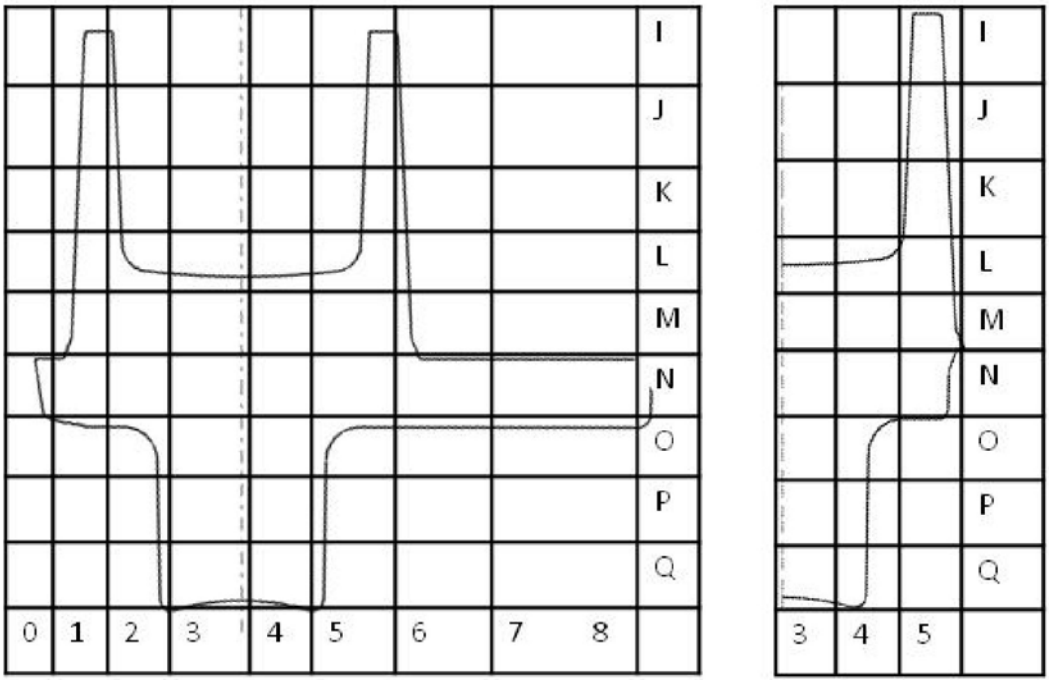

Fig. 4.33. Microstructure observation positions.

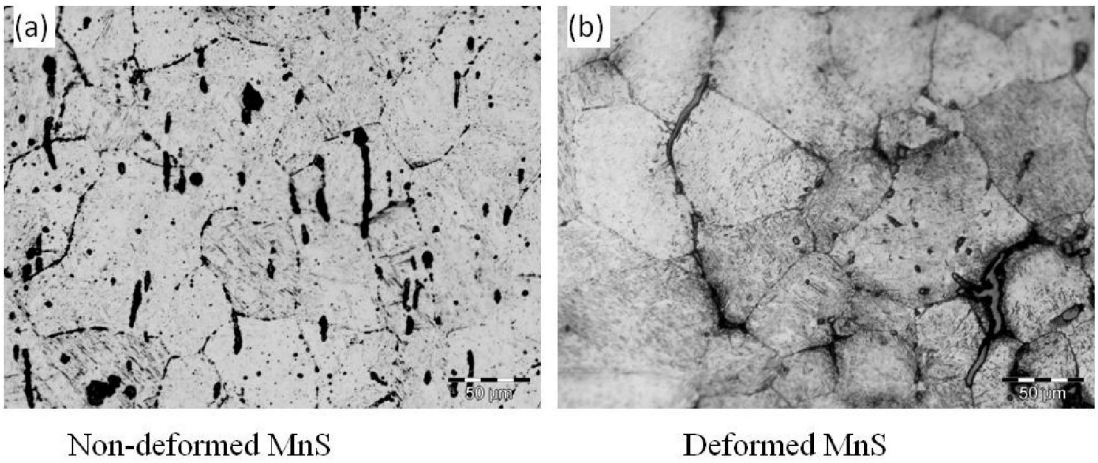

Fig. 4.34. MnS inclusions observed in the thixoforged parts. (a) Non-deformed MnS and (b) deformed MnS inclusions.

From the results of CLSM in situ observation on C38LTT, it can be concluded that in the semi-solid state, the MnS inclusions were not totally dissolved. During forming, the MnS inclusions located in the matrix were not deformed (Fig. 4.34 (a)), while the MnS inclusions located in the grain boundaries were deformed with the arrangement and the deformation of the solid grains (Fig. 4.34 (b)). During the preparation of the thixoforged parts for microstructure observation, as the inclusions are very brittle, they are easily broken and removed from the parts during polishing, leading to the voids. Therefore, the microporosities observed on the thixoforged parts could not be confirmed (Fig. 4.35) whether they are MnS inclusions or microporosities.

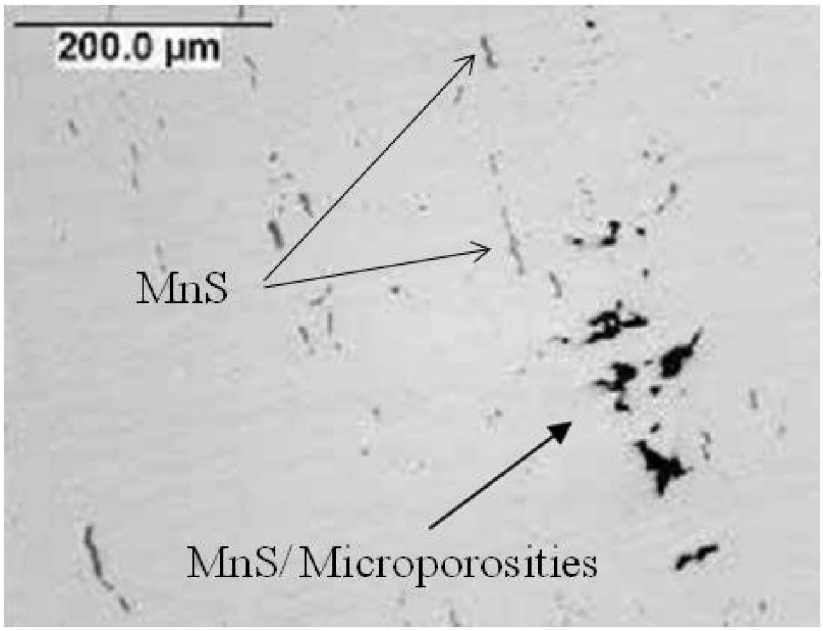

Fig. 4.35. Micrograph before etching.

In general, the microstructures at various positions of the thixoforged parts which are cooled by air are similar (Table. 4.8): ferritic-pearlitic with numerous MnS inclusions on grain boundaries and inside ferrite grains. The near surface microstructure exhibits more ferrite, which corresponds to the decarburization (I1, J1, K1, L1, M1, N1, O2, P2, Q2, Q3). During heating, the billet surface decarburizes as it is in contact with the atmosphere. The depth of the decarburization is around 80µm.

Table. 4.8. Microstructure of the thixoforged parts at different positions. (air cooling)

I1	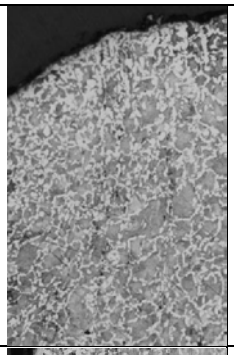	J1	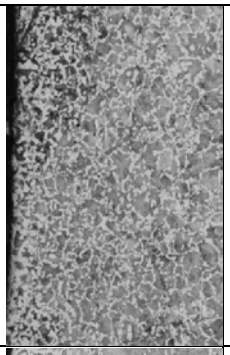	K1	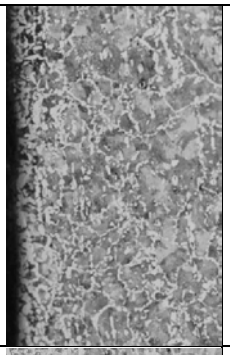	L1	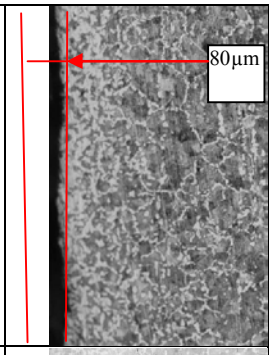
M1	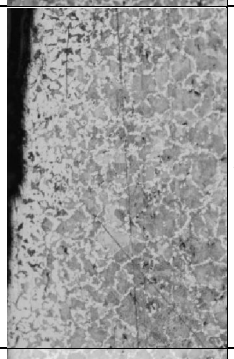	N1	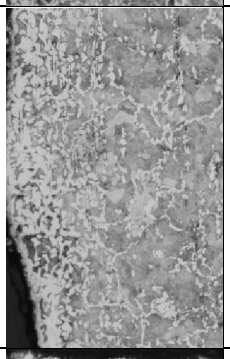	O2	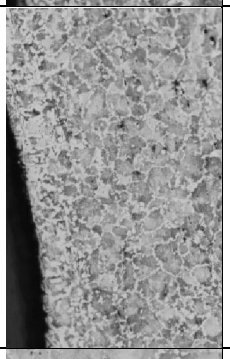	P2	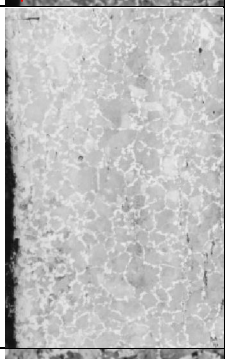
Q2	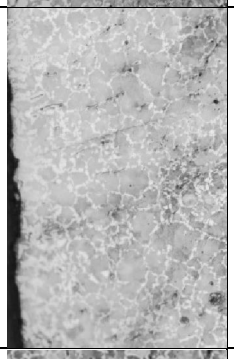	L3	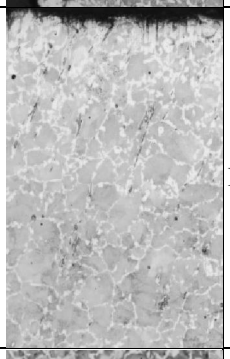	M3	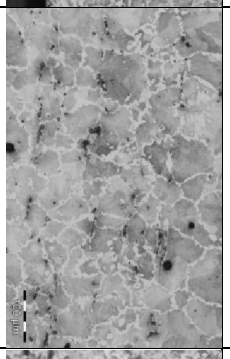	N3	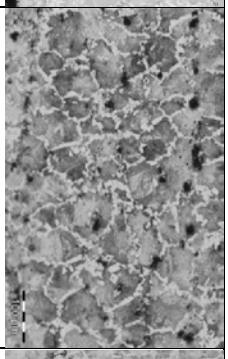
O3	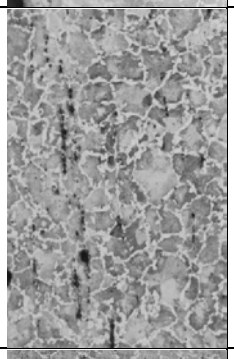	P3	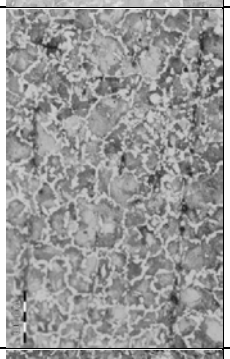	Q3	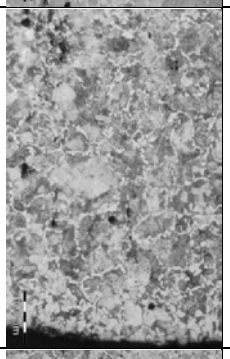	N4	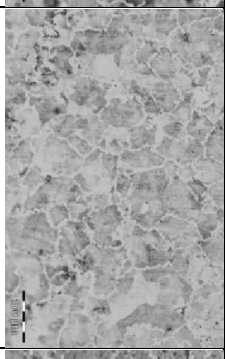
N5	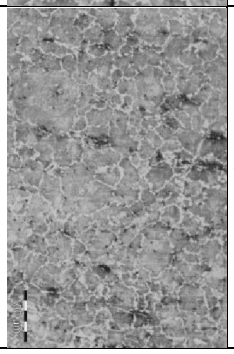	N6	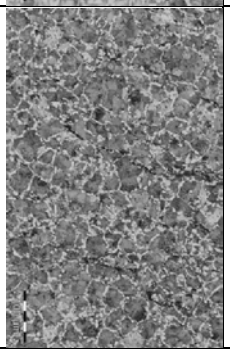	N7	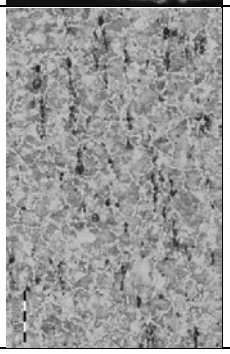	N8	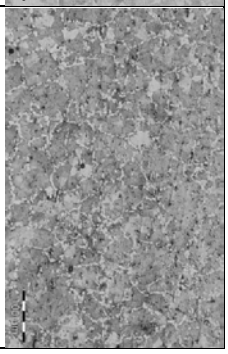

The estimation of grain size was carried out on quenched parts adopting the mean lineal intercept method as outlined in ASTM E112-96. The parts were etched by the etchant Béchet-Beaujard. Fig. 4. 36 presents the microstructure of a quenched part. Both large grains and small grains are observed in large quantities. The average big grain size is ~103±13µm while the average small grain size is ~ 76± 8µm. In addition, by comparing the average grain size of the thixoforged parts under different initial billet temperatures, few differences are observed, which means the initial billet temperature does not have a great influence on the grain size.

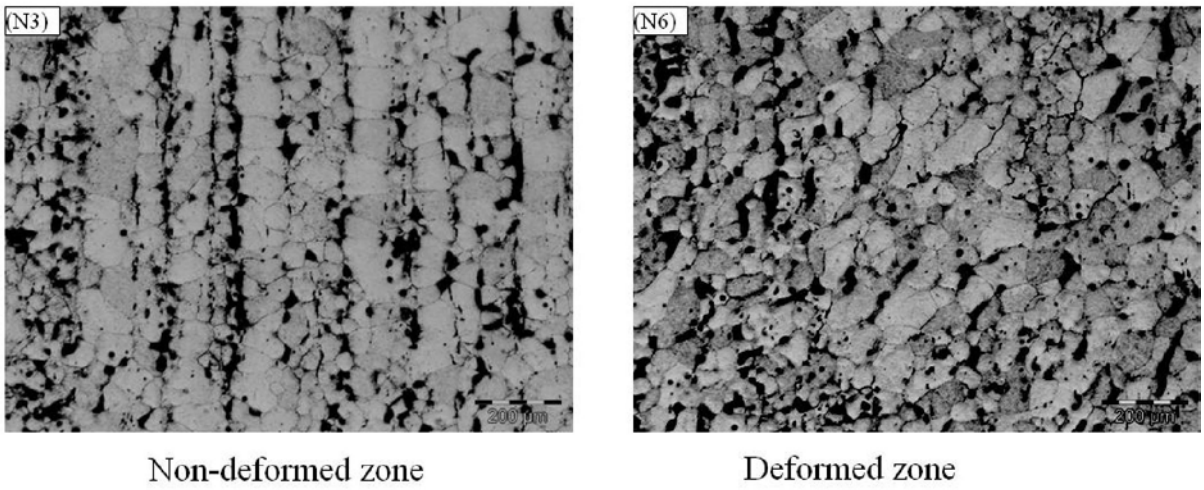

Fig. 4.36. Microstructure of (a) non-deformed zone and (b) deformed zone.

2.2.3. Mechanical properties

The hardness of the parts thixoforged at the billet temperature of 1420°C was analysed by Vickers hardness tests, because the microstructure of the parts formed under various billet temperatures is similar. Vickers hardness tests were carried out under a 3 kg load, dwell time of 10s. Table. 4.9 presents a summary of the hardness results at various positions, corresponding to Fig. 4.33. It can be seen that the variation of the hardness is small. Similar results were obtained by CREAS. In addition, the hardness of the part which was normalized at 950°C for 2h was also carried out at CREAS. After normalization, the hardness decreases to ~270 – 290 HV. Meanwhile, the ultimate strength of the parts was also obtained at CREAS. Table. 4.10 summaries the mechanical properties of the thixoforged parts after air cooling and after normalization. As stated by CREAS, the mechanical properties of the thixoforged parts were improved as compared to that of the classical forged parts.

Table. 4.9. Hardness of thixoforged part (T billet = 1420°C).

	0	1	2	3	4	5	6	7	8
I		325.6				315.5			
J		324.9				313.8			
K		318.9				312.3			
L		323.4	326.9	305.5	335.3	316.8			
M		323.4	308.4	318.8	307.5	312.5			
N	318.8	313.8	314.1	324.0	316.4	311.4	314.3	313.7	314.2
O			324.9	304.3	311.2				
P			316.1	301.9	319.5				
Q			318.3	306.1	318.8				

Table. 4.10. Mechanical properties of the thixoforged parts.

		HV	HRC	Rm (MPa)
Thixoforged part after air cooling	Body	302	29.8	950
	Arm	317	31.9	1000
Thixoforged part after normalisation	Body	271	26	850
	Arm	297	29.3	931

2.3. Conclusions

It is not possible to observe the microstructure of the material in the semi-solid state by quenching because of the insufficient achievable cooling rate and the metallurgy of the material. The melting mechanisms of 100Cr6 and C38LTT are not the same as those of M2, the liquid phase is not obtained by the melting of alloying elements carbides.

The study on the material flow and the microstructure of the thixoforge 100Cr6 parts shows that the heterogeneous material flow has been observed in the extruded parts. Three material flow zones (small deformation zone, classical hot forging zone and the semi-solid forming zone) have been investigated. Different material flow zones may result from the thermal exchange.

- Classical hot forging material flow zone. During forming, at the interface of the material and the die and air, the material is cooled to the solid state by the heat transfer between the material and die, and the material and air, therefore, a classical material flow of hot forging is observed near the interface of the die and material and at the top of the extruded parts.
- The less deformed or non-deformed zone in the cone. The material in this zone is in the solid state due to the heat exchange between the material and die. During forming, the

semi-solid materials are mainly deformed, since the material always follows the minimum energy paths.

- The semi-solid material flow zone. During forming, the material inside the billet is still in the semi-solid state. Therefore, a semi-solid material flow zone is observed inside of the extruded parts.

By studying the results of parts (C38LTT) thixoforged for Thixofranc project, the results show:

- the possibility to thixoforge a complicated part in one operation.
- hot cracks that can occur when the forming temperature exceeds the critical temperature (1450°C).
- heterogeneous material flow which is similar to that of thixo-extruded 100Cr6 parts.

The full filling of the material in the portion of arm may result from several effects. First, when the material comes into contact with the die, the material at the interface is cooled to the solid state due to the heat transfer. However, energy will be generated due to the friction and the dispersion of the material at the entrance of the arm. Therefore, the material will remain in the semi-solid state, or even with a higher liquid fraction. As a result, the arm cavity can be fully filled by the semi-solid material.

3. Conclusions

In chapter 3, the microstructures of the material in the semi-solid state are studied by various techniques. In this chapter, the study is mainly dedicated to the thixoforging experiments.

As presented in chapter 3, it is possible to observe the microstructure of the M2 grade in the semi-solid state at room temperature, but it is impossible for 100Cr6 and C38LTT. Thixoforging of M2 doesn't present a great industrial interest. However, we performed the thixoforging experiments on M2 steel grade in order to study the material flow, microstructure evolution etc during thixoforging process. M2 is utilize as a model material. At the same time, the thixoforging experiments of C38LTT and 100Cr6, which are most preferred material in industrial applications, were carried out in Thixofranc. An automobile-like component (C38LTT) with a complex geometry has been thixoforged under industrial conditions in Thixofranc.

By analyzing the microstructure of thixoforged M2 parts, the mechanisms of material flow during the thixoforming process were proposed: (1) breakdown of solid skeleton at the beginning of the forming, (2) liquid-like flow, (3) liquid-like flow combining with sliding and rotating of solid grains, (4) solid grains sliding and rotating between each other and (5) plastic deformation of grains. The mechanisms may also be applied to the thixoforging of C38LTT and 100Cr6.

After studying the results of thixoforged parts in different aspects (microstructure, material flow, mechanical properties etc), the heterogeneous material flows were observed in all the thixoforged parts. The parts exhibit different material flow zones, these last ones being influenced by the process conditions. The heterogeneous material flow may result from the material behavior which is affected by the material temperature, the microstructure of the material etc. The heterogeneous temperature distribution can result from the induction heating process due to the penetration depth and the edge effect. Therefore, the local material behavior varies with material temperature, resulting in a heterogeneous material flow. Meanwhile, the thermal exchange between the material and dies can also lead to a heterogeneous temperature distribution of the material. For example, the material which is in contact with the die solidifies quickly by the thermal exchange, leading to a hot forging material flow. The heterogeneous microstructure which results from the manufacturing

process or the induction heating process, may also affect the material flow. Because the heterogeneous microstructure can cause the difference in local liquid fraction, which in turn influences the material behavior. Because of the thixotropic effect and the heat due to deformation energy dissipation, to plastic shear is associated to a softening of the material (decrease of the viscosity due to thixotropic effect and increase of the liquid fraction).

This is very different from the hot forging process. During the thixoforging process, the local material behavior may change significantly, which is affected by the thermal exchange, thermal distribution, material dispersion, etc. Therefore, it is necessary to have an accurate control on all aspects (thermal exchange, thermal distribution, material dispersion, etc.) for the thixoforging experiments and simulations.

References

1. Rouff C: **Contribution à la caractérisation et à la modélisation du comportement d'un acier à l'état semi-solide. Application au thixoforgeage.** Thesis. L'Ecole Nationale Supériure d'Arts et Métiers, Docteur de L'Ecole National Supérieure d'Arts et Métiers; 2003.

2. Becker E, Bigot R, Langlois L: **Thermal exchange effects on steel thixoforming processes.** *The International Journal of Advanced Manufacturing Technology* 2009, **48:**913-924.

3. Becker E, Favier V, Bigot R, Cezard P, Langlois L: **Impact of experimental conditions on material response during forming of steel in semi-solid state.** *Journal of Materials Processing Technology* 2010, **210:**1482-1492.

4. Tzimas E, Zavaliangos A: **Mechanical behavior of alloys with equiaxed microstructure in the semisolid state at high solid content.** *Acta Materialia* 1999, **47:**517-528.

5. Neag A, Favier V, Bigot R, Pop M: **Microstructure and flow behaviour during backward extrusion of semi-solid 7075 aluminium alloy.** *Journal of Materials Processing Technology* 2012, **212:**1472-1480.

6. De Freitas ER, Ferracini Junior EG, Piffer VP, Ferrante M: **Microstructure, material flow and tensile properties of A356 alloy thixoformed parts.** *Materials Research* 2004, **7:**593-603.

7. Cézard P: **Impact des effets thermiques sur le comportement du matériau lors de la mise en forme des aciers à l'état semi-solide : Analyses expérimentale et numérique.** Thesis. L'Ecole Nationale Supériure d'Arts et Métiers, Docteur de l'Ecole National Supérieure d'Arts et Métiers; 2006.

8. Carole R: **Contribution à la caractérisation et à la modelisation du comportement d'un acier à l'état semi-solide application au thixoforgeage.** Arts et Métiers ParisTech, Docteur de L'école nationale supérieure d'arts et métiers; 2003.

9. Püttgen W, Bleck W, Hirt G, Shimahara H: **Thixoforming of steels – A status report.** *Advanced Engineering Materials* 2007, **9:**231-245.

10. Atkinson H, Rassili A: **A review of the semi-solid processing of steel.** *International Journal of Material Forming* 2010, **3:**791-795.

11. Kirkwood DH, Suéry M, Kapranos P, Atkinson HV, Young KP: *Semi-solid Processing of Alloys.* Springer; 2010.

12. Becker E: **Investigations experimentales et numeriques pour l'identification des parametres clefs du procede de thixoforgeage de l'acier sur le produit mis en forme.** Thesis. L'Ecole Nationale Supériure d'Arts et Métiers, Docteur de L'Ecole National Supérieure d'Arts et Métiers; 2008.

13. Hirt G, Kopp R (Eds.): **Thixoforming - semi-solid metal processing**. Aachen: Wiley-VCH Verlag GmbH & Co. KGaA; 2009.

General conclusion

The objective of this thesis was the characterization of the microstructure of different steel grades at each step of the thixoforging process in order to better understand the influence of process parameters and mechanisms of deformation during the entire forming process. Our approach was divided into two parts. The first part was focused on the characterization of the microstructure in the semi-solid state using various techniques. In the second part, we mainly characterized the microstructure and the material flow of the thixoforged parts obtained under various process conditions.

The bibliography has been synthesized and studied in chapter 1. First, the semi-solid forming process has been described with various forming routes and their advantages as well as the rheological behavior of semi-solid microstructures with high and low solid fractions. Subsequently, the mechanisms leading to the thixotropic behavior have been explained and the industrial applications of the semi-solid forming introduced. It can be concluded that the morphology of the materials is influenced by the forming process and has an effect on the material flow and the mechanical properties of the parts. Therefore, it is necessary to study the microstructure of the material during the entire thixoforging process (as-received state, heating stage, forming stage). Thus, our studies originated from the characterization of the microstructure of the material, especially the liquid fraction, grain size, shape factor etc.

Chapter 2 presented the materials studied, the different techniques used for microstructure characterization from the most conventional to the newest approaches (fraction of liquid, grain size and etc.) as well as the experimental devices for thixoforming process. The principle, advantages and limitations of each technique have been studied for our experimental work. Meanwhile, the die tools, induction coils and the acquisition systems have been designed and chosen for thixoforging experiments.

The results of the experiments were mainly presented in chapter 3 and chapter 4.

Chapter 3 mainly focused on the microstructure characterization of the material in the semi-solid state. The billets were induction heated to the semi-solid state. The microstructure with spherical solid particles could be obtained directly by induction heating the as-received hot formed M2 bars, which therefore suggests that these initial M2 bars can be used for the thixoforging process directly. Multi-step heating cycles were applied for a homogeneous billet heating. It is suggested that a more suitable microstructure for thixoforging process can be obtained by heating the billet to the semi-solid state as quickly as possible, followed by a low

heating rate to the desired temperature. A prolonged holding time may improve the shape factor of the solid particles, but may not be preferable for industrial applications. The liquid fraction as a function of temperature has been evaluated by various techniques that provided approximate results. The Thermo-Calc software can be used to predict the variation of liquid fraction as a function of temperature, especially for semi-solid forming applications in industries. The DSC is an attractive method for the evaluation of the liquid fraction, although an error may be induced by the approximation of the partial area method. Another limitation of DSC for the semi-solid process studies is that the microstructure evolution can not be characterised by this technique. The quantitative metallography on specimens quenched from the semi-solid state can give microstructure information, about the liquid fraction variation and the microstructure. The diffusion rate after quenching the material from the semi-solid state to the room temperature depends on the considered material. For a material with few alloying elements (C38LTT or 100Cr6 for example), it will be difficult or even impossible to evaluate the liquid fraction and reveal the microstructure in the semi-solid state by image analysis after quenching. Moreover, the quantitative metallography method can only provide 2D microstructure information. The X-ray microtomography is able to provide the microstructure information in 3D. The contrast of the obtained images depends on the chemical contents of the investigated materials; if the latter contains heavy elements, some images with a good contrast can be obtained, as for the high speed tool steel grade M2. However, when there is not a high amount of heavy elements in the material considered, for example a low carbon steel grade, the microstructure may not be revealed by this technique. In addition, the X-ray microtomography permits a real in situ observation at high temperatures. By comparing the results obtained by quantitative metallographic method and 3D X-ray microtomography on M2 steel grade, the agreement was acceptable. Therefore, when the cooling speed is high enough to preserve the microstructure in the semi-solid state, with no diffusion, the quantitative metallographic method (2D microstructure characterization after quenching) is a good solution for the estimation of the liquid volume fraction in the semi-solid state. This comparison is of great importance because even though high-energy X-ray microtomography has proven to be a powerful tool, it is not as easy to use, nor as ubiquitous, as SEM and EDS techniques that are more readily accessible in laboratories. For microstructures that are difficult to be characterized by quenching (image analysis, X-ray

microtomography etc.), it is finally possible to use a CSLM which permits in situ observations directly at high temperature.

The results of thixoforging experiments were detailed and discussed in chapter 4. These experiments were performed to study the influence of the process parameters on the microstructure, the final part geometry, the load as a function of displacement, the material flows etc. Deformation mechanisms were observed. They can be composed of 5 major steps: breakdown of the interconnected solid-liquid structure, liquid flow, liquid flow incorporating solid particles, solid particles sliding among each other and plastic deformation of solid particles. The last two deformation mechanisms become prevailing when the liquid fraction decreases. Two main phenomena distinguishing thixoforming from hot forging were observed: the liquid segregation and the great heterogenization of the material flow. The first one is linked to the deformation mechanism mentioned above. It may lead to a heterogeneous liquid fraction during forming and heterogeneous chemical composition of the thixoforged part. The inevitable thermal gradient within the part being thixoforged and the segregation phenomenon are sources of heterogeneity of the liquid fraction and associated flow stress of the material. The thermal gradient is due to thermal exchange with the die and dissipated energy associated with deformation flow. The maximum liquid fraction is obtained “far” from the die contact and in the more deformed and more quickly deformed zones. This phenomenon can lead to a concentration of the plastic flow in bands or zones as was observed in all the cases studied in chapter 4. This phenomenon is an advantage of thixoforging when it comes to filling narrow areas in parts.

Perspectives

- Plugins development for 3D image analysis.

This work proposed new techniques for microstructure characterization, especially when 3D information is needed and when the microstructures are difficult to characterize after quenching. However, 3D image analysis is time-consuming. Therefore, it is necessary to develop some plugins which can treat the images automatically or at least semi-automatically.

- Numerical modeling development for optimization of the thixoforging process.

Up to now, the experiments have been performed on several steel grades which can not cover all the applications. For industrial applications, the development of a numerical model

based on the experimental achievements will be of great interest and even crucial for the future.

- Toward industrialization of steel thixoforging:

Industrialization of thixoforging needs to provide to industry a methodology with associated tools in order to design the complete thixoforging process including die design, choice of the heating device and heating driving parameters, determination of the thixoforging process parameters (initial temperature, forming velocity etc). The introduction of the thixoforging in the manufacturing layout of a part also implies the choice of adapted material and defining adapted detail geometry.

In order to develop methodology to implement thixoforging, simulation is necessary. The model used for thermal exchange and material flow therefore needs to be accurate enough in order to well represent the heterogeneity within the part as it is being thixoforged. The great softening effect associated with temperature and plastic flow is difficult to control numerically because of problem of convergence. The development of numerical simulation of thixoforging may not be restricted to finding accurate behaviour law but also needs development of numerical algorithm, like explicit calculations.

In the sensitivity of the plastic flow to process parameters and material lies an advantage of thixoforging, for example, in the case of forming narrow parts. But this sensitivity is also a disadvantage in the induced potential non robustness of the process, the necessary accuracy of the models, simulation, die design rules, choice of the processing parameters etc.

The first results obtained during this thesis are therefore very promising and clearly show the interest of thixoforging steel parts. The future works will focus on two complementary aspects: on the one hand, the development of a relevant numerical tool for a good simulation of this process, and on the other hand, the elaboration of reliable dies as well as the choice of the best steel grades and thixoforging parameters from all the results and techniques evoked during this work.

CARACTERISATION DES PROPRIETES D'EMPLOI DES ACIERS THIXOFORGES : VERS LA MAITRISE DU PROCESSUS DE FABRICATION

RESUME : Le thixoforgeage est un procédé de mise en forme innovant permettant l'élaboration de pièces complexes à l'état semi-solide. Il nécessite moins d'opérations et des efforts plus faibles que les autres procédés de mise en forme plus classiques. L'objectif de ce travail et de caractériser la microstructure de plusieurs nuances d'acier à chaque étape du procédé afin de mieux comprendre l'influence des différents paramètres et mécanismes de déformation, car la microstructure à l'état semi-solide, et en particulier la fraction de liquide, est très importante. Plusieurs techniques 2D et 3D (analyses MEB-EDS, CSLM, microtomographie X) ont été utilisées pour évaluer la fraction de liquide des aciers étudiés (M2, C38LTT et 100Cr6). Les résultats obtenus pour l'acier M2 montrent une bonne corrélation entre les observations 2D MEB-EDS et les analyses 3D en microtomographie après trempe, ce qui indique que ces deux techniques sont très efficaces pour caractériser l'état semi-solide des aciers fortement alliés. Le microscope CSLM est utilisé quant à lui pour observer directement l'état semi-solide à haute température : apparition du liquide, processus de solidification etc. Des essais de thixoforgeage ont ensuite été réalisés pour étudier l'influence des différents paramètres du procédé sur la microstructure, la géométrie finale des pièces, les écoulements de matière etc. Après avoir analysé la microstructure des pièces thixoforgées, des mécanismes permettant d'expliquer les écoulements de matière sont proposés. Qui plus est, la comparaison avec la simulation du procédé de forgeage à chaud montre que ces écoulements sont très différents, ce qui est dû au comportement du matériau. Ce dernier est très sensible aux paramètres du procédé : il est donc nécessaire de bien maîtriser et contrôler toutes les étapes lors de la mise en forme.

Mots clés : aciers, thixoforgeage, microstructure, MEB-EDS, CSLM, microtomographie X, écoulements de matière.

METALLURGICAL CHARACTERIZATION OF THIXOFORGED STEEL PARTS FOR A BETTER CONTROLLED MANUFACTURING PROCESS

ABSTRACT: The thixoforging process is an innovative forming process for the manufacturing of complex parts in the semi-solid state, in fewer forming steps and with a decreased forming force. The objective of this work is to characterize the microstructure of different steel grades at each step of the thixoforging process in order to better understand the influence of the process parameters and the mechanisms of deformation, as the microstructure of the material in the semi-solid state, especially the volume fraction of liquid, is very important. Several 2D and 3D techniques (SEM-EDS analyses, CSLM, X-ray microtomography) have been used to evaluate the liquid fraction of various steel grades (M2, C38LTT and 100Cr6). The results for M2 steel show a good agreement between 2D SEM - EDS observations and 3D X-ray microtomography after quenching, which proves that both techniques are efficient in characterizing high-alloyed steels in the semi-solid state. The CSLM technique is used to observe the microstructure directly at high temperature, with the apparition of liquid and the solidification. Thixoforging experiments are finally performed in order to study the influence of the process parameters on the microstructure: the final part geometry, the material flow etc. After analyzing the microstructure of the thixoforged parts, some mechanisms of material flow are proposed. Moreover, by comparing the results between the thixoforging experiments and the hot forging simulations, it is found that the material flow is very different from that of hot forging process, which results from the material behavior. The latter is very sensitive to the process parameters; an accurate process control is necessary.

Keywords: steel, thixoforging, microstructure, SEM-EDS, CSLM, X-ray microtomography, material flows.

ARTS ET MÉTIERS ParisTech

ParisTech INSTITUT DES SCIENCES ET TECHNOLOGIES PARIS INSTITUTE OF TECHNOLOGY